REPUBLIC OF CAMEROON
Peace-Work-Fatherland
****
UNIVERSITY OF YAOUNDE I
****
FACULTY OF SCIENCE
****
POSTGRADUATE SCHOOL
OF SCIENCE, TECHNOLOGY AND
GEOSCIENCES
****
RESEARCH AND POSTGRADUATE
TRAINING UNIT FOR CHEMISTRY AND
APPLICATIONS

REPUBLIQUE DU CAMEROUN
Paix-Travail-Patrie
****
UNIVERSITE DE YAOUNDE I
****
FACULTE DES SCIENCES
****
CENTRE DE RECHERCHE ET DE
FORMATIONDOCTORALE EN SCIENCES,
TECHNOLOGIES ET GEOSCIENCES
****
UNITE DE RECHERCHE ET DE
FORMATION
DOCTORALE CHIMIE ET APPLICATIONS

DEPARTMENT OF ORGANIC CHEMISTRY

DEPARTEMENT DE CHIMIE ORGANIQUE

CHEMICAL INVESTIGATION OF TWO CAMEROONIAN MEDICINAL PLANTS WITH ANTILEISHMANIAL AND ANTIBACTERIAL ACTIVITIES: *RUMEX NEPALENSIS* SPRENG *(POLYGONACEAE)*AND *SYMPHONIA GLOBULIFERA* LINN. F. (CLUSIACEAE)

THESIS

Presented and publicly defended in view of the requirement of Doctorate/Ph.D in Organic Chemistry

By:

NGUENGANG TCHUINKEU Ruland

Registration number: 12Y339

Master in Organic Chemistry

Under the supervision of:

LENTA NDJAKOU Bruno

Professor

Academic Year 2024 - 2025

REPUBLIQUE DU CAMEROUN
****
Paix - Travail - Patrie
****
UNIVERSITE DE YAOUNDE I
****
CENTRE DE RECHERCHE ET DE FORMATION DOCTORALE EN SCIENCES, TECHNOLOGIE ET GEOSCIENCES
****
UNITE DE RECHERCHE DE FORMATION DOCTORALE EN CHIMIE ET APPLICATIONS
****

REPUBLIC OF CAMEROON
****
Peace - Work - Fatherland
****
THE UNIVERSITY OF YAOUNDE I
****
POSTGRADUATE SCHOOL OF SCIENCE, TECHNOLOGY AND GEOSCIENCES
****
DOCTORAL RESEACH UNIT IN CHEMESTRY AND APPLICATIONS
****

DEPARTEMENT DE CHIMIE ORGANIQUE
DEPARTMENT OF ORGANIC CHEMISTRY

ATTESTATION DE CORRECTION DE MEMOIRE DE THESE DE DOCTORAT/ *Ph.D* DE MONSIEUR NGUENGANG TCHUINKEU RULAND

TITRE DE LA THÈSE: CHEMICAL INVESTIGATION OF TWO CAMEROONIAN MEDICINAL PLANTS WITH ANTILEISHMANIAL AND ANTIBACTERIAL ACTIVITIES: *RUMEX NEPALENSIS* SPRENG (POLYGONACEAE) AND *SYMPHONIA GLOBULIFERA* LINN.F. (CLUSIACEAE)

Nous soussignés, enseignants ci-dessous nommés, membres du jury de soutenance de thèse de Doctorat/ *Ph.D* de Monsieur **NGUENGANG TCHUINKEU RULAND**, Matricule **12Y339**, attestons que ce candidat a bel et bien pris en compte dans la mouture finale de sa thèse, toutes corrections et recommandations qui lui ont été faites au cours de sa soutenance en date du 16 Juin 2025.

En foi de quoi, la présente attestation de correction lui est délivrée pour servir et valoir ce que de droit.

Fait à Yaoundé le 29.07.2025

Président :
Pr ATCHADÉ Alex

Rapporteur :
Pr LENTA Bruno

Membres:
Pr MVOT AKAK C.
Pr Meli Lannang

UNIVERSITÉ DE YAOUNDÉ I
Faculté des Sciences
Division de la Programmation et du Suivi des Activités Académiques

THE UNIVERSITY OF YAOUNDE I
Faculty of Science
Division of Programming and Follow-up of Academic Affaires

LISTE DES ENSEIGNANTS PERMANENTS **LIST OF PERMANENT TEACHING STAFF**

ANNÉE ACADEMIQUE 2022/2023
(Par Département et par Grade)
DATE D'ACTUALISATION 30 septembre 2024

ADMINISTRATION

DOYEN : OWONO OWONO Luc Calvin, *Professeur*
VICE-DOYEN / DPSAA: NDJIGUI Paul-Désiré, *Professeur*
VICE-DOYEN / DSSE : NYEGUE Maximilienne Ascension, *Professeur*
VICE-DOYEN / DRC : NOUNDJEU Pierre, *Maître de Conférences*
Chef Division Administrative et Financière : NDOYE FOE Florentine Marie Chantal, *Maître de Conférences*
Chef Division des Affaires Académiques, de la Recherche et de la Scolarité DAARS : AJEAGAH Gideon AGHAINDUM, *Professeur*

1- DÉPARTEMENT DE BIOCHIMIE (BC) (44)

N°	NOMS ET PRÉNOMS	GRADE	OBSERVATIONS
1.	BIGOGA DAIGA Jude	Professeur	En poste
2.	FEKAM BOYOM Fabrice	Professeur	En poste
3.	KANSCI Germain	Professeur	En poste
4.	MBACHAM FON Wilfred	Professeur	En poste
5.	MOUNDIPA FEWOU Paul	Professeur	*Chef de Département*
6.	NGUEFACK Julienne	Professeur	En poste
7.	NJAYOU Frédéric Nico	Professeur	En poste
8.	OBEN Julius ENYONG	Professeur	En poste
9.	ACHU Merci BIH	Maître de Conférences	En poste
10.	AKINDEH MBUH NJI	Maître de Conférences	En poste
11.	ATOGHO Barbara MMA	Maître de Conférences	En poste
12.	AZANTSA KINGUE GABIN BORIS	Maître de Conférences	En poste
13.	BELINGA née NDOYE FOE F. M. C.	Maître de Conférences	*Chef DAF / FS*
14.	DAKOLE DABOY Charles	Maître de Conférences	En poste
15.	DONGMO LEKAGNE Joseph Blaise	Maître de Conférences	En poste
16.	DJUIDJE NGOUNOUE Marceline	Maître de Conférences	En poste
17.	DJUIKWO NKONGA Ruth Viviane	Maître de Conférences	En poste
18.	EFFA ONOMO Pierre	Maître de Conférences	*VD/FS/Univ Ebwa*
19.	EWANE Cécile Annie	Maître de Conférences	En poste
20.	KENGNE NOUEMSI Anne Pascale	Maître de Conférences	En poste
21.	KOTUE TAPTUE Charles	Maître de Conférences	En poste
22.	LUNGA Paul KEILAH	Maître de Conférences	En poste
23.	MANANGA Marlyse Joséphine	Maître de Conférences	En poste

DÉPARTEMENT DE BIOCHIMIE (BC) (SUITE)

24.	MBONG ANGIE M. Mary Anne	Maître de Conférences	En poste
25.	MOFOR née TEUGWA Clotilde	Maître de Conférences	*Doyen FS / UDs*
26.	NANA Louise épouse WAKAM	Maître de Conférences	En poste
27.	NGONDI Judith Laure	Maître de Conférences	En poste
28.	Palmer MASUMBE NETONGO	Maître de Conférences	En poste
29.	PECHANGOU NSANGOU Sylvain	Maître de Conférences	En poste
30.	TCHANA KOUATCHOUA Angèle	Maître de Conférences	En poste

31.	BEBEE Fadimatou	Chargée de Cours	En poste
32.	BEBOY EDJENGUELE Sara Nathalie	Chargé de Cours	En poste
33.	FONKOUA Martin	Chargé de Cours	En poste
34.	FOUPOUAPOUOGNIGNI Yacouba	Chargé de Cours	En poste
35.	KOUOH ELOMBO Ferdinand	Chargé de Cours	En poste
36.	MBOUCHE FANMOE Marceline J.	Chargée de Cours	En poste
37.	OWONA AYISSI Vincent Brice	Chargé de Cours	En poste
38.	WILFRED ANGIE ABIA	Chargé de Cours	En poste

39.	BAKWO BASSOGOG Christian Bernard	Assistant	En Poste
40.	ELLA Fils Armand	Assistant	En Poste
41.	EYENGA Eliane Flore	Assistant	En Poste
42.	MADIESSE KEMGNE Eugenie Aimée	Assistant	En Poste
43.	MANJIA NJIKAM Jacqueline	Assistant	En Poste
44.	WOGUIA Alice Louise	Assistant	En Poste

2- DÉPARTEMENT DE BIOLOGIE ET PHYSIOLOGIE ANIMALES (BPA) (50)

1.	AJEAGAH Gideon AGHAINDUM	Professeur	*DAARS/FS*
2.	DIMO Théophile	Professeur	En Poste
3.	DJIETO LORDON Champlain	Professeur	En Poste
4.	DZEUFIET DJOMENI Paul Désiré	Professeur	En Poste
5.	ESSOMBA née NTSAMA MBALA	Professeur	*CD et Vice Doyen/FMSB/UYI*
6.	KEKEUNOU Sévilor	Professeur	*Chef de Département*
7.	NJAMEN Dieudonné	Professeur	En poste
8.	NOLA Moïse	Professeur	En poste
9.	TAN Paul VERNYUY	Professeur	En poste
10.	TCHUEM TCHUENTE Louis Albert	Professeur	*Inspecteur de service / Coord.Progr./MINSANTE*
11.	ZEBAZE TOGOUET Serge Hubert	Professeur	En poste

12.	ALENE Désirée Chantal	Maître de Conférences	*Vice Doyen/ Uté Ebwa*
13.	ATSAMO Albert Donatien	Maître de Conférences	En poste
14.	BILANDA Danielle Claude	Maître de Conférences	En poste
15.	DJIOGUE Séfirin	Maître de Conférences	En poste

DÉPARTEMENT DE BIOLOGIE ET PHYSIOLOGIE ANIMALES (BPA) (SUITE)

16.	GOUNOUE KAMKUMO Raceline épse FOTSING	Maître de Conférences	En poste
17.	JATSA BOUKENG Hermine épse MEGAPTCHE	Maître de Conférences	En Poste
18.	KANDEDA KAVAYE Antoine	Maître de Conférences	En Poste
19.	LEKEUFACK FOLEFACK Guy B.	Maître de Conférences	En poste
20.	MAHOB Raymond Joseph	Maître de Conférences	En poste
21.	MBENOUN MASSE Paul Serge	Maître de Conférences	En poste
22.	MEGNEKOU Rosette	Maître de Conférences	En poste
23.	MOUNGANG Luciane Marlyse	Maître de Conférences	En poste
24.	NOAH EWOTI Olive Vivien	Maître de Conférences	En poste
25.	MONY Ruth épse NTONE	Maître de Conférences	En Poste
26.	MVEYO NDANKEU Yves Patrick	Maître de Conférences	En Poste
27.	NGUEGUIM TSOFACK Florence	Maître de Conférences	En poste
28.	NGUEMBOCK	Maître de Conférences	En poste
29.	TAMSA ARFAO Antoine	Maître de Conférences	En poste
30.	TOMBI Jeannette	Maître de Conférences	En poste

31.	AMBADA NDZENGUE GEORGIA ELNA	Chargé de Cours	En poste
32.	BASSOCK BAYIHA Etienne Didier	Chargé de Cours	En poste
33.	ETEME ENAMA Serge	Chargé de Cours	En poste
34.	FEUGANG YOUMSSI François	Chargé de Cours	En poste
35.	FOKAM Alvine Christelle Epse KENGNE	Chargé de Cours	En poste
36.	FOSSI TANKOUA Olivia Epse DJEUTCHOUANG SAYANG	Chargé de Cours	En poste
37.	GONWOUO NONO Legrand	Chargé de Cours	En poste
38.	KOGA MANG DOBARA	Chargé de Cours	En poste
39.	LEME BANOCK Lucie	Chargé de Cours	En poste
40.	MAPON NSANGOU Indou	Chargé de Cours	En poste
41.	METCHI DONFACK MIREILLE FLAURE EPSE GHOUMO	Chargé de Cours	En poste
42.	NGOUATEU KENFACK Omer Bébé	Chargé de Cours	En poste
43.	NJUA Clarisse YAFI	Chargée de Cours	*Chef Div. Uté Bamenda*
44.	NWANE Philippe Bienvenu	Chargé de Cours	En poste
45.	TADU Zephyrin	Chargé de Cours	En poste
46.	YEDE	Chargé de Cours	En poste
47.	YOUNOUSSA LAME	Chargé de Cours	En poste

48.	KODJOM WANCHE Jacguy Joyce	Assistante	En poste
49.	NDENGUE Jean De Matha	Assistant	En poste
50.	ZEMO GAMO Franklin	Assistant	En poste

3- DÉPARTEMENT DE BIOLOGIE ET PHYSIOLOGIE VÉGÉTALES (BPV) (32)			
1.	AMBANG Zachée	Professeur	*Chef de Département*
2.	DJOCGOUE Pierre François	Professeur	En poste
3.	MBOLO Marie	Professeur	En poste
4.	MOSSEBO Dominique Claude	Professeur	En poste
5.	YOUMBI Emmanuel	Professeur	En poste
6.	ZAPFACK Louis	Professeur	En poste
7.	ANGONI Hyacinthe	Maître de Conférences	En poste
8.	BIYE Elvire Hortense	Maître de Conférences	En poste
9.	MAHBOU SOMO TOUKAM. Gabriel	Maître de Conférences	En poste
10.	MALA Armand William	Maître de Conférences	En poste
11.	MBARGA BINDZI Marie Alain	Maître de Conférences	*DAAC /UDla*
12.	NGALLE Hermine BILLE	Maître de Conférences	En poste
13.	NGONKEU MAGAPTCHE Eddy L.	Maître de Conférences	*CT / MINRESI*
14.	TONFACK Libert Brice	Maître de Conférences	En poste
15.	TSOATA Esaïe	Maître de Conférences	En poste
16.	ONANA JEAN MICHEL	Maître de Conférences	En poste
17.	DJEUANI Astride Carole	Chargé de Cours	En poste
18.	GONMADGE CHRISTELLE	Chargée de Cours	En poste
19.	MAFFO MAFFO Nicole Liliane	Chargé de Cours	En poste
20.	MANGA NDJAGA JUDE	Chargé de Cours	En poste
21.	NNANGA MEBENGA Ruth Laure	Chargé de Cours	En poste
22.	NOUKEU KOUAKAM Armelle	Chargé de Cours	En poste
23.	NSOM ZAMBO EPSE PIAL ANNIE CLAUDE	Chargé de Cours	*En détachement/UNESCO MALI*
24.	GODSWILL NTSOMBOH NTSEFONG	Chargé de Cours	En poste
25.	KABELONG BANAHO Louis-Paul-Roger	Chargé de Cours	En poste
26.	KONO Léon Dieudonné	Chargé de Cours	En poste
27.	LIBALAH Moses BAKONCK	Chargé de Cours	En poste
28.	LIKENG-LI-NGUE Benoit C	Chargé de Cours	En poste
29.	TAEDOUNG Evariste Hermann	Chargé de Cours	En poste
30.	TEMEGNE NONO Carine	Chargé de Cours	En poste
31.	DIDA LONTSI Sylvere Landry	Assistant	En poste
34.	METSEBING Blondo-Pascal	Assistant	En poste

4- DÉPARTEMENT DE CHIMIE INORGANIQUE (CI) (27)			
1.	GHOGOMU Paul MINGO	Professeur	*Ministre Chargé de Mission PR*
2.	NANSEU NJIKI Charles Péguy	Professeur	En poste
3.	NDIFON Peter TEKE	Professeur	*CT MINRESI*
4.	NENWA Justin	Professeur	En poste
5.	NGOMO Horace MANGA	Professeur	*Vice Chancelor/UB*
6.	NJIOMOU C. épse DJANGANG	Professeur	En poste
7.	NJOYA Dayirou	Professeur	En poste
8.	ACAYANKA Elie	Maître de Conférences	En poste
9.	EMADAK Alphonse	Maître de Conférences	En poste
10	KAMGANG YOUBI Georges	Maître de Conférences	En poste
11	KEMMEGNE MBOUGUEM Jean C.	Maître de Conférences	En poste
12	KENNE DEDZO GUSTAVE	Maître de Conférences	En poste
13	MBEY Jean Aime	Maître de Conférences	En poste
14	NDI NSAMI Julius	Maître de Conférences	*Chef de Département*
15	NEBAH Née NDOSIRI Bridget NDOYE	Maître de Conférences	*Sénatrice/SENAT*
16	NYAMEN Linda Dyorisse	Maître de Conférences	En poste
17	PABOUDAM GBAMBIE AWAWOU	Maître de Conférences	En poste
18	TCHAKOUTE KOUAMO Hervé	Maître de Conférences	En poste
19	BELIBI BELIBI Placide Désiré	Maître de Conférences	*Chef Service/ ENS Bertoua*
20	CHEUMANI YONA Arnaud M.	Maître de Conférences	En poste
21	KOUOTOU DAOUDA	Maître de Conférences	En poste
22	MAKON Thomas Beauregard	Chargé de Cours	En poste
23	NCHIMI NONO KATIA	Chargée de Cours	En poste
24	NJANKWA NJABONG N. Eric	Chargé de Cours	En poste
25	PATOUOSSA ISSOFA	Chargé de Cours	En poste
26	SIEWE Jean Mermoz	Chargé de Cours	En Poste
27	BOYOM TATCHEMO Franck W.	Assistant	En Poste

5- DÉPARTEMENT DE CHIMIE ORGANIQUE (CO) (33)			
1.	Alex de Théodore ATCHADE	Professeur	*DEPE/Univ. Bertoua*
2.	DONGO Etienne	Professeur	*Vice-Doyen/FSE/UYI*
3.	NGOUELA Silvère Augustin	Professeur	*Chef de Département UDS*
4.	PEGNYEMB Dieudonné Emmanuel	Professeur	*Recteur UBertoua/ Chef de Département*
5.	MBAZOA née DJAMA Céline	Professeur	En poste
6.	MKOUNGA Pierre	Professeur	En poste

DÉPARTEMENT DE CHIMIE ORGANIQUE (CO) (SUITE)

7.	AMBASSA Pantaléon	Maître de Conférences	En poste
8.	EYONG Kenneth OBEN	Maître de Conférences	En poste
9.	FOTSO WABO Ghislain	Maître de Conférences	En poste
10.	KAMTO Eutrophe Le Doux	Maître de Conférences	En poste
11.	KENMOGNE Marguerite	Maître de Conférences	En poste
12.	MVOT AKAK CARINE	Maître de Conférences	En poste
13.	NGO MBING Joséphine	Maître de Conférences	*Chef de Cellule MINRESI*
14.	NGONO BIKOBO Dominique Serge	Maître de Conférences	*C.E.A/ MINESUP*
15.	NOTE LOUGBOT Olivier Placide	Maître de Conférences	*Dir ENS/Uté Bertoua*
16.	NOUNGOUE TCHAMO Diderot	Maître de Conférences	En poste
17.	TABOPDA KUATE Turibio	Maître de Conférences	En poste
18.	TAGATSING FOTSING Maurice	Maître de Conférences	En poste
19.	OUAHOUO WACHE Blandine M.	Maître de Conférences	En poste
20.	ZONDEGOUMBA Ernestine	Maître de Conférences	En poste

21.	MESSI Angélique Nicolas	Chargé de Cours	En poste
22.	MUNVERA MFIFEN Aristide	Chargé de Cours	En poste
23.	NGNINTEDO Dominique	Chargé de Cours	En poste
24.	NGOMO Orléans	Chargée de Cours	En poste
25.	NONO NONO Éric Carly	Chargé de Cours	En poste
26.	OUETE NANTCHOUANG Judith Laure	Chargée de Cours	En poste
27.	SIELINOU TEDJON Valérie	Chargé de Cours	En poste
28.	TCHAMGOUE Joseph	Chargé de Cours	En poste
29.	TSAFFACK Maurice	Chargé de Cours	En poste
30.	TSAMO TONTSA Armelle	Chargé de Cours	En poste
31.	TSEMEUGNE Joseph	Chargé de Cours	En poste
32	NDOGO ETEME Olivier	Assistant	En poste
33	NGUEMDJO CHIMEZE Valery Wilfried	Assistant	En poste

6- DEPARTEMENT DES ENERGIES RENOUVELABLES (ER) (1)			
1.	BODO Bertrand	Professeur	*Chef de Département*

7- DÉPARTEMENT D'INFORMATIQUE (IN) (22)			
1.	ATSA ETOUNDI Roger	Professeur	*Chef de Division MINESUP*
2.	FOUDA NDJODO Marcel Laurent	Professeur	*Inspecteur Général/ MINESUP*

DÉPARTEMENT D'INFORMATIQUE (IN) (SUITE)

3.	NDOUNDAM Réné	Maître de Conférences	En poste
4.	TSOPZE Norbert	Maître de Conférences	En poste

5.	ABESSOLO ALO'O Gislain	Chargé de Cours	*Chef de Cellule MINFOPRA*
6.	AMINOU HALIDOU	Chargé de Cours	*Chef de Département*
7.	DJAM Xaviera YOUH - KIMBI	Chargé de Cours	En Poste
8.	DOMGA KOMGUEM Rodrigue	Chargé de Cours	En poste
9.	EBELE Serge Alain	Chargé de Cours	En poste
10.	EKODECK Stéphane Gaël Raymond	Chargé de Cours	En poste
11.	HAMZA Adamou	Chargé de Cours	En poste
12.	JIOMEKONG AZANZI Fidel	Chargé de Cours	En poste
13.	KOUOKAM KOUOKAM E. A.	Chargé de Cours	En poste
14.	MELATAGIA YONTA Paulin	Chargé de Cours	En poste
15.	MESSI NGUELE Thomas	Chargé de Cours	En poste
16.	MONTHE DJIADEU Valery M.	Chargé de Cours	En poste
17.	NZEKON NZEKO'O ARMEL JACQUES	Chargé de Cours	En poste
18.	OLLE OLLE Daniel Claude Georges Delort	Chargé de Cours	*Sous-Directeur ENSET Ebolowa*
19.	TAPAMO Hyppolite	Chargé de Cours	En poste

20.	BAYEM Jacques Narcisse	Assistant	En poste
21.	MAKEMBE. S . Oswald	Assistant	*Directeur CUTI*
22.	NKONDOCK. MI. BAHANACK.N.	Assistant	En poste

8- DÉPARTEMENT DE MATHÉMATIQUES (MA) (34)

1.	AYISSI Raoult Domingo	Professeur	*Chef de Département*

2.	KIANPI Maurice	Maître de Conférences	En poste
3.	MBANG Joseph	Maître de Conférences	En poste
4.	MBEHOU Mohamed	Maître de Conférences	*Chef de Division/ENSPY*
5.	MBELE BIDIMA Martin Ledoux	Maître de Conférences	*Chef de Département de modélisation et applications industrielles/ENSPY*
6.	NOUNDJEU Pierre	Maître de Conférences	*VDRC/FS/UYI*
7.	TAKAM SOH Patrice	Maître de Conférences	En poste
8.	TCHAPNDA NJABO Sophonie B.	Maître de Conférences	*Directeur/AIMS Rwanda*
9.	TCHOUNDJA Edgar Landry	Maître de Conférences	En poste

10.	AGHOUKENG JIOFACK Jean Gérard	Chargé de Cours	*Chef Cellule MINEPAT*
11.	BOGSO ANTOINE Marie	Chargé de Cours	En poste

DÉPARTEMENT DE MATHÉMATIQUES (MA) (SUITE)

12.	BITYE MVONDO Esther	Chargé de Cours	En poste
13.	CHENDJOU Gilbert	Chargé de Cours	En poste
14.	DJIADEU NGAHA Michel	Chargé de Cours	En poste
15.	DOUANLA YONTA Herman	Chargé de Cours	En poste
16.	KIKI Maxime Armand	Chargé de Cours	En poste
17.	KOKOMO AYISSI Eric Brice	Chargé de Cours	En poste
18.	LOUMNGAM KAMGA Victor	Chargé de Cours	En poste
19.	MBAKOP Guy Merlin	Chargé de Cours	En poste
20.	MBATAKOU Salomon Joseph	Chargé de Cours	En poste
21.	MENGUE MENGUE David Joël	Chargé de Cours	*Chef Dpt /ENS Université d'Ebolowa*
22.	MBIAKOP Hilaire George	Chargé de Cours	En poste
23.	NGUEFACK Bernard	Chargé de Cours	En poste
24.	NIMPA PEFOUKEU Romain	Chargée de Cours	En poste
25.	OGADOA AMASSAYOGA	Chargée de Cours	En poste
26.	POLA DOUNDOU Emmanuel	Chargé de Cours	*En stage*
27.	TENKEU JEUFACK Yannick Léa	Chargé de Cours	En poste
28.	TCHEUTIA Daniel Duviol	Chargé de Cours	En poste
29.	TETSADJIO TCHILEPECK M. Eric.	Chargé de Cours	En poste

30.	FOKAM Jean Marcel	Assistant	En poste
31.	GUIDZAVAI KOUCHERE Albert	Assistant	En poste
32.	MANN MANYOMBE Martin Luther	Assistant	En poste
33.	MEFENZA NOUNTU Thiery	Assistant	En poste
34.	NYOUMBI DLEUNA Christelle	Assistant	En poste

9- DÉPARTEMENT DE MICROBIOLOGIE (MIB) (24)

1.	ESSIA NGANG Jean Justin	Professeur	*Chef de Département*
2.	NYEGUE Maximilienne Ascension	Professeur	*VICE-DOYEN / DSSE*
3.	SADO KAMDEM Sylvain Leroy	Professeur	*VICE-DOYEN / DSSE*

4.	ASSAM ASSAM Jean Paul	Maître de Conférences	En poste
5.	BOUGNOM Blaise Pascal	Maître de Conférences	En poste
6.	KOUITCHEU MABEKU Epse KOUAM Laure Brigitte	Maître de Conférences	En poste
7.	MUNE MUNE Martin Alain	Maître de Conférences	En poste
8.	RIWOM Sara Honorine	Maître de Conférences	En poste
9.	NJIKI BIKOÏ Jacky	Maître de Conférences	En poste
10.	TCHIKOUA Roger	Maître de Conférences	*Chef de Service de la Scolarité*

11.	ESSONO Damien Marie	Chargé de Cours	En poste
12.	LAMYE Glory MOH	Chargé de Cours	En poste
13.	MEYIN A EBONG Solange	Chargé de Cours	En poste

DÉPARTEMENT DE MICROBIOLOGIE (MIB) (SUITE)

14.	MONI NDEDI Esther Del Florence	Chargé de Cours	En poste
15.	NKOUDOU ZE Nardis	Chargé de Cours	En poste
16.	NKOUE TONG Abraham	Chargé de Cours	En poste
17.	TAMATCHO KWEYANG Blandine Pulchérie	Chargé de Cours	En poste
18.	SAKE NGANE Carole Stéphanie	Chargé de Cours	En poste
19.	TOBOLBAÏ Richard	Chargé de Cours	En poste

20.	EZO'O MENGO Fabrice Télésfor	Assistant	En poste
21.	EHETH Jean Samuel	Assistant	En poste
22.	MAYI Marie Paule Audrey	Assistant	En poste
23.	NGOUENAM Romial Joël	Assistant	En poste
24.	NJAPNDOUNKE Bilkissou	Assistant	En poste

10. DEPARTEMENT DE PHYSIQUE(PHY) (42)

1.	BEN- BOLIE Germain Hubert	Professeur	En poste
2.	BIYA MOTTO Frédéric	Professeur	*DG/HYDRO Mekin*
3.	DJUIDJE KENMOE épouse ALOYEM	Professeur	En poste
4.	EKOBENA FOUDA Henri Paul	Professeur	*Vice-Recteur. Uté Ngaoundéré*
5.	ESSIMBI ZOBO Bernard	Professeur	En poste
6.	HONA Jacques	Professeur	En poste
7.	NANA ENGO Serge Guy	Professeur	En poste
8.	NANA NBENDJO Blaise	Professeur	En poste
9.	NDJAKA Jean Marie Bienvenu	Professeur	*Chef de Département*
10.	NJANDJOCK NOUCK Philippe	Professeur	En poste
11.	NOUAYOU Robert	Professeur	En poste
12.	SAIDOU	Professeur	*Chef de centre/IRGM/MINRESI*
13.	SIMO Elie	Professeur	En poste
14.	TABOD Charles TABOD	Professeur	*Doyen FSUniv/Bda*
15.	TCHAWOUA Clément	Professeur	En poste
16.	WOAFO Paul	Professeur	En poste
17.	ZEKENG Serge Sylvain	Professeur	En poste
18.	ENYEGUE A NYAM épse BELINGA	Maître de Conférences	*Chef de Division de la formation continue et à distance/ENSPY*
19.	FEWO Serge Ibraïd	Maître de Conférences	En poste
20.	FOUEJIO David	Maître de Conférences	*Chef Cell/ MINADER*
21.	MBINACK Clément	Maître de Conférences	En poste
22.	MBONO SAMBA Yves Christian U.	Maître de Conférences	En poste

DEPARTEMENT DE PHYSIQUE(PHY) (SUITE)

23.	MELI'I Joelle Larissa	Maître de Conférences	En poste
24.	MVOGO ALAIN	Maître de Conférences	En poste
25.	NDOP Joseph	Maître de Conférences	En poste
26.	SIEWE SIEWE Martin	Maître de Conférences	En poste
27.	VONDOU Derbetini Appolinaire	Maître de Conférences	En poste
28.	WAKATA née BEYA Annie Sylvie	Maître de Conférences	*Directeur/ENS/UYI*
29.	WOULACHE Rosalie Laure	Maître de Conférence	*En stage depuis février 2023*
30.	ABDOURAHIMI	Chargé de Cours	En poste
31.	AYISSI EYEBE Guy François Valérie	Chargé de Cours	En poste
32.	CHAMANI Roméo	Chargé de Cours	En poste
33.	DJIOTANG TCHOTCHOU Lucie Angennes	Chargée de Cours	En poste
34.	EDONGUE HERVAIS	Chargé de Cours	En poste
35.	KAMENI NEMATCHOUA Modeste	Chargé de Cours	En poste
36.	LAMARA Maurice	Chargé de Cours	En poste
37.	NGA ONGODO Dieudonné	Chargé de Cours	En poste
38.	OTTOU ABE Martin Thierry	Chargé de Cours	Directeur Unité de production des réactifs/IMPM
39.	TEYOU NGOUPO Ariel	Chargé de Cours	En poste
40.	TOGUEU MOTCHEYO Alain Bertrand	Chargé de Cours	En poste
41.	WANDJI NYAMSI William	Chargé de Cours	En poste
42.	SOUFFO TAGUEU Merimé	Assistant	En poste

11- DÉPARTEMENT DE SCIENCES DE LA TERRE (ST) (34)

1.	EKOMANE Emile	Professeur	*Chef Div./Uté Ebolowa*
2.	GANNO Sylvestre	Professeur	En poste
3.	NDJIGUI Paul-Désiré	Professeur	*Vice-Doyen /DPSAA*
4.	NGOS III Simon	Professeur	En poste
5.	NKOUMBOU Charles	Professeur	En poste
6.	ONANA Vincent Laurent	Professeur	*Chef de Département/Uté. Eb.*
7.	YENE ATANGANA Joseph Q.	Professeur	*Chef Div. /MINTP*

8.	BISSO Dieudonné	Maître de Conférences	*Chef de Département*
9.	Elisé SABABA	Maitre de Conférences	En poste
10.	EYONG John TAKEM	Maitre de Conférences	En poste
11.	FUH Calistus Gentry	Maître de Conférences	*Sec. d'Etat/MINMIDT*

DÉPARTEMENT DE SCIENCES DE LA TERRE (ST) (SUITE)

12.	MBIDA YEM	Maitre de Conférences	En poste
13.	MBESSE Cécile Olive	Maître de Conférences	En poste
14.	METANG Victor	Maître de Conférences	En poste
15.	NGO BIDJECK Louise Marie	Maître de Conférences	En poste
16.	NGUEUTCHOUA Gabriel	Maître de Conférences	*CEA/MINRESI*
17.	NJILAH Isaac KONFOR	Maître de Conférences	En poste
18.	TCHAKOUNTE Jacqueline épse NUMBEM	Maître de Conférences	*Chef. Cell /MINRESI*
19.	TCHOUANKOUE Jean-Pierre	Maître de Conférences	En poste
20.	TEMGA Jean Pierre	Maître de Conférences	En poste
21.	ZO'O ZAME Philémon	Maître de Conférences	*DG/ART*

22.	ANABA ONANA Achille Basile	Chargé de Cours	En poste
23.	BEKOA Etienne	Chargé de Cours	En poste
24.	MAMDEM TAMTO Lionelle Estelle, épouse BITOM	Chargée de Cours	En poste
25.	NGO BELNOUN Rose Noël	Chargée de Cours	En poste
26.	NGO'O ZE ARNAUD	Chargé de Cours	En poste
27.	NOMO NEGUE Emmanuel	Chargé de Cours	En poste
28.	NTSAMA ATANGANA Jacqueline	Chargée de Cours	En poste
29.	TCHAPTCHET TCHATO De P.	Chargé de Cours	En poste
30.	TEHNA Nathanaël	Chargé de Cours	En poste
31.	FEUMBA Roger	Chargé de Cours	En poste
32.	MBANGA NYOBE Jules	Chargé de Cours	En poste

33.	KOAH NA LEBOGO Serge Parfait	Assistant	En poste
34.	TENE DJOUKAM Joëlle Flore, épouse KOUANKAP NONO	Assistante	En poste

Répartition chiffrée des Enseignants de la Faculté des Sciences de l'Université de Yaoundé I

NOMBRE D'ENSEIGNANTS					
DÉPARTEMENT	**Professeurs**	**Maîtres de Conférences**	**Chargés de Cours**	**Assistants**	**Total**
BCH	8 (01)	15 (11)	13 (03)	7 (05)	**44 (20)**
BPA	14 (01)	16 (09)	18 (04)	4 (02)	**49 (16)**
BPV	6 (01)	12 (02)	13 (07)	3 (00)	**32 (10)**
CI	7 (01)	15 (04)	5 (01)	1 (00)	**27 (05)**
CO	6 (01)	18 (04)	11 (04)	2 (00)	**33 (09)**

Répartition chiffrée des Enseignants de la Faculté des Sciences de l'Université de Yaoundé I (suite)

ER	01 (00)		/	/	**01 (00)**
IN	2 (00)	2 (00)	14 (01)	4 (00)	**22 (01)**
MAT	1 (00)	8 (00)	17 (01)	7 (02)	**34 (02)**
MIB	2 (01)	7 (03)	8 (04)	7 (02)	**24 (11)**
PHY	15 (01)	15 (04)	11 (01)	2 (00)	**42 (06)**
ST	8 (00)	17 (03)	15 (04)	3 (01)	**34 (07)**
Total	**69 (07)**	**125 (40)**	**125 (30)**	**40 (12)**	**349 (88)**

Soit un total de **342 (88)** dont :

- Professeurs **69 (07)**
- Maîtres de Conférences **123 (41)**
- Chargés de Cours **120 (30)**
- Assistants **30 (09)**
- () = Nombre de Femmes **88**

DECLARATION

I, the undersigned, **NGUENGANG TCHUINKEU Ruland** (Master in Organic Chemistry, Registration number 12Y339), certify that the work presented in this thesis and entitled «Chemical investigation of two Cameroonian medicinal plants with antileishmanial and antibacterial activities: *Rumex nepalensis* Spreng (Polygonaceae) and *Symphonia globulifera* Linn. f. (Clusiaceae)» was carried out by me., in the Laboratory of Natural Substances of Therapeutic Interest and Organic Synthesis (LASUNITSO) at the Higher Teacher Training College (HTTC), University of Yaoundé 1 under the supersivion of **LENTA NDJAKOU Bruno** (Professor). This work has not yet been the subject of any submission for the acquisition of any academic degree.

Student Supervisor

DEDICATION

To my entire family and my in-laws.

ACKNOWLEDGEMENTS

I express my deepest gratitude to:

Professor LENTA NDJAKOU Bruno, for his expertise, dedication, exceptional support, unwavering guidance and mentorship that have been pivotal in the successful completion of this thesis. His dedication to my education and personal growth has made a lasting impact on my life, and I truly appreciate his unwavering commitment to my success. In many ways, he has been a father figure to me, providing not only academic knowledge but also invaluable life lessons;

Professor PEGNYEMB Dieudonné Emmanuel, Head of the Department of Organic Chemistry at the Faculty of Science of the University of Yaoundé 1, for his proactive approach, unwavering commitment and constant accessibility in facilitating the Department's efficient operations;

All the lecturers of the Department of Organic Chemistry of the Faculty of Science and the Higher Teacher Training College University of Yaoundé 1 for the intellectual and moral training they gave me.

Professor SEWALD Norbert and **Dr FRESE Marcel** from the University of Bielefeld (Germany), and all the principal investigator from the University of Yaoundé 1, for their support, advice and collaboration in the construction of this work;

Professor CHOUNA Jean Rodolph of the University of Dschang, for his expertise, availability, and multiple advice throughout this work;

Professor NGOUELA Silvère, Professor AWANTU FUSI Engelbert, BANKEU KEZETAS Jean Jules and **Dr FONGANG FOTSING Yannick Stéphane**, for their contribution to this work;

Dr TCHENITEGNI TOUSSIE Billy, who has been with me from the start to the completion of my doctoral thesis. Not only did we work together effectively, but we also forged a strong and meaningful social connection**;**

STRESER Nicole, for her encouragement, availability, and support throughout this work;

MATULA Calvin, for his availability, and support throughout this work;

Drs MADIESSE Eugenie, **JOUDA Jean-Bosco**, **TCHAMGOUE Joseph**, and **BITCHAGNO Gabin**, for their contribution throughout this work;

All the laboratory seniors: **Drs ATEBA Joël**, **NGATCHOU Jules, TCHUENMOGNE TCHUENTE Aimé, MBA'NING Brice MITTERANT**, **DONFACK VOUFFO Erik**, **NGAMGWE Rosine**, **Flaure ESSOUNG, DIETAGOUM Stephanie**, **KAGHO Donald, WALEGUELE Claire**, **WONKAM NKWENTI Argan Kelly, GARBA Jean Koffi, BOUZEKO Larissa, DONGMO JUMETA Johanne Kevine, CHOUNA DON Suzy Ardo**, **Mrs TSAKOU TAFOUO Armelle and GOUNI Clemence** for their welcome, advice and constant assistance;

My laboratory mates: **l MENATCHE NJOPNU Joël**, **YOUMBI Tatiana**, **MATEFO Ingrid**, **NGASSAM Elfried**, **FEUMBOU NOUSSI Alix**, **DIFFO Gaelle**, **KADJI, Andrel SAIDOU TSILA Sylveste, POSSI DJILA Landry Franck and BEKOU Larissa** for the close bond we have cultivated over these extended years and for the various types of assistance you have extended to me;

Mr NANA Victor, for helping with the harvest of the plant;

The **Deutscher Akademischer Austauschdienst** (**DAAD**) through **YaBiNaPA project N° 57316173**, for the grant that enables us to have various material and financial resources;

My cherished wife **Mrs NGUENGANG Jenny Brondella**, whose steadfast support and boundless love have been the cornerstone of my work;

My entire family and in-laws, for their unwavering support and encouragement;

My friends, for their invaluable support and encouragement.

TABLE OF CONTENTS

DECLARATION xiii
DEDICATION xiv
ACKNOWLEDGEMENTS xv
TABLE OF CONTENTS xvii
LIST OF ABBREVIATIONS, ACRONYMS AND SYMBOLS xxii
LIST OF TABLES xxiii
LIST OF FIGURES xxv
LIST OF SCHEMES xxix
ABSTRACT 1
RESUME 3
GENERAL INTRODUCTION 5
PART I:LITERATURE REVIEW 7
I.1. OVERVIEW ON LEISHMANIASIS 8
I.1.1. Definition 8
I.1.2. Epidemiology 8
I.1.3. The vector of leishmaniasis 9
I.1.4. The parasite 9
I.1.5. Treatment of leishmaniasis 9
I.2. OVERVIEW ON BACTERIA 11
I.2.1. Definition 11
I.2.2. Epidemiology 12
I.2.3. Classification of Bacteria 12
I.2.4. Identification of Bacteria 13
I.2.5. Treatment of bacterial infections 13
I.3. OVERVIEW ON THE INVESTIGATED PLANTS 14
I.3.1. Overview on the Clusiaceae family 14
I.3.1.1. Introduction 14
I.3.1.2. Overview on the genus *Symphonia* 15
I.3.1.2.1. Overview on *S. globulifera* 15
I.3.2. General overview on the Polygonaceae family 17
I.3.2.1. Overview on the genus *Rumex* 17
I.3.2.1.1. Overview on *Rumex nepalensis* Spreng 18

I.4. USES OF THE INVESTIGATED PLANTS 18
I.4.1. Uses of *S. globulifera* species in folk medecine 18
I.4.2. Uses of plants of the genus *Rumex* in folk medecine 19
I.5. PREVIOUS CHEMICAL AND BIOLOGICAL INVESTIGATIONS ON THE SELECTED PLANTS 20
I.5.1. Previous chemical investigations on the studied plants 20
I.5.1.1. Previous chemical investigations on plants of *Symphonia globulifera* 20
1.5.1.1.1. Benzophenones (Polycyclic polyprenylated acylphloroglucinols, PPAPs) 21
1.5.1.1.2. Xanthones 26
1.5.1.1.3. Flavonoids 29
I.5.1.2. Previous chemical investigations on plants of the genus *Rumex* 30
I.5.1.2.1. Quinones 31
I.5.1.2.2. Flavonoids 33
I.5.1.2.3. Naphtalenes 35
I.5.1.2.4. Triterpenoids 36
I.5.1.2.5. Stibenoids 37
I.5.1.2.6. Carotenoids 38
I.5.1.2.7. Other phenolic compounds 39
I.5.2. Previous biological investigations on the studied plants 40
I.5.2.1. Previous biological investigations on *S. globulifera* 40
I.5.2.2. Previous biological investigations on plants of the genus *Rumex* 42
I.6. Biosynthesis of benzophenones (Polycyclic polyprenylated acylphloroglucinols, PPAPs) 43
PART II:**RESULTS AND DISCUSSION** 46
II.1. Chemical study of *Rumex nepalensis* Spreng and *Symphonia globulifera* Linn. f. 47
II.1.1. Extraction of plant material 47
II.1.2. Antileishmanial screening 47
II.1.3. Antibacterial screening 47
II.1.4. Isolation of compounds 48
II.1.5. Structural elucidation of the isolated compounds 51
II.1.5.1. Phenylisobenzofuranone 51
II.1.5.1.1. Structural elucidation of compound RBR48-1 51
II.1.5.2. Polyprenylated benzophenones 59
II.1.5.2.1. Structural elucidation of compound SYE25-6M 59
II.1.5.2.2. Structural elucidation of compound SYE27-28-16Ma/b 66
II.1.5.2.3. Structural identification of compound SYE44-4-5mi 75

II.1.5.3. Tocotrienol derivative 80
II.1.5.3.1. Structural elucidation of compound SYE70- 45-48 80
II.1.5.4. Phenolic derivatives 86
II.1.5.4.1. Structural identification of compound RBR3C 86
II.1.5.4.2. Structural identification of compound RBR2 93
II.1.5.4.3. Structural identification of compound RBR1a 97
II.1.5.4.4. Structural identification of compound RBR6b 102
II.1.5.4.5. Structural identification of compound RBR7a2 106
II.1.5.4.6. Structural identification of compound RBR10R1 110
II.1.5.4.7. Structural identification of compound RBR147-19 115
II.1.5.4.8. Structural identification of compound RBR15 120
II.1.5.4.9. Structural identification of compound RBR95-35b 125
II.1.5.4.10. Structural identification of compound RBR95-23a/b 130
II.1.5.4.11. Structural identification of compound RBR9a 135
II.1.5.4.12. Structural identification of compound RBR64 140
II.1.5.4.13. Structural identification of compound RBR17 145
II.1.5.4.14. Structural elucidation of compound SYEF137 151
II.1.5.4.15. Structural elucidation of compound SYEF171 157
II.1.5.4.16. Structural elucidation of compound SYE26-8M 161
II.1.5.4.17. Structural elucidation of compound SYEF1310b 166
II.1.5.4.18. Structural elucidation of compound SYEF26-48D 171
II.1.5.4.19 Structural elucidation of compound SYEF23 177
II.1.5.5. Furanones derivative derivative 181
II.1.5.5.1. Structural identification of compound RBR9N2 181
II.1.5.5.2. Structural identification of compound RBR9N1 186
II.1.5.6. Triterpenoid derivative derivative 190
II.1.5.6.1. Structural elucidation of compound SYE22-22 190
II.1.5.7. Steroids 191
II.1.5.7.1. Structural identification of compound RBR5 191
II.1.5.7.2. Structural identification of compound RBR4 192
II.1.5.7.3. Structural identification of compound RBR86-57D 193
II.2. PREPARATION OF THE HEMISYNTHETIC DERIVATIVES 194
II.2.1. Allylation and acetylation of emodin (117) 194
II.2.1.1. Structural elucidation of compound RBR3Al1 (143) 195
II.2.1.2. Structural elucidation of compound RBR3Al2 (144) 197

II.2.1.3. Structural elucidation of compound RBR3Al3 (145) 200
II.2.1.4. Structural elucidation of compound RBR3Al4 (146) 203
II.2.1.5. Structural elucidation of compound RBR3Ace1 (147) 205
II.2.2. Nitration of emodin (117) and catalytic hydrogenation of 1,6,8-trihydroxy-3-methyl-2,4,5,7-tetranitro anthraquinone (148) 207
II.2.2.1. Structural identification of compound (STEP1 new3) (148) 207
II.2.2.2. Structural identification of compound (RBR3amin19b) (148) 209
II.2.3. Acid hydrolysis 210
II.3. CHEMOPHENETIC SIGNIFICANCE OF THE ISOLATED COMPOUNDS 210
II.4. BIOLOGICAL ACTIVITIES OF THE ISOLATED COMPOUNDS 212
II.4.1. Antileishmanial activity of extracts, fractions, and isolated compounds 212
II.4.1.1. S. globulifera 213
II.4.2. Antibacterial activity of extracts, fractions, and isolated compounds 213
II.4.2.1. S. globulifera 214
II.4.2.2. R. nepalensis 215
CONCLUSION AND PERSPECTIVES 219
PART III:MATERIAL AND METHODS 223
III.1. APPARATUS AND PLANT MATERIALS 224
III.1.1. Apparatus 224
III.1.1.1. Evaporation, weighing and chromatographies 224
III.1.1.2. Mass spectra 224
III.1.1.3. Nuclear Magnetic Resonance (NMR) spectra 225
III.1.1.4. Optical rotation measurement and Infrared spectrum 225
III.1.2. Plant materials 225
III.2. SOME CHARACTERISTIC TESTS USED IN THE IDENTIFICATION OF SECONDARY METABOLITES 225
III.2.1. Ferric chloride test 225
III.2.2. Shinoda test 226
III.2.3. Bornträger test 226
III.2.4. Libermann-Burchard test 226
III.3. EXTRACTION, FRACTIONATION, ISOLATION AND PURIFICATION OF COMPOUNDS 226
III.3.1. Extraction 227
III.3.1.1. Preparation of *R. nepalensis* crude extract 227
III.3.1.2. Preparation of *S. globulifera* crude extract 227

III.3.2. Fractionnation of crude extracts and isolation of compounds 227
III.3.2.1. Fractionnation of crude extract and isolation of compounds from *R. nepalensis* 227
III.3.2.1.1. Study of the sub-fraction F1 227
III.3.2.1.2. Study of the sub-fraction F2 227
III.3.2.1.3. Study of the sub-fraction F3 228
III.3.2.1.4. Study of the sub-fraction F4 228
III.3.2.2. Fractionnation of crude extract and isolation of compounds from *S. globulifera* 228
III.4. EVALUATION OF BIOLOGICAL ACTIVITIES 230
III.4.1. Antileishmanial assay 230
III.4.2. Antibacterial assay 231
III.4.3. Cytotoxicity assay 231
III.5. PHYSICAL AND CHEMICAL CHARACTERISTICS OF THE ISOLATED COMPOUNDS 233
REFERENCES 241
ANNEXE 261

LIST OF ABBREVIATIONS, ACRONYMS AND SYMBOLS

CC	Column Chromatography
CDC	Centers for Disease Control and Prevention
CL	Cutaneous Leishmaniasis
COSY	Correlation Spectroscopy
d	Doublet
DEPT	Distortionless Enhancement by Polarization Transfer
DMSO	Dimethyl Sulfoxide
EI	Electron Impact
ESI	Electro Spray Ionization
ESIMS	Electro Spray Ionization Mass Spectrum
HMBC	Heteronuclear Multiple Bond Correlation
HMQC	Heteronuclear Single Quantum Coherence
HRESI	High Resolution Electrospray Ionization
IC_{50}	Inhibitory Concentration 50
IR	Infrared
J	Coupling Constant in Hertz
VL	Visceral Leishmaniasis
m	Multiplet
MIC	Minimal Inhibitory Concentration
NMR ^{13}C	Carbon 13 Nuclear Magnetic Resonance
NMR ^{1}H	Proton Nuclear Magnetic Resonance
q	Quartet
s	Singlet
SI	Selectivity Index
TLC	Thin Layer Chromatography
t	Triplet
WHO	World Health Organization
δ	Chemical shift in ppm

LIST OF TABLES

Table 1: Sub-family, tribes and genera of Clusiaceae 15
Table 2: Places where *S. globulifera* has already been collected in Cameroon 17
Table 3: Places where *R. nepalensis* has already been collected in Cameroon 18
Table 4a: Traditional uses of *S. globulifera* in folk medicine 19
Table 4b: Traditional uses of some species of the genus *Rumex* *19*
Table 5: Some polyprenylated benzophenones isolated from *S. globulifera* 22
Table 6: Some xanthones isolated from *S. globulifera* 27
Table 7: Biflavonoids isolated from *S. globulifera* 30
Table 8: Some anthraquinones isolated from the *Rumex* genus 32
Table 9: Some flavonoids isolated from *Rumex species* 34
Table 10: Some naphtalenes isolated from *Rumex species* 36
Table 11: Some triterpenoids isolated from *R. japonicus* 37
Table 12: Some stibenoids isolated from the *Rumex* genus 38
Table 13: Some carotenoids isolated from *Rumex* species 39
Table 14: Other phenolic compounds isolated from *Rumex species* 40
Table 15: Some of the biological activities from the crude extract from different parts of *S. globulifera* 41
Table 16: Some of the biological activities from the secondary metabolites isolated from different parts of *S. globulifera* 41
Table 17: Some of the biological activities from the crude extract from plants of the genus *Rumex* ... 42
Table 18: Some of the biological activities from compounds isolated from plants of the genus *Rumex* 43
Table 19: ^{1}H (600 MHz) and ^{13}C (150 MHz) spectroscopic data of RBR48-1 in DMSO-d_6 58
Table 20: ^{1}H (600 MHz) and ^{13}C (150 MHz) NMR data of SYE25-6M in acetone-d_6 65
Table 21: ^{1}H (600 MHz) and ^{13}C (150 MHz) NMR data of SYE27-28-16Ma/b in acetone-d_6, ^{13}C (125 MHz), ^{1}H (500 MHz)] 74
Table 22: Comparative ^{1}H (600 MHz) and ^{13}C (150 MHz) NMR data of SYE44-4-5mi and guttiferone K in MeOH-d_4 79
Table 23: ^{1}H (600 MHz) and ^{13}C (150 MHz) NMR data of SYE70- 45-48 in DMSO-d_6 86
Table 24: Comparative NMR data of RBR3C [^{1}H (600 MHz), ^{13}C (150 MHz)] and emodin [^{1}H (400 MHz), ^{13}C (100 MHz)] in DMSO-d_6 92
Table 25: Comparative NMR data of RBR2 [^{1}H (600 MHz), ^{13}C (150 MHz)] in $CDCl_3$and pyscion [^{1}H (400 MHz), ^{13}C (100 MHz)] in DMSO-d_6 97
Table 26: Comparative NMR data of RBR1a [^{1}H (600 MHz), ^{13}C (150 MHz)] and chrisophanol [^{1}H (400 MHz), ^{13}C (100 MHz)] in DMSO-d_6 102
Table 27: ^{1}H (600 MHz) and ^{13}C (150 MHz) NMR data of RBR1a compared to those of citreorosein [^{13}C (125 MHz), ^{1}H (500 MHz)] in DMSO-d_6 106
Table 28: ^{1}H (600 MHz) and ^{13}C (150 MHz) NMR data of RBR7a2 compared to those of questinol [RMN ^{13}C (100 MHz), RMN ^{1}H (400 MHz)] in DMSO-d_6 110
Table 29: ^{1}H (600 MHz) and ^{13}C (150 MHz) NMR data of RBR10R1 in DMSO-d_6 compared to questin [^{13}C (125 MHz), ^{1}H (500 MHz), DMSO-d_6] 115

Table 30: ^{1}H (600 MHz) and ^{13}C (150 MHz) NMR data of RBR147-19 in DMSO-d_6 compared to those of emodic acid [^{13}C (125 MHz), ^{1}H (500 MHz), DMSO-d_6] 120
Table 31: ^{1}H (600 MHz) and ^{13}C (150 MHz) NMR data of RBR147-19 in DMSO-d_6 compared to those of emodic acid [^{13}C (75 MHz), ^{1}H (300 MHz) CD_3COCD_3] 125
Table 32: ^{1}H (600 MHz) and ^{13}C (150 MHz) NMR data of RBR95-35b in DMSO-d_6 compared to emodin-6-*O*-*β*-D-glucoside [^{13}C (75.5 MHz), ^{1}H (300 MHz), DMSO-d_6]..... 130
Table 33: ^{1}H (600 MHz) and ^{13}C (150 MHz) NMR data of RBR95-23a/b in DMSO-d_6 compared to physcionin (Ref a) and chrysophanein (Ref b) (Tsamo *et al*., 2021) [^{13}C (150 MHz), ^{1}H (600 MHz), DMSO-d_6] 135
Table 34: ^{1}H (600 MHz) and ^{13}C (150 MHz) NMR data of RBR9a in DMSO-d_6 compared to emodin bianthrone [^{1}H (400 MHz), DMSO-d_6] 140
Table 35: ^{1}H (600 MHz) and ^{13}C (150 MHz) NMR data of RBR64 in DMSO-d_6 compared to Epicatechin 3-*O*-gallate [DMSO-d_6, RMN ^{13}C (125 MHz), RMN ^{1}H (500 MHz)]..... 145
Table 36: ^{1}H (600 MHz) and ^{13}C (150 MHz) NMR data of RBR17 in DMSO-d_6 compared to epicatechin 3-(6"-*O*-methyl) gallate [^{13}C (68 MHz), ^{1}H (270 MHz), CD_3OD] 150
Table 37: ^{1}H (500 MHz) and ^{13}C (125 MHz) NMR data of SYEF137 in DMSO-d_6 compared to those of gaboxanthone [^{13}C (100.6 MHz), ^{1}H (400.1 MHz), $CDCl_3$] 156
Table 38: ^{1}H (500 MHz) and ^{13}C (125 MHz) NMR data of SYEF171 in Acetone-d_6 compared to xanthone V2 [DMSO-d_6, RMN ^{13}C (25.2 MHz), RMN ^{1}H (60 MHz)] 161
Table 39: ^{1}H (600 MHz) and ^{13}C (150 MHz) NMR data of SYE26-8M in DMSO-d_6 compared to symphonin [^{13}C (100.6 MHz), ^{1}H (400.1 MHz) $CDCl_3$] 166
Table 40: ^{1}H (500 MHz) and ^{13}C (125 MHz) NMR data of SYEF1310b in acetone-d_6 compared to 1,5-dihydroxy-3-methoxyxanthone [^{13}C (73.47 MHz), ^{1}H (300.13) MHz), DMSO-d_6] 171
Table 41: ^{1}H (500 MHz) and ^{13}C (125 MHz) NMR data of SYEF26-48D in DMSO-d_6 compared to pyranojacareubin [$CDCl_3$, RMN ^{13}C (125 MHz), RMN ^{1}H (500 MHz)]..... 177
Table 42: ^{1}H (500 MHz) and ^{13}C (125 MHz) NMR data of SYEF23 in acetone-d_6 compared to kaempferol [^{13}C (100 MHz), ^{1}H (400 MHz), acetone-d_6] 181
Table 43: ^{1}H (600 MHz) and ^{13}C (150 MHz) NMR data of RBR9N2 in DMSO-d_6 compared to those of 5-Hydroxy-7-methoxy-1(3H)-isobenzofuranone [^{13}C (15.03 MHz), ^{1}H (90 MHz), DMSO-d_6]..... 186
Table 44: ^{1}H (600 MHz) and ^{13}C (150 MHz) NMR data of RBR9N2 in DMSO-d_6 compared to 3-hydroxy-*γ*-butyrolactone [^{13}C (125 MHz), ^{1}H (500 MHz), DMSO-d_6]..... 189
Table 45: Criteria of evaluation of the antileishmanial activity of extracts, fractions and pure compounds 212
Table 46: Criteria of evaluation of the cytotoxicity activity 212
Table 47: Antileishmanial and cytotoxic activities of extract, fractions, and compounds from the stem bark of *S. globulifera*..... 213
Table 48: Criteria of evaluation of the antibacterial activity of extracts and pure compounds..... 214
Table 49: Antibacterial activity of extract, fractions, and compounds (MIC in $\mu g.mL^{-1}$) 215
Table 50: Antibacterial activity of extract, fractions, and compounds (1−20) (MIC in $\mu g.mL^{-1}$). 217
Table 51 : Antibacterial activity of emodin (2) and derivatives (21−27) (MIC in $\mu g.mL^{-1}$) 218
Table 52: Chromatogram of the *n*-hexane fraction 229

LIST OF FIGURES

Figure 1: The leaves, stem bark, fruits and seeds of *S. globulifera* 16
Figure 2: Picture of *Rumex nepalensis* Spreng 18
Figure 3: (+) HRESI mass spectrum of RBR48-1 51
Figure 4: IR spectrum of RBR48-1 52
Figure 5: ^{1}H NMR of RBR48-1 (DMSO-d_6, 600 MHz) 53
Figure 6: ^{13}C NMR spectrum of RBR48-1 (DMSO-d_6, 150 MHz) 54
Figure 7: DEPT spectrum of RBR48-1 54
Figure 8: COSY spectrum of RBR48-1 56
Figure 9: HMQC spectrum of RBR48-1 56
Figure 10: HMBC spectrum of RBR48-1 57
Figure 11: HRESI mass spectrum of SYE25-6M 59
Figure 12: IR spectrum of SYE25-6M 60
Figure 13: ^{1}H NMR of SYE25-6M (acetone-d_6, 600 MHz) 61
Figure 14: ^{13}C NMR spectrum of SYE25-6M (acetone-d_6, 150 MHz) 62
Figure 15: HMBC spectrum of SYE25-6M 63
Figure 16: NOESY spectrum of SYE25-6M 64
Figure 17: (+) HRESI mass spectrum of SYE27-28-16Ma/b 66
Figure 18: IR spectrum of SYE27-28-16Ma/b 67
Figure 19: UV spectrum of SYE27-28-16Ma/b 67
Figure 20: ^{1}H NMR of SYE27-28-16Ma/b (acetone-d_6, 600 MHz) 69
Figure 21: ^{13}C NMR spectrum of SYE27-28-16Ma/b (acetone-d_6, 150 MHz) 71
Figure 22: HMBC spectrum of SYE27-28-16Ma/b 73
Figure 23: (+) ESI mass spectrum of SYE44-4-5mi 75
Figure 24: Comparative ^{1}H NMR of SYE25-6M (Acetone-d_6, 600 MHz) and that of SYE44-4-5mi (MeOH-d_4, 600 MHz) 76
Figure 25: Superposition of ^{13}C NMR spectrum of SYE25-6M (Acetone-d_6, 150 MHz) and SYE44-4-5mi (MeOH-d_4, 150 MHz) 77
Figure 26: HMBC spectrum of SYE44-4-5mi 78
Figure 27: (+) HRESI mass spectrum of SYE70- 45-48 80
Figure 28: IR spectrum of SYE70- 45-48 81
Figure 29: UV spectrum of SYE70- 45-48 81
Figure 30: ^{1}H NMR of SYE70- 45-48 (DMSO-d_6, 600 MHz) 82
Figure 31: ^{13}C NMR spectrum of SYE70- 45-48 (DMSO-d_6, 150 MHz) 83
Figure 32: HMBC spectrum of SYE70- 45-48 84
Figure 33: NOESY spectrum of SYE70- 45-48 85
Figure 34: (-) ESI mass spectrum of RBR3C 87
Figure 35: ^{1}H NMR of RBR3C (DMSO-d_6, 600 MHz) 88
Figure 36: ^{13}C NMR spectrum of RBR3C (DMSO-d_6, 150 MHz) 89
Figure 37: DEPT spectrum of RBR3C 89
Figure 38: HMQC spectrum of RBR3C 90
Figure 39: HMQC spectrum of RBR3C 91
Figure 40: HMBC spectrum of RBR3C 92

Figure 41: (-) ESI mass spectrum of RBR2 93
Figure 42: Compared ^{1}H NMR of RBR3C (DMSO-d_6, 600 MHz) and RBR2 ($CDCl_3$, 600 MHz) 94
Figure 43: compared ^{13}C NMR spectrum of RBR3C (DMSO-d_6, 150 MHz) and RBR2 ($CDCl_3$, 150 MHz). 95
Figure 44: HMBC spectrum of RBR2 96
Figure 45: (-) ESI mass spectrum of RBR1a 98
Figure 46: Compared ^{1}H NMR of RBR3C (DMSO-d_6, 600 MHz) and RBR1a (DMSO-d_6, 600 MHz). 99
Figure 47: Compared ^{13}C NMR spectrum of RBR3C (DMSO-d_6, 150 MHz) and RBR1a (DMSO-d_6, 150 MHz) 100
Figure 48: Compared DEPT spectrum of RBR3C and RBR1a 100
Figure 49: HMBC spectrum of RBR1a 101
Figure 50: (-) ESI mass spectrum of RBR6b 103
Figure 51: Comparative ^{1}H NMR of RBR3C (DMSO-d_6, 600 MHz) and RBR6b (DMSO-d_6, 600 MHz) 103
Figure 52: ^{13}C NMR spectrum of RBR3C (DMSO-d_6, 150 MHz) and RBR6b (DMSO-d_6, 150 MHz) 104
Figure 53: HMBC spectrum of RBR6b 105
Figure 54: (-) HRESI mass spectrum of RBR7a2 107
Figure 55: Comparative ^{1}H NMR of RBR6b and RBR7a2 (DMSO-d_6, 600 MHz) 108
Figure 56: Comparative ^{13}C NMR spectrum of RBR6b and RBR7a2 (DMSO-d_6, 150 MHz) 108
Figure 57: HMBC spectrum of RBR7a2 109
Figure 58: (-) HRESI mass spectrum of RBR10R1 111
Figure 59: Comparative ^{1}H NMR of RBR3C (DMSO-d_6, 600 MHz) and RBR10R1 (DMSO-d_6, 600 MHz) 112
Figure 60: Comparative ^{13}C NMR spectrum of RBR3C and RBR10R1 (DMSO-d_6, 150 MHz) 113
Figure 61: HMBC spectrum of RBR10R1 114
Figure 62: (-) HRESI mass spectrum of RBR147-19 116
Figure 63: Superposition of ^{1}H NMR of RBR3C (DMSO-d_6, 600 MHz) and RBR147-19 (DMSO-d_6, 600 MHz). 117
Figure 64: Comparative ^{13}C NMR spectrum of RBR3C and RBR147-19 (DMSO-d_6, 150 MHz). 118
Figure 65: HMBC spectrum of RBR147-19 119
Figure 66: (-) ESI mass spectrum of RBR15 121
Figure 67: Comparative ^{1}H NMR of RBR3C and RBR15 (DMSO-d_6, 600 MHz) 122
Figure 68: Comparative ^{13}C NMR spectrum of RBR3C (DMSO-d_6, 150 MHz) and RBR15 (DMSO-d_6, 150 MHz) 123
Figure 69: HMBC spectrum of RBR15 124
Figure 70: (-) ESI mass spectrum of RBR95-35b 126
Figure 71: Comparative ^{1}H NMR of RBR3C and RBR95-35b (DMSO-d_6, 600 MHz) 127
Figure 72: Comparative ^{13}C NMR spectrum of RBR3C and RBR95-35b (DMSO-d_6, 150 MHz) 128
Figure 73: HMBC spectrum of RBR95-35b 129
Figure 74: (+) ESI mass spectrum of RBR95-23a/b 131
Figure 75: Comparative ^{1}H NMR of RBR95-35b (DMSO-d_6, 600 MHz) and RBR95-23a/b (DMSO-d_6, 600 MHz) 132
Figure 76: Comparative ^{13}C NMR spectrum of RBR95-35b and RBR95-23a/b (DMSO-d_6, 150 MHz) 133

Figure 77: HMBC spectrum of RBR95-23a/b 134
Figure 78: (+) ESI mass spectrum of RBR9a 136
Figure 79: Comparative ^{1}H NMR of RBR3C and RBR9a (DMSO-d_6, 600 MHz) 137
Figure 80: Comparative ^{13}C NMR spectrum of RBR3C (DMSO-d_6, 150 MHz) and RBR9a (DMSO-d_6, 150 MHz) 138
Figure 81: HMBC spectrum of RBR9a 139
Figure 82: (+) ESI mass spectrum of RBR64 141
Figure 83: ^{1}H NMR of RBR64 (DMSO-d_6, 600 MHz) 142
Figure 84a: ^{13}C NMR spectrum of RBR64 (DMSO-d_6, 150 MHz) 143
Figure 85: (+) ESI mass spectrum of RBR17 146
Figure 86: Comparative ^{1}H NMR of RBR64 and RBR17 (DMSO-d_6, 600 MHz) 146
Figure 87: Comparative ^{13}C NMR spectrum of RBR64 and RBR17 (DMSO-d_6, 150 MHz) 147
Figure 88: HMBC spectrum of RBR17 148
Figure 89: (+) ESI mass spectrum of SYEF137 151
Figure 90: ^{1}H NMR of SYEF137 (DMSO-d_6, 500 MHz) 152
Figure 91: ^{13}C NMR spectrum of SYEF137 (DMSO-d_6, 150 MHz) 153
Figure 92: DEPT 135 spectrum of SYEF137 153
Figure 93: HMBC spectrum of SYEF137 155
Figure 94: (+) HRESI mass spectrum of SYEF171 157
Figure 95: Comparative ^{1}H NMR of SYEF137 (DMSO-d_6, 500 MHz) and SYEF171 (Acetone-d_6, 500 MHz) 158
Figure 96: Comparative of ^{13}C NMR spectrum of SYEF137 (DMSO-d_6, 125 MHz) and SYEF171 (Acetone-d_6, 125 MHz) 159
Figure 97: HMBC spectrum of SYEF171 160
Figure 98: (+) HRESI mass spectrum of SYE26-8M 162
Figure 99: Comparative ^{1}H NMR of SYEF137 and SYE26-8M (DMSO-d_6, 500 MHz) 163
Figure 100: Comparative ^{13}C NMR spectrum of SYEF137 and SYE26-8M (DMSO-d_6, 125 MHz) 164
Figure 101: HMBC spectrum of SYE26-8M 165
Figure 102: (+) ESI mass spectrum of SYEF1310b 167
Figure 103: ^{1}H NMR of SYEF1310b (Acetone-d_6, 600 MHz) 168
Figure 104: ^{13}C NMR spectrum of SYEF1310b (Acetone-d_6, 150 MHz) 169
Figure 105: DEPT 135 of SYEF1310b 169
Figure 106: HMBC spectrum of SYEF1310b 170
Figure 107: (+) ESI mass spectrum of SYEF26-48D 172
Figure 108: ^{1}H NMR of SYEF26-48D (DMSO-d_6, 600 MHz) 173
Figure 109: ^{13}C NMR spectrum of SYEF26-48D (DMSO-d_6, 150 MHz) 174
Figure 110: DEPT 135 of SYEF26-48D 174
Figure 111: HMBC spectrum of SYEF26-48D 176
Figure 112: (-) ESI mass spectrum of SYEF23 178
Figure 113: ^{1}H NMR of SYEF23 (Acetone-d_6, 600 MHz) 179
Figure 114: ^{13}C NMR spectrum of SYEF23 (Acetone-d_6, 150 MHz) 180
Figure 115: DEPT 135 of SYEF23 180
Figure 116: (-) ESI mass spectrum of RBR9N2 182
Figure 117: ^{1}H NMR of RBR9N2 (DMSO-d_6, 600 MHz) 183
Figure 118: ^{13}C NMR spectrum of RBR9N2 (DMSO-d_6, 150 MHz) 184
Figure 119: HMBC spectrum of RBR9N2 185

Figure 120: (+) ESI mass spectrum of RBR9N1 186
Figure 121: ^{1}H NMR of RBR9N1 (DMSO-d_6, 600 MHz) 187
Figure 122: Comparative ^{13}C NMR spectrum of RBR9N1 (DMSO-d_6, 150 MHz) and RBR9N2 (DMSO-d_6, 150 MHz) 188
Figure 123: HMBC spectrum of RBR9N1 189
Figure 124: ^{1}H NMR of SYE22-22 ($CDCl_3$, 600 MHz) 190
Figure 125: ^{1}H NMR of RBR5 (DMSO-d_6, 600 MHz) 191
Figure 126: ^{1}H NMR of RBR4 (DMSO-d_6, 600 MHz) 192
Figure 127: ^{1}H NMR of RBR86-57 (DMSO-d_6, 600 MHz) 193
Figure 128: Comparative ^{1}H NMR of RBR3C (DMSO-d_6, 600 MHz) and RBRAl1 ($CDCl_3$, 600 MHz) 196
Figure 129: HRESI mass spectrum of RBRAl1 196
Figure 130: HMBC spectrum of RBRAl1 197
Figure 131: Comparative ^{1}H NMR of RBR3C (DMSO-d_6, 600 MHz) and RBRAl2 ($CDCl_3$, 600 MHz) 198
Figure 132: (+) HRESI mass spectrum of RBRAl2 199
Figure 133: HMBC spectrum of RBRAl2 199
Figure 134: (+) HRESI mass spectrum of RBRAl3 200
Figure 135: Comparative ^{1}H NMR of RBRAl2 ($CDCl_3$, 600 MHz) and RBRAl3 ($CDCl_3$, 600 MHz) 201
Figure 136: Comparative ^{13}C NMR spectrum of RBRAl2 and RBRAl3 ($CDCl_3$, 600 MHz) 201
Figure 137: HMBC spectrum of RBRAl3 203
Figure 138: Comparative ^{1}H NMR of RBR3C (DMSO-d_6, 600 MHz) and RBRAl4 ($CDCl_3$, 600 MHz) 204
Figure 139: HRESI mass spectrum of RBRAl4 205
Figure 140: Comparative of ^{1}H NMR of RBR3C (DMSO-d_6, 600 MHz) and RBR3Ace1 (acetone-d_6, 600 MHz) 206
Figure 141: ESI mass spectrum of RBR3Ace1 206
Figure 142: Comparative ^{1}H NMR of RBR3C (DMSO-d_6, 600 MHz) and STEP1 new3 (DMSO-d_6, 600 MHz) 208
Figure 143: (-) ESI mass spectrum of STEP1 new3 208
Figure 144: Comparative ^{1}H NMR of STEP1 new3 and RBR3amin19b (DMSO-d_6, 600 MHz) 209
Figure 145: (-) HRESI mass spectrum of RBR3amin19b 210

LIST OF SCHEMES

Scheme 1: Basic skeletons of natural polyprenylated benzophenones 21
Scheme 2: Skeleton of xanthones (Gales and Damas, 2005) 26
Scheme 3: Basic skeleton of flavonoids 30
Scheme 4: Basic skeleton of anthraquinones 31
Scheme 5: Biosynthesis of benzophenones from acyl-CoA 45
Scheme 6: Protocol of extraction and isolation of compounds from the root of *R. nepalensis* 49
Scheme 7: Protocol of extraction and isolation of compounds from the stem bark of *S. globulifera* 50
Scheme 8: Key HMBC and COSY correlations of RBR48-1 55
Scheme 9: Key HMBC correlations of SYE25-6M 63
Scheme 10: Key HMBC correlations of SYE27-28-16Ma/b 72
Scheme 11: Key HMBC correlations of SYE44-4-5mi 78
Scheme 12: Key HMBC correlations of SYE70- 45-48 84
Scheme 13: Key HMBC correlations of RBR3C 90
Scheme 14: Key HMBC correlations of RBR2 95
Scheme 15: Key HMBC correlations of RBR1a 101
Scheme 16: Key HMBC correlations of RBR6b 105
Scheme 17: Key HMBC correlations of RBR7a2 109
Scheme 18: Key HMBC correlations of RBR10R1 113
Scheme 19: Key HMBC correlations of RBR147-19 118
Scheme 20: Key HMBC correlations of RBR15 123
Scheme 21: Key HMBC correlations of RBR95-35b 128
Scheme 22: Key HMBC correlations of RBR95-23a/b 134
Scheme 23: Key HMBC correlations of RBR9a 138
Scheme 24: Key HMBC correlations of RBR17 148
Scheme 25: Key HMBC correlations of SYEF137 154
Scheme 26: Key HMBC correlations of SYEF171 159
Scheme 27: Key HMBC correlations of SYE26-8M 164
Scheme 28: Key HMBC correlations of SYEF1310b 170

Scheme 29: Key HMBC correlations of SYEF26-48D 175
Scheme 30: Key HMBC correlations of RBR9N2..... 184
Scheme 31: Key HMBC correlations of RBRN2..... 188
Scheme 32: Allylation and acetylation of hydroxyl groups of emodin (117). 195
Scheme 33: Key HMBC correlations of RBR3Al1 195
Scheme 34: HMBC spectrum of RBRAl2 198
Scheme 35: HMBC spectrum of RBRAl2 202
Scheme 36: Nitration and amination of aromatic protons of emodin (117).. 207

ABSTRACT

This thesis reports the chemical investigation of two Cameroonian medicinal plants with antileishmanial and antibacterial activities: *Rumex nepalensis* Spreng (Polygonaceae) and *Symphonia globulifera* Linn. f. (Clusiaceae). The roots of *R. nepalensis* were chopped, air-dried and ground to yield 8.5 kg of powder. The obtained powder was macerated for 48 hours three times at room temperature with 30 L of CH_2Cl_2−MeOH (1:1, v/v). The extract was freed from solvent under vacuum to yield 500.7 g of crude extract. The stem bark of *S. globulifera* was equally chopped, air dried and then ground to give 10.3 kg of powder, which was extracted by maceration using methanol for 48 h, three times each. The extract was freed from solvent using a rotavapor to yield 638.7 g of MeOH extract. The methanol extract of the stem bark of *S. globulifera* displayed good *in vitro* activity against the parasite strain *Leishmania donovani* NR-48822 promastigotes (IC_{50} = 43.11 μg/mL) and the CH_2Cl_2−MeOH (1:1, v/v) root extract of *R. nepalensis* exhibited significant antibacterial activity against five bacterial strains including *Salmonella typhi CPC, Staphylococcus aureus ATCC43300, S. aureus ATCC25923, Pseudomonas aeruginosa HM801* and *Klebsiella Pneumoniae* (clinical isolate) with MICs ranging from 62.5 to 31.25 μg/mL. Part of the crude extracts were separately dissolved in water and successively partitioned with *n*-hexane, EtOAc and *n*-BuOH to yied 03 fractions. These fractions were assessed for their activity against the same strains of parasite and bacteria. From the most active fractions (*n*-hexane and ethyl acetate soluble fraction) thirty-two (32) compounds were isolated. These compounds were isolated using different chromatographic techniques and characterized by usual spectroscopic and spectrometric techniques (IR, MS, 1D and 2D NMR). Four new benzophenones, trivially named guttiferones U-W and one new tocotrienol named globuliferanol, were isolated from *S. globulifera*. From *R. nepalensis,* one new phenylisobenzofuranone, trivially named berquaertiide and two others known furanones, named 5-Hydroxy-7-methoxy-1(3*H*)-isobenzofuranone and 3-hydroxy-γ-butyrolactone, were isolated for the first time from natural sources. The twenty five remaining compounds were grouped into three classes of secondary metabolites including twenty-one phenolic derivatives [guttiferone K, emodin, physcion, chrisophanol, citreorosein, questinol, questin, emodic acid, 1,3,6-trihydroxy-8-methyl-anthraquinone, emodin-6-*O*-β-D-glucopyranoside, physcionin, chrysophanein, emodin bianthrone, catechin 7-*O*-gallate, epicatechin 3-(6"-*O*-methyl) gallate, gaboxanthone, xanthone V2, symphonin, 1,5-dihydroxy-3-methoxyxanthone, pyranojacareubin, kaempferol], three steroids (β-sitosterol, stigmasterol, β-sitosterol-3-*O*-β-D-glucopyranoside) and one triterpenoid (lupeol). Some isolated compounds were assessed for

both their antileishmanial and cytotoxic activities against the *L. donovani* and Vero cells. Guttiferone K exhibited the best potency (IC_{50} = 3.30 μg/mL), but with low selectivity to Vero cells. All the isolated compounds were also assessed for their antibacterial activity. Emodin was the most active compound against all the tested strains of bacteria (MIC ranging from 15.7 to 1.9 μg/mL), while the citreorosein, 1,3,6-trihydroxy-8-methyl-anthraquinone, questin, the mixture of physcionin and chrysophanein displayed good activities on at least one of the tested strains. In addition, seven analogues of emodin (6-allyloxyemodin, 6,8-diallyloxyemodin, 1,6-diallyloxyemodin, 1,6,8-triallyloxyemodin, 1,6,8-triacetylemodin, 1,6,8-trihydroxy-3-methyl-2,4,5,7-tetranitro anthraquinone and 5-amino-1,6,8-trihydroxy-3-methyl-2,4,7-trinitro anthraquinone) were prepared and further assessed for their antibacterial activity. The 1,6,8-trihydroxy-3-methyl-2,4,5,7-tetranitro anthraquinone and the 5-amino-1,6,8-trihydroxy-3-methyl-2,4,7-trinitro anthraquinone were most active than emodin against *Salmonella enterica and Klebsiella pneumonia* with MIC values of 125 and 15.6 μg/mL, respectively.

Keywords: Polygonaceae, Clusiaceae, *Rumex nepalensis* Spreng, *Symphonia globulifera* Linn. f., chemophenetic significance, antileishmanial activity, antibacterial activity, cytotoxicity

RESUME

Cette thèse rapporte l'investigation chimique de deux plantes médicinales camerounaises à activités antileishmaniale et antibactérienne: *Rumex nepalensis* Spreng (Polygonaceae) et *Symphonia globulifera* Linn. f. (Clusiaceae). Les racines de *R. nepalensis* ont été récoltées, séchées à l'air et broyées pour obtenir 8,5 kg de poudre. La poudre obtenue a été macérée trois fois pendant 48 heures à température ambiante avec un mélange de 30 L de CH_2Cl_2−MeOH (1:1, v/v). L'extrait a été débarrassé du solvant sous vide pour donner 500,7 g d'extrait brut. L'écorce du tronc de *S. globulifera* a été également récoltée, séchée à l'air, puis broyée pour donner 10,3 kg de poudre, qui a été extraite par macération à l'aide de méthanol trois fois pendant 48 heures. L'extrait obtenu a ensuite été débarrassé du solvant sous vide pour obtenir 638,7 g d'extrait de MeOH. L'extrait méthanolique de l'écorce du tronc de *S. globulifera* a montré une bonne activité antileishmaniale *in vitro* sur la souche parasitaire *Leishmania donovani* NR-48822 promastigotes (CI_{50} = 43.11 μg/mL) tandis que l'extrait au mélange de CH_2Cl_2−MeOH (1:1, v/v) des racines *R. nepalensis* a présenté une activité antibactérienne significative contre cinq souches bactériennes *Salmonella typhi CPC, Staphylococcus aureus ATCC43300*, *Staphylococcus aureus ATCC25923*, *Pseudomonas aeruginosa HM801*, *Klebsiella Pneumoniae* (clinical isolate) avec des CMI allant de 62.5 à 31.25 μg/mL. Une partie des extraits bruts a été dissoute dans de l'eau et a successivement été partitionnée avec le *n*-hexane, l'acétate d'éthyle, et le *n*-BuOH et a conduit à l'obtention de 03 fractions. Ces fractions ont été évaluées pour leur activité contre les mêmes souches de parasite et de bactéries. Les fractions les plus actives (la fraction à l'hexane et la fraction soluble à l'acétate d'éthyle) ont conduit à l'isolement de trente-deux (32) composés. Ces composés ont été isolés à l'aide de différentes techniques chromatographiques et ont été tous caractérisés par les techniques spectroscopiques et spectrométriques usuelles (IR, SM, RMN 1D et 2D). Quatre nouvelles benzophénones, nommées guttiférone U-W et un tocotriénol nommé globuliféranol, ont été isolés de *S. globulifera*. De *R. nepalensis*, une nouvelle phénylisobenzofuranone, trivialement appelée berquaertiide, ainsi que les deux autres furanones connus, nommés 5-hydroxy-7-methoxy-1(3*H*)-isobenzofuranone et 3-hydroxy-γ-butyrolactone, sont isolés pour la prémière fois de source naturelle. Les vingt cinq autres composés appartiennent à trois classes de métabolites secondaires incluant vingt-et-un dérivés phénoliques [guttiferone K, emodine, physcione, chrisophanol, citreoroseine, questinol, questine, acide émodique, 1,3,6-trihydroxy-8-methyl-anthraquinone, emodine-6-*O*-β-D-glucopyranoside, physcionine, chrysophaneine, emodine bianthrone, catechine 7-*O*-gallate, epicatechine 3-(6"-*O*-methyl) gallate,

gaboxanthone, xanthone V2, symphoninee, 1,5-dihydroxy-3-methoxyxanthone, pyranojacareubin, kaempferol], trois phytostéroïdes (*β*-sitosterol, stigmasterol, *β*-sitosterol-3-*O*-*β*-D-glucopyranoside) et un triterpénoïde (lupeol). Certains composés isolés ont été évalués à la fois pour leurs activités antileishmaniales et cytotoxiques contre *L. donovani* et les cellules Vero, respectivement. La guttiferone K a présenté la meilleure activité (CI_{50} = 3,30 μg/mL), mais avec une faible sélectivité envers les cellules Vero. Tous les composés isolés ont également été évalués pour leur activité antibactérienne. L'émodine était le plus actif contre toutes les souches bactériennes testées (CMI allant de 15,7 à 1,9 μg/mL), tandis que la citréoroseine, le 1,3,6-trihydroxy-8-méthyl-anthraquinone, la questine, le mélange de phydcionine et de chrysophaneine ont montré de bonnes activités sur au moins une des souches testées. De plus, sept analogues de l'émodine (6-allyloxyemodine, 6,8-diallyloxyemodine, 1,6-diallyloxyemodine, 1,6,8-triallyloxyemodine, 1,6,8-triacetylemodine, 1,6,8-trihydroxy-3-methyl-2,4,5,7-tetranitro anthraquinone and 5-amino-1,6,8-trihydroxy-3-methyl-2,4,7-trinitro anthraquinone) ont été préparés et évalués davantage pour leur activité antibactérienne. Le 1,6,8-trihydroxy-3-méthyl-2,4,5,7-tétranitro anthraquinone et le 5-amino-1,6,8-trihydroxy-3-méthyl-2,4,7-trinitro anthraquinone étaient plus actifs que l'emodin contre *Salmonella enterica* et *Klebsiella pneumonia* avec des CMI (125 et 15,6 μg/mL, respectivement).

Mots clés: Polygonaceae, Clusiaceae, *Rumex nepalensis* Spreng, *Symphonia globulifera* Linn. f., contribution chimiophénétique, activité antileishmaniale, activité antibactérienne, cytotoxici

GENERAL INTRODUCTION

Infectious diseases represented a threat for human lives since the beginning of human existence. Among infectious diseases, bacterial diseases and leismaniasis remain one of the main causes of mortality in the lower income countries. In fact, about 12 to 15 million people are infected and 350 million are at risk of acquiring leishmaniasis. An estimated 1.5 to 2 million new cases occur each year, and it causes 70,000 deaths per year (Torres-Guerrero *et al*., 2017). In addition, bacterial diseases like typhoid, for example, is estimated to affect between 11 to 21 million people each year and cause 128,000 to 161,000 deaths (WHO, 2020). Many infectious diseases were overcome through the discovery of antibiotic and antiparasitic agents. However, the antibiotic-resistant strains and antileishmanial resistant strains are now emerging and are more problematic than the existing ones. In addition, the poor use of some drugs that leads to increasing cases of parasite and bacterial resistance are worrisome. Therefore, there is an urgent need to search for novel antileishmanial and antibacterial drug. Most chemical drugs that are widely used today were isolated from natural sources, and natural products still continue to be an important raw material for the development of new drugs (Kim et *al*., 2016). It is in this perspective that we undertook in the frame of our thesis, the chemical investigation and the evaluation of the antileishmanial and antibacterial activities of extracts, fractions, and secondary metabolites from *Symphonia globulifera* (Clusiaceae) and *Rumex berquaertii* (Polygonaceae).

Our interest in these two species was justified firstly by their uses in folk medicine. Plants of the genus *Rumex* are commonly used in India to treat skin infections (Getie *et al*., 2003), inflammation of the gastrointestinal tract, and against digestive disorders (Vazquez *et al*., 1997). It is also used as laxative or as antidiarrheal agents (Loi *et al*., 2004), and as a treatment for upper respiratory tract diseases (nasal sinuses and throat) (Süleyman *et al*., 1999). Parts of *S. globulifera* are used in African and South American folk medicines to treat diabetes, stomach troubles, cough, malaria, intestinal worms, jaundice, fever, and scabies (Ssegawa et *al*., 2007; Fromentin et *al*., 2014; Majekodunmi et *al*., 2017). In Cameroon, its bark and heartwood are used as laxatives for pregnant women and as general tonics (Irvine *et al*., 1961). In Panama, its fresh latex is used as a cataplasm against skin diseases and body pain (Gupta *et al*., 2005). The decoction of the bark is traditionally rubbed on the skin for the treatment of cutaneous leishmaniasis in Colombia (Lopez *et al*., 2001). Secondly, both plants were reported to exhibit good antileishmanial and antibacterial activities (Lenta et *al*., 2007; Mkounga et *al*., 2009; Vasas et *al*., 2015) and during their preliminary screening. Thirdly, and to the best of our

knowledge *R. nepalensis* and the stem bark of *S. globulifera* have not yet been investigated for their antileishmanial properties. Furthermore, the studies conducted by Andrade et *al*., (1990) demonstrated the susceptibility of visceral leishmaniasis patients to bacterial infections, thereby providing an additional motivation for the study of these plants for their antileishmanial and antibacterial properties.

The objective of this work was to search for potential extracts, fractions, or compounds with antileishmanial or antibacterial activity that can serve as starting point for the development of new therapeutic agents.

Specifically, this work consisted to:

- harvest, extract, fractionnate and asses for antileishmanial and antibacterial activities;
- isolate, purify, and characterize secondary metabolites from the most active fractions;
- perfom *in vitro* antileishmanial and antibacterial, cytotoxicity and toxicity assays in view to formulate a phytodrug.

This thesis, which summarizes the essential of our work, has three main parts: a first part which covers the bibliographic study with a brief overview on leishmaniasis and a brief botanical description as well as the previous chemical and biological works on the studied plants, a second part devoted to results and discussion, and a third part which describes the equipment and the various techniques used as well as the work methodology.

PART I:

LITERATURE REVIEW

I.1. OVERVIEW ON LEISHMANIASIS

I.1.1. Definition

Leishmaniasis is a parasitic infection affecting the monocyte-macrophage system. The causative pathogen is a flagellated protozoan known as *Leishmania*, which falls under the family Trypanosomatidae and the genus *Leishmania* (Akhoundi *et al*., 2016). There are four main forms of the disease including visceral leishmaniasis (VL, also known as kala-azar), post-kala-azar dermal leishmaniasis, cutaneous leishmaniasis (CL) and mucocutaneous leishmaniasis. While cutaneous leishmaniasis (CL) is the most frequently occurring form of the disease, visceral leishmaniasis (VL) is the most severe and can be nearly fatal if left untreated. (WHO, 2020; Desjeux, 2004).

I.1.2. Epidemiology

Leishmaniasis is widely distributed across 88 tropical, subtropical and temperate countries, with more than 350 million people at risk. An estimated 12 million patients suffer from leishmaniasis, with 0.2-0.4 million of new VL and 0.7-1.2 million of new CL cases per year worldwide (Alvar *et al*., 2012). The disease mainly affects poor people in Africa, Asia and Latin America, and is associated with malnutrition, population migration, poor residency conditions, frail immune system and lack of resources (Alvar *et al*., 2006). The disease is prevalent both in South and Central America, Southern Europe, Africa, Middle East, Central Asia and Indian subcontinent. Of the 16 categories of neglected tropical diseases assessed for the period from 2005 to 2013, leishmaniasis ranks next to malaria as the second worst in the agestandardized disability-adjusted life years and second only to dengue fever in the rate of daily increase, from 5.7 to 5.9 million (Murray *et al*., 2015). In Africa, the disease has been reported in Niger, Mali, Nigeria, Senegal, Cameroon, Burkina Faso, Mauritania, Gambia, Guinea, Algeria. Algeria has 90% of CL cases in Northen Africa. Today, more than 1 billion people live in areas endemic for leishmaniasis and are at risk of infection. An estimated 30,000 new cases of VL and more than 1 million new cases of CL occur annually (WHO, 2017).

Also, cutaneous leishmaniasis is endemic in northern Cameroon. 326 cases were reported in the town of Garoua. In a survey carried out in the North region near Mokolo (50 km west of Maroua) of 887 people, 162 people were found with leishmanian scars and 14 cases with active leishmaniasis (Kimutai *et al*., 2009). In addition, cases may occur in areas bordering Chad (including in the N'Djamena vicinity). Other cases have been reported from the eastern areas in the past. An identified focus of visceral leishmaniasis has been reported from Kousseri in the

Extreme-Nord with 46 patients presenting symptoms of VL out of 120 examined (Kimutai *et al*., 2009).

I.1.3. The vector of leishmaniasis

Leishmaniasis is transmitted through the bite of female sandflies (Akhoundi *et al*., 2016). Countries of Africa, Europe and Asia (Old World) are affected by sandflies of the genus *Phlebotomus*, while countries of America (New world) are affected by *Lutzomyia* species (Reithinger *et al*., 2007; Kevric *et al*., 2015; Borghi *et al*., 2017).

I.1.4. The parasite

The parasite is categorized in two main groups: species occurring in Europe, Africa and Asia, and those occurring in America (Cox, 1993). Human infection is caused by about 21 of 30 species that infect mammals. These include the *L. donovani* complex with 3 species (*L. donovani*, *L. infantum*, and *L. chagasi*), the *L. mexicana* complex with 3 main species (*L. mexicana*, *L. amazonensis*, and *L. venezuelensis*), *L. tropica*, *L. major*, *L. aethiopica*, and the subgenus *Viannia* with 4 main species (*L. (V.) braziliensis*, *L. (V.) guyanensis*, *L. (V.) panamensis*, and *L. (V.) peruviana*) (Alvar and *al.*, 2012). Many of the leishmania species infecting human are zoonotic, having a complex variation in domestic and wild mammal reservoir hosts, while other species of the parasite are anthroponotic, having human-to-human transmission in the presence of the vector (Alvar and *al.*, 2012).

I.1.5. Treatment of leishmaniasis

The available antileishmanial drugs have a limited spectrum and efficacy. These drugs developed for treating leishmaniasis can be classified into distinct groups: the first-line drugs and altenative drugs (Kobets *et al*., 2012; Singh *et al*., 2014).

- **First Line Drugs**

Pentavalent antimonials have been the mainstay of treatment for all forms of leishmaniasis worldwide for a period spanning over five decades.

Pentavalent antimonials (Sb_V) have been the first-line drug for more than 70 years. There are two formulations of the drug available: meglumine antimoniate (**1**) and sodium stibogluconate (**2**) known in pharmacies as Glucantime and Pentostam, respectively (Kobets *et al*., 2012; Singh *et al*., 2014).

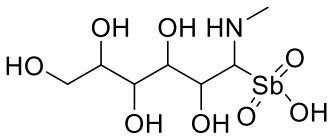

1

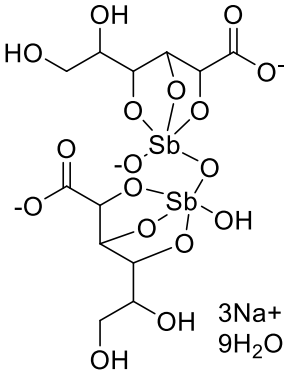

2

Additionally, the identification of multiple genes in clinical isolates that show resistance to antimonials implies a complex, multifaceted resistance mechanism, emphasizing the urgent necessity for alternative therapeutic approaches for this disease. (Singh *et al*., 2006).

- **Alternative Drugs**

Several alternative drugs, including amphotericin B (**3**), pentamidine (**4**), miltefosine (**5**), paromomycin (**6**) (Kobets *et al*., 2012; Singh *et al*., 2014) have been introduced.

- **Amphotericin B**

It is the first drug of choice which is extensively employed in endemic regions where antimonials resistance is common. There are three commercially available lipid-associated formulations of amphotericin B (**3**): liposomal amphotericin B (L-AMB), amphotericin B lipid complex (ABLC) and amphotericin B colloidal dispersion (ABCD) known in pharmacies as Ambisome™, Abelcet® and Amphocil™/Amphotec™, respectively (Kobets *et al*., 2012; Singh *et al*., 2014).

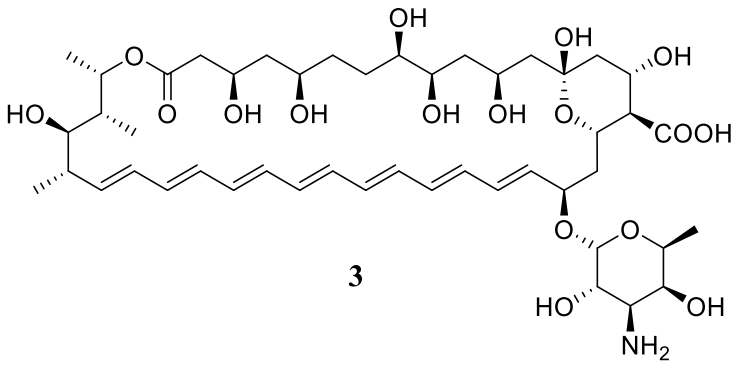

3

- **Pentamidine**

Pentamidine (**4**), as the isethionate salt (Pentacarinat®) and previously as the methylsuphonate salt (Lomidine®), has served as an alternative treatment for both VL and CL (Croft and Yardley, 2002).

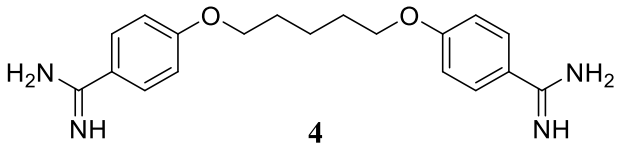

4

- **Miltefosine**

Miltefosine, an alkylphospholipid derivative also known as hexadecylphosphocholine, represents the first orally administered effective antileishmanial agent (Kobets *et al*., 2012).

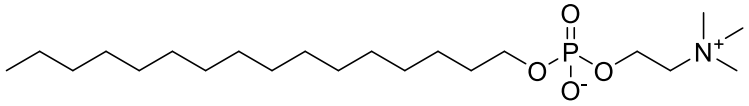

5

- **Paromomycin**

It is a treatment that, despite its high cost, proves to be highly effective in the fight against leishmaniasis (Singh *et al*., 2014).

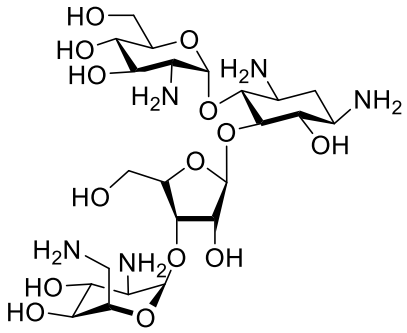

6

I.2. OVERVIEW ON BACTERIA

I.2.1. Definition

Bacteria are prokaryotic single-celled microorganisms, among the most ancient and abundant life forms on Earth. They are characterized by their lack of a true nucleus and membrane-bound organelles, setting them apart from eukaryotic cells. Bacteria exist in various

shapes, sizes, and metabolic capabilities, allowing them to thrive in a wide range of environments (Madigan *et al*., 2017).

These microorganisms have a profound impact on our world, influencing human health, global biogeochemical cycles, and even industrial processes. They can be found in soil, water, air, and the human body, and their metabolic activities are critical to the planet's equilibrium (Slonczewski *et al*., 2017).

I.2.2. Epidemiology

Bacterial infections kill over 7 million people annually, and it may kill up to 10 million people by the year 2050 (Yadav *et al*., 2021) if appropriate measures are not taken. Common bacterial infections include respiratory infections (e.g., pneumonia, tuberculosis), diarrheal diseases, and healthcare-associated infections (HAIs) (CDC, 2021). The epidemiology of bacterial diseases is influenced by the emergence of new pathogens and the reemergence of old ones. This includes the rise of antibiotic-resistant bacteria, which pose a growing threat to public health (Ventola, 2015).

I.2.3. Classification of Bacteria

Bacteria are classified into different types based on their Gram staining characteristics, which reveal differences in the structure of their cell walls. The two primary groups are Gram-positive and Gram-negative bacteria (Madigan *et al*., 2017).

- **Gram-Positive Bacteria**

- These bacteria have a thick layer of peptidoglycan in their cell walls, which retains the crystal violet stain used in Gram staining. They appear purple under the microscope.
- Common Gram-positive bacteria include *Staphylococcus*, *Streptococcus*, *Bacillus*, and *Clostridium*.

- **Gram-Negative Bacteria**

- Gram-negative bacteria have a thinner layer of peptidoglycan surrounded by an outer membrane. They do not retain the crystal violet stain and appear pink under the microscope.
- Well-known Gram-negative bacteria include *Escherichia coli*, *Salmonella*, *Pseudomonas*, *Klebsiella* and *Neisseria*.

I.2.4. Identification of Bacteria

The identification of bacteria typically involves a combination of techniques, including morphological, biochemical, serological, and molecular methods. These methods help to determine the type or species of a bacterium:

- **Morphological and Staining Characteristics**: Bacterial identification often begins with observing the shape, arrangement, and staining properties of bacteria. Common staining methods include Gram staining and acid-fast staining (Madigan *et al*., 2017).
- **Biochemical Tests**: Biochemical tests are used to assess the metabolic characteristics of bacteria, such as their ability to ferment specific sugars or produce certain enzymes. The results are compared to databases of known bacteria (Collee *et al*., 1996).
- **Serological Identification**: Serological tests involve the use of antibodies to detect specific bacterial antigens. This method is often used in clinical diagnostics (Bailey *et al*., 1986).
- **Genetic Analysis**: Molecular techniques, such as polymerase chain reaction (PCR) and DNA sequencing, are increasingly used for bacterial identification. These methods analyze bacterial DNA for species-specific markers (Persing *et al*., 1993).
- **Matrix-Assisted Laser Desorption/Ionization Time-of-Flight Mass Spectrometry (MALDI-TOF MS)**: MALDI-TOF MS is a rapid and accurate method for bacterial identification based on the mass spectrometry analysis of microbial proteins (Seng *et al*., 2009).
- **Whole Genome Sequencing (WGS)**: WGS involves sequencing the entire genome of a bacterium, allowing for the most precise identification and analysis of genetic markers (Köser *et al*., 2014).

I.2.5. Treatment of bacterial infections

Antibiotics are the mainstay of bacterial infection treatment. They work by targeting specific aspects of bacterial physiology, such as cell wall synthesis, protein synthesis, or DNA replication (Mandell *et al*., 2014). To select the most appropriate antibiotic, laboratory tests are performed to determine the susceptibility of the infecting bacterium to various antibiotics. This helps to ensure the effectiveness of treatments (CLSI 2021). In some cases, a combination of antibiotics may be used to treat severe or resistant infections. Combining antibiotics with different mechanisms of action can be more effective (Weinstein *et al*., 2020).

The progress of bacterial-resistance to available antibiotics is alarming and makes the treatment of even simple bacterial infections difficult (Aslam *et al*., 2018). Also, the absence of an effective vaccine and the development of resistance to drugs used to treat leishmaniasis, along with their high cost, requirement for injection, and potential toxicity, pose significant concerns, particularly in regions where the disease is endemic in developing countries (Oryan, 2015). These concerns require a continuous search for new and efficient lead antibacterial and antileishmanial agents. In this context, plants can play a key role in the discovery of new lead drugs since in most African countries, people have been relying mainly on medicinal plants to treat themselves from bacterial diseases and other infections. Plants have been reported as an important source of bioactive molecules (Stafford 2002).

I.3. OVERVIEW ON THE INVESTIGATED PLANTS

The two investigated plants belong to two families including Clusiaceae and Polygonaceae.

I.3.1. Overview on the Clusiaceae family

I.3.1.1. Introduction

The clusioid clade belongs to the order Malpighiales and is represented by five families: Bonnetiaceae, Calophyllaceae, Clusiaceae, Hypericaceae and Podostemaceae (APG IV, 2016). Calophyllaceae, Clusiaceae and Hypericaceae were previously known as Clusiaceae or Guttiferae (Cronquist, 1981), but the latest molecular studies showed that the family in this circumscription was not monophyletic (Ruhfel *et al*., 2013).

Clusiaceae are either terrestrial or hemiphytic trees, shrubs or lianas frequently with adventitious roots, usually glabrous and evidently lacticiferous, with white, cream, yellow or orange exudate. Their flowers are hermaphroditic or unisexual (Cabral *et al*., 2016a). The family occurs in most neotropical habitats from sea level to 3.5 m altitude (Stevens, 2006).

The Clusiaceae family was divided into two subfamilies: Kielmeyeroideae and Clusioideae (Gustafsson *et al*., 2002). In order to resolve issues related to ancestry, it was decided to elevate the status of subfamily *Kielmeyeroideae*, revalidating family Calophyllaceae, composed of fourteen genera (Wurdack and Davis, 2009). The remainder of the Clusiaceae constitutes the subfamily Clusioideae, which was divided into three distinctive tribes in the most recent classification of the Clusiaceae: Clusieae (neotropical), Garcinieae (pantropical) and Symphonieae (pantropical) composed of 14 genera and about 800 neo- and paleotropical

species (Ruhfel *et al*., 2011). In Brazil, the family is represented by 131 species (BFG, 2015). 9 gives a summary of the classification of the Clusiaceae (Cabral *et al*., 2017).

Table 1: Sub-family, tribes and genera of Clusiaceae

Sub-family	Tribes	Genera
Clusoideae	Clusieae	*Clusia, Dystovomita, Tovomita, Chrysochlamys, Tovomitidium*
	Garcinieae	*Garcinia, Allanblackia*
	Symphonieae	*Pentadesma, Moronobea Platonia, Montrouziera, Symphonia, Lorostemon, Thysanostemon*

I.3.1.2. Overview on the genus *Symphonia*

The genus *Symphonia* consists of some 17 species distributed from South America to Africa and Madagascar (Dick *et al*., 2003). It is a genus of tropical woody plants specifically trees with stilt roots and bright yellow exudate. The perulae ist present, protecting the terminal buds, resulting in groups of scars on the branches. Leaves are opposite with secondary conspicuous veins. They have hermaphrodite flowers that are axillary and solitary with inflorescent terminal. Their sepals and petals are five in number with contorted, free but tube-like closure forming a chamber. Stamens are arranged in fascicles of three stamens each, all united at the base, forming a staminal tube with five carnose lobes to which the long anthers are abaxially attached. Furthermore, they are made up of ovaries with five locules, style terminating in a head of five radiating branches, stigmas forming cylindrical lobes, each with an apical pore. Lastly, the fruits are berries with 1 to 8 seeds with hairy like testa (Cabral *et al*., 2017).

Amongst the *Symphonia* species, *S. globulifera is* broadly distributed across the Neotropics and equatorial Africa (Dick and Heuertz, 2008). Of the 17 accepted species of *Symphonia*, only *S. globulifera* can be found outside of Madagascar (Newman and Cragg., 2012).

I.3.1.2.1. Overview on *S. globulifera*

Some of the vernacular names of this plant are, “boarwood”, “hog gum”, "chew stick” (English) “manil marécage”, “palétuvier jaune” (French Guiana), “barillo” (Guatemala, Honduras), “cerillo” (Costa Rica, Panama), “machare” (Colombia), “mani”, “paraman” (Venezuela), “mataki” (Surinam), “manni” (Guiana), “anany” (Brazil), and “brea-caspi”

(Peru). *S. globulifera* plants are generally tall trees (canopy trees) more than 15 m high with opposite leaves exhibiting characteristic aerial roots and producing bright yellow latex. The flowers are red with a red staminal column and black anthers and organized as a sympodium. Fruits are drupes of about 4–5 cm, ovoid or globular. Seeds are intensively red inside (Dick *et al*., 2003).

S. globulifera is easy to recognize. The filaments fuse to form a staminal tube with five carnose triangular lobes at the apex and the anthers are attached abaxially to the lobes. The flowers have petals that firmly enclose the staminal tubes and the ovary. There are four anthers per fascicle and the ovary has four ovules per locule. The combination of these characters is found only in this species in the Neotropics (Abdul-Salim, 2002). The plants flowering occurs from May to February and its fruiting from May to June and September to January (Cabral *et al*., 2017).

This species is also characterized by important morphological variations, which seem to be dependent of its ecological distribution (Kumar *et al*., 2013). Indeed, at least three varieties exist, var. *angustifolia* Maguire, var. *macoubea* Vesque, and var. *major* Diels (Kumar *et al*., 2013), and a small number of supposed subspecies such as *Symphonia*. However, none of these differences has been yet considered sufficient to merit splitting into more than one species (Fromentin *et al*., 2013). Figure 1 below gives a representation of the leaves, stem bark, fruits and seeds of *S. globulifera.*

Figure 1: The leaves, stem bark, fruits and seeds of *S. globulifera*

S. globulifera has a remarkable distribution, occurring naturally in the rainforest of tropical America and Africa. In tropical America it occurs from Mexico through Brazil to Peru and in tropical Africa, it occurs from Guinea Bissau to Tanzania, Western Zambia and Angola, possibly also in Madagascar, Gabon, Nigeria, Uganda, Cameroon, Tanzania, Zambia, (Oyen, 2005). Guinea Bissau and Angola are some of the African countries in which these plants can be found (Cottet *et al*., 2014). According to the information collected from the National Herbarium of

Cameroon, *S. globulifera* has already been collected in different localities in Cameroon (Table 2).

Table 2: Places where *S. globulifera* has already been collected in Cameroon

Regions	Localities
West	Bangangte and Bafoussam
South	The Dja Faunal Reserve
Centre	Nomayos
South West	Bakossi National park
Littoral	Nkongsamba

I.3.2. General overview on the Polygonaceae family

The Polygonaceae, known informally as the knotweed family or smartweed, namely, buckwheat family, in the Order of Caryophyllales, is a family of dicotyledonous flowering plants, consisting of about 48 genera with more than 1200 species, worldwide distributed. Plants are usually herbaceous, shrubs or small trees (Xu *et al*., 2017).

The largest genera are *Eriogonum* (240 species), *Rumex* (250 species), *Coccoloba* (120 species), *Persicaria* (100 species) and *Calligonum* (80 species) (Craig *et al*., 2005; Rao *et al*., 2011; John *et al*., 1993). The genus *Rumex* is of interest in this study.

I.3.2.1. Overview on the genus *Rumex*

The genus *Rumex* is the largest one of the family Polygonaceae with more than 250 species distributed worldwide (Rao *et al*., 2011). It is mostly perennial herbs with sturdy roots, paniculate inflorescences and triangular fruits that are enveloped in the enlarged inner perianth. The name "Rumex" originated from the Greek word–"dart" or "spear", alluding to the shape of leaves (Liddell *et al*., 1940). Some common species of the genus *Rumex* are *R. acetosa, R. trisetifer, R. patientia, R. crispus, R. japonicus, R. dentatus* and *R. nepalensis* Spreng the species of focus in this study.

I.3.2.1.1. Overview on *Rumex nepalensis* Spreng

Also known as *R. berquaertii* De Wild, it is characterized by a perennial herb up to 150 cm high, erect, branching in the upper half. The basal leaves are made of cordate base, hooked teeth, broad, flat and cauline. They are inflorescence in whorls of many-flowers. The fruits are nut, long, dark brown with thicker below and the middle (Figure 2) (Abbasi *et al*., 2015)

Figure 2: Picture of *Rumex nepalensis* Spreng

According to the information collected from the National Herbarium of Cameroon, *R. nepalensis* has already been collected in different localities in Cameroon (Table 3).

Table 3: Places where *R. nepalensis* has already been collected in Cameroon

Regions	Localities
Littoral	Mont Manengouba (Nkongsamba)
Ouest	Route Bafou – Baranka
Nord-ouest	Bambili, Bamenda, Klanluk (Oku)
Est	Mont Okou
Sud-Ouest	Kumba, Mueba, Bakossi, Buea, Ehumseh, Mejel, Bakossi

I.4. USES OF THE INVESTIGATED PLANTS

I.4.1. Uses of *S. globulifera* species in folk medecine

S. globulifera species have been reported to possess medicinal properties for the treatment of many human ailments in different areas. Some uses of *S. globulifera* in folk medicine are in table 4a:

Table 4a: Traditional uses of *S. globulifera* in folk medicine

Species	Parts	Uses
S. globulifera	Latex	- Used traditionally for their effectiveness against dermatoses (Grenand *et al*., 2004).
	Bark	- Used by the Masango, Gabon, as an emetic to treat chest complaints and decoctions of *S. globulifera* bark are produced to cure the serious problem of scabies (Akendengué and Louis, 1994). - Presents broad applications in Uganda ranging from treating coughs and prehepatic jaundice to fever and intestinal worms (Ssegawa and Kasenene, 2007) - Used In Cameroon, as laxative for pregnant women and as a general tonic (Irvine, 1961). Also used in the North West region of Cameroon, by traditional healers to treat malaria (Nkengfack *et al*., 2002).
	Leaves	- Used in Nigeria as a decoction and are applied on the body to treat skin disease, which is the largest application followed by malaria and diabetes (Ajibesin *et al*., 2008)

I.4.2. Uses of plants of the genus *Rumex* in folk medecine

Several species of the genus *Rumex* have been reported to possess medicinal properties for the treatment of many human ailments in different areas (Table 4b).

Table 4b: Traditional uses of some species of the genus *Rumex*

Species	Uses
R. acetosella (leaves, aerial parts, seeds)	- Applied in Hungary and in Romania for constipation, diarrhoea, kidney disorders, swellings, sores, rashes and wounds, ringworm and as an astringent (Dénes *et al*., 2013).
R. dentatus (leaves and root)	- Used for the treatment of several diseases (foot and mouth infections, asthma, cough, jaundice, fever, weakness and scabies) by local communities in Pakistan (Abbasi *et al*., 2015).
Rumex nepalensis Spreng (root and leaves)	- Used in East Africa (Cameroon) as remedies for various types of stomach disorder and cancer (Munavu *et al*., 1984; Tamokou *et al.*, 2013); -Used in China for the treatment of dysentery, haemostasis, and tinea (Mei *et al*., 2009); - The fresh young leaves are used in India to treat skin disorders, colic and syphilic ulcers (Gautam *et al*., 2010; Khare, 2007).
R. hastatus (nd)	- Used in India for the treatment of sexually transmitted diseases, including AIDS (Sahreen *et al*., 2014).
R. patientia (nd)	- Used in Egyptian as a tonic and analgesic and for the treatment of hepatic diseases, constipation, poor digestion, spleen disorders, flatulence, asthma, bronchitis, dyspepsia, vomiting and piles, among others (El-Hawary *et al*., 2011).

I.5. PREVIOUS CHEMICAL AND BIOLOGICAL INVESTIGATIONS ON THE SELECTED PLANTS

I.5.1. Previous chemical investigations on the studied plants

I.5.1.1. Previous chemical investigations on plants of *Symphonia globulifera*

Previous chemical studies carried out on the *S. globulifera* species revealed the presence of numerous secondary metabolites, which belong to the following classes of compounds: biflavonoids, xanthones and benzophenones (Polycyclic polyprenylated acylphloroglucinols, PPAPs) which are the main class of compounds of this species (Fromentin *et al.*, 2015).

1.5.1.1.1. Benzophenones (Polycyclic polyprenylated acylphloroglucinols, PPAPs)

A large part of the benzophenones isolated from species of the Clusiaceae family consists of highly oxygenated substances, whose structures are characterized by the presence of a bicyclo core [3.3.1] nonane-2,4,9-trione, generally bonded to a substituted phenyl group (Wu *et al*., 2014). Benzophenones isolated from this species are mainly polyprenylated benzophenones (Polycyclic polyprenylated acylphloroglucinols, PPAPs) (Ciochina *et al.*, 2006). Depending on the position of the exocyclic acyl group, the PPAPs are divided into four subclasses, that is, type A (acyl group at C_1), type B (acyl group at C_3), type C (acyl group at C_5) and type D without the eight membered ring (Wu *et al.*, 2014). Scheme 1 below gives a classification of the skeleton of natural polyprenylated benzophenones.

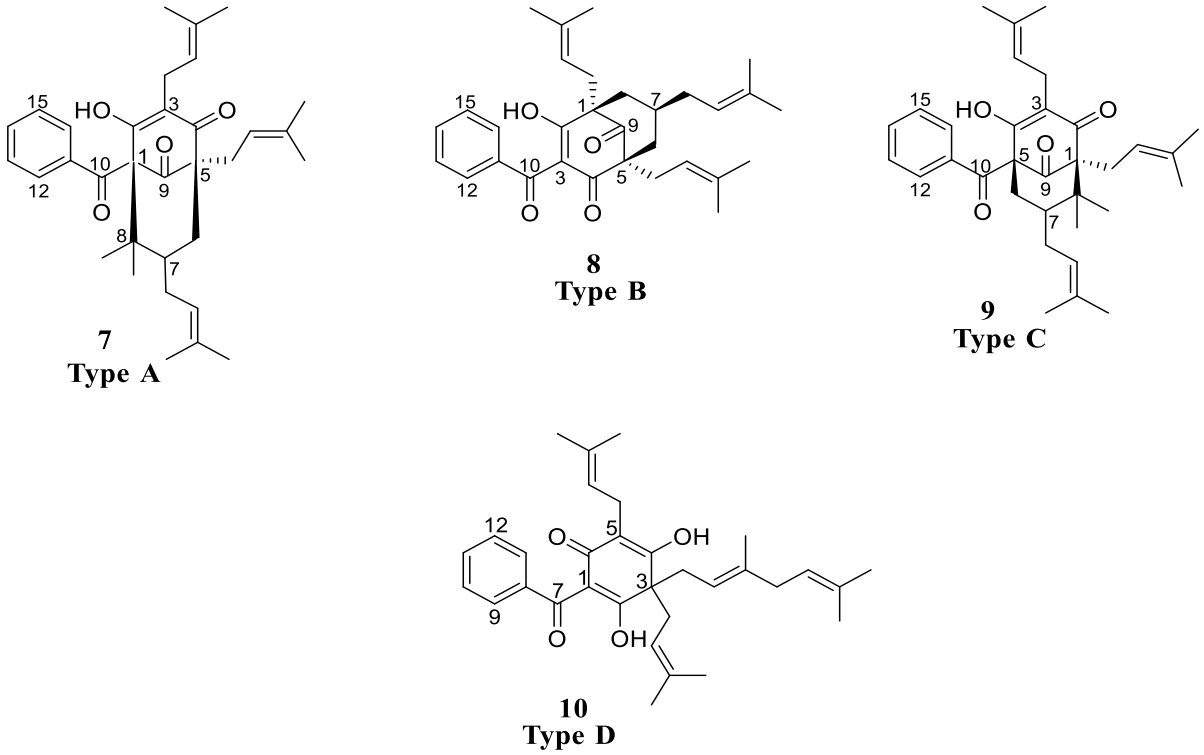

Scheme 1: Basic skeletons of natural polyprenylated benzophenones

All the polyprenylated benzophenones isolated in this species belong to the type B group (Fromentin *et al.*, 2015). (Table5)

Table 5: Some polyprenylated benzophenones isolated from *S. globulifera*

Structures	Sources	References
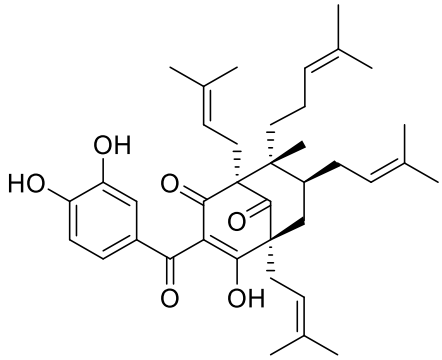 Guttiferone A **(11)**	Seeds, roots and leaves	Ngouela *et al.*, 2006 Gustafson *et al.*, 1992 Lenta *et al.*, 2007
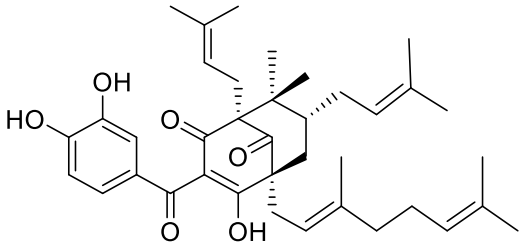 Guttiferone B **(12)**	Roots	Gustafson *et al.*, 1992
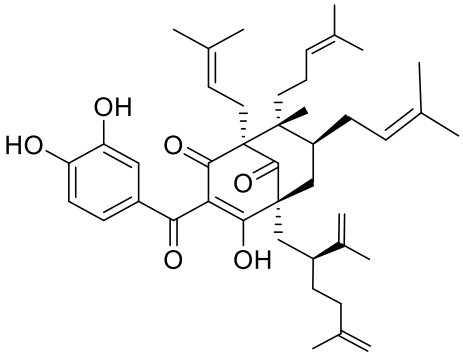 Guttiferone C **(13)**		

Some polyprenylated benzophenones isolated from *S. globulifera* (continued)

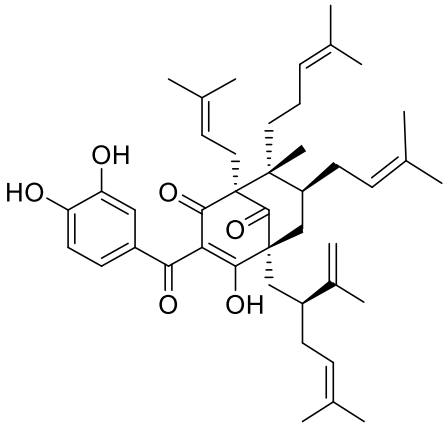 Guttiferone D **(14)**	Roots	Gustafson et al., 1992
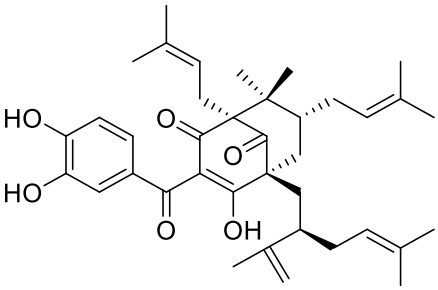 Guttiferone F **(15)**	Leaves	Lenta *et al.*, 2007
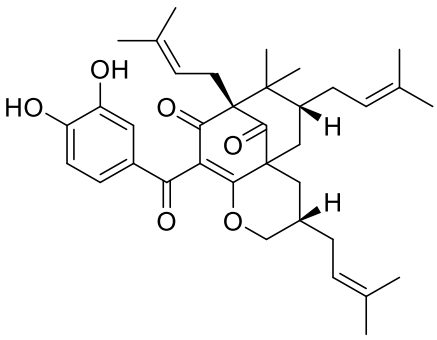 Cambogin **(16)** 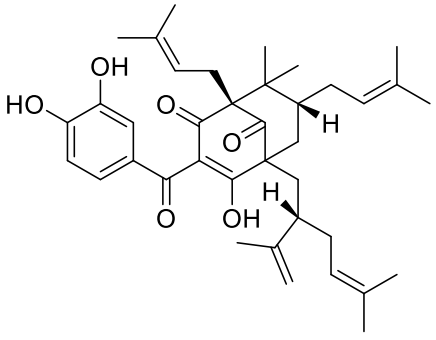 Garcinol **(17)**	Leaves	Lenta *et al.*, 2007

Some polyprenylated benzophenones isolated from *S. globulifera* (continued)

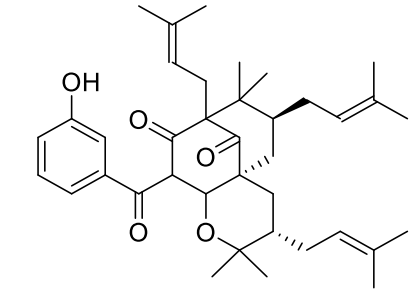 14-Deoxy-7-epi-isogarcinol **(18)** 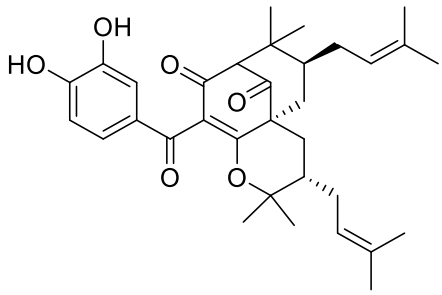 7-epi-isogarcinol **(19)**	Root barks	Marti *et al.*, 2010
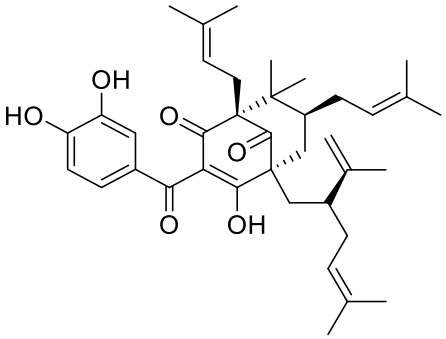 7-epi-garcinol **(20)** 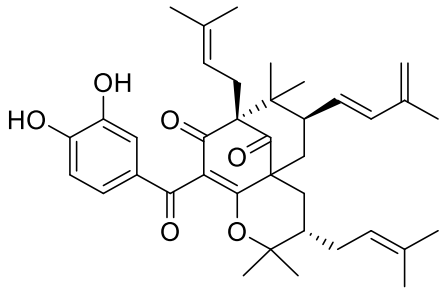 Symphonone A **(21)**	Root barks	Marti *et al.*, 2010

Some polyprenylated benzophenones isolated from *S. globulifera* (continued)

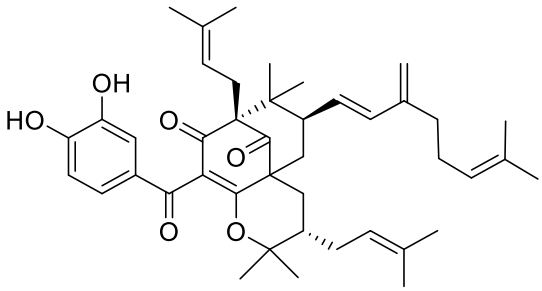 Symphonone B **(22)** 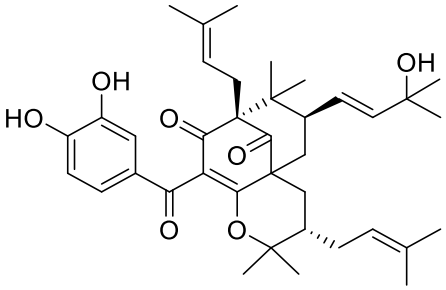 Symphonone C **(23)**	Root barks	Marti *et al.*, 2010
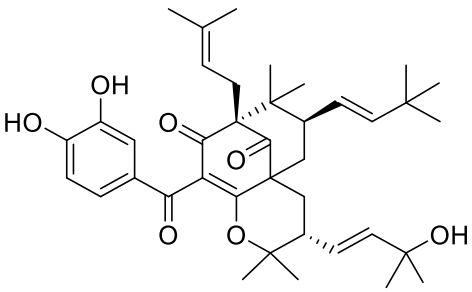 Symphonone D **(24)** 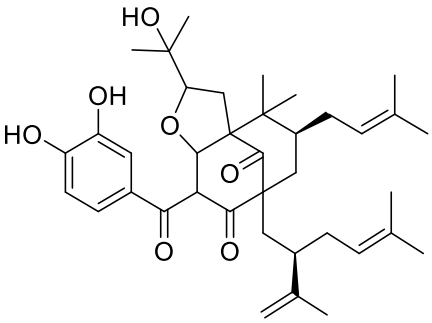 Symphonone G **(25)**	Root barks	Marti *et al.*, 2010

Some polyprenylated benzophenones isolated from *S. globulifera*. (continued)

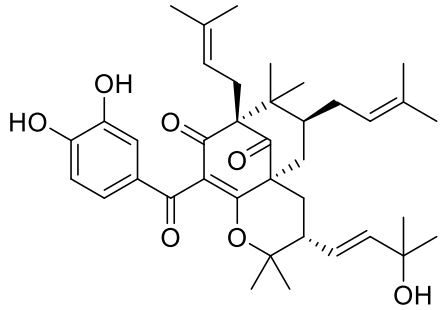 7-*Epi*-coccinone **(26)**	Root barks	Marti *et al.*, 2010
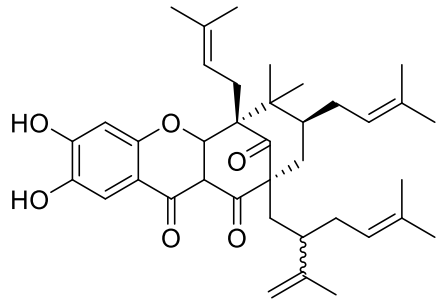 Symphonone H **(27)**		

1.5.1.1.2. Xanthones

Xanthones are secondary metabolites commonly occurring in higher plant families, fungi, and lichen (Cardona *et al.*, 1990). They constitute an important class of oxygenated heterocycles with a C_{13} basic skeleton whose role is well known in medicinal Chemistry (Yoshikawa *et al.*, 2002). Chemically, xanthones are compounds with an oxygen-containing dibenzo-γ-pyrone heterocyclic scaffold (scheme 2) (Gales and Damas, 2005).

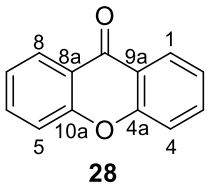

28

Scheme 2: Skeleton of xanthones (Gales and Damas, 2005)

The structure of some xanthones isolated from different parts of *S. globulifera* is shown in table 6 below:

Table 6: Some xanthones isolated from *S. globulifera*

Structures	Sources	References
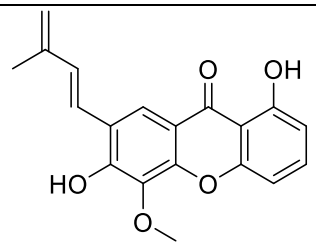 Globulixanthone A **(29)**	Root bark	Nkengfack *et al.*, 2002
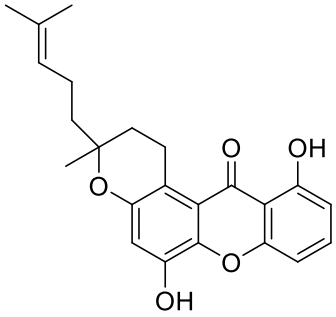 Globulixanthone B **(30)** 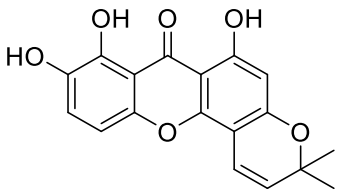 Globulixanthone C **(31)**	Roots	Nkengfack *et al.*, 2002
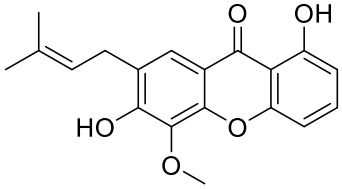 Globulixanthone D **(32)**	Roots	Nkengfack *et al.*, 2002
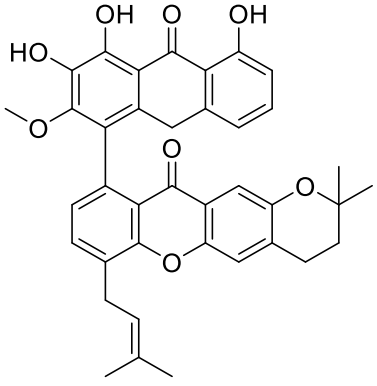 Globulixanthone E **(33)**	Roots	Nkengfack *et al.*, 2002

Some xanthones isolated from *S. globulifera (continued)*

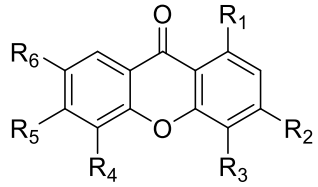 $R_1 = R_2 = R_6 = OH$; $R_4 = R_5 = H$; R_3 = prenyl Mbarraxanthone **(34)** $R_1 = R_6 = OH$; $R_2 = R_3 = R_4 = R_5 = H$ 1,7-dihydroxyxanthone **(35)** $R_1 = R_4 = R_5 = OH$; $R_2 = R_3 = R_6 = H$ 1,5,6-trihydroxyxanthone **(36)** 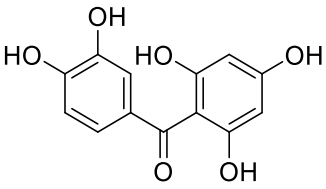 Maclurin **(37)**	Heart wood	Locksley *et al.*, 1966
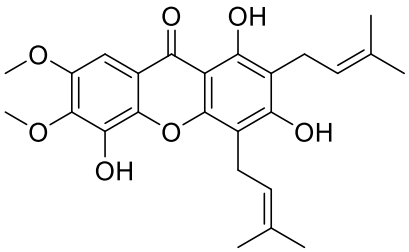 Globuliferin **(38)** 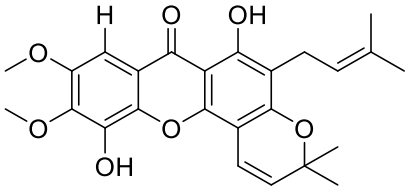 Symphonin **(39)** 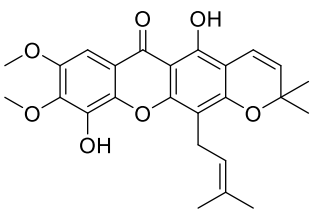 Gaboxanthone **(40)**	Seeds	Ngouela *et al.*, 2006

Some xanthones isolated from *S. globulifera (continued)*

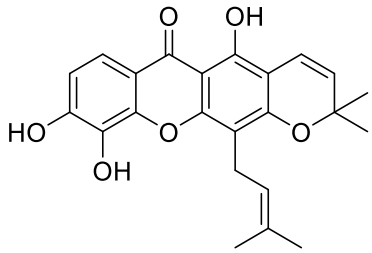 Xanthone V1 **(41)**	Leaves	Lenta *et al.*, 2007
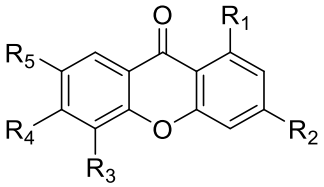 $R_1 = R_2 = R_3 = R_4 = OH$; $R_5 = H$ 1,3,5,6-Tetrahydroxyxanthone **(42)** $R_1 = R_2 = R_4 = R_5 = OH$; $R_3 = H$ Norathyriol **(43)**	Heart wood and twigs	Mkounga *et al.*, 2009 Locksley *et al.*, 1966
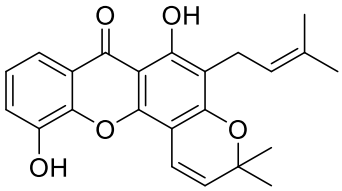 Ananixanthone **(44)**	bark	Bayma *et al.*, 1998
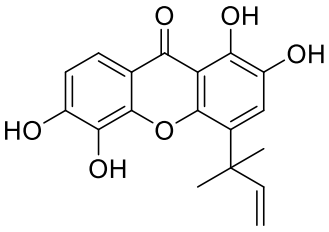 Symphoxanthone **(45)**	Heart wood	Locksley *et al.*, 1966

1.5.1.1.3. Flavonoids

Flavonoids are a class of polyphenolic secondary metabolites found in plants, and thus commonly consumed in diets. Chemically, flavonoids have 15-carbon in their basic skeleton, which consists of two phenyl rings (A and B) and a heterocyclic ring (C). This carbon structure is arranged in C_6-C_3-C_6 (D'Amelia *et al.*, 2018). Scheme 3 shows the basic skeleton of flavonoids.

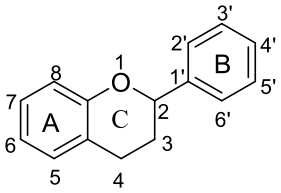

46

Scheme 3: Basic skeleton of flavonoids

Some biflavonoids have been isolated from the leaves and twigs of *S. globulifera* (Fromentin *et al*., 2015) and are flavonoid dimers formed by the covalent bond (C-C or C-O-C) between two monoflavonoids (Gontijo *et al*., 2017). (table 7)

Table 7: Biflavonoids isolated from *S. globulifera*

Structures	Sources	References
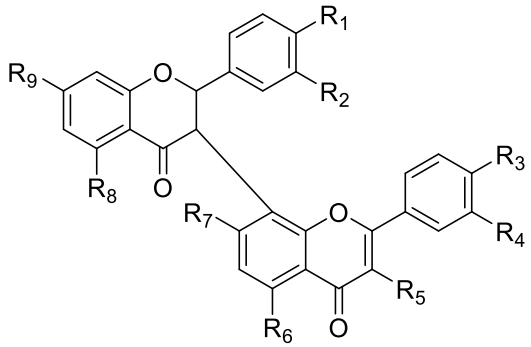 $R_1 = R_3 = R_4 = R_6 = R_7 = R_8 = R_9$ =OH; $R_2 = R_5 = H$ Morelloflavone **(47)**	Leaves	Diel *et al.*, 2022
$R_1 = R_3 = R_4 = R_6 = R_7 = R_8 = R_9 = R_5$ = OH; R_2 = H Biflavonoid GB2 **(48)** $R_1 = R_3 = R_4 = R_6 = R_7 = R_8 = R_9 = R_5 = R_2$ = OH Maniflavanone GB3 **(49)**	Twigs	Mkounga *et al.*, 2009

I.5.1.2. Previous chemical investigations on plants of the genus *Rumex*

Prior chemical investigations conducted on plants belonging to the *Rumex* genus has led to the isolation and characterization of numerous secondary metabolites. Among these, the most notable compounds include anthraquinones, naphthalenes, flavonoids, stilbenoids, triterpenes, carotenoids and other phenolic compounds (Vasas *et al*., 2015).

I.5.1.2.1. Quinones

Quinones represent a class of natural compounds, within which anthracenosides are secondary metabolites derived from anthraquinone and are characterized by the presence of two hydroxy groups at positions 1 and 8 in their structure. Depending on their oxidation state, anthraquinones, anthrones and bianthrones are distinguished. These compounds are considered as the oxidized version of hydroxyanthracene compounds, sharing a fundamental C-14 skeleton resembling that of anthracene-9,10-dione (Bruneton, 1999). Also known as emodols, anthraquinones constitute the largest subgroup of quinones and serve as the oxidized form of anthracenosides. Scheme 4 illustrates the basic structure of anthraquinones.

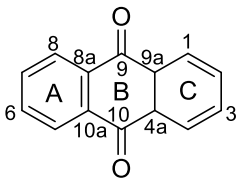

50

Scheme 4: Basic skeleton of anthraquinones

The structure of some anthraquinones isolated from different parts of the *Rumex* genus is shown in table 8 below:

Table 8: Some anthraquinones isolated from the *Rumex* genus

Structures	Species and sources	References
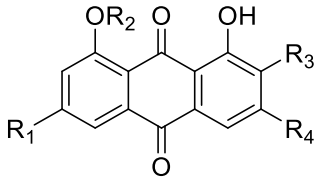 R_1 = OH; R_2 = H; R_3 = H; R_4 = CH_3 Emodin **(51)** R_1 = H; R_2 = H; R_3 = H; R_4 = CH_3 Chrysophanol **(52)** R_1 = OCH_3; R_2 = H; R_3 = H; R_4 = CH_3 Physcion **(53)** R_1 = OH; R_2 = H; R_3 = COOH; R_4 = CH_3 Endocrocin **(54)** R_1 = OH; R_2 = glc; R_3 = H; R_4 = CH_3 Emodin-8-*O*-*β*-D-glucopyranoside **(55)** R_1 = H; R_2 = glc; R_3 = H; R_4 = CH_3 Chrysophanein **(56)** R_1 = OH; R_2 = H; R_3 = H; R_4 = CH_2OH Citreoresin **(57)**	*R. nepalensis* (roots)	Gautam *et al*., 2010; Liang *et al*., 2010
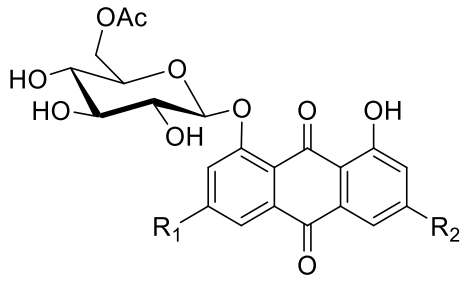 R_1 = H; R_2 = CH_3 Chrysophanol-8-*O*-*β*-D-(6′-*O*-acetyl) glucopyranoside **(58)** R_1 = OH; R_2 = CH_3 Emodin-8-*O*-*β*-D-(6′-*O*-acetyl) glucopyranoside **(59)**	*R. nepalensis* (roots)	Liang *et al*., 2010

Some anthraquinones isolated from the *Rumex* genus (*continued)*

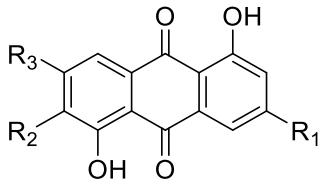 $R_1 = CH_3$; $R_2 = H$; $R_3 = H$ Ziganein **(60)** $R_1 = OH$; $R_2 = CH_2OH$; $R_3 = H$ 1,3,5-Trihydroxy-6-hydroxymethylanthraquinone **(61)** $R_1 = OCH_3$; $R_2 = H$; $R_3 = CH_3$ Przewalsquinone **(62)**	*R. crispus* (roots) *R. nepalensis* (roots)	Günaydin *et al.*, 2002; Gautam *et al.*, 2010
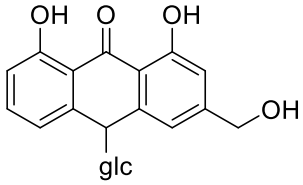 Barbaloin **(63)** 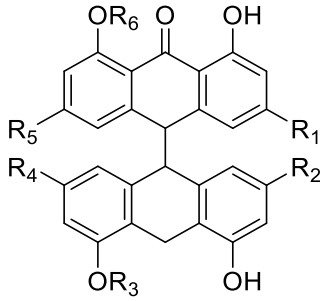 $R_1 = COOH$; $R_2 = COOH$; $R_3 = R_6 = glc$; $R_4 = R_4 = H$ (R+) Sennoside A **(64)** $R_1 = COOH$; $R_2 = COOH$; $R_3 = R_6 = glc$; $R_4 = R_4 = H$ (*Meso*) Sennoside B **(65)**	*R. confertus* (roots)	Wegiera *et al.*, 2007

I.5.1.2.2. Flavonoids

Flavonoids are secondary metabolites that contribute to the diverse colors observed in the flowers and fruits of numerous plant species. Structurally, they have a basic skeleton with fifteen carbon atoms (C15) and make two aromatic rings linked by a chain with three carbon atoms corresponding to diphenylpropane (**66**) (Dacosta, 2003).

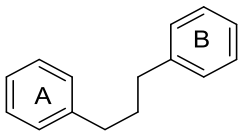

66

Table 9 below shows some examples of flavonoids isolated from plants of the the *Rumex* genus.

Table 9: Some flavonoids isolated from *Rumex species*

Structures	Sources	References
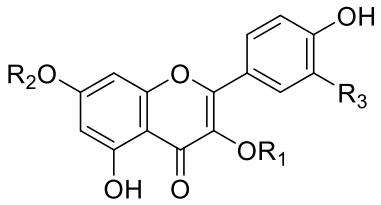 R_1 = H; R_2 = H; R_3 = OH quercetin **(67)** R_1 = glc; R_2 = H; R_3 = H Astragalin **(68)** R_1 = rha; R_2 = H; R_3 = OH Quercitrin **(69)** R_1 = glc; R_2 = H; R_3 = OH Isoquercitrin **(70)**	*R. japonicus* (fruits)	Tavares *et al*., 2010
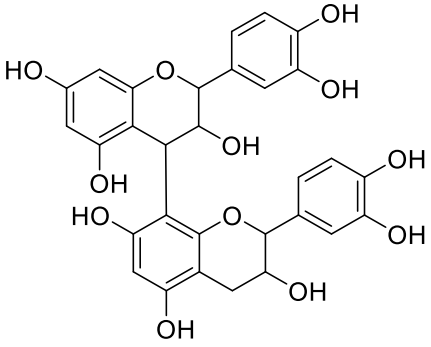 (2*R*, 2′*R*, 3*R*, 3′*S*, 4*R*), Procyanidin B1 **(71)** (2*R*, 2′*R*, 3*R*, 3′*R*, 4*R*), Procyanidin B2 **(72)** (2*R*, 2′*R*, 3*S*, 3′*S*, 4*R*), Procyanidin B3 **(73)** (2*R*, 2′*R*, 3*S*, 3′*R*, 4*S*), Procyanidin B4 **(74)**	*R. acetosa* (herb)	Bicker *et al*., 2009

Some flavonoids isolated from *Rumex species (continued)*

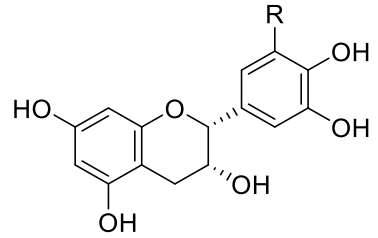 R = H: Epicatechin **(75)** R = OH: Epigallocatechin **(76)**	*R. hymenosepalus* (roots)	Rivero-Cruz *et al*., 2005
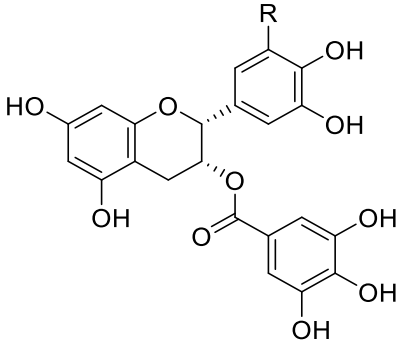 R = H: Epicatechin-3-*O*-gallate **(77)** R = OH: Epigallocatechin-3-*O*-gallate **(78)**	*R. vesicarius*	El-Hawary *et al*., 2011

I.5.1.2.3. Naphtalenes

Naphthalenes belong to the class of chemical compounds known as polycyclic aromatic hydrocarbons (PAHs). They are characterized by the presence of two fused benzene rings, which creates a bicyclic structure (**79**) (Goss and Schwarzenbach, 2001) (Table 10).

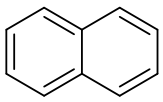

79

Table 10: Some naphtalenes isolated from *Rumex species*

Structures	Sources	References
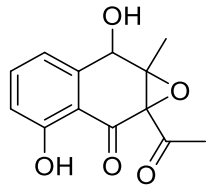 3-acetyl-2-methyl-1,5-dihydroxy-2,3-epoxynaphthoquinol **(80)**	*R. japonicus* (roots)	Zee *et al*., 1998
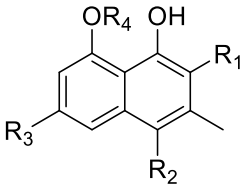 R1 = $COCH_3$; R2 = Cl; R3 = H; R4 = glc Patientoside A (81) R1 = R2 = Cl; R3 = H; R4 = glc Patientoside B (82)	*R. patientia (roots)*	Kuruüzüm et al., 2001
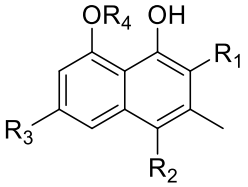 R1 = $COCH_3$; R2 = H; R3 = COOH; R4 = glc rumexoside (83) R1 = $COCH_3$; R2 = H; R3 = OCH_3; R4 = glc-glc Orientaloside (84) R1 = $COCH_3$; R2 = H; R3 = H; R4 = glc Nepodin monoglucoside (85)	*R. patientia (roots)*	Demirezer et al., 2001

I.5.1.2.4. Triterpenoids

Triterpenoids are a subclass of terpenes, which are natural compounds produced by plants and some fungi. They consist of three isoprene units and have a characteristic structure that includes multiple cyclic rings (John and Mary, 2020). Table 11 displays a collection of some triterpenoids that have been isolated from *R. japonicus*.

Table 11: Some triterpenoids isolated from *R. japonicus*

Structures	Sources	References
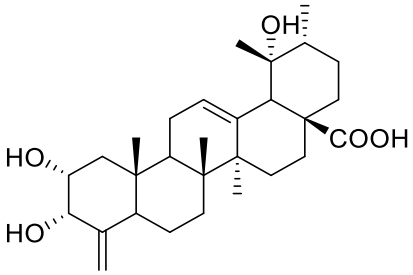 2*α*, 3*α*, 19*α*-Trihydroxy-24-norurs-4 (23), 12-dien-28-oic **(86)**	*R. japonicus* (stem)	Jang *et al*., 2005
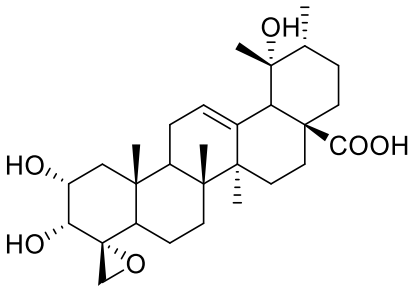 4 (*R*), 23-Epoxy- 2*α*, 3*α*, 19*α*-trihydroxy-24-norurs-12-dien-28-oic **(87)**		
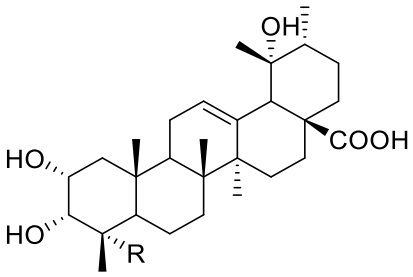 R = CH_3: Tormentic acid **(88)** R = CH_2OH: Myrianthic acid **(89)**		

I.5.1.2.5. Stibenoids

Stilbenoids are a class of natural chemical compounds that belong to the polyphenols. They are characterized by the presence of two phenyl groups linked by a carbon-carbon double bond (C=C) in a *trans*-configuration (**90**) (Agati *et al*., 2012). Some stilbenes isolated from species of *Rumex* genus are presented in table 12.

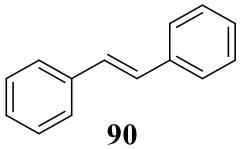

90

Table 12: Some stibenoids isolated from the *Rumex* genus

Structures	Sources	References
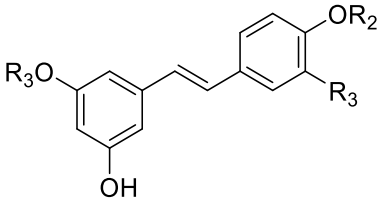 $R_1 = R_2 = R_3 = H$: *Trans*-resveratrol **(91)** $R_1 = CH_3$; $R_2 = R_3 = H$: Pinostibene **(92)** $R_1 = H$; $R_2 = CH_3$; $R_3 = H$: Dexoxyrhapontigenin **(93)**	*R. bucephalophorus* (roots)	Kerem *et al*., 2003
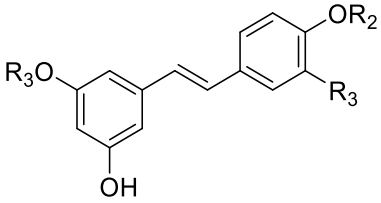 R_1 = glc; $R_2 = H$; $R_3 = H$: Piceid **(94)** R_1 = ara; $R_2 = H$; $R_3 = H$: Rumexoid **(95)**	*R. bucephalophorus* (roots)	Kerem *et al*., 2006
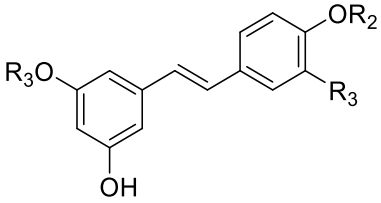 $R_1 = R_2 = H$; $R_3 = OH$ 4-[(*E*)-2-(3,5-Dihydroxyphenyl) ethenyl]-1,2-benzenediol **(96)** $R_1 = H$; R_2 = glc; $R_3 = H$ 4-[(*E*)-2-(3,5-Dihydroxyphenyl) ethenyl] phenyl-hexopyranoside **(97)** $R_1 = H$; R_2 = glc; $R_3 = OH$ 4-[(*E*)-2-(3,5-Dihydroxyphenyl) ethenyl]-2-hydroxyphenyl-hexopyranoside **(98)**	*R. hymenosepalus* (roots)	Rivero-Cruz *et al*., 2005

I.5.1.2.6. Carotenoids

Carotenoids represent a large group of yellow-orange pigments that consist of eight isoprenoid units joined to form a conjugated double bond system in the carotenoid molecule. The conjugated polyene structure is responsible for the observed colour of each carotenoid. The

all-*trans* (all-*E*) configuration is the predominant system in naturally-occurring carotenoids, however, *cis-trans* (*Z-E*) isomers have also been detected in minute concentrations in bread and durum wheats (Abdel-Aal *et al*., 2007a). Table 13 below shows some carotenoids isolated from *Rumex* species.

Table 13: Some carotenoids isolated from *Rumex* species

Structures	Sources	References
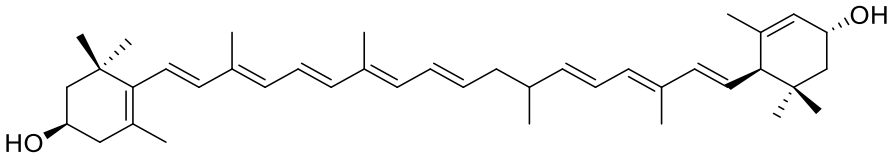 Lutein **(99)** 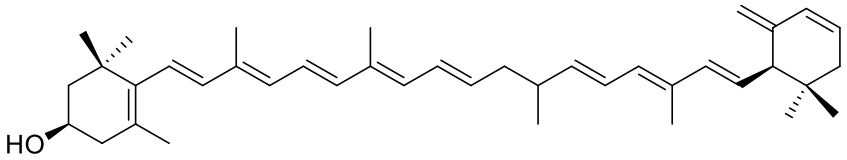 Anhydrolutein Ⅰ **(100)** 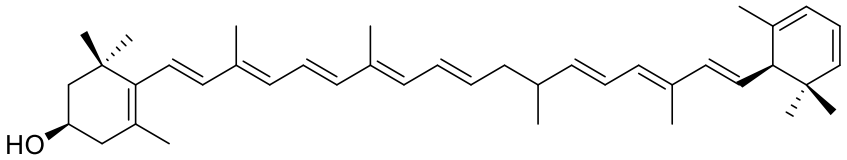 Anhydrolutein Ⅰ Ⅰ **(101)**	*R. rugosus* (steam)	Molnár *et al*., 2005
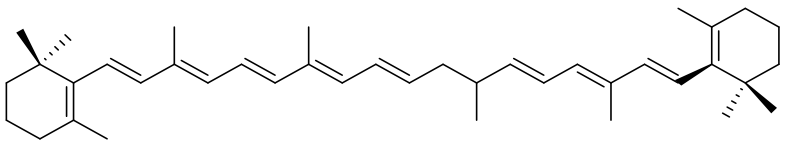 *β*-Carotene **(102)**	*R. vesicarius* (leaves)	Bélanger *et al*., 2010

I.5.1.2.7. Other phenolic compounds

Other phenolic compounds isolated from plants of the genus *Rumex* are listed in **table 14** below.

Table 14: Other phenolic compounds isolated from *Rumex species*

Structures	Sources	References
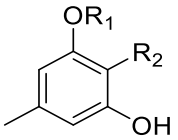 R_1 = H; R_2 = H: Orcinol **(103)**	*R. patientia* (roots)	Demirezer *et al*., 2001
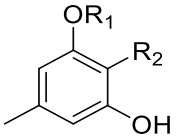 R1 = H; R2 = Ac: 2-Acetylorcinol (104) R1 = glc; R2 = H: Sakakin (105) R1 = glc; R2 = Ac: Pinostibene (106)	*R. alpinus (roots)*	Berg and Labadie, 1981
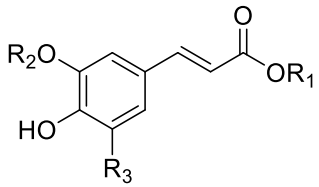 R1 = H; R2 = H; R3 = H Caffeic acid (107) R1 = CH_3; R2 = H; R3 = H 1-Methylcaffeic acid (108) R1 = glc; R2 = H; R3 = H 1-O-Caffeoyl-β-D-glucopyranoside (109) R1 = H; R2 = CH3; R3 = OCH3	*R. aquaticus (aerial parts)*	Yoon et al., 2005

I.5.2. Previous biological investigations on the studied plants

I.5.2.1. Previous biological investigations on *S. globulifera*

Some of the biological activities from the crude extract as well as the secondary metabolites isolated from different parts of *S. globulifera* are are listed in table 15 and 16 below.

Table 15: Some of the biological activities from the crude extract from different parts of *S. globulifera*

Source	Extracts	Activities	References
S. globulifera (leaves)	Methanolic extract	Significant activity against *Leishmania donovani* MHOM/ET/67/L82 axenic amastigotes (IC_{50} = 0.2 μg/mL).	Lenta *et al.*, 2007
S. globulifera (stem bark)	Methanolic extract	Activity against strains of Gram-positive bacteria, namely *Staphylococcus aureus* (ATCC 6538), (MIC = 100 μg/mL for each organism) and Gram-negative bacteria *Escherichia coli* (ATCC 8739) (MIC = 150 μg/mL).	Mkounga *et al.*, 2009

Table 16: Some of the biological activities from the secondary metabolites isolated from different parts of *S. globulifera*

Source	Compounds	Activities	References
S. globulifera (leaves)	Guttiferone A **(11)** and F **(15)**	Strong leishmanicidal activity *in vitro* (IC_{50} = 0.2 μg/mL and 0.16 μg/mL, respectively).	Lenta *et al.*, 2007
		Potent anticholinesterase activities towards butyl cholinesterase (BChE) (IC_{50} = 2.77 and 3.50 μg/mL, respectively).	
	Xanthone VI **(41)**	Interesting antiparasitic activity (IC_{50} = 1.4 μg/mL).	
	Gaboxanthone (40), symphonin (39), globuliferin (38) and guttiferone A (11)	Activities against the Plasmodium parasites (IC50 = 3.53, 1.29, 3.86 and 3.17 µg/mL, respectively).	
	Biflavonoïd GB2 (48) and manniflavanone GB3 (49)	Activity against Gram-negative bacteria Escherichia coli (MIC = 7.50 and 4.50 µg/mL, respectively).	

Some of the biological activities from the secondary metabolites isolated from different parts of *S. globulifera (continued)*

S. globulifera (root bark)	***Globulixanthone C (31), D (32) and E (33)***	Antimicrobial potential with minimum inhibitory concentration against Gram-positive Staphylococcus aureus (ATCC 6538) (MIC = 14.05, 8.0 and 4.51 mg/mL, respectively).	Nkengfack *et al.*, 2002

I.5.2.2. Previous biological investigations on plants of the genus *Rumex*

Biological assays carried out on extracts and secondary metabolites isolated from the genus *Rumex* revealed interesting biological activities. Some of them are listed in **table 17** and **18** below:

Table 17: Some of the biological activities from the crude extract from plants of the genus *Rumex*

Source	Extracts/Fractions	Activities	References
R. nepalensis (roots)	Chloroform and ethyl acetate extracts	Anti-inflammatory activity (significant activity when applied at 0.5 and 1.0 mg/ear).	Gautam *et al*., 2010
	Methanolic extract	Antibacterial activity against *Shigella dysenteriae* (diameter of zone of inhibition = 21.5 mm at 1000 μg/disc).	Ghosh *et al*., 2003a
R. japonicus	Ethyl acetate fraction	Strong antibacterial effect against *B. subtilis*, *B. cereus* and *E. coli* with ampicillin as positive control [zones of inhibition = 15 ± 0.33 mm (*B. subtilis*); 17 ± 0.33 mm (*B. cereus*); and 20 ± 0.88 mm (*E. coli*)].	Elzaawely *et al*., 2005
R. abyssinicus (roots)	Dichloromethane extract	Antiplasmodial activity against chloroquine-resistant *P. falciparium* strain W2 (IC_{50} =3.1 μg/mL).	Muganga *et al*., 2010

Table 18: Some of the biological activities from compounds isolated from plants of the genus *Rumex*

Source	Compounds	Activities	References
R. nepalensis (roots)	Emodin **(51)**, 1,3,5-trihydroxy-6-hydroxymethylanthraquinone **(61)**, przewalsquinone **(62)**	Anti-inflammatory activity (65.3%, 57.7%, and 43.2%, respectively reduction in ear oedema).	Gautam *et al*., 2010
	Emodin (**51**), chrysophanol (**52**), physcion (**53**)	Antidiabetic activity (significantly decreased collagen IV and fibronectin production at 10 μg/mL).	Yang *et al*., 2013
R. nepalensis and *R. hastatus*	Nepodin monoglucoside (**85**), chrysophanol-8-*O*-β-D-(6′-*O*-acetyl) glucopyranoside **(58)**, epicatechin-3-*O*-gallate **(77)**	Potent inhibitory activity against *Mycobacterium tuberculosis* (MIC = 26.6, 4.1 and 10.2 μg/mL, respectively).	Liang *et al*., 2010
R. acetosa *(aerial parts)*	Emodin (51)	Antigenotoxic effects (19.6% in the case of methylnitronitrosoguanidine and 43.5% in the case of 4-nitroquinoline 1-oxide).	Lee et *al*., 2005

Through this study, a total of thirty-two compounds were isolated, including five previously undiscovered compounds, among which three novel derivatives of polyprenylated benzophenones. Consequently, it becomes imperative to provide the biosynthesis of this class of compounds.

Given that PPAPs represent one of the classes predominantly isolated in this study, we aimed to explore their biosynthetic origin.

I.6. Biosynthesis of benzophenones (Polycyclic polyprenylated acylphloroglucinols, PPAPs)

The biosynthesis of acylphloroglucinols includes the condensation of three malonyl-CoA molecules and one acyl-CoA molecule. The product, a tetraketide intermediate, is then transformed through Dieckmann condensation, resulting in the formation of an acylphloroglucinol (**110**) (Liu *et al*., 2003; Klingauf *et al*., 2005). Monocyclic polyprenylated acylphloroglucinols (MPAPs) undergo cyclization to yield both type A and type B PPAPs via a common precursor (Scheme 5) (Cuesta-Rubio *et al*., 2001). The process begins when one of the geminal prenyl groups within an MPAP reacts with prenyl pyrophosphate, leading to the generation of a tertiary carbocation (**110**). An attack on the pendant carbocation (or the

corresponding pyrophosphate) at C (1) of **110** would result in the formation of a type A PPAP, while an attack at C (5) would yield a type B PPAP (Scheme 5). Furthermore, a single diastereomer of **110** has the potential to generate either a type A PPAP with an exo 7-prenyl group or a type B PPAP with an endo 7-prenyl group. In most cases, type A PPAPs are characterized by the presence of exo 7-prenyl groups, whereas type B PPAPs are predominantly distinguished by their endo 7-prenyl groups. A comparable mechanism is suggested for the biosynthesis of hyperforin (Adam *et al*., 2002). On the other hand, the most probable pathway for the biosynthesis of type C PPAPs would involve the initial MPAP with a quaternary center carrying the acyl group (as illustrated in Scheme 5) (Karppinen *et al.*, 2007).

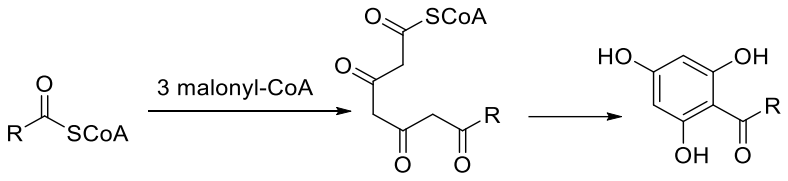

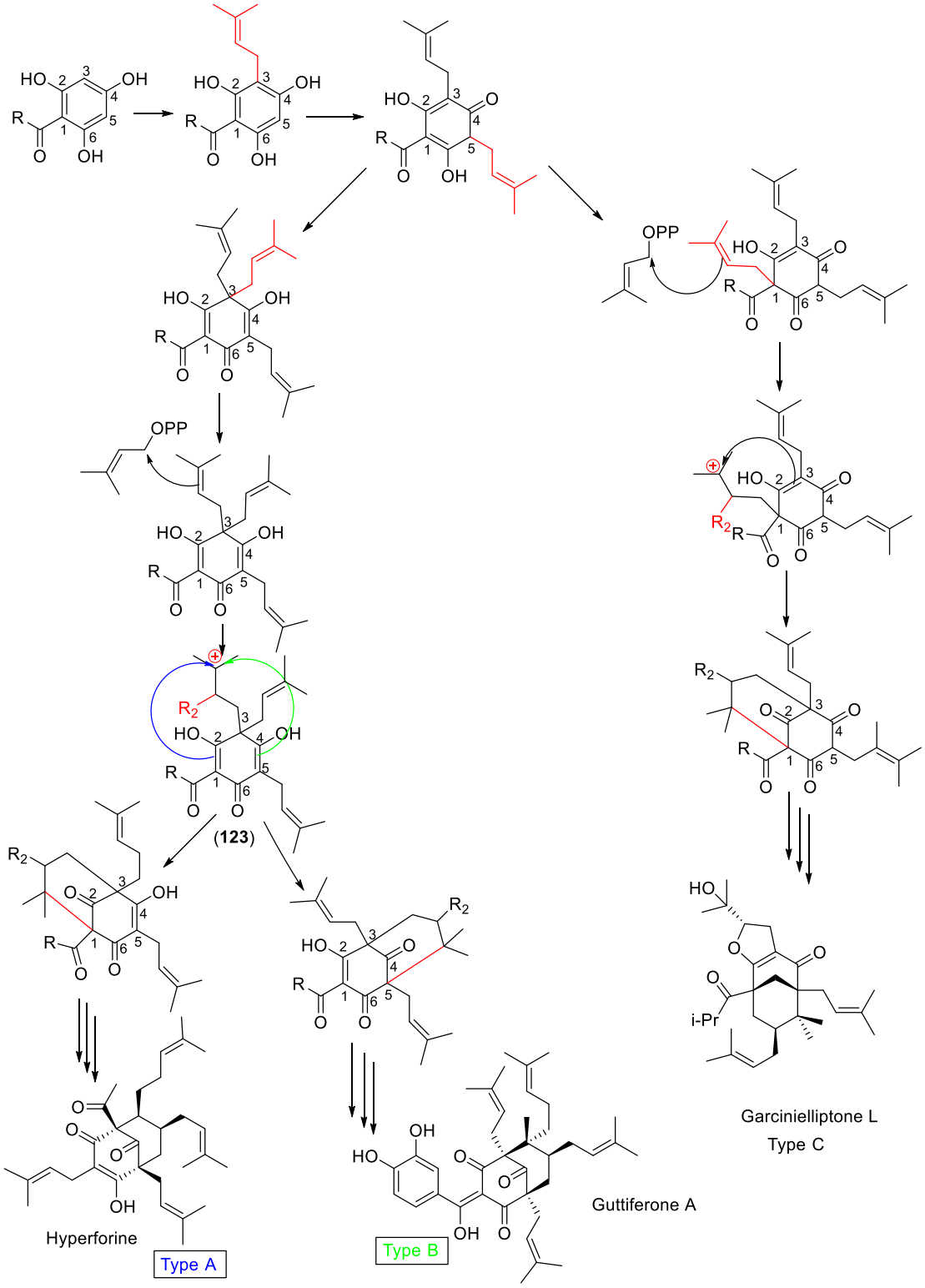

Scheme 5: Biosynthesis of benzophenones from acyl-CoA

The main groups of R and R_2 are as follows:

R = *iso*-butyle, *iso*-propyle, *sec*-butyle, phenol, tri-hydroxy benzyle, phenyl or catechol;
R_2 = phenyl, geranyl or lavandulyl.

PART II:

RESULTS AND DISCUSSION

II.1. Chemical study of *Rumex nepalensis* Spreng and *Symphonia globulifera* Linn. f.

II.1.1. Extraction of plant material

The roots of *R. nepalensis* were harvested in May 2016 in Bamenda, Northwest Region of Cameroon, and identified at the Cameroon National Herbarium, Yaoundé, with voucher specimen number N° 7665/SRFCam. They were chopped, air-dried and ground to yield 8.5 kg of powder. The obtained powder was macerated for 48 hours three times at room temperature (about 26 °C) with 30 L of CH_2Cl_2–MeOH (1:1). The extract was freed from solvent under vacuum to yield 500.7 g of crude extract.

The stem bark of *S. globulifera* was equally harvested in May 2016 in Bangangte (West region of Cameroon) and identified by Mr. Nana Victor, a retired botanist at the National Herbarium of Cameroon, where a voucher specimen (29529 SRFK) was already available. The stem bark of *S. globulifera* was chopped, air dried and then ground to give 10.3 kg of powder, which was extracted by maceration using methanol for 48 h, three times each. The extract was freed from solvent using a rotavapor to yield 638.7 g of MeOH extract.

Because of the observations made in the study conducted by Andrade et *al*., (1990), which demonstrated the vulnerability of visceral leishmaniasis patients to bacterial infections, we carried out antileishmanial and antibacterial screenings on these obtained extracts.

II.1.2. Antileishmanial screening

The methanol extract of the stem bark of *S. globulifera* displayed good *in vitro* activity against *Leishmania donovani* NR-48822 promastigotes with IC_{50} value of 43.11 μg/mL (Table 46).

II.1.3. Antibacterial screening

The methanol extract of the stem bark of *S. globulifera* Linn f. was assessed for their antibacterial activity against seven bacterial strains: *Salmonella typhi CPC, S. enterica NR13555, Staphylococcus aureus ATCC43300*, *S. aureus ATCC25923*, *Klebsiella pneumoniae clinical isolate, K. pneumoniae NR41388*, and *Pseudomonas aeruginosa HM801* (Table 49) and exhibited moderate activity with MIC values ranging from 125.0 to 250.0 μg.mL^{-1}, except on *S. enterica NR13555* and *K. pneumoniae NR41388*, which was not susceptible to this crude extract.

The CH_2Cl_2–MeOH (1:1, v/v) root extract of *R. nepalensis* was subjected to preliminary screening on seven bacteria strains: *S. typhi CPC, S. enterica NR13555, S. aureus ATCC43300, S. aureus ATCC25923, P. aeruginosa HM801, K. Pneumoniae NR41388,* and *K. Pneumoniae* (clinical isolate). This extract exhibited significant antibacterial activities with 31.25 ≤MIC≤ 62.5 $\mu g.mL^{-1}$against five of the tested strains (Table 50).

II.1.4. Isolation of compounds

Part of the CH_2Cl_2–MeOH (1:1, v/v) root extract of *R. nepalensis* (490.1 g) was suspended in distillated water and successively partitioned with *n*-hexane, EtOAc, and *n*-BuOH to afford 20.5 g, 130.1 g, and 110.5 g of each fraction, respectively. Part of the EtOAc soluble fraction (125 g), which was the most active fraction was subjected to silica gel column chromatography (CC), MPLC using normal phase pre-packed silica gel columns as stationary and Sephadex LH-20 and led to the isolation of twenty secondary metabolites (Scheme 6).

Part of the methanol extract of the stem bark of *Symphonia globulifera* (628.2 g) was dissolved in distillated water and successively partitioned with *n*-hexane, EtOAc, and *n*-BuOH. After evaporation of each solvent under reduced pressure, 146.8 g of *n*-hexane, 76.2 g of EtOAc, and 42.3 g of *n*-BuOH fractions were obtained. A part of the soluble *n*-hexane fraction of *S. globulifera* (140.1 g), which was the most active fraction was purified through silica gel column chromatography (CC), MPLC using normal phase pre-packed silica gel columns as stationary and Sephadex LH-20 and led to the isolation of fifteen secondary metabolites (Scheme 7).

Schemes 6 and 7 below summarized the experimental protocols of extraction and purification of both plant extracts.

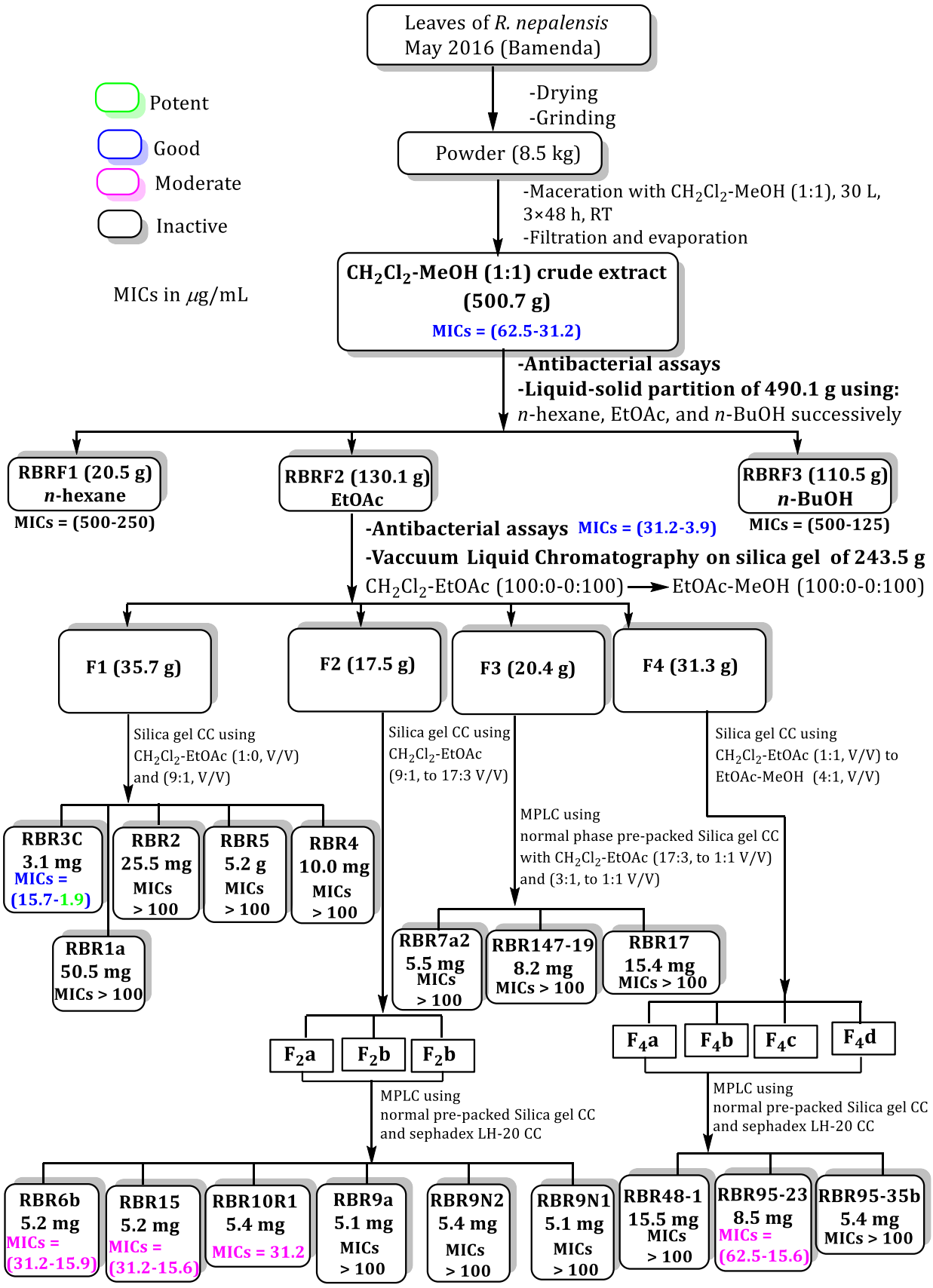

Scheme 6: Protocol of extraction and isolation of compounds from the root of *R. nepalensis*

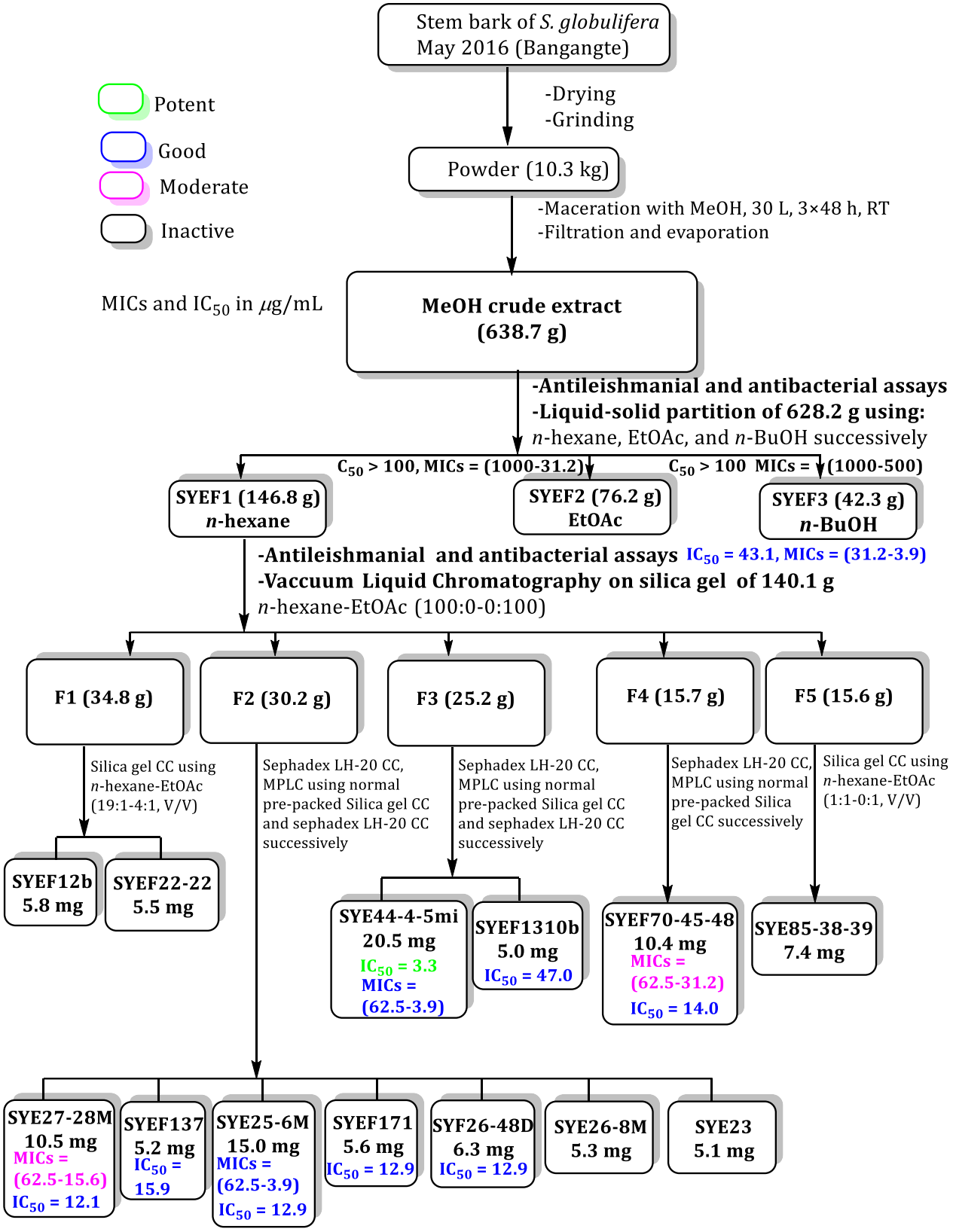

Scheme 7: Protocol of extraction and isolation of compounds from the stem bark of *S. globulifera*

II.1.5. Structural elucidation of the isolated compounds

A total of thirty-two different compounds were fully characterized using physical and spectroscopic methods (MS, IR, NMR).

II.1.5.1. Phenylisobenzofuranone

II.1.5.1.1. Structural elucidation of compound RBR48-1

Compound RBR48-1 was obtained as a brown oil in CH_2Cl_2-MeOH (7:3). It was soluble in DMSO, $[\alpha]_{589}^{20}$ + 6.1 (*c* 0.5, MeOH).

Its molecular formula, $C_{23}H_{24}O_{11}$, was deduced from its HRESIMS (Figure 3), which showed the sodium adduct peak $[M+Na]^+$ at *m/z* 499.1205 (calcd for $C_{23}H_{24}O_{11}Na^+$, 499.1211), corresponding to twelve degrees of unsaturation.

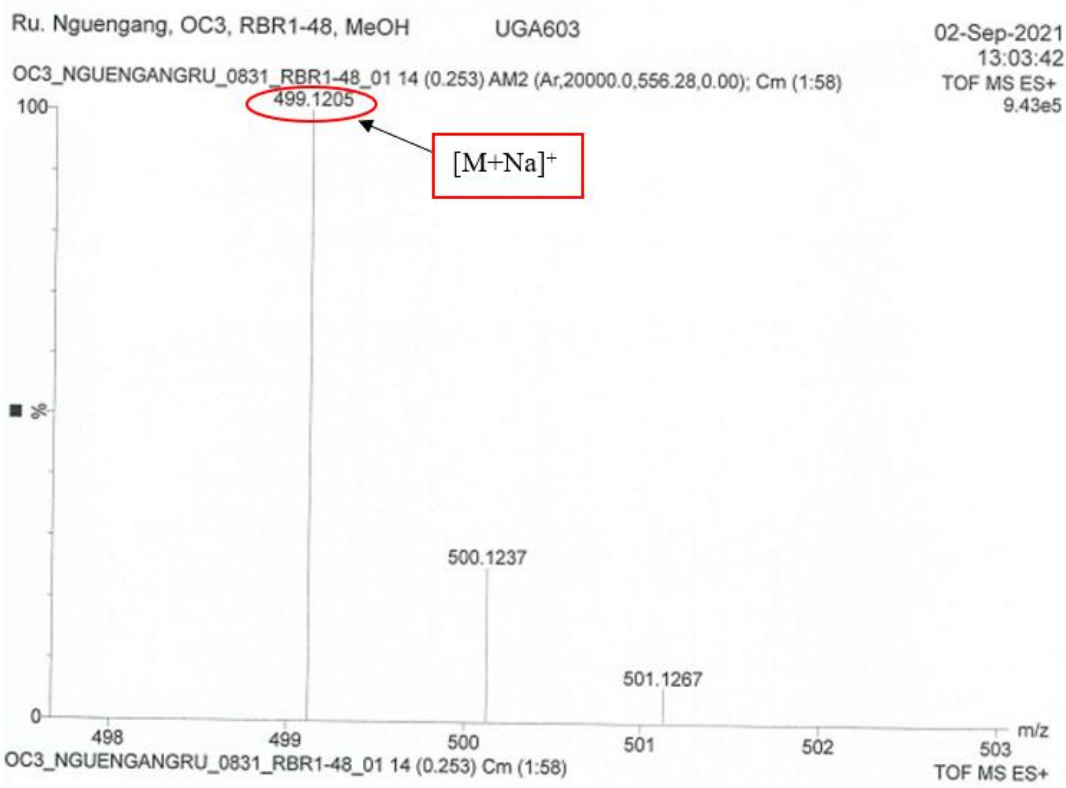

Figure 3: (+) HRESI mass spectrum of RBR48-1

Its IR spectrum (Figure 4) showed characteristic absorption bands of hydroxy (3264–3733 cm^{-1}), conjugated carbonyl ester (1733 cm^{-1}), and aromatic ring (1615 cm^{-1}) functional groups (Hayasaka *et al.,* 2011).

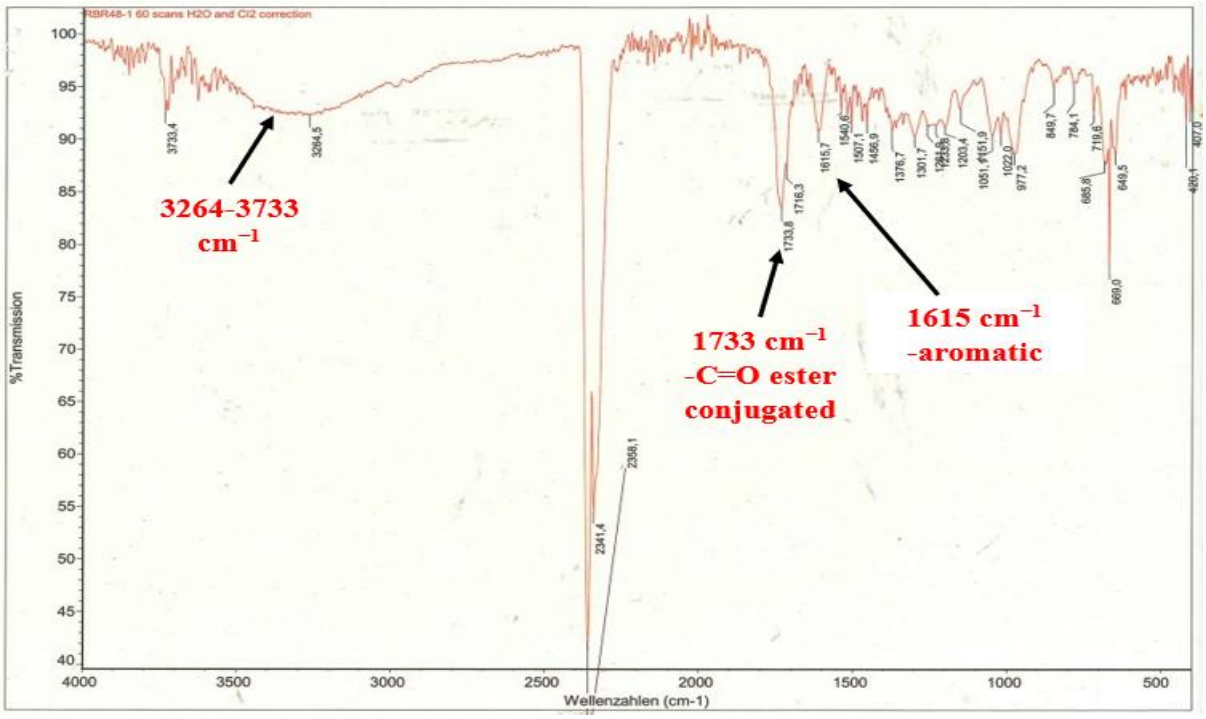

Figure 4: IR spectrum of RBR48-1

Its ^{1}H NMR spectrum (Figure 5) exhibited resonances of:

- two pairs of meta-coupled protons at δ_H [6.60 (1H, br s, H-5) and 6.72 (1H, br s, H-7)] and [5.71 (1H, d, J = 2.8 Hz, H-6′) and 6.33 (1H, d, J = 2.8 Hz, H-4′)], suggesting the presence of two tetra-substituted aromatic rings;
- one methyl group attached to an aromatic ring at δ_H 2.29 (3H, s, H-8);
- a singlet of a strongly deshielded oxymethine proton at δ_H 6.49 (1H, s, H-3);
- the protons of the methyl of an acetyl group at δ_H 2.02 (3H, s, H-2‴) (Pavia *et al*., 2015);
- the sugar moiety between 1.04 and 5.19 with a doublet of three protons at δ_H 1.04 (3H, d, J = 6.2 Hz, H-6″) and the anomeric proton at δ_H 5.19 (1H, d, J = 1.8 Hz, H-1″) suggesting the presence of a deoxyhexose unit (Agrawal 1992).

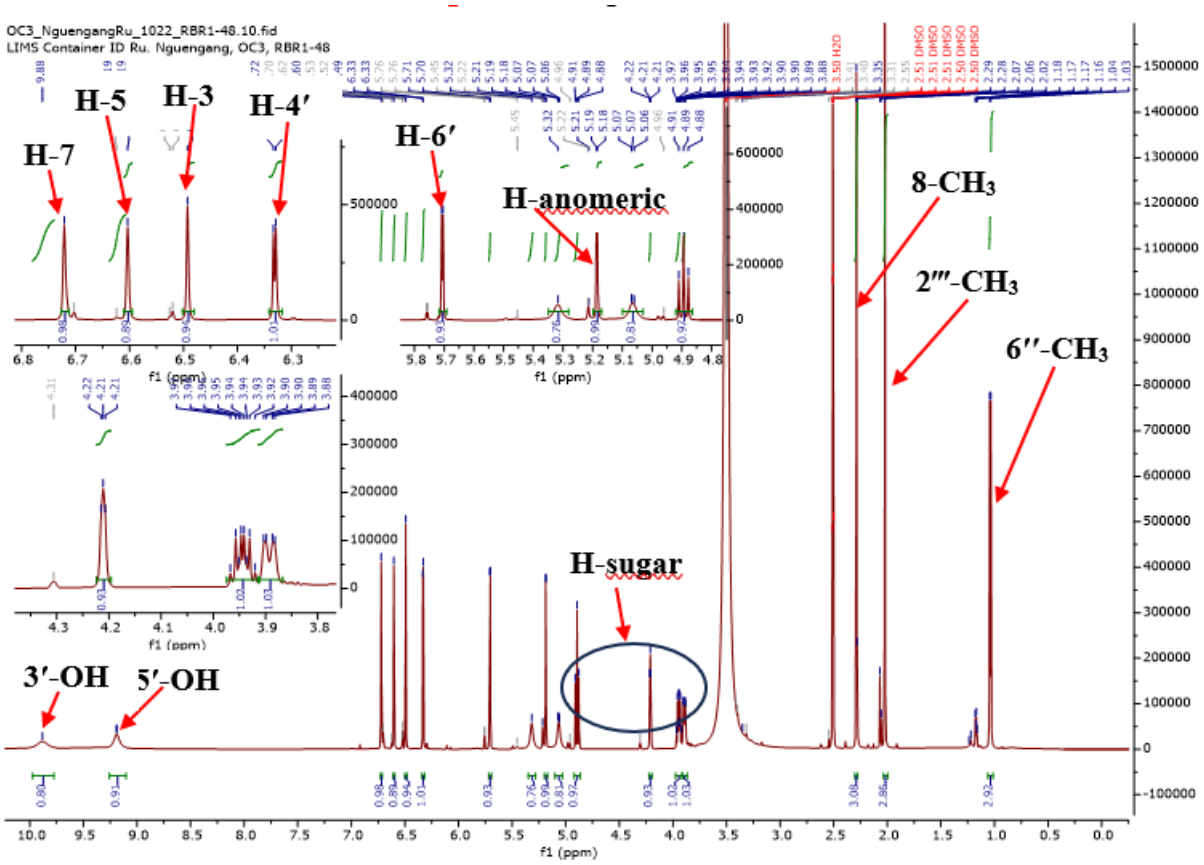

Figure 5: ^{1}H NMR of RBR48-1 (DMSO-d_6, 600 MHz)

Its ^{13}C NMR spectrum (Figure 6) revealed 23 carbon resonances, which were sorted by DEPT (Figure 7) and HSQC (Figure 9**)** techniques into:

- three methyls [including one methyl group attached to the aromatic ring at δ_C 22.1 (C-8)]);
- ten methine carbons [including six oxymethines and four aromatic methines]
- ten quaternary carbons [including two carbonyl functions at δ_C 168.5 (lactone, C-1) and 170.6 (ester, C-1‴)];

The comparison of the ^{13}C chemical shifts of the sugar moiety with those from literature (Agrawal 1992) confirmed the presence of the rhamnopyranosyl moiety.

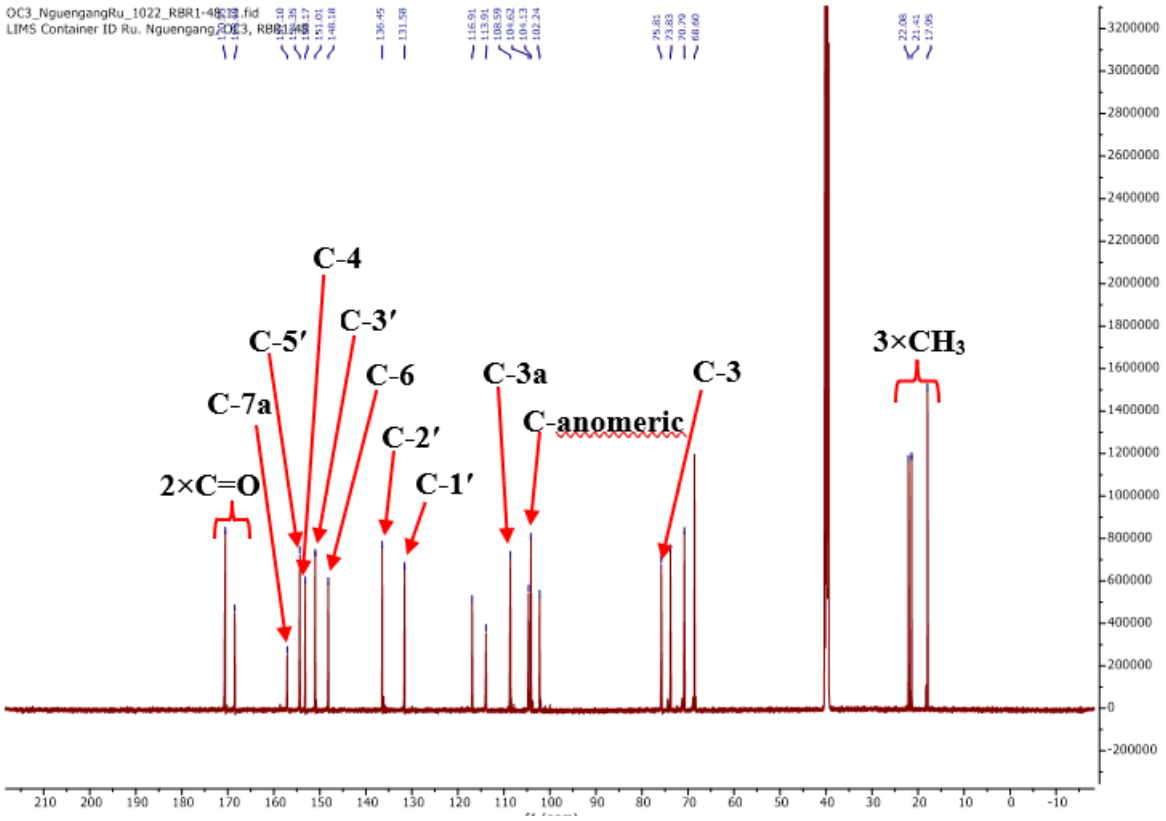

Figure 6: ^{13}C NMR spectrum of RBR48-1 (DMSO-d_6, 150 MHz)

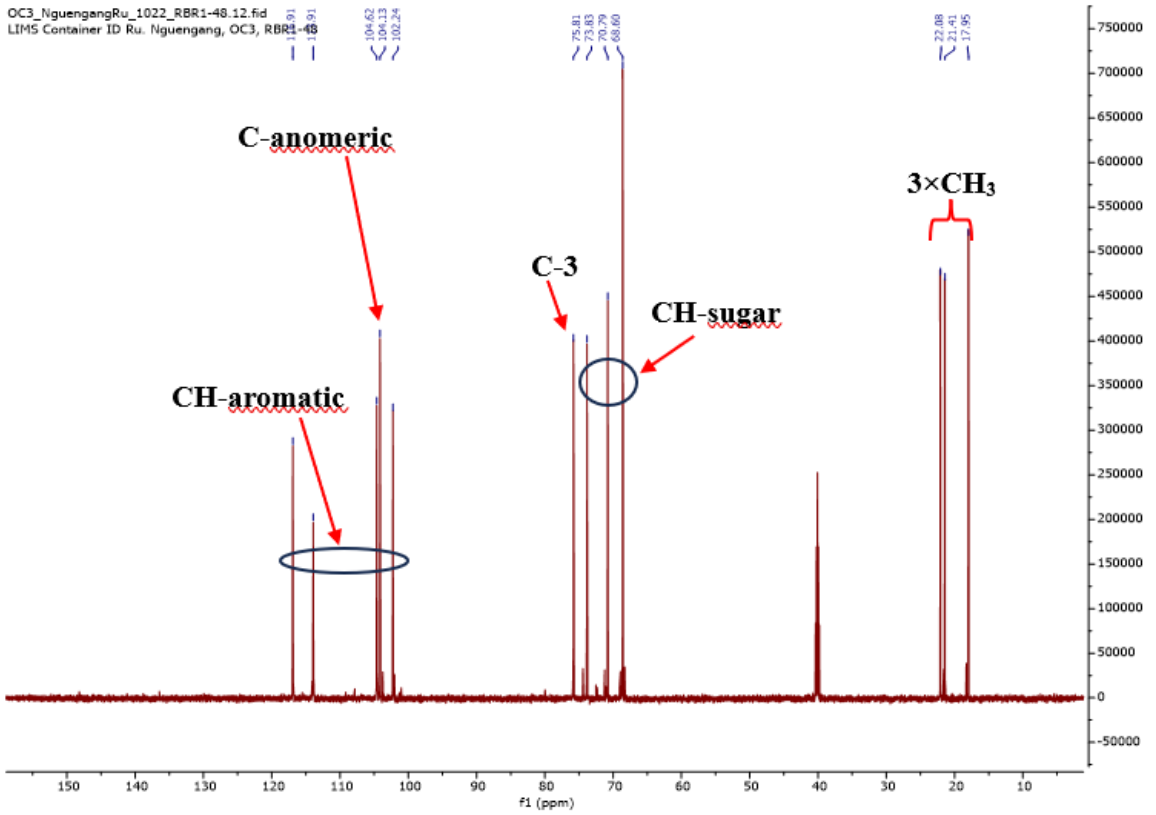

Figure 7: DEPT spectrum of RBR48-1

Correlations observed on its COSY (Figure 8) and HMBC (Figure 9) spectra clearly indicated the presence of 1(3H)-isobenzofuranone unit (Hayasaka *et al*., 2011), 3,5-dihydroxyphenyl and 4-OAc-rhamnopyranosyl moieties (Yang *et al*., 2003).

The 1(3H)-isobenzofuranone moiety was established by HMBC correlations (Figure 10) of H-3/C-1 (δ_C 168.5) and C-4 (δ_C 153.2), H-7/C-1 (δ_H 168.5), and H-5/C-3a (δ_C 108.6).

The 1(3H)-isobenzofuranone moiety was connected to the 3,5-dihydroxyphenyl moiety through the HMBC correlations of H-3/C-2′ (δ_C 136.5) and C-6′ (δ_C 102.2), while the location of the methyl group on the benzofuranone moiety was established by the HMBC correlations of H-5/C-8 (δ_C 22.1), H-7/C-8 (δ_H 22.1), and H-8/C-5 (δ_C 114.0), C-6 (δ_C 148.2), and C-7 (δ_C 117.0). Furthermore, the 3,5-dihydroxyphenyl moiety was connected to the sugar moiety through the HMBC correlation of H-1″/C-2′ (δ_C 136.5), while the acetyl group was attached to the sugar moiety through the HMBC correlation of H-4″/C-1‴ (δ_C 170.6).

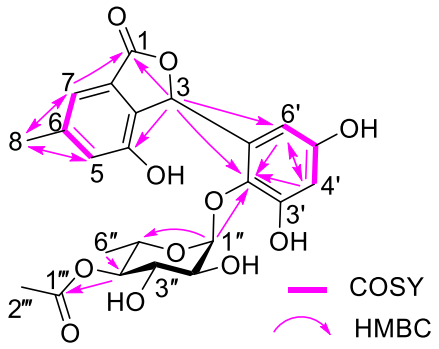

Scheme 8: Key HMBC and COSY correlations of RBR48-1

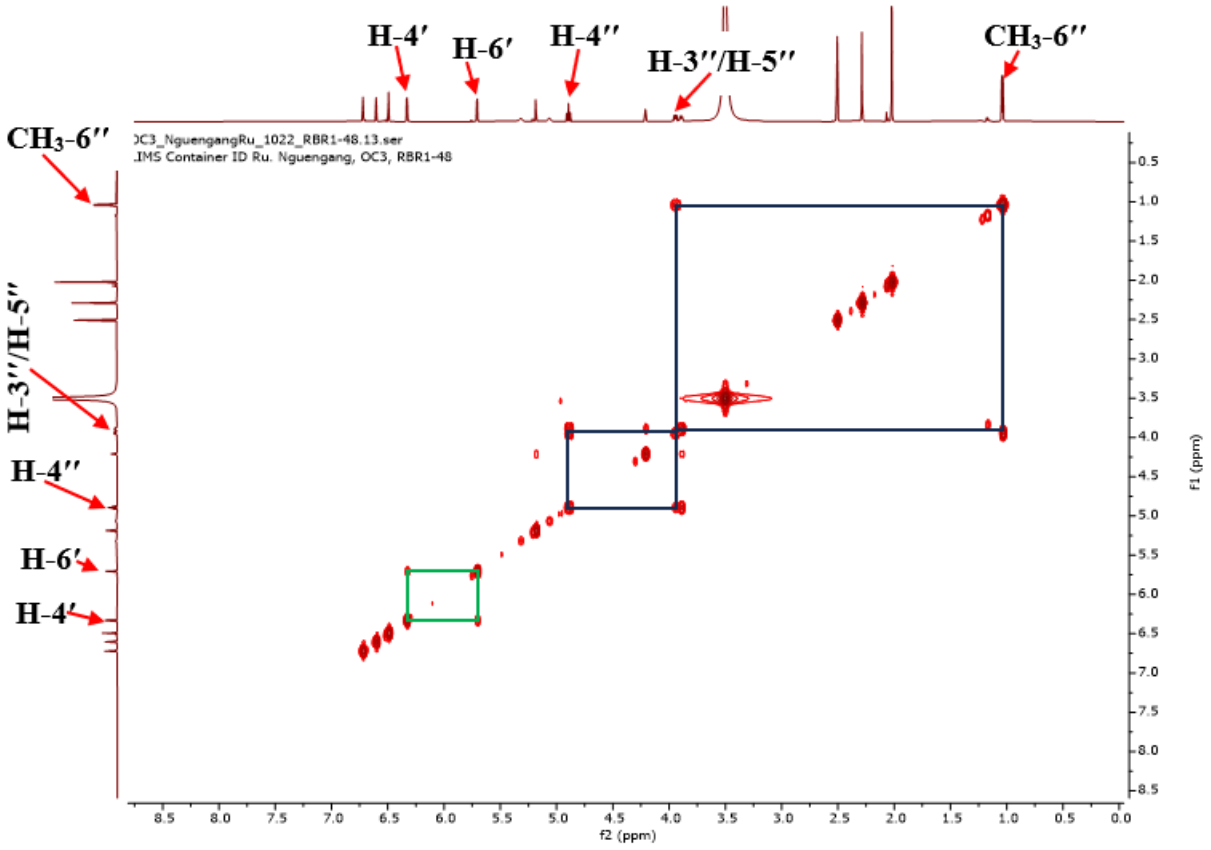

Figure 8: COSY spectrum of RBR48-1

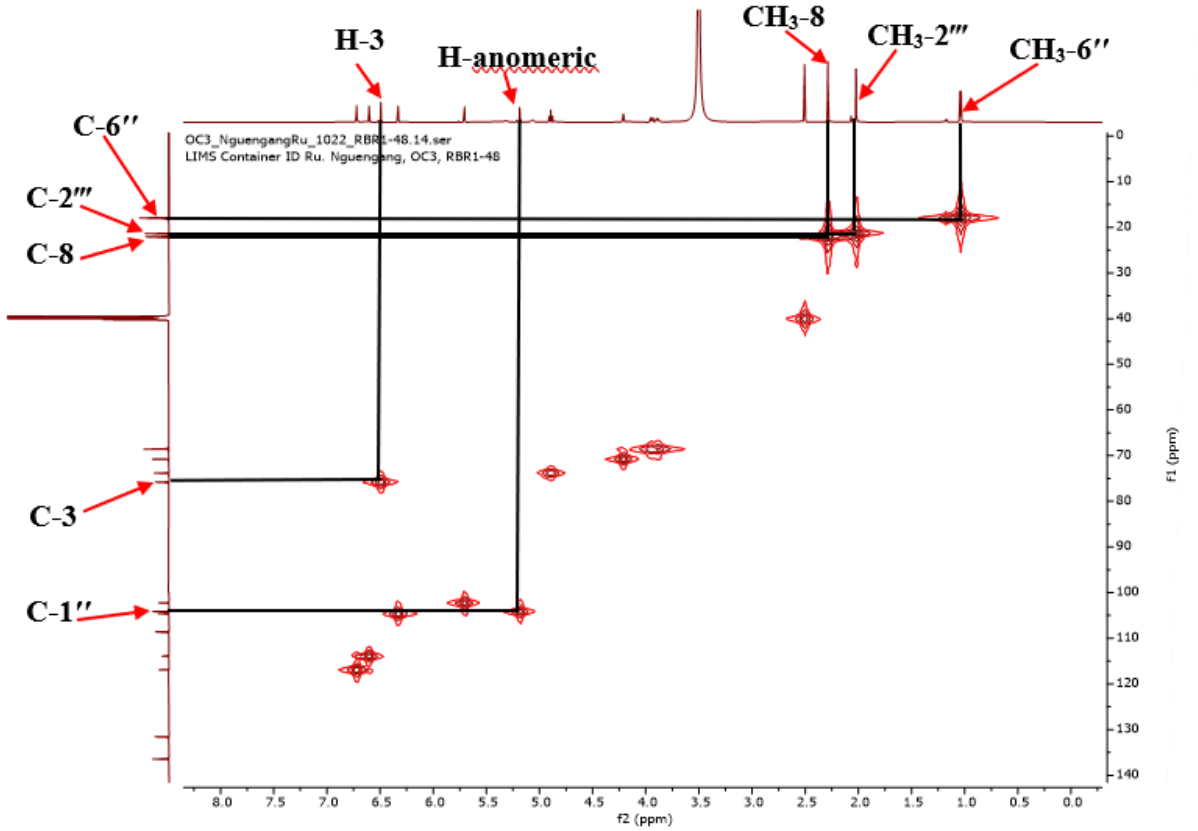

Figure 9: HMQC spectrum of RBR48-1

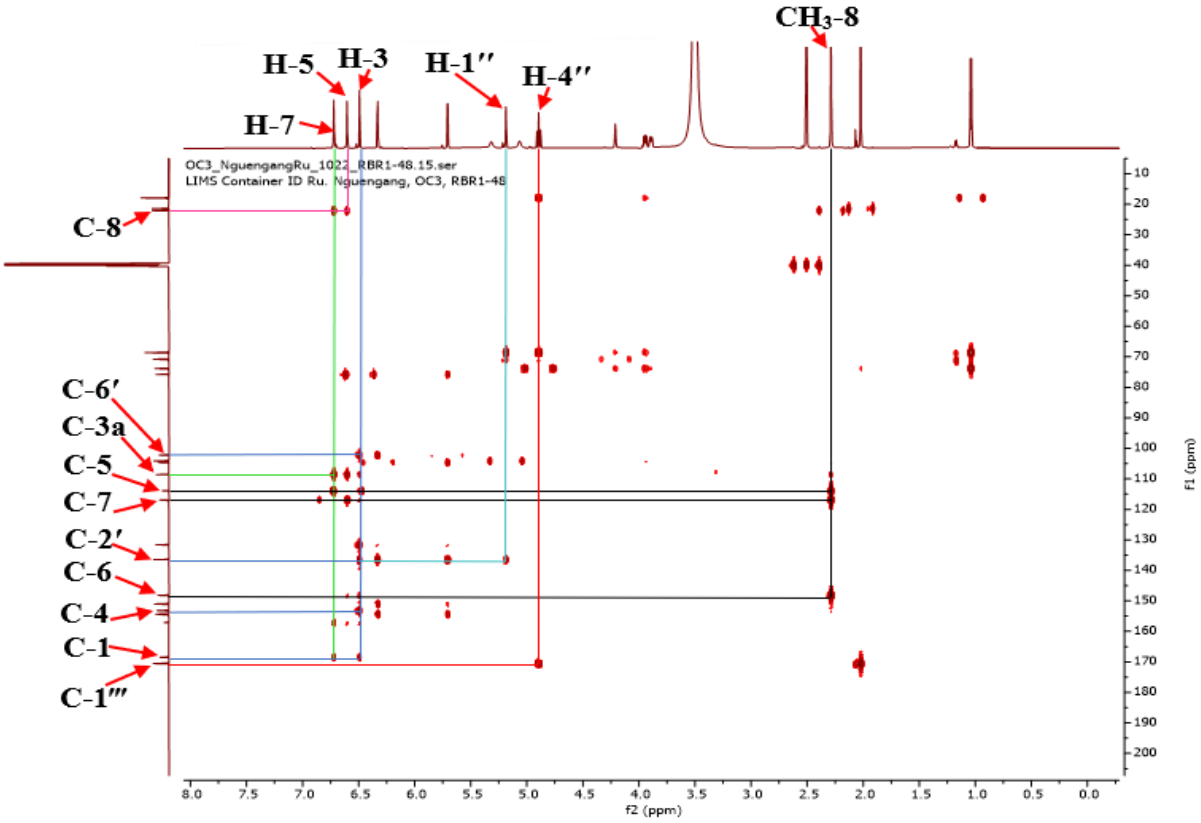

Figure 10: HMBC spectrum of RBR48-1

Based on the above evidence, the structure of RBR48-1, was characterized as a new phenylisobenzofuranone, 4''-*O*-4-hydroxy-6-methyl-3-(3',5'-dihydroxyphenyl)-1(3H)-isobenzofuranone-α-L-rhamnopyranoside, trivially named berquaertiide (**111**).

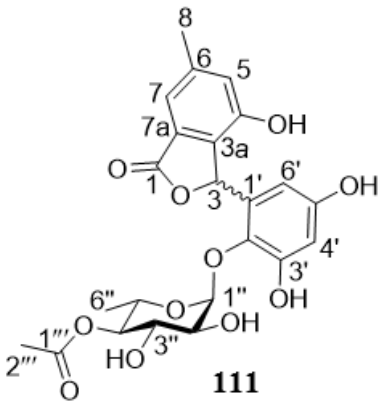

111

Table 19: ^{1}H (600 MHz) and ^{13}C (150 MHz) spectroscopic data of RBR48-1 in DMSO-*d*$_6$

Position	δ_C	δ_H (m, *J* in Hz)	HMBC correlations
1	168.5	-	
3	75.8	6.49 (1H, s)	C-1, C-4, C-1′, C-2′, C-6′
3a	108.6	-	
4	153.2	-	
5	114.0	6.60 (1H, br s)	C-3a, C-7, C-8
6	148.2	-	
7	117.0	6.72 (1H, br s)	C-1, C-3a, C-5, C-7a, C-8
7a	157.1	-	
8	22.1	2.29 (3H, s)	C-5, C-6, C-7
1′	131.6	-	
2′	136.5	-	
3′	151.0	-	
4′	104.6	6.33 (1H, d, 2.8)	C-2′, C-3′, C-5′, C-6′
5′	154.4	-	
6′	102.2	5.71 (1H, d, 2.8)	C-3, C-2′, C-4′, C-5′
OH-3′	-	9.88	
OH-5′	-	9.19	
1″	104.1	5.19 (1H, d, 1.8)	C-2′, C-2″, C-5″
2″	70.8	4.21 (1H, t, 2.5)	C-3″, C-4″
3″	68.6	3.89 (1H, dd, 10.0, 3.1)	C-4″
4″	73.8	4.89 (1H, t, 9.7)	C-5″, C-6″, C-1
5″	68.6	3.94 (1H, m)	C-1″, C-3″, C-4″, C-6″
6″	18.0	1.04 (3H, d, 6.2)	C-4″, C-5″
1‴	170.6	-	
2‴	21.4	2.02 (3H, s)	
OH-2″	-	5.32 (1H, br s)	
OH-3″	-	5.07 (1H, br s)	

II.1.5.2. Polyprenylated benzophenones

II.1.5.2.1. Structural elucidation of compound SYE25-6M

Compound **SYE25-6M** was obtained as a yellowish finely divided solid in the *n*-hexane-EtOAc (3:2, v/v) mixture. It was soluble in acetone, $[\alpha]_{589}^{20}$ + 93 (*c* 0.5, MeOH).

Its molecular formula, $C_{38}H_{50}O_6$, was deduced from the HRESIMS (Figure 11), which showed the sodium adduct peak $[M+Na]^+$ at *m/z* 625.3494 (calcd for $C_{38}H_{50}O_6Na^+$, 625.3500), corresponding to 14 degrees of unsaturation.

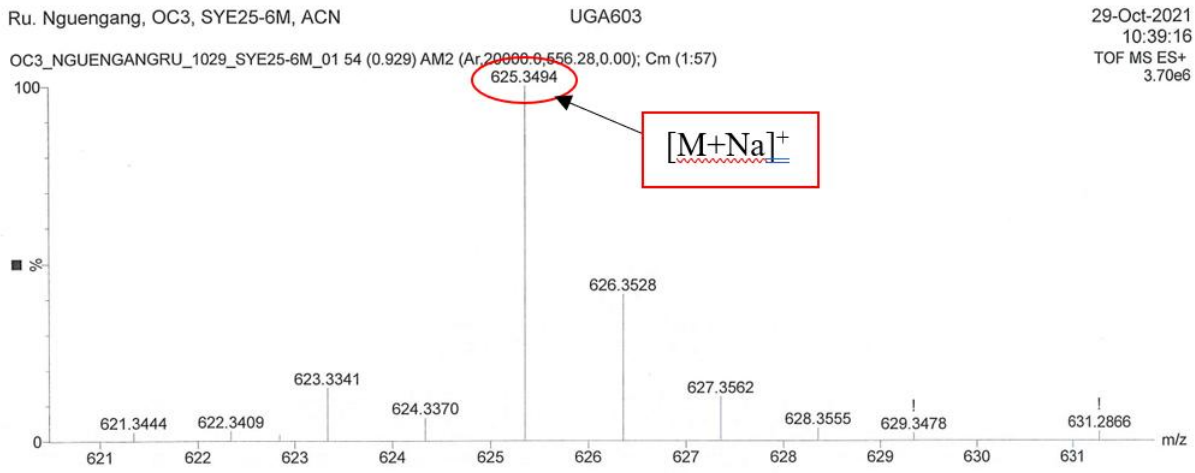

Figure 11: HRESI mass spectrum of SYE25-6M

Its IR spectrum (Figure 12) showed characteristic absorption bands for hydroxy (3735 cm^{-1}), vinyl (2974 cm^{-1}), conjugated carbonyl ketone (1725 cm^{-1}) and aromatic ring (1646 cm^{-1}) functional groups.

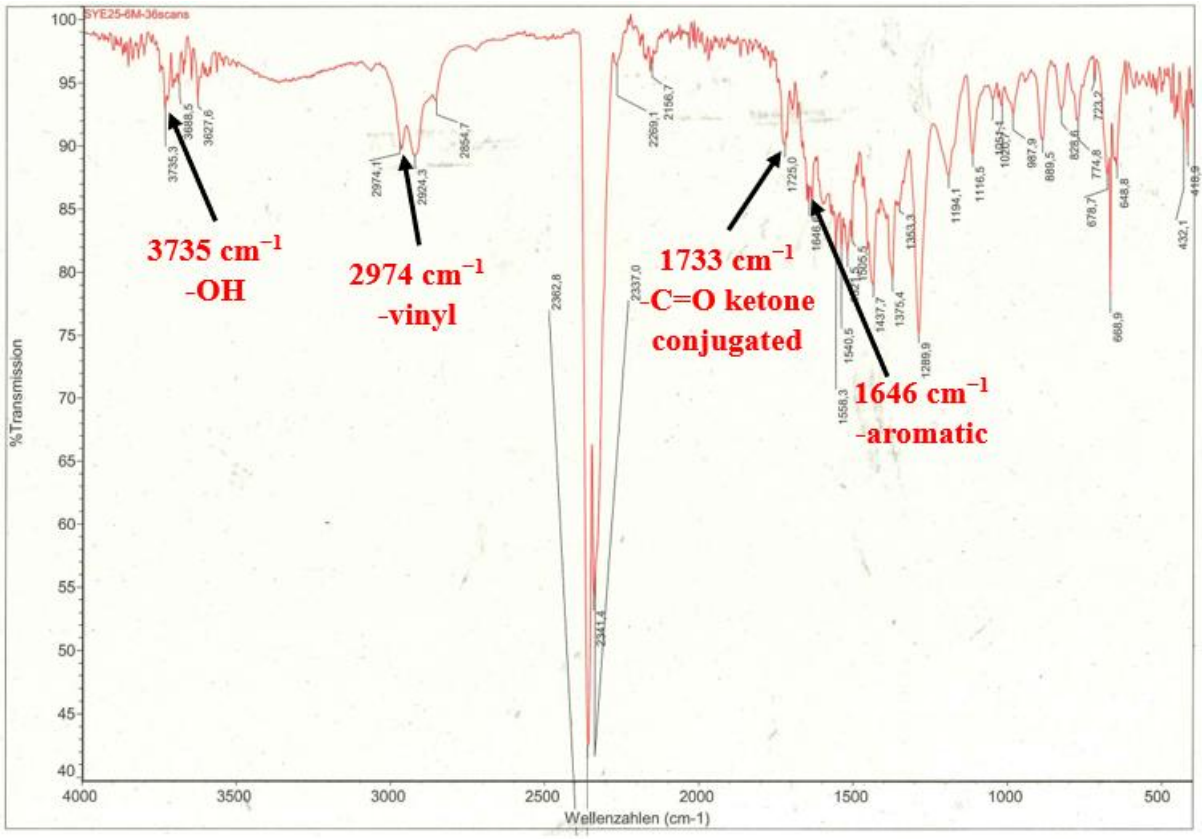

Figure 12: IR spectrum of SYE25-6M

Its ^{1}H NMR spectrum (Figure 13) exhibited:

- signals of an ABX pattern at δ_H 6.81 (1H, d, J = 8.3 Hz, H-15), 7.06 (1H, dd, J = 8.3, 2.1 Hz, H-16), and 7.23 (1H, d, J = 2.1 Hz, H-12);
- the characteristic signals of three isopent-2-enyl groups at δ_H {[2.05 (2H, m, H-29), 5.06 (1H, m, H-30), 1.65 (3H, s, H-32), and 1.53 (3H, s, H-33)], [2.68 (2H, m, H-17), 5.15 (1H, m, H-18), 1.71 (3H, s, H-20), and 1.65 (3H, s, H-21)], [1.91 (2H, m, H-34), 5.11 (1H, m, H-35), 1.68 (3H, s, H-37), and 1.60 (3H, s, H-38)]};
- signals of one isopent-3-enyl unit at δ_H [2.05 (2H, m, H-24), 1.91 (2H, m, H-25), 1.70 (3H, s, H-27), and 4.66 (2H, brs, H-28)];
- The resonances of one tertiary methyl group at δ_H 1.16 (3H, s, H-22), two methylenes at δ_H 1.28 (2H, m, H-23) and 2.05 (2H, m, H-7), and one methine at δ_H 1.87 (1H, m, H-6).

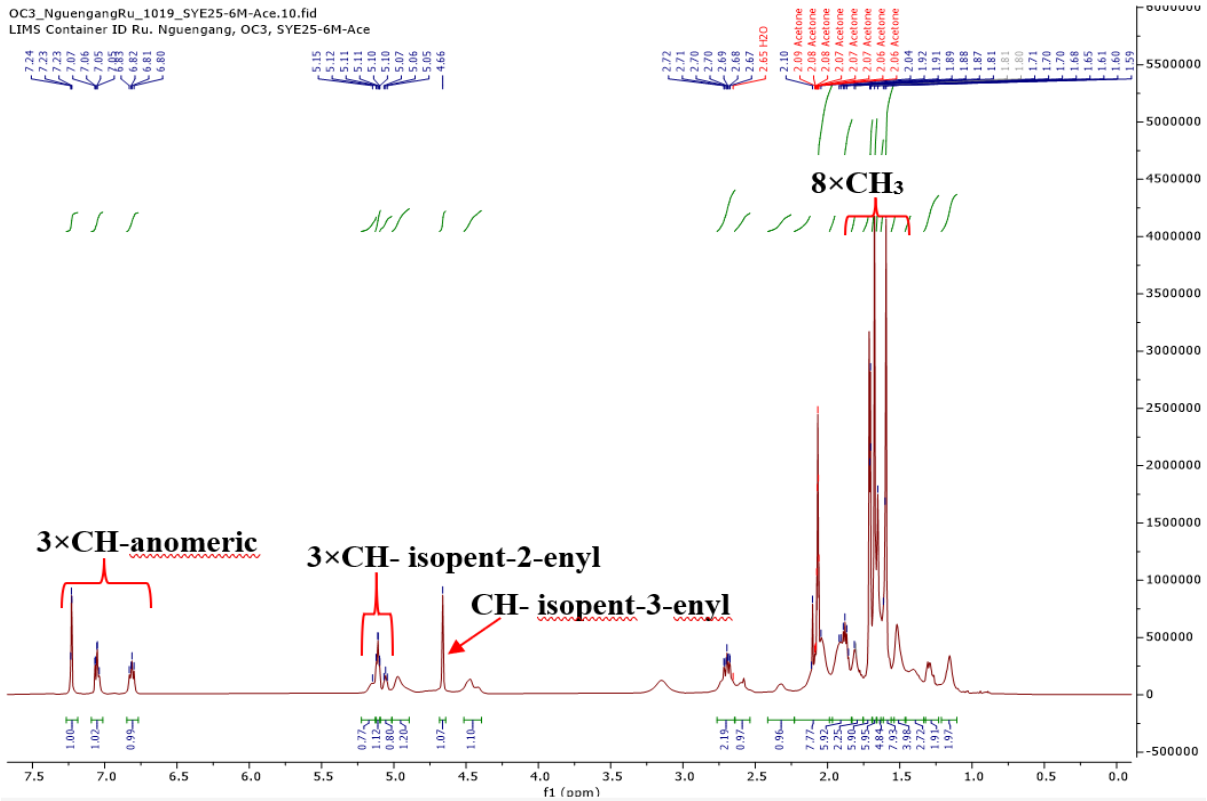

Figure 13: ^{1}H NMR of SYE25-6M (acetone-d_6, 600 MHz)

Its ^{13}C NMR spectrum (Figure 14) revealed 38 carbon signals, which were sorted by DEPT and HSQC techniques into:

- eight methyls, eight methylenes, seven methines [including three aromatic carbons at δ_C 116.6 (C-12), 114.2 (C-15), and 123.9 (C-16)], and fifteen quaternary carbons;
- typical signals of a bicyclo[3.3.1]nonane ring system that included one ketone [$\boldsymbol{\delta}_C$ 208.8 (C-9)], an enolized 1,3-diketone [δ_C 196.5 (C-1), 193.9 (C-10), 116.1 (C-2), and 191.9 (C-3)], three quaternary carbons [δ_C 70.3 (C-4), 51.8 (C-5), and 57.8 (C-8)], one methine at δ_C 39.7 (C-6), and a methylene at δ_C 43.3 (C-7) (Bailly and Vergoten, 2021).

All these spectral data were closely related to those of guttiferone A, a polyisoprenylated benzophenone (Gustafson *et al*., 1992). The discrepancy between guttiferone A and compound **SYE25-6M** was the isomerization of one isopent-2-enyl unit into an isopent-3-enyl unit. In addition, the Δ^{1-2} enol group in guttiferone A was present as $\Delta^{2-(10)}$ in compound **SYE25-6M**.

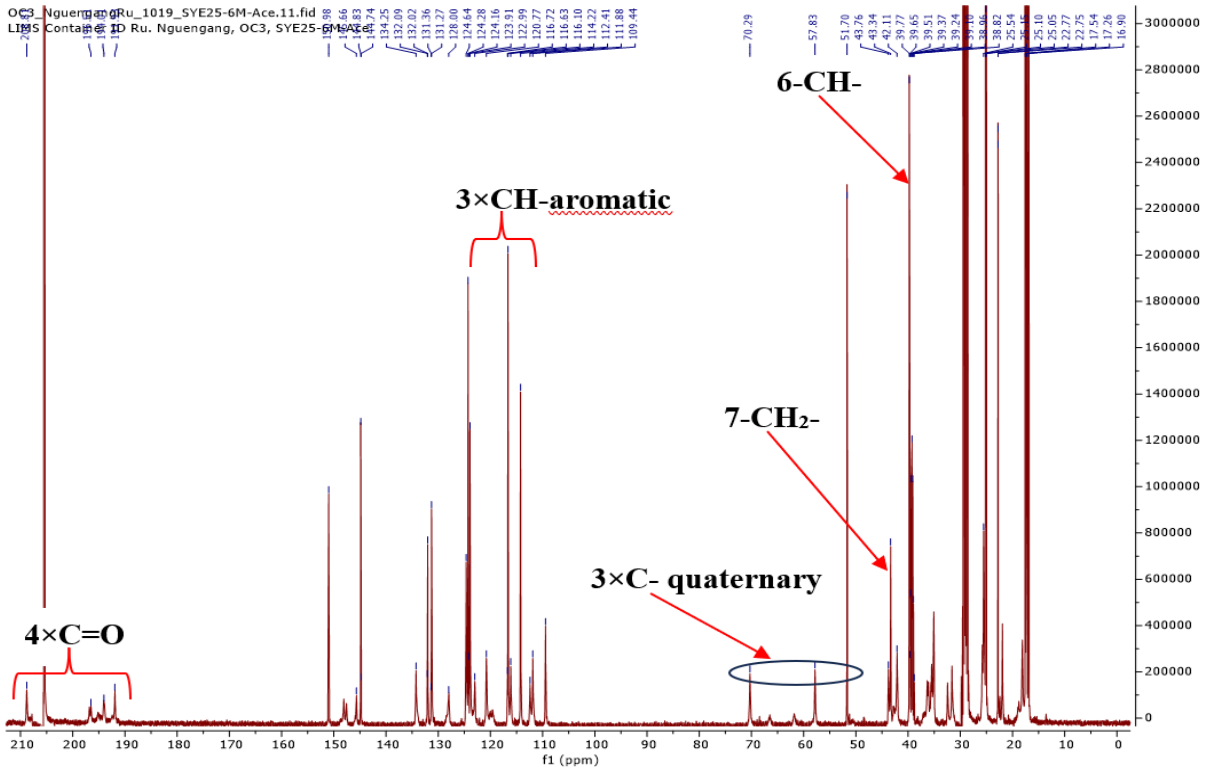

Figure 14: ^{13}C NMR spectrum of SYE25-6M (acetone-d_6, 150 MHz)

The HMBC correlations (Figure 15) between proton H-12 (δ_H 7.23) and carbons C-10 (δ_C 193.9), C-14 (δ_C 150.9) and C-16 (δ_C 123.9) as well as proton H-15 (δ_H 6.81) and carbons C-13 (δ_C 144.8) and C-11 (δ_C 132.0) indicated the presence of a catechol unit and supported the presence of the $\Delta^{2-(10)}$ enol group in the structure. The isopent-3-enyl unit was located at C-6 following the HMBC correlations of H-24 (δ_H 2.05), H-25 (δ_H 1.91), and H-22 (δ_H 1.16) with C-6 (39.7). Additional HBMC correlations of H-17 (δ_H 2.68) with C-3 (δ_C 191.9) and C-9 (δ_C 208.8), H-34 (δ_H 1.91) with C-23 (δ_C 35.0) and C-5 (δ_C 51.8), and H-29 (δ_H 2.05) with C-8 (δ_C 57. 8) allowed the junction of isoprenyl groups at C-4 (δ_C 70.3), C-23 (δ_C 35. 0), and C-8 (δ_C 57. 8), respectively. The bicyclic ring system in **SYE25-6M** required that the isopentenyl groups on C-4 and C-8 be equatorial (Gustafson *et al.*, 1992). Furthermore, the lack of NOESY correlation between H-17 (δ_H 2.68) and H-22 (δ_H 1.16) suggested that the isopentenyl unit fixed at C-4 (δ_C 70.3) and the methyl group at C-5 (δ_C 51.8) were on the opposite sides. Nevertheless, the NOESY spectrum displayed an important correlation between CH_3-22 (δ_H 1.16) and H-24 (δ_H 2.05), suggesting a relative *Cis*-configuration with the methyl group (Figure 16).

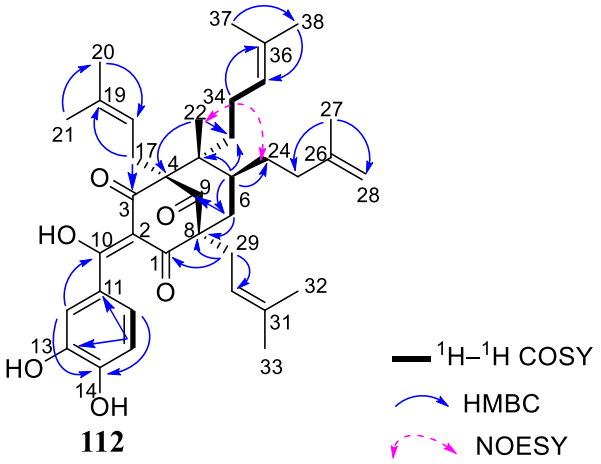

Scheme 9: Key HMBC correlations of SYE25-6M

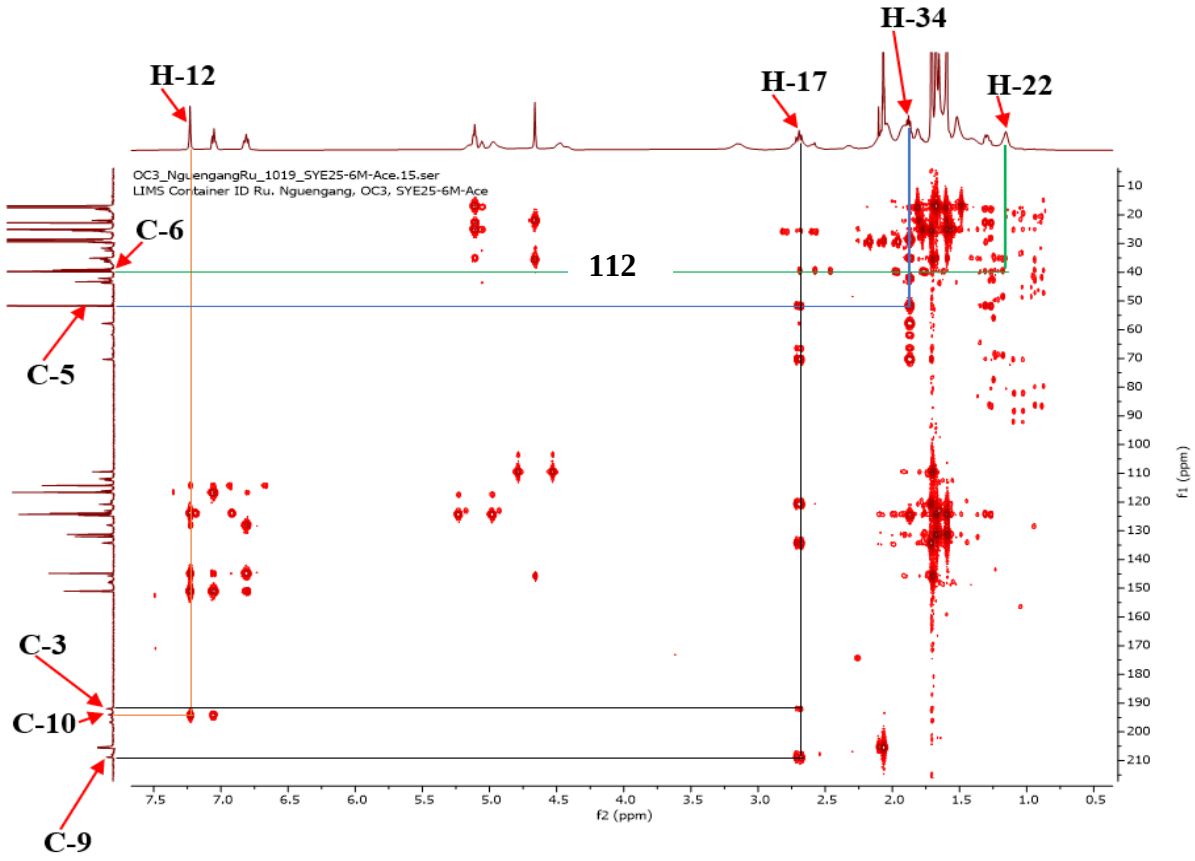

Figure 15: HMBC spectrum of SYE25-6M

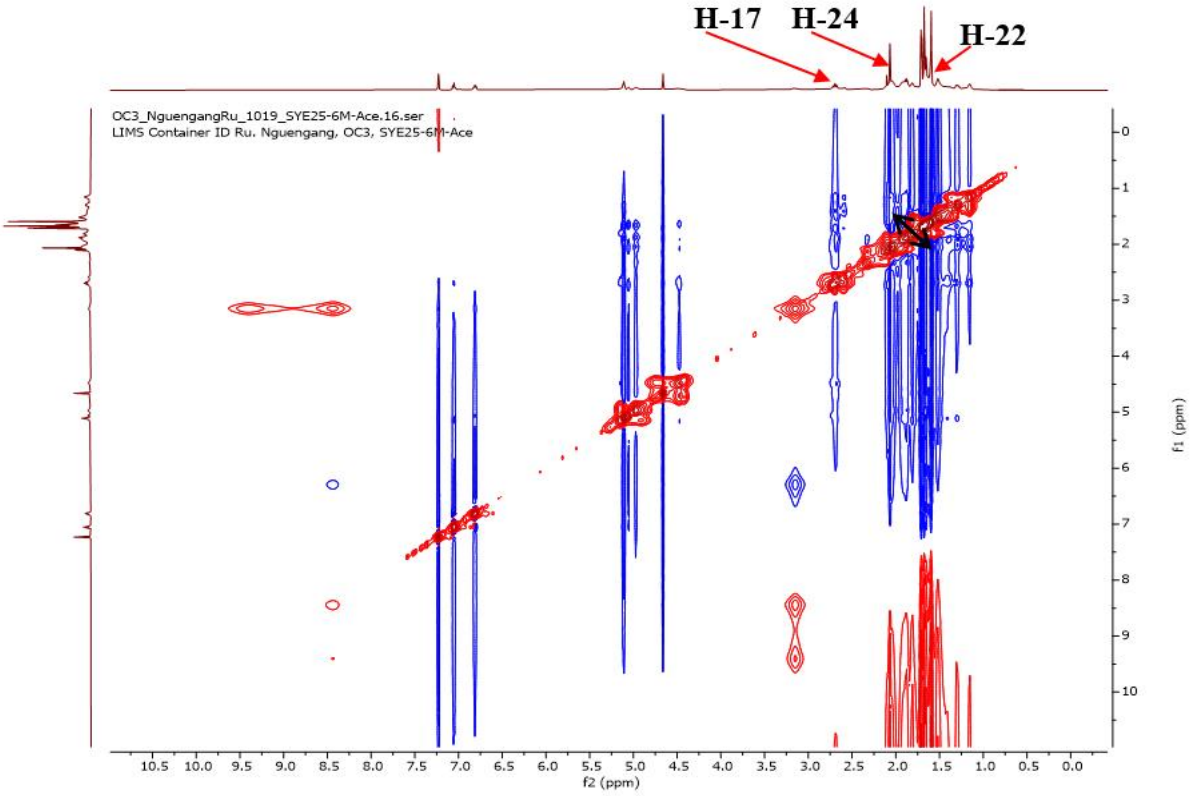

Figure 16: NOESY spectrum of SYE25-6M

These informations suggested that the relative stereochemistry of compound **SYE25-6M** could be identical to that of guttiferone A. This was further confirmed by the comparison of their optical rotation signs. Therefore, compound **SYE25-6M** was concluded to be a new polyprenylated acylphloroglucinol derivative named guttiferone U (**112**) with the structure as shown.

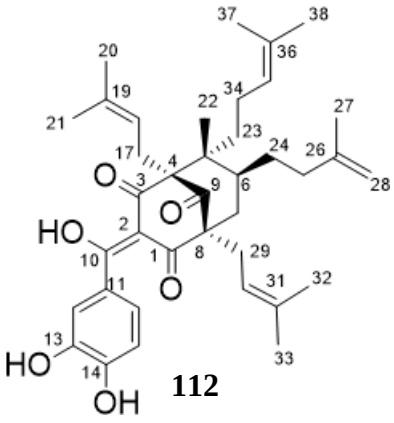

112

Table 20: ^{1}H (600 MHz) and ^{13}C (150 MHz) NMR data of SYE25-6M in acetone-d_6

Guttiferone U		
Position	δ_C	δ_H **(m, *J* in Hz)**
1	196.5	-
2	116.1	-
3	191.9	-
4	70.3	-
5	51.8	-
6	39.7	1.87 (m)
7	43.3	2.05 (m)
8	57.8	-
9	208.8	-
10	193.9	-
11	132.0	-
12	116.6	7.23 (d, 2.2)
13	144.8	-
14	150.9	-
15	114.2	6.81 (d, 8.3)
16	123.9	7.06 (dd, 8.3, 2.1)
17	25.2	2.68 (m)
18	120.7	5.15 (brs)
19	134.3	-
20	25.2	1.71 (s)
21	17.5	1.65 (s)
22	18.1	1.16 (s)
23	35.0	1.28 (m);1.31 (m)
24	28.4	2.05 (m)
25	35.4	1.91 (m)
26	145.6	-
27	21.9	1.70 (br s)
28	109.4	4.66 (br s)
29	28.4	2.05 (m)
30	123.9	5.06 (m)
31	134.2	-
32	25.1	1.65 (br s)
33	17.2	1.53 (br s)
34	22.7	1.91 (m)
35	124.3	5.11 (m)
36	131.2	-
37	25.0	1.68 (s)
38	16.9	1.60 (br s)

II.1.5.2.2. Structural elucidation of compound SYE27-28-16Ma/b

Compounds **SYE27-28-16Ma** and **SYE27-28-16Mb** were obtained as an optically active mixture of a yellowish finely divided solid in the *n*-hexane-EtOAc (3:2, v/v) mixture with the same R_f on thin-layer chromatography (TLC) in different solvent systems. It was soluble in acetone, $[\alpha]_{589}^{20}$ + 93 (*c* 0.5, MeOH). It was present as a 1:1 mixture based on the NMR peak intensities of each component. The HR-ESIMS (Figure 17) showed a sodium adduct peak at *m/z* 693.4141 $[M + Na]^+$ (calcd for $C_{43}H_{58}O_6Na^+$, 693.4126) corresponding to the molecular formula, $C_{43}H_{58}O_6$, a mass which was 68 a.m.u higher than that of compound **SYE25-6M**, suggesting the presence of an additional prenyl side chain (C_5H_9) when compared to **SYE25-6M**.

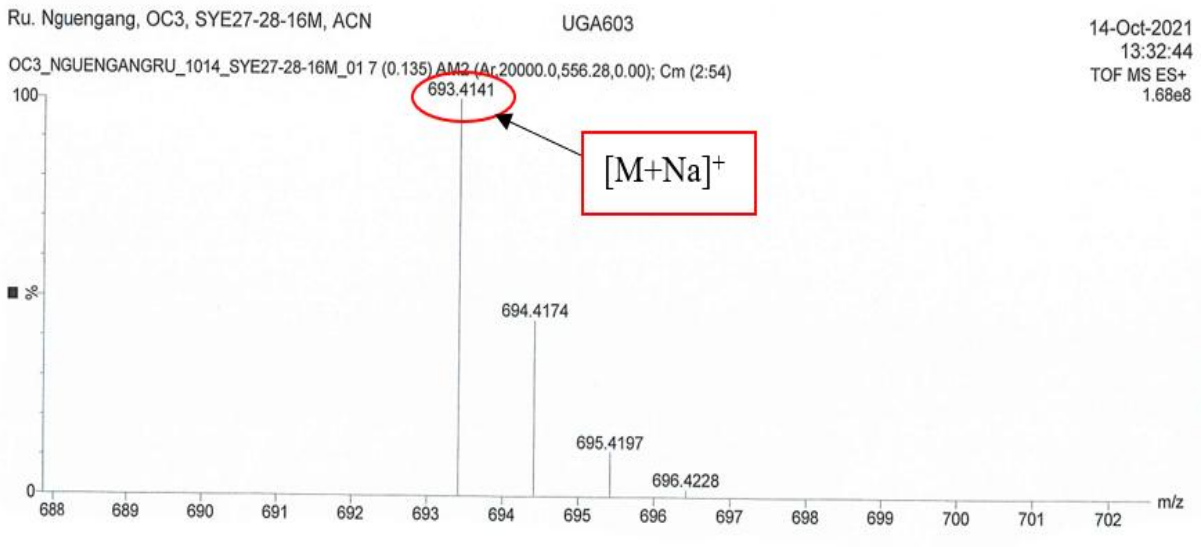

Figure 17: (+) HRESI mass spectrum of SYE27-28-16Ma/b

The IR spectrum (Figure 18) of **SYE27-28-16Ma/b** exhibited strong absorption bands at 3300 (hydroxy groups), 1729, and 1669 (for non-conjugated and conjugated carbonyl groups), and 1699 cm^{-1} (C=C). The UV spectrum (Figure 19) displayed characteristic absorptions at λ_{max} 340 and 370 nm for the aromatic ring and conjugated carbonyl chromophores, respectively (Gustafson *et al*., 1992).

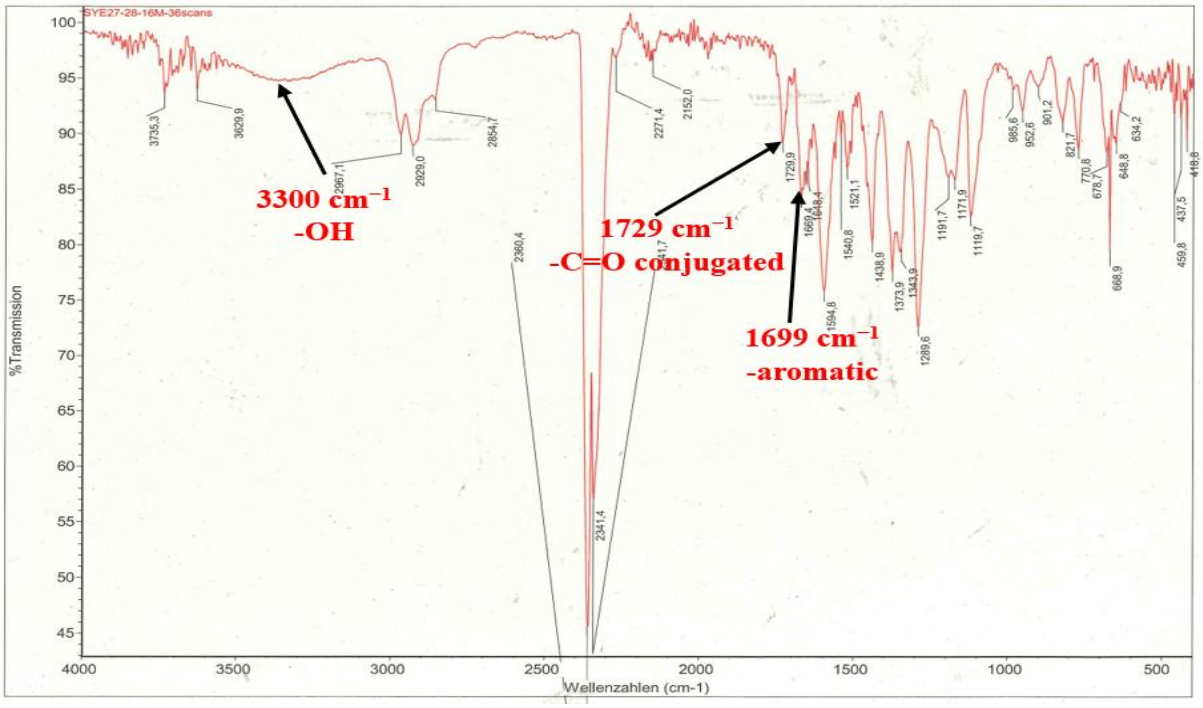

Figure 18: IR spectrum of SYE27-28-16Ma/b

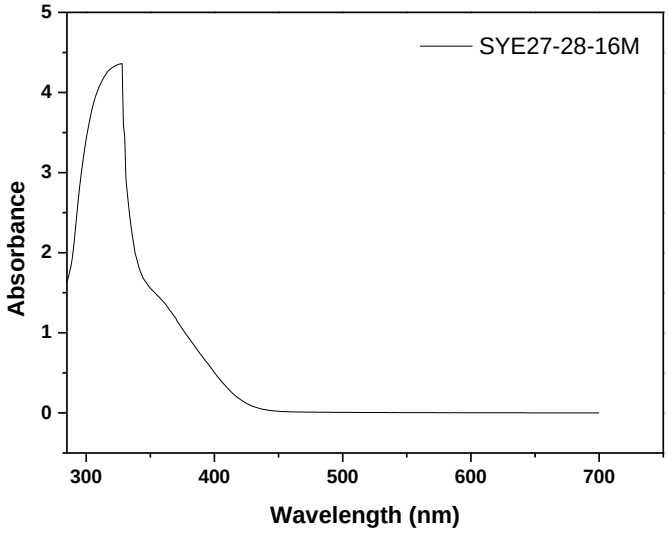

Figure 19: UV spectrum of SYE27-28-16Ma/b

The analysis of the NMR spectra (Figure 20 to Figure 22) confirmed that **SYE27-28-16Ma/b** is a polyprenylated benzophenone derivatives. The ^{1}H NMR spectrum (Figure 20) of the mixture exhibited:

- signals of two ABX substitution patterns as pairs of duplicated signals at δ_H 7.39/7.38 (1H, d, J = 2.0 Hz, H-12), 7.14/7.07 (1H, dd, J = 8.2, 2.0 Hz, H-16), and 6.85/6.82 (1H, d, J = 8.2 Hz, H-15);

- the characteristic signals of seven isopent-2-enyl groups {[δ_H 2.59/2.54 (2H, m, H-17), 4.95/4.95 (2H, m, H-18), 1.56/1.56 (6H, s, H-20), and 1.70/1.70 (6H, brs, H-21)], [δ_H 2.80/2.80 (2H, m, H-24), 5.02/5.02 (2H, m, H-25), 1.71/1.71 (6H, s, H-27), and 1.71/1.71 (6H, brs, H-28)], [δ_H 2.10/2.10 (2H, m, H-34), 5.22/5.22 (2H, m, H-35), 1.77/1.77 (6H, brs, H-37), and 1.63/1.63 (6H, brs, H-38)], [δ_H 1.94 (2H, m, H-39, **SYE27-28-16Ma**), 5.12 (1H, m, H-40, **SYE27-28-16Ma**), 1.67 (3H, brs, H-42, **SYE27-28-16Ma**), and 1.60 (3H, brs, H-43, **SYE27-28-16Ma**)]};
- signals of one isopent-3-enyl unit [δ_H 1.94 (2H, m, H-39, **SYE27-28-16Mb**), 1.21 (2H, m, H-40, **SYE27-28-16Mb**), 1.74 (3H, brs, H-42, **SYE27-28-16Mb**), and 4.79 (2H, brs, H-43, **SYE27-28-16Mb**)];
- And the signals of two isopentyl units [δ_H 3.00/3.05 (2H, m, H-29), 1.10/1.10 (2H, m, H-30), 0.99/0.99 (6H, s, H-32), and 1.27/1.29 (3H, s, H-33)].

The duplication of all these data in association with the mass data confirmed that **SYE27-28-16Ma/b** was a mixture of two polyisoprenylated benzophenone isomers.

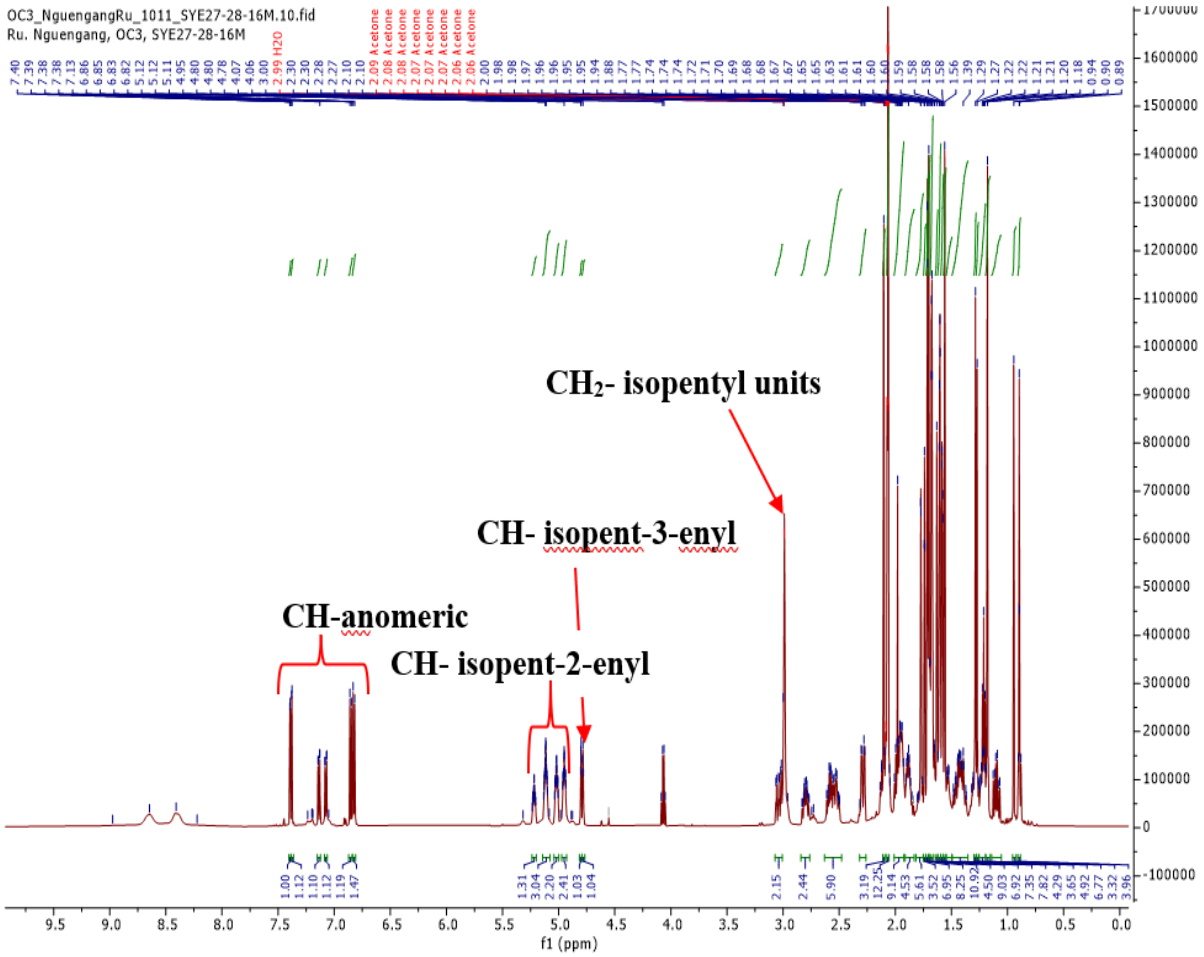

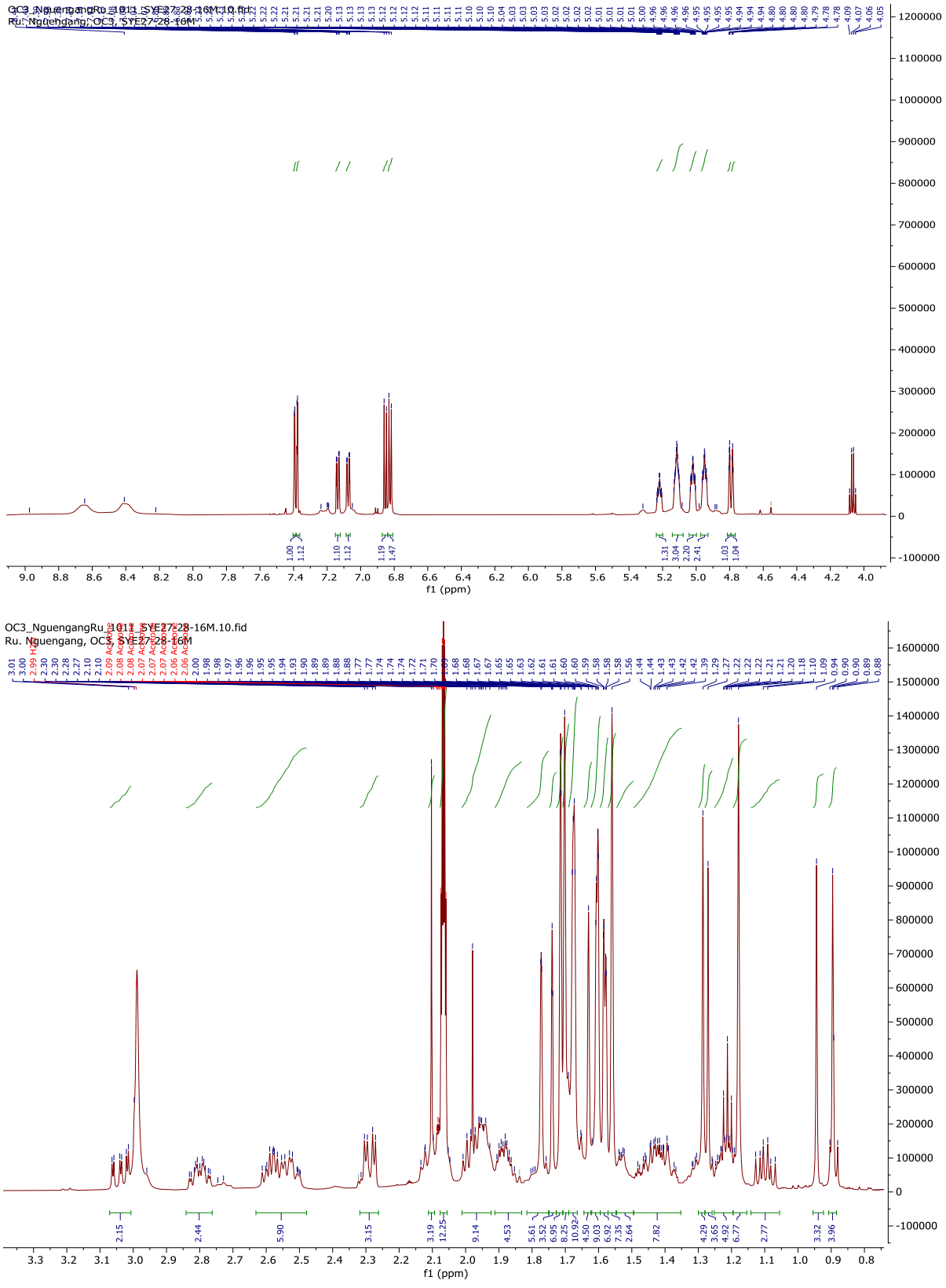

Figure 20: ^{1}H NMR of SYE27-28-16Ma/b (acetone-d_6, 600 MHz)

The ^{13}C NMR spectrum of **SYE27-28-16Ma/b** (Figure 21) displayed:

- characteristic signals for a bicyclo[3.3.1]nonane ring as pairs of carbons at δ_C 170.3/170.5 (C-1), 125.6/125.9 (C-2), 193.3/193.6 (C-3), 68.9/69.0 (C-4), 48.3/48.4 (C-5), 2×39.4 (C-6), 38.1/38.3 (C-7), 51.2/51.5 (C-8), and 206.2/206.3 (C-9) (Bailly and Vergoten, 2021; Nguyen *et al*., 2022).

In addition, the combination of the DEPT 135 and HSQC confirmed the presence:

- of seven isopent-2-enyl units, one isopent-3-enyl with the characteristic signals at δ_C/δ_H [22.4/1.94 (C-39/H-39), 35.4/1.21 (C-40/H-40), 145.0 (C-41), 21.5/1.74 (C-42/H-42) and 110.4/4.79 (C-43/H-43)];
- and one dimethylpyrane moiety identified by the signals at δ_C/δ_H {[28.3/0.89 (C-29/H-29), 41.8/1.10 (C-30/H-30), 86.2 (C-31), 27.9/0.89 (C-32/H-32) and 20.6/1.27 (C-33/H-33) for **SYE27-28-16Ma**], [28.3/0.94 (C-29/H-29), 42.9/1.10 (C-30/H-30, 86.5 (C-31), 28.0/0.89 (C-32/H-32) and 20.7/1.29 (C-33/H-33) for **SYE27-28-16Mb**]}.

All these data indicated that the structures of **SYE27-28-16Ma/b** were closely related to shomburgkianone I (Nguyen *et al*., 2022).

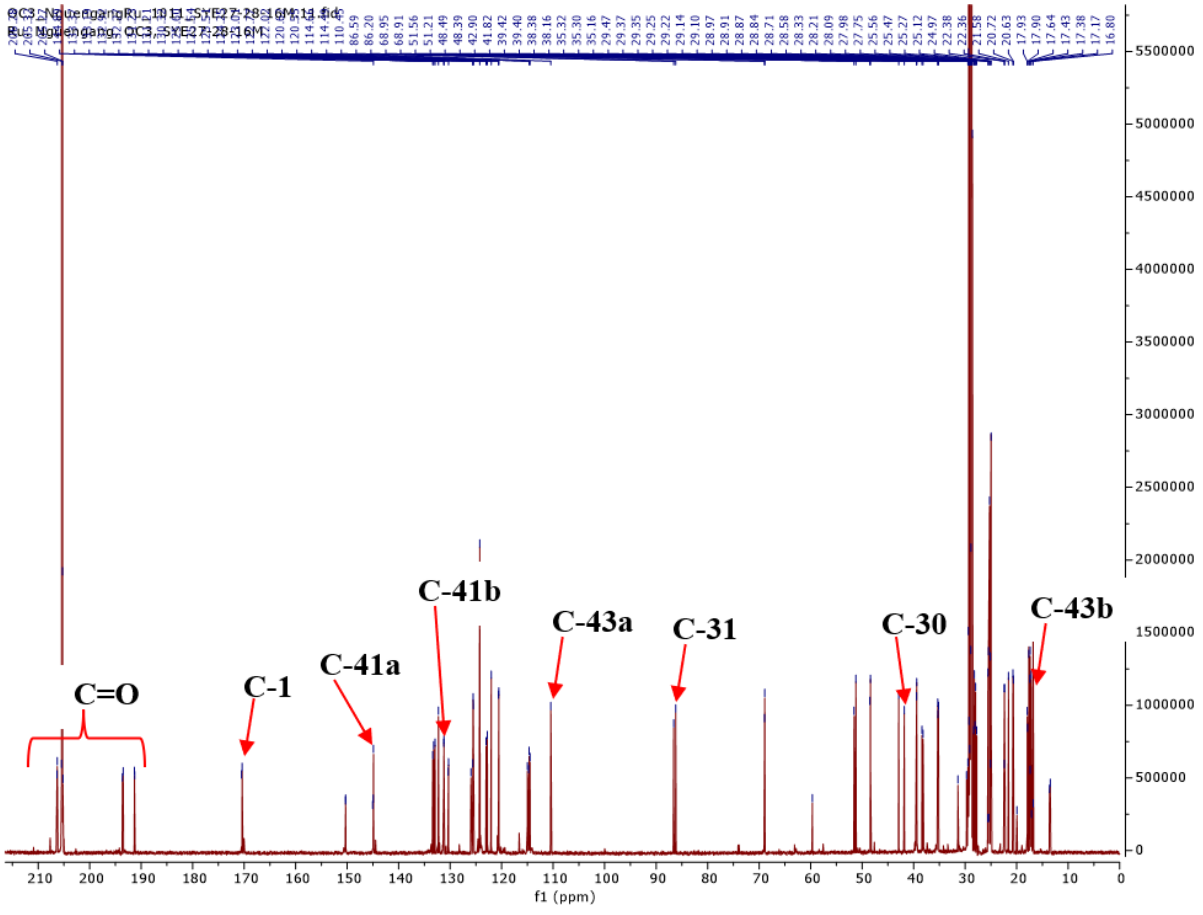

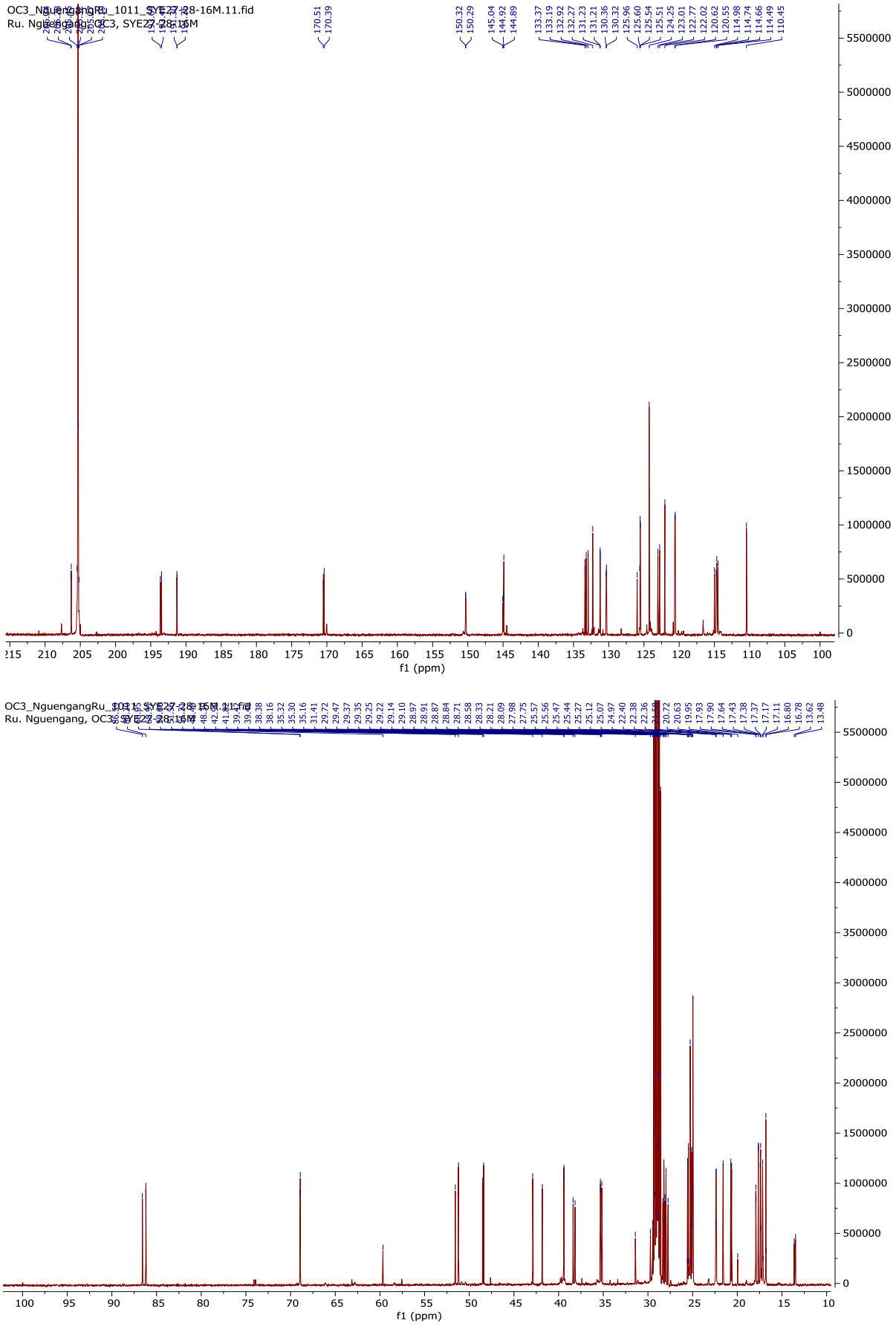

Figure 21: ^{13}C NMR spectrum of SYE27-28-16Ma/b (acetone-d_6, 150 MHz)

The location of the dimethylpyrane moiety on the bicyclo unit was deduced by the HMBC correlation (Figure 22) of H-29 (δ_H 3.00/3.05)/C-8 (δ_C 51.2/51.5), C-1 (δ_C 170.3/170.5), C-30 (δ_C 41.8/42.9), and C-31 (δ_C 86.5). All these evidences suggested that the only difference between compounds **SYE27-28-16Ma** and **SYE27-28-16Mb** was the isomerization of one isopent-2-enyl unit in **SYE27-28-16Ma** into an isopent-3-enyl unit in **SYE27-28-16Mb**. The two isopentenyl units were located at C-23 by the HMBC correlation of H-39/C-23 (Figure 2). The locations of additional isoprenyl groups were evidenced by the HMBC correlations of H-17/C-3 and C-9, H-39/C-23, H-24/C-6 and C-7 and H-35/C-30. The relative configurations of the different stereogenic centers in **SYE27-28-16Ma** (**113**) and **SYE27-28-16Mb** (**144**) were deduced in the same manner to that of **SYE25-6M** (Gustafson *et al*., 1992).

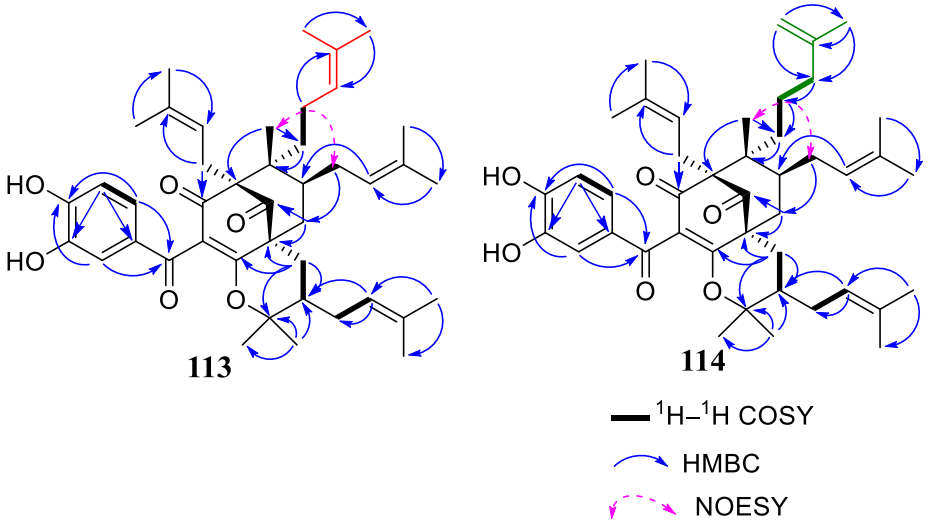

Scheme 10: Key HMBC correlations of SYE27-28-16Ma/b

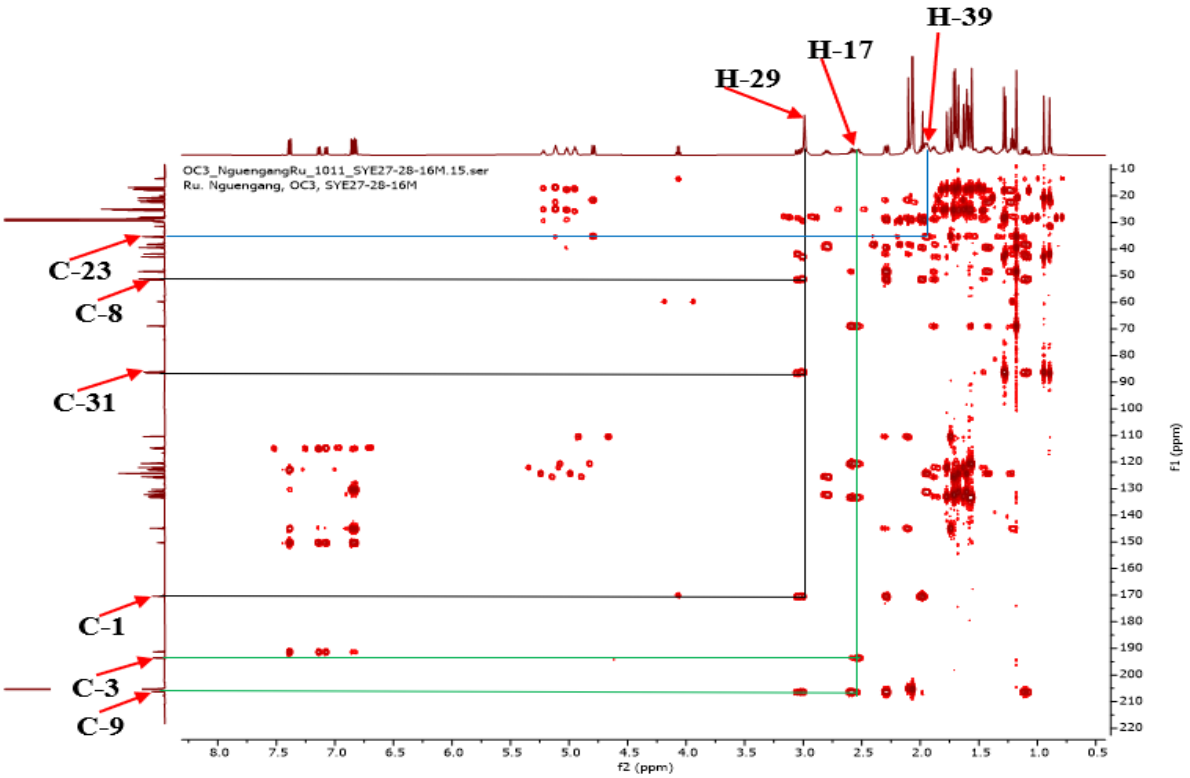

Figure 22: HMBC spectrum of SYE27-28-16Ma/b

Based on the above data, compounds **SYE27-28-16Ma** and **SYE27-28-16Mb** were found to be new polyisoprenylated benzophenone isomers named guttiferones V (**113**) and W (**114**), respectively.

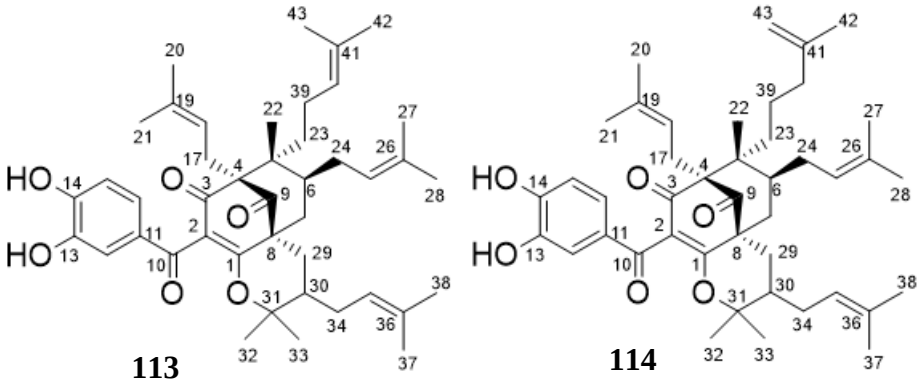

113 **114**

Table 21: ^{1}H (600 MHz) and ^{13}C (150 MHz) NMR data of SYE27-28-16Ma/b in acetone-d_6, ^{13}C (125 MHz), ^{1}H (500 MHz)]

	Guttiferone V		Guttiferone W	
Position	δ_C	δ_H **(m, *J* in Hz)**	δ_C	δ_H **(m, *J* in Hz)**
1	170.3	-	170.5	-
2	125.6	-	125.9	-
3	193.4	-	193.6	-
4	68.9	-	69.0	-
5	48.3	-	48.4	-
6	39.4	1.88 (m)	39.4	1.86 (m)
7	38.1	2.31 (m)	38.3	2.28 (m)
8	51.2	-	51.5	-
9	206.2	-	206.3	-
10	191.2	-	191.3	-
11	130.3	-	130.4	-
12	114.7	7.39 (d, 2.0)	114.9	7.38 (d, 2.0)
13	144.8	-	144.9	-
14	150.2	-	150.3	-
15	114.4	6.85 (d, 8.2)	114.6	6.82 (d, 8.2)
16	122.7	7.14 (dd, 8.2, 2.0)	123.0	7.07 (dd, 8.2, 2.0)
17	24.9	2.59 (m)	24.9	2.54 (m)
18	120.5	4.95 (m)	120.6	4.95 (m)
19	133.1	-	133.3	-
20	25.4	1.56 (br s)	25.5	1.56 (br s)
21	17.3	1.70 (br s)	17.4	1.70 (br s)
22	17.9	1.18 (br s)	17.9	1.18 (br s)
23	35.1	1.21 (m); 1.43 (m)	35.3	1.21 (m); 1.43 (m)
24	28.8	2.80 (m)	28.9	2.80 (m)
25	125.5	5.02 (m)	125.5	5.02 (m)
26	132.2	-	132.2	-
27	25.2	1.71 (br s)	25.2	1.71 (br s)
28	17.6	1.71 (br s)	17.6	1.71 (br s)
29	28.3	3.00 (d, 3.3); 3.05 (dd, 14.0, 3.3)	28.3	3.00 (d, 3.3); 3.05 (dd, 14.0, 3.3)
30	41.8	1.10 (m)	42.9	1.10 (m)
31	86.2	-	86.5	-
32	27.9	0.89 (br s)	28.0	0.89 (br s)
33	20.6	1.27 (br s)	20.7	1.29 (br s)
34	29.2	2.10 (br s)	29.3	2.10 (br s)
35	122.0	5.22 (m)	122.0	5.22 (m)
36	132.9	-	132.9	-
37	25.0	1.77 (br s)	25.1	1.77 (br s)
38	17.11	1.63 (br s)	17.2	1.63 (br s)
39	22.4	1.94 (m)	22.4	1.94 (m)
40	124.2	5.12 (m)	35.4	1.21 (m)
41	131.2	-	145.0	-
42	24.9	1.67 (br s)	21.5	1.74 (br s)
43	16.7	1.60 (br s)	110.4	4.79 (br s)

II.1.5.2.3. Structural identification of compound SYE44-4-5mi

Compound **SYE44-4-5mi** was obtained as a yellowish finely divided solid in the *n*-hexane-EtOAc (3:2, v/v) mixture. Its ESIMS (Figure 23) showed the protonated molecular ion peak $[M+H]^+$ at *m/z* 603.4. This mass was identical to that of **SYE25-6M** suggesting that there are isomers.

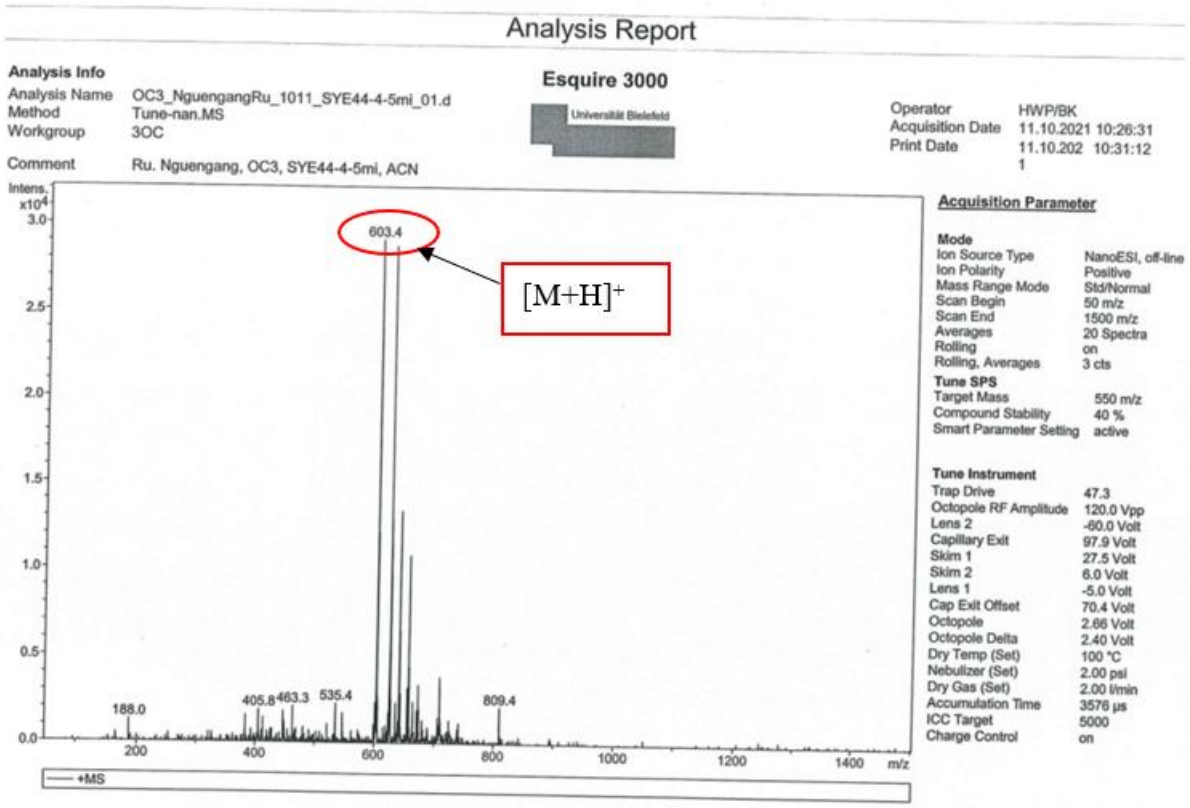

Figure 23: (+) ESI mass spectrum of SYE44-4-5mi

Comparison of the ^{1}H (Figure 24) and ^{13}C NMR spectra (Figure 25) of **SYE44-4-5mi** to that of **SYE25-6M** revealed many similarities.

The main discrepancy between the ^{1}H NMR of **SYE44-4-5mi** and that of **SYE25-6M** was the absence of signals of one isopent-3-enyl unit at δ_H [2.05 (2H, m, H-24), 1.91 (2H, m, H-25), 1.70 (3H, s, H-27), and 4.66 (2H, brs, H-28)] and the presence of characteristic signals of one additional isopent-2-enyl groups at δ_H [2.11 (2H, m, H-24), 4.93 (1H, m, H-25), 1.67 (3H, s, H-27), and 1.50 (3H, s, H-28)].

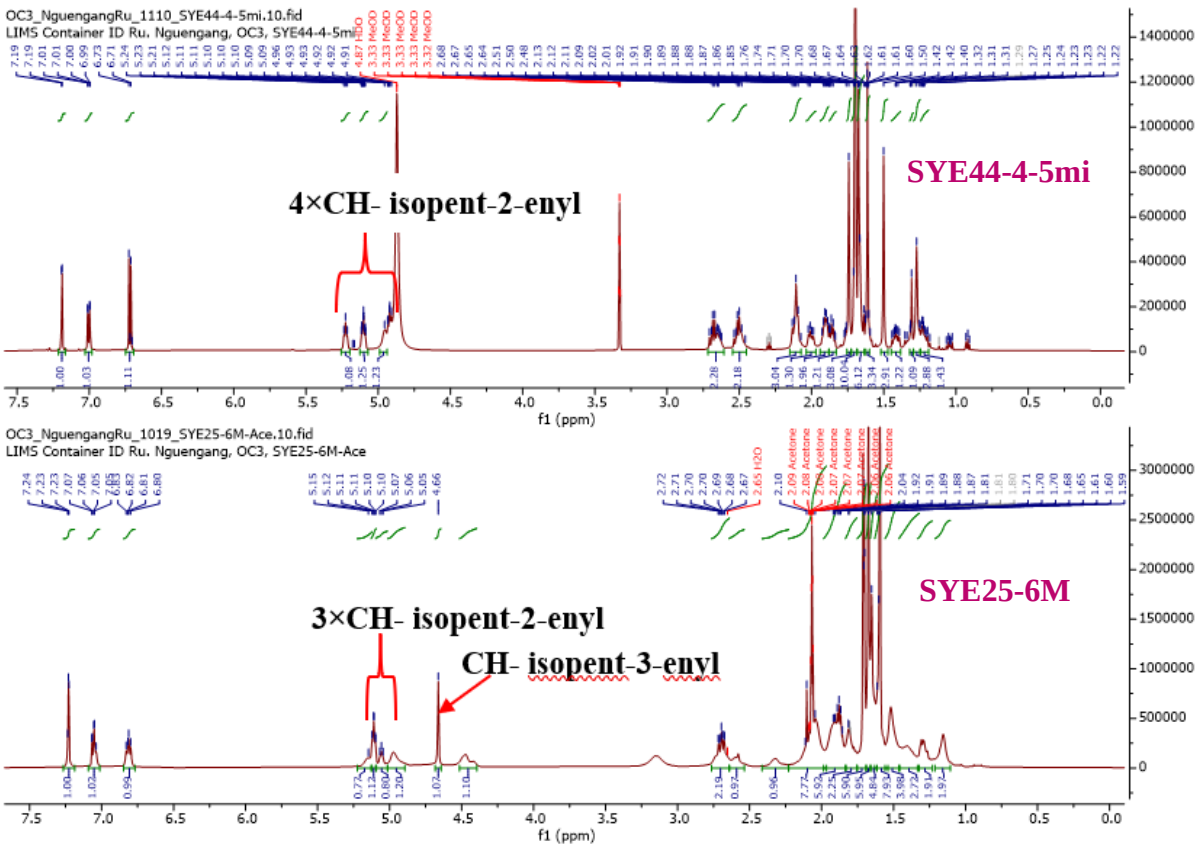

Figure 24: Comparative ^{1}H NMR of SYE25-6M (Acetone-d_6, 600 MHz) and that of SYE44-4-5mi (MeOH-d_4, 600 MHz)

This suggestion was confirmed after examination of the broad band decoupled ^{13}C spectrum (Figure 89) which showed characteristic signals of guttiferone U (**1**).

However, significant differences were recognized in the signals of C-25, C-26, and C-28 carbons. In fact, the C-26 (δ 132.3) and C-28 (δ 18.8) had resonances in the higher fields than that of **SYE25-6M** C-26 (δ 145.6) and C-28 (δ 109.4), while the C-25 had resonances at lower field (δ 124.2) than that of **SYE25-6M** (δ 35.4), confirming the presence of one additional isopent-2-enyl groups and the absence one isopent-3-enyl unit.

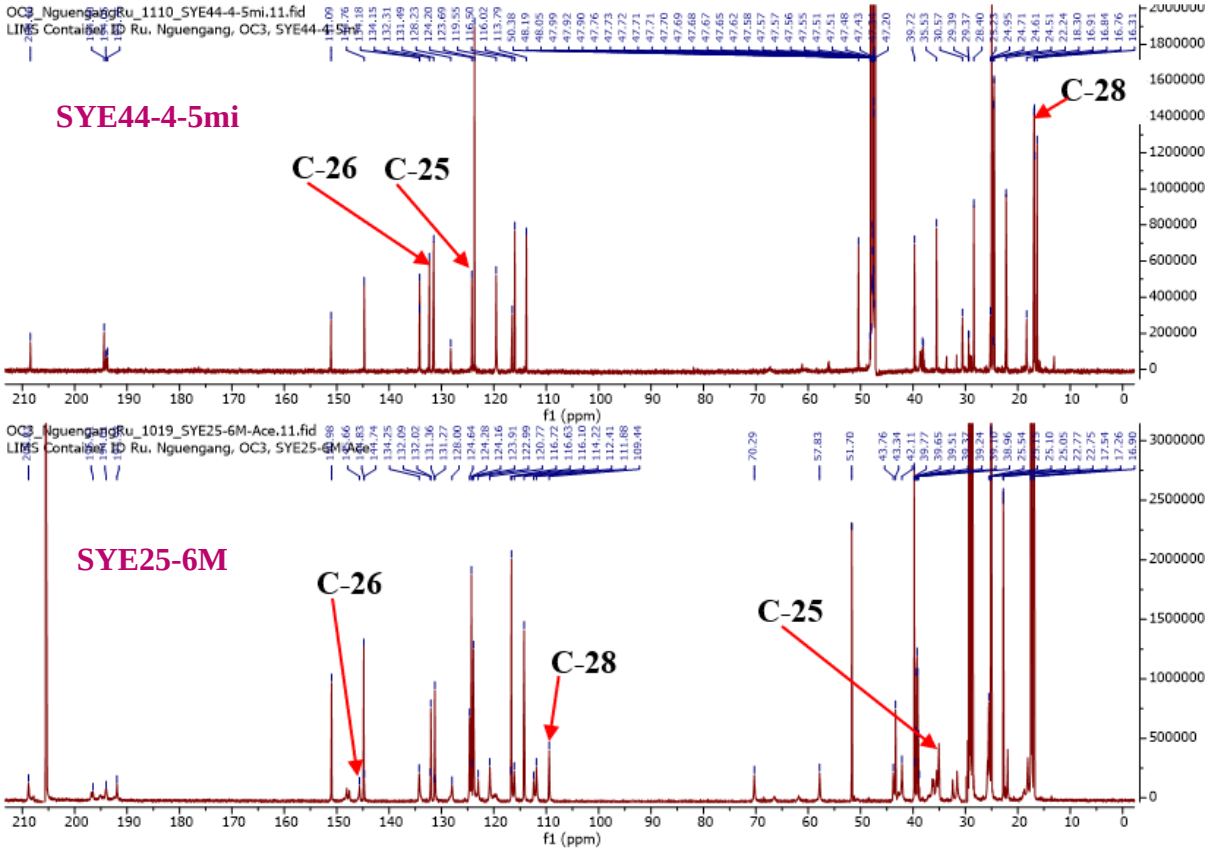

Figure 25: Superposition of ^{13}C NMR spectrum of SYE25-6M (Acetone-d_6, 150 MHz) and SYE44-4-5mi (MeOH-d_4, 150 MHz)

The HMBC correlations (Figure 26) of proton H-12 (δ_H 7.19)/C-10 (δ_C 194.4), C-14 (δ_C 151.1) and C-16 (δ_C 123.7) as well as proton H-15 (δ_H 6.72)/C-13 (δ_C 144.7) and C-11 (δ_C 128.2) also indicated the presence of a catechol unit and supported the presence of the $\Delta^{2-(1)}$ enol group in the structure. HBMC correlations of H-24 (δ_H 2.11)/C-6 (39.7), H-17 (δ_H 2.67)/C-3 (δ_C 193.8) and C-9 (δ_C 208.5), H-23 (δ_H 1.21/1.42)/C-5 (δ_C 50.4) and C-6 (δ_C 39.7), and H-29 (δ_H 2.51)/C-1 (δ_C 194. 0) allowed the junction of isoprenyl groups at C-6 (39.7), C-4 (δ_C 70.3), C-23 (δ_C 35. 0), and C-8 (δ_C 57. 8). The bicyclic ring system in **SYE44-4-5mi** required that the isopentenyl groups on C-4 and C-8 be equatorial (Gustafson *et al*., 1992).

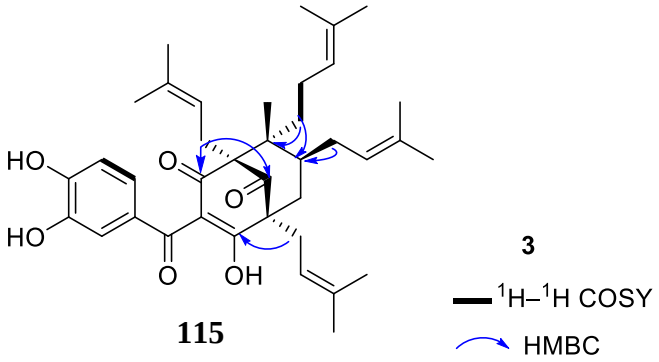

Scheme 11: Key HMBC correlations of SYE44-4-5mi

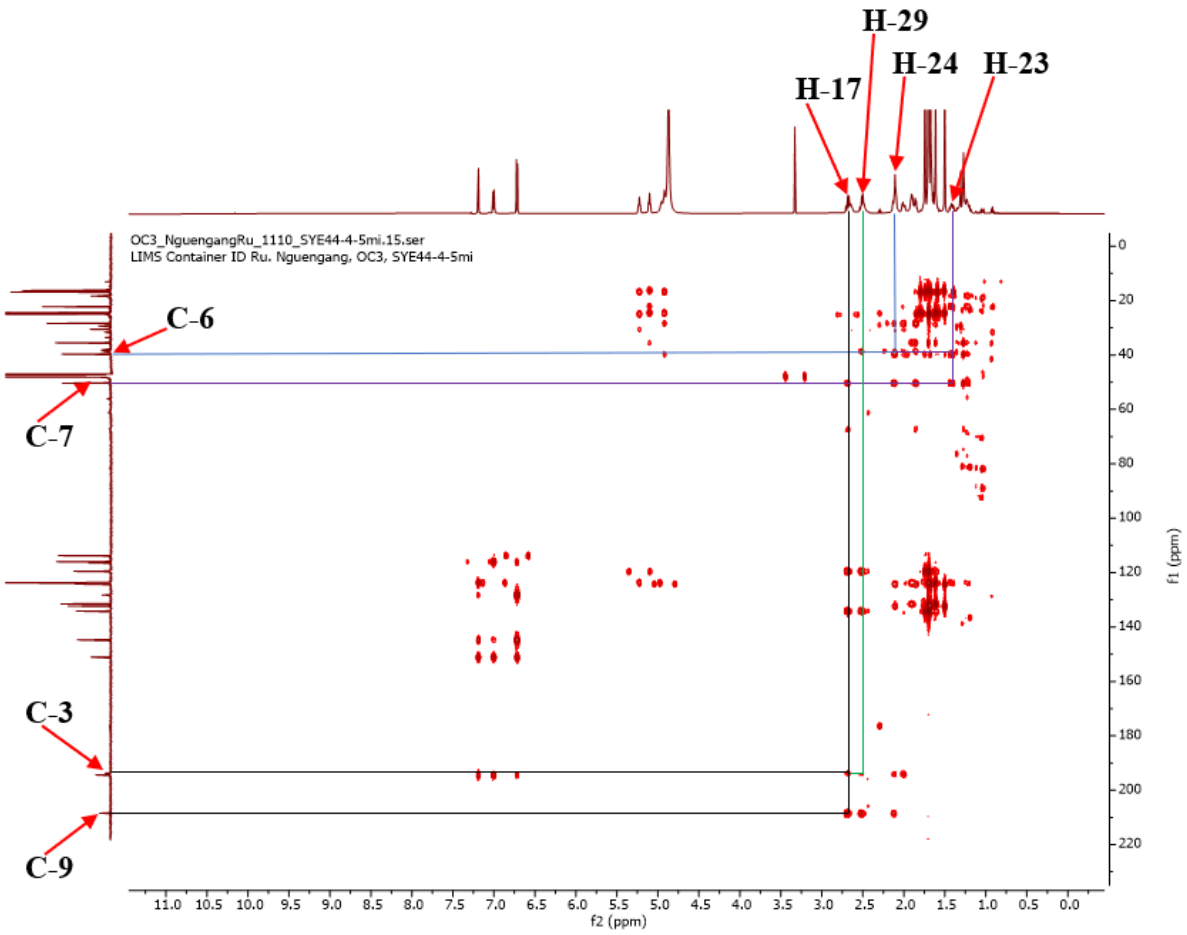

Figure 26: HMBC spectrum of SYE44-4-5mi

All these data were similar to those described in the literature for guttiferone K (**115**), previously isolated from the fruits of *Rheedia calcicola* by Cao *et al*., (2007).

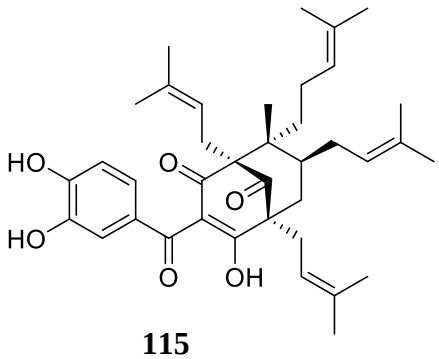

115

Table 22: Comparative ^{1}H (600 MHz) and ^{13}C (150 MHz) NMR data of SYE44-4-5mi and guttiferone K in MeOH-d_4

	SYE44-4-5mi		Guttiferone K (Cao *et al*., 2007)	
Position	δ_C	δ_H **(m, *J* in Hz)**	δ_C	δ_H **(m, *J* in Hz)**
1	194.0	-	196.7	-
2	116.5	-	119.9	-
3	193.8	-	191.0	-
4	67.4	-	69.4	-
5	50.4	-	51.6	-
6	39.7	1.86 (q, 7.4 Hz)	42.0	1.75 (m)
7	38.7	2.00 (m); 2.1 (m)	43.2	2.03 (dd, 13.3, 3.3 Hz), 1.44 (dd, 13.3, 12.9 Hz)
8	nd	-	64.1	-
9	208.5	-	209.2	-
10	194.4	-	196.7	-
11	128.2	-	130.3	-
12	116.0	7.19 (d, 2.1)	117.4	7.20 (d, 2.1)
13	144.7	-	146.5	-
14	151.1	-	152.6	-
15	113.8	6.72 (d, 8.3)	115.3	6.69 (d, 8.4)
16	123.7	7.00 (dd, 8.2, 2.2)	125.1	6.95 (dd, 8.4, 2.1)
17	25.2	2.67 (m)	26.7	2.73 (dd, 13.0, 7.8 Hz), 2.65 (dd, 13.0, 4.3 Hz)
18	119.5	4.95 (m)	121.5	4.88 (m)
19	134.2	-	135.2	-
20	16.3	1.61 (br s)	18.5	1.69 (s)
21	24.6	1.70 (br s)	26.4	1.62 (s)
22	18.3	1.27 (s)	16.4	0.81 (s)
23	35.5	1.21 (m); 1.42 (m)	37.6	1.68 (m)
24	28.4	2.11 (m)	30.2	2.07 (m); 1.77 (m)
25	124.2	4.93 (m)	123.7	5.00 (br t, 7.0)
26	132.3	-	134.7	-
27	16.8	1.50 (s)	18.3	1.67 (s)
28	24.5	1.67 (br s)	26.0	1.57 (s)
29	30.6	2.51 (d, 8.1 Hz)	31.8	2.51 (dd, 14.5, 8.8 Hz), 2.44 (dd, 14.5, 4.8 Hz)
30	119.5	5.23 (t, 7.3 Hz)	121.1	5.10 (br t, 7.1 Hz)
31	134.1	-	135.7	-
32	16.9	1.70 (br s)	18.4	1.67 (s)
33	25.0	1.74 (s)	26.4	1.71 (s)
34	22.2	1.91 (dt, 11.4, 5.6 Hz)	25.3	1.97 (m)
35	123.7	5.10 (m)	125.6	5.04 (br t, 6.9)
36	131.5	-	132.7	-
37	24.6	1.74 (s)	26.1	1.66 (s)
38	16.3	1.61 (br s)	18.0	1.59 (s)

II.1.5.3. Tocotrienol derivative

II.1.5.3.1. Structural elucidation of compound SYE70- 45-48

Compound **SYE70- 45-48** was isolated as a brown oil, $[\alpha]_{589}^{20}$: + 21.5 (*c* 0.5, MeOH). Its molecular formula, $C_{26}H_{40}O_4$, with seven degrees of unsaturation was deduced from its HR-ESIMS (Figure 27), which showed the sodium adduct peak $[M + Na]^+$ at *m/z* 439.2816 (calcd for $C_{26}H_{40}O_4Na^+$, 439.2819).

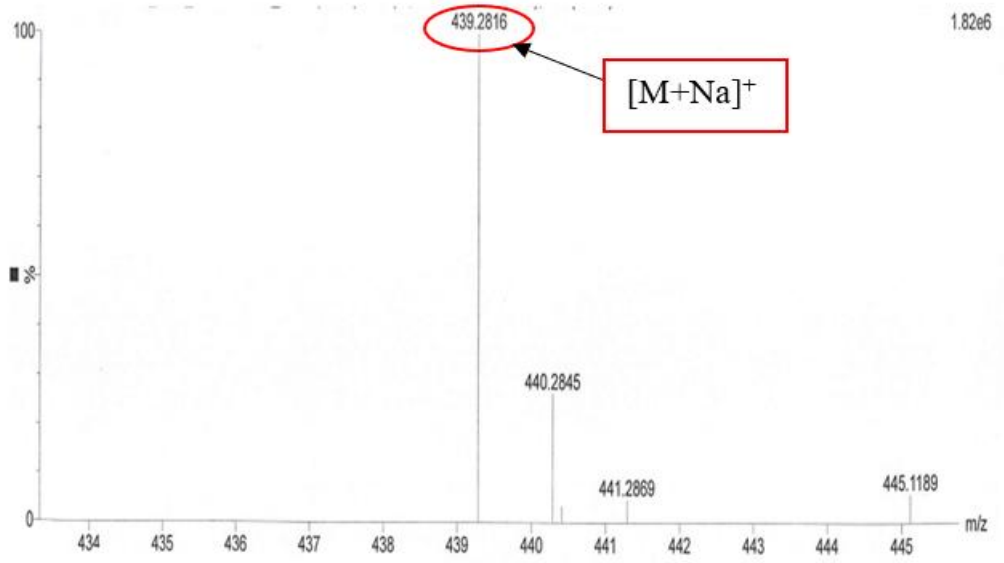

Figure 27: (+) HRESI mass spectrum of SYE70- 45-48

The vibrational absorption bands at 3364, 1685, and 1620 cm^{-1} in the IR spectrum (Figure 28) were consistent with those of the hydroxy, conjugated carbonyl, and olefinic groups, respectively.

The UV spectrum (Figure 29) showed an absorption band at λ_{max} 320 nm.

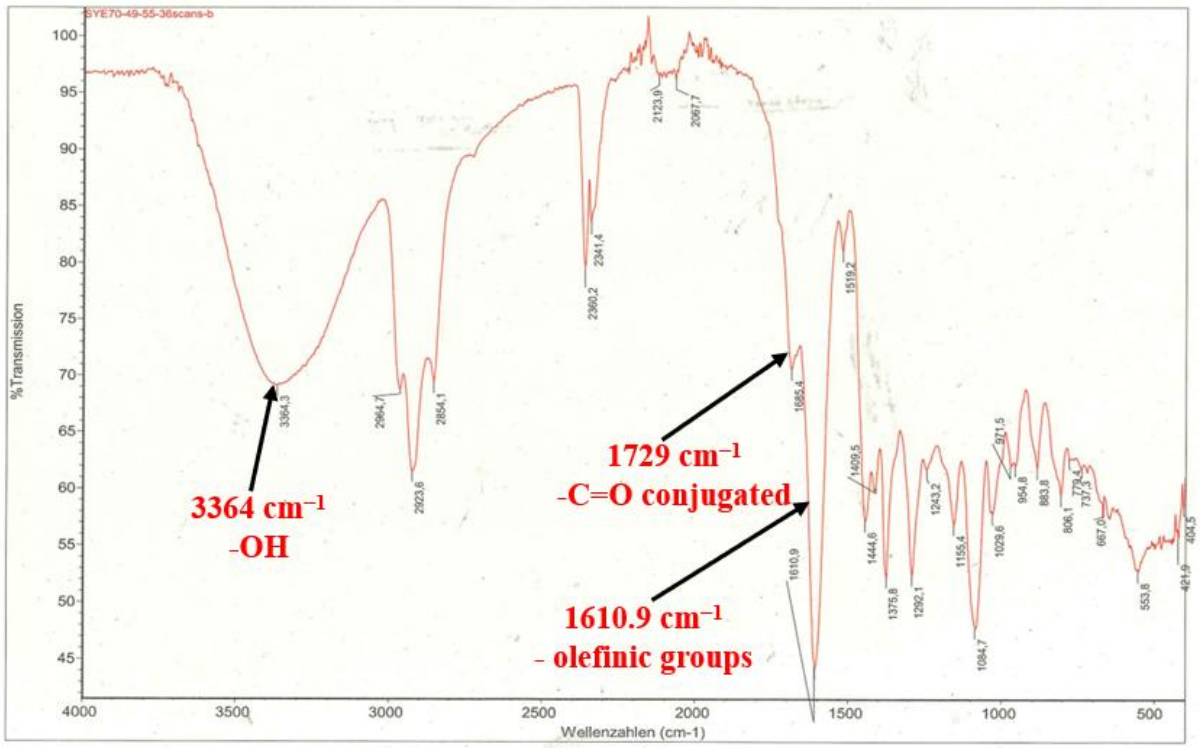

Figure 28: IR spectrum of SYE70- 45-48

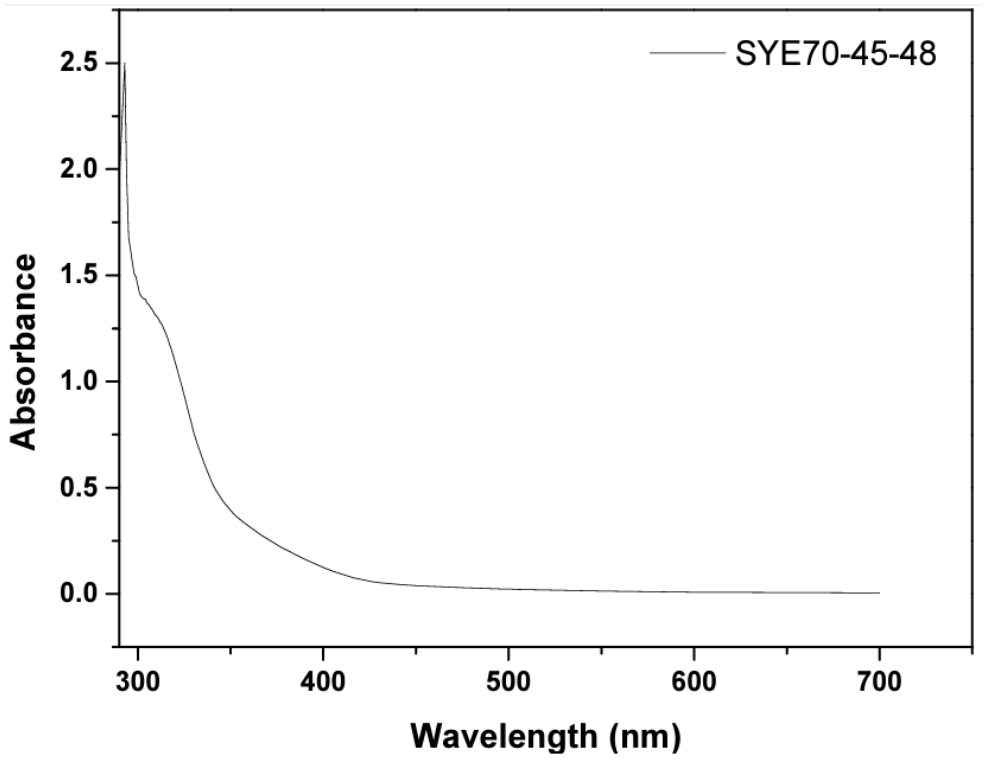

Figure 29: UV spectrum of SYE70- 45-48

The ^{1}H NMR spectrum (Figure 30) exhibited the signals of:

- protons of two free hydroxy groups at δ_H [5.53 (1H, d, J = 6.5 Hz, OH-6) and 5.32 (1H, s, OH-7)];
- three olefinic protons at δ_H [5.12 (1H, t, J = 7.1 Hz, H-2′) and 5.06 (2H, m, H-6′ and H-10′)];
- one oxymethine at δ_H 3.90 (1H, d, J = 6.3 Hz H-6);
- eight methylene protons at δ_H [1.73 (1H, dd, J = 14.0, 6.2 Hz, H-3a)/1.22 (1H, m, H-3b), 2.03 (2H, m, H-4), 1.63 (1H, m, H-12a)/1.53 (1H, m, H-12b), and 2.03–2.05 (10H, m, H-1′, H-4′, H-5′, H-8′ and H-9′)];
- six methyls {including four methyl linked to sp^2 carbons at [δ_H 1.63 (3H, s, H-15′), 1.58 (3H, m, H-12′), and 1.55 (6H, s, H-13′/H-14′)]; and two sp^3 carbons at [1.28 (3H, s, H-11) and 1.17 (3H, s, H-10)]}.

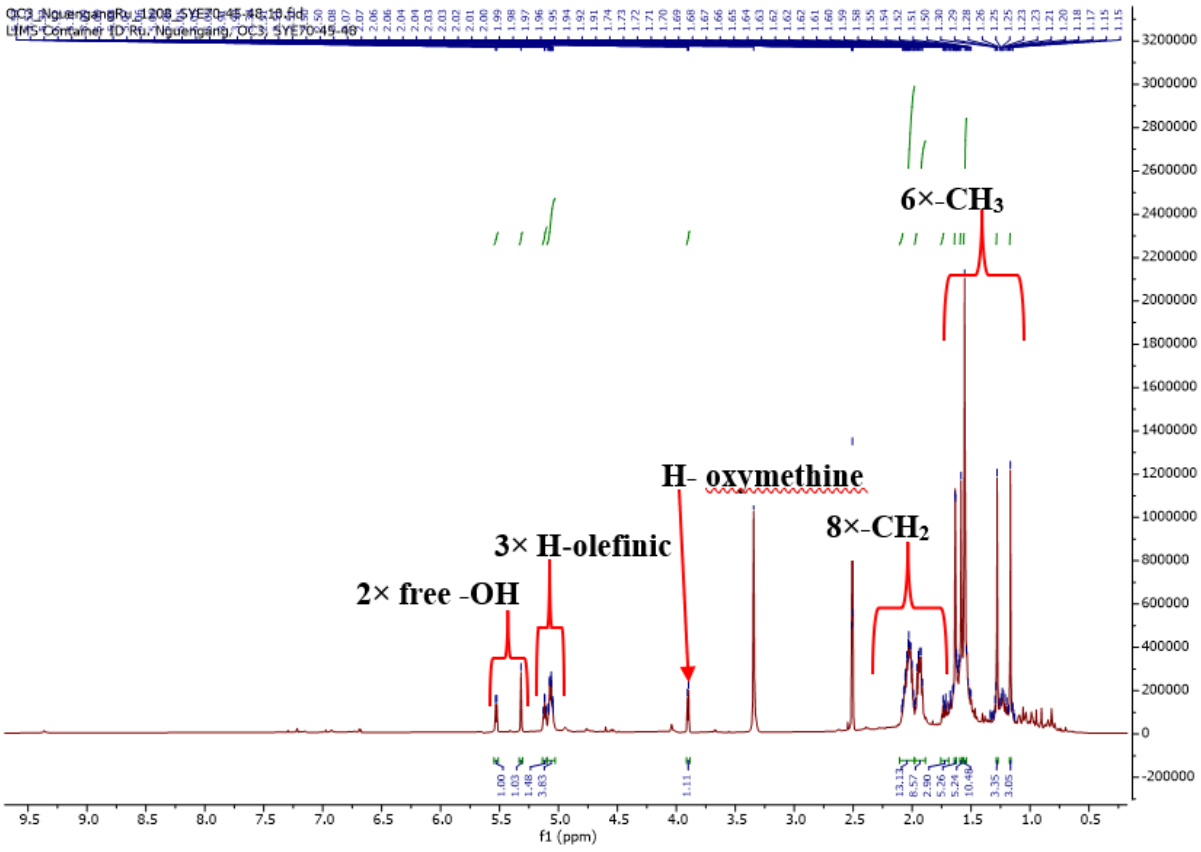

Figure 30: ^{1}H NMR of SYE70- 45-48 (DMSO-d_6, 600 MHz)

Its ^{13}C NMR (Figure 31) spectrum exhibited the signals for 26 carbons, which were sorted by DEPT and HSQC into eight methylenes, four methines and eight quaternary carbons, [among which one α,β-conjugated carbonyl at δ_C 198.8 (C-5)] and six methyl groups.

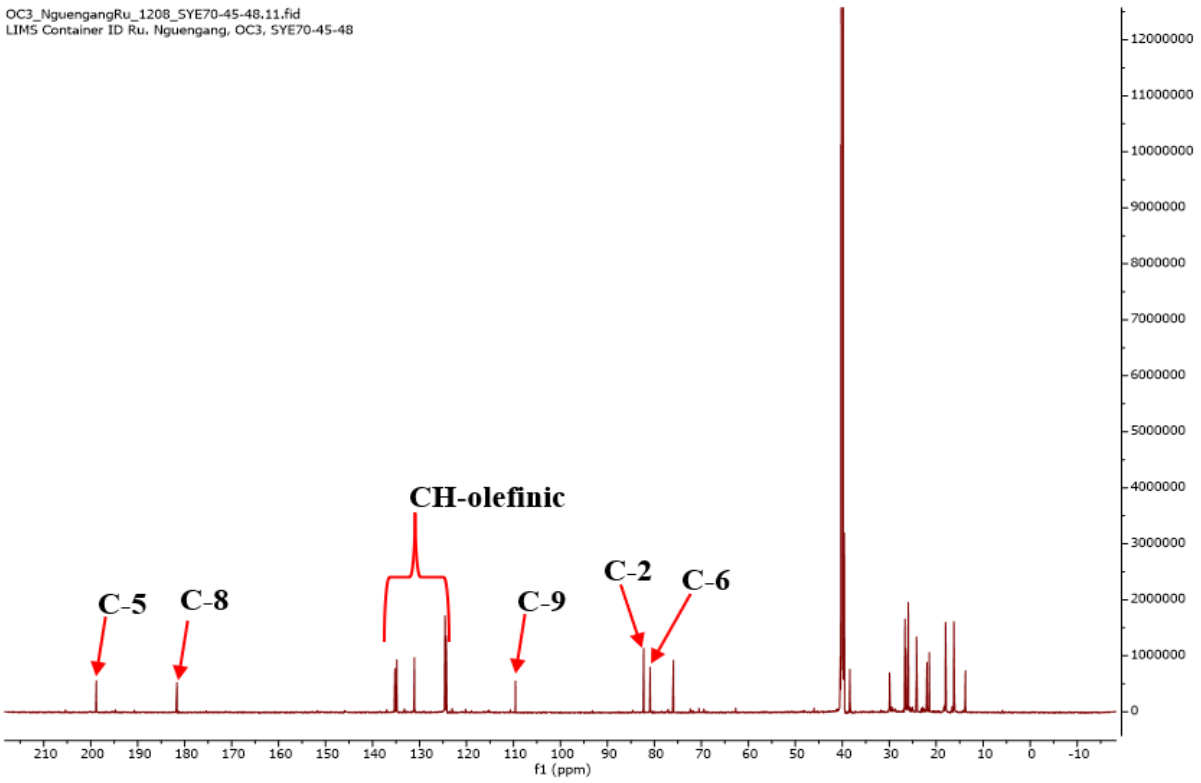

Figure 31: ^{13}C NMR spectrum of SYE70- 45-48 (DMSO-*d*$_6$, 150 MHz)

The 6,7-dihydroxy-2,2,7-trimethyl-3,4,6,7-tetrahydrocyclopenta[*b*]pyran-5(2*H*)-one and farnesyl moieties were built based on the correlations observed in the ^{1}H–^{1}H COSY and HMBC spectra (Figure 32) (Ohnmacht *et al*., 2008; Zeutsop *et al*., 2021).

The farnesyl unit was located at C-2 as proven by the HMBC correlations of H-3 (δ_H 1.73/1.22) and H-11 (δ_H 1.28) with carbons C-12 (δ_C 38.3) and C-2 (δ_C 82.2), and of H-1′ (δ_H 2.03) and H-12 (δ_H 1.63/1.53) with C-2 (δ_C 82.2). All of the above evidence indicated that compound **SYE70- 45-48** is an unusual tocotrienol with a C5/C6 membered ring.

The NOESY spectrum displayed a correlation (Figure 33) between H-6 (δ_H 3.90) and H-10 (δ_H 1.17), suggesting their *Cis*-orientation. Furthermore, the lack of a NOESY correlation between H-10 (δ_H 1.17) and H-11(δ_H 1.28), which was biogenetically α-oriented in tocotrienol derivatives (Zeutsop *et al*., 2021; Collakova *et al*., 2021), allowed us to suggest a β-orientation for H-6 (δ_H 3.90) and H-10 (δ_H 1.17). Thus, compound **SYE70- 45-48** was characterized as 12-farnesyl-6,7-dihydroxy-7-methyl-3,4,6,7-tetrahydrocyclopenta[*b*]pyran-5(2*H*)-one, trivially named globuliferanol.

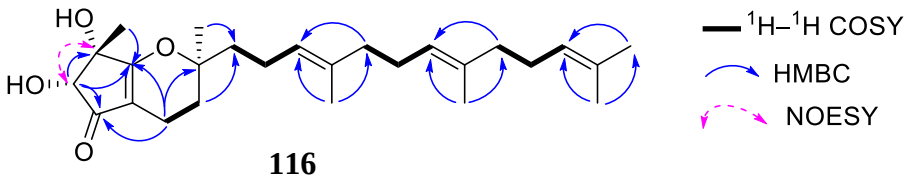

116

Scheme 12: Key HMBC correlations of SYE70- 45-48

Thus, compound **SYE70- 45-48** was characterized as 12-farnesyl-6,7-dihydroxy-7-methyl-3,4,6,7-tetrahydrocyclopenta[*b*]pyran-5(2*H*)-one, trivially named globuliferanol (**116**).

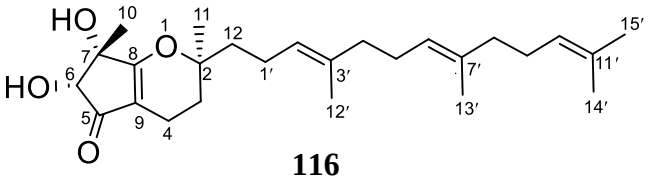

116

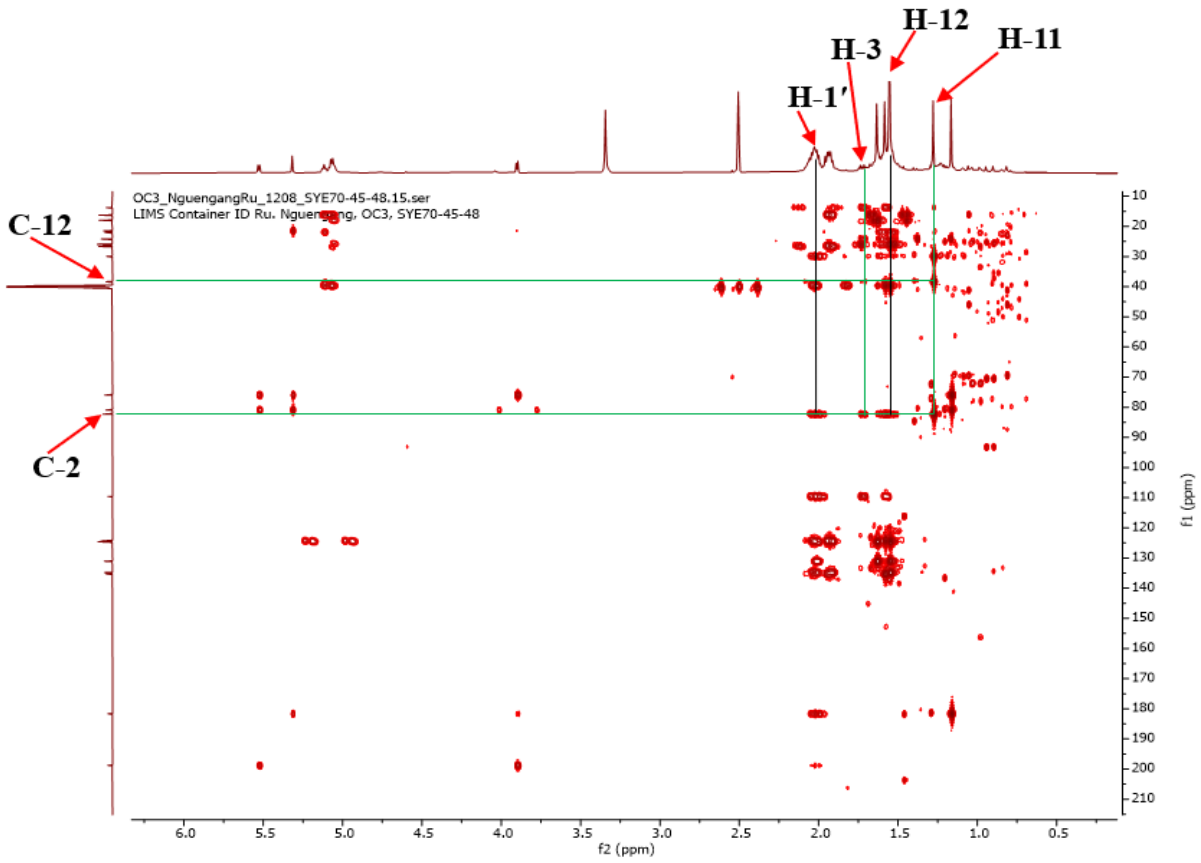

Figure 32: HMBC spectrum of SYE70- 45-48

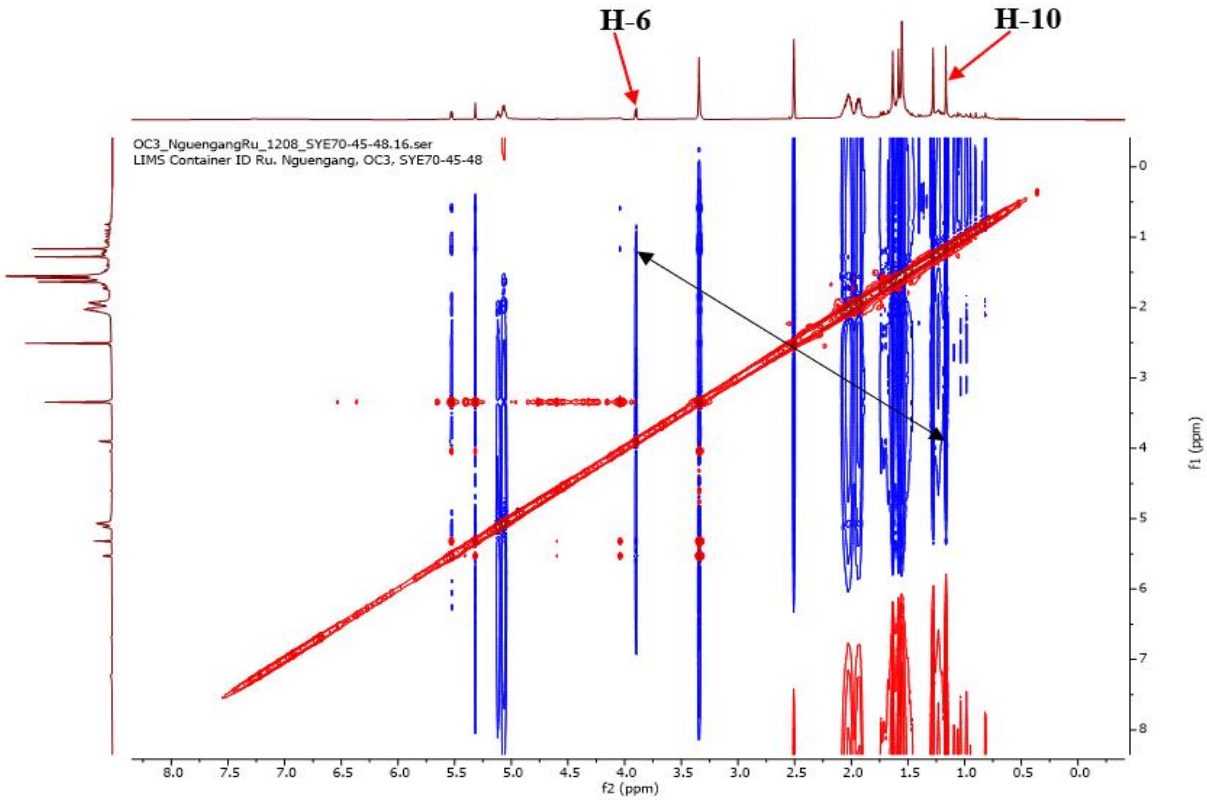

Figure 33: NOESY spectrum of SYE70- 45-48

Table 23: ^{1}H (600 MHz) and ^{13}C (150 MHz) NMR data of SYE70- 45-48 in DMSO-d_6

Globuliferanol		
Position	**δ_C**	**δ_H (m, *J* in Hz)**
2	82.2	
3	29.9	1.73 (dd, 14.0, 6.2)/1.22 (m)
4	13.7	2.03 (m)
5	198.8	
6	80.9	3.90 (d, 6.3)
7	75.9	
8	181.6	
9	109.5	
10	21.4	1.17 (s)
11	24.1	1.28 (s)
12	38.3	1.63 (m)/1.53 (brs)
1′	21.9	2.03 (m)
2′	124.2	5.12 (t, 7.1)
3′	135.2	
4′	39.5	2.03 (m)
5′	26.6	2.03 (m)
6′	124.3	5.06 (m)
7′	134.8	
8′	39.6	2.03 (m)/1.93 (q, 6.3)
9′	26.4	2.04 (m, 2H)
10′	124.5	5.06 (m)
11′	131.0	
12′	16.22	1.58 (m)
13′	16.25	1.55 (s)
14′	18.0	1.55 (s)
15′	25.9	1.63 (s)
OH-6	-	5.53 (d, 6.5)
OH-7	-	5.32 (s)

II.1.5.4. Phenolic derivatives

II.1.5.4.1. Structural identification of compound RBR3C

RBR3C was obtained as red finely divided solid in CH_2Cl_2-EtOAc (1:0, v/v). It was soluble in dichloromethane and reacted positively to Bornträger test, characteristic of anthraquinones and quinones.

Its molecular formula, $C_{15}H_{10}O_5$, implying eleven degrees of unsaturation, was deduced from the combination of its NMR and ESIMS (Figure 34), which showed the dehydrogenated adduct peak $[M-H]^-$ at *m/z* 269.8 to those of the NMR spectra (Figure 35 to 40).

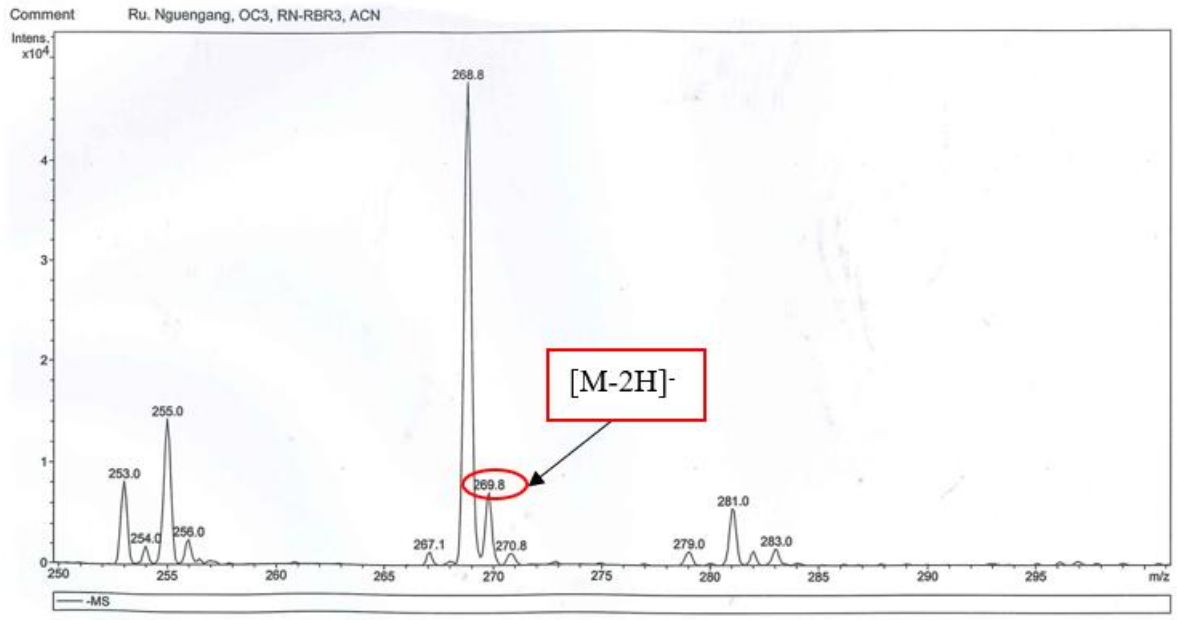

Figure 34: (-) ESI mass spectrum of RBR3C

Its ^{1}H NMR spectrum (Figure 35) exhibited from downfield to upfield, resonances of:

- Two chelated hydroxy protons at δ_H 12.10 (1H, s, OH-1) and 12.03 (1H, s, OH-8);
- Four doublets of one proton each at δ_H 7.50 (1H, d, J = 1.6 Hz, H-4), 7.18 (1H, d, J = 1.6 Hz, H-2), 7.12 (1H, d, J = 2.4 Hz, H-5) and 6.60 (1H, d, J = 2.4 Hz, H-7) corresponding to two couples of *meta* coupled aromatic protons. This was confirmed by the ^{1}H–^{1}H COSY spectrum, which showed cross-peak correlations between H-4 and H-2; H-5 and H-7 (Figure 39);
- One singlet at δ_H 2.42 (3H, s, 3-CH_3), attributable to a methyl attached to a Csp^2-hybridized carbon.

The presence of an anthraquinone skeleton was strongly supported by the two chelated hydroxy groups.

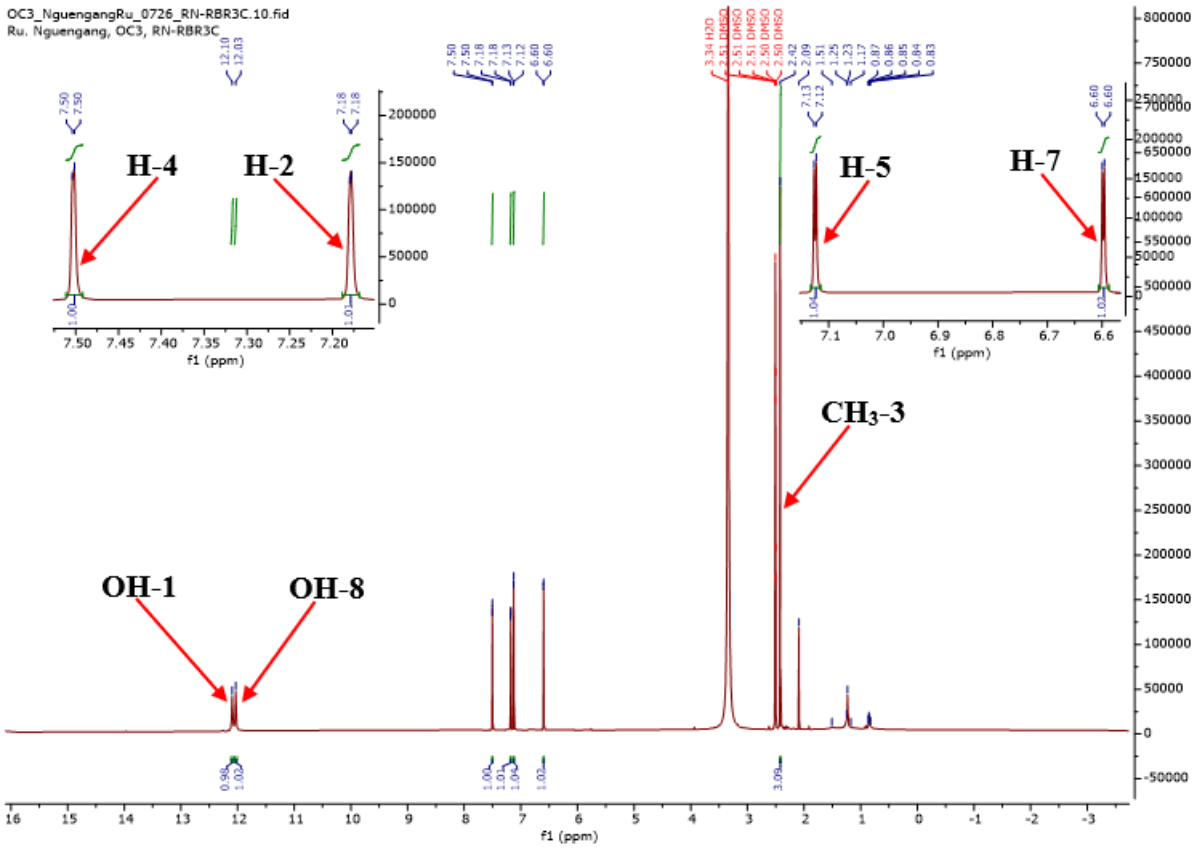

Figure 35: ^{1}H NMR of RBR3C (DMSO-*d*$_6$, 600 MHz)

Its ^{13}C NMR spectrum (Figure 36) revealed 15 carbon resonances of anthraquinone type skeleton (Chun-Nan *et al.*, 1990; Ayer and Trifonov, 1994), which were sorted by DEPT (Figure 37) and HSQC (Figure 38) experiments into:

- ten quaternary carbons at δ_C 166.2 (C-6), 164.9 (C-8), 161.9 (C-1), 148.7 (C-3), 135.6 (C-10a), 133.3 (C-4a), 113.9 (C-9a), 109.4 (C-8a) including two carbonyls at δ_C 190.1 (C-9) and 181.9 (C-10). The signal of the carbonyl groups confirmed the presence of two chelated hydroxy group, and thus suggested the anthraquinone skeleton (Chun-Nan *et al.*, 1990 ; Ayer and Trifonov, 1994);
- four aromatic methine groups at δ_C 124.6 (C-2), 120.9 (C-4), 109.3 (C-5) and 108.4 (C-7);
- one methyl group at δ_C 22.0 (CH_3-3).

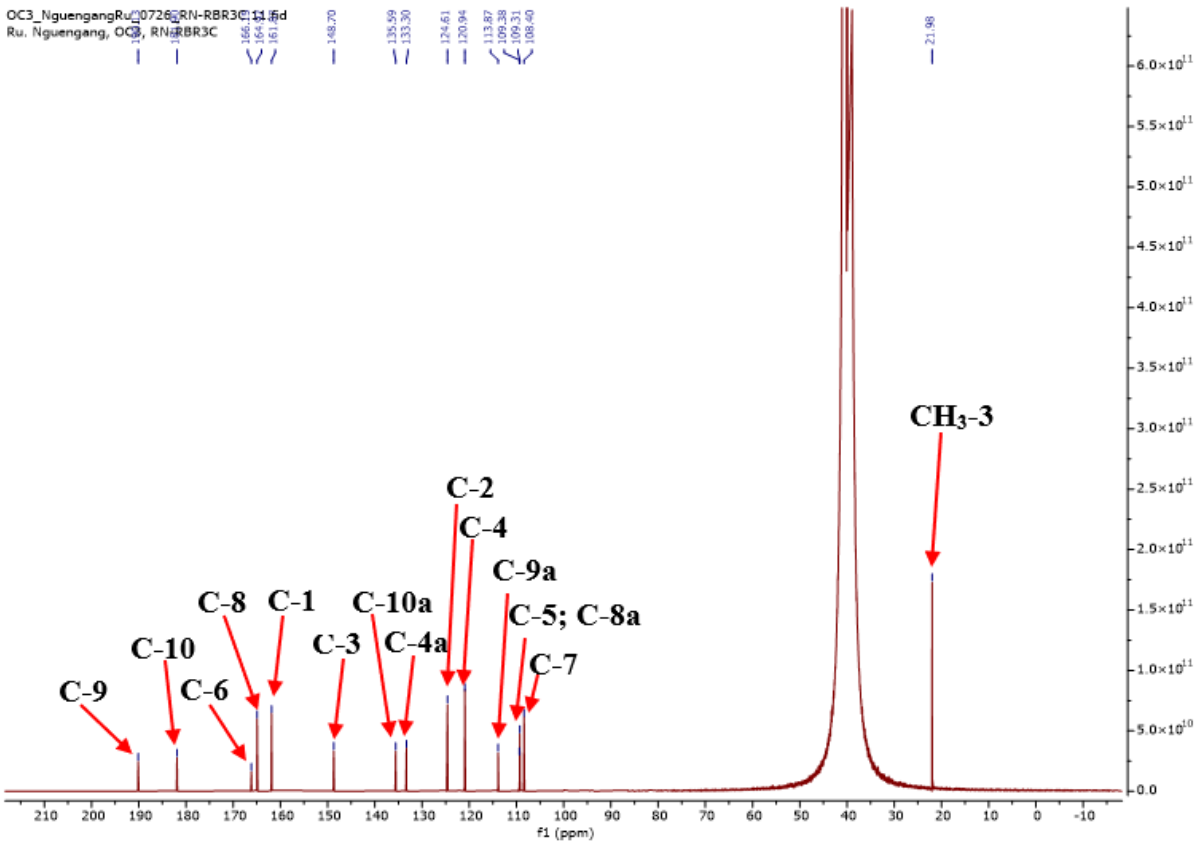

Figure 36: ^{13}C NMR spectrum of RBR3C (DMSO-d_6, 150 MHz)

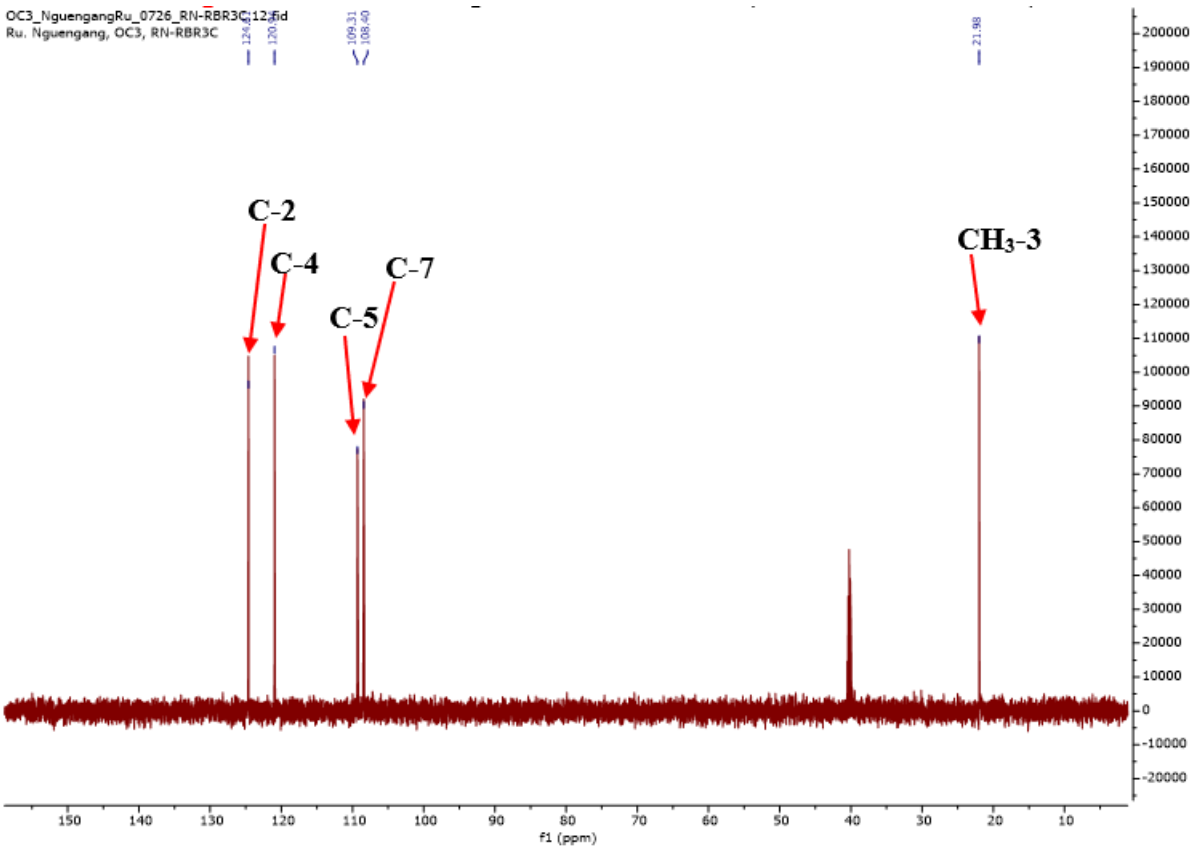

Figure 37: DEPT spectrum of RBR3C

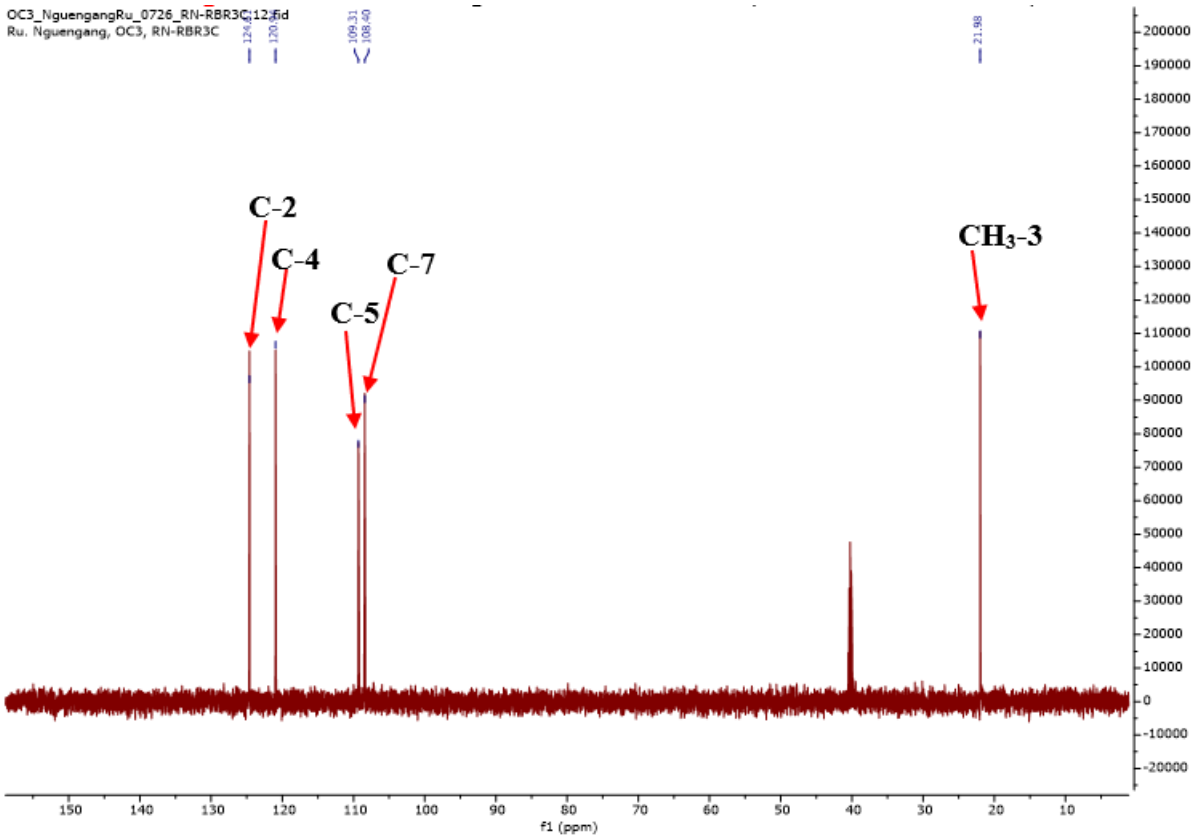

Figure 38: HMQC spectrum of RBR3C

The position of the different substituents was determined by the correlations observed on the HMBC spectrum (Figure 40) between protons:

- H-5 (δ_H 7.12, 1H, d, J = 2.4 Hz) and carbon C-10 (δ_C 181.9);
- H-7 (δ_H 6.60, 1H, d, J = 2.4 Hz) and carbons C-5 (δ_C 109.3) and C-6 (166.2);
- 3-CH_3 (δ_H 2.42, s, 3H) and carbons C-4 (δ_C 120.9) and C-2 (124.6).

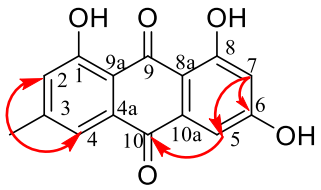

Scheme 13: Key HMBC correlations of RBR3C

All these data, compared with those described in the literature, were in agreement with those of 3-methyl-1,6,8-trihydroxyanthraquinone (emodin) (**117**), previously isolated from *Rumex japonicus* by Guo *et al.*, (2011).

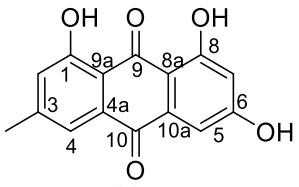

117

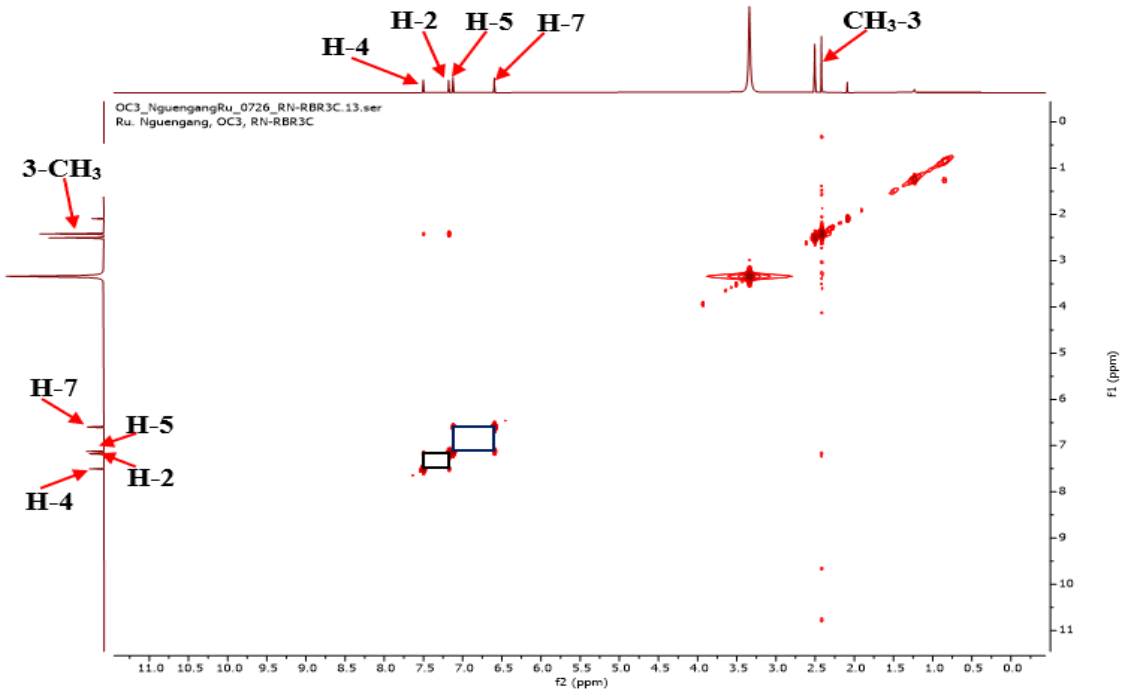

Figure 39: HMQC spectrum of RBR3C

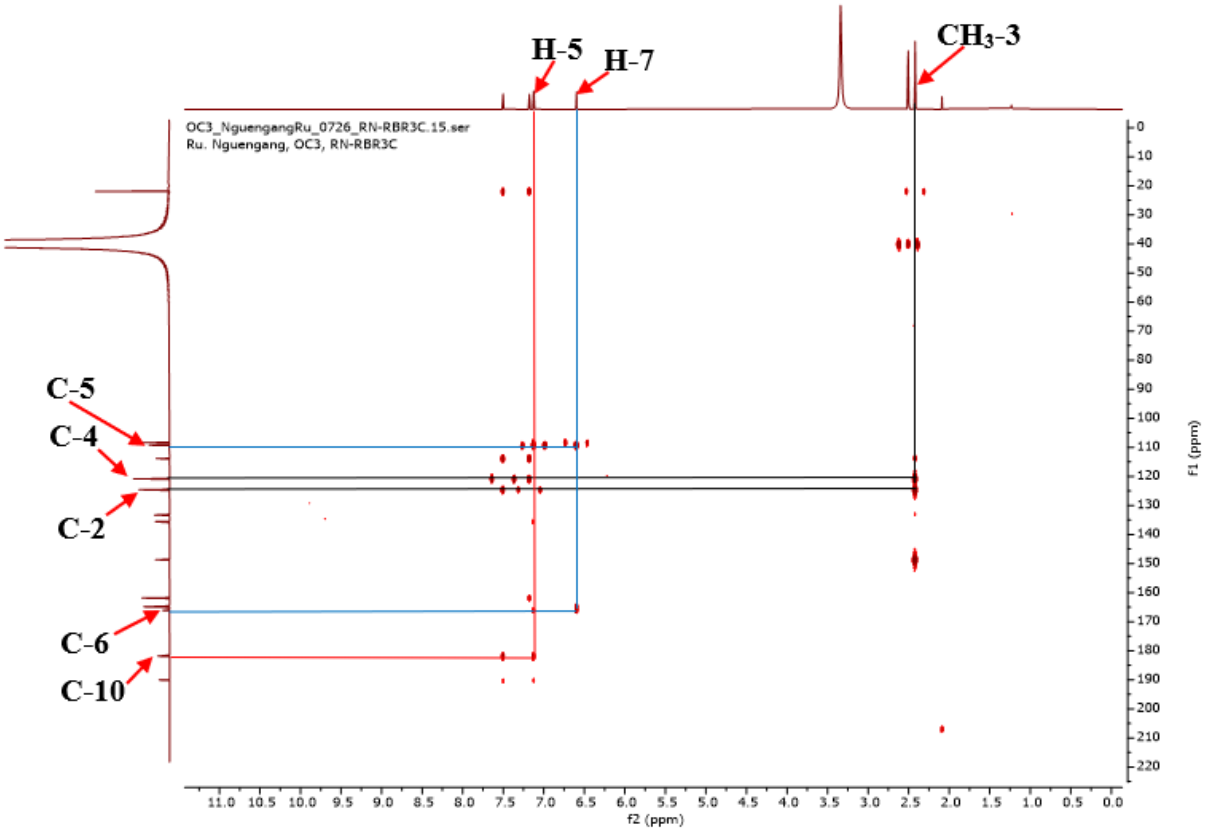

Figure 40: HMBC spectrum of RBR3C

Table 24: Comparative NMR data of RBR3C [^{1}H (600 MHz), ^{13}C (150 MHz)] and emodin [^{1}H (400 MHz), ^{13}C (100 MHz)] in DMSO-*d*$_6$

	RBR3C		Emodin (Guo *et al.*, 2011)	
Position	δ_C	δ_H (m, *J* in Hz)	δ_C	δ_H (m, *J* in Hz)
1	161.9	-	161.1	-
2	124.6	7.18 (1H, d, 1.6)	123.9	7.15 (1H, d, 1.2)
3	148.7	-	148.0	-
4	120.9	7.50 (1H, d, 1.6)	120.2	7.48 (1H, d, 1.2)
4a	133.3	-	132.6	-
5	109.3	7.12 (1H, d, 2.4)	108.7	7.11 (1H, d, 2.0)
6	166.2	-	164.1	-
7	108.4	6.60 (1H, d, 2.4)	107.7	6.59 (1H, d, 2.0)
8	164.9	-	165.2	-
8a	109.4	-	108.5	-
9	190.1	-	189.4	-
9a	113.9	-	113.1	-
10	181.9	-	181.0	-
10a	135.6	-	134.9	-
CH_3-3	22.0	2.42 (3H, s)	21.4	2.38 (3H, s)
OH-1	-	12.10 (1H, s)	-	12.07 (1H, s)
OH-8	-	12.03 (1H, s)	-	12.00 (1H, s)

II.1.5.4.2. Structural identification of compound RBR2

RBR2 was obtained as yellow powder in CH_2Cl_2-EtOAc (1:0, v/v). It was soluble in dichloromethane and reacted positively to Bornträger test, characteristic of anthraquinones and quinones.

Its molecular formula, $C_{16}H_{12}O_5$, implying eleven degrees of unsaturation, was deduced from the combination of its NMR and ESIMS (Figure 41), which displayed the dehydrogenated adduct peak $[M-H]^-$ at *m/z* 283.8 to those of the NMR spectra (Figure 42 to 44).

The mass difference of 14 amu between RBR3C and RBR2 suggested the apparition of a CH_2 in RBR2.

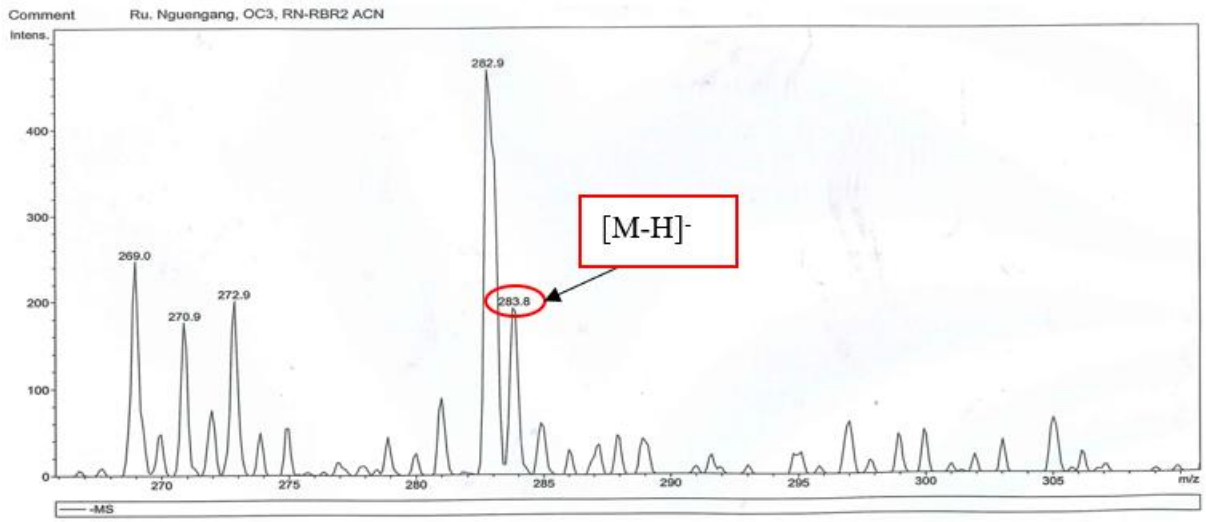

Figure 41: (-) ESI mass spectrum of RBR2

The ^1H NMR spectrum of RBR2 was very similar to that of RBR3C (Figure 42). In fact, the ^1H NMR spectrum of RBR2 displayed signals of two chelated hydroxy protons at δ_H 12.22 (1H, s, OH-1) and 12.03 (1H, s, OH-8), two couples of meta coupled aromatic protons at δ_H 7.54 (1H, br s, H-4), 7.28 (1H, dd, J = 2.6, 1.4 Hz, H-5), 7.00 (1H, br s, H-2) and 6.60 (1H, dd, J = 2.6, 1.4 Hz, H-7) and one singlet signal of methyl group at δ_H 2.37 (3H, s, CH_3-3). The only difference observed on both spectra proton was the presence of one singlet signal of methoxy group at δ_H 3.86 ppm (3H, s, OCH_3-6) of RBR2 (Figure 42).

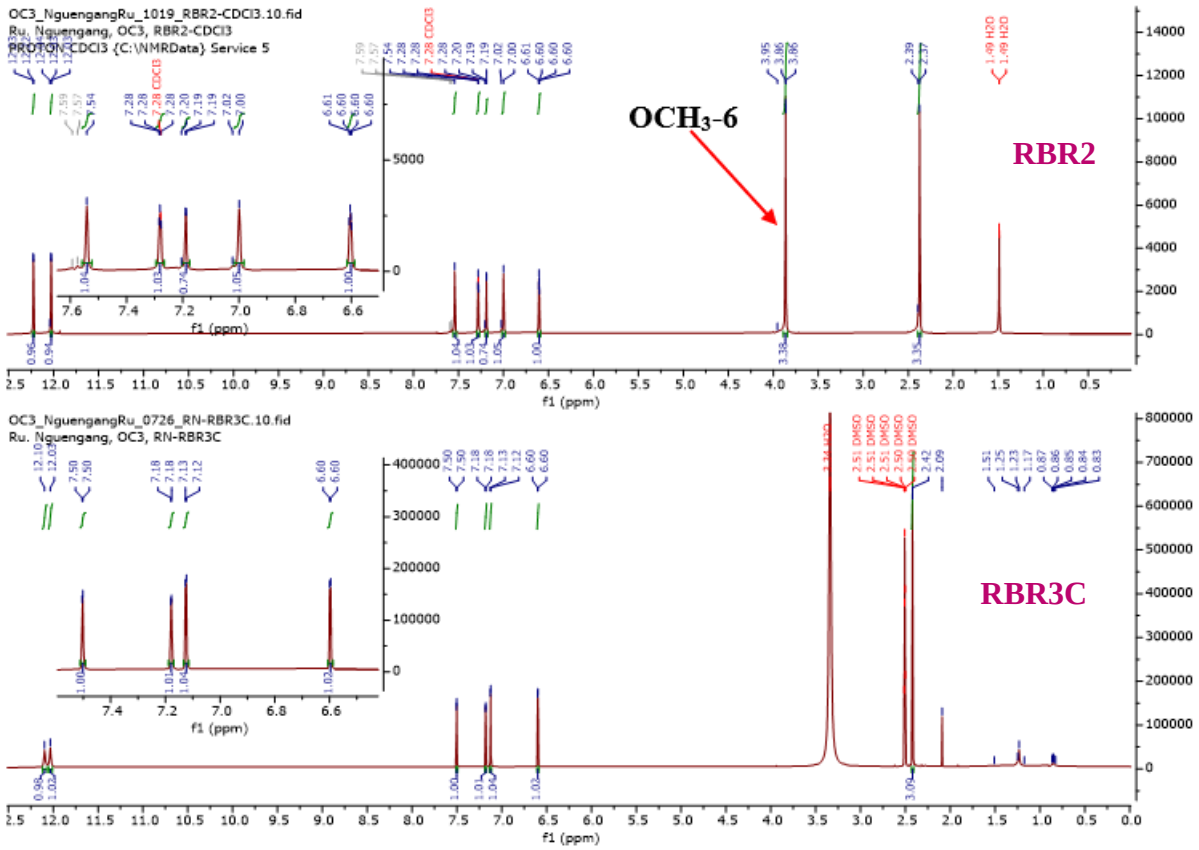

Figure 42: Compared ^{1}H NMR of RBR3C (DMSO-*d*$_6$, 600 MHz) and RBR2 ($CDCl_3$, 600 MHz)

The broad band decoupled ^{13}C spectrum (Figure 43) showed similar signals. The only discrepancy was the presence of the signal of one methoxy group at δ_C 56.1 (OCH_3-6) in comparison to that of RBR3C (Figure 43).

In addition, the C-6 has resonance at higher field (δ_C 164.9) than that of RBR3C (δ_C 166.2) indicatind the linkage of the methoxy group at that position (Figure 43).

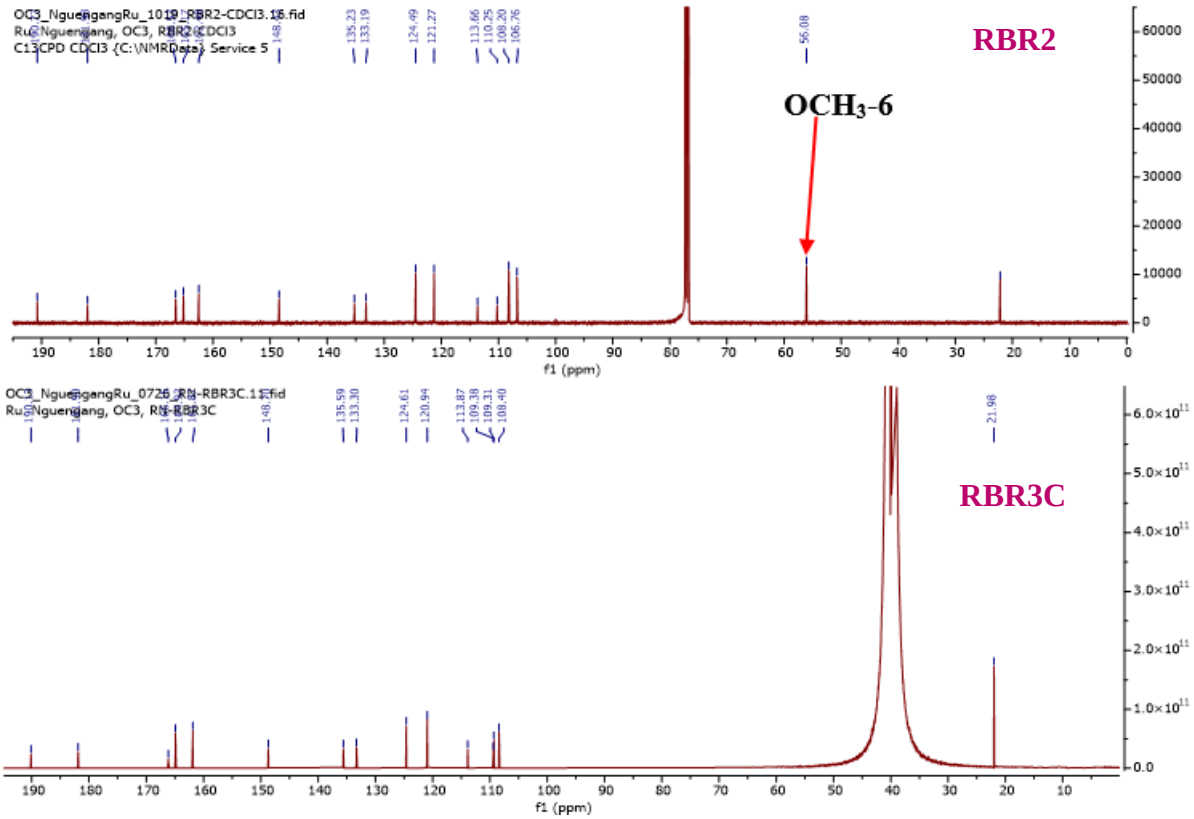

Figure 43: compared ^{13}C NMR spectrum of RBR3C (DMSO-d_6, 150 MHz) and **RBR2 ($CDCl_3$, 150 MHz).**

The location of the methoxy group was determined by the correlation observed on the HMBC spectrum (Figure 44) of RBR2 between the proton OCH_3-6 (δ_H 3.86, s, 3H) and the carbon C-6 (δ_C 164.9).

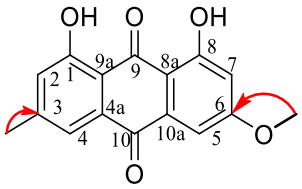

Scheme 14: Key HMBC correlations of RBR2

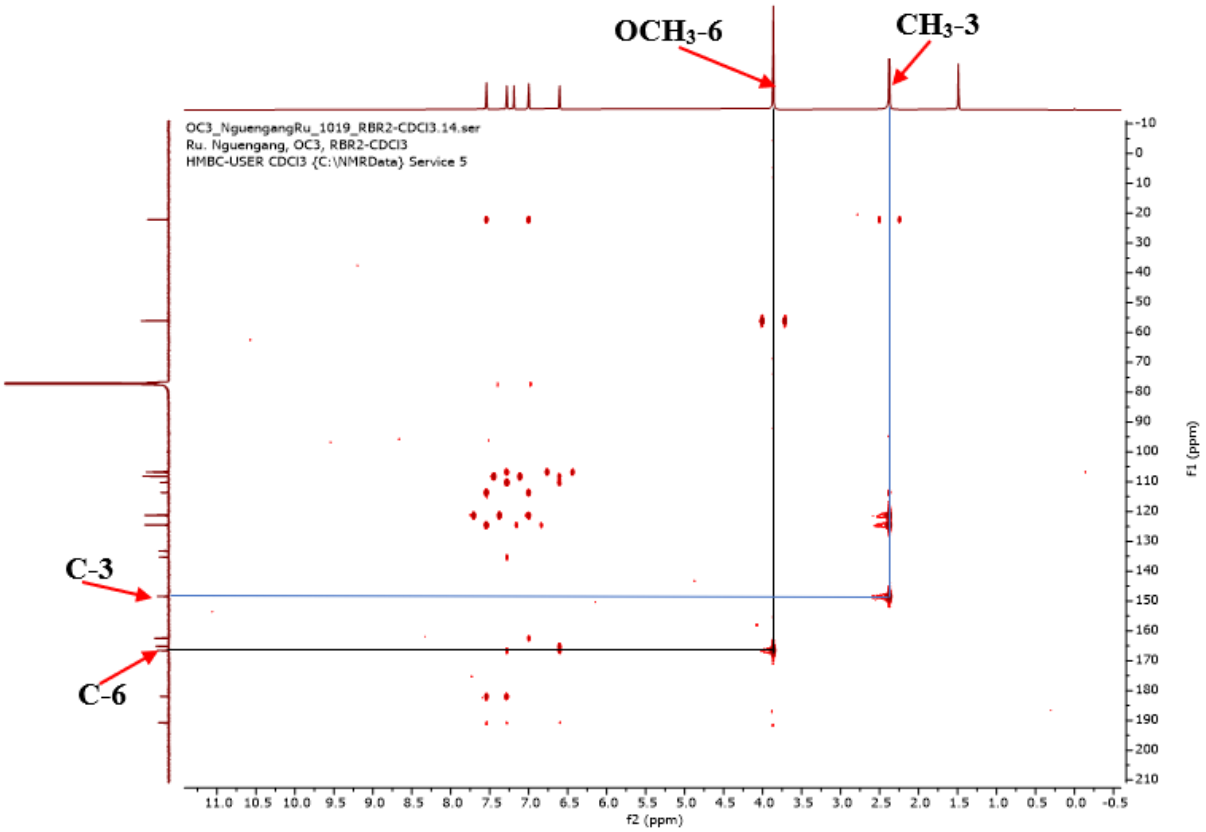

Figure 44: HMBC spectrum of RBR2

Based on these data and by comparison with those in literature, RBR2 was identified as 1,8-dihydroxy-6-methoxy-3-methylanthraquinone (physcion) (**118**), previously isolated from *Rumex japonicus* by Guo and collaborators (2011).

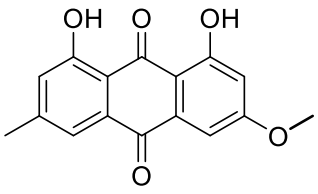

118

Table 25: Comparative NMR data of RBR2 [^{1}H (600 MHz), ^{13}C (150 MHz)] in $CDCl_3$and pyscion [^{1}H (400 MHz), ^{13}C (100 MHz)] in DMSO-d_6

	RBR2		Physcion (Guo *et al*., 2011)	
Position	δ_C	δ_H (m, *J* in Hz)	δ_C	δ_H (m, *J* in Hz)
1	165.2	-	165.1	-
2	121.3	7.00(1H, br s)	121.2	7.08(1H, br s)
3	148.4	-	148.4	-
4	124.5	7.54 (1H, br s)	124.4	7.63 (1H, br s)
4a	133.2	-	133.2	-
5	108.2	7.28 (1H, dd,2.6, 1.4)	108.2	7.37(1H, d, 2.4)
6	166.5	-	166.5	-
7	106.8	6.60 (1H, dd, 2.6, 1.4)	106.8	6.69 (1H, d, 2.4)
8	162.5	-	162.4	-
8a	110.3	-	110.2	-
9	190.8	-	190.7	-
9a	113.7	-	113.7	-
10	182.0	-	181.9	-
10a	135.2	-	135.2	-
6-OCH_3	56.1	3.86 (3H, s)	56.1	3.94 (3H, s)
3-CH_3	22.2	2.37(3H, s)	22.2	2.46 (3H, s)
1-OH	-	12.22 (1H, s)	-	12.31 (1H, s)
8-OH	-	12.03 (1H, s)	-	12.11 (1H, s)

II.1.5.4.3. Structural identification of compound RBR1a

RBR1a was obtained as light yellow amorphous powder CH_2Cl_2-EtOAc (1:0, v/v). It was soluble in dichloromethane and reacted positively to Bornträger test, characteristic of anthraquinones and quinones.

Its molecular formula $C_{15}H_{10}O_4$, implying eleven degrees of unsaturation was deduced from the combination of the data from the ESIMS spectrum (Figure 45) which showed the dehydrogenated adduct peak $[M-H]^-$ at *m/z* 253.0 to those of the NMR spectra (Figure 46 to 49). The mass difference of 16 amu between RBR3C and RBR2 suggested the absence of an oxygen atom in RBR1a.

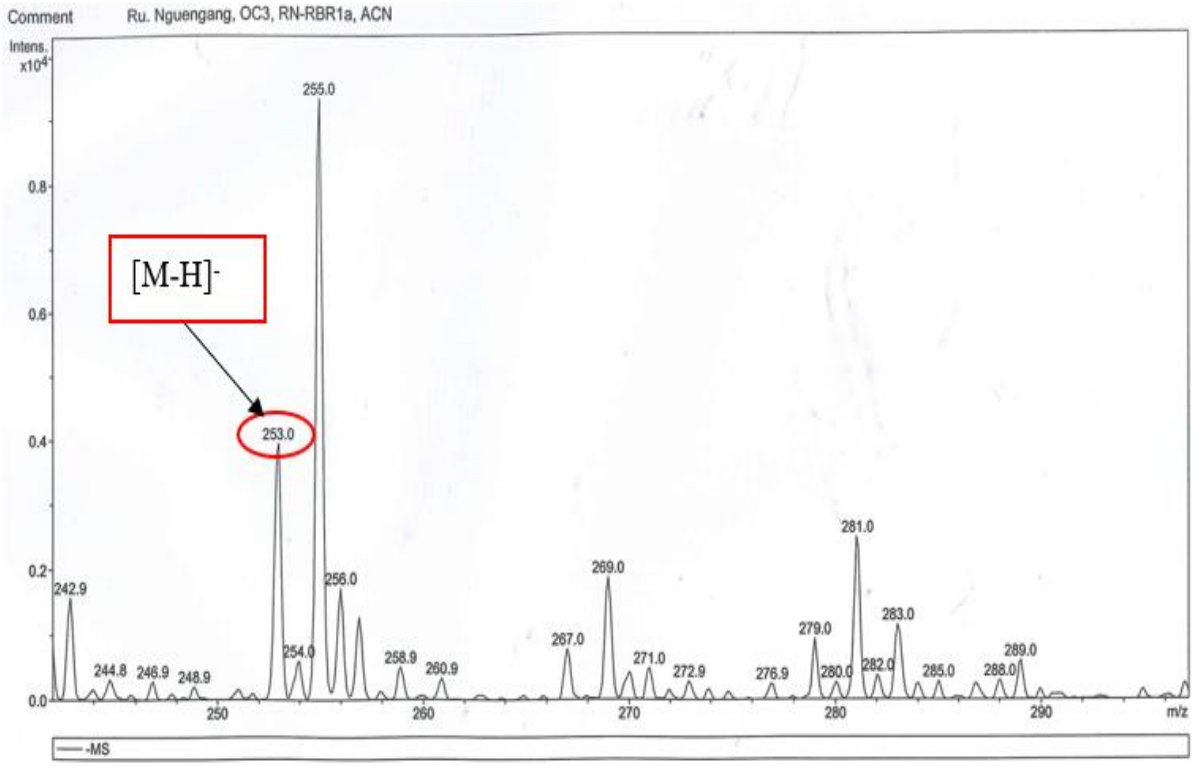

Figure 45: (-) ESI mass spectrum of RBR1a

The ^{1}H NMR spectrum of RBR1a showed similarities to that of RBR3C (Figure 46). In fact, the ^{1}H NMR spectrum of RBR1a displayed a signal of two chelated hydroxy protons at δ_H 11.93 (1H, s, OH-1) and 11.93 (1H, s, OH-8), four signals of aromatic protons at δ_H 7.72 (1H, dd, J = 7.5, 1.1 Hz, H-5), 7.56 (1H, d, J = 1.7 Hz, H-4), 7.39 (1H, dd, J = 8.4, 1.1 Hz, H-7) and 7.23 (1H, d, J = 1.7 Hz, H-2) and one singlet signal of methyl group at δ_H 2.45 (3H, s, -CH_3-3). The only difference in its ^{1}H NMR spectrum was the presence of additional signal of one aromatic proton at δ_H 7.81 (1H, br t, J = 7.9 Hz, H-6), which formed an ABC system with the two other protons at δ_H 7.72 (1H, dd, J = 7.5, 1.1 Hz, H-5) and 7.39 (1H, dd, J = 8.4, 1.1 Hz, H-7) according to their coupling constants (Figure 46).

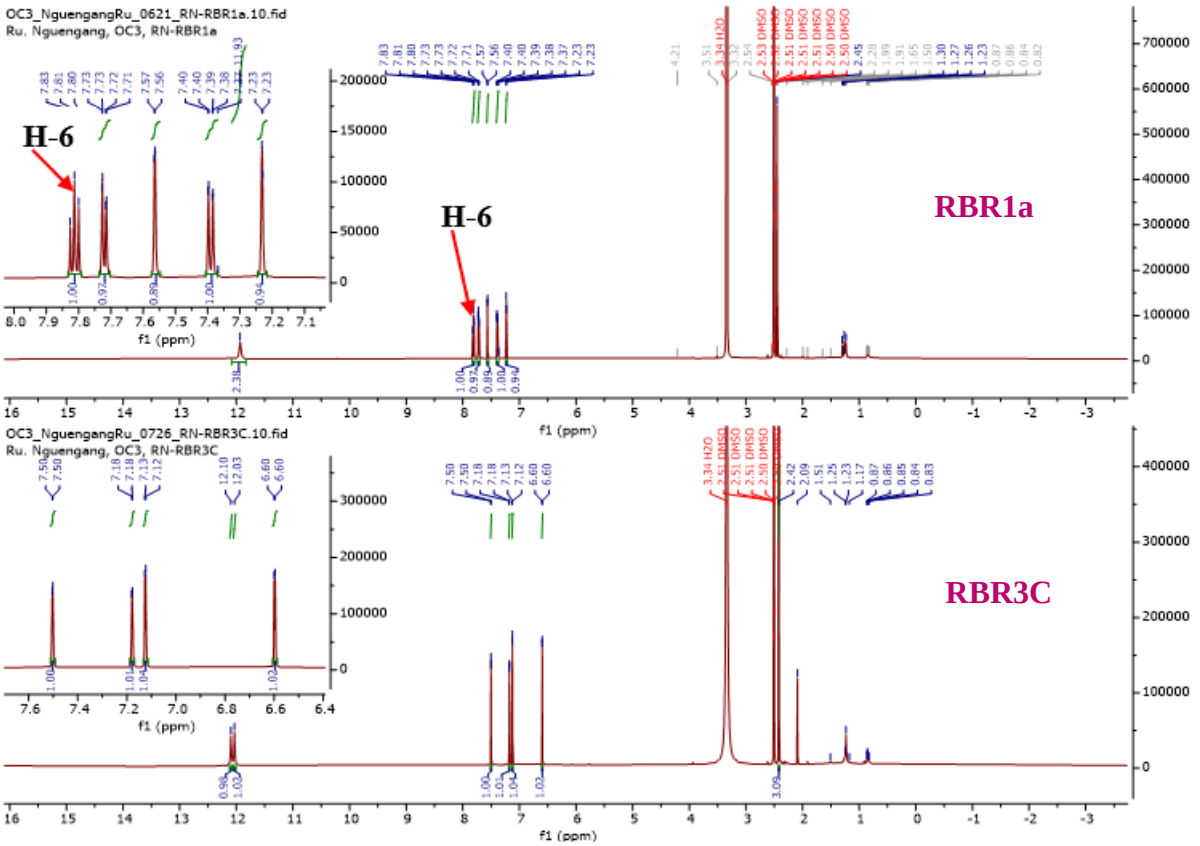

Figure 46: Compared ^{1}H NMR of RBR3C (DMSO-d_6, 600 MHz) and RBR1a (DMSO-d_6, 600 MHz).

After examination of the broadband decoupled ^{13}C and DEPT 135 spectra (Figure 47 and Figure 48) similar signals were observed. The only difference was the presence of signal for one methine group at δ_C 137.8 (C-6) in RBR1a instead of signals of the aromatic carbon with *O*-function at δ_C 166.2 (C-6) in comparison to that of RBR3C (Figure 47).

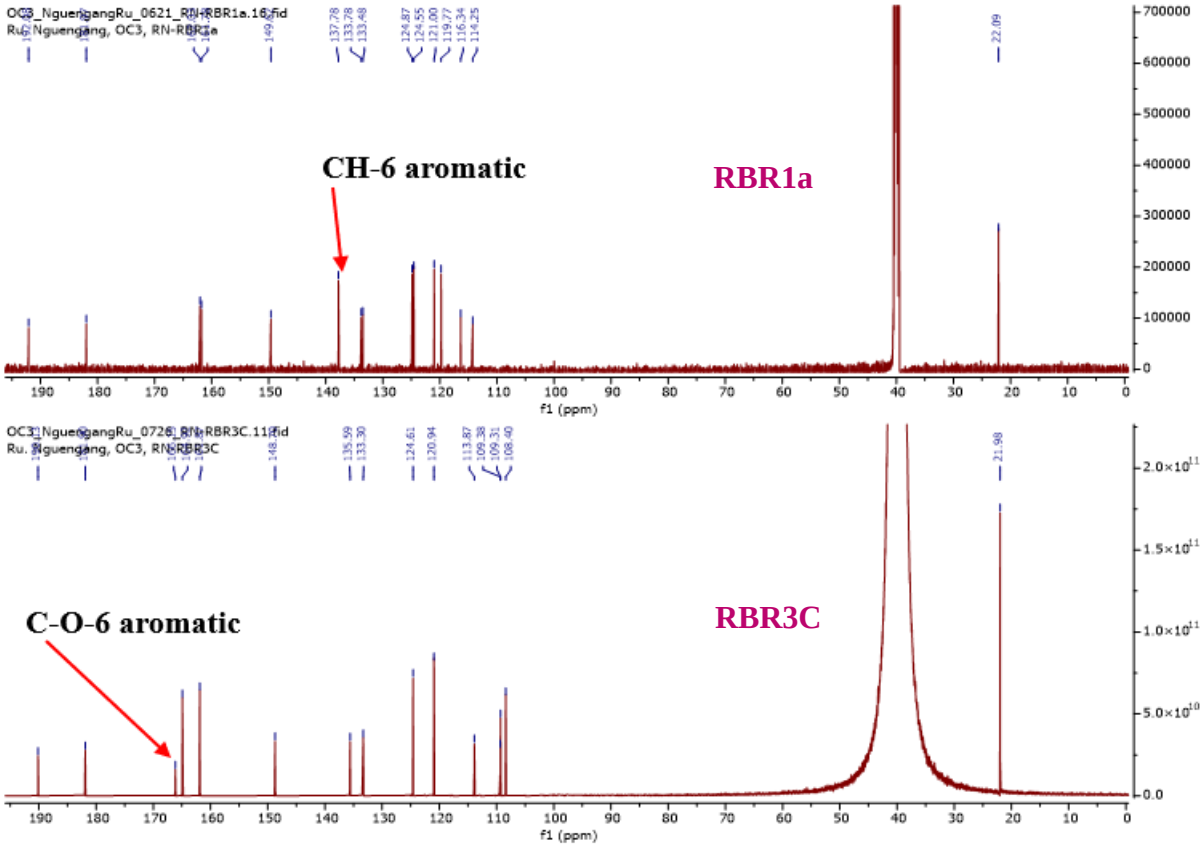

Figure 47: Compared ^{13}C NMR spectrum of RBR3C (DMSO-d_6, 150 MHz) and RBR1a (DMSO-d_6, 150 MHz)

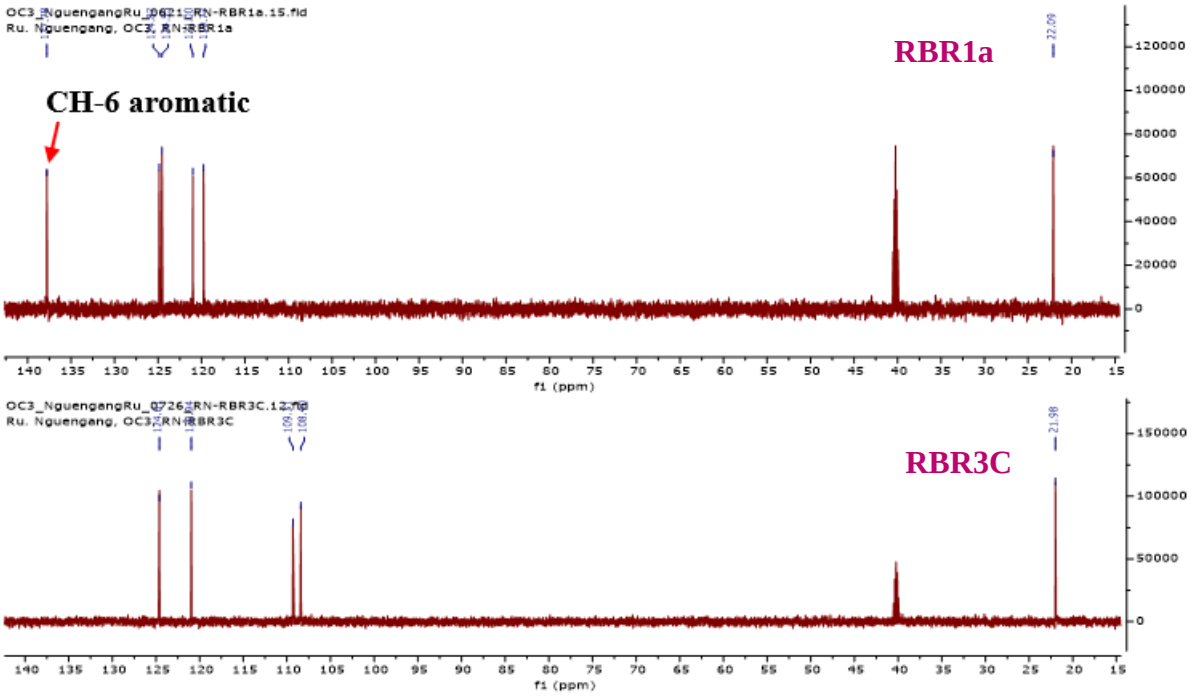

Figure 48: Compared DEPT spectrum of RBR3C and RBR1a

The proton at δ_H 7.81 (1H, br t, J = 7.9 Hz, H-6) was assigned to C-6 based on the HMBC correlations of H-6 to C-10a (δ_C 133.8) and C-8 (δ_C 161.8) observed on the HMBC spectrum (Figure 49) of RBR1a.

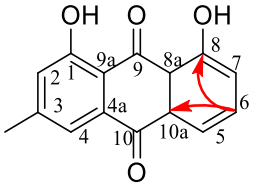

Scheme 15: Key HMBC correlations of RBR1a

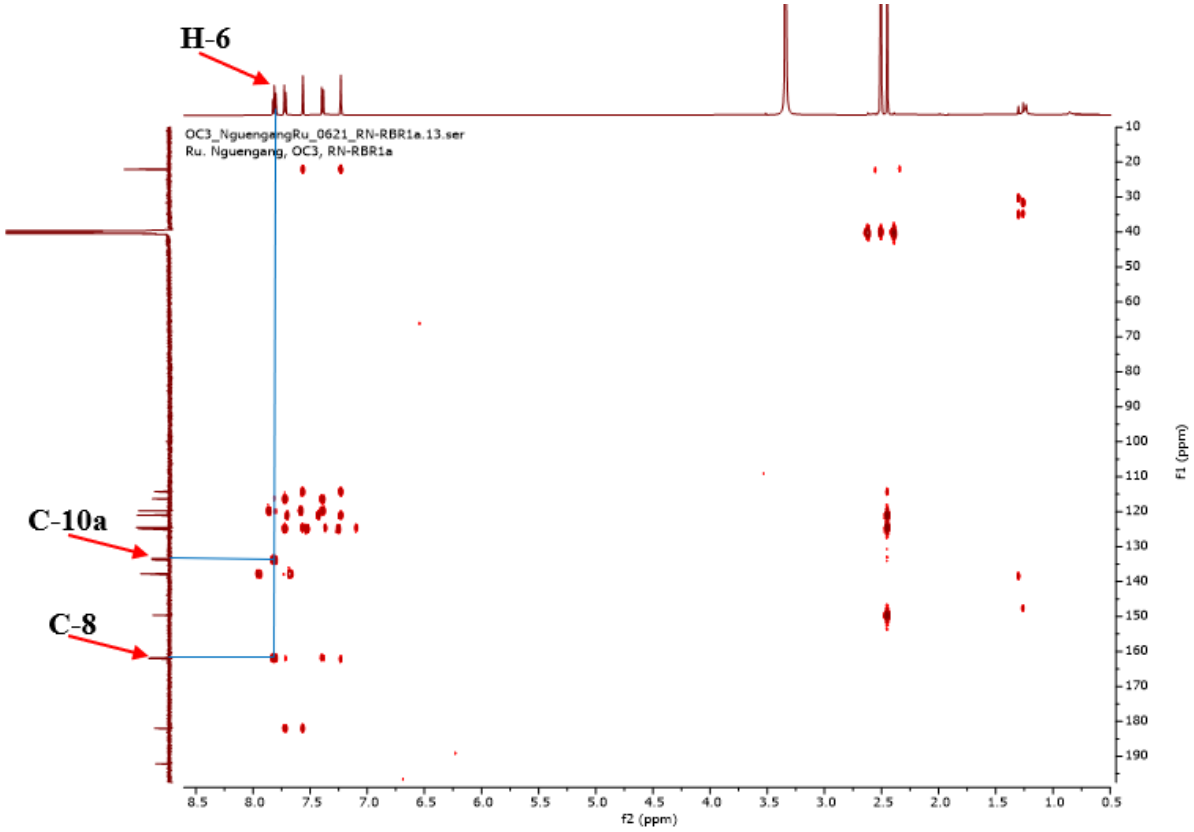

Figure 49: HMBC spectrum of RBR1a

Based on the above data and by comparison with those described in the literature, RBR1a was identified as 1,8-dihydroxy-3-methylanthraquinone (chrisophanol) (**119**), previously isolated from *Rumex japonicus* by Guo and collaborators (2011).

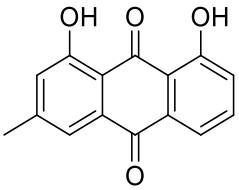

119

Table 26: Comparative NMR data of RBR1a [^{1}H (600 MHz), ^{13}C (150 MHz)] and chrisophanol [^{1}H (400 MHz), ^{13}C (100 MHz)] in DMSO-d_6

	RBR1a		Chrisophanol (Guo *et al*., 2011)	
Position	δ_C	δ_H (m, *J* in Hz)	δ_C	δ_H (m, *J* in Hz)
1	162.0	-	161.1	-
2	124.6	7.23 (1H, d, 1.7)	124.2	7.22 (1H, d, 0.8)
3	149.6	-	149.0	-
4	121.0	7.56 (1H, d, 1.7)	120.4	7.55 (1H, d, 0.8)
4a	133.5	-	132.8	-
5	119.8	7.72 (1H, dd, 7.5, 1.1)	119.2	7.71 (1H, d, 7.6)
6	137.8	7.81 (1H, br t, 7.9)	137.2	7.80 (1H, dd, 8.4, 7.6)
7	124.9	7.39 (1H, dd, 8.4, 1.1)	123.9	7.38 (1H, d, 8.4)
8	161.8	-	161.4	-
8a	116.3	-	115.7	-
9	192.1	-	191.4	-
9a	114.3	-	113.6	-
10	182.0	-	181.3	-
10a	133.8	-	133.2	-
CH_3-3	22.1	2.45 (3H, s)	21.6	2.44 (3H, s)
OH-1	-	11.93 (1H, s)	-	11.96 (1H, s)
OH-8	-	11.93 (1H, s)	-	11.86 (1H, s)

II.1.5.4.4. Structural identification of compound RBR6b

RBR6b was obtained as yellow powder in CH_2Cl_2-EtOAc (1:1, v/v). It was soluble in dichloromethane and reacted positively to Bornträger test, characteristic of anthraquinones and quinones.

Its molecular formula, $C_{15}H_{10}O_6$, implying eleven degrees of unsaturation, was established by combination of its NMR and ESIMS data (Figure 50), which showed the dehydrogenated adduct peak $[M-H]^-$ at *m/z* 285.7 to those of the NMR spectra (Figure 51 to 53).

The mass difference of 16 amu between RBR3C and RBR6b suggested the presence of an additional oxygen atom in RBR6b.

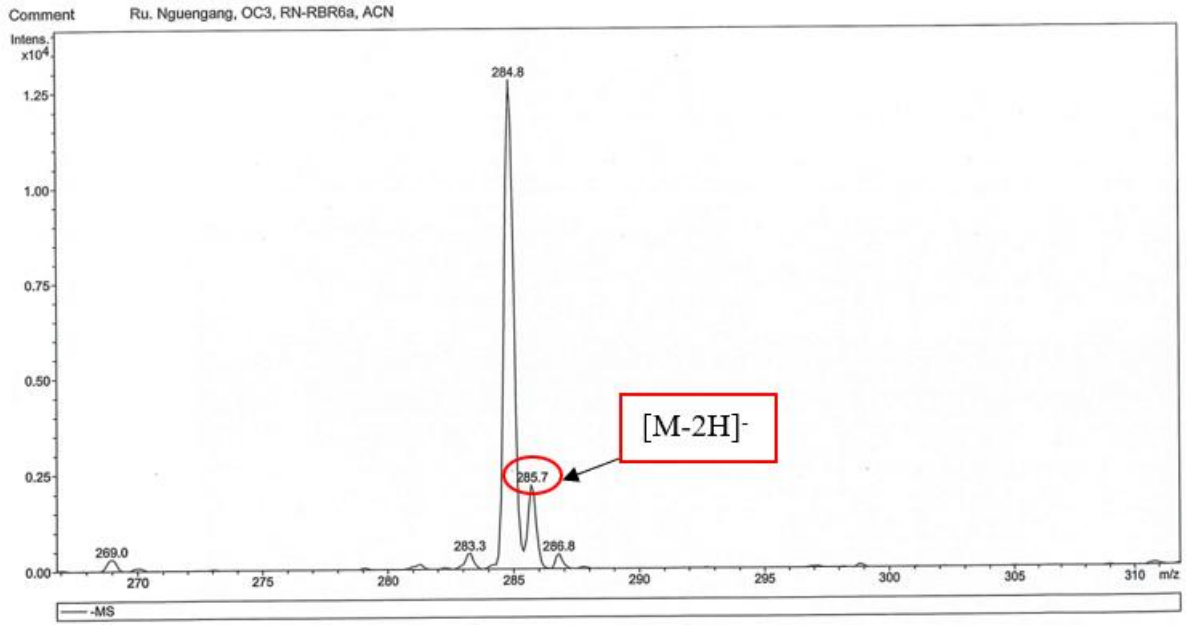

Figure 50: (-) ESI mass spectrum of RBR6b

The ^{1}H NMR spectrum of RBR6b was close to that of emodin (RBR3C) (Figure 51). The main difference between the ^{1}H NMR of RBR6b and that of RBR3C was the presence of one broad singlet signal of oxymethylene group at δ_H 4.61 (2H, br s, CH_2O-3) in RBRR6b instead the of signal of one methyl group at δ_H 2.42 (3H, s, CH_3-3) (Figure 51).

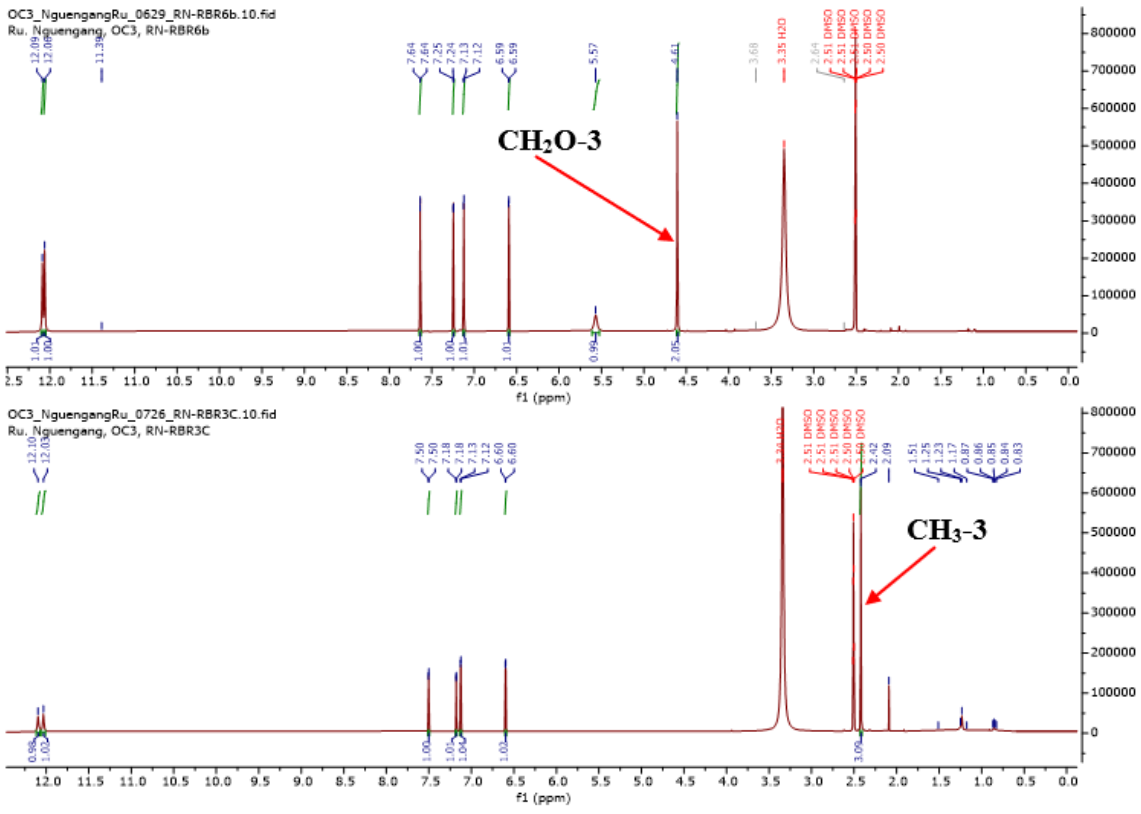

Figure 51: Comparative ^{1}H NMR of RBR3C (DMSO-d_6, 600 MHz) and RBR6b (DMSO-d_6, 600 MHz)

The ^{13}C spectrum of RBR6b was also close to that of RBR3C with little discrepancies (Figure 52). The only difference was the presence of signal of one hydroxymethyl group at δ_C 62.5 (3-CH_2O-) in RBR6b instead of signal of one methyl group at δ_C 22.0 (3H, s, CH_3-3) (Figure 52).

In addition, the C-3 had resonance at lower field (δ_C 153.3) in RBR3C than that of RBR6b (δ_C 148.7) (Figure 52).

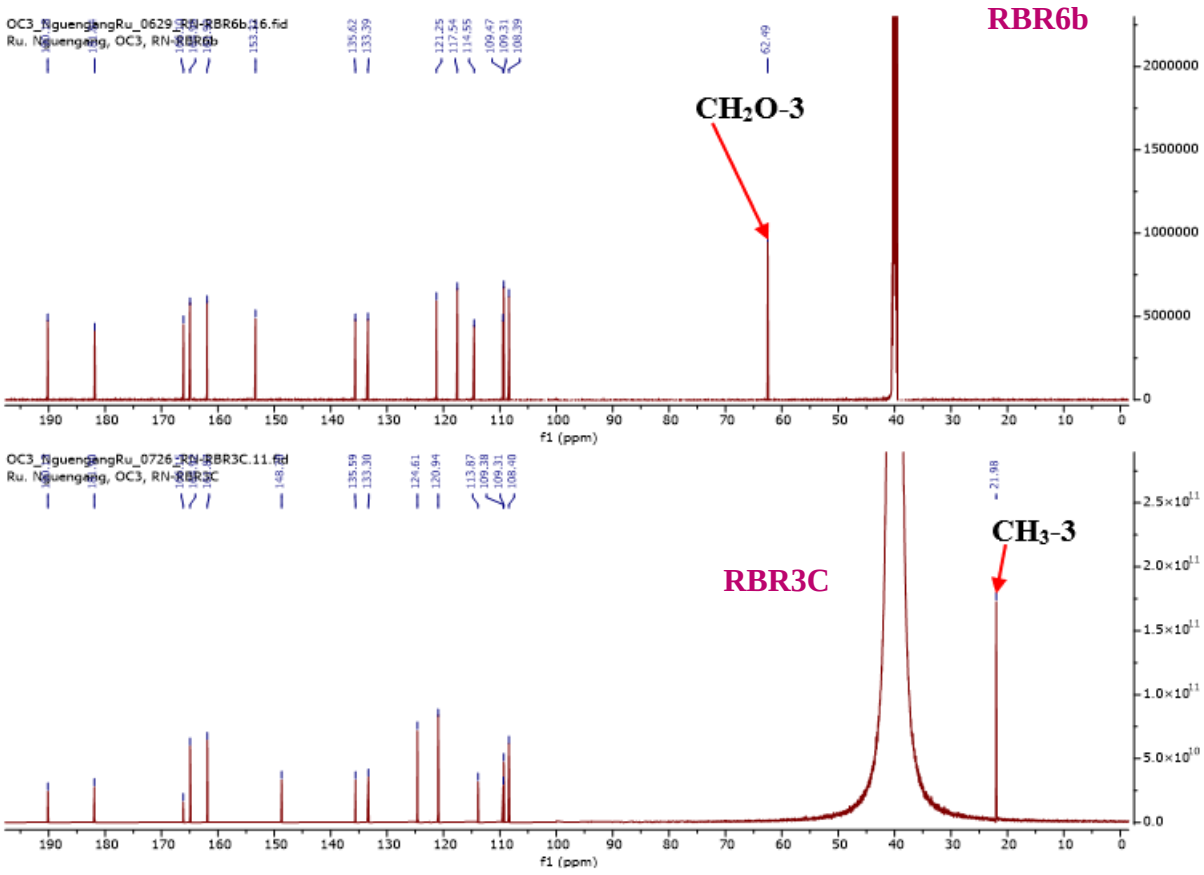

Figure 52: ^{13}C NMR spectrum of RBR3C (DMSO-*d*$_6$, 150 MHz) and RBR6b (DMSO-*d*$_6$, 150 MHz)

The location of the hydroxymethyl group was determined by the correlation observed on the HMBC spectrum (Figure 53) of RBR6b between protons the proton OCH_2-3 (δ_H 4.61, br s, 2H) and the carbon C-3 (δ_C 153.3); C-2 (δ_C 121.2) and C-4 (δ_C 117.5).

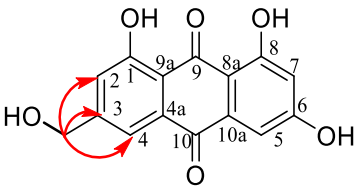

Scheme 16: Key HMBC correlations of RBR6b

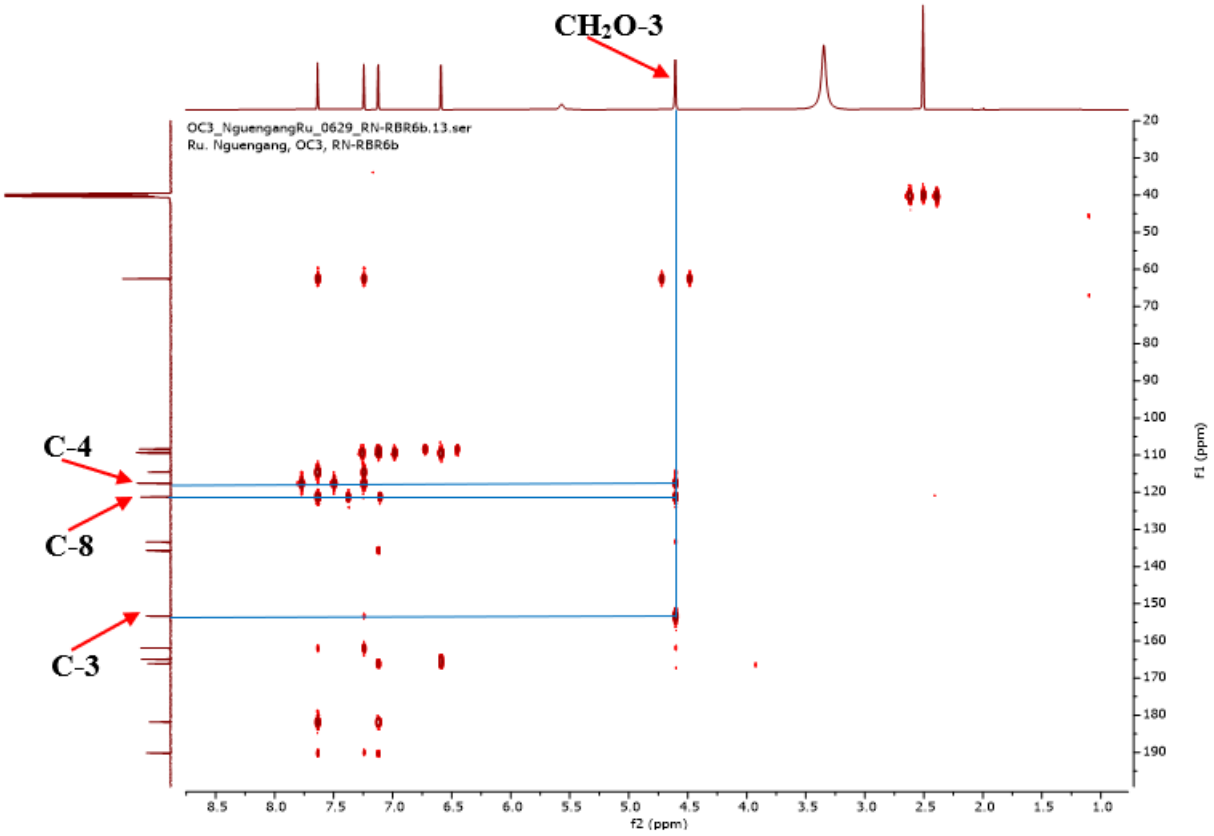

Figure 53: HMBC spectrum of RBR6b

All these data, compared with those described in the literature, was in agreement with that of 3-hydroxymethyl-1,6,8-trihydroxyanthraquinone (citreorosein) (**120**), previously isolated from endophyte fungal genus *Fusarium sp.* of *meniran* leaves (*Phyllanthus niruri Linn.*) by Yuniati *et al*., (2018).

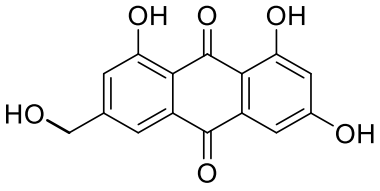

120

Table 27: ^{1}H (600 MHz) and ^{13}C (150 MHz) NMR data of RBR1a compared to those of citreorosein [^{13}C (125 MHz), ^{1}H (500 MHz)] in DMSO-d_6

	RBR6b		Citreorosein (Yuniati *et al.*, 2018)	
Position	δ_C	δ_H **(m, *J* in Hz)**	δ_C	δ_H **(m, *J* in Hz)**
1	161.9	-	161.6	-
2	121.2	7.24 (1H, d, 1.5)	120.8	7.21 (1H, d, 2.5)
3	153.3	-	152.9	-
4	117.5	7.64 (1H, d, 1.5)	117.1	7.64 (1H, d, 2.0)
4a	133.4	-	135.2	-
5	109.3	7.12 (1H, d, 2.4)	108.8	7.13 (1H, s)
6	166.1	-	165.6	-
7	108.4	6.59 (1H, d, 2.4)	107.9	6.59 (1H, d, 2.0)
8	164.9	-	164.5	-
8a	109.5	-	109.0	-
9	190.2	-	189.7	-
9a	114.5	-	114.1	-
10	181.8	-	181.5	-
10a	135.6	-	130.0	-
OCH_2-6	62.5	4.61 (2H, br s)	62.0	4.62 (2H, s)
OH-6		5.57 (1H, s)		5.65 (1H, s)
OH-1	-	12.06 (1H, s)	-	13.11
OH-8	-	12.09 (1H, s)	-	11.87

II.1.5.4.5. Structural identification of compound RBR7a2

RBR7a2 was obtained as light yellow amorphous powderin in CH_2Cl_2-EtOAc (3:1, v/v). It was soluble in dichloromethane and reacted positively to Bornträger test, characteristic of anthraquinones and quinones.

Its molecular formula, $C_{16}H_{12}O_6$, with eleven degrees of unsaturation, was deduced from the HRESIMS spectrum (Figure 29) which showed the dehydrogenated adduct peak $[M-H]^-$ at *m/z* 299.0559 (calcd for $C_{16}H_{11}O_6$, 299.0561). The mass difference of 14 amu between RBR6b and RBR7a2 suggested the apparition of a CH_2 in RBR6b.

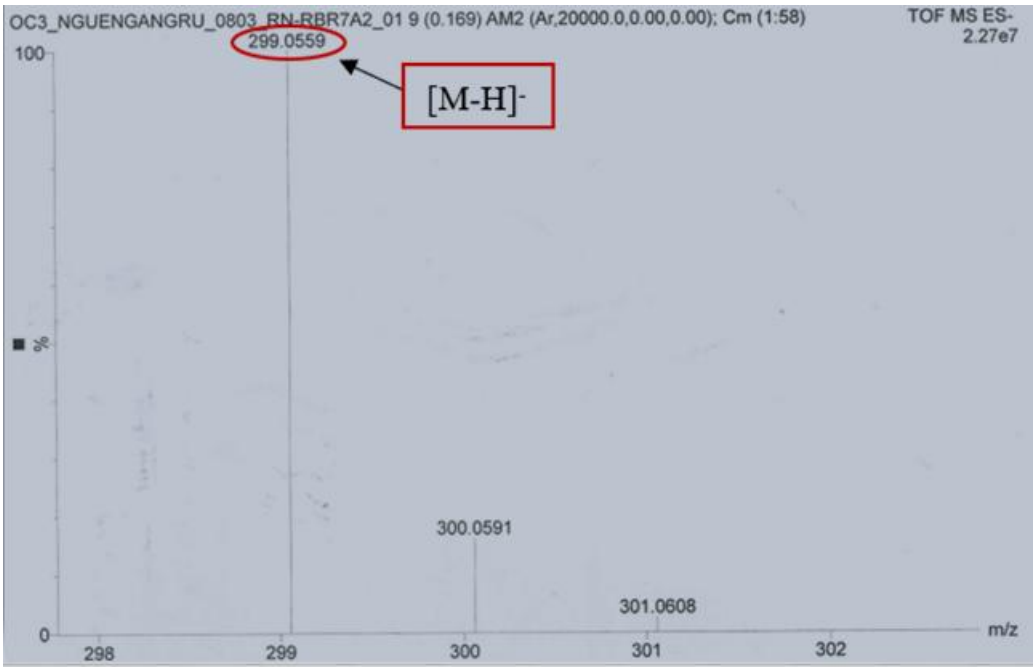

Figure 54: (-) HRESI mass spectrum of RBR7a2

The ^{1}H NMR spectrum (Figure 55) showed one signal with regard to chelated hydroxy protons at δ_H 13.34 (1H, s, OH-1), one free hydroxy proton at δ_H 5.52 (1H, s, OH-6), together with two couples of meta coupled aromatic protons at δ_H 7.60 (1H, d, J = 1.6 Hz, H-4), 7.22 (2H, d, J = 2.0 Hz, H-2, 5) and 6.85 (1H, d, J = 2.3 Hz, H-7). The ^{13}C NMR spectrum (Figure 56) showed characteristic signals for citreorosein at δ_C 165.2 (C-6), 164.0 (C-8), 162.2 (C-1), 151.8 (C-3), 137.3 (C-10a), 132.6 (C-4a), 115.6 (C-9a), 112.9 (C-8a), 186.7 (C-9), 182.9 (C-10), 121.4 (C-2), 116.3 (C-4), 107.7 (C-5), 108.4 (C-7), 22.0 (3-CH3), 62.5 (3-OCH2-). It was observed that the structures of RBR7a2 was close to citreorosein (**RBR6b**) from the above NMR data. The main discrepancy between the ^{1}H NMR of **RBR7a2** and that of **RBR6b** was the presence of one singlet signal of a methoxy group at δ_H 3.92 ppm (3H, s, OCH_3-8) in RBRR7a2 instead of signal of one chelated hydroxy proton at δ_H 12.09 (1H, s, OH-8) (Figure 55). This suggestion was confirmed with the presence of additional signal of one methoxy group at δ_C 56.8 (3H, s, OCH_3-8) in ^{13}C NMR spectra (Figure 56) of **RBR7a2**.

In addition, the C-9 has resonance at higher field (δ_C 186.7) than that of RBR6b (δ_C 190.2) confirming the presence of only one chelated hydroxy group in RBRR7a2 instead of two (Figure 56).

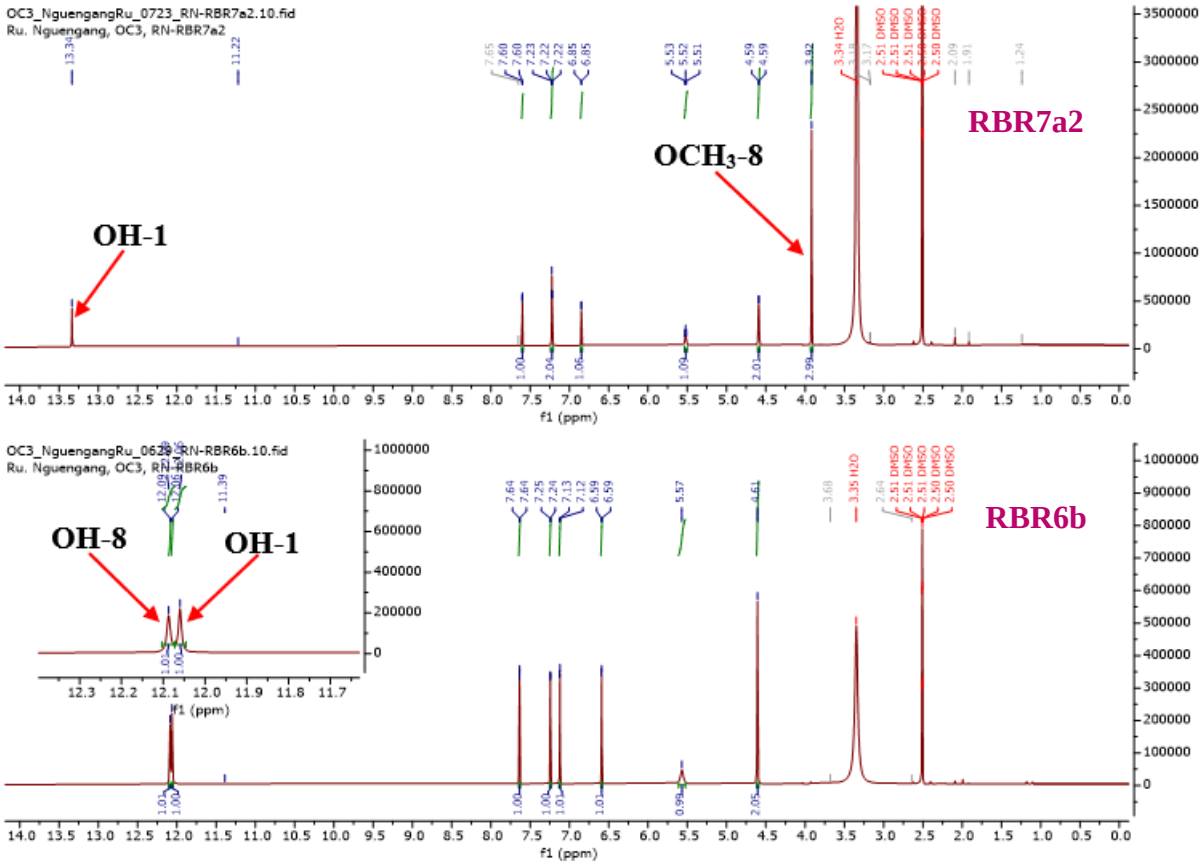

Figure 55: Comparative ^{1}H NMR of RBR6b and RBR7a2 (DMSO-*d*$_6$, 600 MHz)

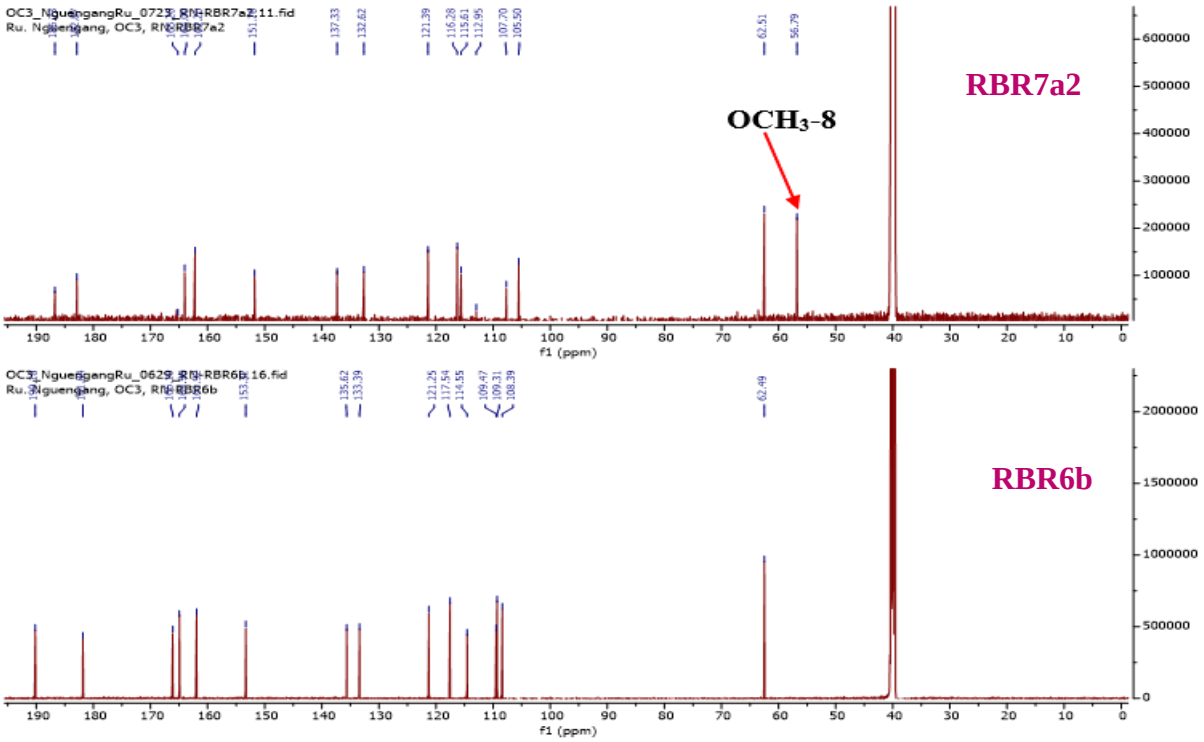

Figure 56: Comparative ^{13}C NMR spectrum of RBR6b and RBR7a2 (DMSO-*d*$_6$, 150 MHz)

The location of the methoxy group was determined by the correlation observed on the HMBC spectrum (Figure 57) of RBR7a2 between the proton OCH_3-8 (δ_H 3.92, s, 3H) and C-8 (δ_C 164.0), proton H-7 [δ_H (6.85, 1H, d, J = 2.3 Hz)] and C-8 (δ_C 164.0).

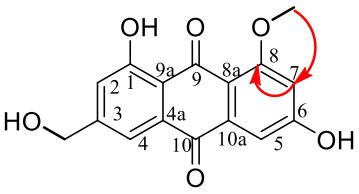

Scheme 17: Key HMBC correlations of RBR7a2

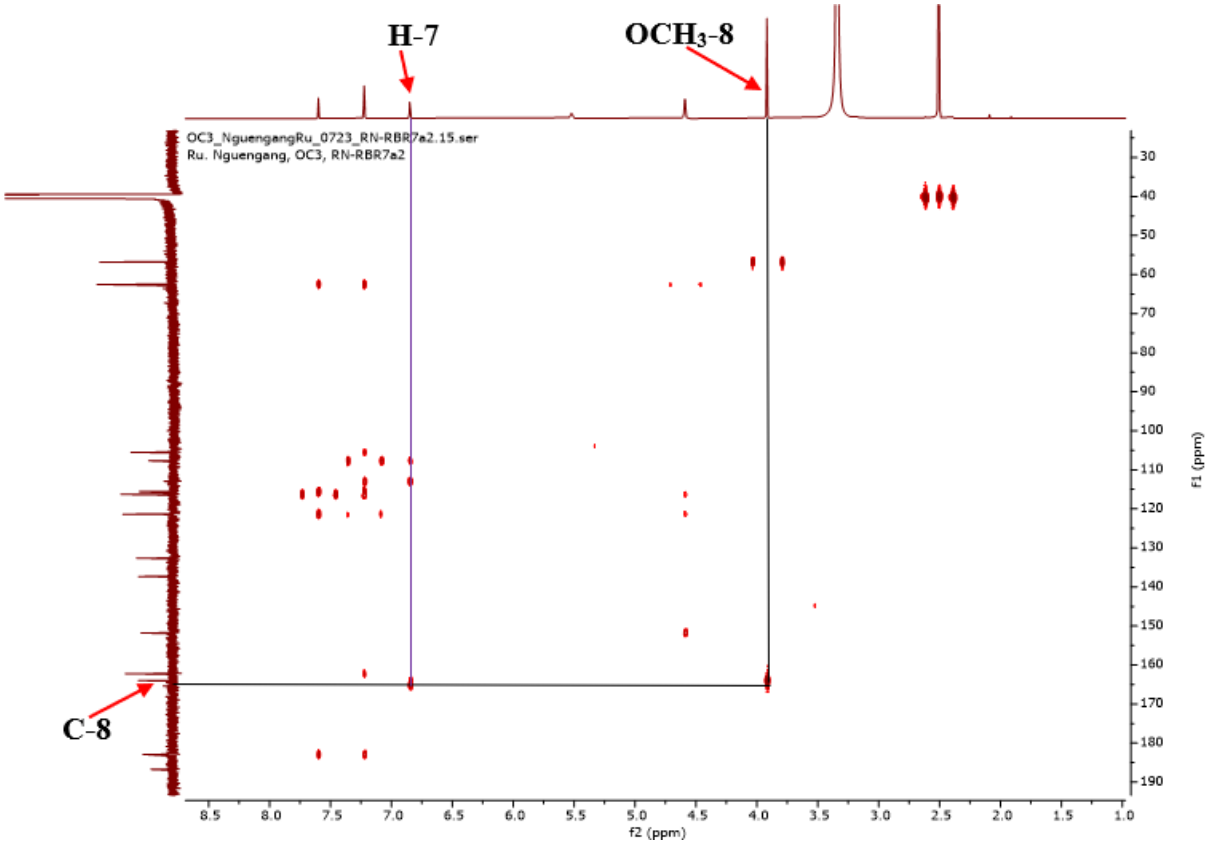

Figure 57: HMBC spectrum of RBR7a2

All these data, compared with those in the literature, led to the identification of RBR7a2 as 3-hydroxymethyl-1,6,8-trihydroxyanthraquinone (questinol) (**121**), previously isolated from Marine-Derived Fungus *Eurotium amstelodami* in lipopolysaccharide-stimulated RAW 264.7 macrophages by Yang and collaborators (2014).

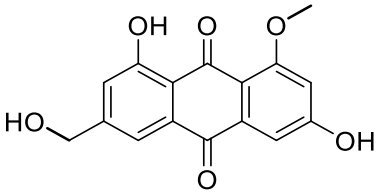

121

Table 28: ^{1}H (600 MHz) and ^{13}C (150 MHz) NMR data of RBR7a2 compared to those of questinol [RMN ^{13}C (100 MHz), RMN ^{1}H (400 MHz)] in DMSO-d_6

	RBR7a2		Questinol (Yang *et al*., 2014)	
Position	δC	δH (m, *J* in Hz)	**δC**	δH (m, *J* in Hz)
1	162.2	-	161.7	-
2	121.4	7.22 (2H, d, 2.0)	120.9	7.20 (1H, d, 1.6)
3	151.8	-	151.2	-
4	116.3	7.60 (1H, br s)	115.8	7.57 (1H, d, 1.6)
4a	132.6	-	132.1	-
5	107.7	7.22 (2H, d, 2.0)	107.2	7.20 (1H, d, 2.3)
6	165.2	-	163.5	-
7	105.5	6.85 (1H, d, 2.3)	105.0	6.83 (1H, d, 2.3)
8	164.0	-	164.8	-
8a	112.9	-	115.1	-
9	186.7	-	186.3	-
9a	115.6	-	112.5	-
10	182.9	-	182.3	-
10a	137.3	-	136.8	-
CH_2O-3	62.5	4.59 (2H, d, 3.9)	62.0	4.58 (2H, s)
OCH_3-6	56.8	3.92 (3H, s)	56.3	3.90 (3H, s)
OH-1	-	13.34 (1H, s)	-	13,31 (1H, s)

II.1.5.4.6. Structural identification of compound RBR10R1

RBR10R1 was obtained as yellow needles in CH_2Cl_2-EtOAc (17:3, v/v). It was soluble in dichloromethane and reacted positively to Bornträger test, characteristic of anthraquinones and quinones.

Its molecular formula, $C_{16}H_{12}O_5$, with eleven degrees of unsaturation, was deduced from the HRESIMS spectrum (Figure 58), which showed the dehydrogenated adduct peak $[M-H]^-$ at *m/z* 283.0608 (calcd for $C_{16}H_{11}O_6$, 283.0612). The mass difference of 14 amu between **RBR3C** and **RBR10R1** suggested the apparition of a CH_2 in **RBR10R1**.

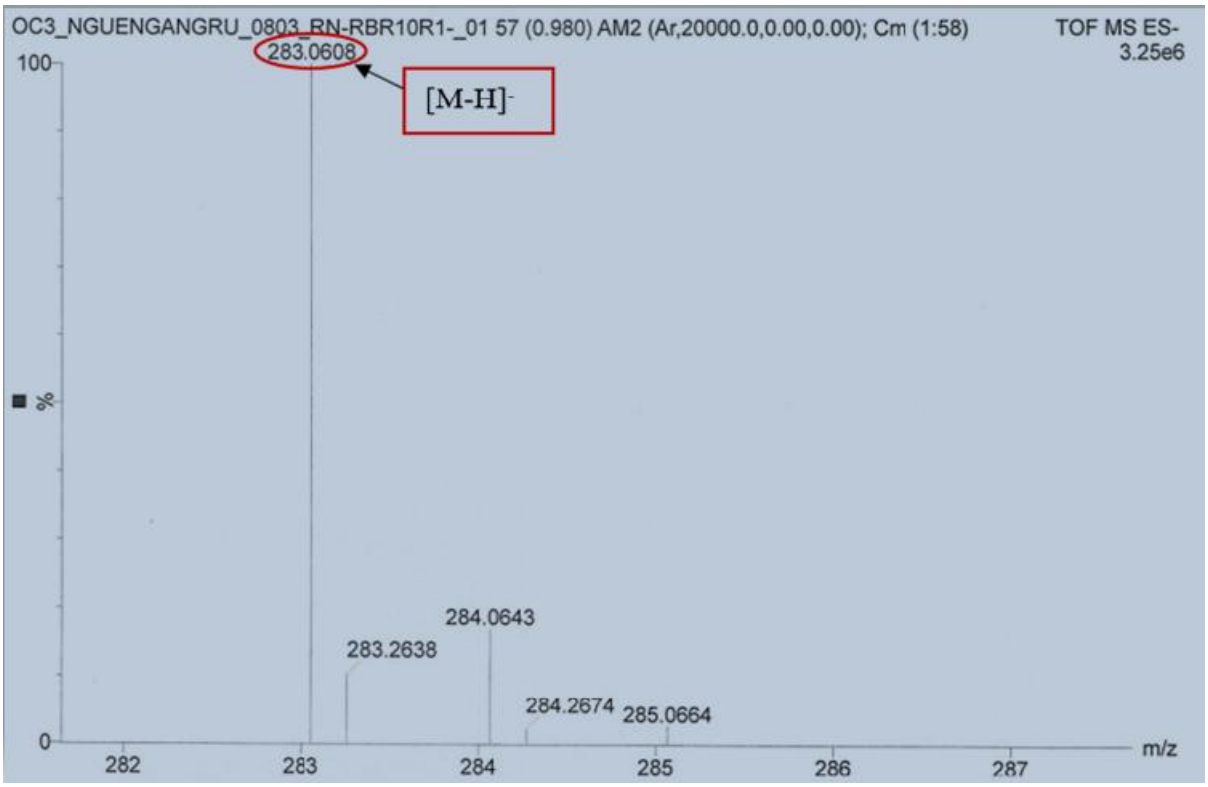

Figure 58: (-) HRESI mass spectrum of RBR10R1

The comparison of the ^{1}H NMR (Figure 59) and ^{13}C NMR (Figure 60) spectra of RBR10R1 with those of RBR3C showed similarities, except the presence of additional signal of one methoxy group. Detailed analysis of the ^{1}H NMR (Figure 59) spectrum of this compound revealed supplementary signal that was assigned to one methoxy group at δ_H 3.91 ppm (3H, s, OCH_3-8) in **RBR10R1** instead of signal of one chelated hydroxy proton at δ_H 12.03 (1H, s, OH-8) (Figure 60).

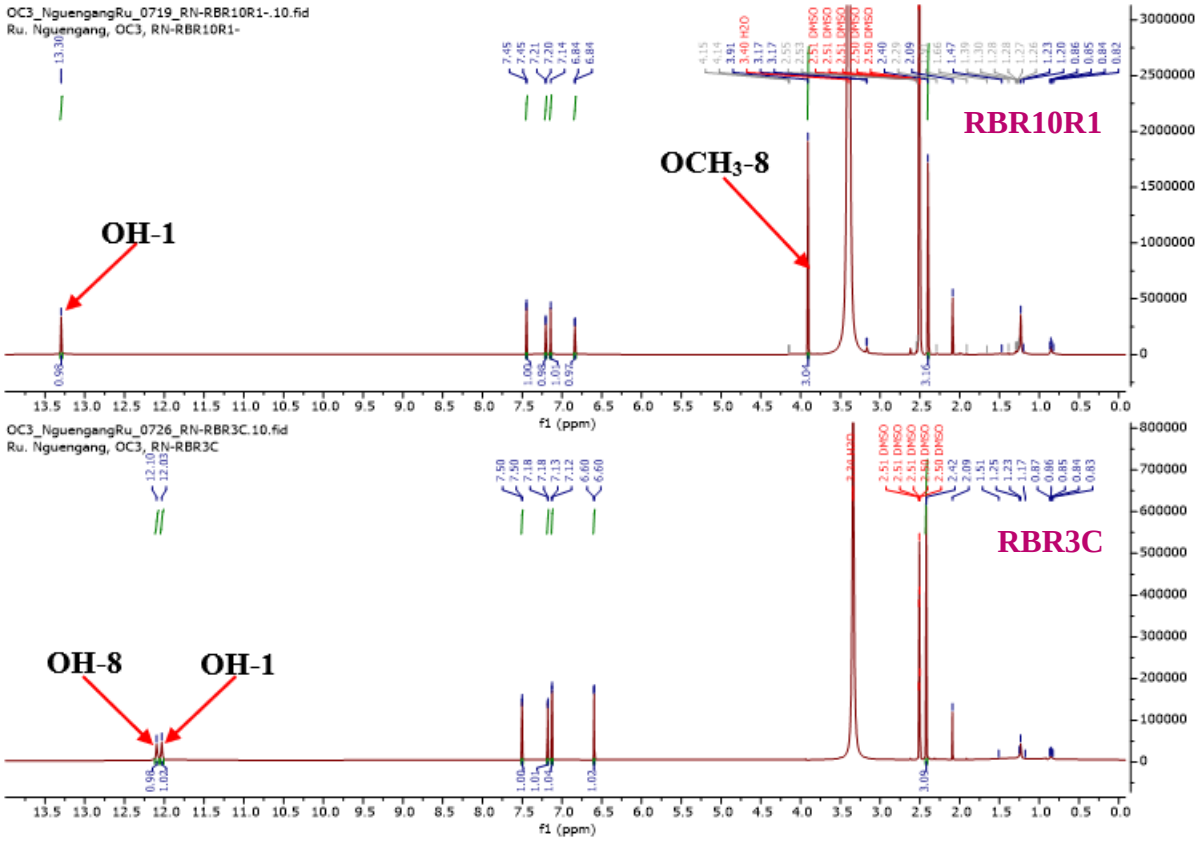

Figure 59: Comparative ^{1}H NMR of RBR3C (DMSO-d_6, 600 MHz) and RBR10R1 (DMSO-d_6, 600 MHz)

The broad band decoupled ^{13}C NMR spectrum (Figure 60) of **RBR10R1** exhibited signals characteristic of emodin. The only difference observed on both spectra was the presence of additional signal of one methoxy group at δ_C 56.8 (3H, s, OCH_3-8) in **RBR10R1** (Figure 60).

In addition, the C-9 had resonance at higher field (δ 186.7) than that of **RBR3C** (δ 190.1) confirming the presence of only one chelated hydroxy group in **RBRR10R1** instead of two (Figure 60).

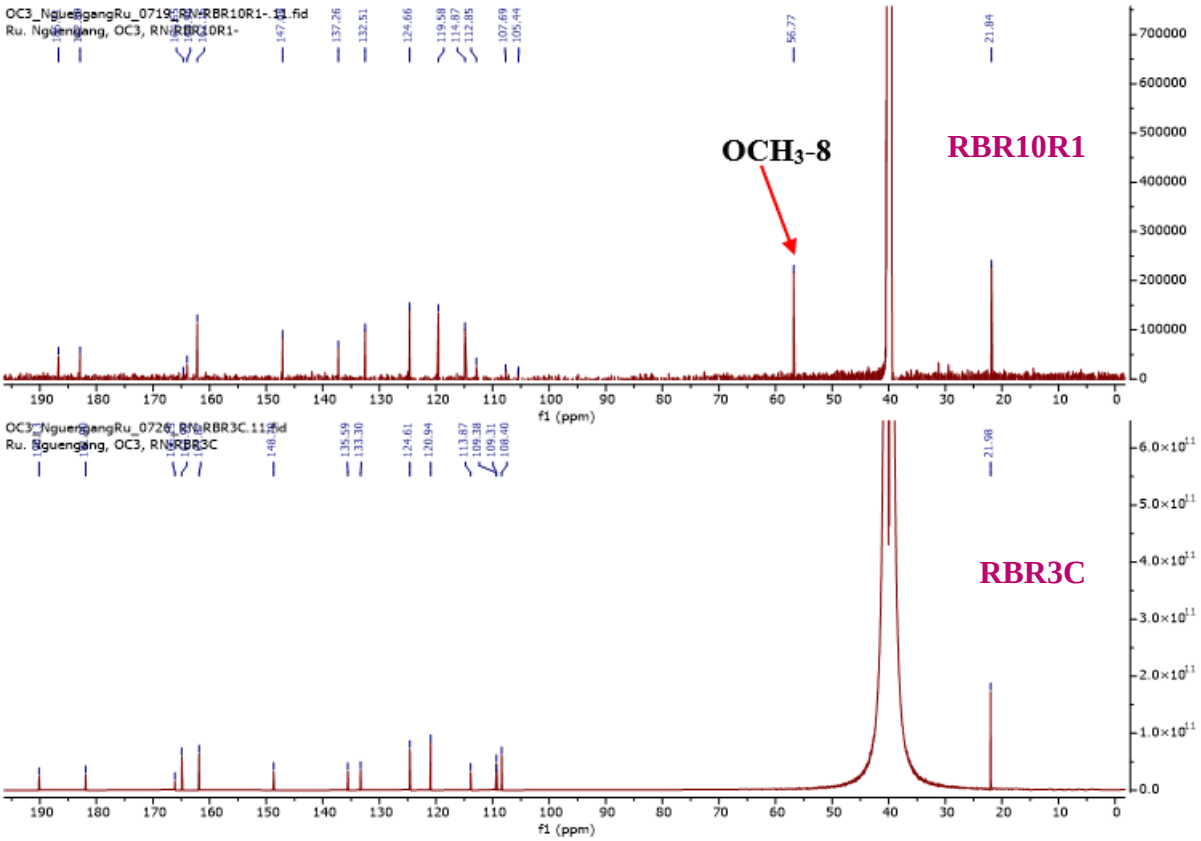

Figure 60: Comparative ^{13}C NMR spectrum of RBR3C and RBR10R1 (DMSO-d_6, 150 MHz)

The location of the methoxy group was determined by the correlations observed on the HMBC spectrum (Figure 40) of RBR10R1 between the proton OCH_3-8 (δ_H 3:91, s, 3H) and C-8 (δ_C 163.9) and proton H-7 [δ_H (6.84, 1H, d, J = 2.2 Hz)] and C-8 (δ_C 163.9) (Figure 61).

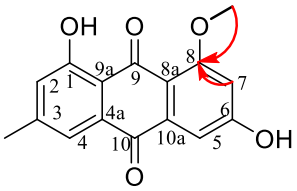

Scheme 18: Key HMBC correlations of RBR10R1

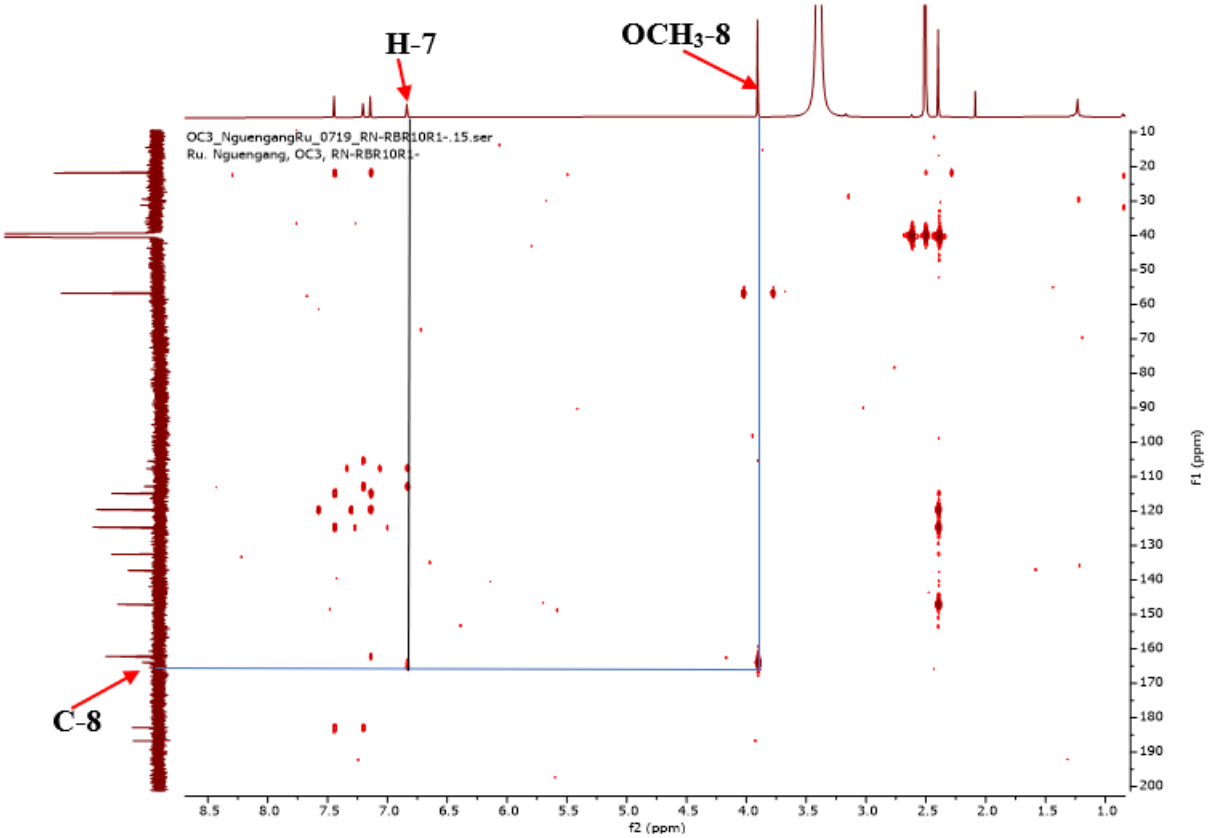

Figure 61: HMBC spectrum of RBR10R1

Based on the above mentionned data, **RBR10R1** was identified as 1,6-dihydroxy-8-methoxy-3-methylanthraquinone (questin) (**122**), previously isolated from deep sea fungus *Emericella* sp SCSIO 05240 by Fredimoses *et al*., (2019).

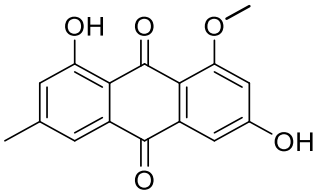

122

Table 29: ^{1}H (600 MHz) and ^{13}C (150 MHz) NMR data of RBR10R1 compared to questin [^{13}C (125 MHz), ^{1}H (500 MHz)] both in DMSO-d_6

	RBR10R1		Questin (Fredimoses *et al*., 2019)	
Position	δ_C	δ_H **(m, *J* in Hz)**	δ_C	δ_H **(m, *J* in Hz)**
1	162.1	-	162.2	-
2	124.7	7.14 (1H, br, s)	124.6	7.14 (1H, d, 1.5)
3	147.1	-	146.7	-
4	119.6	7.45 (1H, d, 1.6)	119.6	7.45 (1H, d, 1.5)
4a	132.5	-	132.5	-
5	107.7	7.21 (1H, d, 2.2)	107.5	7.22 (1H, d, 2.0)
6	164.7	-	164.6	-
7	105.4	6.84 (1H, d, 2.2)	105.5	6.86 (1H, d, 2.0)
8	163.9	-	163.9	-
8a	112.8	-	112.5	-
9	186.7	-	186.9	-
9a	114.9	-	114.9	-
10	182.9	-	182.6	-
10a	137.3	-	137.3	-
CH_3-3	21.8	2.40 (3H, s)	21.8	2.40 (3H, s)
OCH_3-8	56.8	3.91 (3H, s)	56.8	3.92 (3H, s)
OH-1	-	13.30 (1H, s)	-	13.26 (1H, s)
OH-6	-	-	-	-

II.1.5.4.7. Structural identification of compound RBR147-19

RBR147-19 was obtained as yellow finely divided solid in CH_2Cl_2-EtOAc (1:1, v/v). It was soluble in dichloromethane and reacted positively to Bornträger test, characteristic of anthraquinones and quinones.

Its molecular formula, $C_{15}H_8O_7$, implying twelve degrees of unsaturation, was deduced from the HRESIMS spectrum (Figure 62), which showed the dehydrogenated adduct peak [M-H]$^-$ at *m/z* 299.0198 (calcd for $C_{16}H_{11}O_6$, 299.0197).

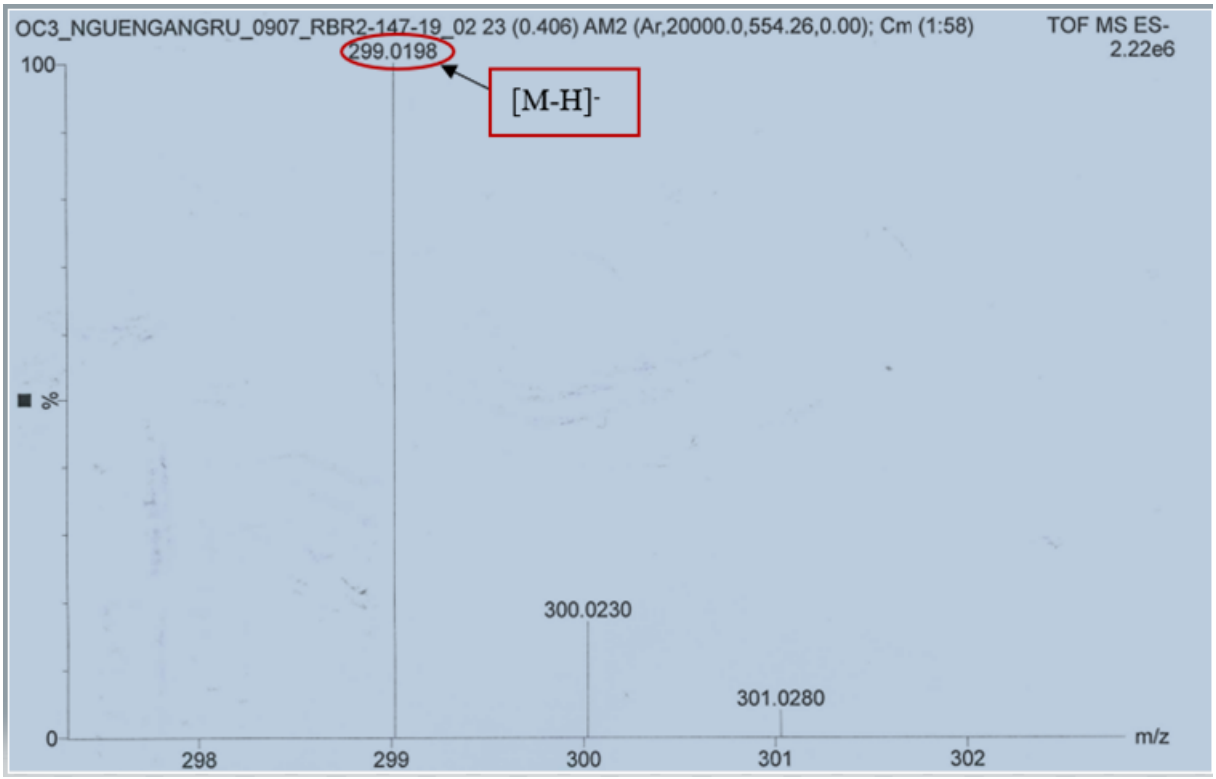

Figure 62: (-) HRESI mass spectrum of RBR147-19

The ^{1}H NMR spectrum of **RBR147-19** was very close to that of **RBR3C** (Figure 63). The only difference between the ^{1}H NMR of **RBR147-19** and that of **RBR3C** was the absence of one singlet signal of methyl group at δ_H 2.42 ppm (3H, s, -CH_3-3) in RBR147-19 (Figure 63).

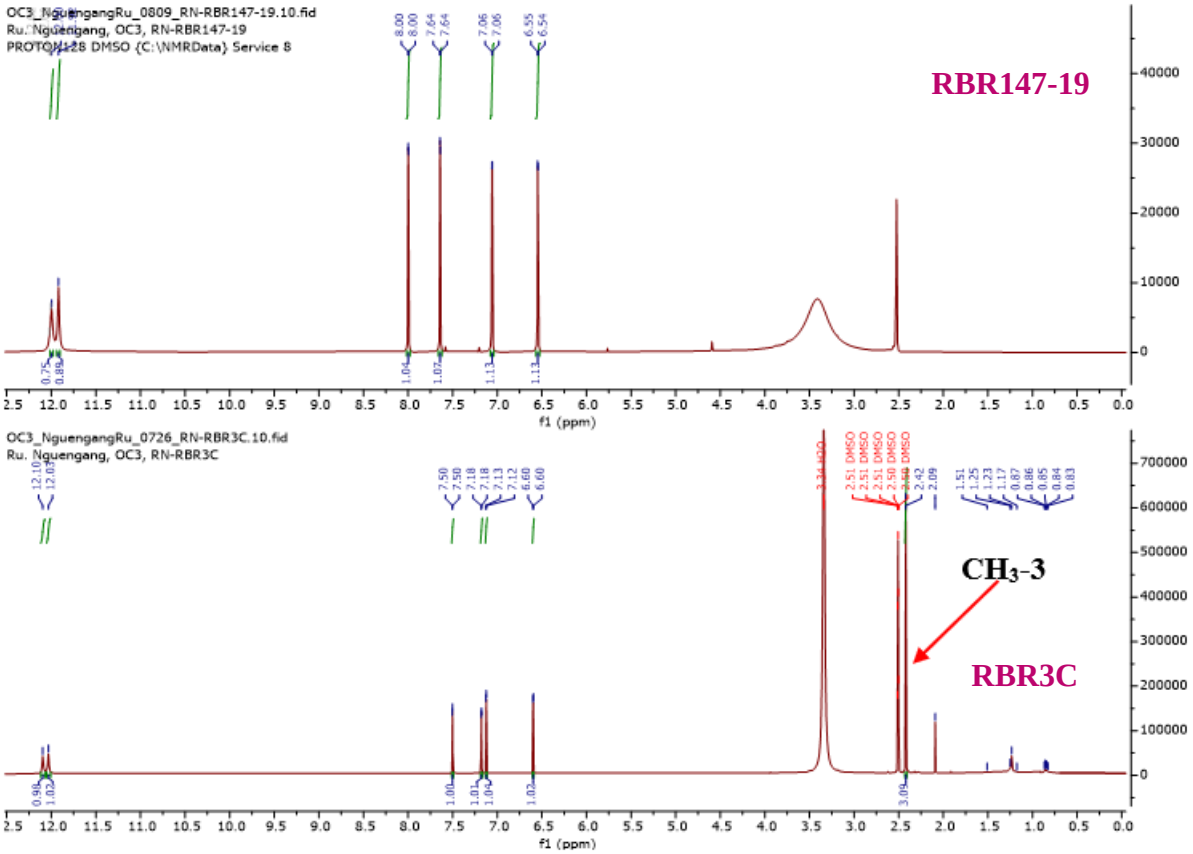

Figure 63: Superposition of ^{1}H NMR of RBR3C (DMSO-d_6, 600 MHz) and RBR147-19 (DMSO-d_6, 600 MHz).

The broad band decoupled ^{13}C NMR spectrum (Figure 64) of RBR147-19 exhibited signals characteristic of emodin:

- Ten quaternary carbons at δ_C 166.4 (C-6), 165.1 (C-8), 161.5 (C-1), 137.9 (C-3), 135.3 (C-10a), 133.8 (C-4a), 118.6 (C-9a), 109.6 (C-8a) including two carbonyls at δ_C 189.6 (C-9) and 181.0 (C-10);
- Four methine groups at δ_C 124.6 (C-2), 119.3 (C-4), 109.6 (C-5) and 108.4 (C-7);
- One methyl group at δ_C 21.8 (3-CH_3).

The only difference was the presence of signal of one carboxylic group at δ_C 165.8 (3-COOH) in RBR147-19 instead of signal of one methyl group at δ_C 22.0 (3H, s, 3-CH3) (Figure 64).

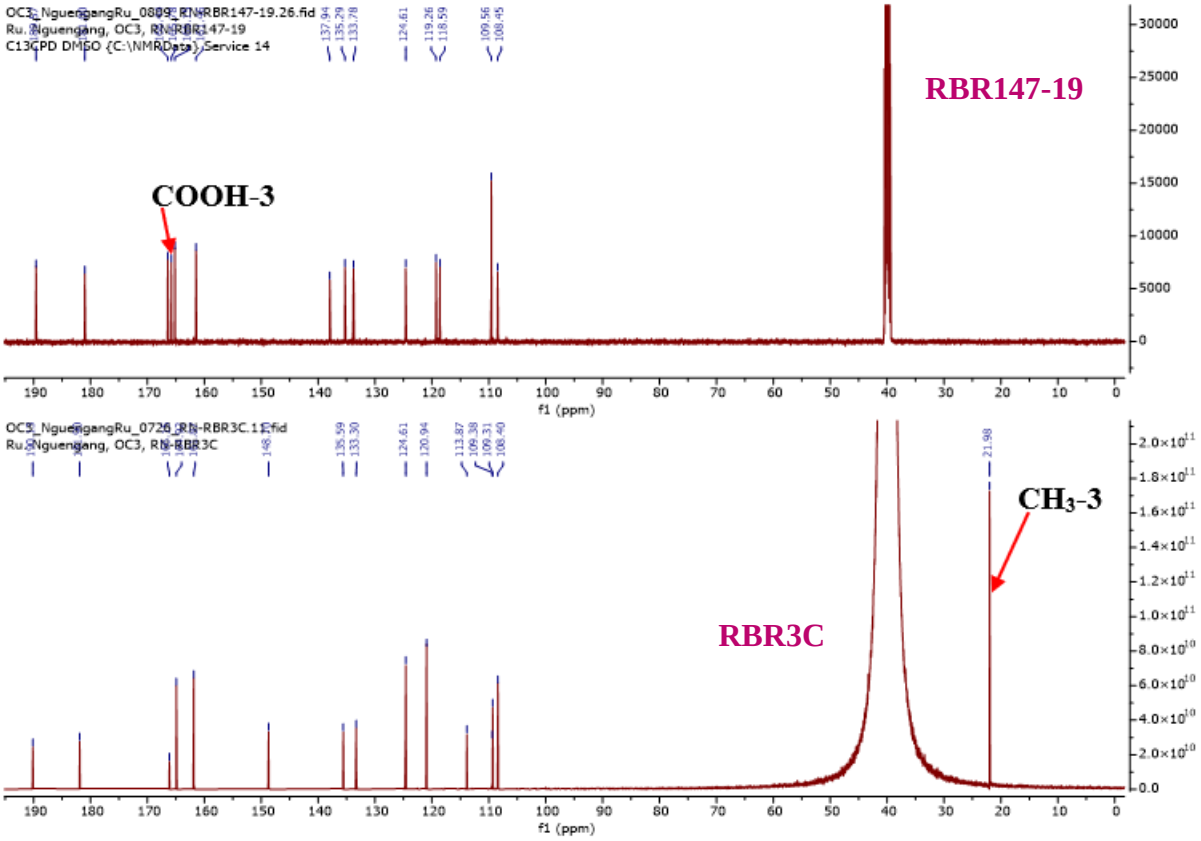

Figure 64: Comparative ^{13}C NMR spectrum of RBR3C and RBR147-19 (DMSO-d_6, 150 MHz).

The location of the carboxylic group was determined by the correlation observed on the HMBC spectrum (Figure 65) of **RBR147-19** between the proton H-2 (δ_H 7.64, 1H, d, J = 1.6 Hz) and H-4 (δ_H 8.00, 1H, d, J = 1.6 Hz) with the carboxyl group at δ_C 165.8.

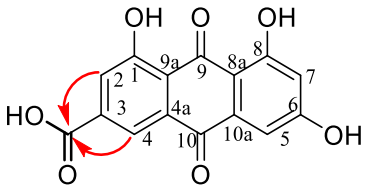

Scheme 19: Key HMBC correlations of RBR147-19

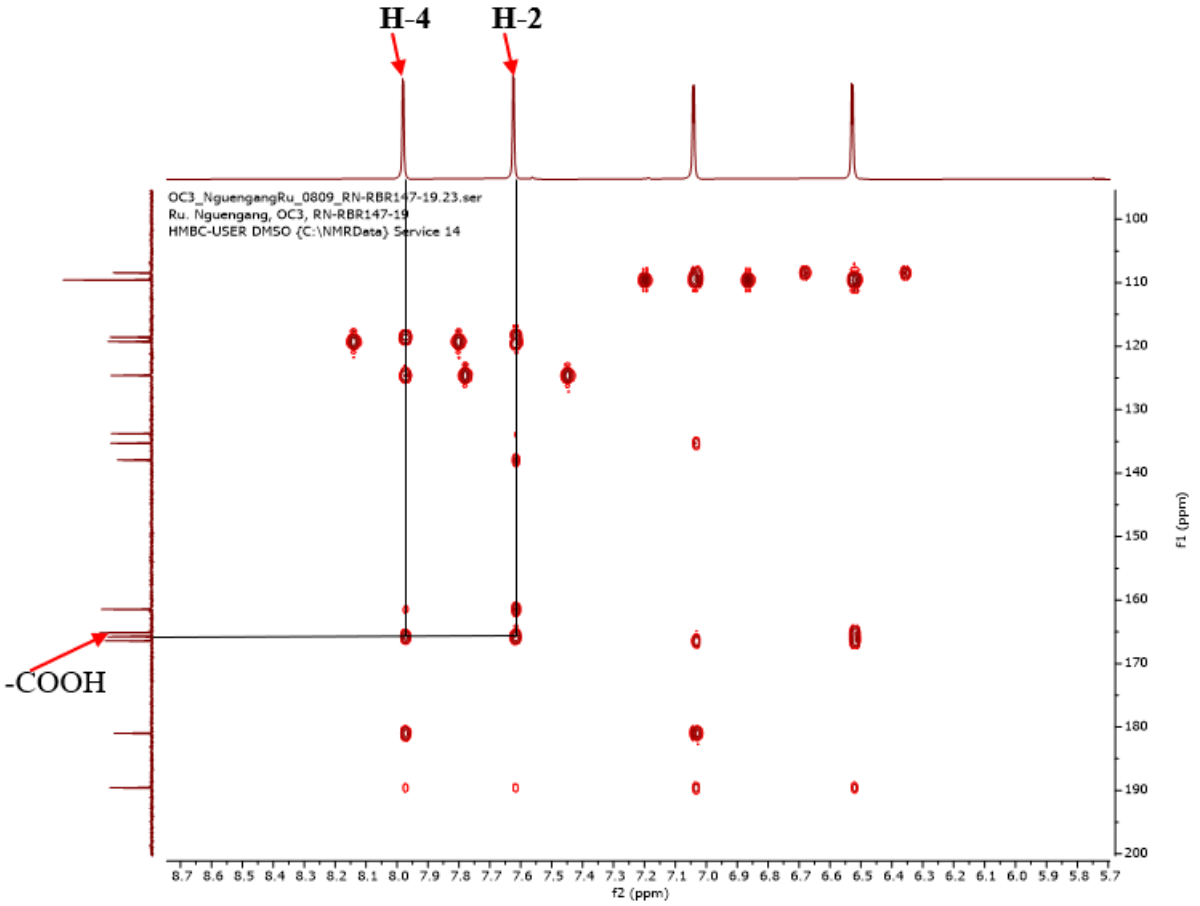

Figure 65: HMBC spectrum of RBR147-19

The above data were in agreement compared with those described in the literature for 1,6,8-trihydroxy-9,10-dioxo-3-anthracenecarboxylic acid (emodic acid) (**123**), previously isolated from microbial extracts for tyrosine kinnase inhibitors by Alvi and collaborators (1997).

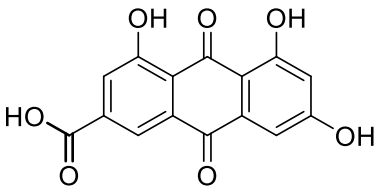

123

Table 30: ^{1}H (600 MHz) and ^{13}C (150 MHz) NMR data of RBR147-19 compared to those of emodic acid [^{13}C (125 MHz), ^{1}H (500 MHz)] both in DMSO-d_6

	RBR147-19		Emodic acid (Alvi *et al*., 1997)	
Position	δ_C	δ_H **(m, *J* in Hz)**	δ_C	δ_H **(m, *J* in Hz)**
1	161.5	-	161.0	-
2	124.6	7.64 (1H, d, 1.6)	124.1	7.60 (1H, d, 1.5)
3	137.9	-	137.4	-
4	119.3	8.00 (1H, d, 1.6)	118.8	7.95 (1H, d, 1.5)
4a	133.8	-	134.8	-
5	109.6	7.06 (1H, d, 2.3)	109.1	7.01 (1H, d, 2.3)
6	166.4	-	166.0	-
7	108.4	6.54 (1H, d, 2.4)	108.0	6.50 (1H, d, 2.3)
8	165.1	-	164.7	-
8a	109.6	-	109.0	-
9	189.6	-	189.1	-
9a	118.6	-	118.1	-
10	181.0	-	180.5	-
10a	135.3	-	133.3	-
COOH-3	165.8		165.3	-
OH-1	-	11.92 (1H, s)	-	11.80 (1H, s)
OH-8	-	12.00 (1H, s)	-	11.96 (1H, s)

II.1.5.4.8. Structural identification of compound RBR15

RBR15 was obtained as yellow needles in CH_2Cl_2-EtOAc (1:1, v/v). It was soluble in dichloromethane and reacted positively to Bornträger test, characteristic of anthraquinones and quinones.

Its molecular formula, $C_{15}H_{10}O_5$, implying eleven degrees of unsaturation, was deduced from the combination of the data from the ESIMS spectrum (Figure 66), which showed the dehydrogenated adduct peak $[M-H]^-$ at *m/z* 269.112 to those of the NMR spectra (Figure 67 to 69). This mass was identical to that of **RBR3C** suggesting that **RBR15** is an isomer of **RBR3C**.

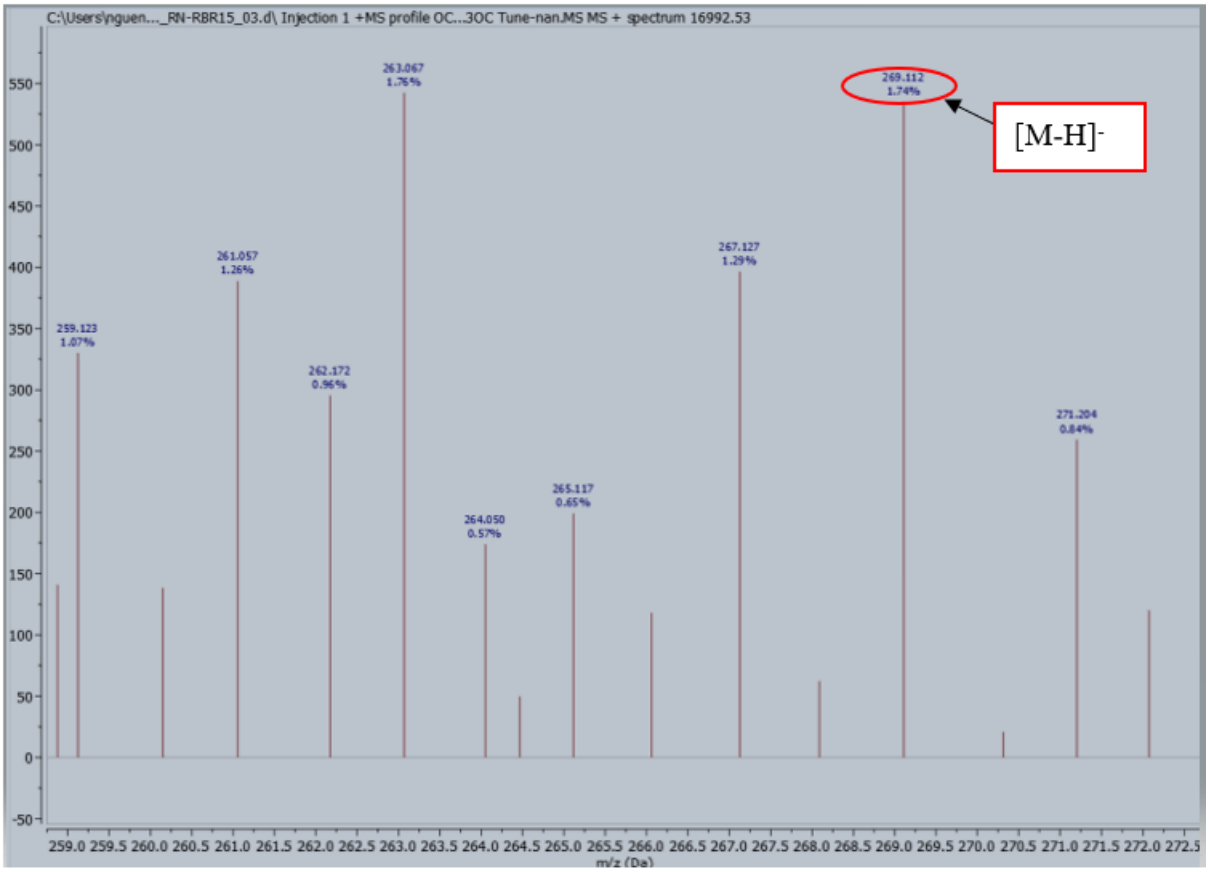

Figure 66: (-) ESI mass spectrum of RBR15

The comparison of the ^{1}H NMR (Figure 67) and ^{13}C NMR spectra (Figure 68) of RBR15 to that of **RBR3C** revealed many similarities. The only difference between the ^{1}H NMR of RBR15 and that of RBR3C was the absence of the signal of one of the chelated hydroxy protons and the appearance of that of a methyl group at δ_H 2.71(3H, s) in **RBR15** (Figure 67).

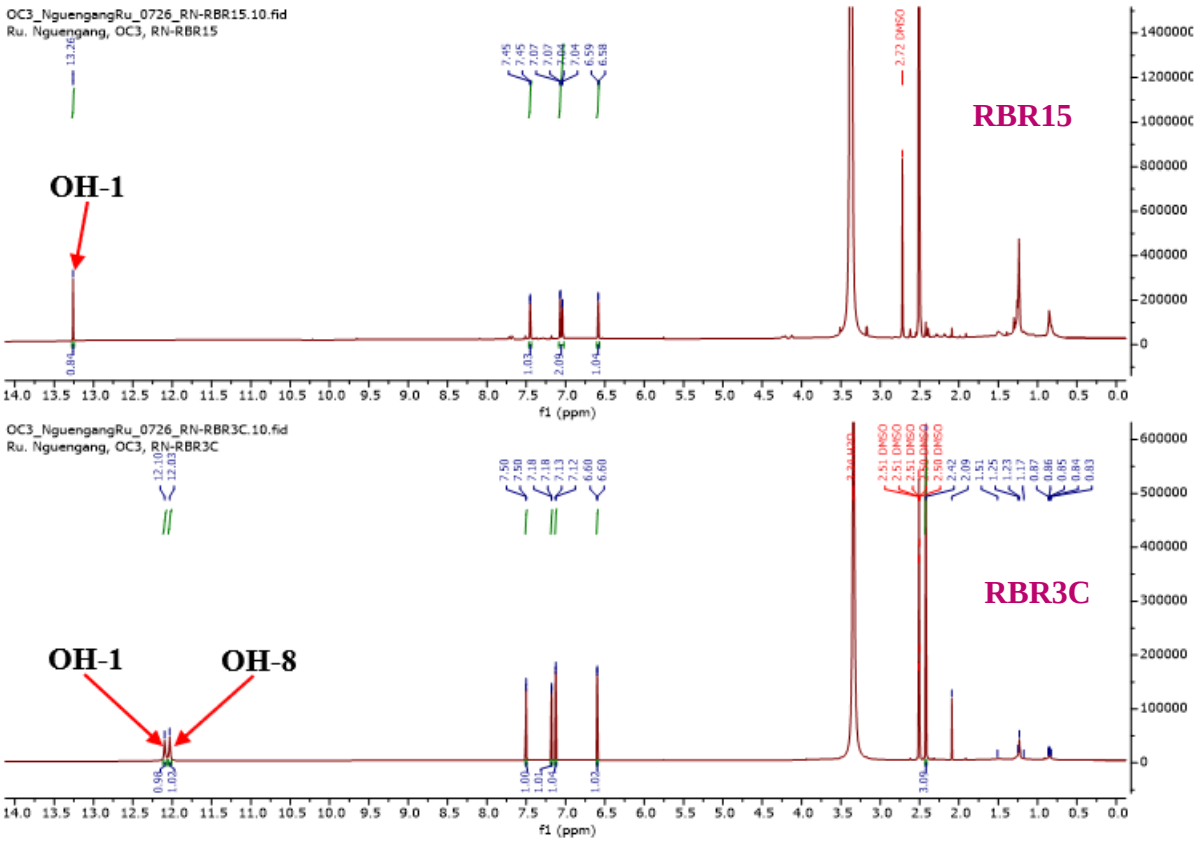

Figure 67: Comparative ^{1}H NMR of RBR3C and RBR15 (DMSO-d_6, 600 MHz)

This suggestion was confirmed after examination of the broad band decoupled ^{13}C spectrum (Figure 68), which showed signals characteristic of emodin.

However, significant differences were recognized in the signals of C-3 and C-8 carbons. In fact, the C-3 here resonated at lower field (δ_C 163.6) than that of RBR3C (δ_C 148.7) while the C-8 here resonated at higher field (δ_C 145.7) than that of RBR3C (δ_C 164.9).

In addition, the C-9 had resonance at higher field (δ_C 188.5) than that of RBR3C (δ_C 190.1) confirming the presence of only one chelated hydroxy group in RBR15 instead of two (Figure 68).

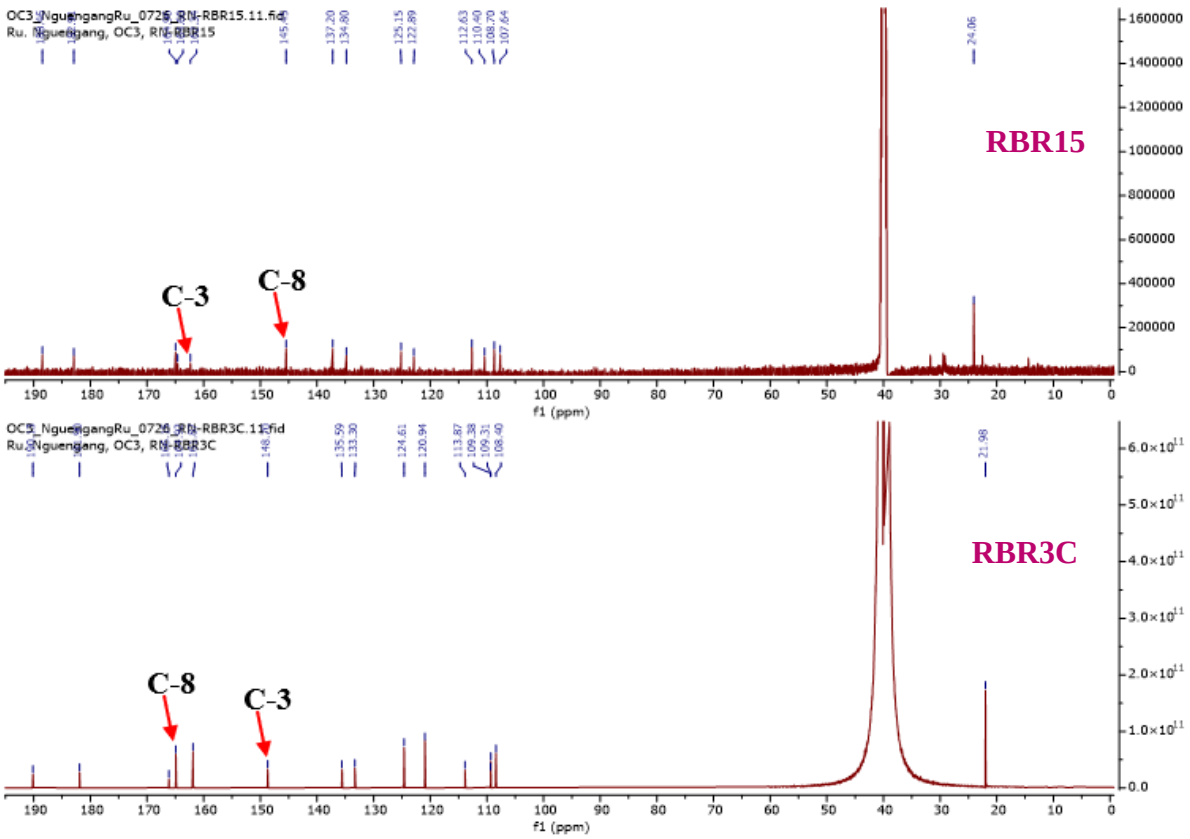

Figure 68: Comparative ^{13}C NMR spectrum of RBR3C (DMSO-d_6, 150 MHz) and RBR15 (DMSO-d_6, 150 MHz)

The location of the methyl group was determined by the correlation observed on the HMBC spectrum (Figure 69) of RBR15 between the proton CH_3-8 (δ_H 2.71, s, 3H) and carbons C-7 (δ_C 125.2), C-8 (145.4) and C-8a (122.9).

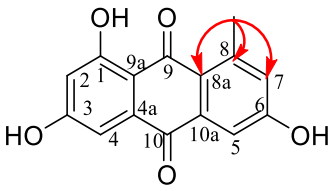

Scheme 20: Key HMBC correlations of RBR15

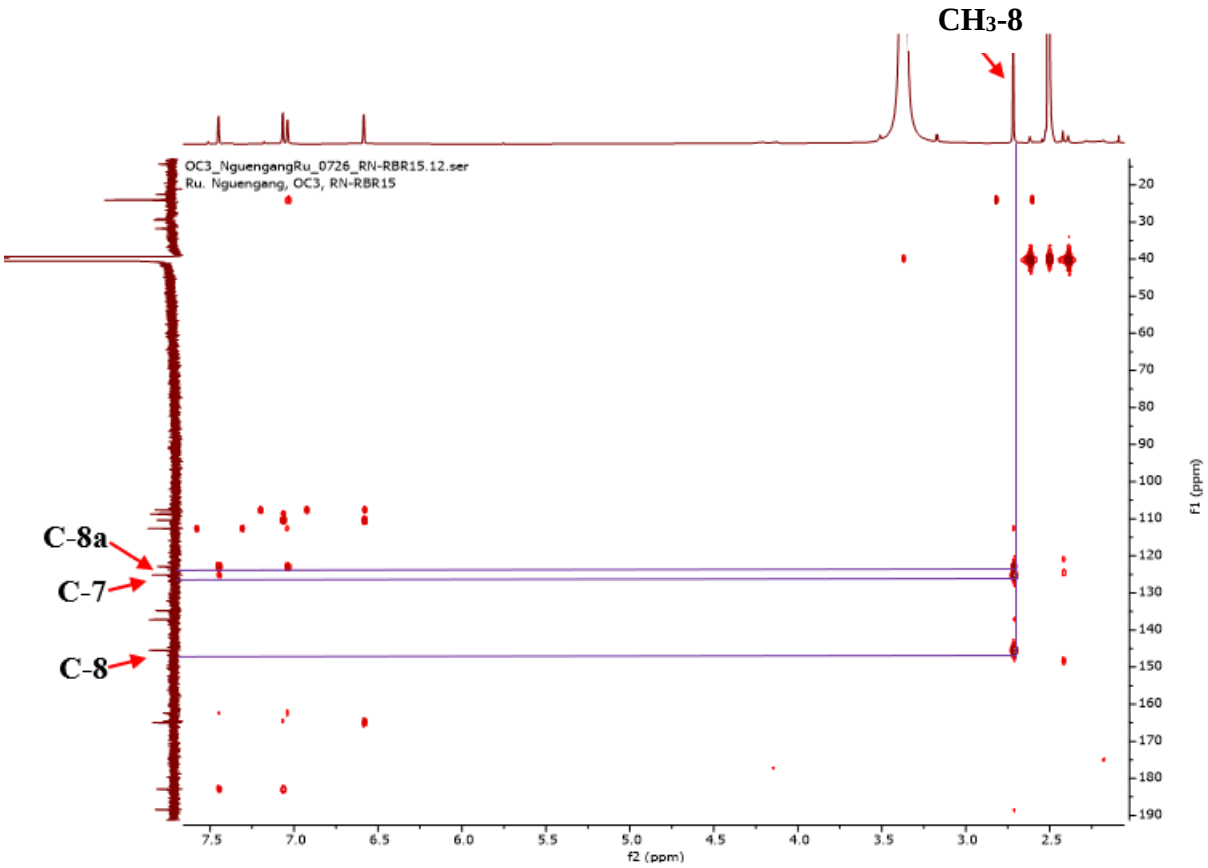

Figure 69: HMBC spectrum of RBR15

All these data were similar to those described in the literature for 1,3,6-trihydroxy-8-methyl-anthraquinone (**124**), previously isolated from *Gladiolus psittascinus* by Ngamba and collaborators (2007).

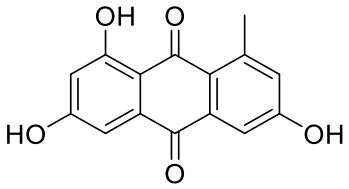

124

Table 31: ^{1}H (600 MHz) and ^{13}C (150 MHz) NMR data of RBR147-19 in DMSO-d_6 compared to those of emodic acid [^{13}C (75 MHz), ^{1}H (300 MHz) CD_3COCD_3]

	RBR15		1,3,6-trihydroxy-8-methyl-anthraquinone (Ngamba *et al.*, 2007)	
Position	δ_C	δ_H **(m, *J* in Hz)**	δ_C	δ_H **(m, *J* in Hz)**
1	165.0	-	164.9	-
2	108.7	7.04 (1H, d, 2.6)	108.2	6.64 (1H, d, 2.4)
3	164.6	-	163.9	-
4	107.6	7.45 (1H, d, 2.6)	106.9	7.19 (1H, d, 2.4)
4a	137.2	-	134.9	-
5	112.6	7.06 (1H, d, 2.4)	112.2	7.57 (1H, d, 2.5)
6	162.3	-	161.7	-
7	125.2	6.58 (1H, d, 2.4)	124.5	7.09 (1H, d, 2.4)
8	145.4	-	145.4	-
8a	122.9	-	123.6	-
9	188.5	-	188.6	-
9a	110.4	-	110.7	-
10	182.9	-	182.4	-
10a	134.8	-	134.9	-
CH_3-3	24.1	2.71(3H, s)	23.2	2.80 (3H, s)
OH-1	-	13.26 (1H, s)	-	13.30 (1H, s)

II.1.5.4.9. Structural identification of compound RBR95-35b

RBR95-35b was obtained as yellow finely divided solid in CH_2Cl_2-EtOAc (1:1, v/v). It was soluble in dichloromethane and reacted positively to Bornträger test, characteristic of anthraquinones and quinones.

Its molecular formula, $C_{21}H_{20}O_{10}$, suggesting twelve degrees of unsaturation was deduced from the combination of the data from the ESIMS spectrum (Figure 70), which showed the dehydrogenated adduct peak $[M-H]^-$ at *m/z* 430.923 with those of the NMR spectra (Figure 71 to 73).

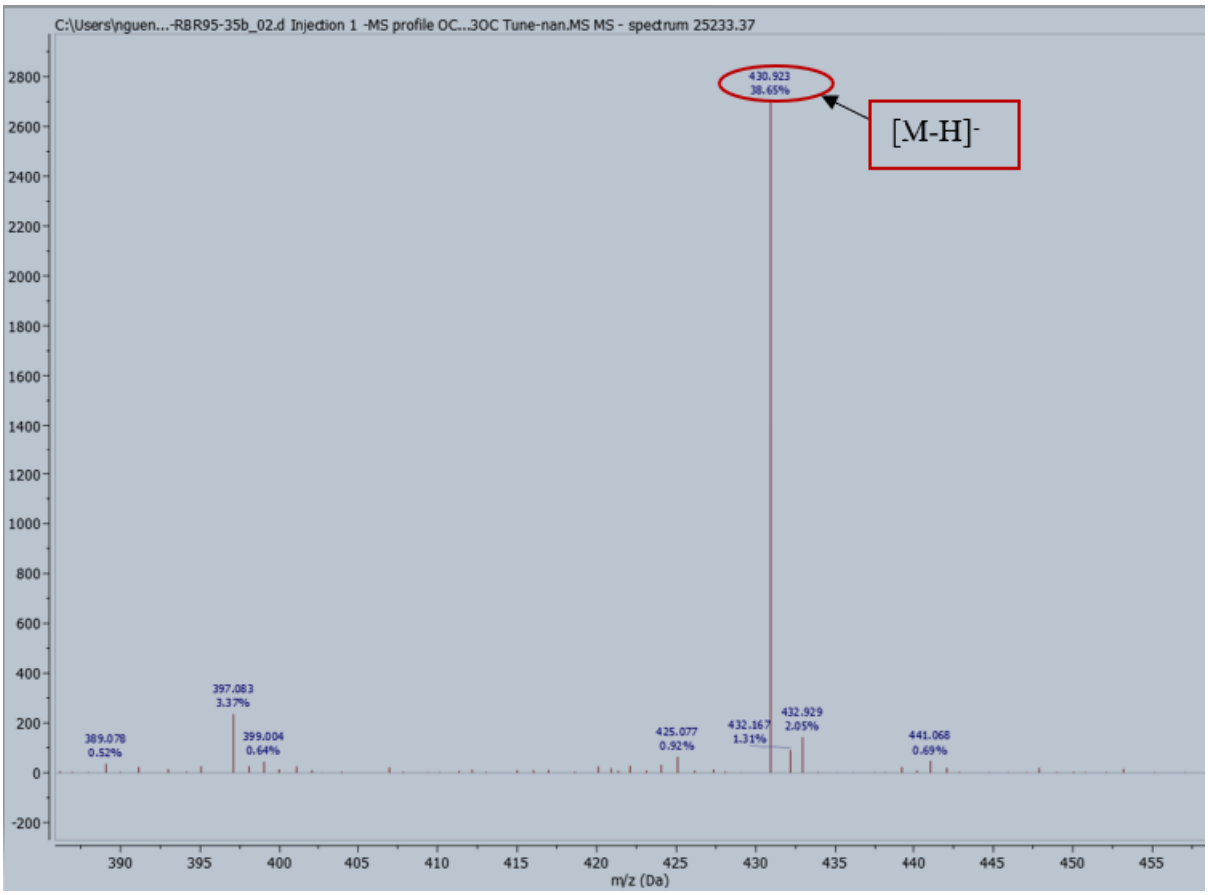

Figure 70: (-) ESI mass spectrum of RBR95-35b

The ^{1}H NMR spectrum of **RBR95-35b** was very close to that of **RBR3C** (Figure 71) and exhibited resonances of four doublets of one proton each at δ_H 7.47 (1H, d, J = 2.4 Hz, H-4), 7.29 (1H, d, J = 2.4 Hz, H-5), 7.17 (1H, m, H-2) and 7.01 (1H, d, J = 2.4 Hz, H-7) corresponding to two couples of *meta* coupled aromatic protons. The only difference between the ^{1}H NMR of **RBR95-35b** and that of **RBR3C** was the presence of an anomeric proton at δ_H 5.06 (1H, d, J = 7.7 Hz, H-1′) and the other proton signals of the sugar moiety at δ_H 5.06-3.25, indicating the presence of sugar moiety attached to one of the hydroxy groups of emodin in RBR95-35b (Figure 71). The β-configuration of the sugar moiety was deduced based on the higher value of its coupling constant.

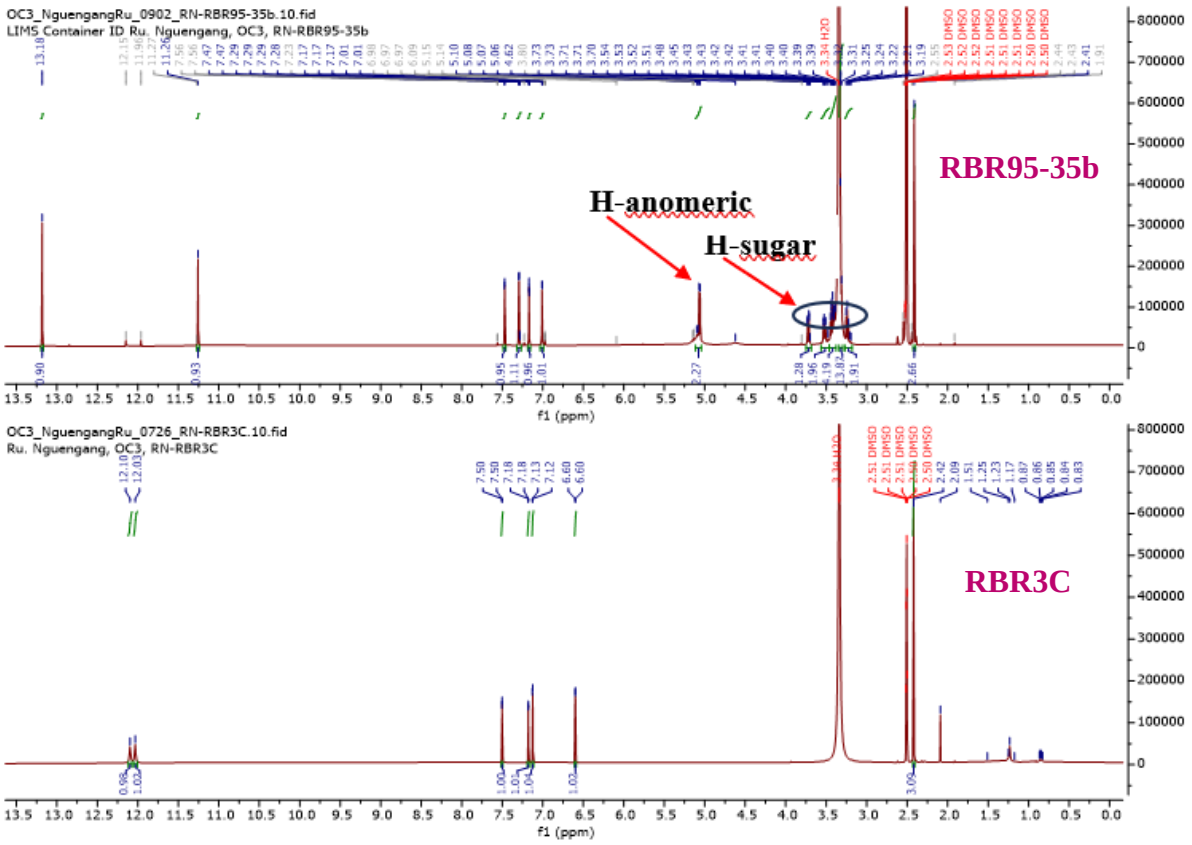

Figure 71: Comparative ^{1}H NMR of RBR3C and RBR95-35b (DMSO-d_6, 600 MHz).

This suggestion was confirmed by the broad band decoupled ^{13}C spectrum (Figure 72), which showed signals characteristic of emodin.

The only difference was the resonances of carbons of the glucose unit. In fact, we observed additional signals of a glucosyl anomeric carbon at δ_C 101.2 (C-1′) and five other glycosyl carbon at δ_C 77.7 (C-5′), 76.9 (C-3′), 73.7 (C-2′), 69.9 (C-4′) and 61.0 (C-6′).

Comparison of the chemical shifts of the sugar with those of the literature allowed its identification to a β-glucopyranosyl unit.

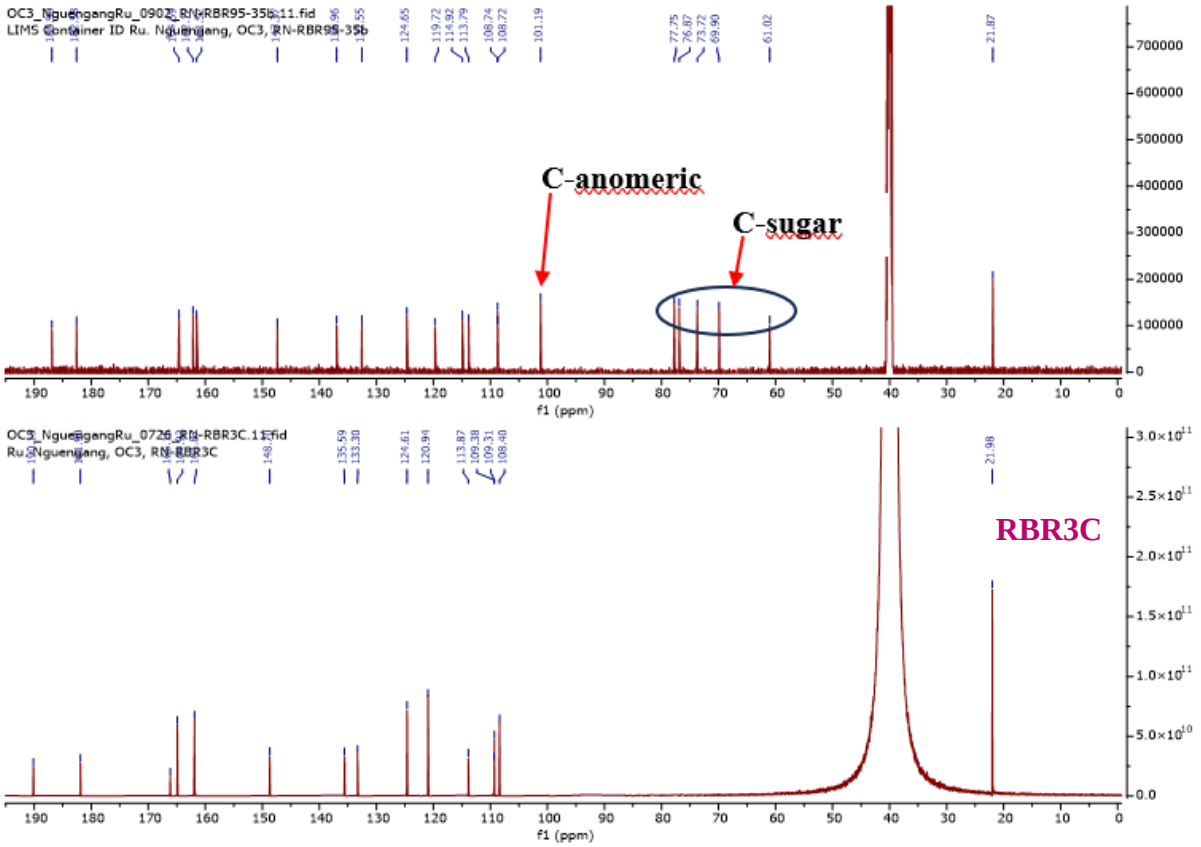

Figure 72: Comparative ^{13}C NMR spectrum of RBR3C and RBR95-35b (DMSO-d_6, 150 MHz)

The location of the β-glucopyranosyl unit was determined by the correlations observed on the HMBC spectrum (Figure 73) of **RBR95-35b** between its anomeric proton at δ_H 5.06 (1H, d, J = 7.7 Hz, H-1′) and carbons C-6 (δ_C 161.5) and proton H-7 (δ_H 7.01, 1H, d, J = 2.4 Hz) and C-6 (161.5).

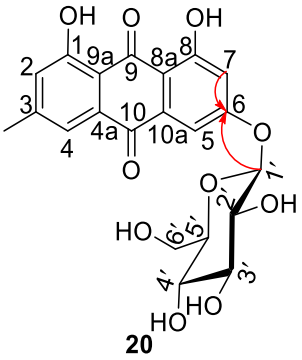

20

Scheme 21: Key HMBC correlations of RBR95-35b

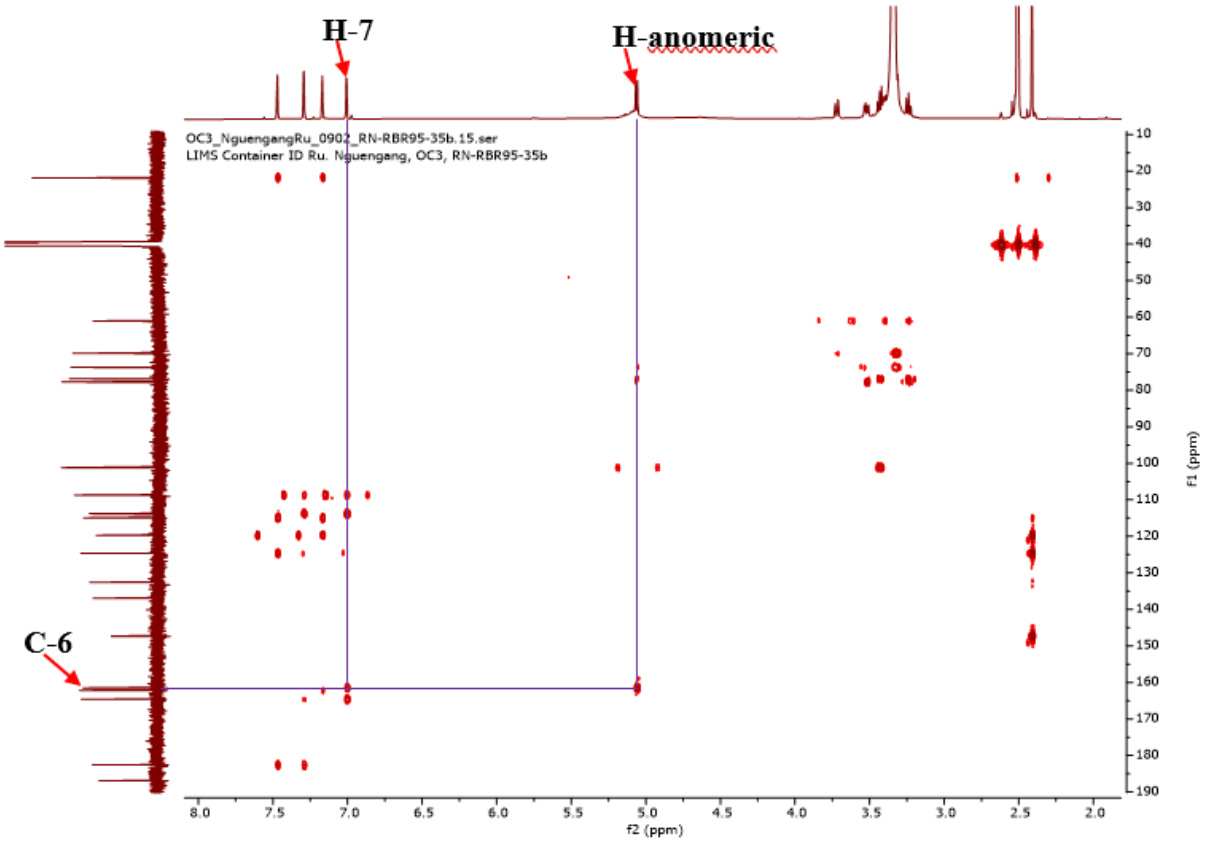

Figure 73: HMBC spectrum of RBR95-35b

The structure **RBR95-35b** was assigned as emodin-6-*O*-*β*-D-glucopyranoside (**125**), previously isolated from roots of *Rumex patientia* by Demirezer and collaborators (2001).

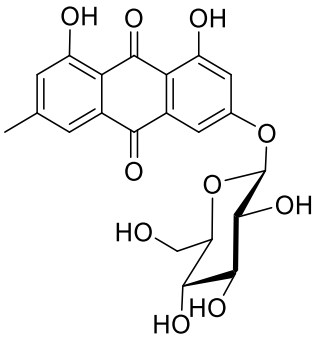

125

Table 32: ^{1}H (600 MHz) and ^{13}C (150 MHz) NMR data of RBR95-35b in DMSO-d_6 compared to emodin-6-*O*-*β*-D-glucoside [^{13}C (75.5 MHz), ^{1}H (300 MHz), DMSO-d_6]

	RBR95-35b		emodin-6-*O*-*β*-D-glucoside (Demirezer *et al.*, 2001)	
Position	δ_C	δ_H **(m, *J* in Hz)**	δ_C	δ_H **(m, *J* in Hz)**
1	162.2	-	161.7	-
2	124.7	7.17 (1H, m)	124.1	7.17 (1H, bs)
3	147.4	-	147.3	-
4	119.7	7.47 (1H, d, 2.4)	119.6	7.50 (1H, bs)
4a	137.0	-	132.2	-
5	107.8	7.29 (1H, d, 2.4)	112.1	7.87 (1H, d, 2.1)
6	161.5	-	159.9	-
7	108.7	7.01 (1H, d, 2.4)	111.9	7.33 (1H, d, 2.1)
8	164.6	-	159.7	-
8a	113.8	-	115.7	-
9	186.9	-	186.8	-
9a	114.9	-	114.6	-
10	182.6	-	182.0	-
10a	132.6	-	135.9	-
CH_3-3	21.9	2.41 (3H, s)	21.38	2.42 (3H, s)
OH-1	-	13.18 (1H, s)	11.5	-
OH-8	-	11.26 (1H, s)	11.3	-
Glc		5.06-3.25		5.07-3.73
1′	101.2	-	100.7	
2′	73.7	-	73.4	
3′	76.9	-	76.6	-
4′	69.9	-	69.7	
5′	77.7	-	77.3	
6′	61.0	-	60.4	

II.1.5.4.10. Structural identification of compound RBR95-23a/b

RBR95-23a/b was obtained as yellow finely divided solid in EtOAc-MeOH (4:1, v/v). It was soluble in dichloromethane and reacted positively to the Bornträger test, characteristic of anthraquinones and quinones.

Its molecular formula, $C_{21}H_{20}O_9$, implying twelve degrees of unsaturation, was deduced from the combination of the data from the ESIMS spectrum (Figure 74) which showed the sodium adduct peak $[M+Na]^+$ at *m/z* 439.1 with those of the NMR spectra (Figure 75 to 77).

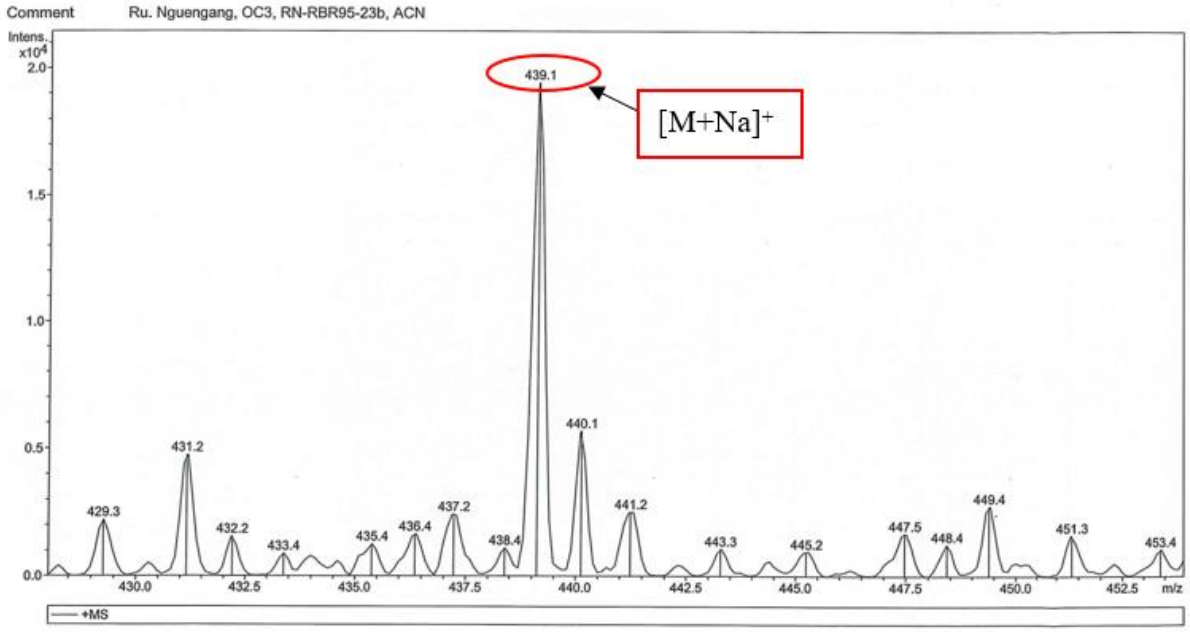

Figure 74: (+) ESI mass spectrum of RBR95-23a/b

It was shown to be a mixture of two anthraquinone glycosides **RBR95-23a** and **RBR95-23b** (1:2) from the interpretation of the NMR data (Figure 75 to 77). The ^{1}H- and ^{13}C-NMR spectra showed a set of duplicated signals corresponding to the common parts of the molecules with some significant differences observed, especially for signals around C-6 (Table 11).

The ^{1}H NMR spectrum of **RBR95-23a/b** was very close to that of **RBR95-35b** (Figure 75). In fact, the ^{1}H NMR spectrum of **RBR95-23a/b** displayed a signal of two chelated hydroxy protons at δ_H 13.07/12.83 (1H, s, OH-1), two couples of *meta* coupled aromatic protons at δ_H 7.86/7.34 (1H, br s/ d, J = 2.6 Hz, H-5), 7.85 (1H, br s, H-6), 7.71/7.17 (1H, d, J = 2.1/2.6 Hz, H-7), 7.48/7.46 (1H, br s, H-4), 7.18/7.16 (1H, dd/br s, J = 1.7, 0.9 Hz, H-2), a glucosyl anomeric proton at δ_H 5.13 (1H, m, H-1′) and the other proton signals of the sugar moiety at δ_H 5.13-3.20 and one singlet signal of methyl group at δ_H 2.40 (3H, s, CH_3-3). The only difference between the ^{1}H NMR of **RBR95-23a/b** and that of **RBR95-35b** was the absence of one singlet signal for one chelated hydroxy protons at δ_H 11.26 (1H, s, OH-8) and the presence of the signal of one additional aromatic proton at δ_H 7.85 (1H, br s, H-6) and the signal of the singlet of one methoxy group at δ_H 3.96 (OCH_3-6) in **RBR95-23a/b** (Figure 75).

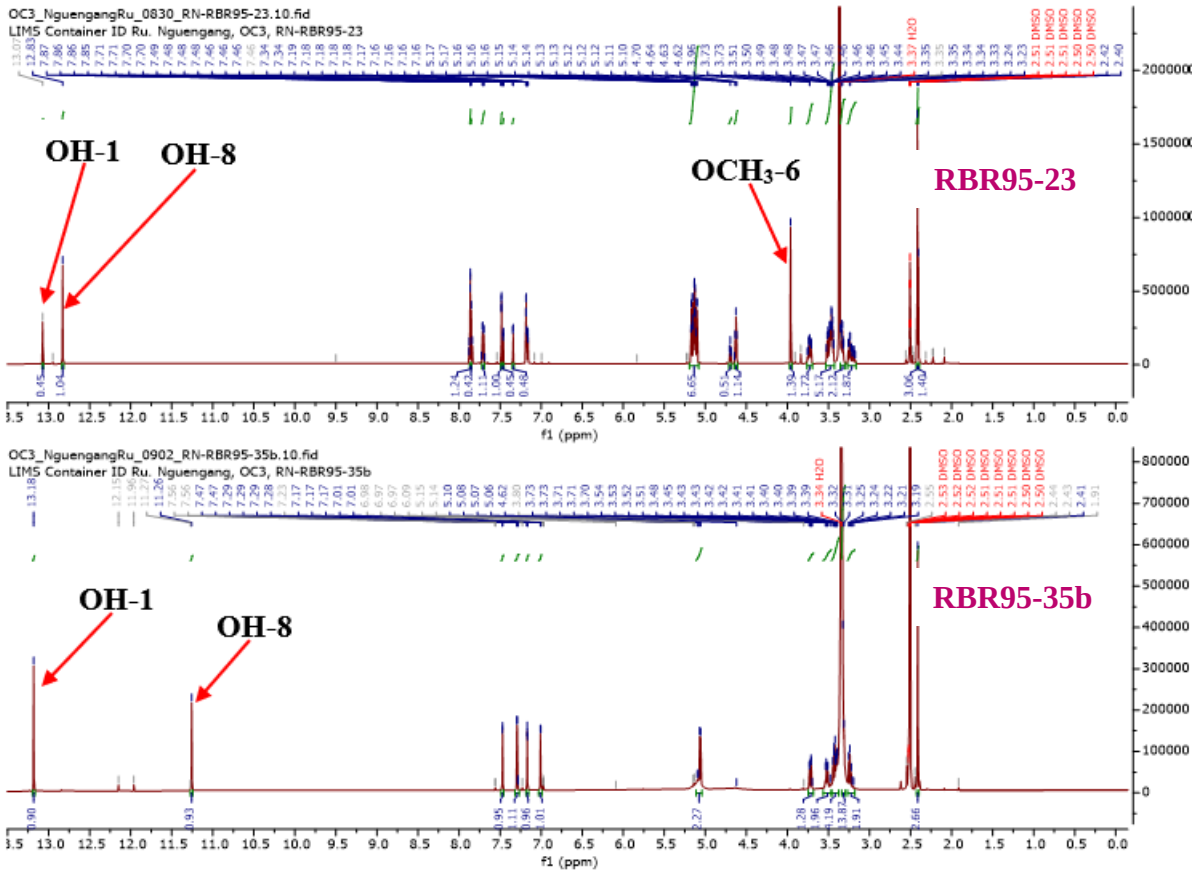

Figure 75: Comparative ^{1}H NMR of RBR95-35b (DMSO-*d*$_6$, 600 MHz) and RBR95-23a/b (DMSO-*d*$_6$, 600 MHz)

Following signals characteristic of emodin observed after examination of the broad-band proton-decoupled ^{13}C spectrum of **RBR95-23a/b** (Figure 76) allowed to confirm this suggestion:

- ten quaternary carbons at δ_C 165.2 (C-6), 161.1/158.7 (C-8), 162.1 (C-1), 148.1/147.6 (C-3), 136.8/135.2 (C-10a), 132.6/132.5 (C-4a), 115.2/114.90 (C-9a), 115.2/114.88 (C-8a) including two carbonyls at δ_C 186.9/188.0 (C-9) and 182.5/182.3 (C-10).
- four methine groups at δ_C 124.7/124.2 (C-2), 119.8 (C-4), 121.0/107.0 (C-5) and 122.9/107.8 (C-7);
- one methyl group at δ_C 21.9 (CH_3-3);
- a glucosyl anomeric carbon at δ_C 101.1/101.0 (C-1′) and five other glucosyl carbon at δ_C 77.9/77.7 (C-5′), 77.0 (C-3′), 73.8/73.7 (C-2′), 70.3/70.0 (C-4′) and 61.2/61.1 (C-6′).

The only difference was the presence of the signal of one additional methine aromatic carbon at δ_C 136.4 (C-6) and the signal of one methoxy group at δ_C 56.5 (OCH_3-6) in RBR95-23a/b (Figure 76).

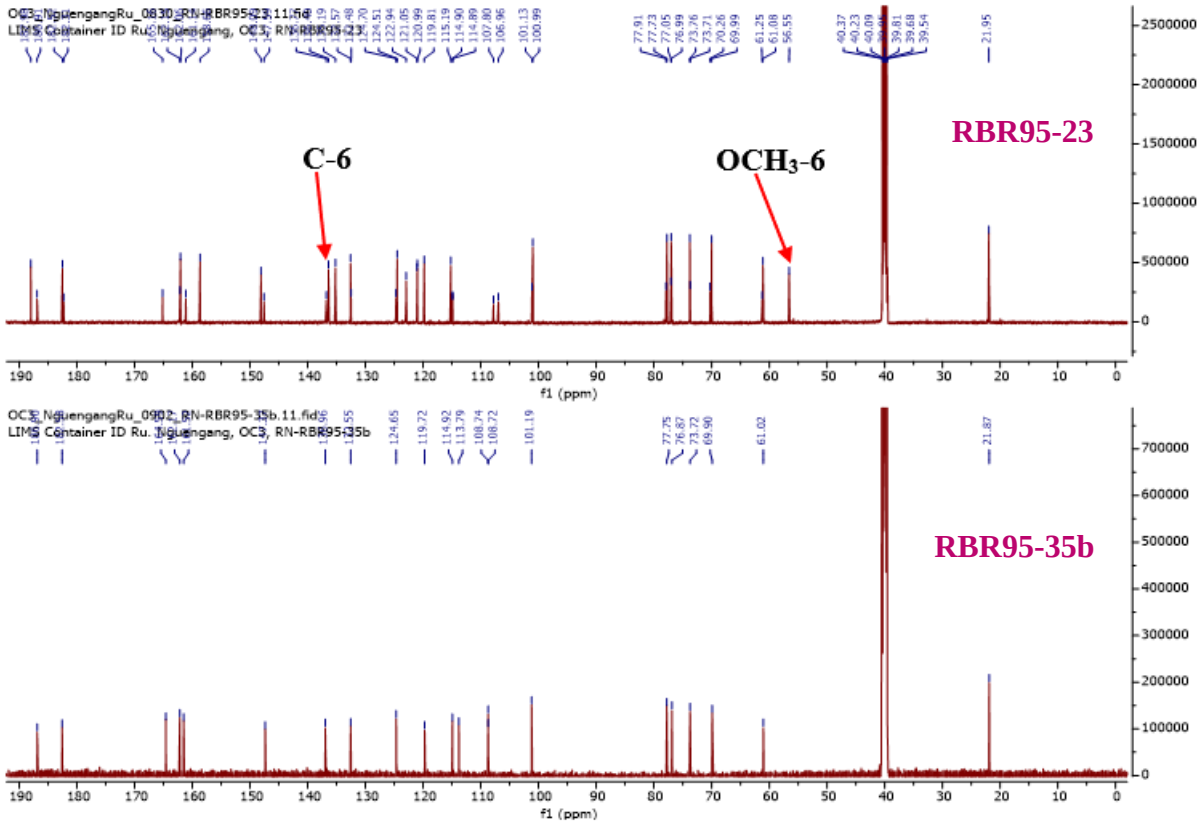

Figure 76: Comparative ^{13}C NMR spectrum of RBR95-35b and RBR95-23a/b (DMSO-*d*$_6$, 150 MHz)

The location of the glucose unit was determined by the correlations observed on the HMBC spectrum (Figure 77) of **RBR95-23a/b** between the anomeric proton at δ_H 5.13 (1H, m, H-1′) and carbons C-8 (δ_C 161.1/158.7) and proton H-6 (δ_H 7.85, br s) and C-8 (δ_C 158.7). In addition, the location of the methoxy group was determined by the correlations observed between the singlet of one methoxy group at δ_H 3.96 (OCH_3-6) and C-6 (δ_C 165.2) and proton H-7 (δ_H 7.17, d, J = 2.6 Hz) and C-6 (δ_C 165.2) and C-8 (δ_C 161.1).

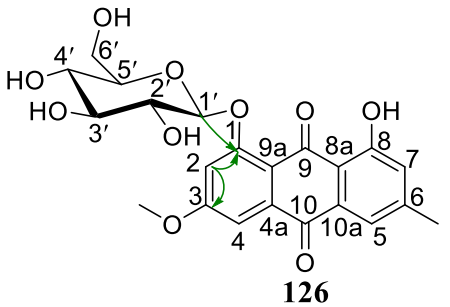

126

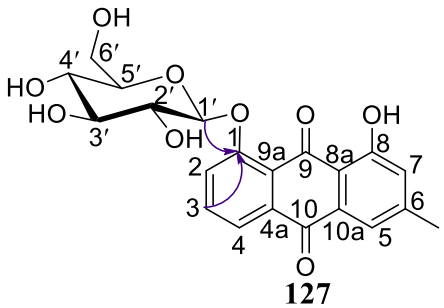

127

Scheme 22: Key HMBC correlations of RBR95-23a/b

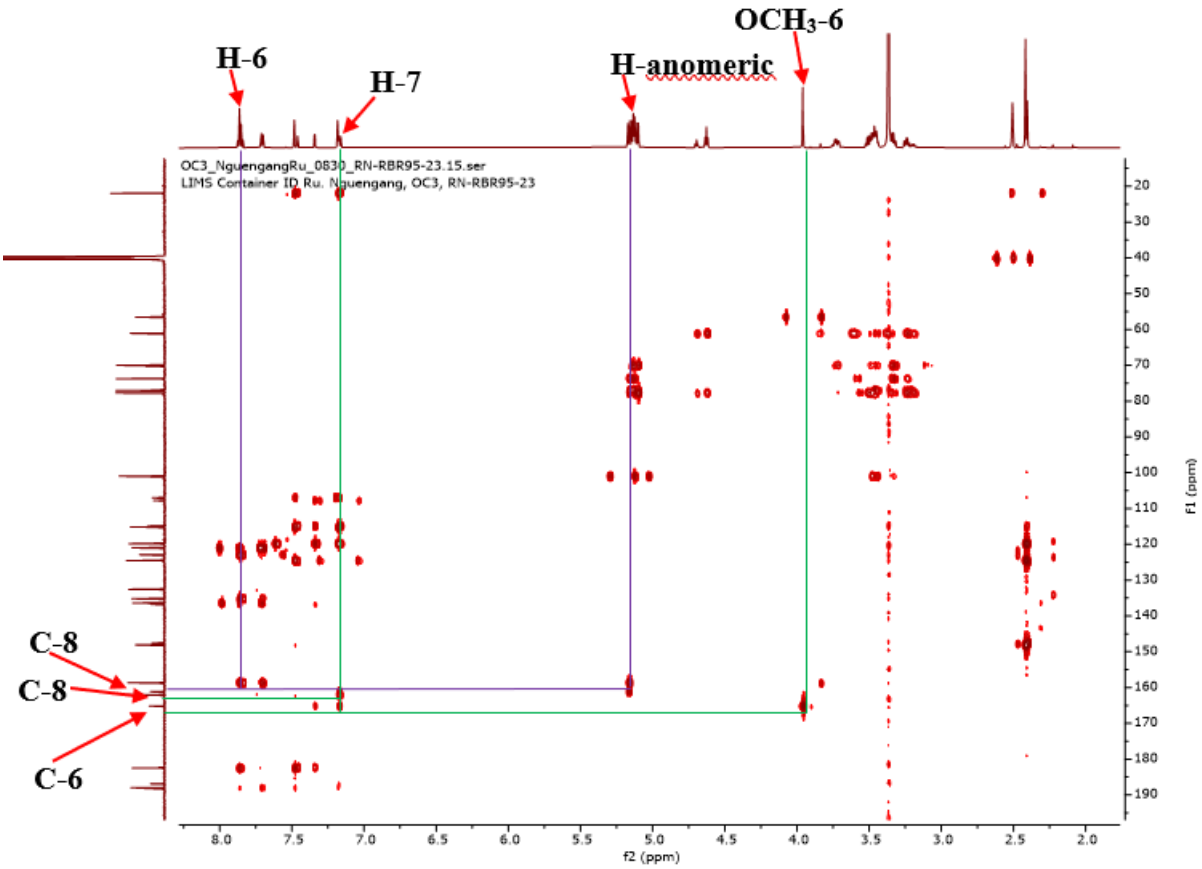

Figure 77: HMBC spectrum of RBR95-23a/b

All these data, compared to those in the literature, led to the identification of RBR95-23a/b as a mixture of physcionin (**126**) and chrysophanein (**127**), previously isolated from *Rumex abyssinicus* Jacq by Tsamo and collaborators (2021).

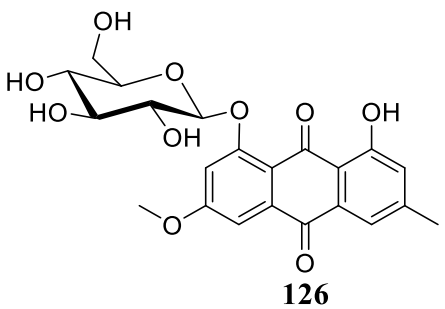

126

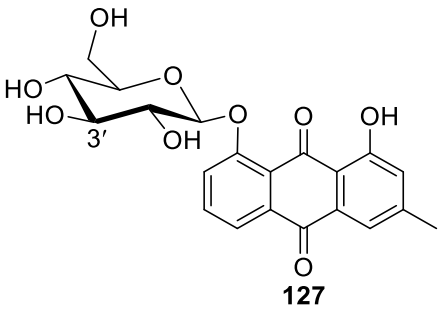

127

Table 33: ^{1}H (600 MHz) and ^{13}C (150 MHz) NMR data of RBR95-23a/b in DMSO-d_6 compared to physcionin (Ref a) and chrysophanein (Ref b) (Tsamo *et al*., 2021) [^{13}C (150 MHz), ^{1}H (600 MHz), DMSO-d_6]

Positions	RBR95-23a		Ref a	RBR95-23b		Ref b
	δ_C	δ_H[a)] (m, *J* in Hz)	δ_C	δ_C	δ_H[b)] (m, *J* in Hz)	δ_C
1	162.1	-	162.1	162.1	-	162.1
2	124.7	7.16 (1H, br s)	124.7	124.5	7.71 (dd, 1.7, 0.9)	124.5
3	147.6	-	147.6	148.1	-	148.1
4	119.8	7.46 (1H, br s)	119.7	119.8	7.48 (1H, br s)	119.8
4a	132.5	-	132.5	132.6	-	132.6
5	107.8	7.34 (1H, d, 2.6)	106.9	121.0	7.86 (1H, m)	121.0
6	165.2	-	165.2	136.4	7.85 (1H, br s)	136.4
7	107.8	7.17 (1H, d, 2.6)	107.9	122.9	7.71 (1H, d, 2.1)	122.9
8	161.1	-	161.2	158.7	-	158.7
8a	114.88	-	114.95	115.2	-	115.3
9	186.9	-	186.9	188.0	-	188.0
9a	114.90	-	114.96	115.2	-	115.2
10	182.3	-	182.4	182.5	-	182.6
10a	136.8	-	135.1	135.2	-	135.2
CH_3-3	21.9	2.40 (3H, s)	21.8	21.9	2.42 (3H, s)	21.9
OCH_3-6	56.5	3.96 (3H, s)	56.6	-	-	-
OH-1	-	13.07 (1H, s)	-	-	12.83 (s)	-
Glc		5.13-3.20			5.13-3.20	
1′	101.1	-	101.1	101.0	-	101.0
2′	73.7	-	73.8	73.8	-	73.7
3′	77.0	-	77.1	77.0	-	77.0
4′	70.3	-	70.3	70.0	-	70.0
5′	77.9	-	77.9	77.7	-	77.8
6′	61.2	-	61.3	61.1	-	61.1

II.1.5.4.11. Structural identification of compound RBR9a

RBR9a was obtained as brown oil in CH_2Cl_2-EtOAc (17:3, v/v). It was soluble in dichloromethane and reacted positively to Bornträger test, characteristic of anthraquinones and quinones.

Its molecular formula, $C_{30}H_{22}O_8$, implying twenty degrees of unsaturation, was deduced from the combination of the data from the ESIMS spectrum (Figure 78), which showed the

protonated molecular ion peak $[M+H]^+$ at *m/z* 511.287 with those of the NMR spectra (Figure 79 to 81).

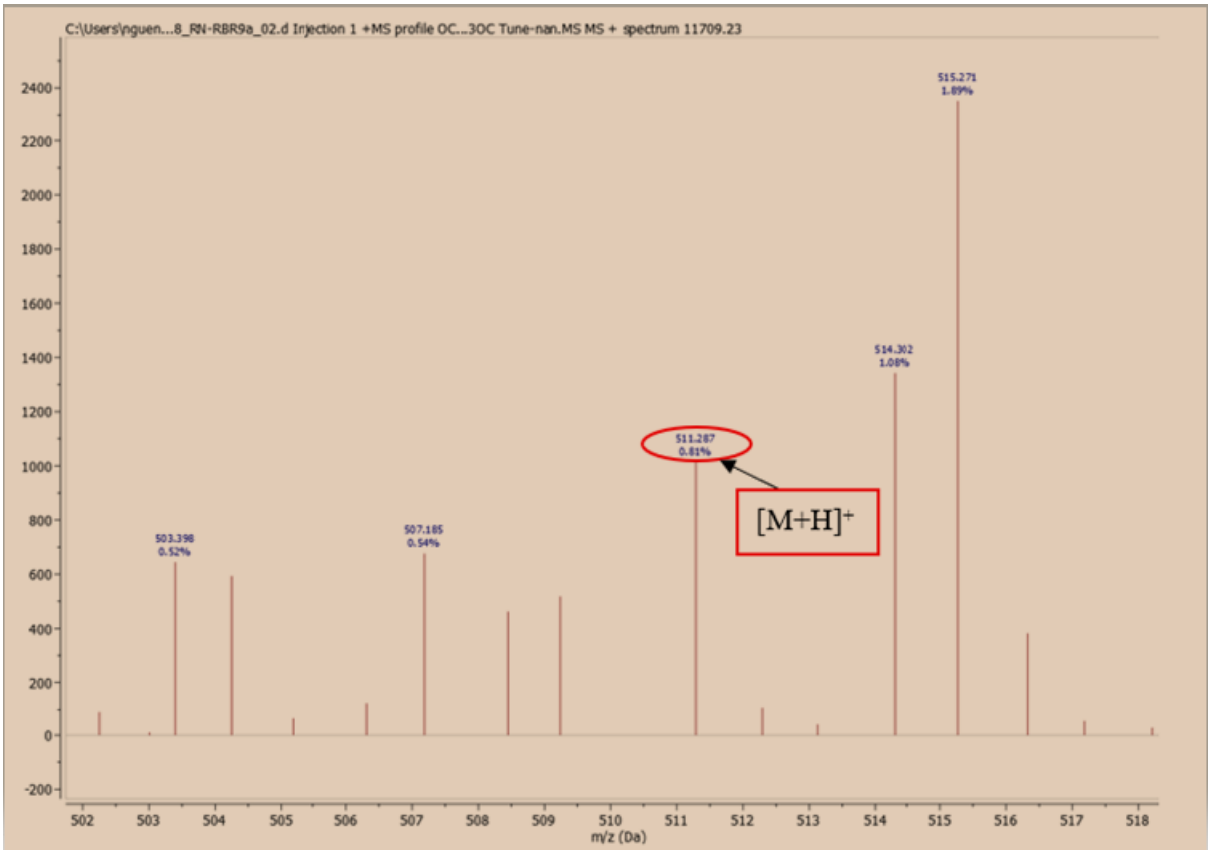

Figure 78: (+) ESI mass spectrum of RBR9a

The ^{1}H NMR spectrum of **RBR9a** was very close to that of **RBR3C** (Figure 79). The only difference between the ^{1}H NMR of **RBR9a** and that of **RBR3C** was the presence of the additional proton at δ_H 4.39 (1H, d, J = 3.7 Hz, H-10) in **RBR9a** (Figure 79).

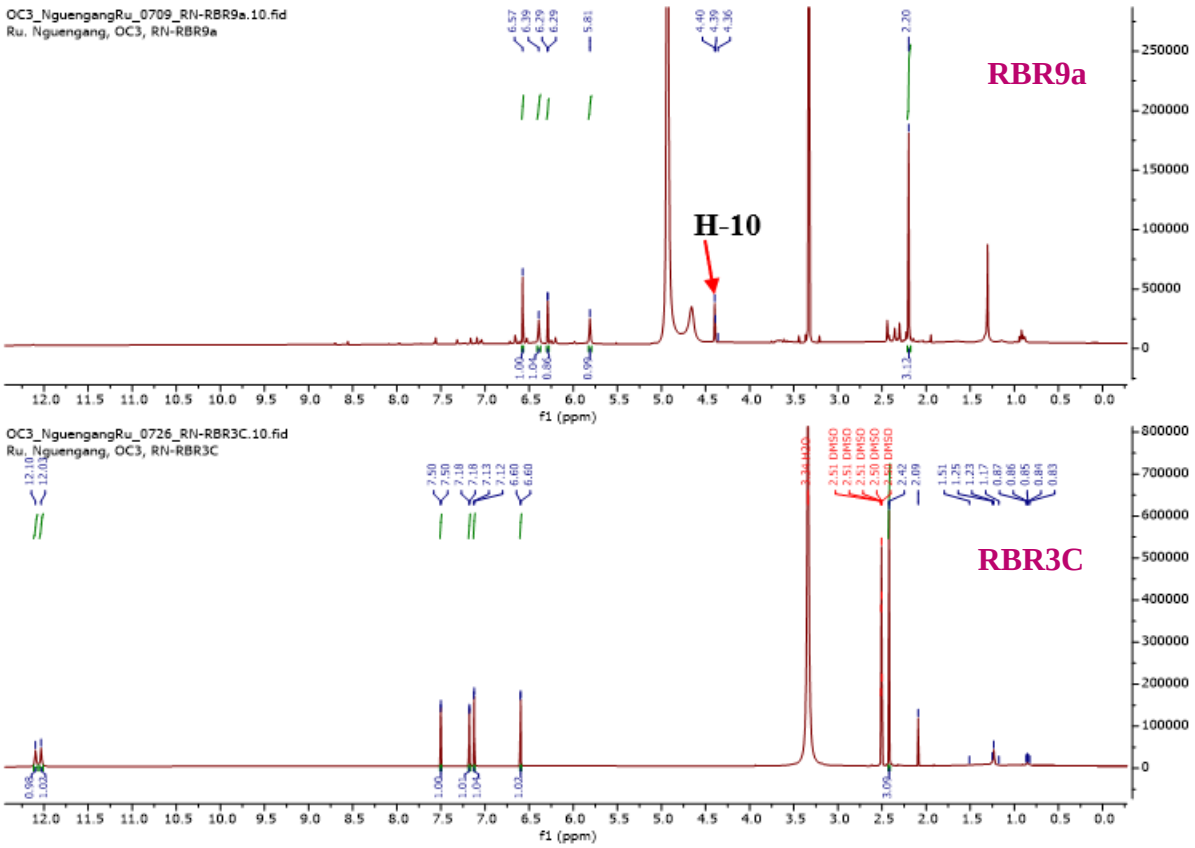

Figure 79: Comparative ^{1}H NMR of RBR3C and RBR9a (DMSO-d_6, 600 MHz)

The ^{13}C NMR spectrum of RBR9a (Figure 80) was also close to that of emodin. The only difference was the presence of signal of one methine group at δ_C 56.2 (C-10) in **RBR9a** instead of signal of one carbonyl group at δ_C 181.9 (C-10) (Figure 80).

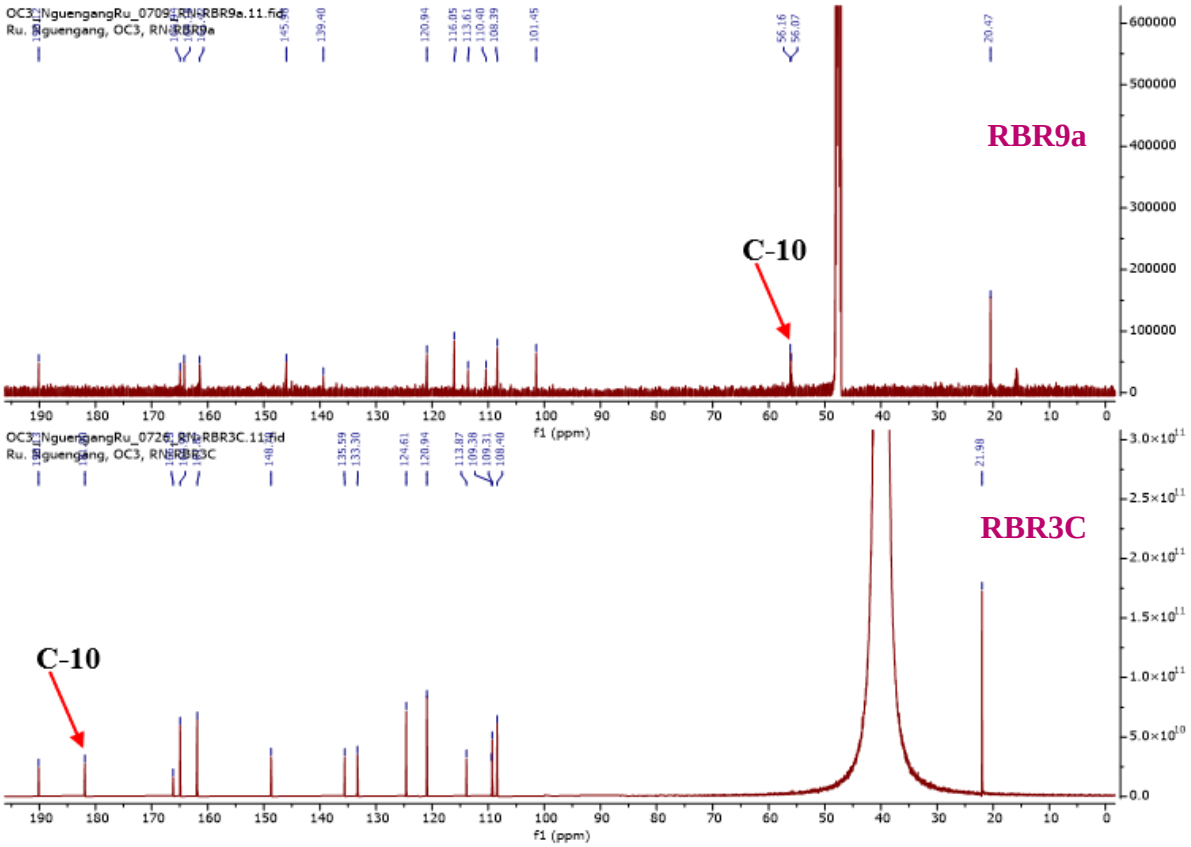

Figure 80: Comparative ^{13}C NMR spectrum of RBR3C (DMSO-d_6, 150 MHz) and RBR9a (DMSO-d_6, 150 MHz)

The position of this methine group was determined by correlations observed on the HMBC spectrum (Figure 81). In fact, on this spectrum, cross peaks were observed between the proton at δ_H 4.39 (1H, d, J = 3.7 Hz, H-10) and carbons C-10a (δ_C 139.4) and C-4a (δ_C 145.0), which means that compound RBR9a is a bianthrone.

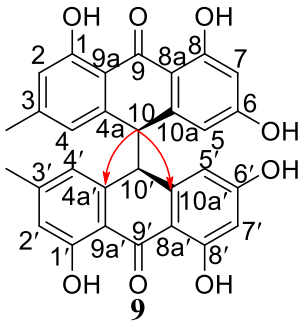

9

Scheme 23: Key HMBC correlations of RBR9a

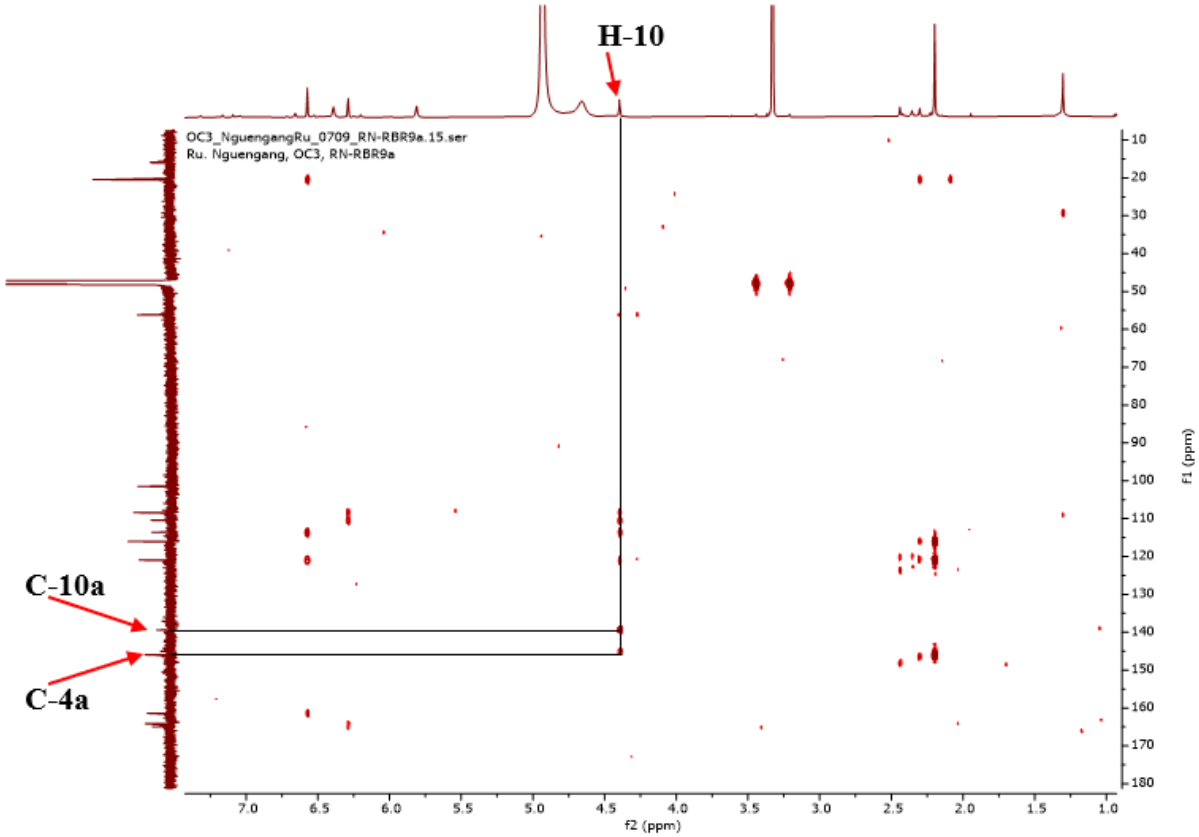

Figure 81: HMBC spectrum of RBR9a

All these data, compared with those described in the literature, was in agreement with that of emodin bianthrone (**128**), previously isolated from *Rhamnus nepalensis* by Mai and collaborators (2001).

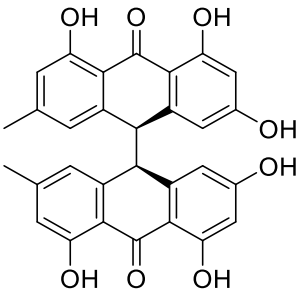

128

Table 34: ^{1}H (600 MHz) and ^{13}C (150 MHz) NMR data of RBR9a in DMSO-d_6 compared to emodin bianthrone [^{1}H (400 MHz), DMSO-d_6]

	RBR9a		Emodin bianthrone (Mai *et al*., 2001)	
Position	δ_C	δ_H **(m, *J* in Hz)**	δ_C	δ_H **(m, *J* in Hz)**
1	161.4	-		-
2	116.1	6.57 (1H, br s)		6.37 (1H, br s)
3	146.0	-		-
4	120.9	5.81 (1H, br s)		6.59 (1H, br s)
4a	145.0	-		-
5	108.4	6.39 (1H, br s)		6.33 (1H, d, 2.0)
6	164.2	-		-
7	101.5	6.29 (1H, d, 2.1)		6.07 (1H, br s)
8	164.9	-		-
8a	110.4	-		-
9	190.1	-		-
9a	113.6	-		-
10	56.2	4.39 (1H, d, 3.7)		4.55 (1H, s)
10a	139.4	-		-
CH_3-3	20.5	2.20 (3H, s)		2.20 (1H, s)
OH-1	-	11.65 (1H, s)		11.75 (1H, s)
OH-8	-	11.94 (1H, s)		12.05 (1H, s)

II.1.5.4.12. Structural identification of compound RBR64

RBR64 was obtained as a yellowish white oil in CH_2Cl_2-EtOAc (1:1, v/v). It was soluble in dichloromethane and reacted positively to ferric chloride test and Shinoda test, characteristic of phenolic compounds and flavonoids, respectively.

Its molecular formula, $C_{22}H_{18}O_{10}$, implying fourteen degrees of unsaturation, was deduced from the combination of the data from the ESIMS spectrum (Figure 82), which showed the sodium adduct peak $[M+Na]^+$ at *m/z* 465.1 with those of the NMR spectra (Figure 83 to 84).

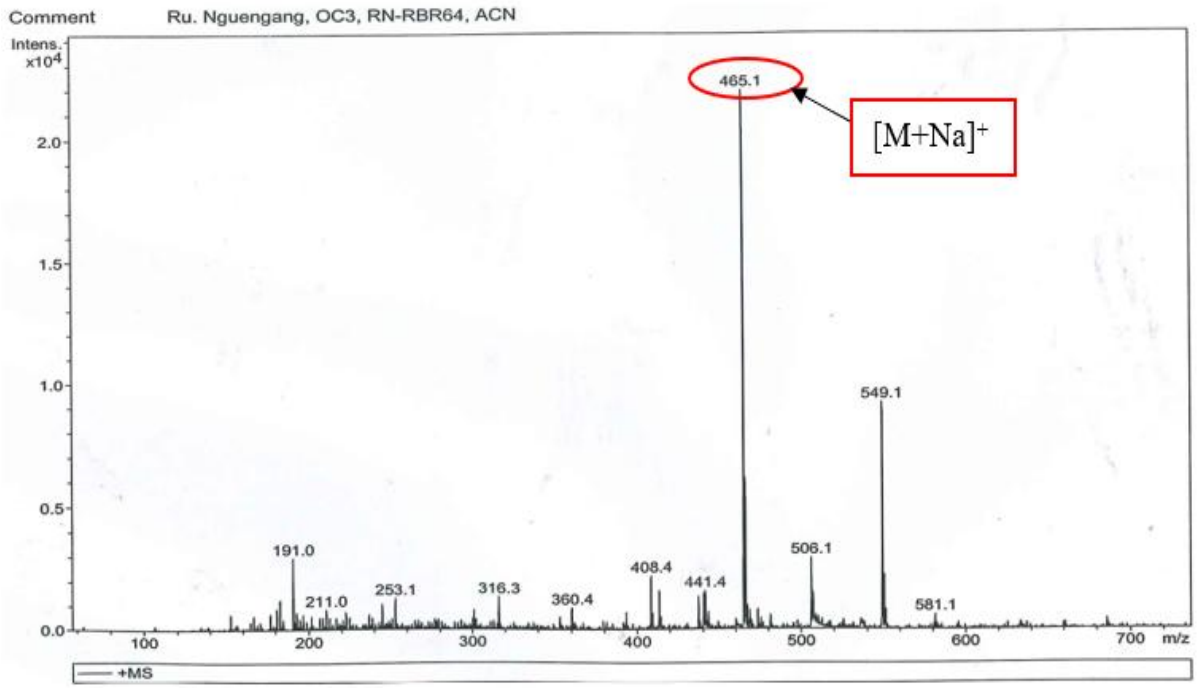

Figure 82: (+) ESI mass spectrum of RBR64

Its ^{1}H NMR spectrum (Figure 83) displayed:

- resonances of protons at δ_H 5.37 (1H, t, J = 3.5 Hz, H-3), 5.05 (1H, brs, H-2), 2.97 (1H, dd, J = 14.5, 4.0 Hz, H-4b) and 2.71 (1H, m, H-4a) suggesting the presence of ring C of flavan-3-ol compound;
- a pair of *meta*-coupled aromatic proton signals at δ_H [5.96 (1H, d, J = 2.3 Hz, H-6), 5.89 (1H, d, J = 2.2 Hz, H-8)] for the A ring and a set of ABX-system protons at δ_H [6.90 (1H, d, J = 2.0 Hz, H-2′), 6.79 (1H, dd, J = 8.3, 2.0 Hz, H-6′) and 6.69 (1H, d, J = 8.1 Hz, H-5′)] suggesting the 5,7, 3′, 4′-tetrahydroxyflavan-3-ol skeleton of RBR64;
- a singlet at 6.85 (2H, s, H-3″, 7″) assigned to the H-3″ and H-7″ of gallic acid.

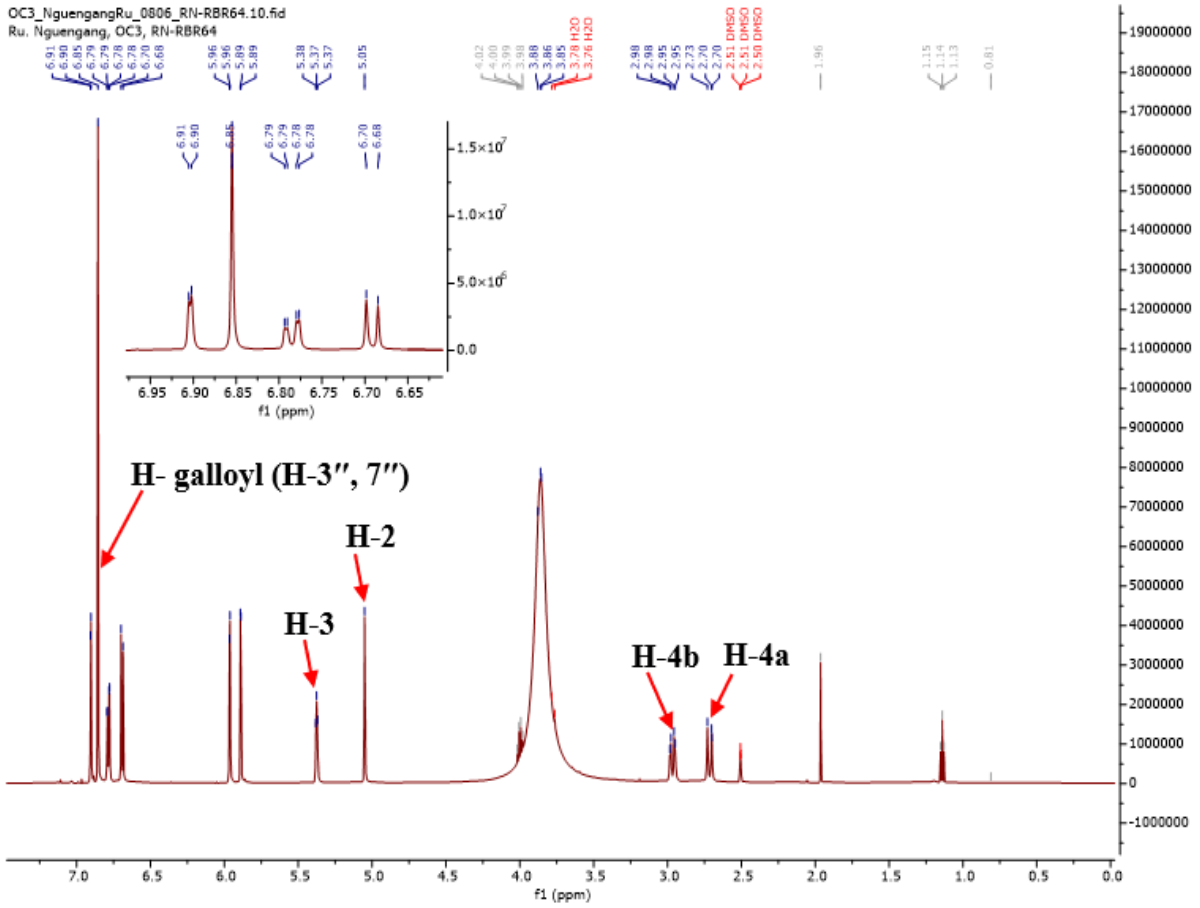

Figure 83: ^{1}H NMR of RBR64 (DMSO-d_6, 600 MHz)

Its ^{13}C NMR spectrum (Figure 84a) confirmed this hypothesis and exhibited 22 signals which were sorted by DEPT and HMQC techniques into:

- Twelve quarternary carbons [including the carbonyl at δ_C 165.7 (C-1″) and other carbons at δ_C

  156.9 (C-5,9), 156.0 (C-7), 145.8 (C-4″, 6″), 145.1 (C-3′), 145.0 (C-4′), 139.0 (C-5″), 129.9 (C-1′), 119.7 (C-2″), 97.8 (C-10)];

- Six aromatic methine carbons at δ_C 118.1 (C-6′), 115.5 (C-5′), 114.7 (C-2′), 109.1 (C-3″, 7″), 96.0 (C-6), 94.8 (C-8);

- Two additional methine carbons at δ_C 76.9 (C-2), 68.7 (C-3) and one methylene carbon at δ_C 26.1 (C-4) characteristics for flavan-3-ol (Michał, 2019).

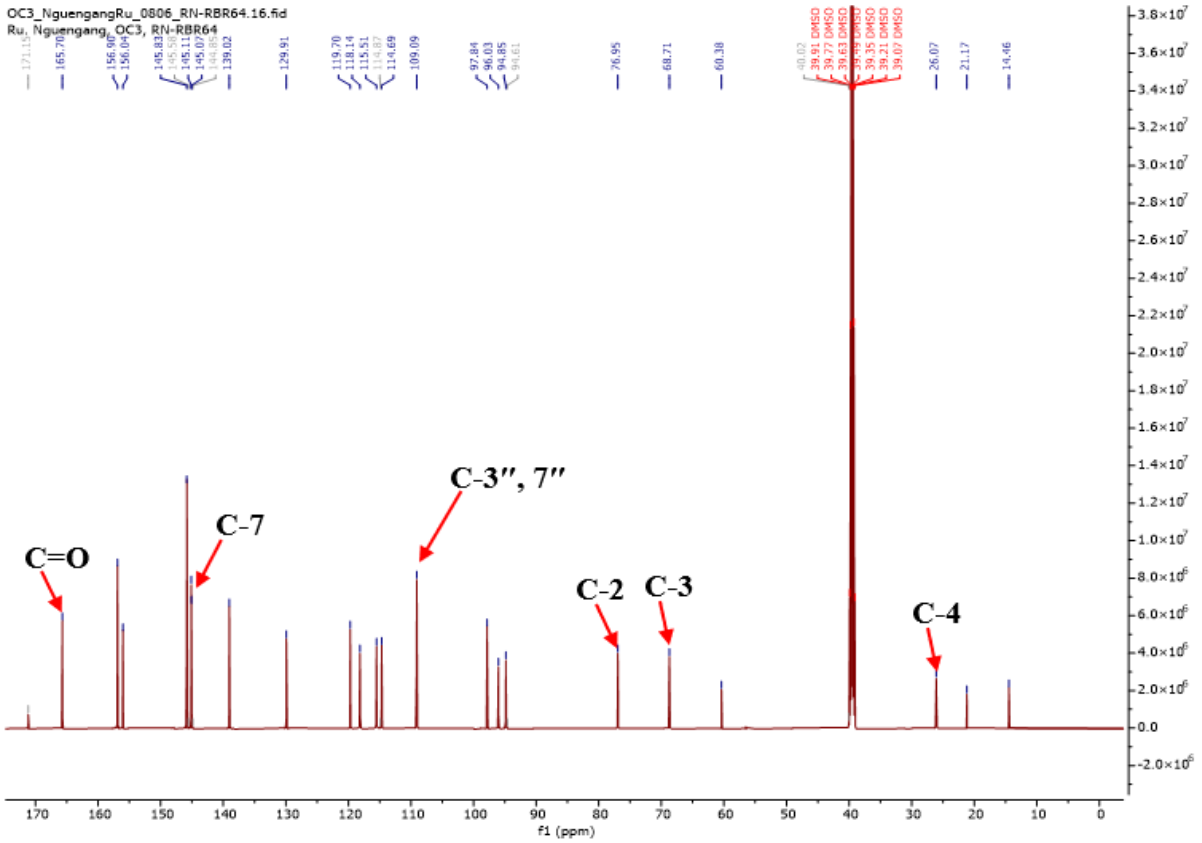

Figure 84a: ^{13}C NMR spectrum of RBR64 (DMSO-d_6, 150 MHz)

The location of the galloyl group was determined by the correlations observed between the proton at δ_H 5.37 (1H, t, J = 3.5 Hz, H-3) and C-1″ (δ_C 165.7) (Figure 84b). The position of the H-2 proton at δ_H 5.05, suggests that the flavan structure possesses the cis-2,3 stereochemistry, this was supported by the small value for the coupling (< 1 Hz) between the H-2 and H-3 protons, which appeared as a broad singlet at H-2 (δ_H 5.05) (Fan *et al*., 2004; Pizzolatti *et al*., 2002).

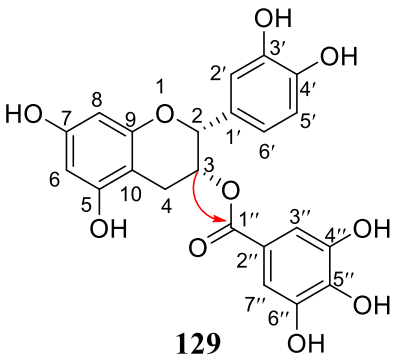

129

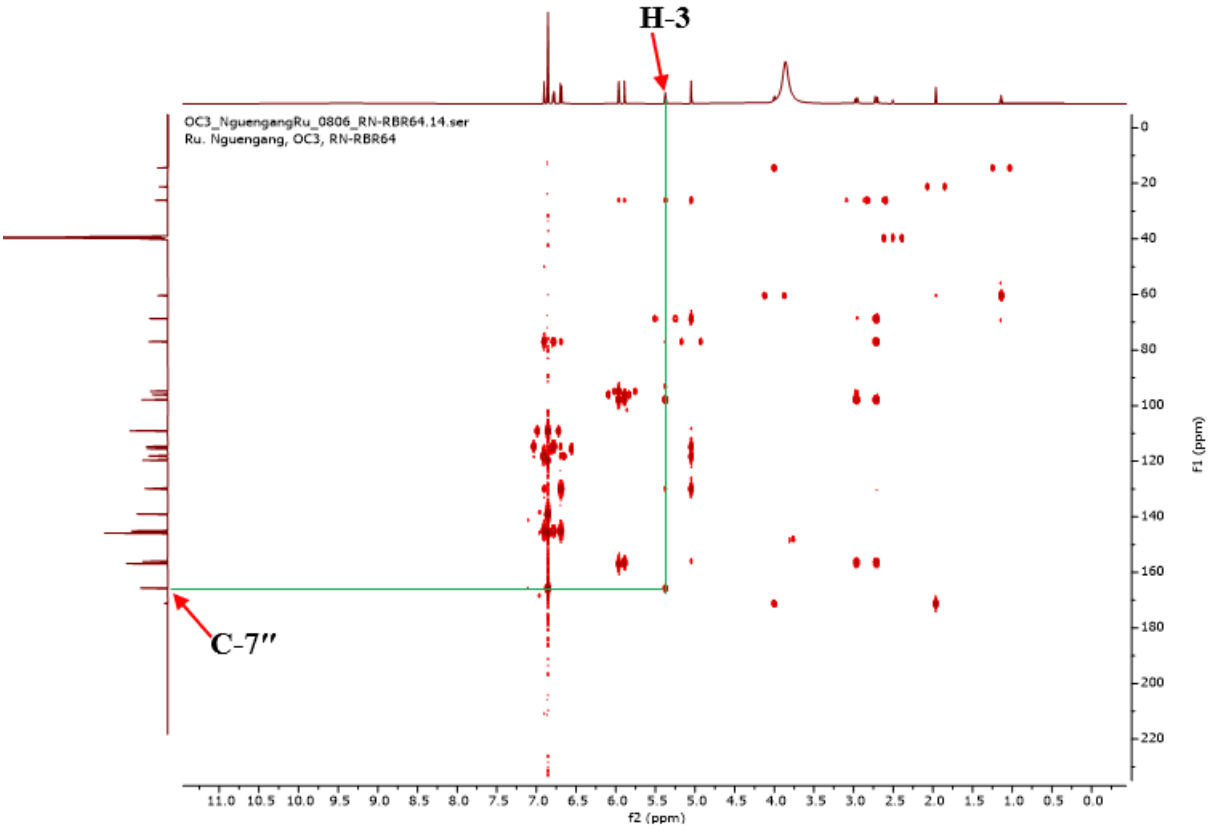

Figure 84b: HMBC spectrum of RBR64

Based on the above data, RBR64 was identified as epicatechin 3-*O*-gallate (**129**), previously isolated from *Polygonum amphibium* by Lee and collaborators (2021).

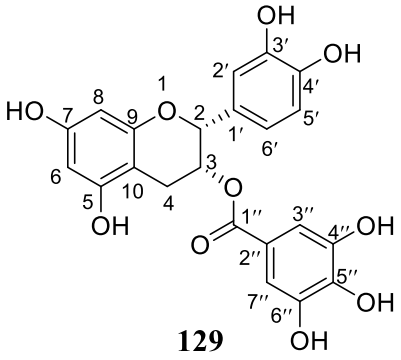

129

Table 35: ^{1}H (600 MHz) and ^{13}C (150 MHz) NMR data of RBR64 in DMSO-d_6 compared to Epicatechin 3-O-gallate [DMSO-d_6, RMN ^{13}C (125 MHz), RMN ^{1}H (500 MHz)]

	RBR64		Epicatechin 3-O-gallate (Lee *et al.*, 2021)	
Position	δ_C	δ_H **(m, *J* in Hz)**	δ_C	δ_H **(m, *J* in Hz)**
1	-	-	-	-
2	76.9	5.05 (1H, br s)	76.5	5.03 (1H, br s, 7.2)
3	68.7	5.37 (1H, t, 3.5)	68.2	5.36 (1H, m)
4	26.1	2.71 (H-4$_a$, m); 2.97 (H-4b, dd, 14.5, 4.0)	25.7	2.68 (H-4$_a$, d, 17.3); 2.94 (H-4b, dd, 17.3, 4.5)
5	156.9	-	155.7	
6	96.0	5.89 (1H, d, 2.3)	95.6	5.84 (1H, d, 2.3)
7	156.0	-	156.6	
8	94.8	5.96 (1H, d, 2.2)	94.4	5.94 (1H, d, 2.3)
9	156.9	-	156.5	-
10	97.8	-	97.3	-
1′	129.9	-	129.4	-
2′	114.7	6.90 (1H, d, 2.0)	114.3	6.86 (1H, d, 2.0)
3′	145.1	-	144.8	-
4′	145.0	-	145.5	-
5′	115.5	6.69 (1H, d, 8.1)	115.1	6.66 (1H, d, 8.3)
6′	118.1	6.79 (1H, dd, 8.3, 2.0)	117.6	6.76 (1H, dd, 8.3, 2.0)
		Galloyl moiety		
1″	165.7	-	165.2	-
2″	119.7	-	119.3	-
3″/7″	109.1	6.85 (2H, s)	108.6	6.83 (2H, s)
4″/6″	145.8	-	145.5	-
5″	139.0	-	138.6	-

II.1.5.4.13. Structural identification of compound RBR17

RBR17 was obtained as a colorless amorphous in CH_2Cl_2-EtOAc (1:1, v/v). It was soluble in dichloromethane and reacted positively to the ferric chloride test and Shinoda test, characteristic of phenolic compounds and flavonoids, respectively.

Its molecular formula, $C_{23}H_{20}O_{10}$, implying fourteen degrees of unsaturation, was deduced from the combination of the data from the ESIMS spectrum (Figure 85), which showed the sodium adduct peak $[M+Na]^+$ at *m/z* 479.1 (calcd for $C_{23}H_{20}O_{10}Na^+$, 479.0954) with those of the NMR spectra (Figure 86 to 88).

The mass difference of 14 amu between RBR64 and RBR17 suggested the apparition of a CH_2 in **RBR17**.

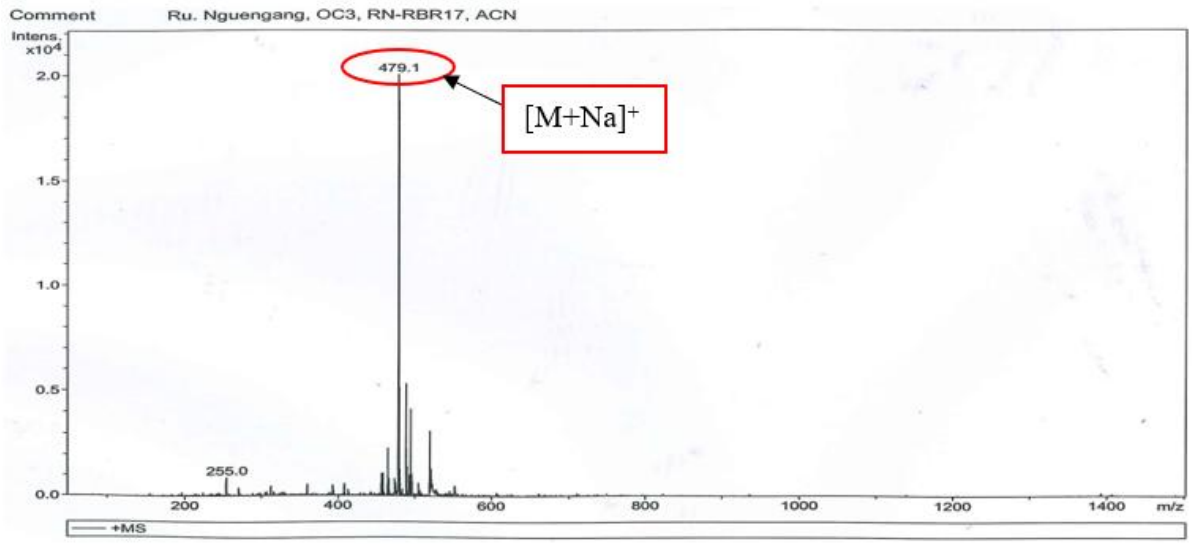

Figure 85: (+) ESI mass spectrum of RBR17

The ^{1}H NMR spectrum of **RBR17** was very close to that of **RBR64** (Figure 86). The only difference between the ^{1}H NMR of **RBR17** and that of **RBR64** was the presence of one singlet signal of methoxy group at δ_H 3.80 ppm (3H, s, 6″-OCH3) in RBR17 and the presence of signals of aromatic proton at δ_H [7.11 (1H, d, J = 1.9 Hz, H-3″), 7.01 (1H, d, J = 1.9 Hz, H-7″)] instead of signal of one singlet at 6.85 (2H, s, H-3″, 7″) of gallic acid (Figure 86).

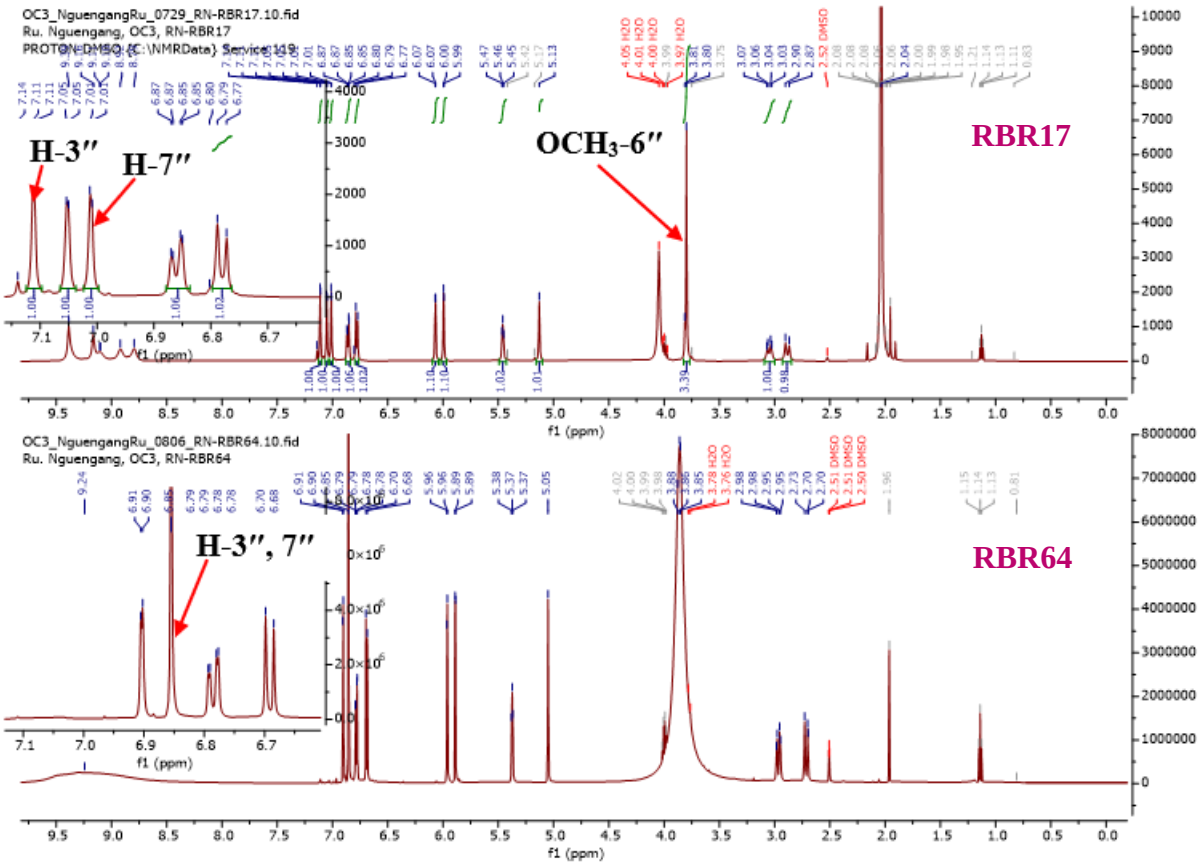

Figure 86: Comparative ^{1}H NMR of RBR64 and RBR17 (DMSO-d_6, 600 MHz)

The ^{13}C NMR data of **RBR17** was also close to those of **RBR64** (Figure 87). The differences was the presence of two signals of two quarternary carbons at δ_C 145.5 (C-4″) and 148.2 (C-6″) in RBR17 instead of only one signal of these two quarternary carbons at δ_C 145.8 (C-4″, 6″) and the presence of two signals of two aromatic methine carbons at δ_C 111.0 (C-3″) and 105.2 (C-7″) in RBR9a instead of only one signal of these two methine aromatic carbons at δ_C 109.1 (C-3″, 7″) suggested the loss of symmetry in the galloyl group (Figure 87). Another difference was the presence of the signal of one methoxy group at δ_C 56.1 (OCH_3-6″) in comparison to that of **RBR64** (Figure 87).

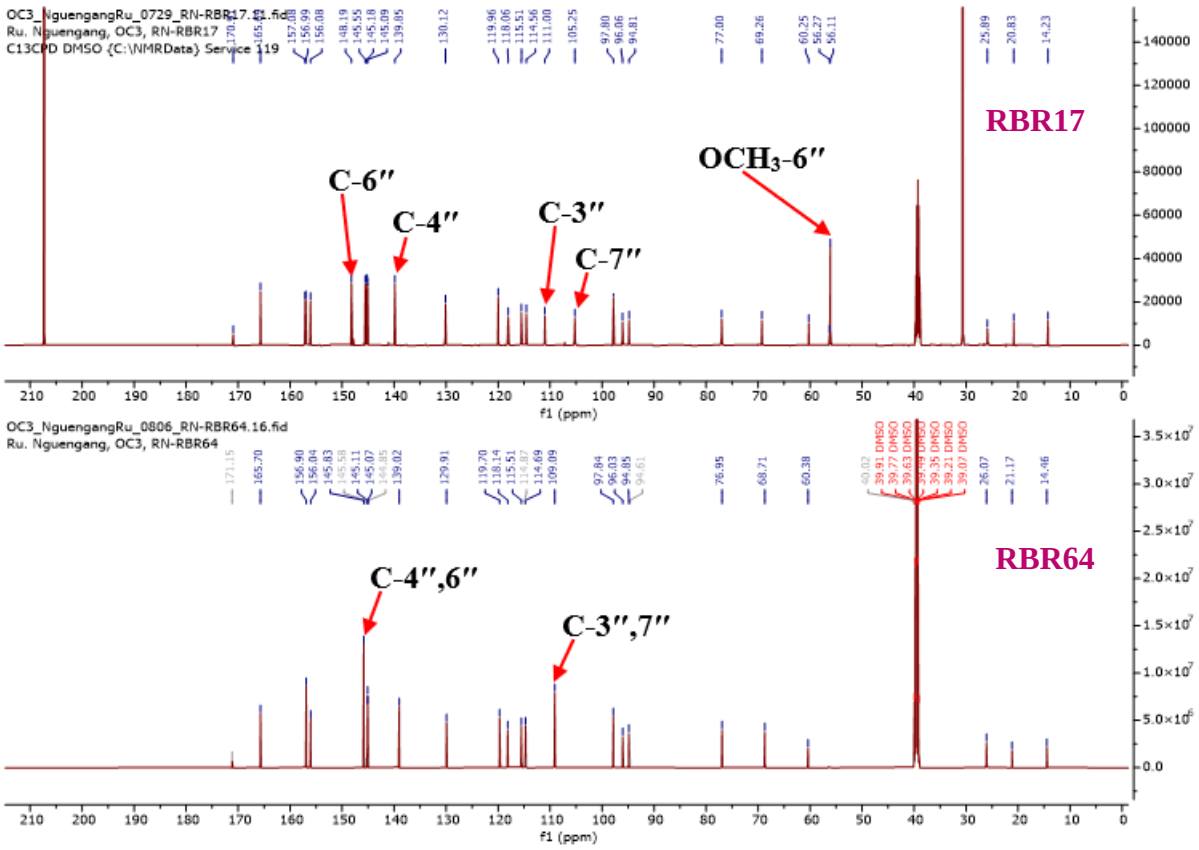

Figure 87: Comparative ^{13}C NMR spectrum of RBR64 and RBR17 (DMSO-*d*$_6$, 150 MHz)

The location of the methoxy group was determined by the correlations observed on the HMBC spectrum (Figure 88) of **RBR17** between the proton OCH_3-6″ [δ_H 3.80 (3H, s)] and the carbon C-6″ (δ_C 148.2) justifying the loss of symmetry in the galloyl group. In addition, the location of this 6"-*O*-methylgalloyl group was determined by the correlations observed between the proton at δ_H 5.46 (1H, t, J = 3.5 Hz, H-3) and C-1″ (δ_C 165.7) (Figure 88). The position of the H-2 proton at δ_H 5.13, equaly suggests that the flavan structure possesses the cis-2,3 stereochemistry, this was supported by the small value for the coupling (< 1 Hz) between the

H-2 and H-3 protons, which appeared as a broad singlet at H-2 (δ_H 5.13) (Fan *et al*., 2004; Pizzolatti *et al*., 2002).

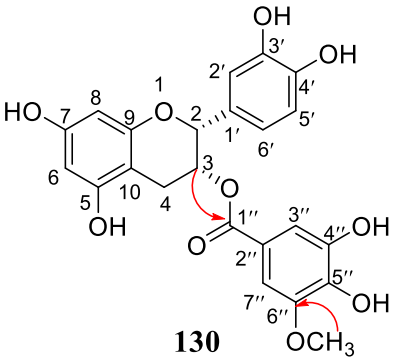

130

Scheme 24: Key HMBC correlations of RBR17

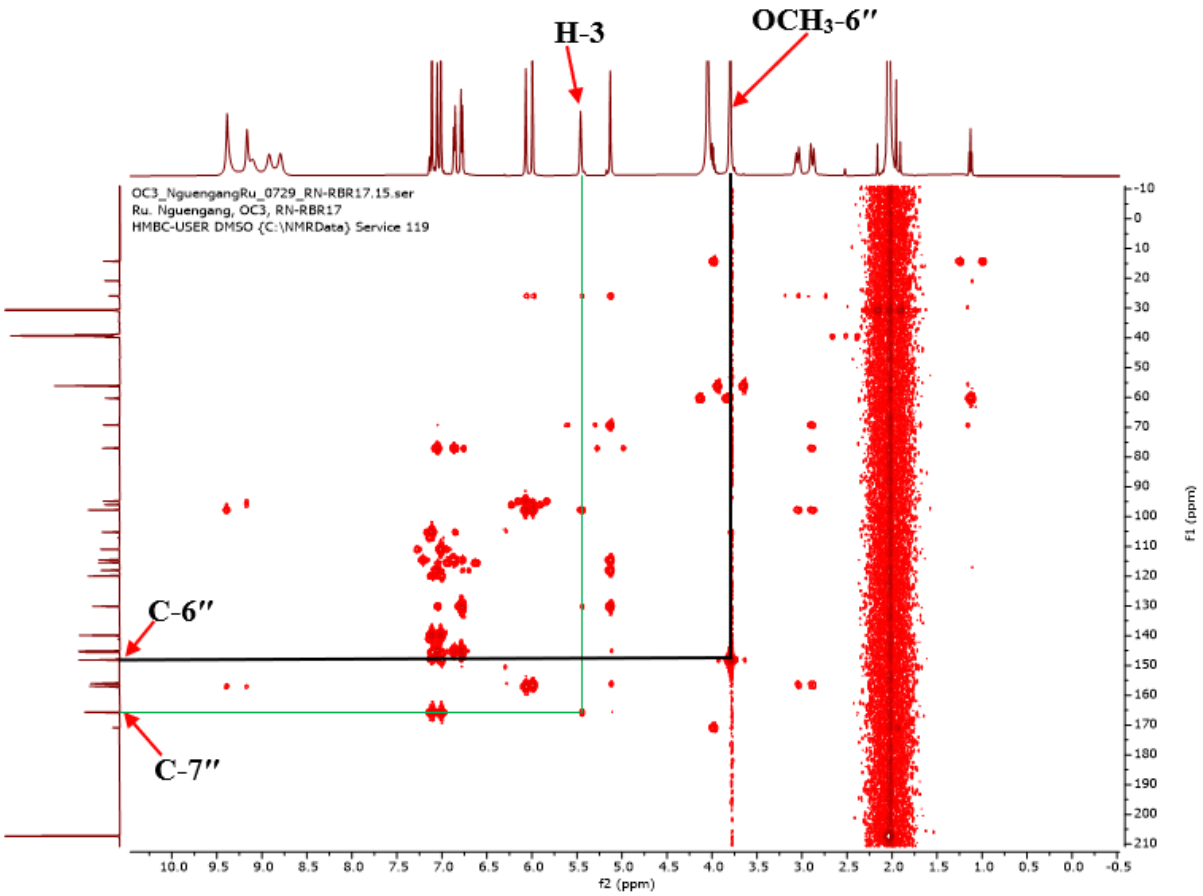

Figure 88: HMBC spectrum of RBR17

RBR17 was identified as epicatechin 3-(6"-*O*-methyl) gallate (**130**), previously synthesized by Asakawa and collaborators (2016).

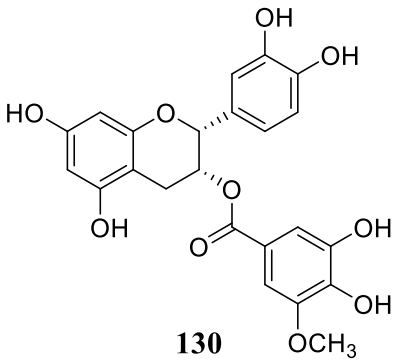

130

Table 36: ^{1}H (600 MHz) and ^{13}C (150 MHz) NMR data of RBR17 in DMSO-d_6 compared to epicatechin 3-(6''-*O*-methyl) gallate [^{13}C (68 MHz), ^{1}H (270 MHz), CD_3OD]

	RBR17		epicatechin 3-(6''-*O*-methyl) gallate (Asakawa *et al*., 2016)	
Position	δ_C	δ_H **(m, *J* in Hz)**	δ_C	δ_H **(m, *J* in Hz)**
1	-	-	-	-
2	77.0	5.13 (1H, br s)	78.5	5.00 (1H, s)
3	69.3	5.46 (1H, d, 3.5)	70.4	5.49 (1H, m)
4	25.9	3.05 (H-4b, m); 2.89 (H-4a, d, 17.0)	26.6	2.99 (H-4_a, dd, 17.5, 4.3); 2.86 (H-4b, dd, 17.5, 3.0)
5	156.9	-	157.8	
6	96.1	6.07 (1H, d, 2.3)	96.5	5.96 (1H, d, 2.6)
7	157.1	-	157.9	
8	94.8	5.99 (1H, d, 2.2)	95.8	5.95 (1H, d, 2.6)
9	156.1	-	157.2	-
10	97.8	-	99.4	-
1′	130.1	-	130.9	-
2′	114.6	7.05 (1H, d, 1.9)	111.9	7.02 (1H, d, 1.9)
3′	145.1	-	140.6	-
4′	145.2	-	146.0	-
5′	115.5	6.78 (1H, d, 8.1)	-	6.50 (1H, s)
6′	118.1	6.86 (1H, dd, 8.3, 1.9)	-	6.50 (1H, s)
		Galloyl moiety		
1″	165.7	-	167.7	-
2″	119.9	-	121.5	-
3″	111.0	7.11 (1H, d, 1.9)	106.8	7.05 (1H, d, 1.9)
4″	145.5	-	146.8	-
5″	139.8	-	133.7	-
6″	148.2	-	149.0	-
7″	105.2	7.01 (1H, d, 1.9)	106.3	7.01 (1H, d, 1.9)
OCH_3-6″	60.5	3.82 (3H, s)	56.6	3.82 (3H, s)

II.1.5.4.14. Structural elucidation of compound SYEF137

SYEF137 was obtained as a yellowish finely divided solid in the *n*-hexane/EtOAc (3:2, v/v) mixture. It was soluble in acetone and reacted positively to the ferric chloride test, characteristic of phenolic compounds. Its molecular formula, $C_{25}H_{26}O_7$, implying 13 degrees of unsaturation, was deduced by a combination of the NMR and ESIMS data (Figure 89) which showed the potassium adduct peak $[M+K]^+$ at *m/z* 477.43 (calcd for $C_{25}H_{26}O_7K^+$, 477.13).

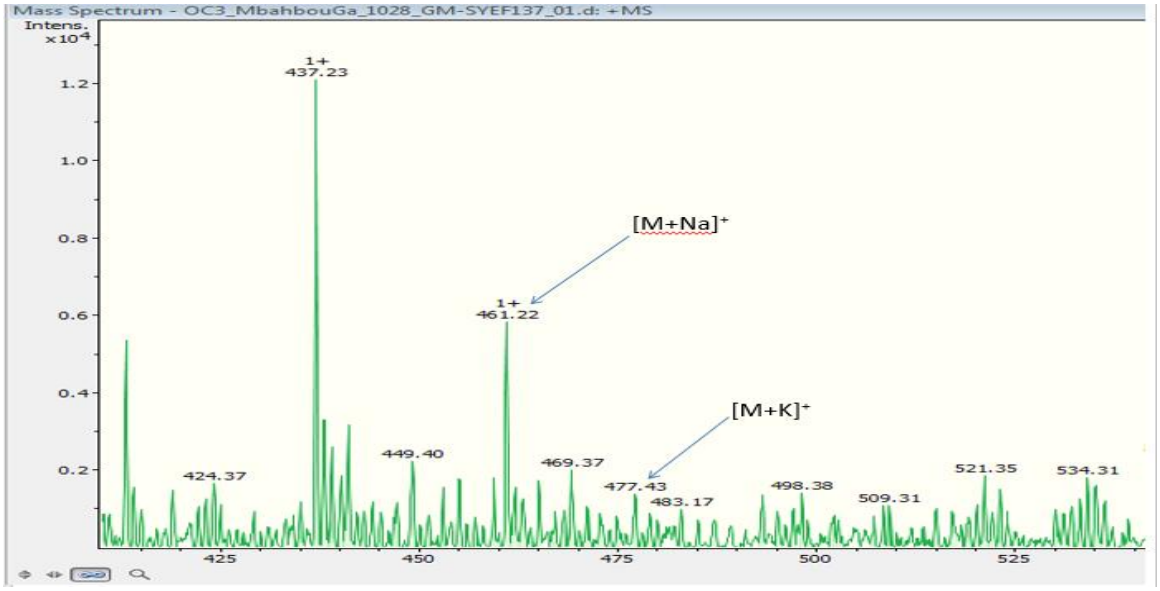

Figure 89: (+) ESI mass spectrum of SYEF137

Its ^{1}H NMR spectrum (Figure 90) displayed the resonances of:

- a singlet of a chelated hydroxy proton at δ_H 13.44 (1H, s, OH-1);
- an aromatic singlet at δ_H 7.12 (1H, s, H-8);
- the protons of a prenyl group (Ngouela *et al*., 2006) at δ_H 1.64 (3H, s, H-14), 1.77 (3H, s, H-15), 5.18 (1H, t, J = 7.1 Hz, H-12) and 3.25 (2H, d, J = 7.2 Hz, H-11);
- the protons of a dimethyl pyran ring (Ngouela *et al*., 2006) at δ_H 5.79 (1H, d, J = 10 Hz, H-2′), 7.06 (1H, d, J = 10 Hz, H-1′) and 1.46 (6H, s, 3′(2×CH_3));
- two methoxy groups at δ_H 3.89 (3H, s, OCH_3-6) and 3.91 (3H, s, OCH_3-7).

All these data showed that the compound SYEF137 is a xanthone carrying two methoxy groups, a prenyl and a 2,2-dimethylchromene moiety.

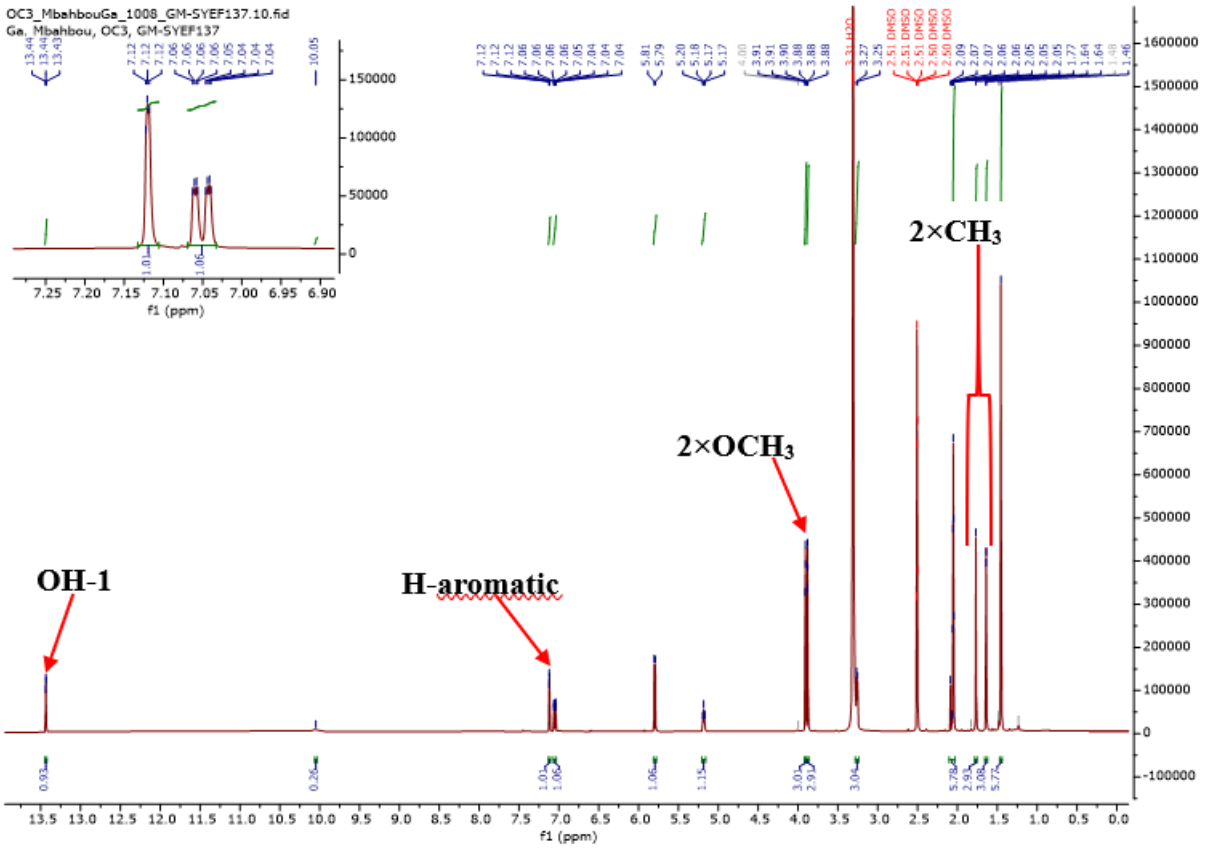

Figure 90: ^{1}H NMR of SYEF137 (DMSO-d_6, 500 MHz)

Its ^{13}C NMR spectrum (Figure 91) exhibited carbon resonances of xanthone type skeleton (Silva and Pinto, 2005), which were sorted by HMQC and DEPT 135 (Figure 92) techniques into:

- fourteen quaternary carbons including carbon of a carbonyl of 1 or 8 hydroxylated xanthone at δ_C 180.5 (C-9) (Silva *et* Pinto., 2005) and the others at δ_C 159.5 (C-1), 157.9 (C-3), 150.6 (C-7), 150.0 (C-4a), 143.3 (C-6), 142.0 (C-10a), 139.9 (C-5), 131.7 (C-13) , 115.5 (C-8a), 110.9 (C-4), 102.6 (C-9a), 101.0 (C-2) and 78.7 (C-3′);
- four carbons of methine groups including three olefinics at δ_C 127.7 (C-2′) and 122.2 (C-12), 115.6 (C-1′) and one aromatic at δ_C 95.9 (C-8);
- one carbon of methylene group at δ_C 21.1 (C-11);
- four carbons of methyl groups at δ_C 25.8 (C-14), 18.0 (C-15) and 28.1 (3′(2×CH_3));
- two carbons of methoxy groups at δ_C 56.1 (7-OCH_3) and 61.1 (6-OCH_3).

All these data suggest that SYEF137 is a dimethoxylated xanthone with a chelated hydroxy group bearing also a prenyl and 2,2-dimethylchromene moiety.

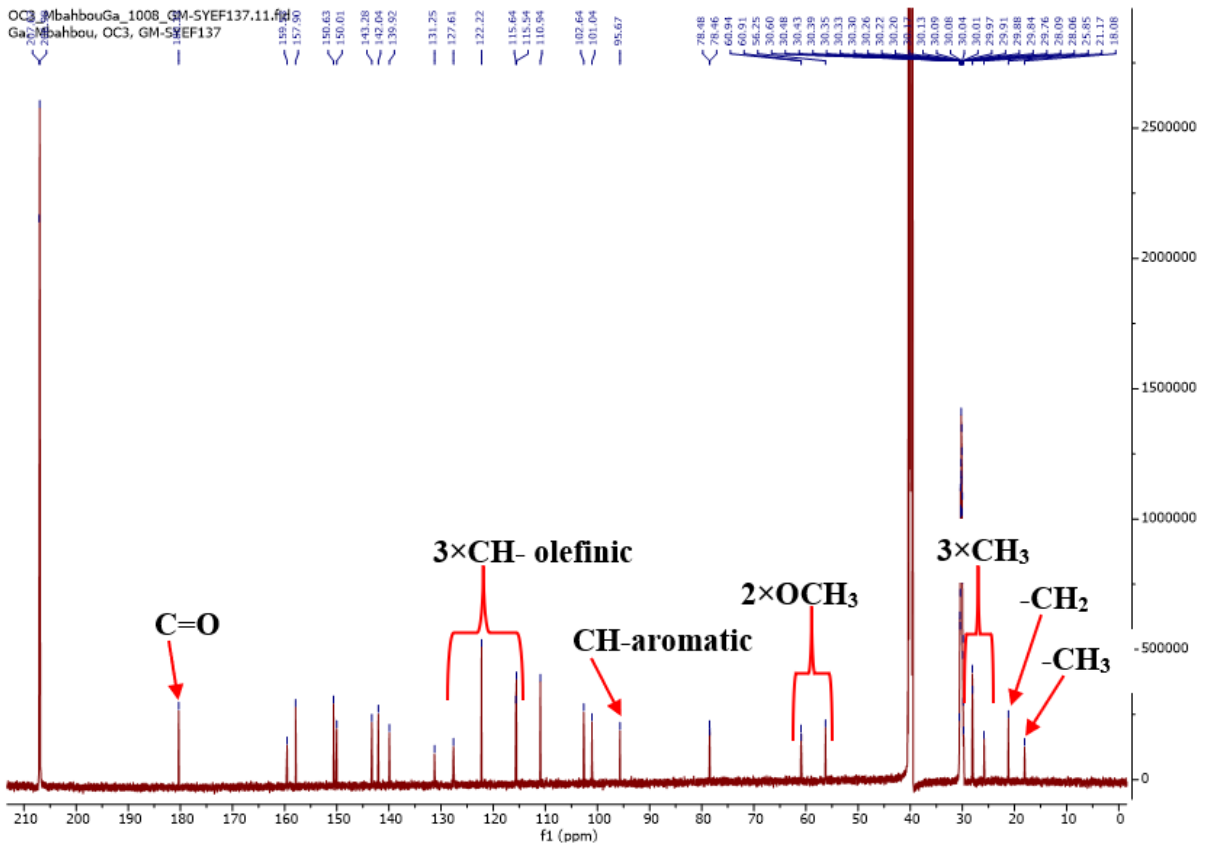

Figure 91: ^{13}C NMR spectrum of SYEF137 (DMSO-*d*$_6$, 150 MHz)

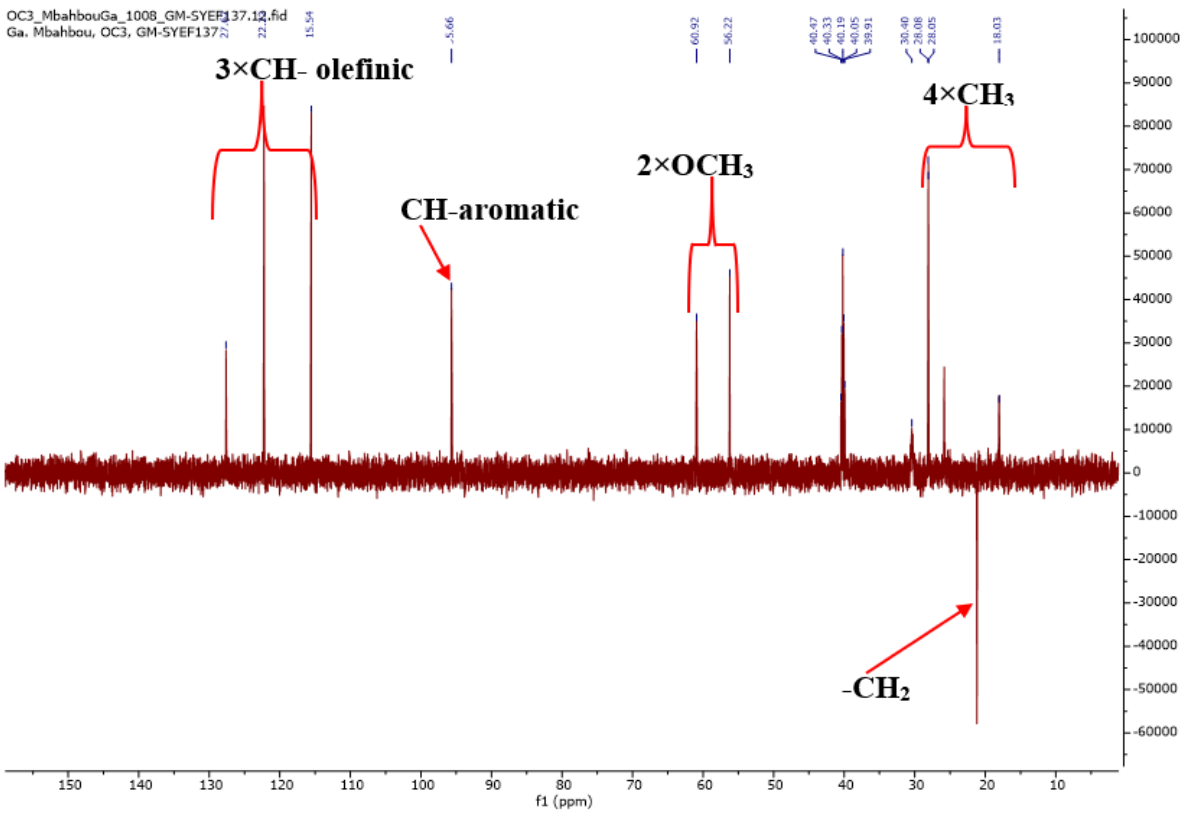

Figure 92: DEPT 135 spectrum of SYEF137

The positions of these groups on the xanthone skeleton were determined by correlations observed on the HMBC spectrum (Figure 93). In fact, on this spectrum, cross peaks were observed between;

- the methoxy protons OCH_3-7 (δ_H 3.90) and the aromatic carbons C-7 (δ_C 150.6), C-8 (δ_C 95.7) suggesting the attachment of the methoxy group to the position C-7;
- the methoxy protons OCH_3-6 (δ_H 3.87) and the aromatic carbon C-6 (δ_C 143.3) suggesting the attachment of the methoxy group to the C-6;
- the protons of the methylene carbon H-11(δ_H 3.25) and carbons C-3 (δ_C 157.9) and C-4 (δ_C 110.9) confirming the attachment of the 3,3-dimethylallyl moiety to the C-4;
- the protons of the methyl groups of the dimethyl pyran ring 3′ (2×CH_3) (δ_H 1.46) and carbon, C-3′ (δ_C 78.5), C-1′ (δ_C 115.6), C-2′ (δ_C 127.6);
- the olefinic proton of the dimethyl pyran ring H-2′ (δ_H 5.79) and carbon 3′ (2×CH_3) (δ_C 28.1), C-3′ (δ_C 78.5), C-2 (δ_C 101.0), C-3 (δ_C 157.9) confirming the linear cyclisation;
- the olefinic proton of the dimethyl pyran ring H-1′ (δ_H 7.04) and carbon 3′ (2×CH_3) (δ_C 28.1), C-3′ (δ_C 78.5), C-2 (δ_C 101.0), C-1 (δ_C 150.0), C-3 (δ_C 157.9) confirming the attachment of the 2,2-dimethylchromene moiety at C-2 and C-3.

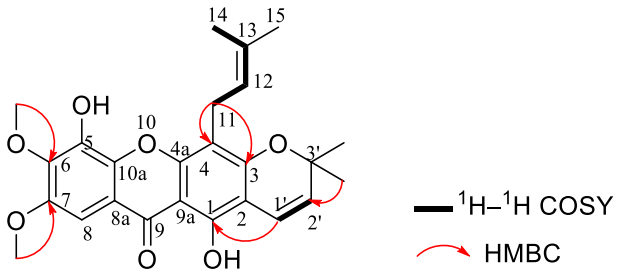

Scheme 25: Key HMBC correlations of SYEF137

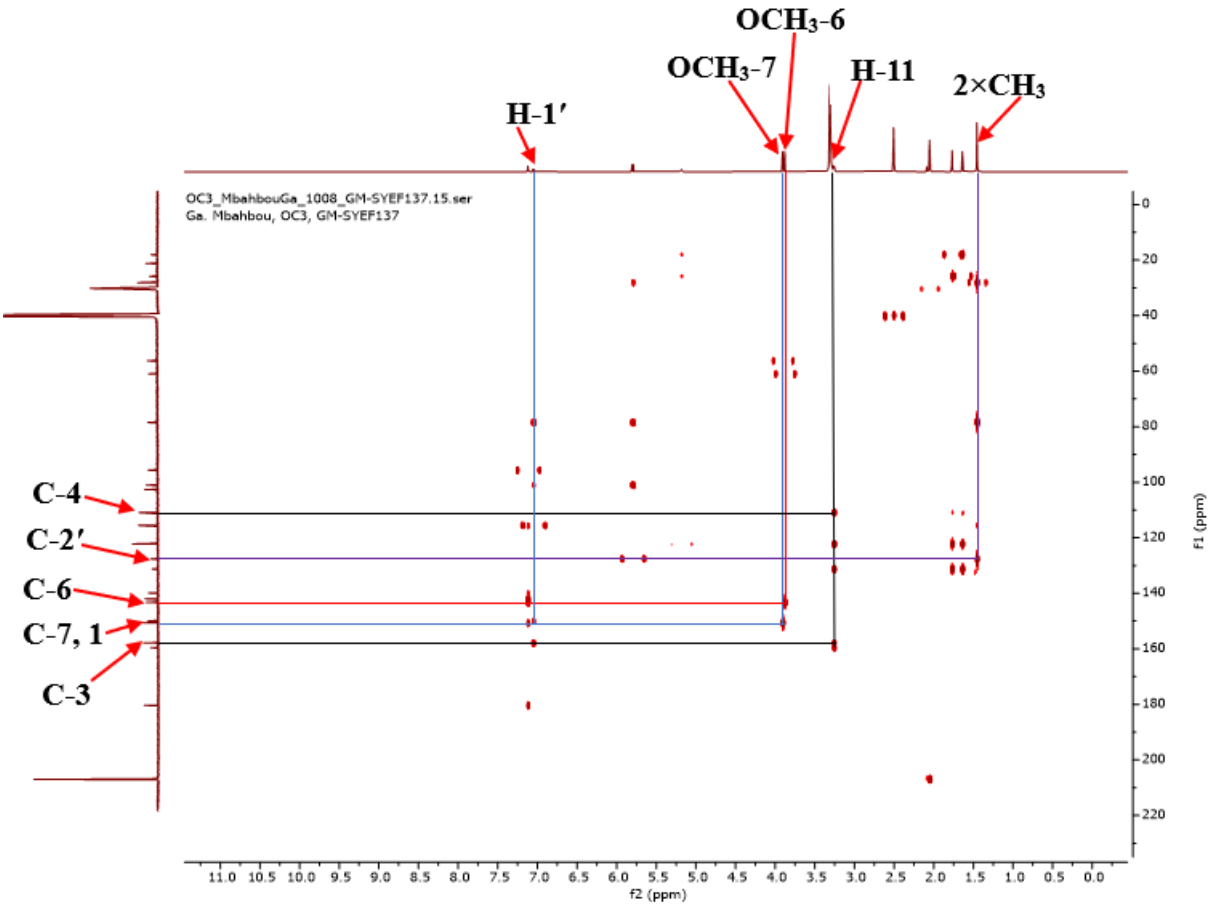

Figure 93: HMBC spectrum of SYEF137

All these data, compared to those described in the literature, were in accordance with that of gaboxanthone (**131**) previously isolated from the seeds of *S. globulifera* by Ngouela and collaborators (2006).

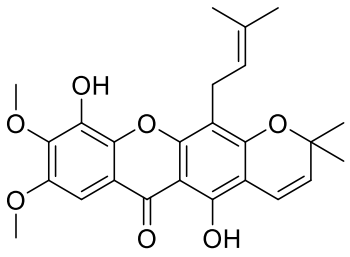

131

Table 37: ^{1}H (500 MHz) and ^{13}C (125 MHz) NMR data of SYEF137 in DMSO-d_6 compared to those of gaboxanthone [^{13}C (100.6 MHz), ^{1}H (400.1 MHz), $CDCl_3$]

	SYEF137		Gaboxanthone (Ngouela et *al.*, 2006)	
Position	δ_C	δ_H **(m, *J* in Hz)**	δ_C	δ_H **(m, *J* in Hz)**
1	159.5	-	158.0	-
2	101.0	-	102.0	-
3	157.9	-	155.6	-
4	110.9	-	107.5	-
4a	150.0	-	153.0	-
5	139.9	-	140.0	-
6	143.3	-	141.1	-
7	150.6	-	149.4	-
8	95.7	7.12 (1H, s)	96.6	7.23 (1H, s)
8a	115.5	-	116.0	-
9	180.3	-	180.0	-
9a	nd			
10a	142.0	-	138.0	-
11	21.17	3.25 (2H, overlapped)	21.6	3.52 (2H, d, 7.2)
12	122.2	5.18 (1H, t, 7.1)	122.3	5.30 (1H, t, 7.2)
13	131.3	-	131.7	-
14	25.9	1.64 (3H, s)	25.8	1.89 (3H, s)
15	18.1	1.77 (3H, s)	17.9	1.70 (3H, s)
1’	115.6	7.04 (1H, d, 10.0)	115.8	6.65 (1H, d, 10.0)
2’	127.6	5.79 (1H, d, 10.0)	127.4	7.04 (1H, d, 10.0)
3’	78.5	-	78.1	-
(2×CH_3)-3’	28.1	1.46 (3H, s)	28.4	1.55 (3H, s)
OCH_3-7	56.1	3.90 (3H, s)	56.2	3.94 (3H, s)
OCH_3-6	61.1	3.89 (3H, s)	61.4	4.06 (3H, s)
OH-1	-	13.43 (1H, s)	-	13.35 (1H, s)
OH-5	-	-	-	4.85 (1H, s)

II.1.5.4.15. Structural elucidation of compound SYEF171

SYEF171 was obtained as a yellowish finely divided solid in the *n*-hexane/EtOAc (3:2, v/v) mixture. It is soluble in acetone and reacted positively to the ferric chloride test, characteristic of phenolic compounds. Its molecular formula, $C_{24}H_{24}O_7$, was deduced from the HRESIMS spectrum (Figure 94) which showed the potassium adduct peak $[M+K]^+$ at *m/z* 463.4534 (calcd for $C_{24}H_{24}O_7K^+$, 463.4530), with 13 degrees of unsaturation. This mass was 14 amu less than that of SYEF137 suggesting the absence of a CH_2 in SYEF171.

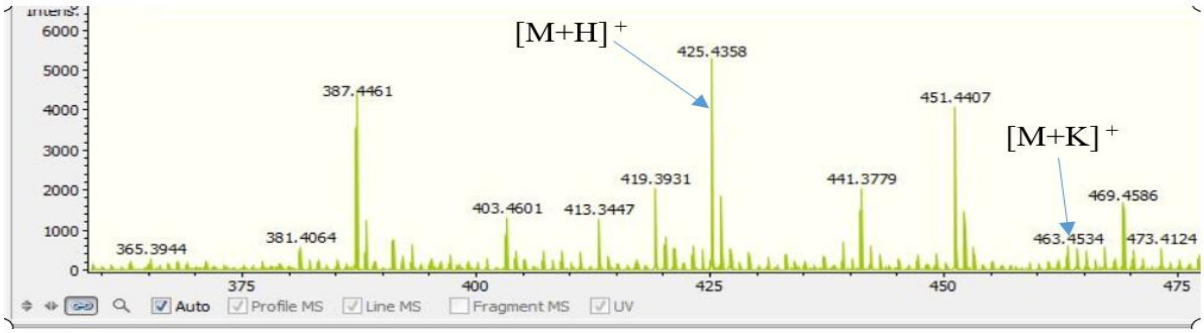

Figure 94: (+) HRESI mass spectrum of SYEF171

Comparison of the ^1H (Figure 95) and ^{13}C NMR (Figure 96) spectra of SYEF171 with those of SYEF137 showed some similarities. The difference between the ^1H NMR spectrum (Figure 95) of SYEF 171 with that of SYEF137 is the diseapperance of the signal of the singlet of the methoxy group at δ_H 3.89 (3H, s) in SYEF171.

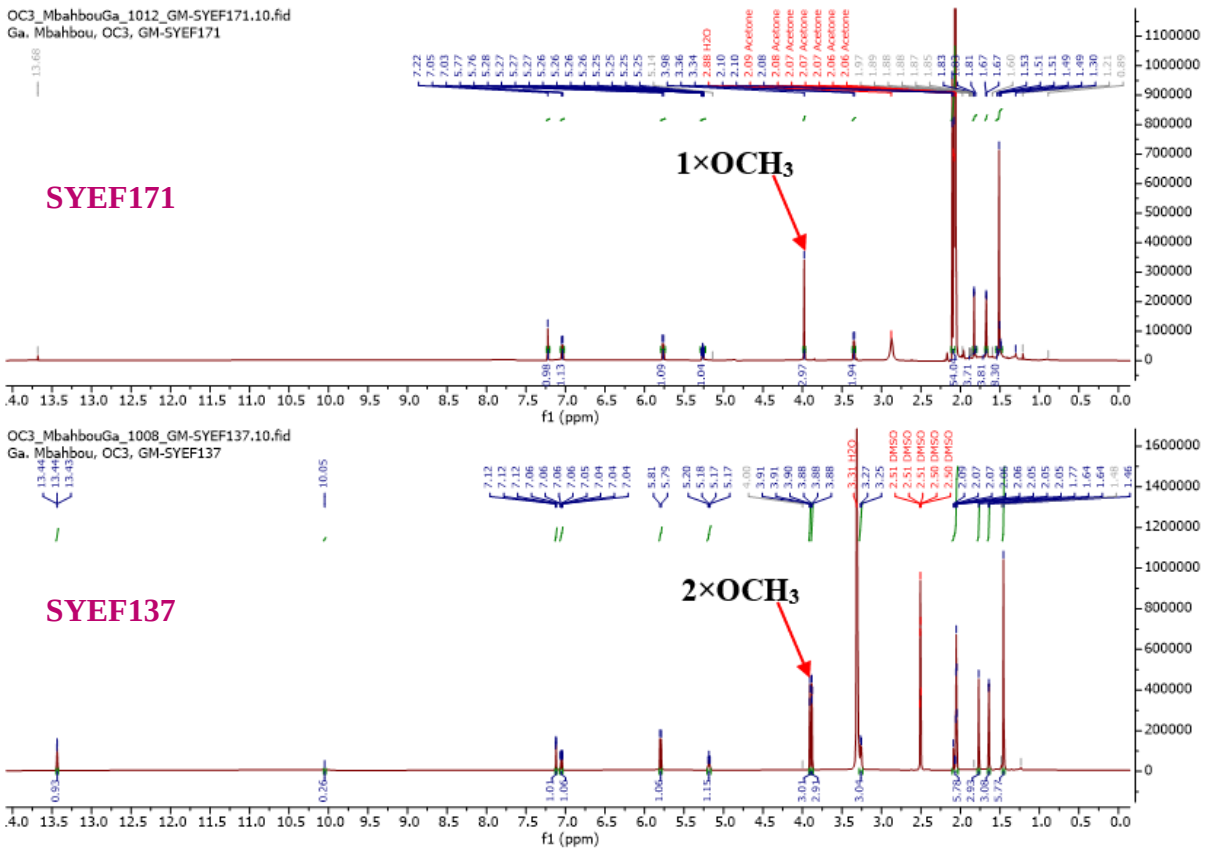

Figure 95: Comparative ^{1}H NMR of SYEF137 (DMSO-d_6, 500 MHz) and SYEF171 (Acetone-d_6, 500 MHz)

The broad band decoupled ^{13}C NMR spectrum (Figure 96) of SYEF171 exhibited characteristic signals of gaboxanthone (**131**):

- fourteen quaternary carbons including carbon of a carbonyl of 1 or 8 hydroxylated xanthone at δ_C 180.0 (C-9) (Silva *et* Pinto., 2005) and the others at δ_C 159.5 (C-1), 157.5 (C-3), 145.8 (C-7), 149.9 (C-4a), 142.3 (C-6), 141.2 (C-10a), 133.0 (C-5), 130.6 (C-13) , 112.1 (C-8a), 110.8 (C-4), 102.5 (C-9a), 101.2 (C-2) and 78.0 (C-3′);
- four carbons of methine groups including three olefinics at δ_C 127.0 (C-2′), 122.3 (C-12) and 115.4 (C-1′) and one aromatic at δ_C 95.9 (C-8);
- one carbon of a methylene group at δ_C 21.1 (C-11);
- four carbons of methyl groups at δ_C 25.0 (C-14), 17.4 (C-15) and 27.2 (3′(2×CH_3));
- one carbon of a methoxy group at δ_C 55.8 (7-OCH_3).

The only difference observed on both spectra was the absence of signal of one methoxy group at δ_C 61.1 (3H, s, OCH_3-6) in SYEF171 (Figure 96).

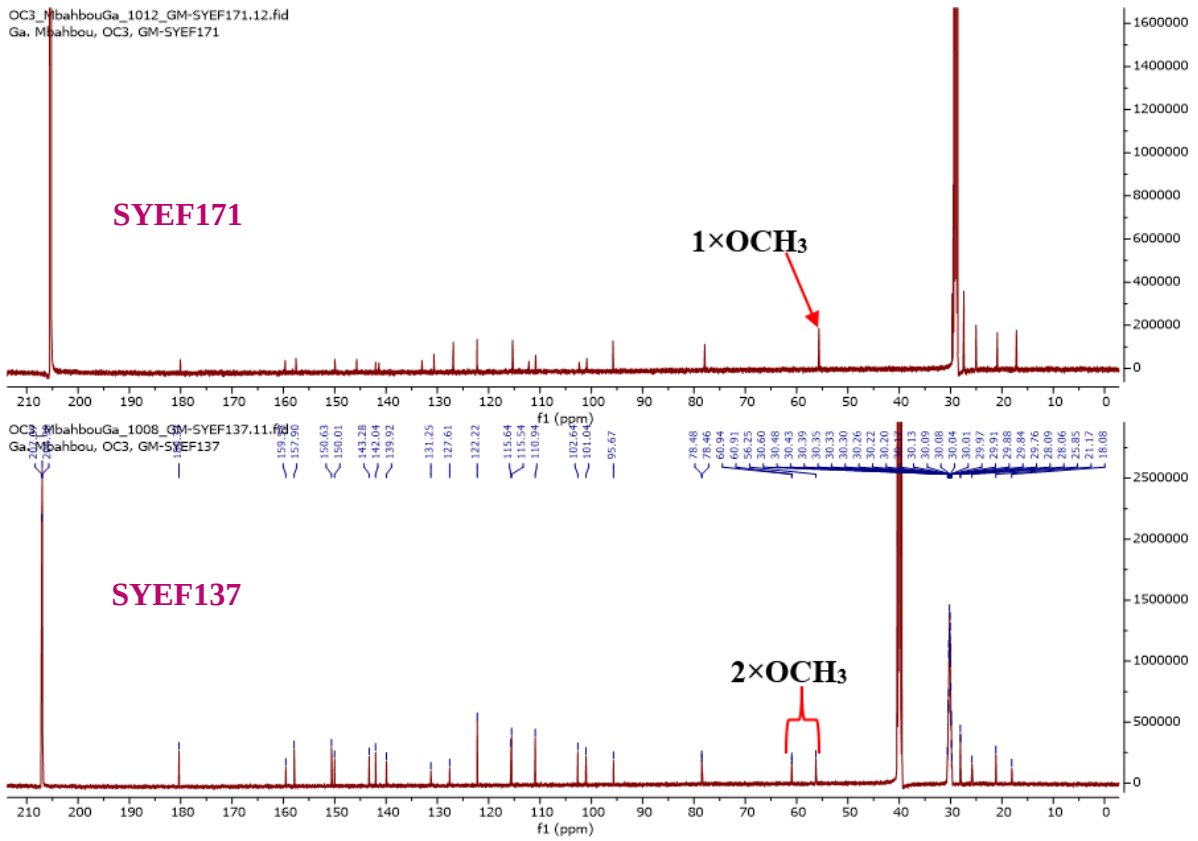

Figure 96: Comparative of ^{13}C NMR spectrum of SYEF137 (DMSO-d_6, 125 MHz) and SYEF171 (Acetone-d_6, 125 MHz)

The position of the remaining methoxy group on the xanthone skeleton was deduced from the correlations observed on the HMBC spectrum of SYEF171 (Figure 97). In fact, on this spectrum, cross peak was observed between the methoxy protons OCH_3-7 (δ_H 3.98) and the aromatic carbon C-7 (δ_C 145.8) confirming the attachment of the methoxy group to C-7 (δ_C 145.8).

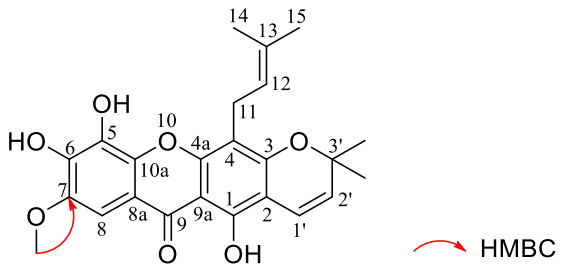

Scheme 26: Key HMBC correlations of SYEF171

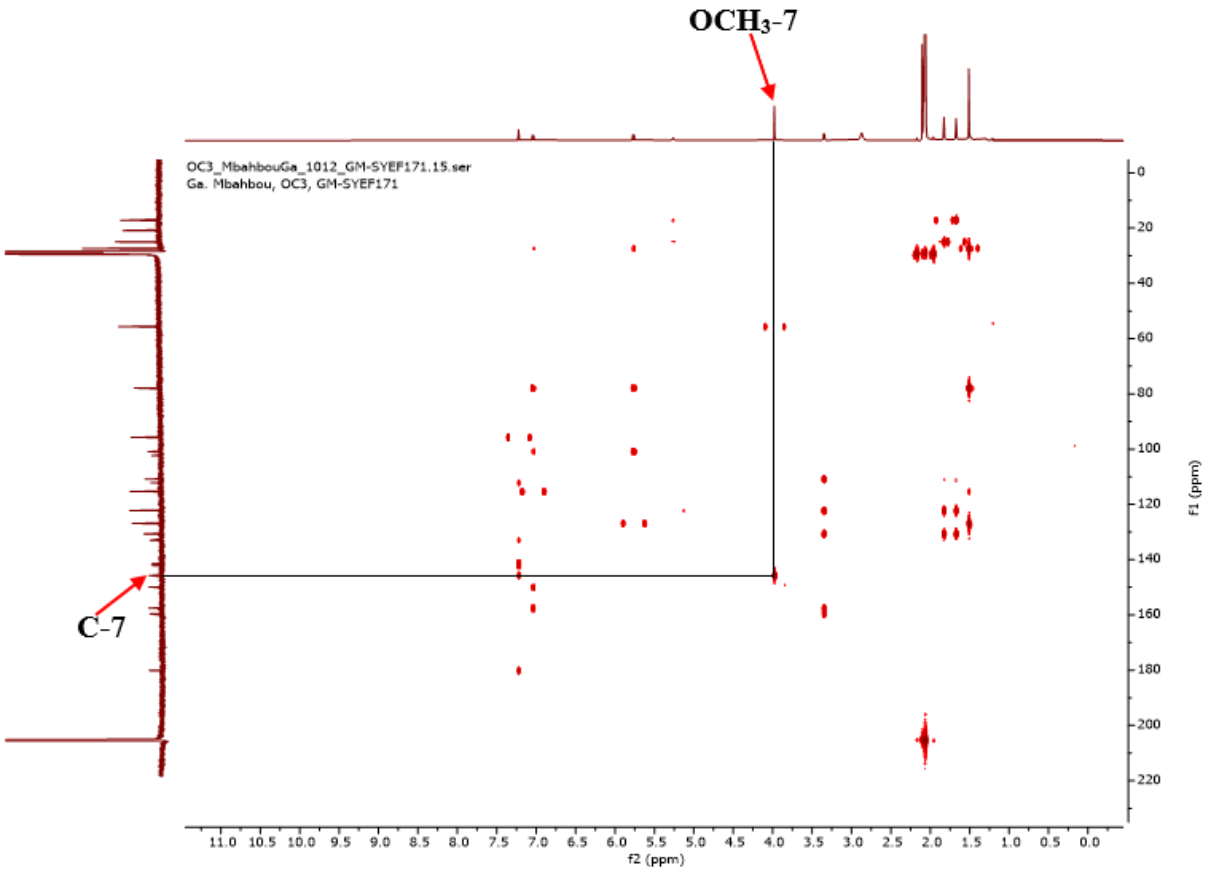

Figure 97: HMBC spectrum of SYEF171

All these data compared with those from literature were in agreement with xanthone V2 (**132**) previously isolated from the root bark of *Vismia guineensis* (Botta et *al*., 1986) and to the best of our knowledge isolated for the first time from *S. globulifera*.

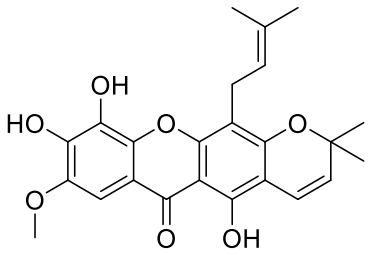

132

Table 38: ^{1}H (500 MHz) and ^{13}C (125 MHz) NMR data of SYEF171 in Acetone-d_6 compared to xanthone V2 [DMSO-d_6, RMN ^{13}C (25.2 MHz), RMN ^{1}H (60 MHz)]

	SYEF171		Xanthone V2 (Botta et *al*., 1986)	
Position	δ_C	δ_H **(m, *J* in Hz)**	δ_C	δ_H **(m, *J* in Hz)**
1	159.5	-	157.9	-
2	101.2	-	104.6	-
3	157.5	-	156.1	-
4	110.8	-	107.9	-
4a	149.9	-	150.7	-
5	133.0	-	133.9	-
6	142.3	-	141.8	-
7	145.8	-	146.1	-
8	95.9	7.21 (1H, s)	96.1	7.14 (1H, s)
8a	112.1	-	112.7	-
9	180.0	-	180.2	-
9a	102.5	-	103.2	-
5a	141.2	-	142.9	-
11	21.2	3.34 (2H, overlapped)	21.7	3.50 (2H, d, 7)
12	122.3	5.26 (1H, t, 7.1)	123.3	5.30 (1H, t, 7.0)
13	130.6	-	131.2	-
14	25.0	1.67 (3H, s)	25.7	1.65 (3H, s)
15	17.4	1.89 (3H, s)	17.9	1.85 (3H, s)
1’	115.4	7.09 (1H, d, 10.0)	116.1	6.65 (1H, d, 10.0)
2’	127.0	5.78 (2H, d, 10.0)	127.8	5.79 (2H, d, 10.0)
3’	78.0	-	78.3	-
(2×Me)-3′	27.2	1.53 (3H, s)	28.2	1.48 (6H, s)
OMe-7	55.8	3.98 (3H, s)	56.2	3.90 (3H, s)
OH-6	-	-	-	-
OH-1	-	13.71 (1H, s)	-	13.45 (s)
OH-5	-	-	-	-

II.1.5.4.16. Structural elucidation of compound SYE26-8M

SYE26-8M was obtained as a yellowish finely divided solid in the *n*-hexane/EtOAc (3:2, v/v) mixture. It is soluble in DMSO and reacted positively to the ferric chloride test, characteristic of phenolic compounds. Its molecular formula, $C_{25}H_{26}O_7$, was deduced from the HRESIMS spectrum (Figure 98), which showed the sodium adduct peak $[M+Na]^+$ at *m/z* 461.1480 (calcd for $C_{25}H_{26}NaO_7$, 461.1480), with 13 degrees of unsaturation. This mass was identical to that of SYEF137 suggesting that SYE26-8M is an isomer of SYEF137.

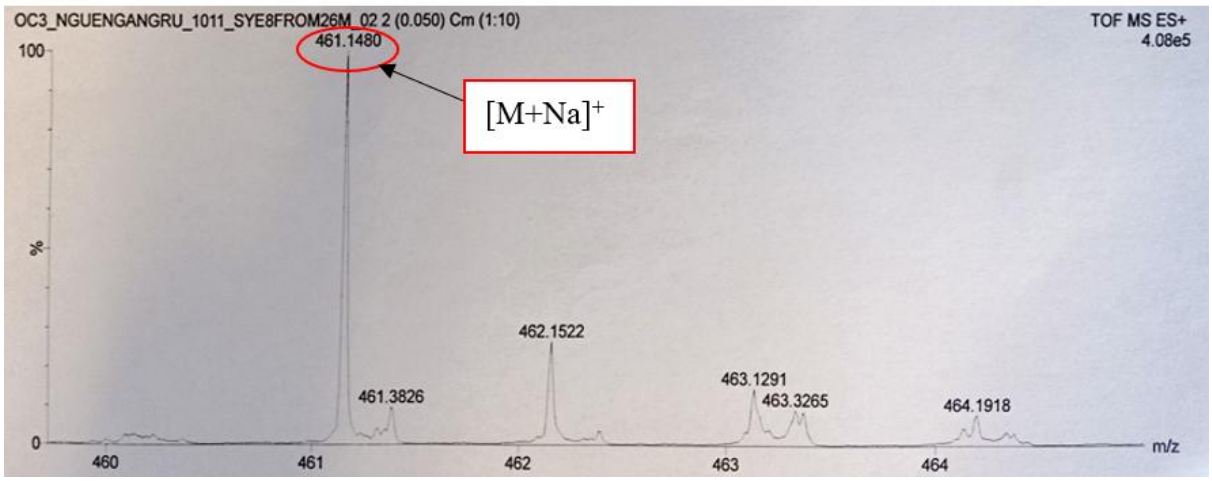

Figure 98: (+) HRESI mass spectrum of SYE26-8M

The ^{1}H NMR spectrum of **SYE26-8M** was close to that of **SYEF137** (Figure 99). In fact, the ^{1}H NMR spectrum of **SYE26-8M** displayed the resonances of:

- a singlet of a chelated hydroxy proton at δ_H 13.42 (1H, s, OH-1);
- an aromatic singlet at δ_H 7.11 (1H, s, H-8);
- the protons of a prenyl group (Ngouela *et al*., 2006) at δ_H 1.64 (3H, s, H-14), 1.76 (3H, s, H-15), 5.18 (1H, m, H-12) and 3.25 (2H, d, J = 7.5 Hz, H-11);
- the protons of a 2,2-dimethylchromene moiety (Ngouela *et al*., 2006) at δ_H 5.80 (1H, d, J = 10 Hz, H-2′), 7.03 (1H, d, J = 10 Hz, H-1′) and 1.45 (6H, s, 3′(2×CH_3));
- two singlets of methoxy groups at δ_H 3.87 (3H, s, OCH_3-6) and 3.90 (3H, s, OCH_3-7).

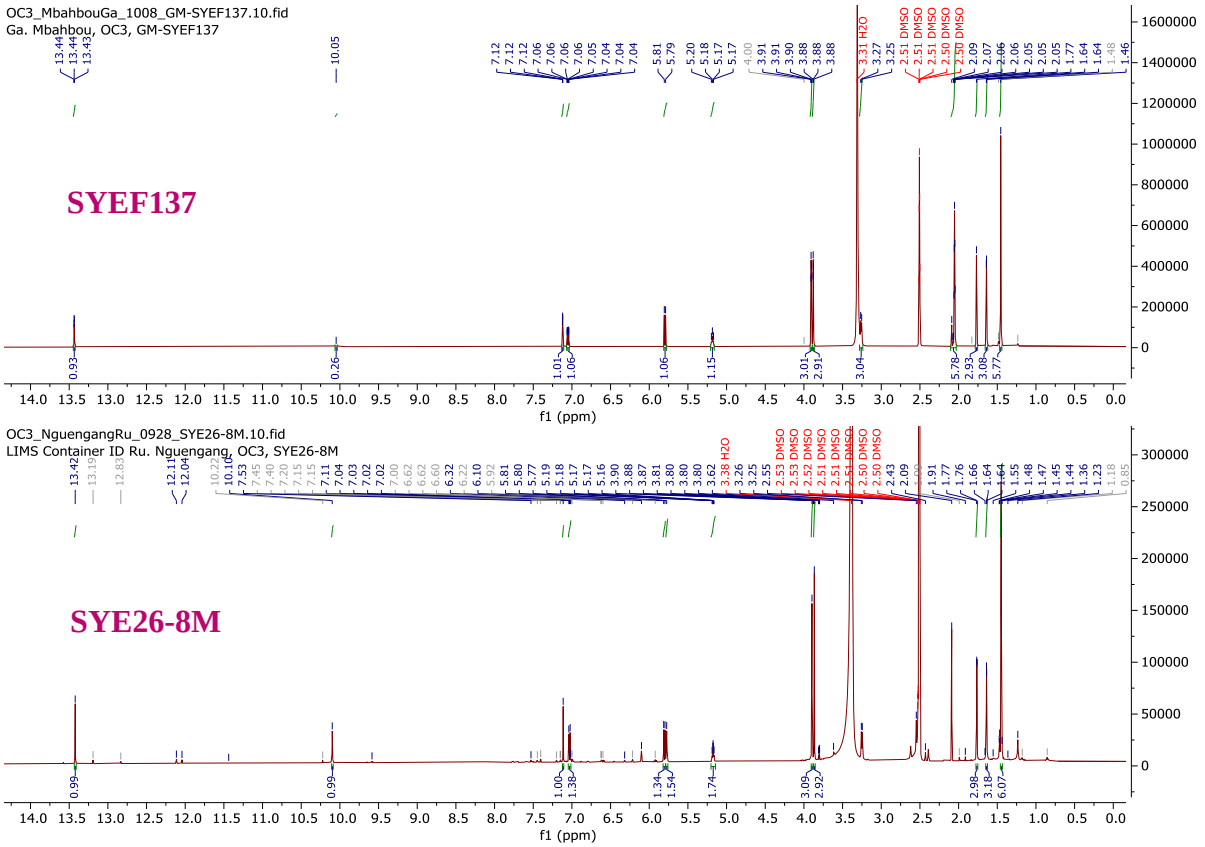

Figure 99: Comparative ^{1}H NMR of SYEF137 and SYE26-8M (DMSO-d_6, 500 MHz)

The broad band decoupled ^{13}C NMR spectrum (Figure 100) of **SYE26-8M** exhibited characteristic signals of gaboxanthone (**123**) given as follows:

- fourteen quaternary carbons including carbon of a carbonyl of 1 or 8 hydroxylated xanthone at δ_C 180.3 (C-9) (Silva *et* Pinto., 2005) and the others at δ_C 159.4 (C-1), 157.9 (C-3), 150.6 (C-7), 150.0 (C-4a), 143.3 (C-6), 139.9 (C-10a), 142.0 (C-5), 131.4 (C-13) , 115.6 (C-8a), 101.1 (C-4), 102.6 (C-9a), 111.0 (C-2) and 78.6 (C-3′);
- four carbons of methine groups including three olefinics at δ_C 127.8 (C-2′) and 122.2 (C-12), 115.5 (C-1′) and one aromatic at δ_C 95.7 (C-8);
- one carbon of methylene group at δ_C 21.2 (C-11);
- four carbons of methyl groups at δ_C 26.0 (C-14), 18.2 (C-15) and 28.2 (3′(2×CH_3));
- two carbons of methoxy groups at δ_C 56.4 (OCH_3-7) and 61.0 (OCH_3-6).

However, significant differences were recognized in the signals of C-2 and C-4 carbons. In fact, the C-4 here resonated at higher field (δ_C 101.1) than that of SYEF137 (δ_C 110.9), while the C-2 here resonated at lower field (δ_C 111.0) than that of SYEF137 (δ_C 101.1) indicated that the 3,3-dimethylallyl group was attached to C-2 while the chromene moiety was attached to C-3 and C-4 of ring A of the xanthone nucleus.

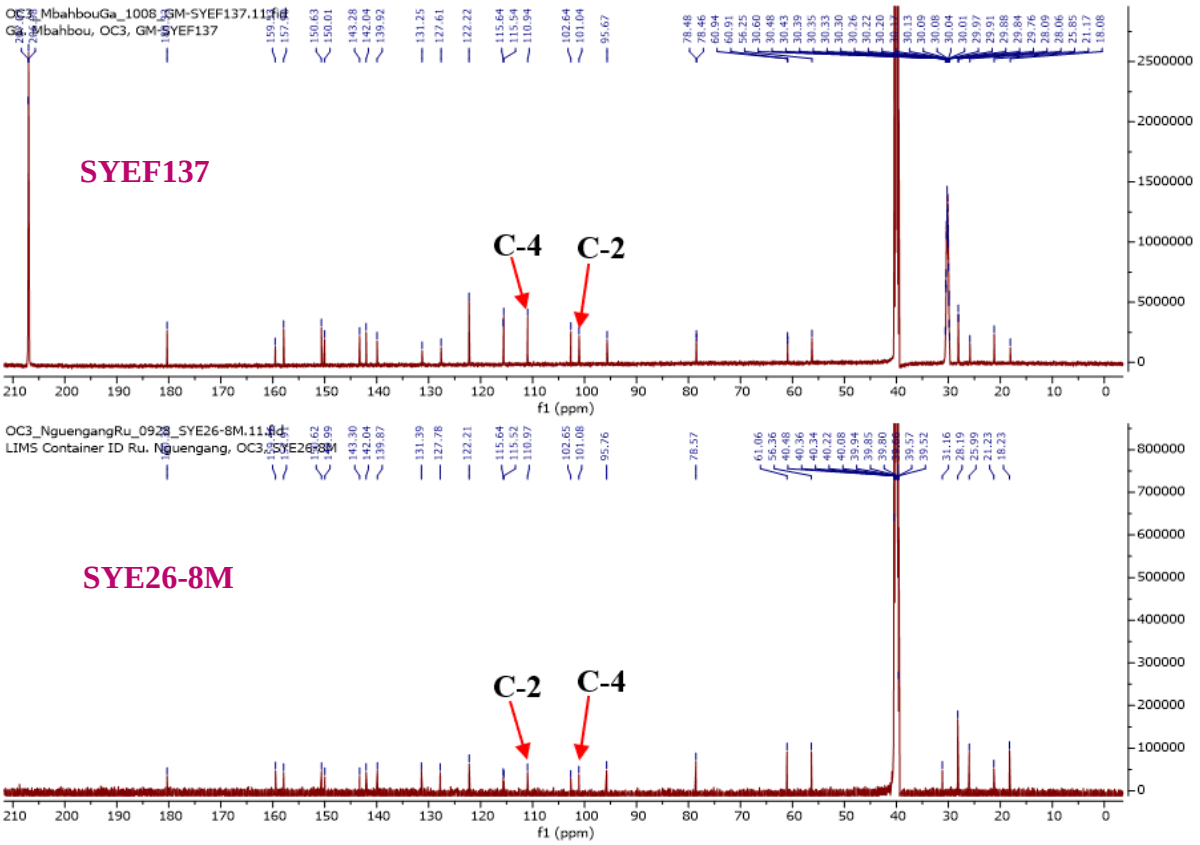

Figure 100: Comparative ^{13}C NMR spectrum of SYEF137 and SYE26-8M (DMSO-*d*$_6$, 125 MHz)

These results were confirmed by the cross-peaks of the methylene proton of the 3,3-dimethylallyl group at δ_H 3.25 (2H, d, J = 7.5 Hz, H-11) with three quaternary carbons C-1 (δ_C 159.4), C-2 (δ_C 111.0) and C-13 (δ_C 131.4) while the protons of the AB system of the 2,2-dimethylchromene moiety (δ_C 7.03 and 5.80) displayed correlations with C-3 (δ_C 157.9) and C-3' (δ_C 78.6) and with C-4 (δ_C 101.1) and C-3' (δ_C 78.6), respectively.

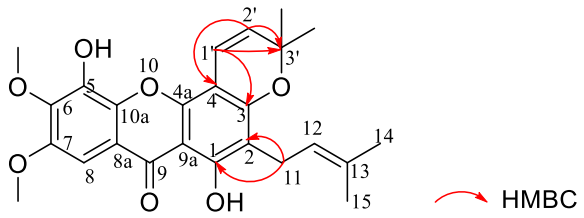

Scheme 27: Key HMBC correlations of SYE26-8M

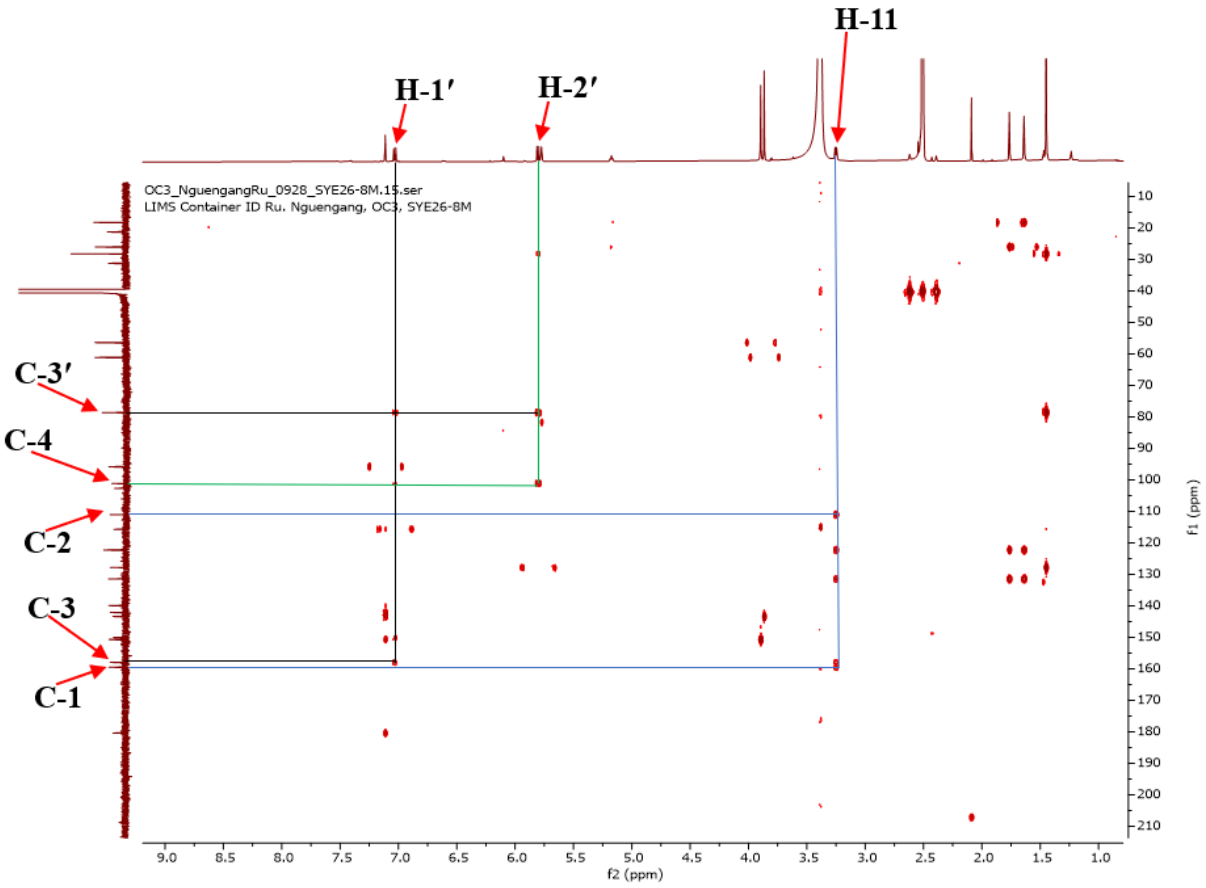

Figure 101: HMBC spectrum of SYE26-8M

All these data, compared to those in the literature, led to the identification of **SYE26-8M** as symphonin (**133**), previously isolated from seeds of *Symphonia globulifera* by Lenta and collaborators (2004).

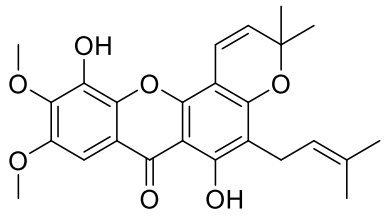

133

Table 39: ^{1}H (600 MHz) and ^{13}C (150 MHz) NMR data of SYE26-8M in DMSO-d_6 compared to symphonin [^{13}C (100.6 MHz), ^{1}H (400.1 MHz) $CDCl_3$]

	SYE26-8M		Symphonin (Lenta et *al*., 2004)	
Position	δ_C	δ_H **(m, *J* in Hz)**	δ_C	δ_H **(m, *J* in Hz)**
1	159.4	-	160.0	-
2	111.0	-	111.7	-
3	157.9	-	158.3	-
4	101.1	-	107.5	-
4a	150.0	-	150.0	-
5	142.0	-	140.9	-
6	143.3	-	140.9	-
7	150.6	-	149.2	-
8	95.7	7.11 (1H, s)	96.9	7.20 (1H, s)
8a	115.6	-	116.0	-
9	180.3	-	180.2	-
9a	102.6	-	103.0	-
10a	139.9	-	137.9	-
11	21.2	3.25 (2H, d, 7.5)	21.8	3.34 (d, 7.2)
12	122.2	5.18 (1H, m)	122.1	5.20 (m)
13	131.4	-	131.5	-
14	26.0	1.64 (3H, s)	25.8	1.60 (3H, s)
15	18.2	1.76 (3H, s)	18.2	1.80 (3H, s)
1’	115.5	7.03 (1H, d, 10.0)	115.5	6.80 (1H, d, 10.0)
2’	127.8	5.80 (1H, d, 10.0)	126.8	5.50 (1H, d, 10.0)
3’	78.2	-	78.0	-
(2×CH_3)-3’	28.2	1.45 (3H, s)	28.2	1.40 (3H, s)
OCH_3-6	61.0	3.87 (3H, s)	61.4	4.04 (3H, s)
OCH_3-7	56.4	3.90 (3H, s)	56.2	3.96 (3H, s)
OH-1	-	13.42 (1H, s)	-	13.20 (1H, s)
OH-5	-	10.10 (1H, s)	-	5.80

II.1.5.4.17. Structural elucidation of compound SYEF1310b

SYEF1310b was obtained as a yellowish finely divided solid in the *n*-hexane/EtOAc (3:2, v/v) mixture. It was soluble in acetone and reacted positively to the ferric chloride test, characteristic of phenolic compounds. Its molecular formula, $C_{14}H_{10}O_5$, implying ten degrees of unsaturation, was deduced from the combination of the data from its ESIMS spectrum (Figure 102), which showed the sodium adduct peak $[M+Na]^+$ at *m/z* 281.0 with those from its NMR spectra (Figure 103 to 106).

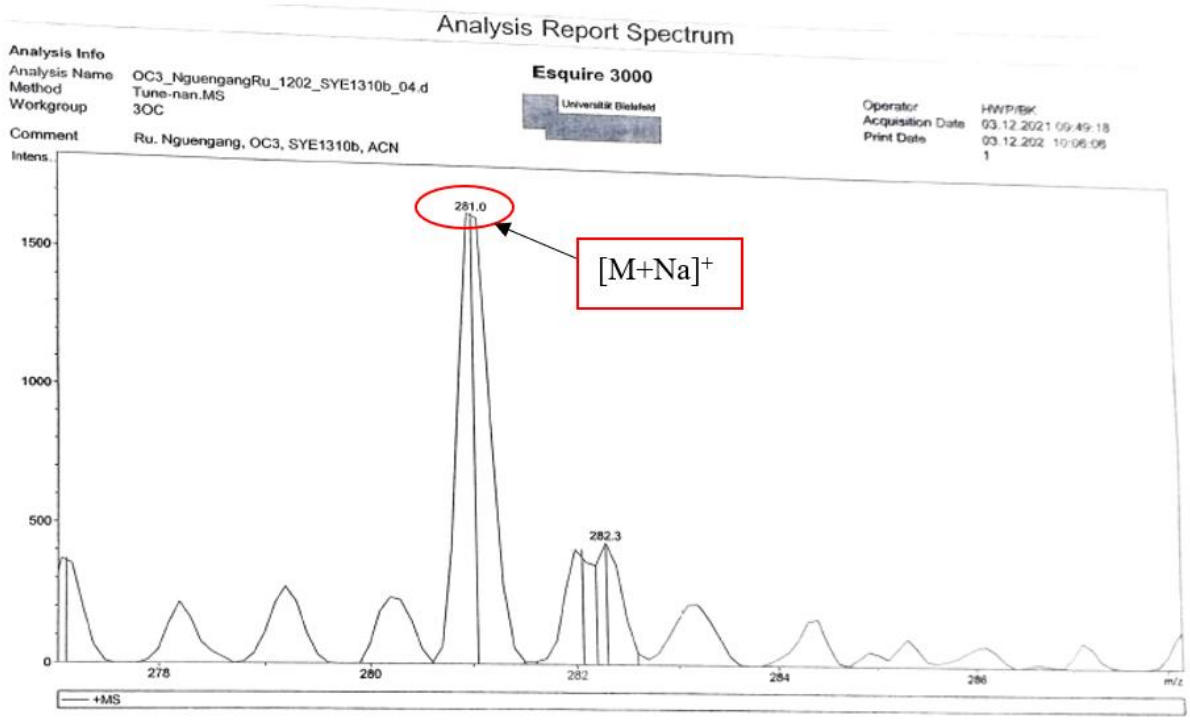

Figure 102: (+) ESI mass spectrum of SYEF1310b

Its ^{1}H NMR spectrum (Figure 103) displayed resonances of:

- one singlet at δ_H 3.97 (3H, s, OCH_3-3), attributable to one methoxy group;
- a chelated hydroxyl proton at δ_H 12.94 (1H, OH-1);
- one couple of *meta*-coupled aromatic protons at δ_H 6.38 (1H, d, J = 2.2 Hz, H-2) and 6.59 (1H, d, J = 2.3 Hz, H-4);
- one aromatic proton at δ_H 7.31 (1H, t, J = 7.9 Hz, H-7), which formed an ABC system with the two other protons at δ_H 7.39 (1H, dd, J = 7.8, 1.6 Hz, H-6) and 7.70 (1H, dd, J = 7.9, 1.5 Hz, H-8) according to their coupling constants.

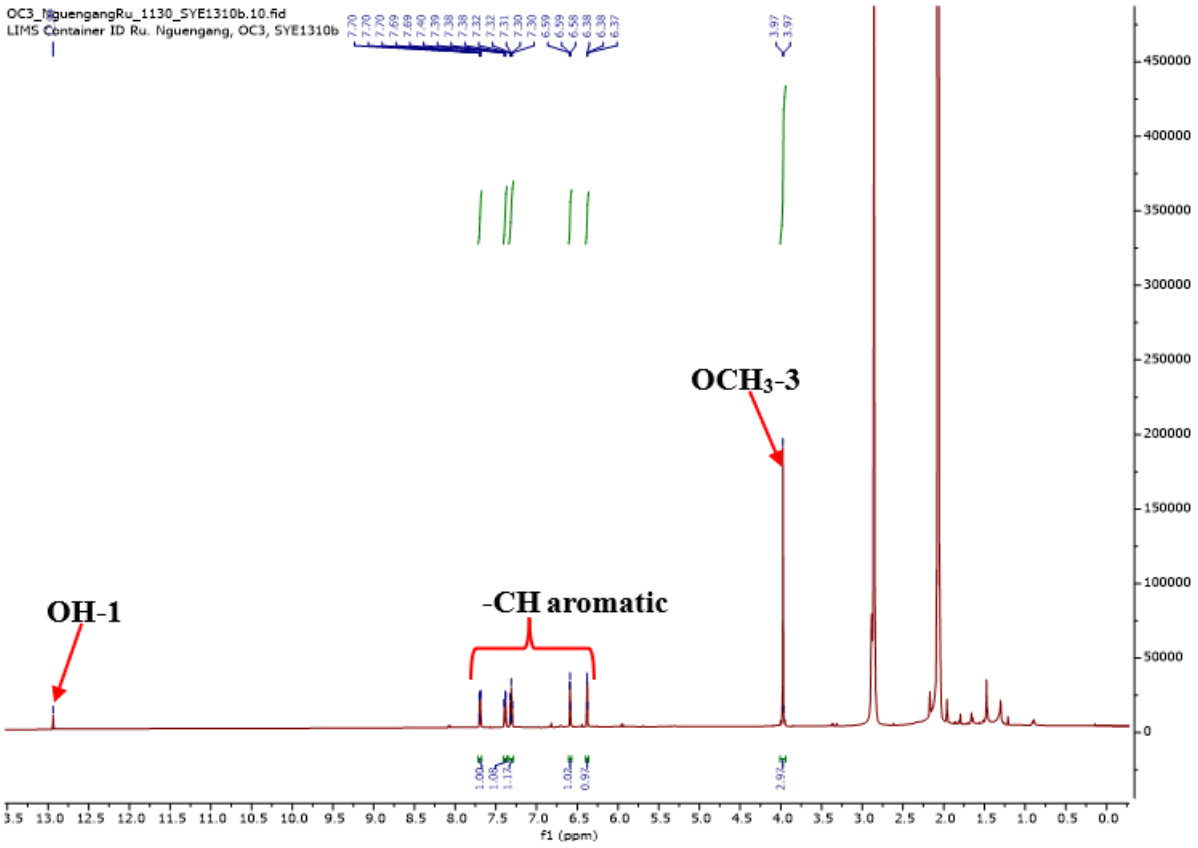

Figure 103: ^{1}H NMR of SYEF1310b (Acetone-d_6, 600 MHz)

Its ^{13}C NMR spectrum (Figure 104) exhibited carbon resonances of xanthone type skeleton (Silva et Pinto, 2005), which were sorted by DEPT 135 (Figure 105) technique into:

- eight quaternary carbons at δ_C 103.4 (C-9a), 121.4 (C-8a), 163.2 (C-1), 145.2 (C-10a), 157.6 (C-4a), 146.0 (C-5), 166.9 (C-3) including a carbonyl of 1 or 8 hydroxylated xanthone at δ_C 180.8 (C-9) (Silva and Pinto, 2005);
- five methine groups at δ_C 96.9 (C-4), 92.5 (C-2), 120.6 (C-6), 124.1 (C-7) and 115.4 (C-8);
- one methoxy group at δ_C 55.6 (3-OCH_3).

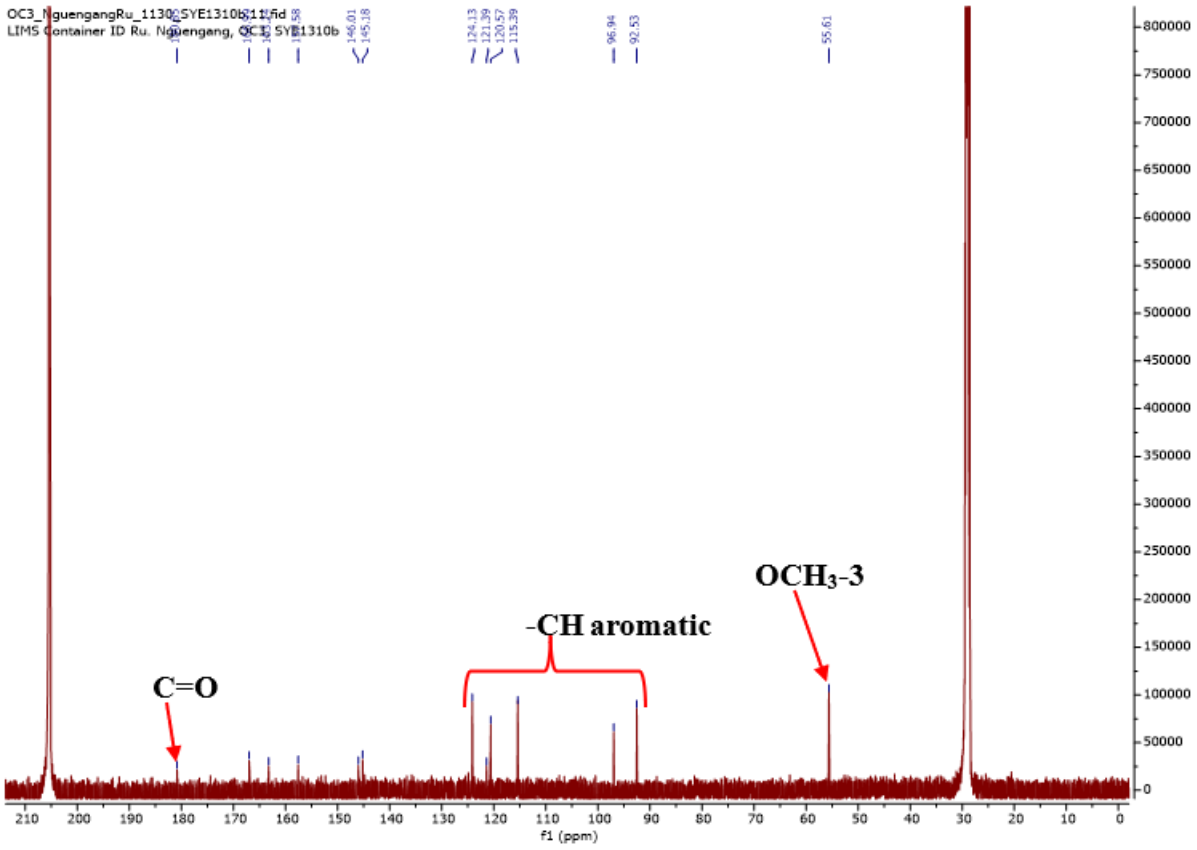

Figure 104: ^{13}C NMR spectrum of SYEF1310b (Acetone-d_6, 150 MHz)

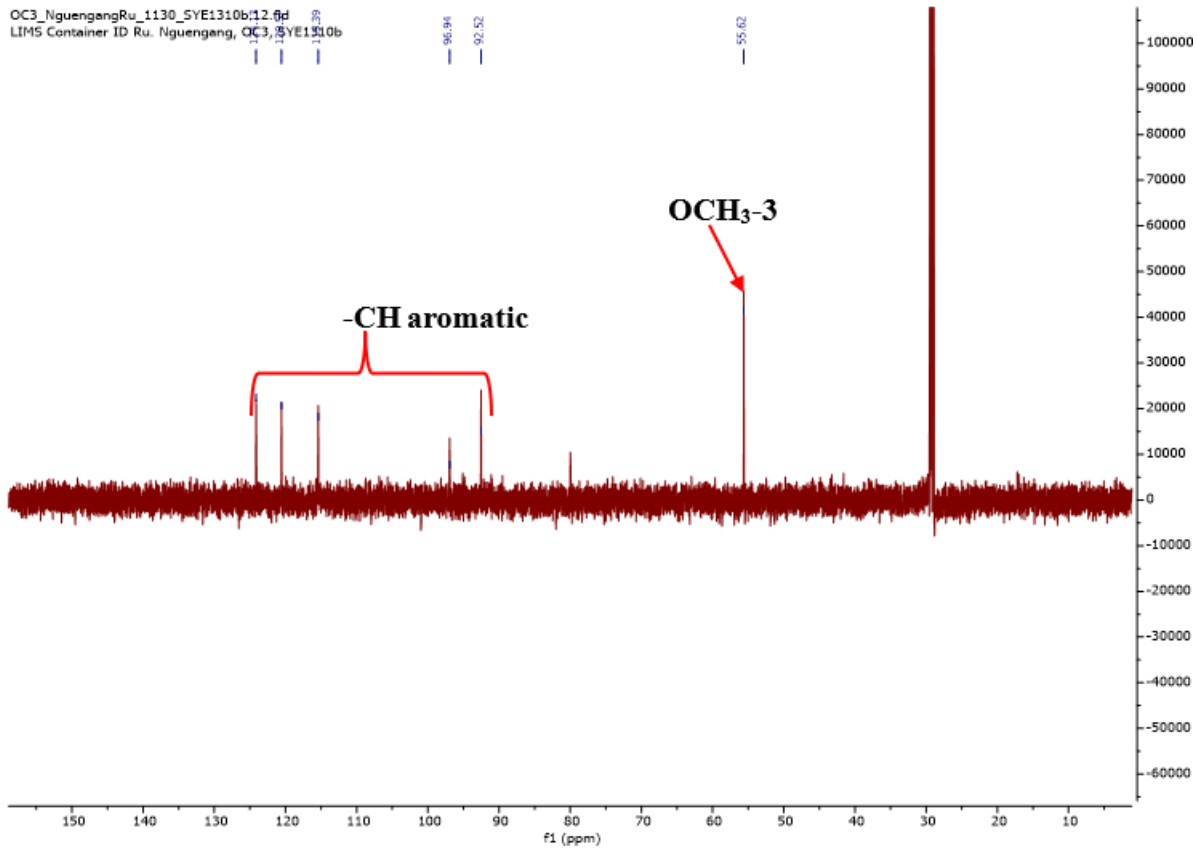

Figure 105: DEPT 135 of SYEF1310b

The position of the different substituents was determined by the correlations observed on the HMBC spectrum (Figure 106) between protons:

- H-7 (δ_H 7.31) and carbons C-5 (δ_C 146.0);
- H-4 (δ_H 6.59) and carbons C-3 (δ_C 166.9), C-4a (157.6);
- 3-OCH_3 (δ_H 3.97) and carbon C-3 (δ_C 166.9).

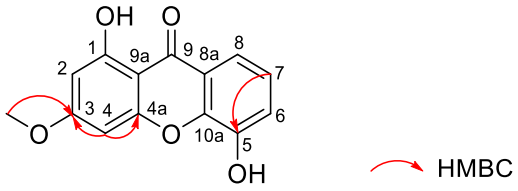

Scheme 28: Key HMBC correlations of SYEF1310b

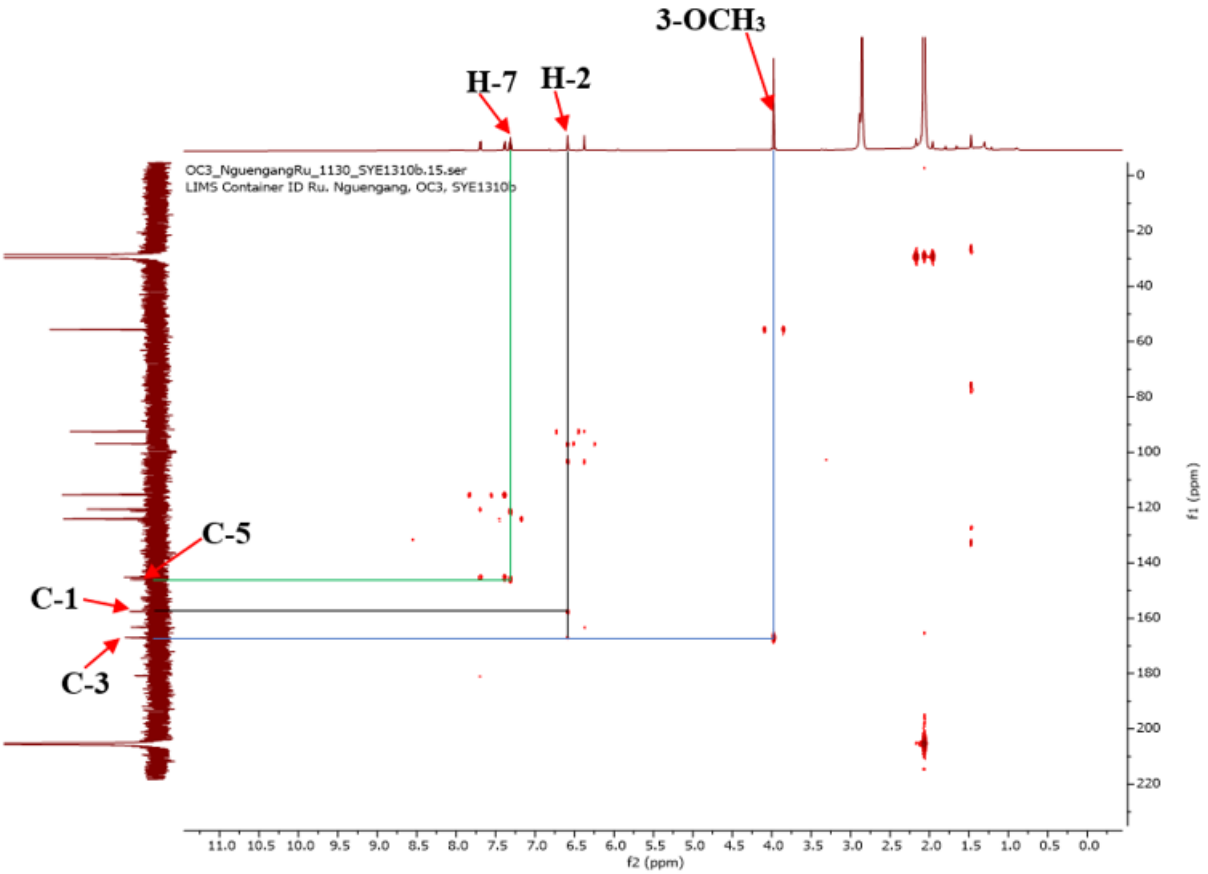

Figure 106: HMBC spectrum of SYEF1310b

All these data, compared with those described in the literature, was in agreement with that of 1,5-dihydroxy-3-methoxyxanthone (**134**), previously isolated from *Centaurium erythraea* by Valentão and collaborators (2002).

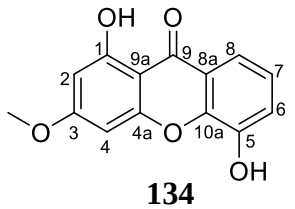

134

Table 40: ^{1}H (500 MHz) and ^{13}C (125 MHz) NMR data of SYEF1310b in acetone-d_6 compared to 1,5-dihydroxy-3-methoxyxanthone [^{13}C (73.47 MHz), ^{1}H (300.13) MHz), DMSO-d_6]

	SYEF1310b		1,5-dihydroxy-3-methoxyxanthone (Valentão *et al.*, 2002)	
Position	δ_C	δ_H **(m, *J* in Hz)**	δ_C	δ_H **(m, *J* in Hz)**
1	163.2	-	162.6	-
2	96.9	6.38 (1H, d, 2.2)	97.1	6.40 (1H, d, 2.2)
3	166.9	-	166.1	-
4	92.5	6.59 (1H, d, 2.3)	92.8	6.64 (1H, d, 2.2)
4a	157.6	-	156.8	-
10a	145.2	-	-	-
5	146.0	-	146.3	-
6	120.6	7.39 (1H, dd, 7.8, 1.6)	120.9	7.33 (1H, dd, 7.8, 1.8)
7	124.1	7.31 (1H, t, 7.9)	124.3	7.27 (1H, t, 1.8)
8	115.4	7.70 (1H, dd, 7.9, 1.5)	114.5	7.56 (1H, dd, 7.8, 1.8)
8a	121.4	-	-	-
9	180.8	-	-	-
9a	103.4	-	103.0	-
OCH_3-3	55.6	3.97 (3H, s)	56.2	3.90 (3H, s)
OH-1	-	12.94 (1H, s)	-	12.87 (1H, s)

II.1.5.4.18. Structural elucidation of compound SYEF26-48D

SYEF26-48D was obtained as a yellowish finely divided solid in the *n*-hexane/EtOAc (3:2, v/v) mixture. It was soluble in DMSO and reacted positively to ferric chloride test, characteristic of phenolic compounds. Its molecular formula, $C_{23}H_{20}O_6$, implying fourteen degrees of unsaturation, was deduced from its NMR and its ESIMS data (Figure 107), which showed the sodium adduct peak $[M+Na]^+$ at *m/z* 415.2 (Figure 108 to 111).

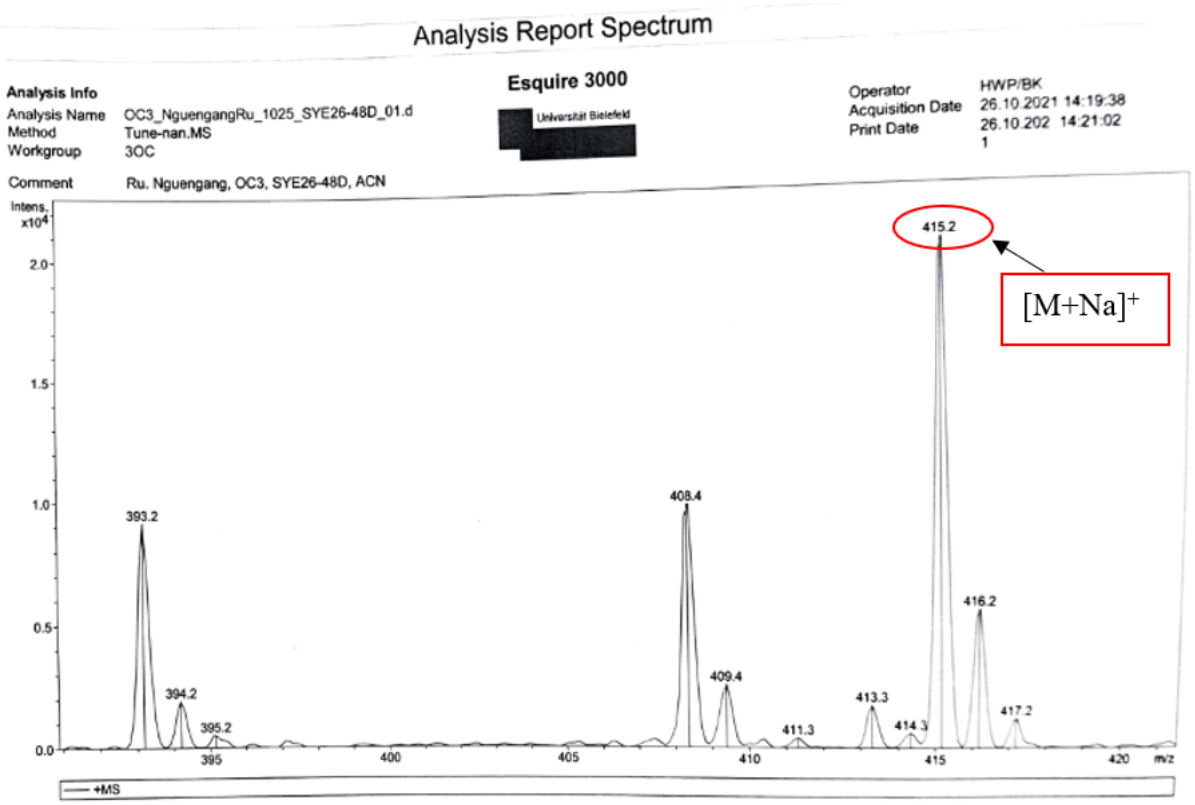

Figure 107: (+) ESI mass spectrum of SYEF26-48D

Its ^{1}H NMR spectrum (Figure 108) displayed resonances of:

- a singlet of a chelated hydroxy proton at δ_H 13.20 (1H, s, OH-1);
- two aromatic singlets at δ_H 7.41 (1H, s, H-1) and 6.22 (1H, s, H-5);
- the protons of two 2,2-dimethylchromene moieties (Ngouela *et al.*, 2006) at δ_H {[5.81 (1H, d, J = 10 Hz, H-12), 7.01 (1H, d, J = 10.1 Hz, H-11) and 1.45 (6H, s, (2×CH_3)-3′)], [5.92 (1H, d, J = 9.9 Hz, H-2′), 6.60 (1H, d, J = 9.9 Hz, H-1′) and 1.47 (6H, s, (2×CH_3)-13))]}.

All of these data showed that the compound **SYEF26-48D** is a xanthone carrying two 2,2-dimethylchromene moieties.

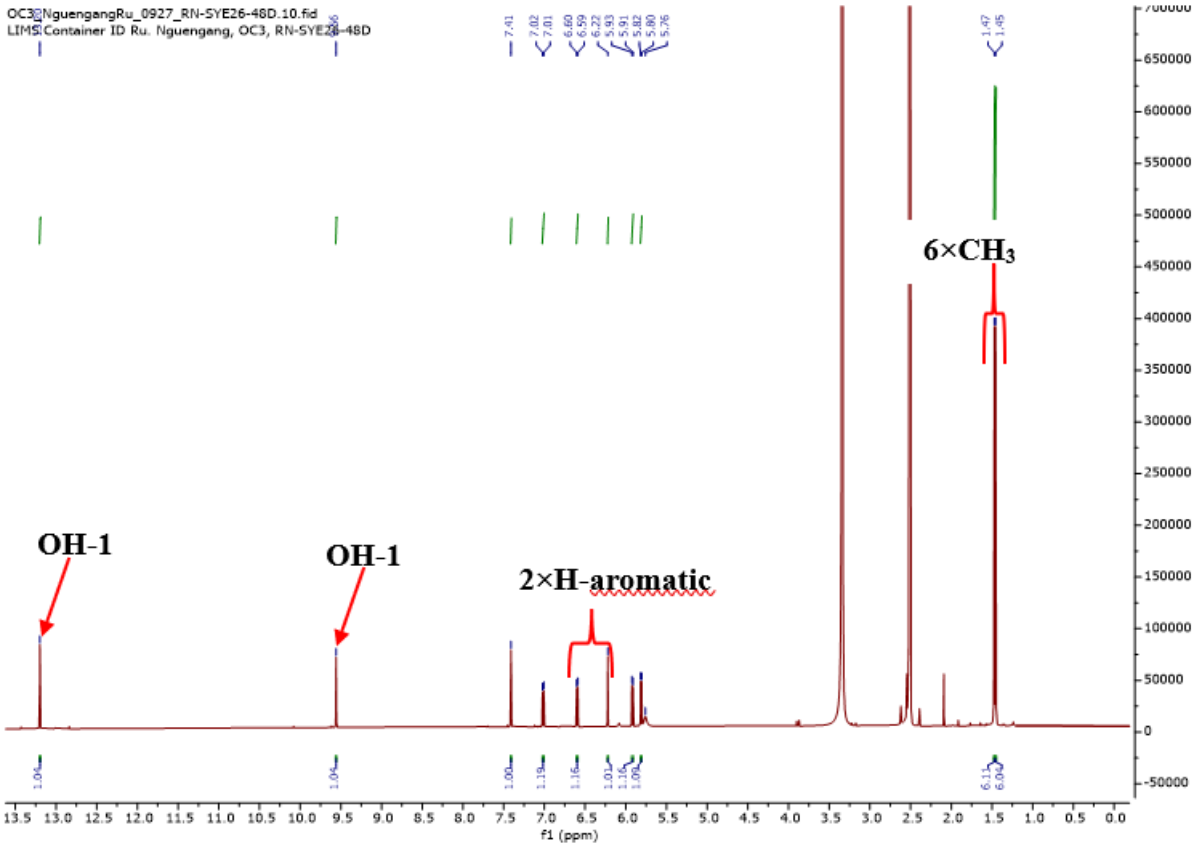

Figure 108: ^{1}H NMR of SYEF26-48D (DMSO-d_6, 600 MHz)

Its ^{13}C NMR spectrum (Figure 109) exhibited carbon resonances of xanthone type skeleton (Silva and Pinto, 2005), which were sorted by the DEPT 135 (Figure 110) technique into:

- thirteen quaternary carbons including carbon of a carbonyl of 1 or 8 hydroxylated xanthone at δ_C 180.3 (C-9) (Silva *et* Pinto., 2005) and the others at δ_C 160.2 (C-8), 151.6 (C-6), 119.1 (C-2), 162.7 (C-10a), 147.0 (C-3), 146.5 (C-4a), 133.7 (C-4), 78.3 (C-13) , 114.1 (C-9a), 103.0 (C-8a), 101.4 (C-7) and 78.8 (C-3′);
- six carbons of methine groups including four olefinics at δ_C 128.0 (C-12), 132.3 (C-2′), 121.5 (C-1′), 115.2 (C-11) and two aromatics at δ_C 112.7 (C-1), δ_C 99.0 (C-5);
- four carbons of methyl groups at δ_C 28.4 [(2×CH_3)-13], 18.0 (C-15) and 28.3 [(2×CH_3)-3′].

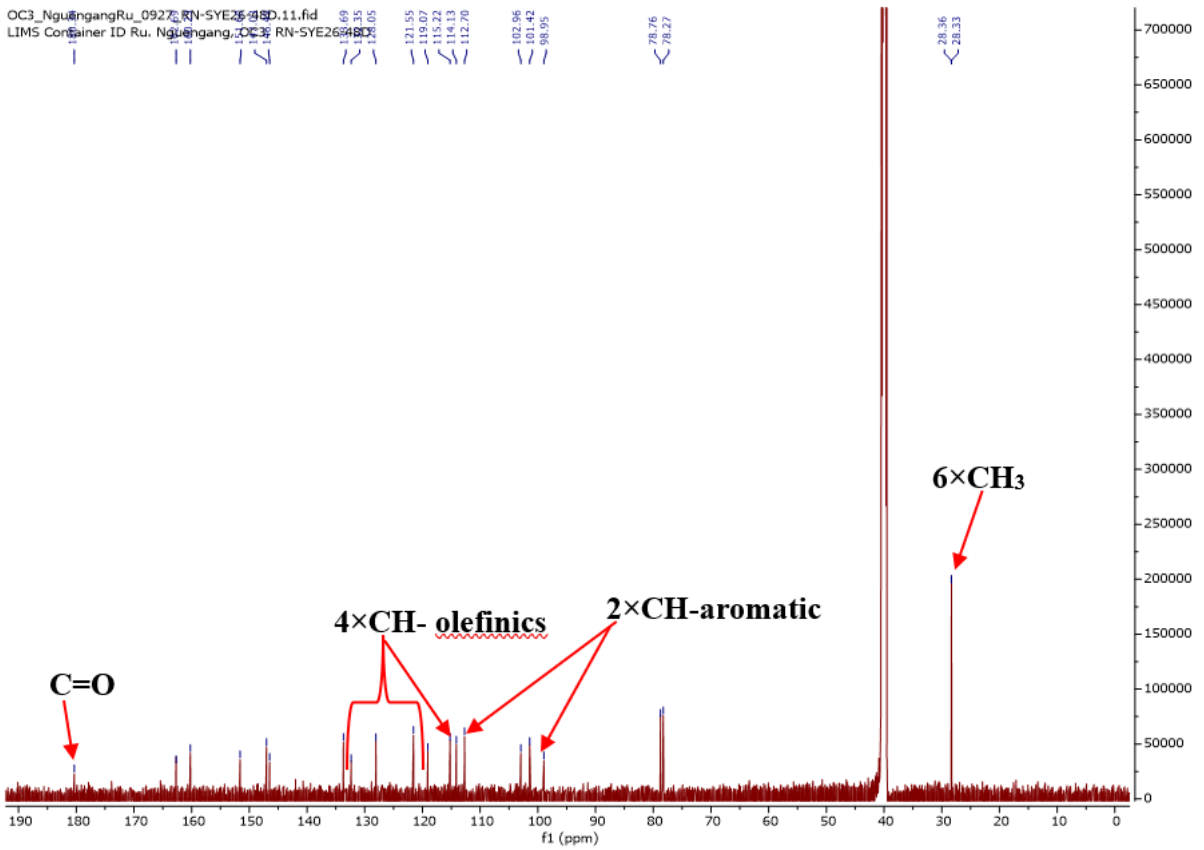

Figure 109: ^{13}C NMR spectrum of SYEF26-48D (DMSO-d_6, 150 MHz)

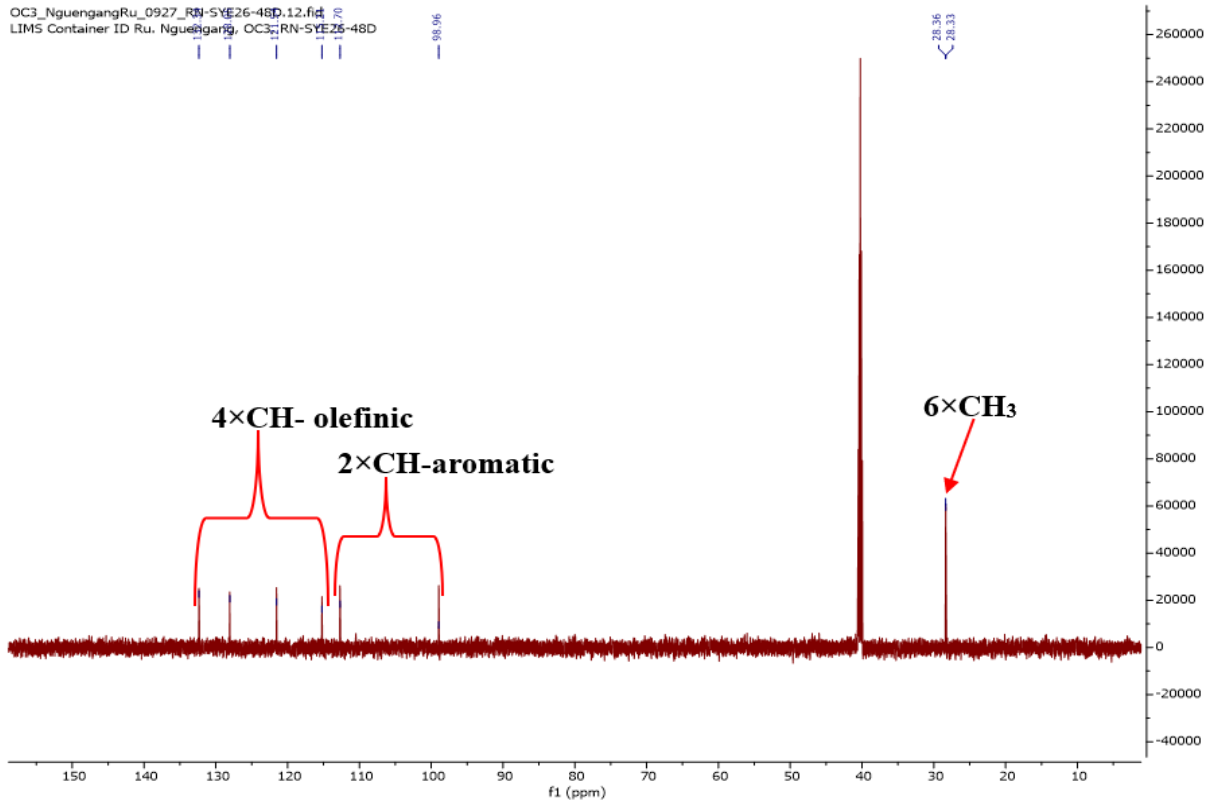

Figure 110: DEPT 135 of SYEF26-48D

The positions of these two 2,2-dimethylchromene moieties on the xanthone skeleton were determined by correlations observed on the HMBC spectrum (Figure 111). In fact, on this spectrum, cross peaks were observed between:

- the protons of the methyl groups of the 2,2-dimethylchromene moieties {[(2×CH_3)-13 (δ_H 1.45) and carbons, C-13 (δ_C 78.8), C-12 (δ_C 128.0)], [(2×CH_3)- 3′ (δ_H 1.47) and carbons, C-3′ (δ_C 78.3), C-2′ (δ_C 132.3)]};
- the olefinic proton of the 2,2-dimethylchromene moieties {[H-12 (δ_H 5.81) and carbon (2×CH_3)-13 (δ_C 28.3), C-13 (δ_C 78.8), C-7 (δ_C 101.4)], [H-2′ (δ_H 5.92) and carbon (2×CH_3)- 3′ (δ_C 28.4), C-3′ (δ_C 78.3), C-2 (δ_C 119.1)} confirming the linear cyclisations;
- the olefinic proton of the dimethyl pyran ring {[H-11 (δ_H 7.01) and carbons C-13 (δ_C 78.8), C-8 (δ_C 160.2), C-6 (δ_C 151.6)], [H-1′ (δ_H 6.60) and carbons C-3′ (δ_C 78.3), C-2 (δ_C 119.1), C-3 (δ_C 147.0), C-1 (δ_C 112.7)} confirming the attachment of two dimethyl pyran rings to C-2 and C-3, C-6 and C-7, respectively.

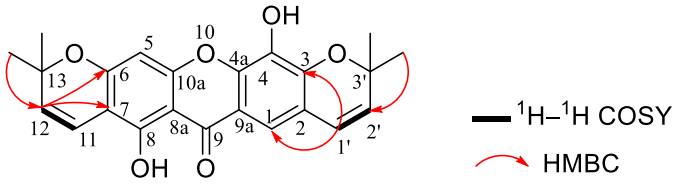

Scheme 29: Key HMBC correlations of SYEF26-48D

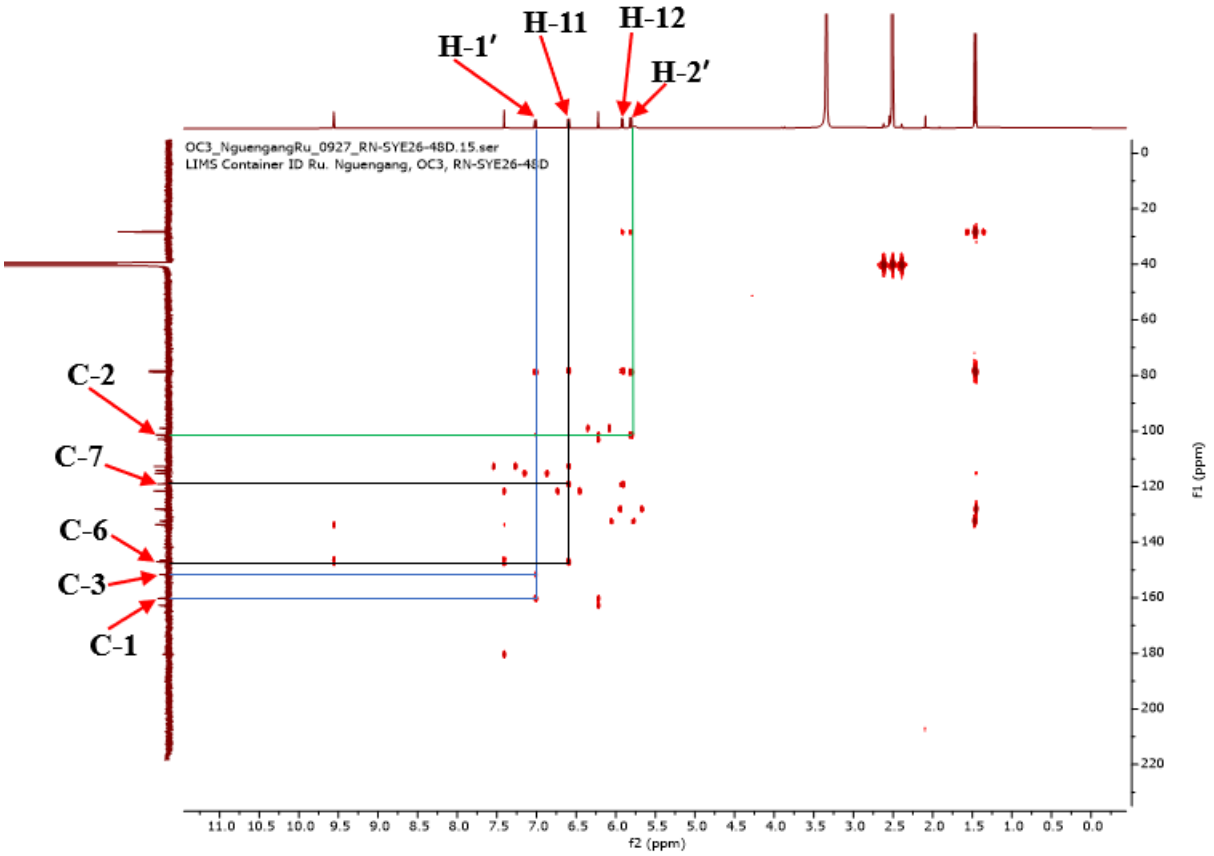

Figure 111: HMBC spectrum of SYEF26-48D

The above data were in agreement with those described in the literature for pyranojacareubin (**135**), previously isolated from the bark of *Calophyllum gracilipes* by Cao and collaborators (1997).

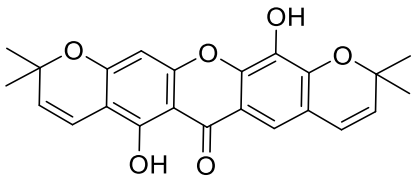

135

Table 41: ^{1}H (500 MHz) and ^{13}C (125 MHz) NMR data of SYEF26-48D in DMSO-d_6 compared to pyranojacareubin [$CDCl_3$, RMN ^{13}C (125 MHz), RMN ^{1}H (500 MHz)]

	SYEF26-48D		Pyranojacareubin (Cao et *al*., 1997)	
Position	δ_C	δ_H **(m, *J* in Hz)**	δ_C	δ_H **(m, *J* in Hz)**
1	112.7	7.41 (1H, s)	112.4	7.46 (1H, s)
2	119.1	-	118.3	-
3	147.0	-	146.0	-
4	133.7	-	133.2	-
4a	146.5	-	146.1	-
5	99.0	6.22 (1H, s)	95.1	6.40 (1H, s)
6	151.6	-	157.4	-
7	101.4	-	104.3	-
8	160.2	-	160.1	-
8a	103.0	-	102.9	-
9	180.3	-	180.2	-
9a	114.1	-	114.2	-
10a	162.7	-	156.8	-
11	115.2	7.01 (1H, d, 10.1)	115.2	6.74 (1H, d, 10.0)
12	128.0	5.81 (1H, d, 10.0)	127.4	5.69 (1H, d, 10.0)
13	78.8	-	77.5	-
(2×CH3) -13	28.4	1.47 (3H, s)	28.2	1.53 (3H, s)
1′	121.5	6.60 (1H, d, 9.9)	121.4	6.43 (1H, d, 10.0)
2′	132.3	5.92 (1H, d, 9.9)	131.3	5.72 (1H, d, 10.0)
3′	78.3	-	78.0	-
(2×CH3) - 3′	28.3	1.45 (3H, s)	28.1	1.48 (3H, s)
1-OH	-	13.20 (1H, s)	-	13.24 (1H, s)

II.1.5.4.19 Structural elucidation of compound SYEF23

SYEF23 was obtained as a yellowish finely divided solid in the *n*-hexane/EtOAc (3:2, v/v) mixture. It was soluble in acetone and reacted positively to ferric chloride test and Shinoda test, characteristic of phenolic compounds and flavonoids. Its molecular formula, $C_{15}H_{10}O_6$, implying eleven degrees of unsaturation, was deduced from its ESIMS data (Figure 112) which showed the deprotonated adduct peak $[M-H]^-$ at *m/z* 284.894 and its NMR data (Figure 113 to 115).

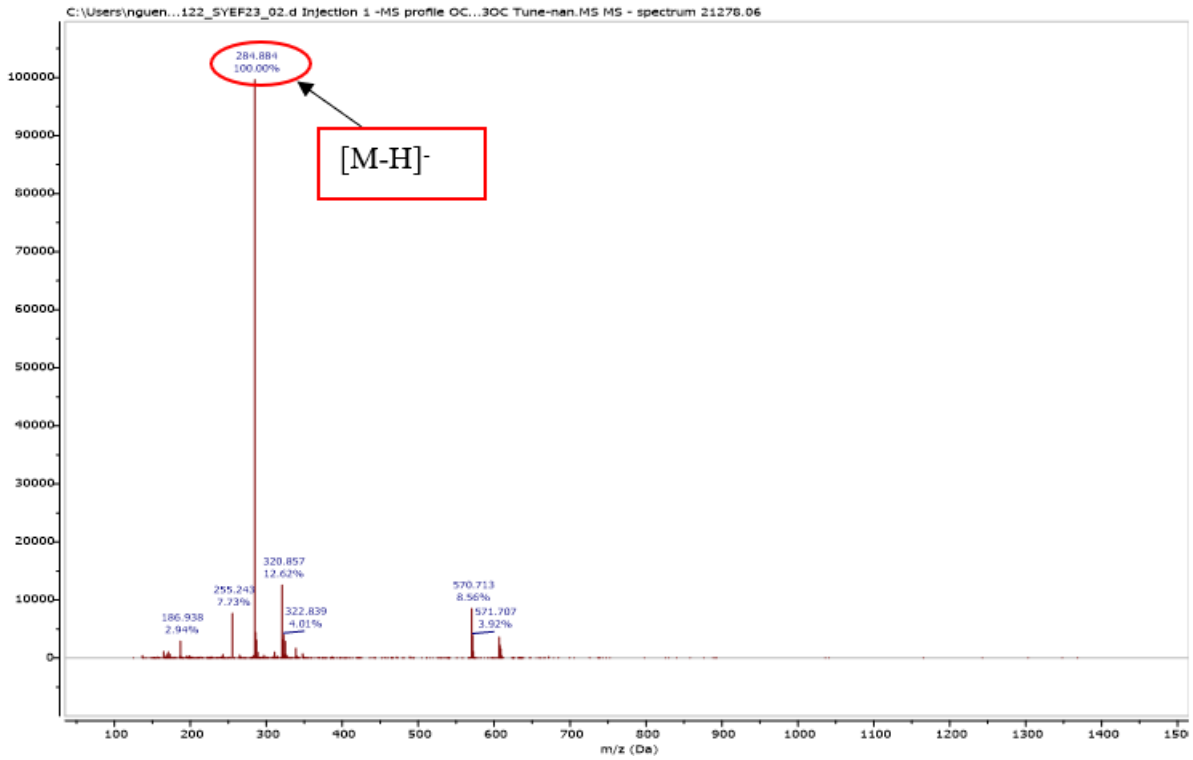

Figure 112: (-) ESI mass spectrum of SYEF23

Its ^{1}H NMR spectrum (Figure 113) displayed resonances of:

- two aromatic protons at δ_H 6.55 (1H, br s, H-8) and 6.29 (1H, br s, H-6);
- two doublets of two protons each at δ_H 8.17 (2H, d, J = 8.4 Hz, H-2′/H-6′) and 7.03 (2H, d, J = 8.5 Hz, H-3′/H-5′) indicating the presence of one AA′BB′ system, characteristic of a *para*-substituted aromatic system (Wei *et al*., 2011);
- resonance of a chelated hydroxy group at δ_H 12.19 (1H, OH).

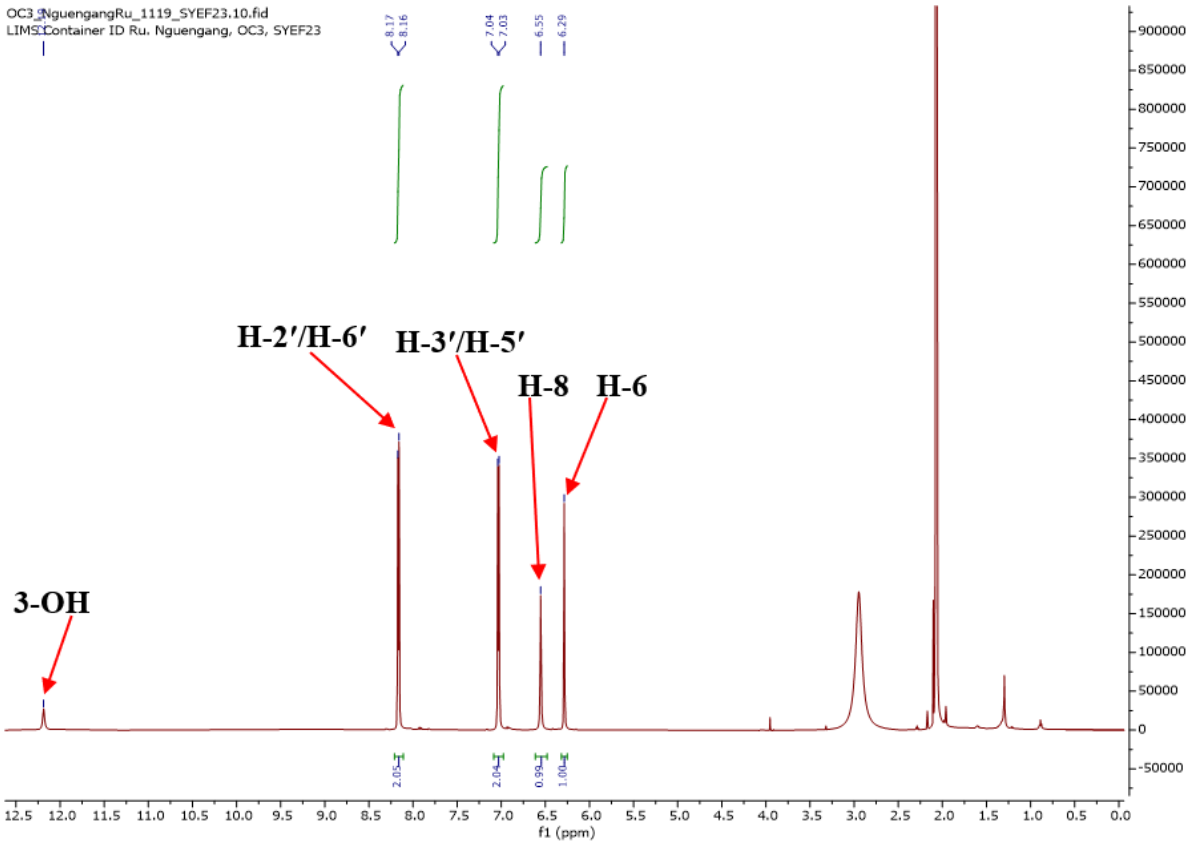

Figure 113: ^{1}H NMR of SYEF23 (Acetone-d_6, 600 MHz)

Its ^{13}C NMR spectrum (Figure 114) exhibited carbon signals, which were sorted by the DEPT 135 (Figure 115) technique into:

- nine quarternary carbons including the carbonyl at δ_C 175.7 (C-4) and carbon at δ_C 135.7 (C-3), characteristics of flavonol (Markham, 1982). The other carbons at δ_C 103.2 (C-10), 122.4 (C-1′), 161.2 (C-9), 146.1 (C-2), 159.2 (C-4′), 156.9 (C-5), 164.1 (C-7);
- six methine groups at δ_C 93.6 (C-8), 98.2 (C-6), 115.4 (C-3′/C-5′) and 129.6 (C-2′/C-6′).

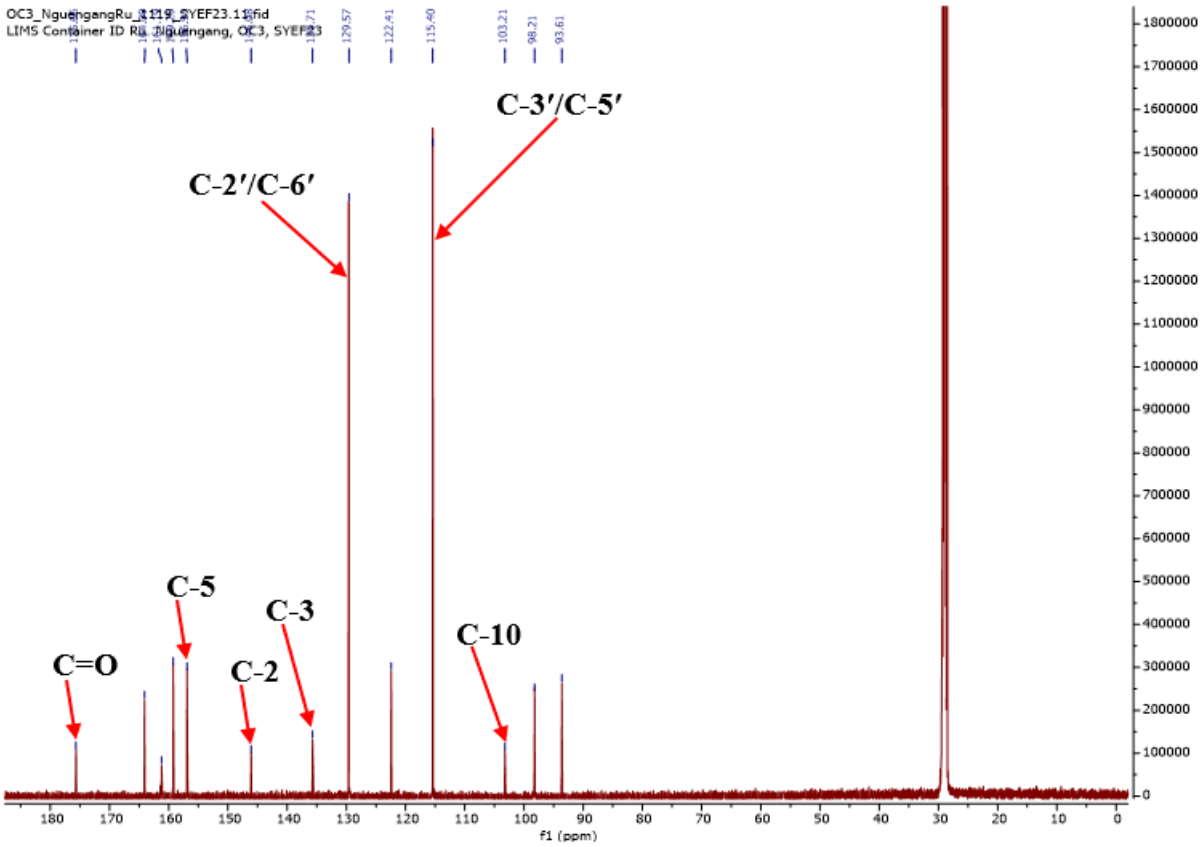

Figure 114: ^{13}C NMR spectrum of SYEF23 (Acetone-d_6, 150 MHz)

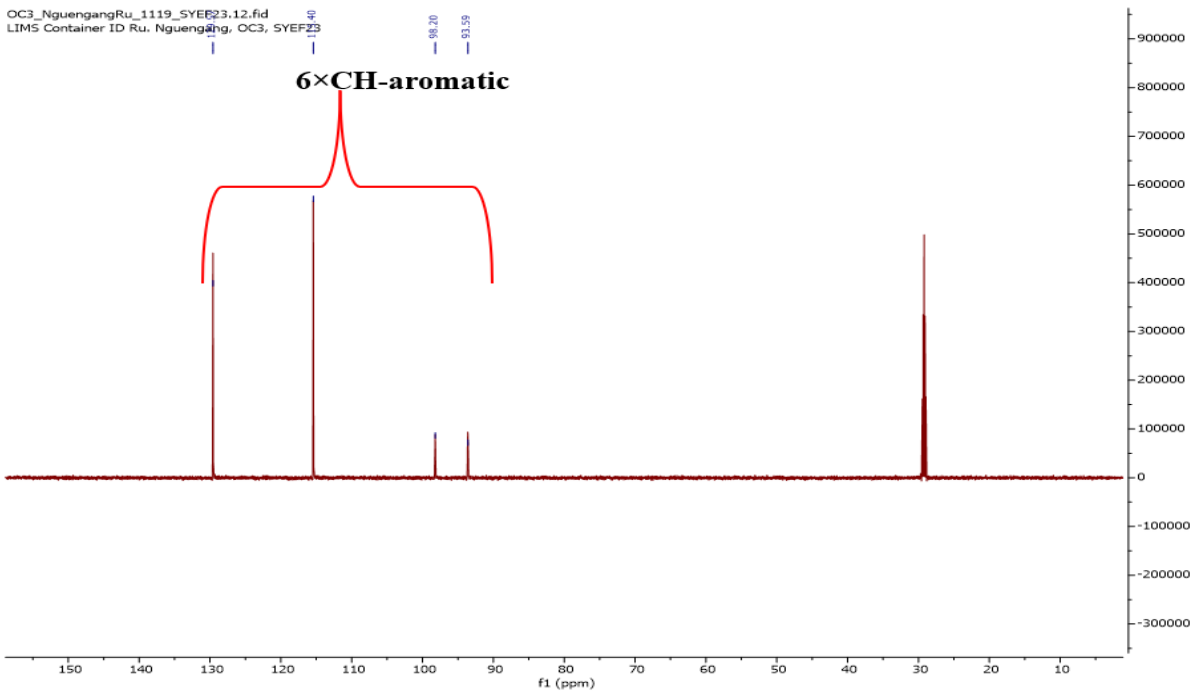

Figure 115: DEPT 135 of SYEF23

All these data were in agreement with those of kaempferol (**136**), previously isolated from *Rosa rugosa* by Xiao and collaborators (2006).

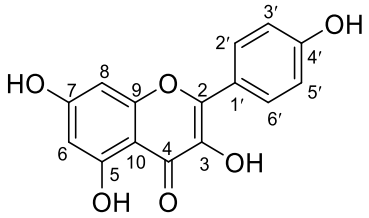

Table 42: ^{1}H (500 MHz) and ^{13}C (125 MHz) NMR data of SYEF23 in acetone-*d*$_6$compared to kaempferol [^{13}C (100 MHz), ^{1}H (400 MHz), acetone-*d*$_6$]

	SYEF23		Kaempferol (Xiao *et al*., 2006)	
Position	δ_C	δ_H **(m, *J* in Hz)**	δ_C	δ_H
1	-	-	-	-
2	146.1	-	146.9	-
3	135.7	-	136.5	-
4	175.7	-	176.5	-
5	156.9	-	157.7	-
6	98.2	6.29 (1H, br s)	98.9	6.27 (1H, d, 2.0)
7	164.1	-	165.0	-
8	93.6	6.55 (1H, br s)	94.3	6.54 (1H, d, 2.0)
9	161.2	-	160.1	-
10	103.2	-	103.9	-
1′	122.4	-	123.1	-
2′, 6′	129.6	8.17 (2H, d, 8.4)	130.3	8.16 (2H, d, 8.8)
3′, 5′	115.4	7.03 (2H, d, 8.5)	116.1	7.03 (2H, d, 8.8)
4′	159.2	-	161.9	

II.1.5.5. Furanones derivative derivative

II.1.5.5.1. Structural identification of compound RBR9N2

RBR9N2 was obtained as a bright shiny needle in CH_2Cl_2-EtOAc (17:3, v/v). It was soluble in dichloromethane and reacted positively to the ferric chloride of phenolic compounds.

Its molecular formula, $C_9H_8O_4$, implying six degrees of unsaturation, was deduced from its ESIMS data (Figure 116), which showed the deprotonated adduct peak $[M-H]^-$ at *m/z* 178.8 and its NMR data (Figure 117 to 119).

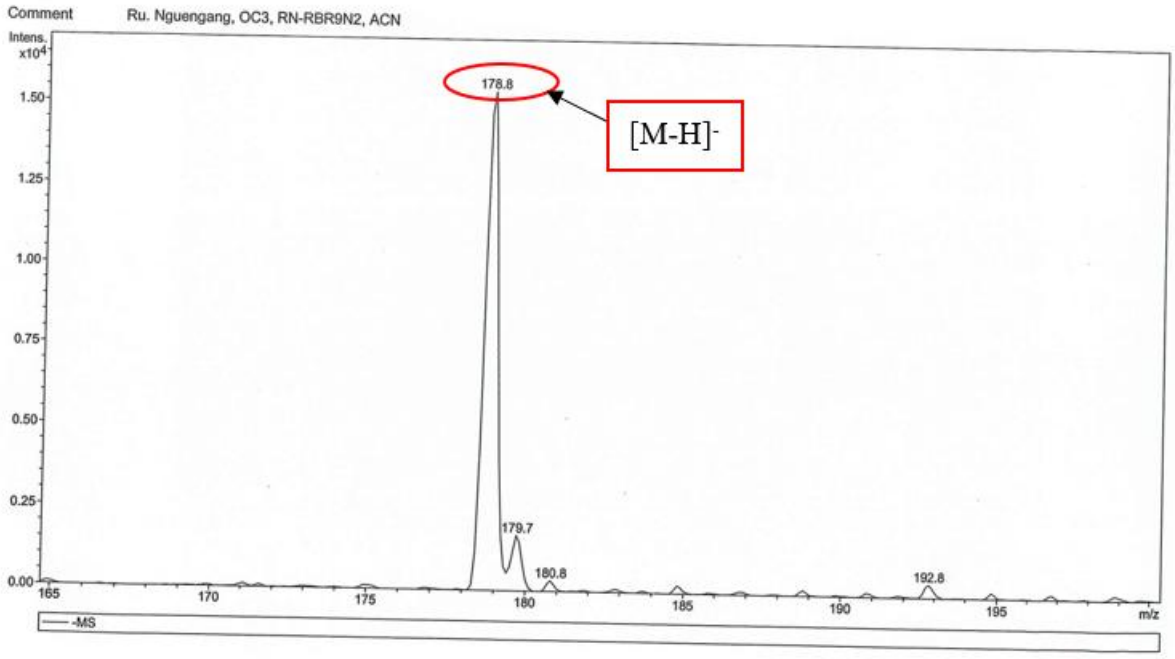

Figure 116: (-) ESI mass spectrum of RBR9N2

Its ^{1}H NMR spectrum (Figure 117) showed the resonances of two pairs of meta-coupled protons at δ_H [6.40 (1H, br s, H-6) and 6.47 (1H, br s, H-4)], suggesting the presence of one di-substituted aromatic rings. It also displayed the resonances of one methoxy group attached to an aromatic ring at δ_H 3.81 (3H, s, H-8) and a singlet of a strongly deshielded oxymethylene proton at δ_H 5.14 (2H, s, H-3).

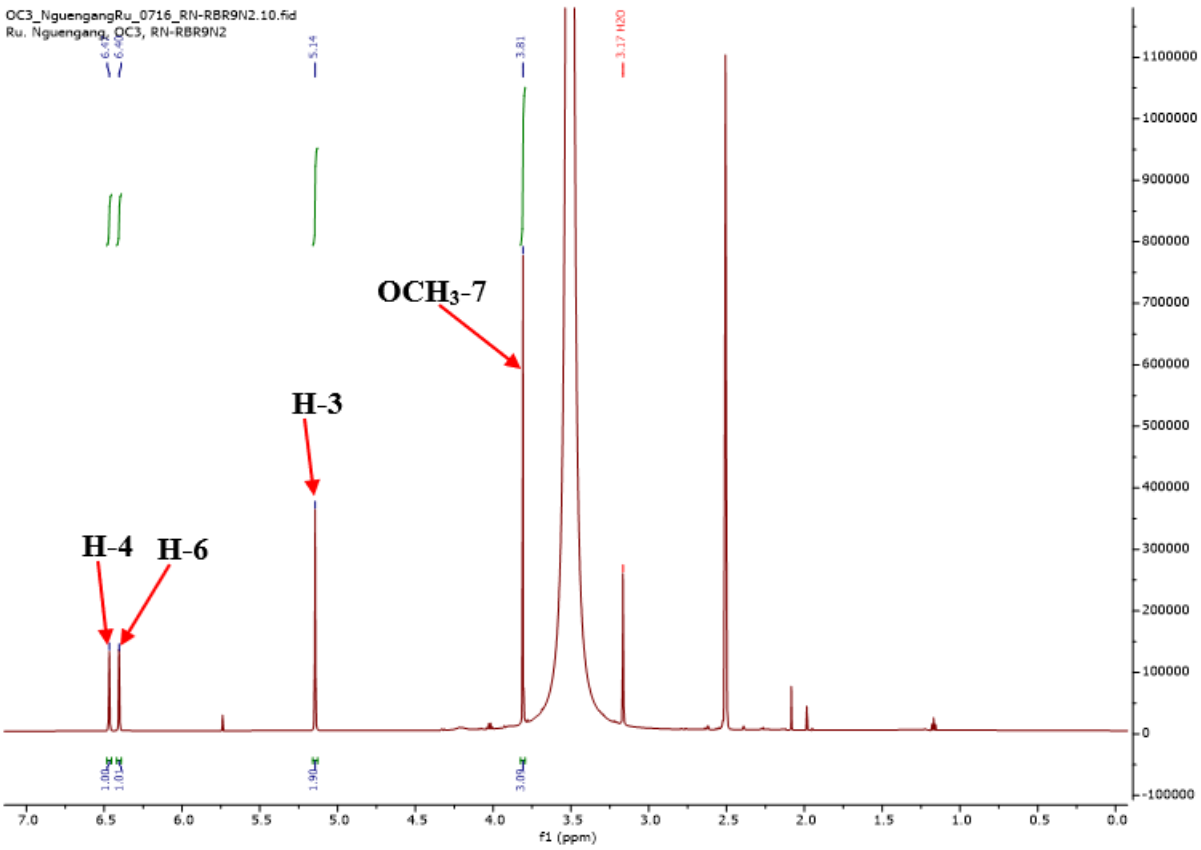

Figure 117: ^{1}H NMR of RBR9N2 (DMSO-d_6, 600 MHz)

Its ^{13}C NMR spectrum (Figure 118) revealed 9 carbon resonances including:

- five quarternary carbons in which the carbonyl at δ_C 168.6 (C-1) (lactone, C-1) and carbon at δ_C 165.9 (C-5), 159.8 (C-7), 152.6 (C-3a), 103.9 (C-7a);
- two aromatic methines at δ_C 101.2 (C-4), 99.4 (C-6);
- one methylene carbon at δ_C 68.9 (C-3) and signal of one methoxy group at δ_C 55.9 (-OCH_3-7).

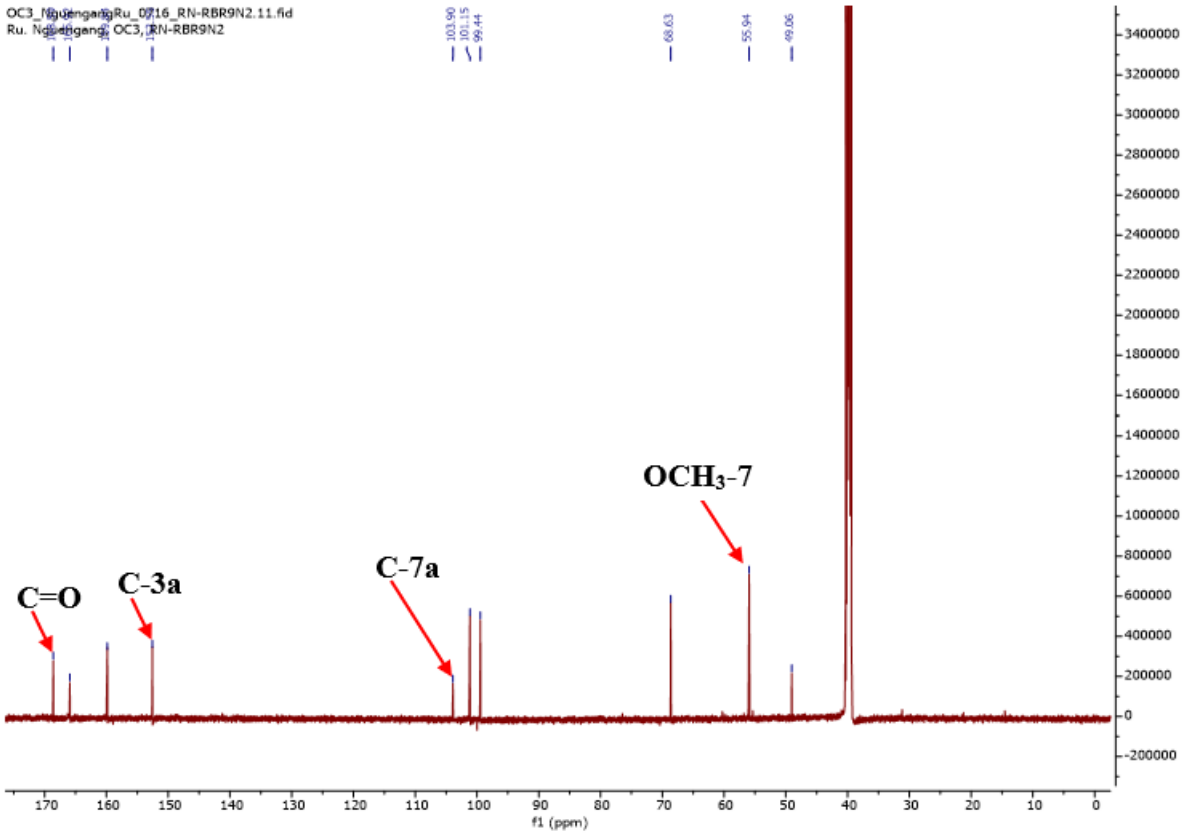

Figure 118: ^{13}C NMR spectrum of RBR9N2 (DMSO-d_6, 150 MHz)

The position of the carbonyl group was determined using the correlations observed on the HMBC spectrum (Figure 119) between proton H-3 (δ_H 5.14) and carbons C-1 (δ_C 168.6). In addition, the position of the different substituents was determined by the correlations observed on the HMBC spectrum (Figure 119) between:

- H-4 (δ_H 6.47), H-6 (δ_H 6.40) and carbons C-5 (δ_C 165.9);
- 7-OCH$_3$ (δ_H 3.81) and carbons C-7 (δ_C 159.8).

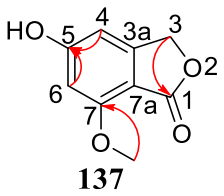

137

Scheme 30: Key HMBC correlations of RBR9N2

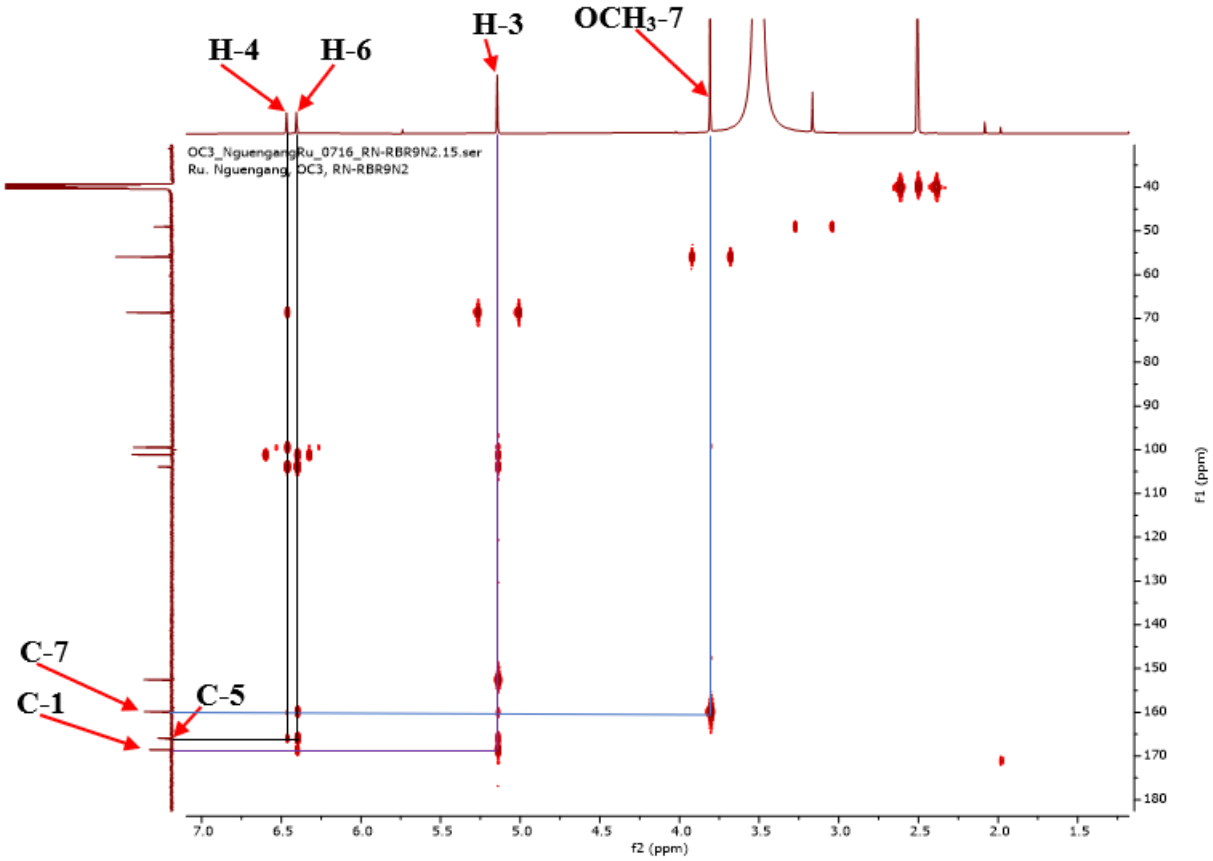

Figure 119: HMBC spectrum of RBR9N2

Based on the above data and by comparison with those described in the literature, RBR9N2 was identified as 5-Hydroxy-7-methoxy-1(3*H*)-isobenzofuranone (**137**), previously synthesized by El-Feraly and collaborators (1985).

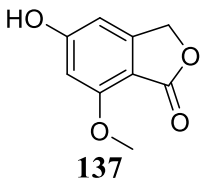

137

Table 43: ^{1}H (600 MHz) and ^{13}C (150 MHz) NMR data of RBR9N2 in DMSO-d_6 compared to those of 5-Hydroxy-7-methoxy-1(3H)-isobenzofuranone [^{13}C (15.03 MHz), ^{1}H (90 MHz), DMSO-d_6]

	RBR9N2		5-Hydroxy-7-methoxy-1(3H)-isobenzofuranone (El-Feraly *et al.*, 1985)	
Position	δ_C	δ_H **(m, *J* in Hz)**	δ_C	δ_H **(m, *J* in Hz)**
1	168.6	-	168.9	
2		-		-
3	68.9	5.14 (2H, s)	68.6	5.17 (2H, s)
3a	152.6	-	151.5	
4	101.2	6.47 (1H, br s)	101.4	6.58 (1H, d, 1.5)
5	165.9	-	166.0	
6	99.4	6.40 (1H, br s)	98.6	6.41 (1H, d, 1.5)
7	159.8	-	157.8	
7a	103.9	-	104.3	
OCH_3	55.9	3.81 (3H, s)	55.7	3.73 (3H, s)

II.1.5.5.2. Structural identification of compound RBR9N1

RBR9N1 was obtained as a yellowish oil in CH_2Cl_2-EtOAc (17:3, v/v).

Its molecular formula, $C_4H_6O_3$, implying two degrees of unsaturation, was deduced from its NMR data and its ESIMS data which showed the sodium adduct peak $[M+Na]^+$ at *m/z* 124.9 (Figure 121 to 123).

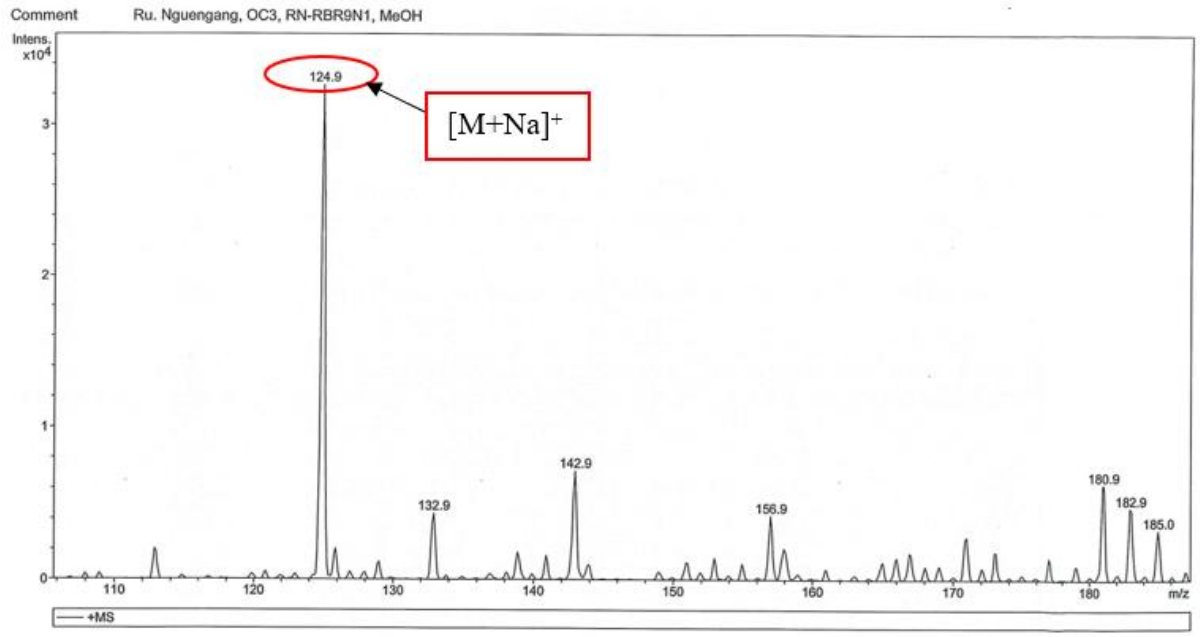

Figure 120: (+) ESI mass spectrum of RBR9N1

It was shown to be a mixture of two compounds **RBR9N1** and **RBR9N2** from the interpretation of the NMR data (Figure 121 to 123).

In fact, the ^{1}H NMR spectrum (Figure 121) of **RBR9N1** displayed a signal of one oxymethine proton at δ_H 4.66 (1H, m, H-3), the signals of a strongly deshielded diastereotopic oxymethylene protons at δ_H 4.41 (1H, dd, J = 9.8, 4.1 Hz, H-4b) and 4.19 (1H, dd, J = 9.8, 1.2 Hz, H-4a) and the signals of diastereotopic methylene protons at δ_H 2.79 (1H, dd, J = 17.5, 5.8 Hz, H-2b) and 2.32 (1H, dt, J = 17.5, 1.3 Hz, H-2a).

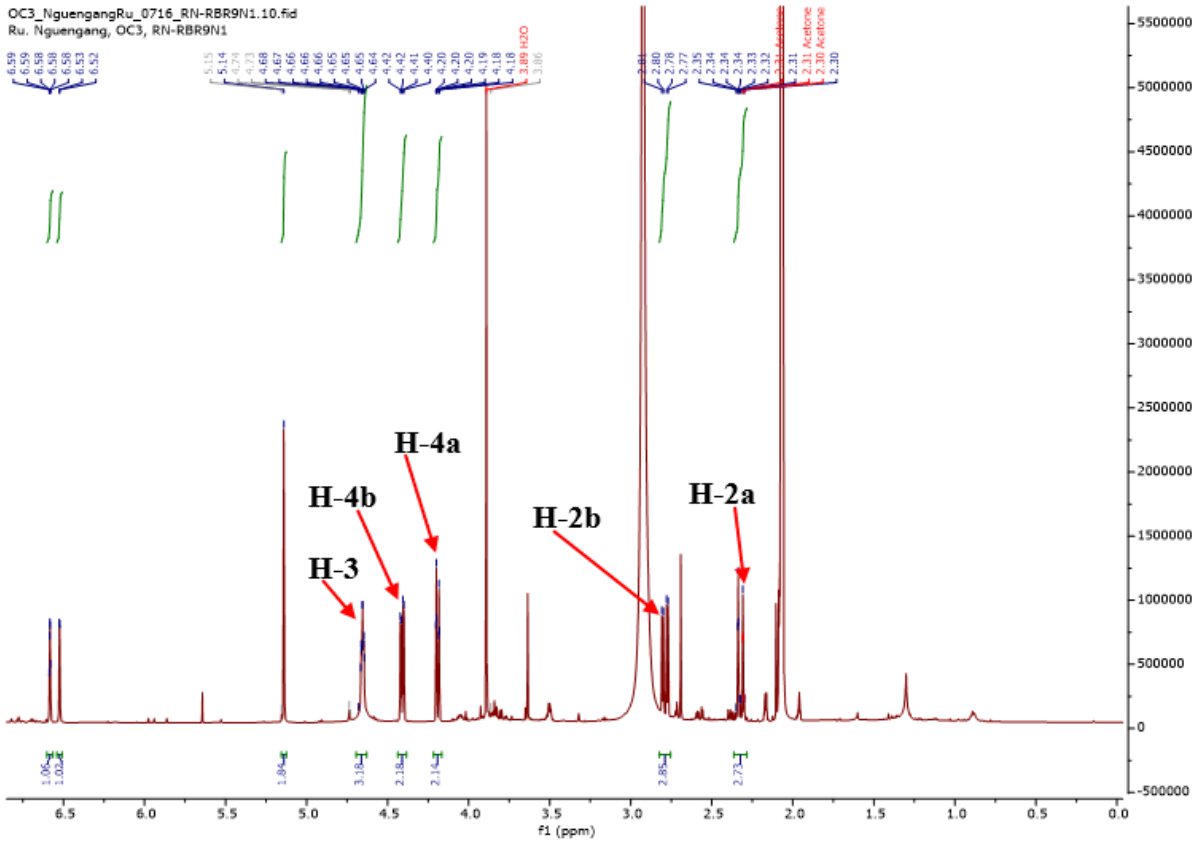

Figure 121: ^{1}H NMR of RBR9N1 (DMSO-d_6, 600 MHz)

Its ^{13}C NMR spectrum (Figure 122) revealed 4 carbon resonances among which:

- one carbonyl at δ_C 175.8 (C-1) (lactone, C-1);
- two methylenes at δ_C 75.8 (C-4), 37.3 (C-2);
- one methine at δ_C 67.1 (C-3).

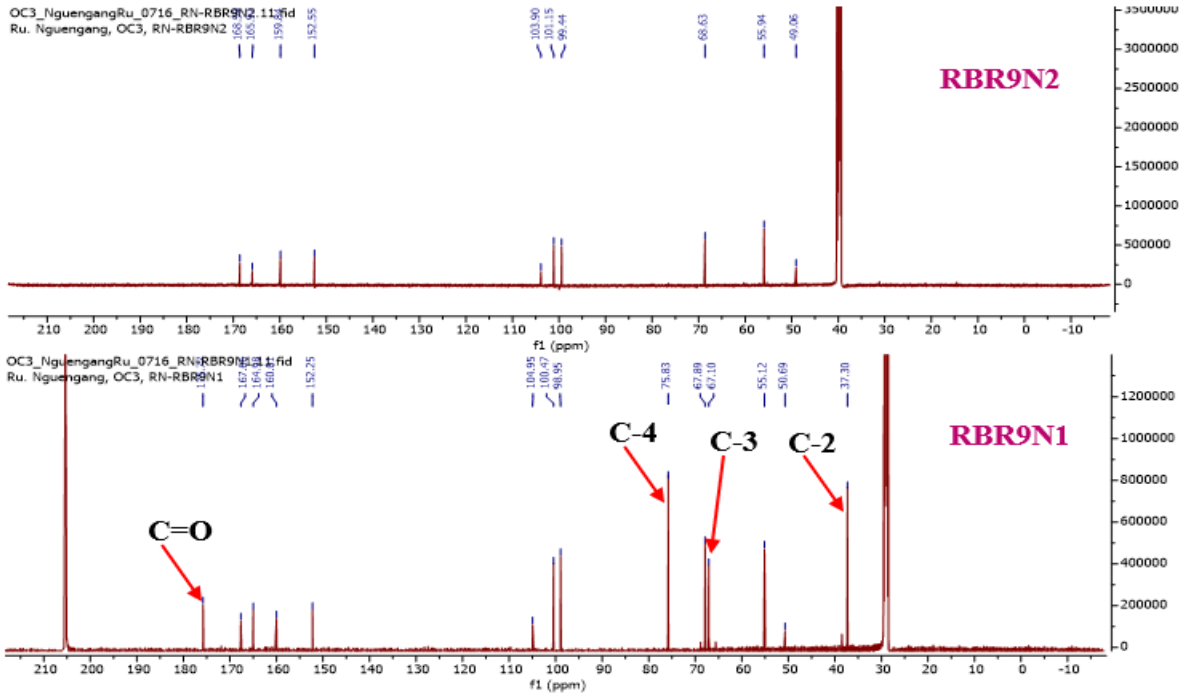

Figure 122: Comparative ^{13}C NMR spectrum of RBR9N1 (DMSO-d_6, 150 MHz) and RBR9N2 (DMSO-d_6, 150 MHz)

The position of the carbonyl group was determined by the correlations observed on the HMBC spectrum (Figure 123) between protons H-2a (δ_H 2.32) and carbons C-1 (δ_C 175.8). In addition, the position of the hydroxy substituents was determined by the correlations observed on the HMBC spectrum (Figure 123) between protons H-4a (δ_H 4.19) and carbons C-3 (δ_C 67.1).

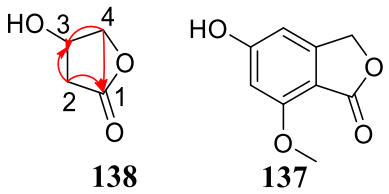

138 **137**

Scheme 31: Some key HMBC correlations of RBRN2

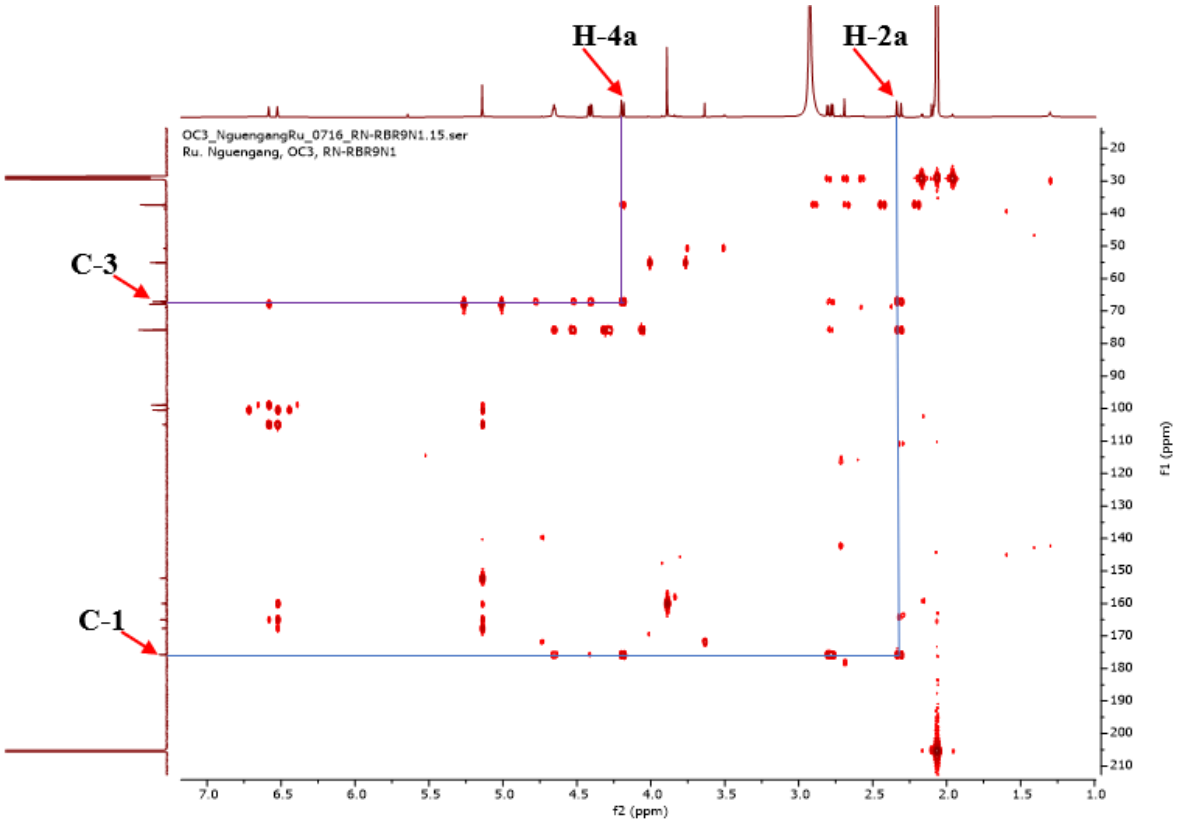

Figure 123: HMBC spectrum of RBR9N1

These data were therefore in accordance with those of 3-hydroxy-*γ*-butyrolactone (**138**), previously synthesized by Zhang and collaborators (2014).

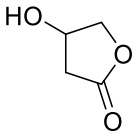

138

Table 44: ^{1}H (600 MHz) and ^{13}C (150 MHz) NMR data of RBR9N2 in DMSO-*d*$_6$ compared to 3-hydroxy-*γ*-butyrolactone [^{13}C (125 MHz), ^{1}H (500 MHz), DMSO-*d*$_6$]

	RBR9N1		3-hydroxy-gamma-butyrolactone (Zhang *et al.*, (2014)	
Position	δ_C	δ_H **(m, *J* in Hz)**	δ_C	δ_H **(m, *J* in Hz)**
1	175.8	-	176.1	
2	37.3	-	37.8	-
2a		2.32 (1H, dt, 17.5, 1.3)		2.45-256 (1H, m)
2b		2.79 (1H, dd, 17.5, 5.8)		2.72 (1H, dd, 18.0, 6.1)
3	67.1	4.66 (1H, m)	67.5	4.64-4.68 (1H, m)
3a		-		
4	75.8	-	76.0	
4a		4.19 (1H, dt, 9.8, 1.2)		4.27 (1H, d, 10.3)
4b		4.41 (1H, dd, 9.8, 4.1)		4.39 (1H, dd, 10.3, 4.5)

II.1.5.6. Triterpenoid derivative derivative

II.1.5.6.1. Structural elucidation of compound SYE22-22

SYE22-22 was obtained as a white finely divided solid in the *n*-hexane/EtOAc (4:1, v/v) mixture. It was soluble in methylene chloride and gave a red colour, which turned purple to the Liebermann-Burchard test characteristic of triterpenoids.

SYE22-22 was identified as lupeol (**139**) thanks to its NMR data (Figure 124) and its TLC profile compared to that of a sample kept in the laboratory.

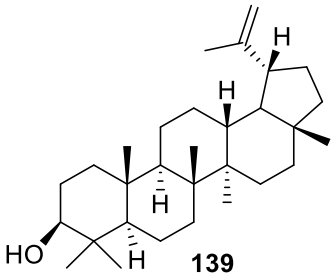

139

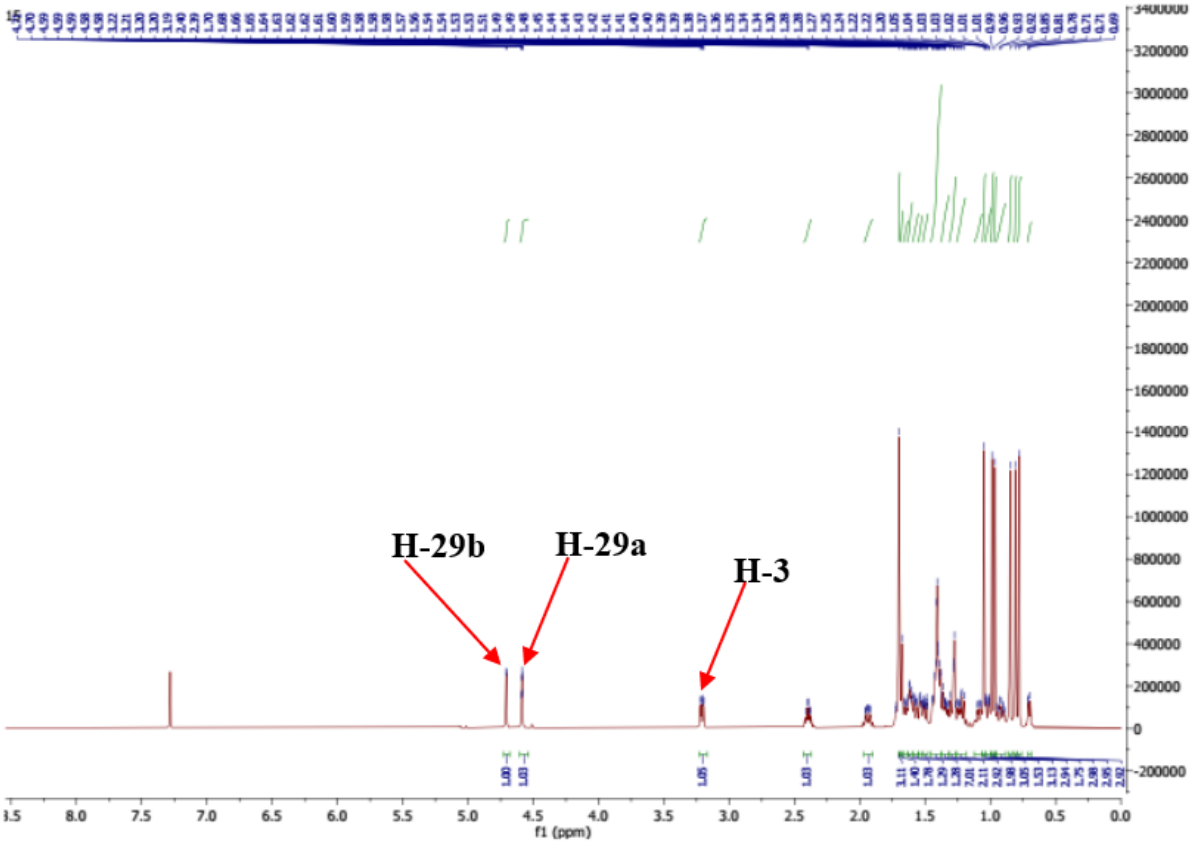

Figure 124: ^{1}H NMR of SYE22-22 ($CDCl_3$, 600 MHz)

II.1.5.7. Steroids

II.1.5.7.1. Structural identification of compound RBR5

RBR5 was obtained as a white powder in CH_2Cl_2-EtOAc (9:1, v/v). It was soluble in dichloromethane and reacted positively to Lieberman Burchard test, characteristic of steroids by given a blue colour that turns quickly to dark green.

RBR5 was identified as *β*-sitosterol (**140**) (Habib *et al*., 2007) thanks to its NMR data and its TLC profile compared to a sample kept in the laboratory. Its proton spectrum (Figure 125) showed characteristic resonances of protons of steroids at δ_H 5.28 (1H, m, H-6) and 3.47 (1H, m, H-3) (Habib *et al*., 2007).

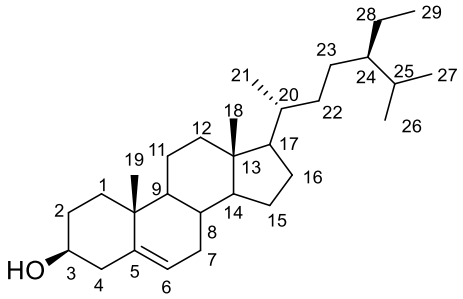

140

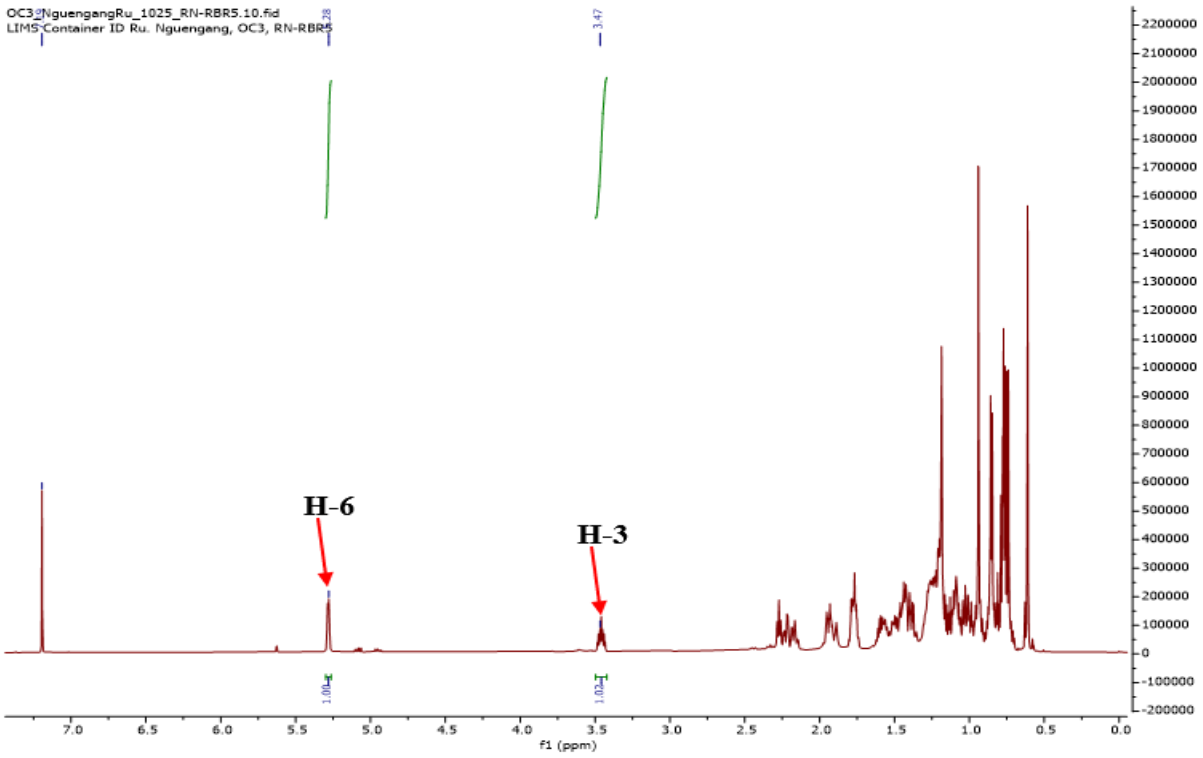

Figure 125: ^{1}H NMR of RBR5 (DMSO-*d*$_6$, 600 MHz)

II.1.5.7.2. Structural identification of compound RBR4

RBR4 was obtained as a white powder in CH_2Cl_2-EtOAc (9:1, v/v). It was soluble in dichloromethane and reacted positively to Lieberman Burchard test, characteristic of steroids by given a blue colour that turns quickly to dark green.

RBR4 was identified as stigmasterol (**141**) (Habib *et al*., 2007) thanks to its NMR data and its TLC profile compared to a sample kept in the laboratory. Its proton spectrum (Figure 126) showed characteristic resonances of protons of steroids at δ_H 5.28 (1H, m, H-6), 3.97 (1H, m, H-3), 5.04 (1H, m, H-22) and 4.53 (1H, m, H-23).

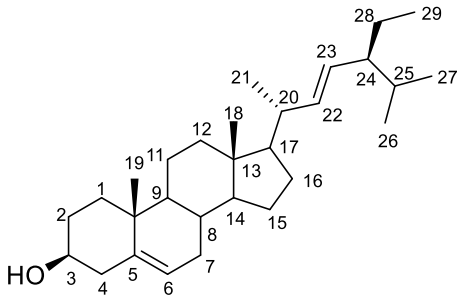

141

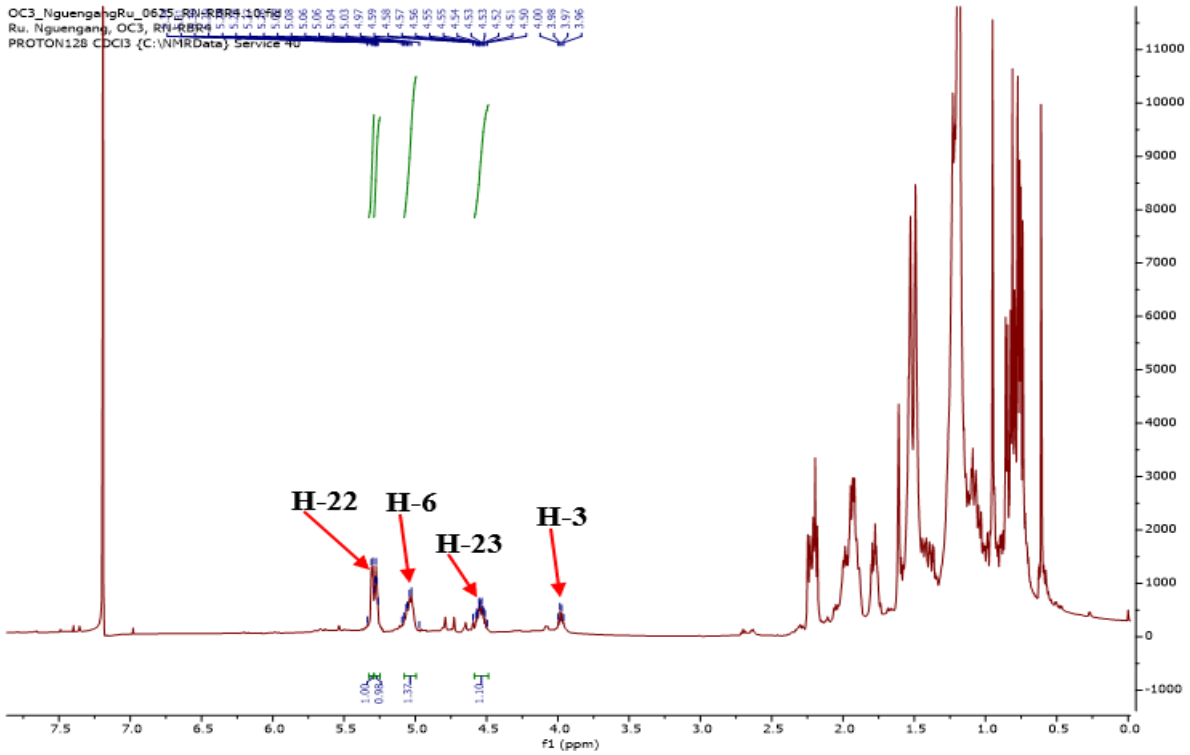

Figure 126: ^{1}H NMR of RBR4 (DMSO-d_6, 600 MHz)

II.1.5.7.3. Structural identification of compound RBR86-57D

RBR87-56D was obtained as a white powder in CH_2Cl_2-EtOAc (1:1, v/v). It was soluble in pyridine and reacted positively to Lieberman Burchard test, characteristic of steroids by given a blue colour that turns quickly to dark green.

RBR87-56D was identified as *β*-sitosterol-3-*O*-*β*-D-glucopyranoside (**142**) thanks to its NMR data (Figure 127) and its TLC profile compared to a sample kept in the laboratory.

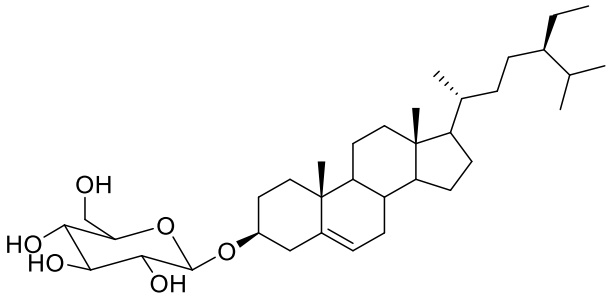

142

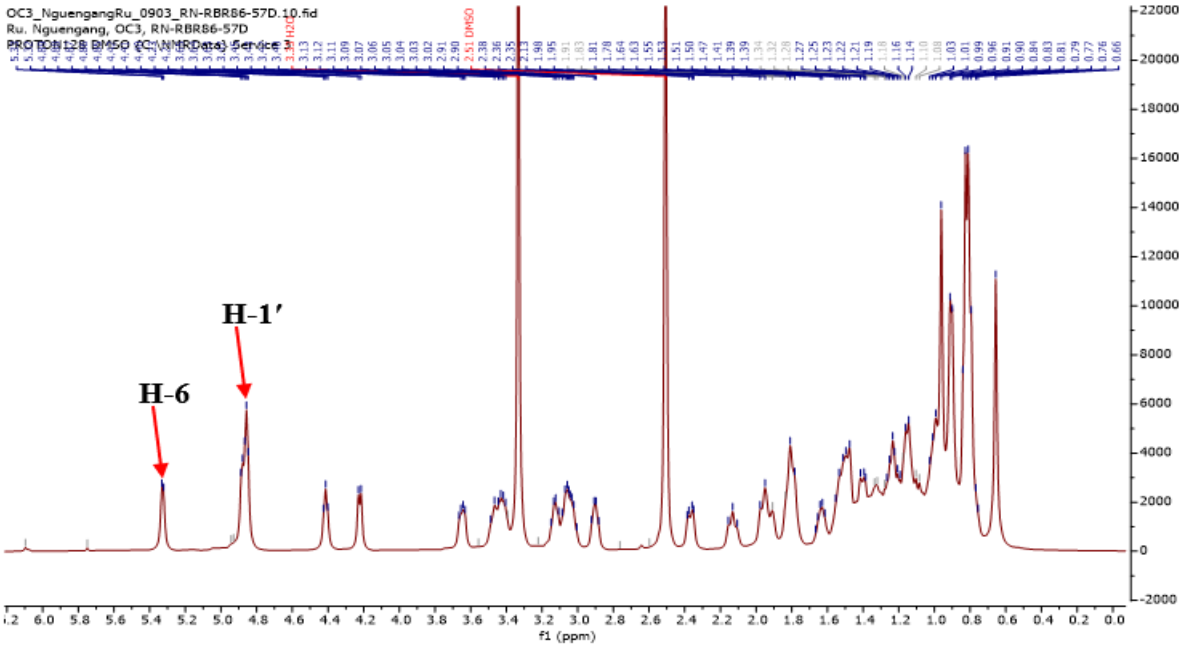

Figure 127: ^{1}H NMR of RBR86-57 (DMSO-d_6, 600 MHz)

A total of thirty-two different compounds were fully characterized using physical and spectroscopic methods (MS, IR, NMR).

They belong to eleven classes of secondary metabolites including:

- one new phenylisobenzofuranone derivative (**RBR48-1**);
- three new polyprenylated benzophenones derivative (**SYE25-6M, SYE27-28-16Ma, SYE27-28-16Mb**) and one known compound (**SYE44-4-5mi**);
- one new tocotrienol derivative (**SYE70- 45-48**);

- twenty-one phenolic derivatives (**RBR1a**, **RBR2**, **RBR3C**, **RBR6b, RBR7a2**, **RBR9a**, **RBR9N2**, **RBR9N1**, **RBR10R1**, **RBR15**, **RBR17**, **RBR64**, **RBR147-19**, **RBR95-23a**, **RBR95-23b**, **RBR95-35b**, **SYE137**, **SYE26-48D**, **SYE26-8M**, **SYE171**, **SYE23**, **SYE1310b**);
- two furanones derivative (**RBR9N1 and RBR9N2**); six steroids (RBR5 = SYEF12a, RBR4 = SYEF12b, RBR86-57D = SYE85-38-39);
- one triterpenoid (**SYE22-22**).

II.2. PREPARATION OF THE HEMISYNTHETIC DERIVATIVES

Owing to the antibacterial potential of emodin (**117**) and the fact that the methylation of its hydroxy groups led to inactive analogue towards methicillin-resistant *S. aureus* at 200 mg/mL (Chalothorn *et al*., 2019), some structural modifications were carried out to evaluate the effect of allylation and acetylation on its antibacterial potency. The first series of analogues were synthesized using the Williamson ether synthesis method for allylation and acetylation (Scheme 40).

II.2.1. Allylation and acetylation of emodin (117)

The allylation of emodin **(117)** was achieved by the treatment with allyl bromide in the presence of K_2CO_3 to yield monoallylated emodin [6-allyloxyemodin (**143**)] (**RBR3Al1**), diallylated emodin [6,8-diallyloxyemodin (**144**) (**RBR3Al2**) and 1,6-diallyloxyemodin (**145**) (**RBR3Al3**)] and fully allylated emodin, 1,6,8-triallyloxyemodin (**146**) (**RBR3Al4**) (Scheme 32).

The acetylation was done with acetic anhydride in the presence of 4-(dimethylamino) pyridine, to give 1,6,8-triacetylemodin (**147**) (RBR3Ace1) (Scheme 32).

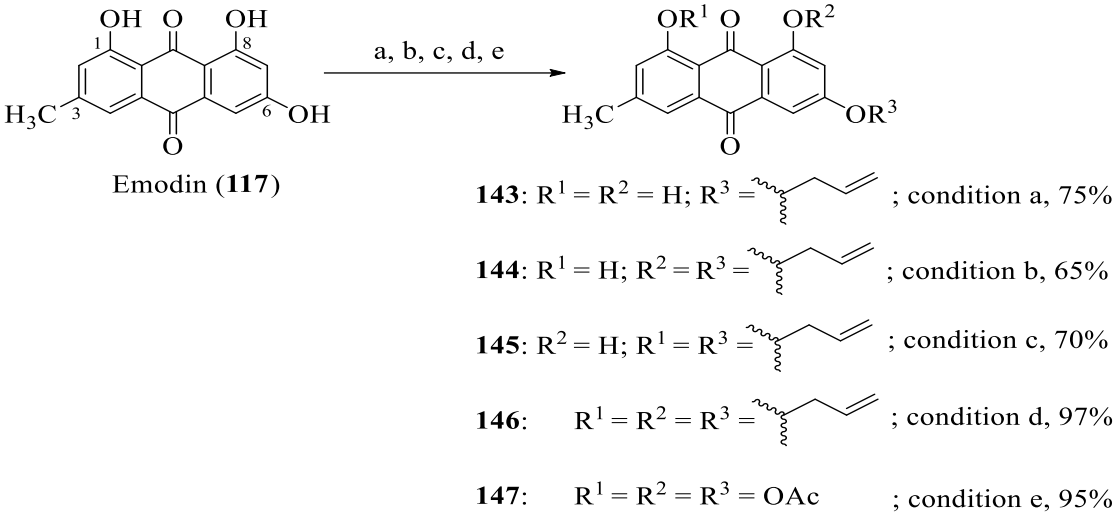

Scheme 32: Allylation and acetylation of hydroxyl groups of emodin (117).

Reagents and conditions: (a) allyl bromide, K_2CO_3, acetone, rt, 2 h; (b) allyl bromide, K_2CO_3, acetone, rt, 8 h; (c) allyl bromide, K_2CO_3, acetone, rt, 12 h; (d) allyl bromide, K_2CO_3, acetone, rt, 24 h; (e) acetic anhydride, 4-(dimethylamino) pyridine, pyridine, rt, 24 h.

II.2.1.1. Structural elucidation of compound RBR3Al1 (143)

RBR3Al1 was obtained as yellowish finely divided solid soluble in dichloromethane. The ^{1}H NMR spectrum of **RBR3Al1** (**143**) was very close to that of **RBR3C** (Figure 128). The only difference was the presence of the signals of one allyl group at δ_H 5.98 (1H, ddt, J = 17.4, 10.6, 5.3 Hz, H-12), 5.39 (1H, dq, J = 17.2, 1.5 Hz, H-13), 5.29 (1H, dq, J = 10.5, 1.3 Hz, H-13′) and 4.60 (2H, dt, J = 5.5, 1.5 Hz, H-11) in **RBR3Al1** (Figure 128). This suggestion was confirmed with the HRESIMS (Figure 129), which showed the sodium adduct peak $[M+Na]^+$ at *m/z* 333.0741 (calcd for $C_{18}H_{14}O_5Na^+$, 333.07335), corresponding to twelve degrees of unsaturation.

The location of the allyl group was determined by the correlation observed on the HMBC spectrum (Figure 130) of RBR3Al1 between the proton H-11 (δ_H 4.60, 2H, dt, J = 5.5, 1.5 Hz) and C-6 (δ_C 165.5).

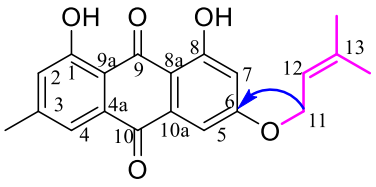

Scheme 33: Key HMBC correlations of RBR3Al1

Based on the above observation, the structure of **RBRAl1**, was characterized as a new monoallylated emodin [6-allyloxyemodin (**143**)].

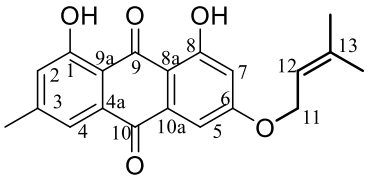

143

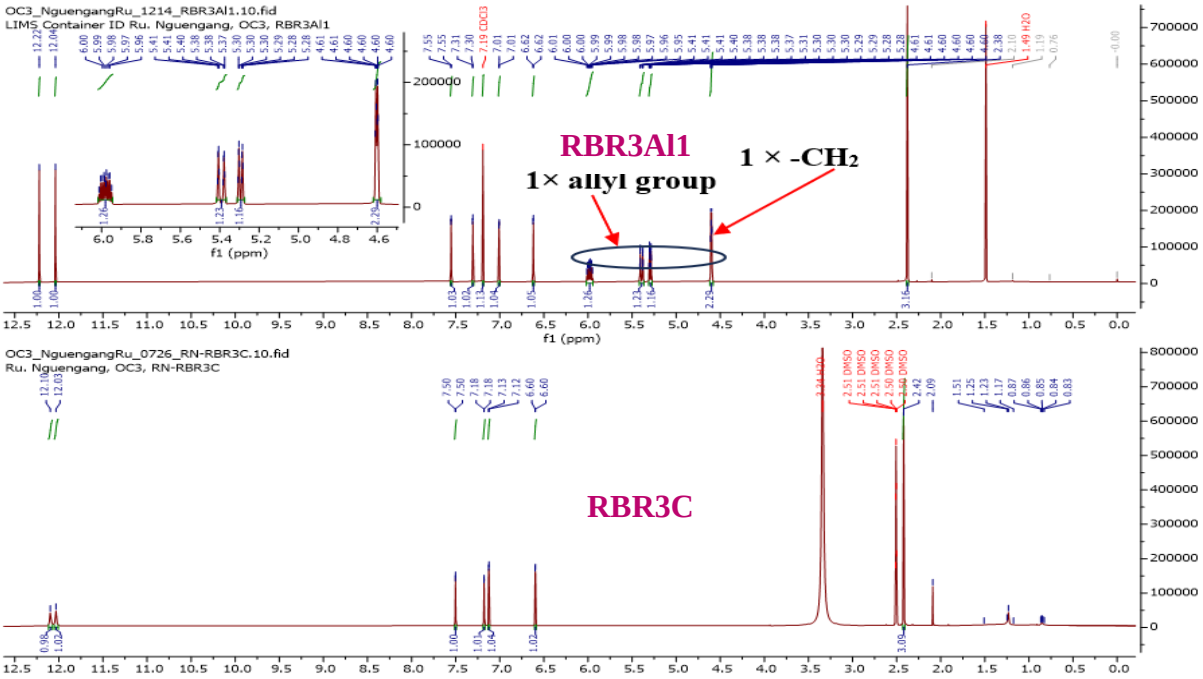

Figure 128: Comparative ^{1}H NMR of RBR3C (DMSO-d_6, 600 MHz) and RBRAl1 ($CDCl_3$, 600 MHz)

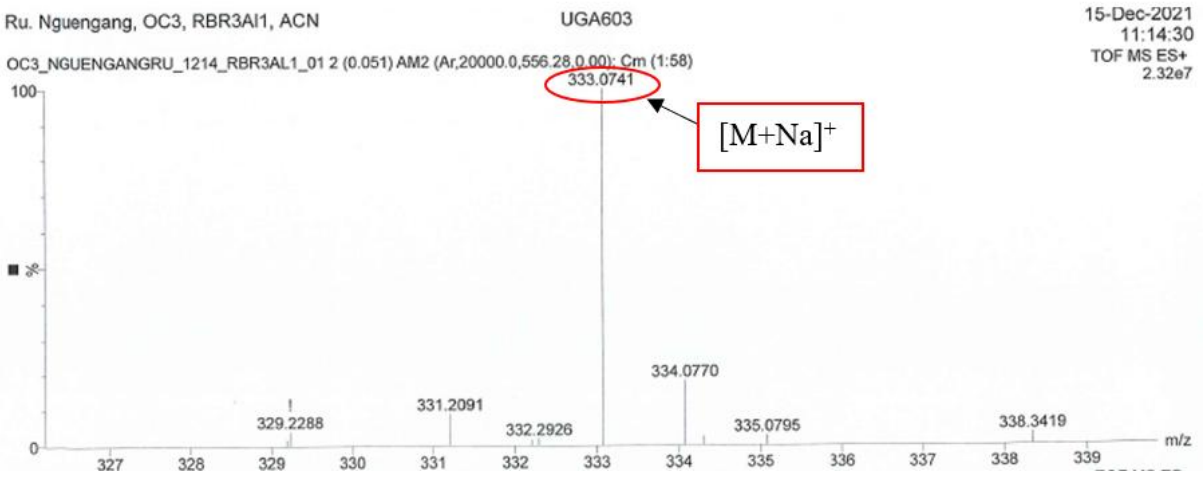

Figure 129: HRESI mass spectrum of RBRAl1

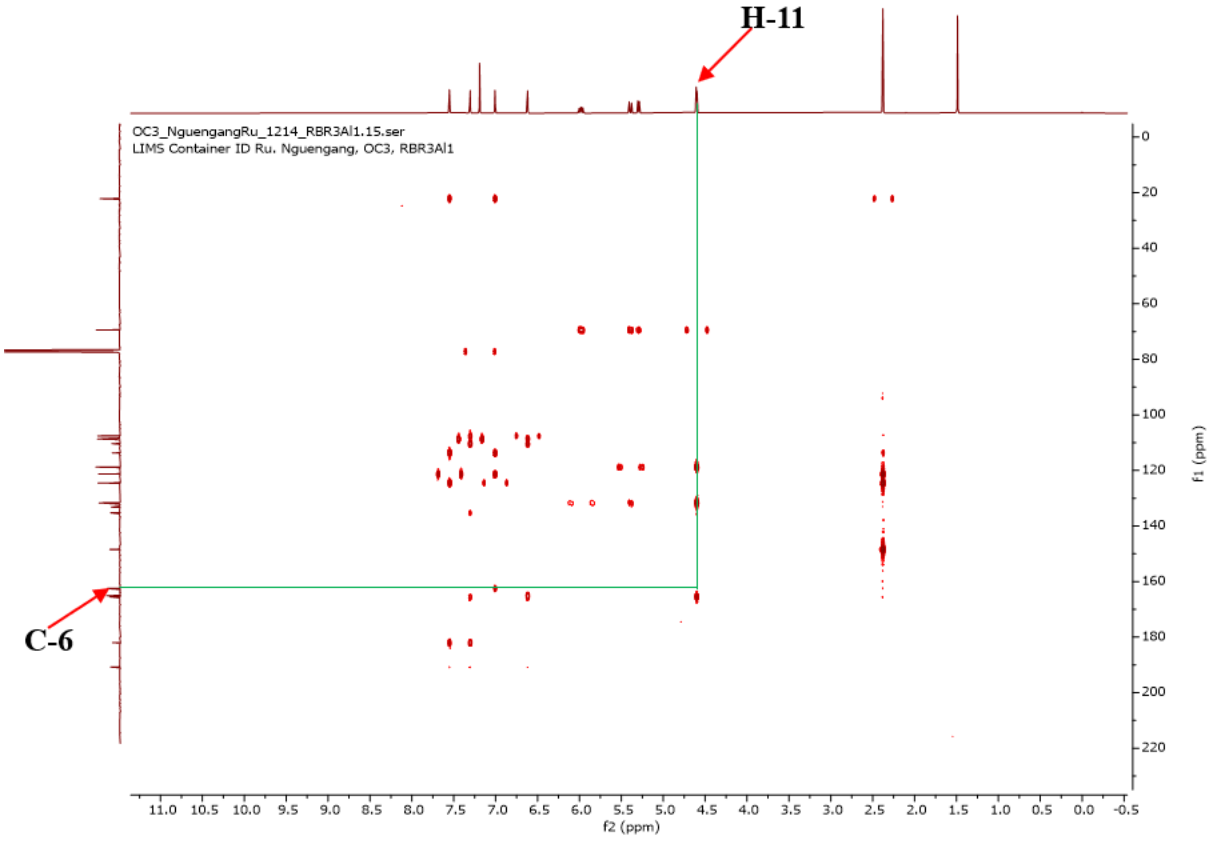

Figure 130: HMBC spectrum of RBRAl1

II.2.1.2. Structural elucidation of compound RBR3Al2 (144)

RBR3Al2 was obtained as yellowish finely divided solid soluble in dichloromethane. The ^{1}H NMR spectrum of **RBR3Al2** (**144**) showed signals characteristic of emodin **(117)** (Figure 131). The only difference was the presence of the signals of two allyl groups at δ_H [6.06 (1H, m, H-12), 5.32 (2H, dq, m, H-13) and 4.64 (2H, dd, J = 5.4, 1.6 Hz, H-11)] and [6.00 (1H, m, H-15), 5.61 (1H, dq, J = 17.3, 1.7 Hz, H-16), 5.40 (1H, dq, J = 17.2, 1.6 Hz, H-16′) and 4.66 (2H, dt, J = 4.7, 1.7 Hz, H-14)] in **RBR3Al2** (Figure 131). This structure was confirmed with the HRESIMS (Figure 132), which showed the sodium adduct peak $[M+Na]^+$ at *m/z* 373.1053 (calcd for $C_{21}H_{18}O_5Na^+$, 373.10465), corresponding to thirteen degrees of unsaturation.

The location of the allyl groups was determined by the correlations observed on the HMBC spectrum (Figure 133) of RBR3Al2 between the proton H-11 (δ_H 4.64, 2H, dd, J = 5.4, 1.6 Hz) and C-6 (δ_C 165.5) and between the proton H-14 (δ_H 4.66, 2H, dt, J = 4.7, 1.7 Hz) and C-8 (δ_C 161.9).

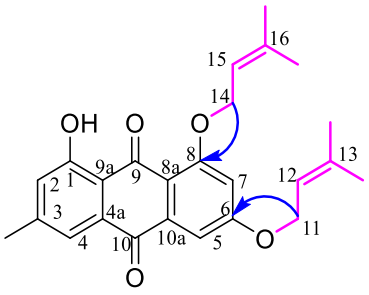

144

Scheme 34: HMBC spectrum of RBRAl2

Therefore, **RBR3Al2** was concluded to be a new diallylated emodin [6,8-diallyloxyemodin (**144**)].

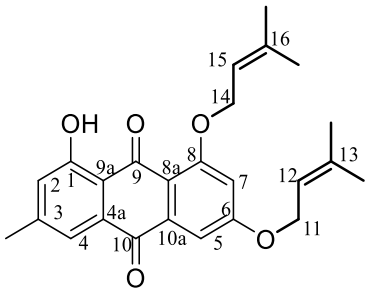

144

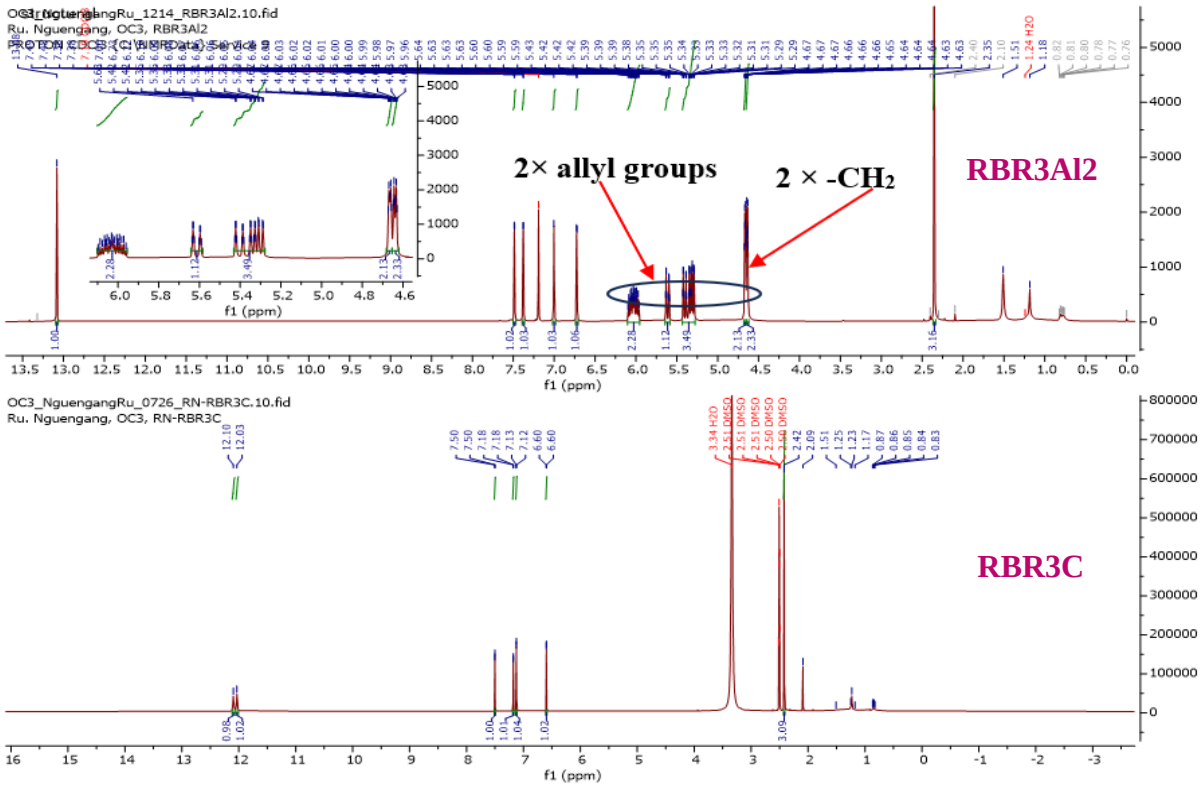

Figure 131: Comparative ^{1}H NMR of RBR3C (DMSO-d_6, 600 MHz) and RBRAl2 ($CDCl_3$, 600 MHz)

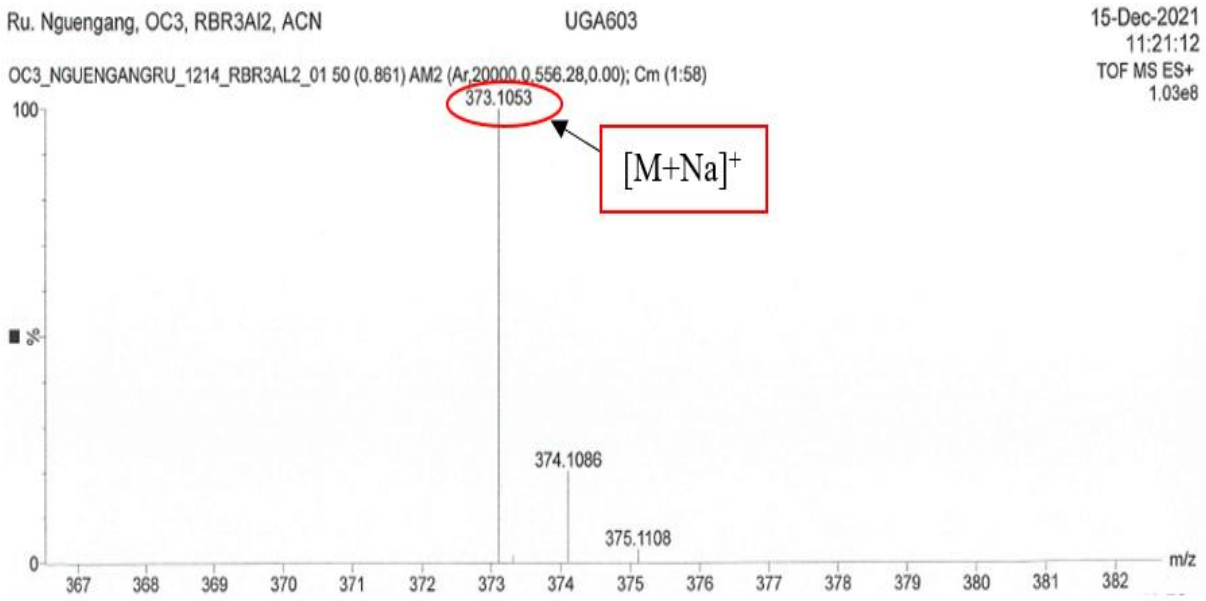

Figure 132: (+) HRESI mass spectrum of RBRAl2

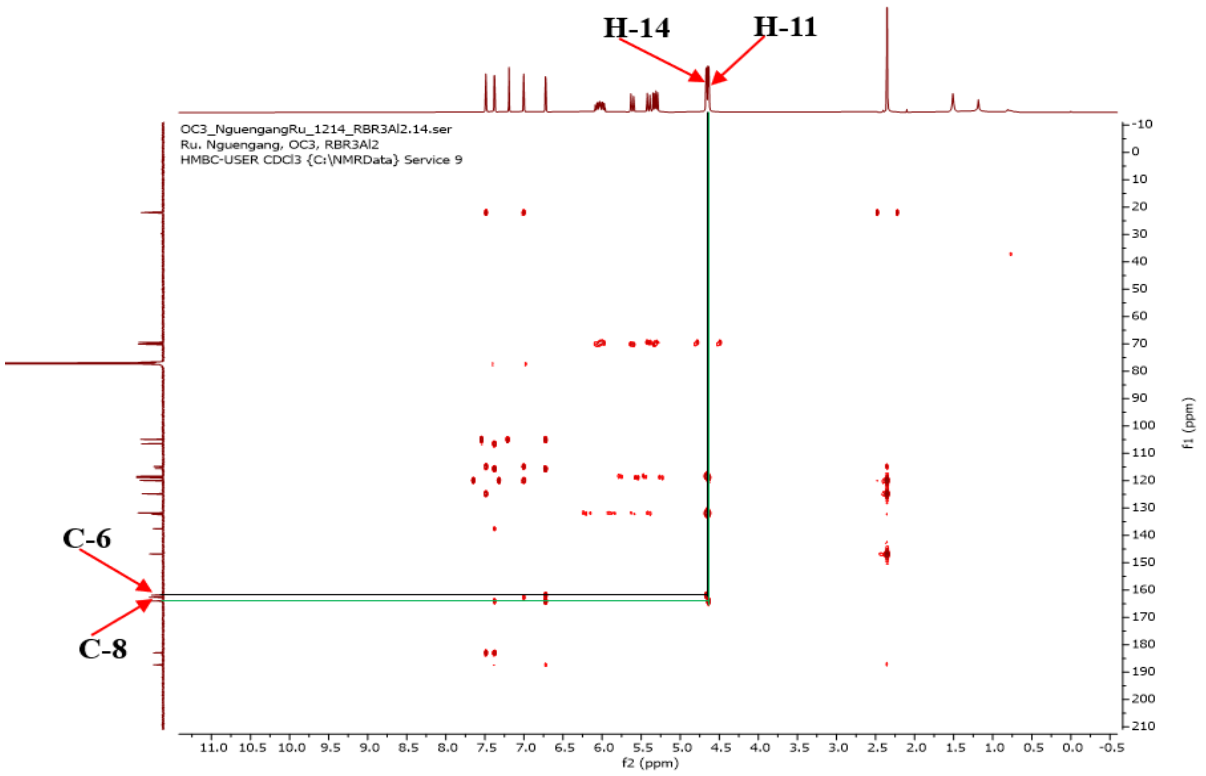

Figure 133: HMBC spectrum of RBRAl2

II.2.1.3. Structural elucidation of compound RBR3Al3 (145)

RBR3Al3 was obtained as yellowish finely divided solid soluble in dichloromethane. Its molecular formula, $C_{21}H_{18}O_5$, was deduced from its HRESIMS data (Figure 134), which showed the sodium adduct peak $[M+Na]^+$ at *m/z* 373.1053 (calcd. for $C_{21}H_{18}O_5Na$, 373.10465), corresponding to 13 degrees of unsaturation. This mass was identical to that of **RBR3Al2** (**144**) suggesting that **RBR3Al3** (**145**) is an isomer of **RBR3Al2** (**144**).

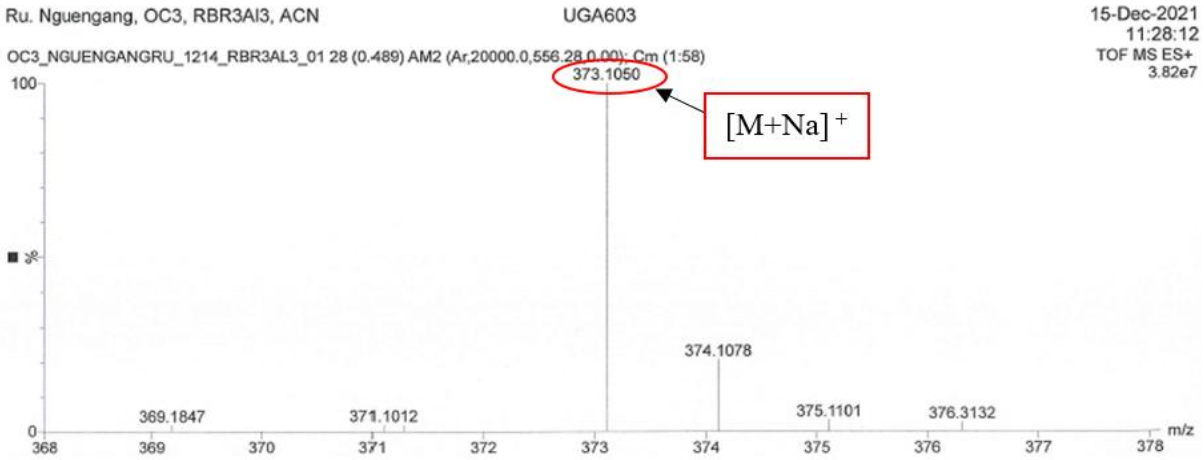

Figure 134: (+) HRESI mass spectrum of RBRAl3

In fact, the ^{1}H NMR spectrum of **RBR3Al3** (**145**) was very close related to that of **RBR3Al2** (**144**) (Figure 135). However, significant differences were recognized in the signals of C-1 and C-8 carbons. In fact, the C-1 here resonated at higher field (δ_C 159.9) than that of **RBR3Al2** (δ_C 162.6) while the C-8 here resonated at lower field (δ_C 165.1) than that of RBR3Al2 (δ_C 161.9) confirming the change of the position of the allyl group at δ_C 161.9 (C-8) (Figure 136).

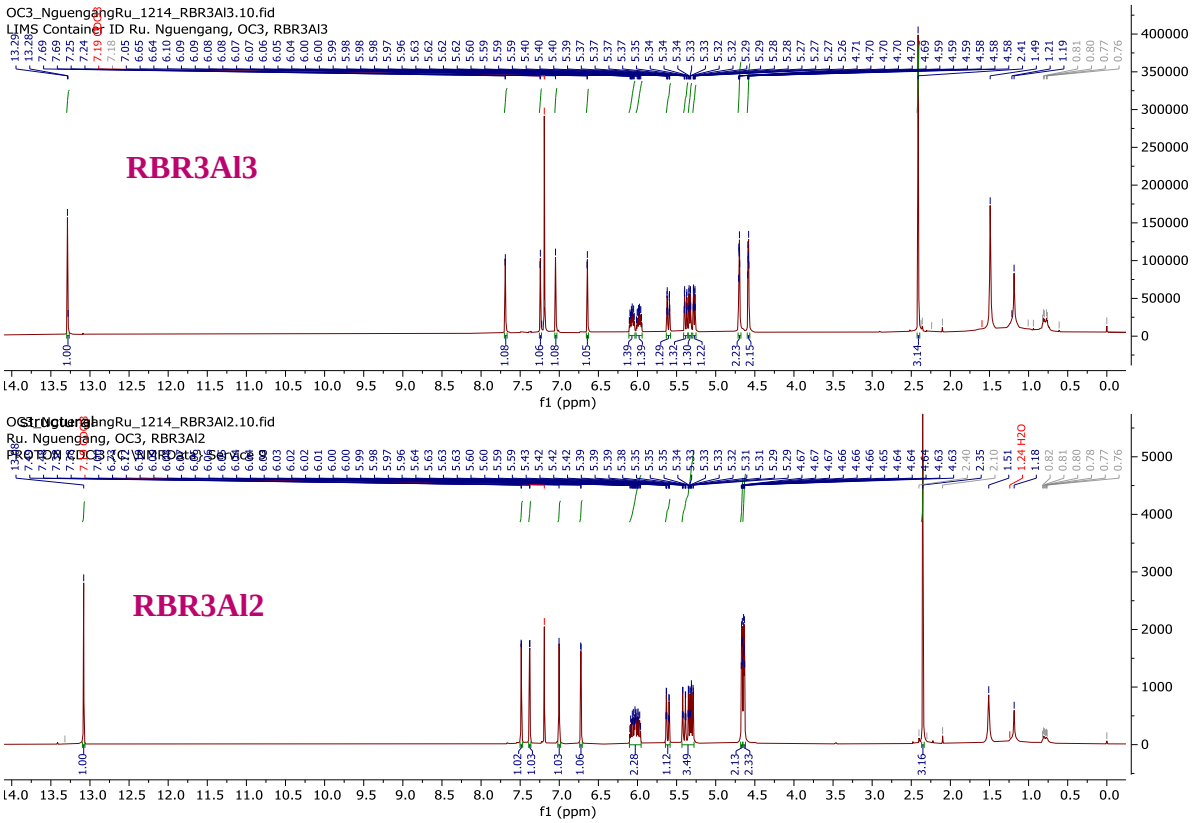

Figure 135: Comparative ^{1}H NMR of RBRAl2 ($CDCl_3$, 600 MHz) and RBRAl3 ($CDCl_3$, 600 MHz)

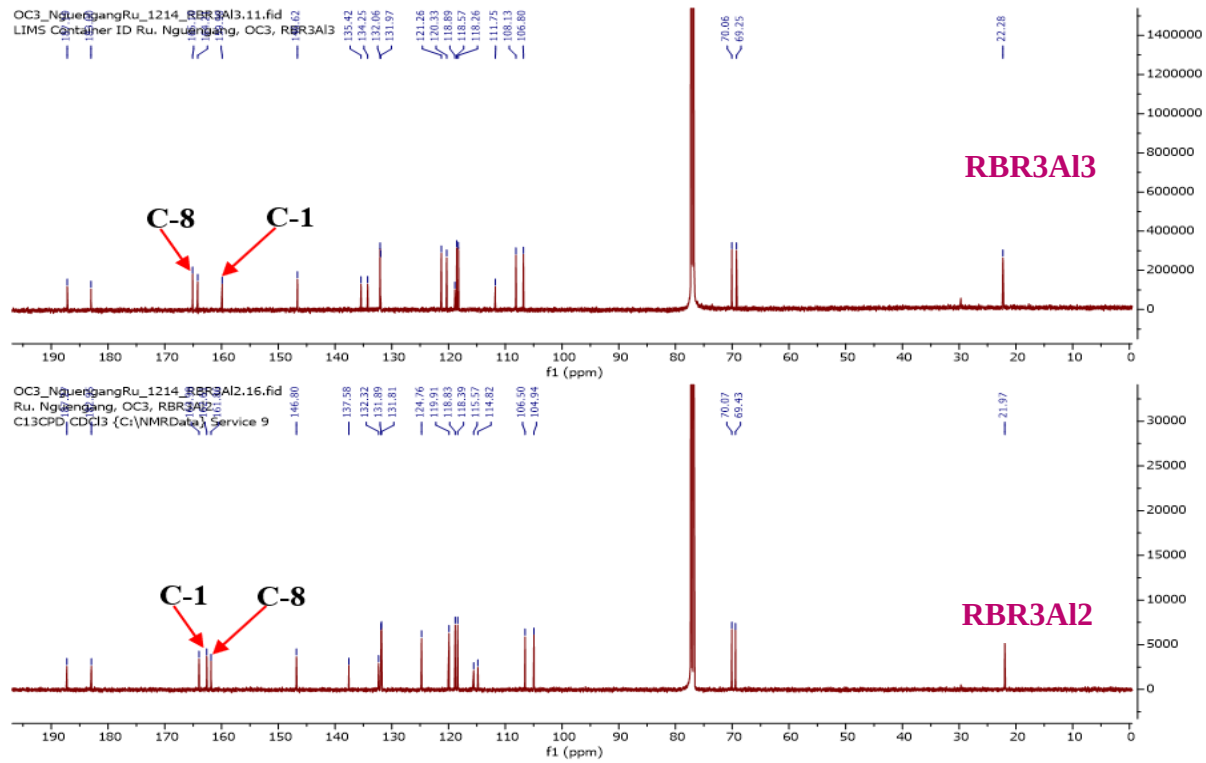

Figure 136: Comparative ^{13}C NMR spectrum of RBRAl2 and RBRAl3 ($CDCl_3$, 600 MHz)

This suggestion was confirmed with the correlation observed on the HMBC spectrum (Figure 137) of **RBR3Al3** between the proton H-11 [δ_H 4.58 (2H, dd, J = 5.5, 1.7 Hz)] and C-6 (δ_C 164.2) and between the proton H-14 [δ_H 4.70 (2H, dt, J = 5.0, 1.8 Hz)] and C-1 (δ_C 159.9).

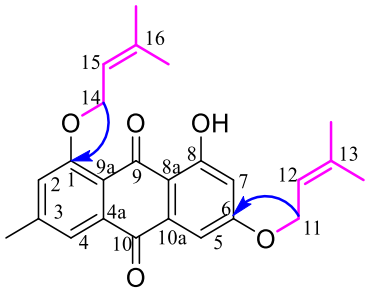

145

Scheme 35: HMBC spectrum of RBRAl2

Thus, compound **RBR3Al3** was characterized as new diallylated emodin [1,6-diallyloxyemodin (**145**)].

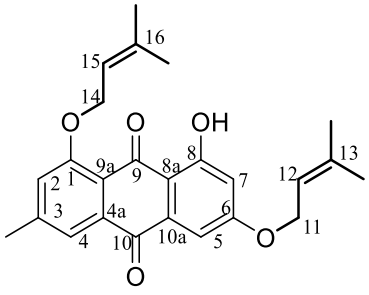

145

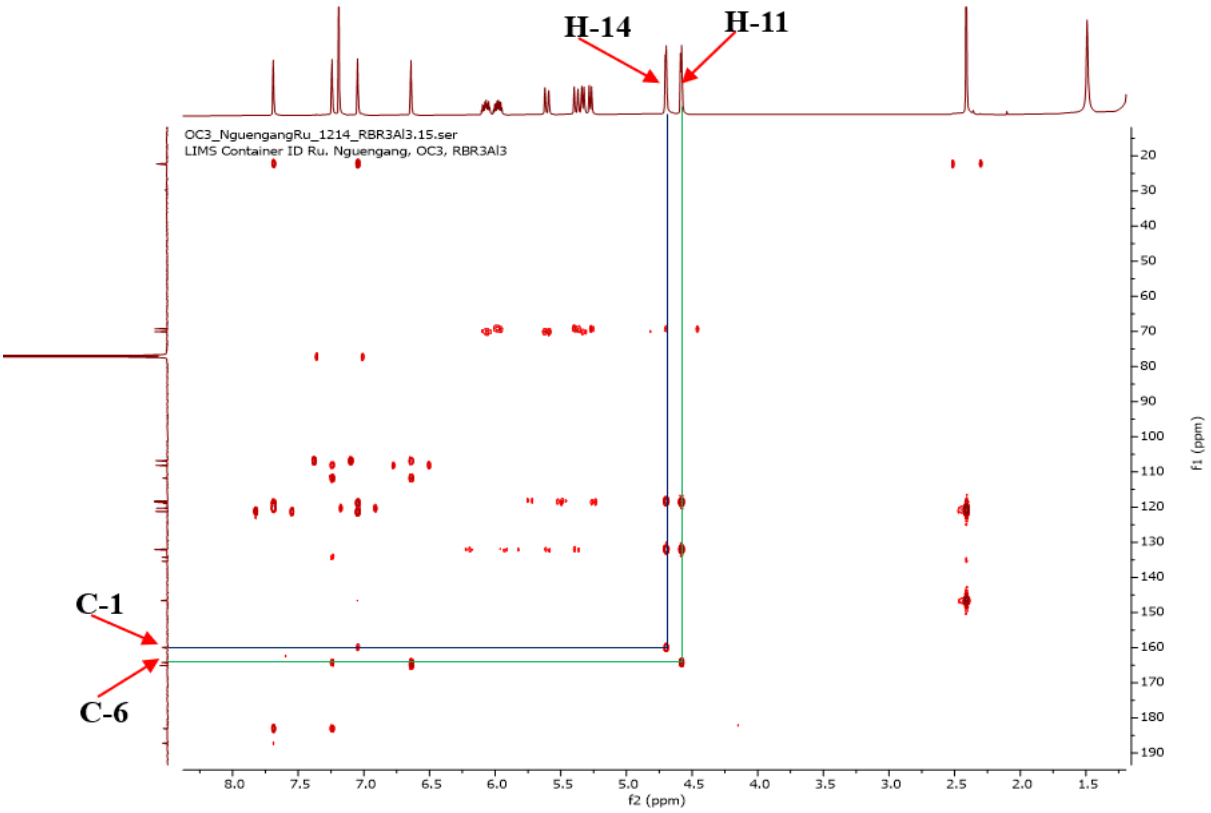

Figure 137: HMBC spectrum of RBRAl3

II.2.1.4. Structural elucidation of compound RBR3Al4 (146)

RBR3Al4 was obtained as yellowish finely divided solid soluble in dichloromethane. The ^{1}H NMR spectrum of **RBR3Al4** (**146**) showed characteristic signals of emodin **(117)** (Figure 138). The only difference was the presence of the signals of three allyl groups at δ_H [6.06 (1H, m, H-12), 5.39 (2H, dq, J = 17.2, 1.5 Hz, H-13) and 4.60 (2H, dt, J = 5.4, 1.5 Hz, H-11)], [6.03 (1H, m, H-15), 5.57 (2H, m, H-16) and 4.64 (2H, dt, J = 4.7, 1.8 Hz, H-14)] and [5.99 (1H, m, H-18), 5.26 (1H, m, H-19) and 4.66 (2H, dt, J = 4.8, 1.8 Hz, H-17)] in RBR3Al4 (Figure 138). This structure was confirmed with the HRESIMS (Figure 139), which showed the protonated adduct peak $[M+H]^+$ at *m/z* 391.1537 (calcd for $C_{24}H_{23}O_5^+$, 391.15400), corresponding to 14 degrees of unsaturation.

Based on the above observations, the structure of RBRAl4, was characterized as a new fully allylated emodin, 1,6,8-triallyloxyemodin (**146**).

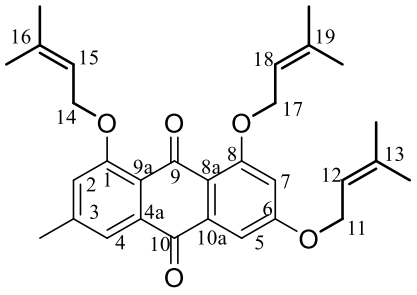

146

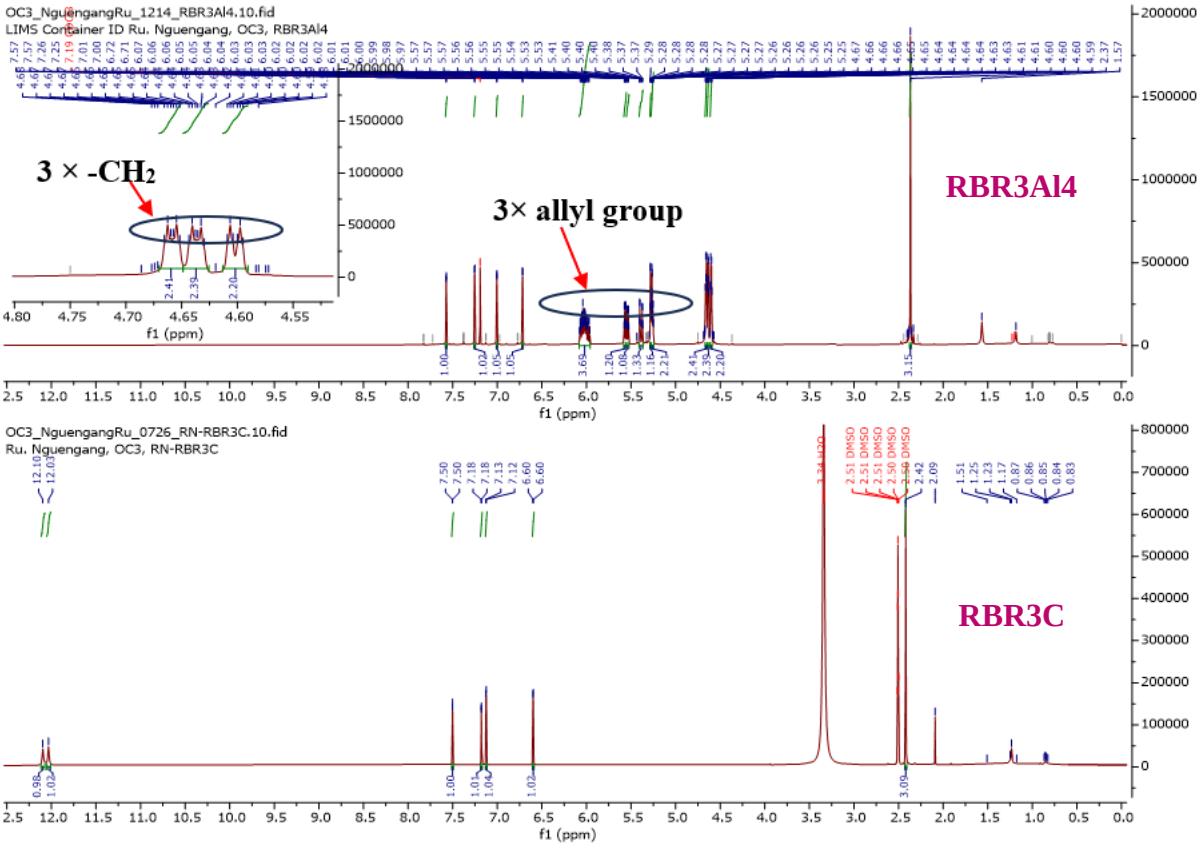

Figure 138: Comparative ^{1}H NMR of RBR3C (DMSO-d_6, 600 MHz) and RBRAl4 ($CDCl_3$, 600 MHz)

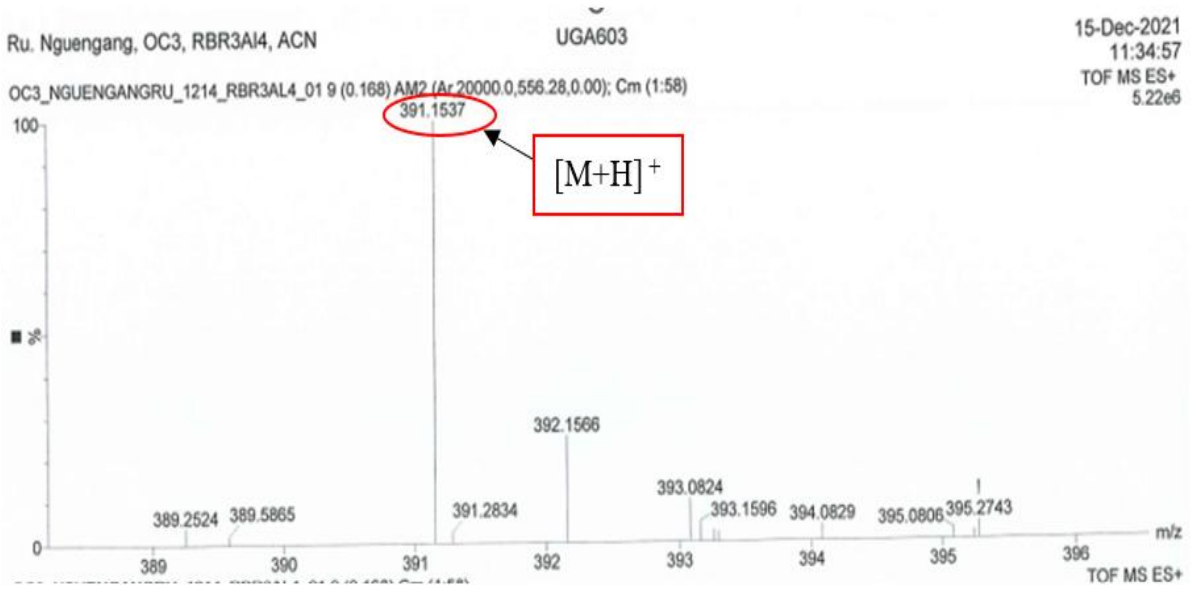

Figure 139: HRESI mass spectrum of RBRAl4

II.2.1.5. Structural elucidation of compound RBR3Ace1 (147)

RBR3Ace1 was obtained as yellow crystals soluble in acetone. The ^{1}H NMR spectrum of **RBR3Ace1** (**147**) was very close to that of emodin **(117)** (Figure 140). The only difference was the presence of additional signals of three methyl group at δ_H [2.41 (3H, s, H-15), 2.40 (3H, s, H-17) and 2.38 (3H, s, H-12)] suggesting the addition of three acethyl groups in RBR3Ace1 (**147**) (Figure 140). This suggestion was confirmed with its molecular formula, $C_{21}H_{16}O_8$, implying fourteen degrees of unsaturation, deduced from its NMR and its ESIMS data (Figure 141), which showed the sodium adduct peak $[M+Na]^+$ at *m/z* 419.1.

Based on the above observation, the structure of RBR3Ace1, was characterized as 1,6,8-triacetylemodin (**147**).

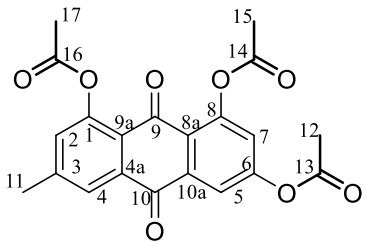

147

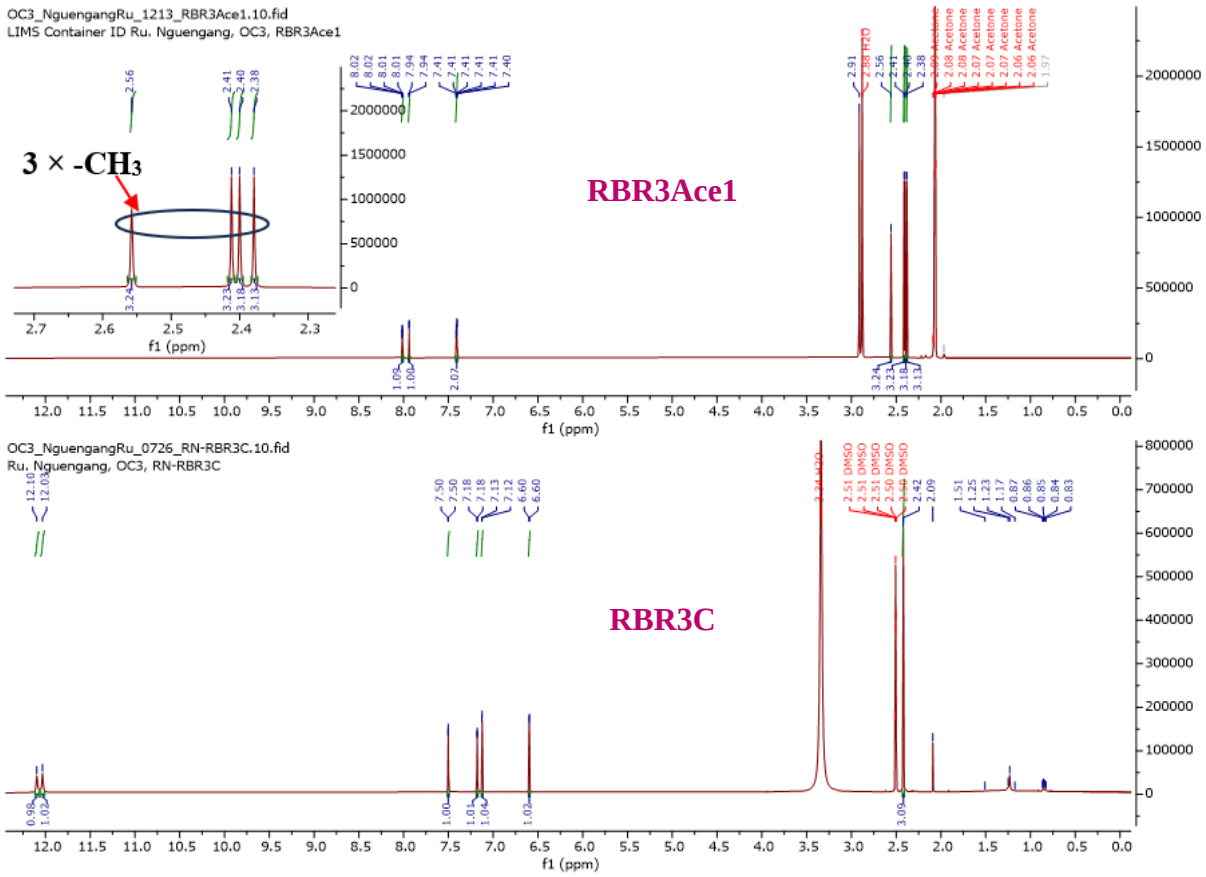

Figure 140: Comparative of ^{1}H NMR of RBR3C (DMSO-d_6, 600 MHz) and RBR3Ace1 (acetone-d_6, 600 MHz)

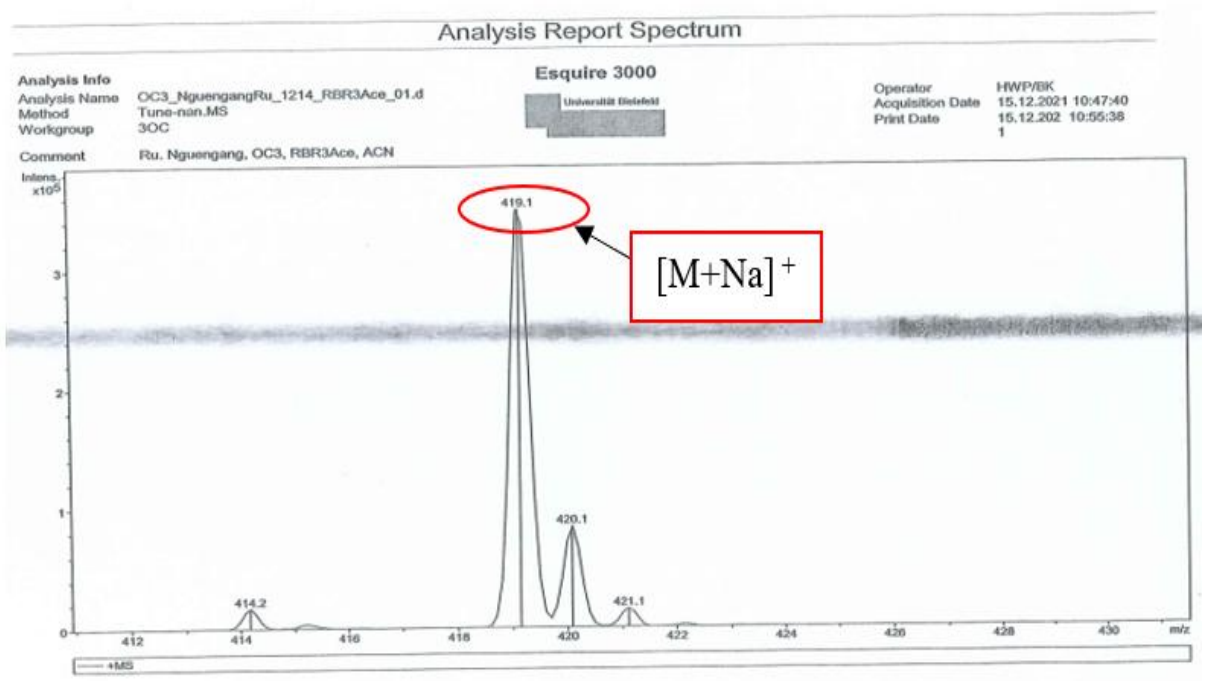

Figure 141: ESI mass spectrum of RBR3Ace1

II.2.2. Nitration of emodin (117) and catalytic hydrogenation of 1,6,8-trihydroxy-3-methyl-2,4,5,7-tetranitro anthraquinone (148)

In addition to the previously prepared derivatives of emodin, nitro and amino derivatives were also prepared (Scheme 36). In fact, the treatment of compound **RBR3C** (**117**) with concentrated HNO_3 in concentrated H_2SO_4 (Teich *et al*., 2004) produced 1,6,8-trihydroxy-3-methyl-2,4,5,7-tetranitro anthraquinone (STEP1 new3) **(148)**. Furthermore, this analogue was treated with H_2 in palladium (Carturan *et al*., 1983) and led to 5-amino-1,6,8-trihydroxy-3-methyl-2,4,7-trinitro anthraquinone **(149)** (RBR3amino19b).

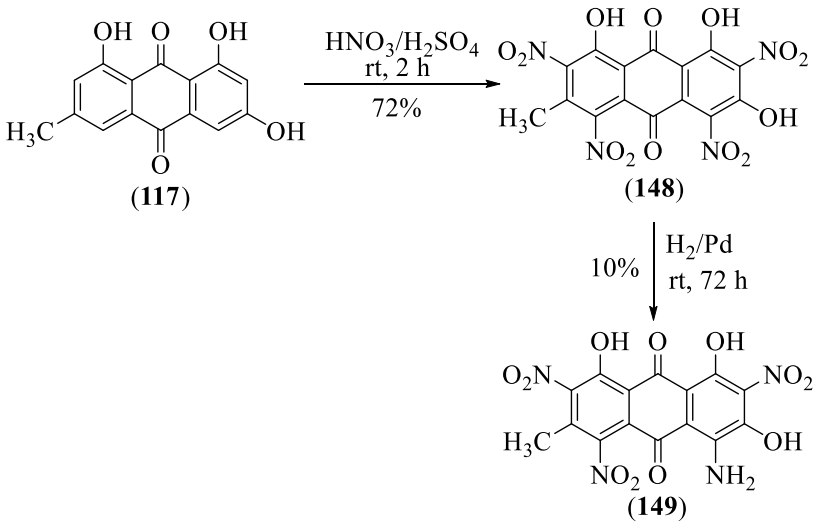

Scheme 36: Nitration and amination of aromatic protons of emodin (117).

II.2.2.1. Structural identification of compound (STEP1 new3) (148)

STEP1 new3 **(26)** was obtained as red finely divided solid soluble in DMSO. The difference between the ^1H NMR of emodin **(117)** and that of **STEP1 new3 (148)** was the diseapperance of signal of aromatic protons suggested the apparition of four nitro groups in **STEP1 new3** (Figure 142). This observation was confirmed with its molecular formula, $C_{15}H_6N_4O_{13}$, implying eleven degrees of unsaturation, deduced from its NMR and its ESIMS data (Figure 143), which showed the deprotonated adduct peak $[M-H]^-$ at *m/z* 448.8.

Based on the above data, **STEP1 new3** was identified as 1,6,8-trihydroxy-3-methyl-2,4,5,7-tetranitro anthraquinone **(148)**, previously synthesized by Teich *et al*., (2004).

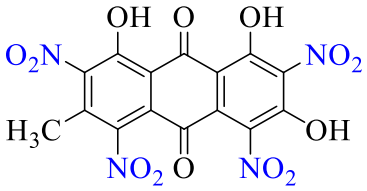

(**148**)

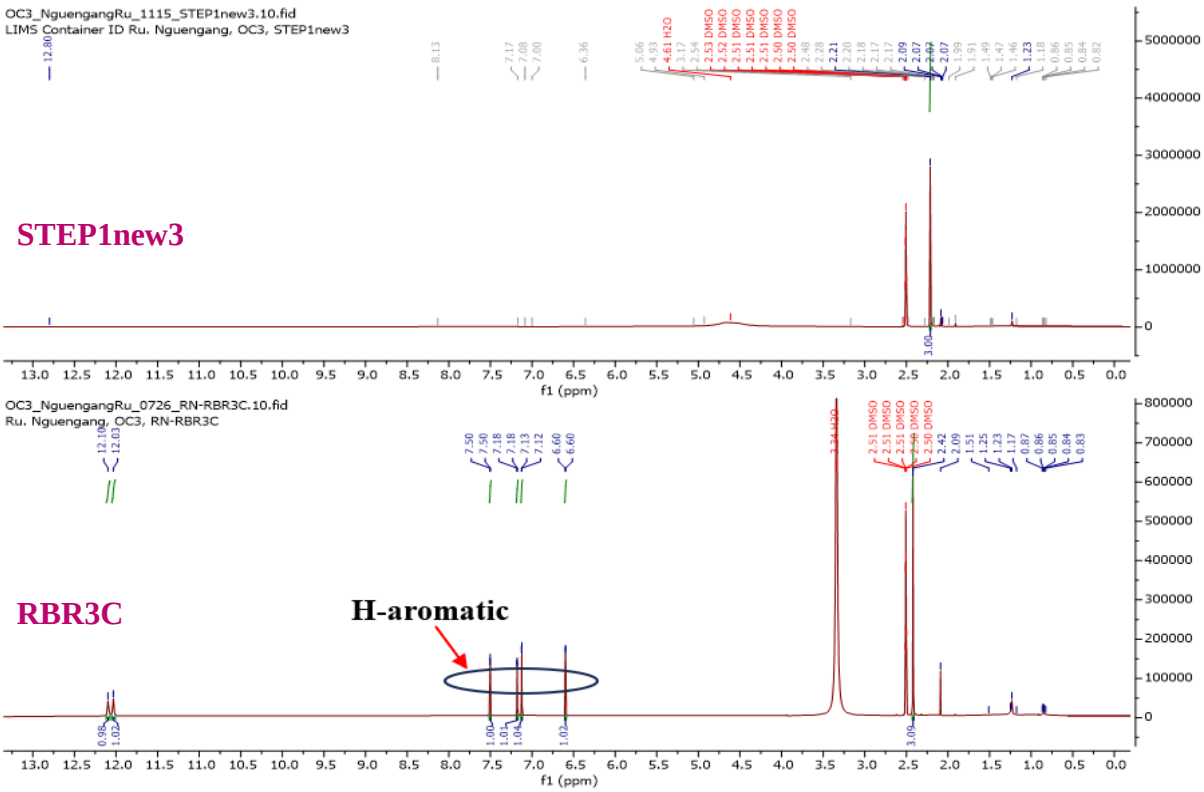

Figure 142: Comparative ^{1}H NMR of RBR3C (DMSO-*d*$_6$, 600 MHz) and STEP1 new3 (DMSO-*d*$_6$, 600 MHz)

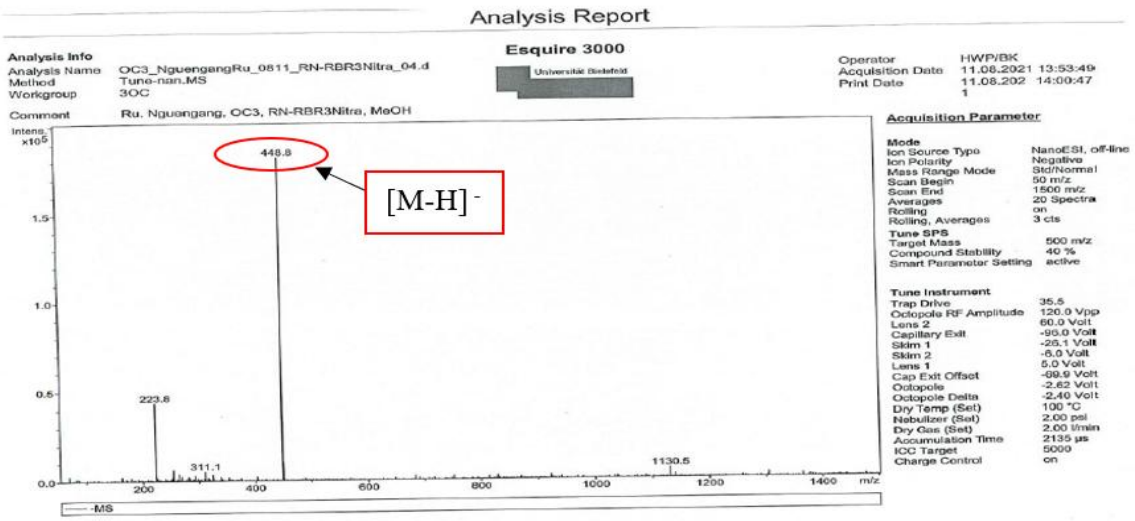

Figure 143: (-) ESI mass spectrum of STEP1 new3

II.2.2.2. Structural identification of compound (RBR3amin19b) (148)

RBR3amin19b (149) was obtained as violet finely divided solid soluble in DMSO. The difference between the ^{1}H NMR of **STEP1 new3 (148)** and that of **RBR3amino19b (149)** was the presence of one additional signal of amino group at δ_H 10.04 (1H, s, NH_2-5) suggesting the reduction of one nitro groups in **RBR3amin19b (149)** (Figure 144). This changed was confirmed by its HRESIMS (Figure 145), which showed the deprotonated molecular ion peak $[M-H]^-$ at *m/z* 419.0113 (calcd for $C_{15}H_7N_4O_{11}^-$, 419.01168), corresponding to eleven degrees of unsaturation.

Based on the above observations, the structure of **RBR3amin19b**, was characterized as a new 5-amino-1,6,8-trihydroxy-3-methyl-2,4,7-trinitro anthraquinone **(149)**.

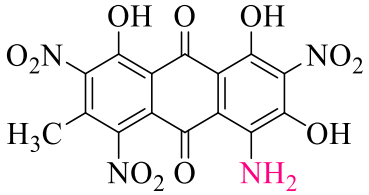

(149)

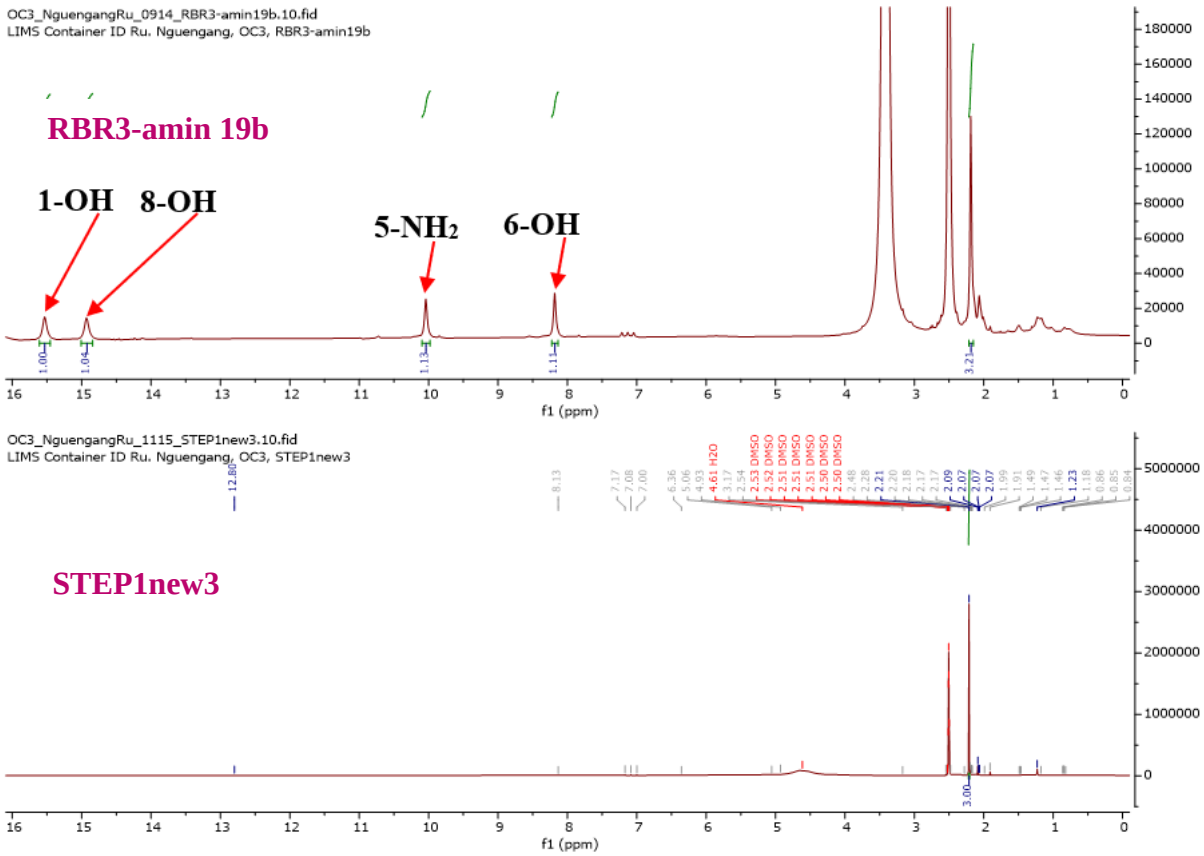

Figure 144: Comparative ^{1}H NMR of STEP1 new3 and RBR3amin19b (DMSO-d_6, 600 MHz)

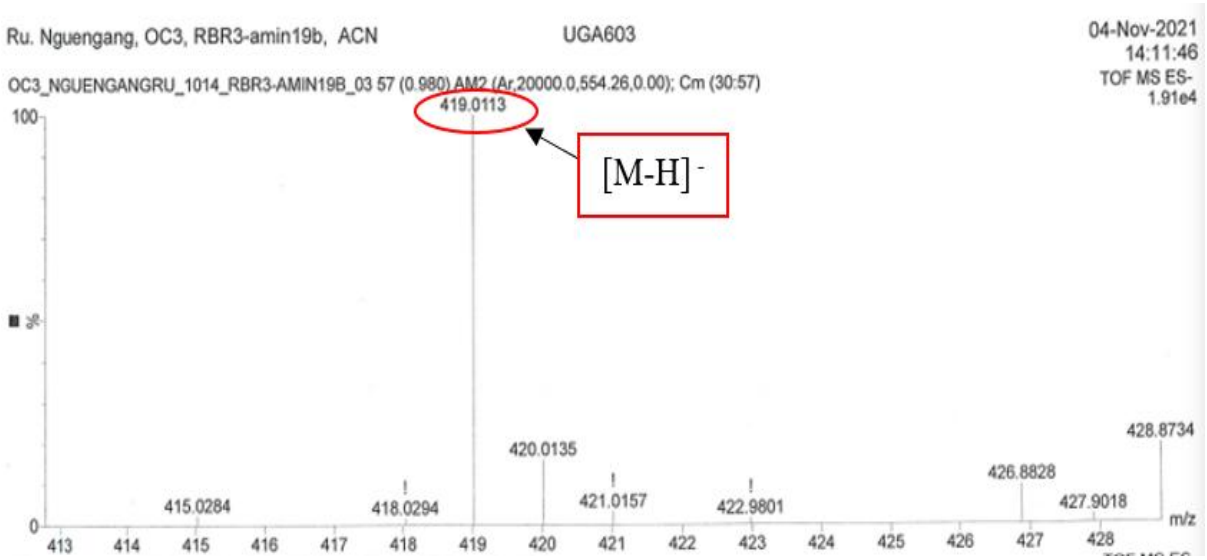

Figure 145: (-) HRESI mass spectrum of RBR3amin19b

II.2.3. Acid hydrolysis

Compound RBR48-1 (**111**) (2 mg) was refluxed in 2 M HCl (5 mL) at 100°C for 4 h. The reaction mixture was poured into water and extracted with EtOAc (5 mL, three times). The aqueous layer was concentrated and used for the sugar identification by TLC and comparison of the optical rotation with L-rhamnose.

II.3. CHEMOPHENETIC SIGNIFICANCE OF THE ISOLATED COMPOUNDS

- ***R. nepalensis***

In the present study, twenty compounds sorted into four classes of secondary metabolites were isolated from the ethyl acetate fraction of the roots of *R. nepalensis* including three furanones (**111**, **137** and **138**) among which one new phenylisobenzofuranone derivative (**111**), twelve anthraquinones (**117–128**), three steroids (**140–142**), and two flavanols (**129** and **130**).

Among these compounds, the furanones (**111**; **137** and **138**) were isolated for the first time from the Polygonaceae family, while the phenylisobenzofuranone derivative (**111**) was found to be a new compound. However, the literature indicates that benzofuranones have already been isolated from other species of the genus *Rumex* such as *R. gmelini* (Hai-peng *et al*., 2009), *R. patientia* (Yuan *et al*., 2001) and *R. vesicarius* (Shah *et al*., 2015). Thus, the presence of phenylisobenzofuranone derivative (**111**) in *R. nepalensis* is not surprising. However, among the anthraquinones isolated (**117–128**), 1,3,6-trihydroxy-8-methyl-anthraquinone (**124**) emodin bianthrone (**128**) and emodic acid (**123**) are newly isolated from the Polygonaceae family while

questin (**122**) and questinol (**121**), were isolated from *Radix Polygoni multiflora* and *Polygonum cuspidatum* (Zhen-li *et al*., 2009; Shen, 2013) two plant species from the Polygonaceae family, but were reported in this study for the first time from the genus *Rumex*. Emodin bianthrone (**128**) were detected in *Japanese knotweed* rhizome (Jug *et al*., 2021) (Polygonaceae), although it is newly isolated from the Polygonaceae family. The anthraquinones (**117–120**; **126–127**) have been previously isolated from *R. acetosa*, *R. confertus* Willd, *R. crispus*, *R. hydrolapathum* Huds, *R. obtusifolius* (Wegiera *et al*., 2007), *R. aquaticus* (Orbán-Gyapai *et al*., 2017) and *R. acetosella* (Choe *et al*., 1998), which exhibited the taxonomic relationships between *R. nepalensis* and these other species and confirm the botanical identification of *R. nepalensis*. The Anthraquinones could be considered as chemotaxonomic markers for this genus. Moreover, the three steroid derivatives (**140–142**) have been isolated from *R. patientia* (Yuan *et al*., 2001), *R. vesicarius* (Al Easa *et al*., 1995) and *R. paulsenianus* (Gusakova *et al*., 1990). Additionally, it is worthy to note that among the two flavanols isolated, epicatechin 3-(6″-*O*-methyl) gallate (**130**) was previously reported from *R. abyssinicus* (Tala *et al*., 2018), while catechin 7-*O*-gallate (**129**) was isolated for the first time from Polygonaceae family.

- ***S. globulifera***

With regard to the chemophenetic contribution, fifteen compounds sorted into five classes of secondary metabolites were isolated from the *n*-hexane soluble fraction of the stem bark of *S. globulifera*, including four polyprenylated benzophenones (**112**−**115**), among which three new derivatives (**112**−**114**), one new tocotrienol derivative (**116**), five xanthones (**131–135**), three steroids (**140–142**), one flavanol (**135**) and one triterpenoid (**139**). The presence of the polyprenylated benzophenones (**112**−**114**) is not surprising since benzophenones (polycyclic polyprenylated acylphloroglucinols) are known to be widespread in the Clusiaceae family (Fromentin *et al*., 2013). Moreover, gaboxanthone (**131**), symphonin (**133**), lupeol (**139**), *β*-sitosterol (**140**), stigmasterol (**141**) and *β*-sitosterol 3-*O*-*β*-D-glucopyranoside (**142**) have been reported from *S. globulifera* (Ngouela *et al*., 2006; Suffredini *et al*., 2017; Téné *et al*., 2021). In addition, the new tocotrienol derivative (**116**) has been isolated for the first time from the genus *Symphonia*. However, the literature indicates that tocotrienol derivatives have already been isolated from other genera of the Clusiaceae family, such as *Garcinia* (Tan *et al*., 2021; Fuentes *et al*., 2018) and *Clusia* (Marques *et al*., 2021). To the best of our knowledge, guttiferone K (**115**), xanthone V2 (**132**), pyranojacareubin (**135**) and kaempferol (**136**) were isolated for the first time from the genus *Symphonia*. However, these compounds have been reported from plants of the Clusiaceae family. In fact, guttiferone K (**115**) has been previously

isolated from the fruits of *Rheedia calcicole* (Cao *et al*., 2007), xanthone V2 (**132**) was also isolated from root bark of *Vismia guineensis* (Botta *et al*., 1986), while pyranojacareubin (**135**) was reported from the bark of *Calophyllum gracilipes* (Cao *et al*., 1997) and kaempferol (**136**) was obtained from the leaves of *V. guineensis* (Mbaveng *et al*., 2008) Mbaveng. 1,5-Dihydroxy-3-methoxyxanthone (**134**) was isolated for the first time from Clusiaceae.

II.4. BIOLOGICAL ACTIVITIES OF THE ISOLATED COMPOUNDS

II.4.1. Antileishmanial activity of extracts, fractions, and isolated compounds

The isolated compounds were assessed for their antileishmanial activity against *Leishmania donovani* 1S (MHOM/SD/62/1S) promastigotes and their cytotoxicity towards RAW 264.7 macrophage cells.

The criteria of evaluation of the antileishmanial activity and cytotoxicity activity of natural products are represented in the tables 45 and 46.

Table 45: Criteria of evaluation of the antileishmanial activity of extracts, fractions and pure compounds

Antileishmanial activity of extracts/Fractions (Camacho, 2003)		**Antileishmanial activity of pure compounds (Nwaka and Hudson, 2006; Sosa *et al*., 2016)**	
IC_{50} (μg/mL)	Qualification	IC_{50} (μg/mL)	Qualification
$IC_{50} < 10$	Potent activity	$IC_{50} < 1$	Hit/lead activity
$10 < IC_{50} < 50$	Good activity	$IC_{50} < 10$	Potent activity
$50 < IC_{50} < 100$	Moderate activity	$10 < IC_{50} < 20$	Moderate activity
$IC_{50} > 100$	Inactive	$IC_{50} > 20$	Inactive

Table 46: Criteria of evaluation of the cytotoxicity activity

Cytotoxicity activity criteria (Camacho, 2003; Nwaka and Hudson, 2006)	
Selectivity Index (SI)	Qualification
SI > 20	Hit selective
SI > 1	Selective
SI < 1	Non selective

II.4.1.1. *S. globulifera*

From the active *n*-hexane fraction (IC_{50} = 43.11 μg/mL) of crude extract of *S. globulifera*, compounds (**112−116, 131−135**) were isolated and assessed *in vitro* for their antileishmanial activity against *L. donovani* NR-48822 promastigotes and for their cytotoxicity toward Raw 264.7 macrophage cells (Table 47). Guttiferone K (**115**) exhibited the best antileishmanial activity against the parasite with an IC_{50} value of 3.30 ± 0.51 μg.mL^{-1} but with weak selectivity toward Raw 264.7 macrophage cells (SI > 1.25), while compounds **112−114**, **116**, **131-132** and **134-135** showed moderate activity with IC_{50} values ranging from 10.80 to 15.98 μg.mL^{-1}. The assessed compounds were more active than the *n*-hexane soluble fraction from which they were obtained. The inactivity of the MeOH crude extract and EtOAc fraction may be due to the antagonistic effect of its constituents. The majority of the active compounds were xanthones or benzophenones, which are known to possess antileishmanial activity.

Table 47: Antileishmanial and cytotoxic activities of extract, fractions, and compounds from the stem bark of *S. globulifera*.

Extracts/ compounds	Antileishmanial activity IC_{50} ± SD (μg/mL)	Macrophages CC_{50} ± SD (μg/mL)	Selectivity index SI ± SD (=$CC5_0/IC_{50}$)
ME	> 100		
HF	43.11 ± 0.01	> 20	
EF	> 100		
BF	> 100		
112	12.91 ± 1.11	28.06 ± 5.72	2.17
113 and 114	12.13 ± 1.08	9.60 ± 0.26	0.79
116	14.03 ± 1.14	> 20	> 1.39
115	3.30 ± 0.51	5.20 ± 0.02	1.57
131	15.97 ± 1.20	> 20	> 1.25
132	12.91 ± 1.11	> 20	> 1.54
135	12.91 ± 1.11	> 20	> 1.54
133	ND	ND	
134	47.04 ± 1.67	> 20	> 0.42
Amphotericin B	0.048		

ND: not determined; **BF**: *n*-butanol fraction; **HF**: *n*-hexane fraction; **ME**: methanol extract; **EF**: ethyl acetate fraction

II.4.2. Antibacterial activity of extracts, fractions, and isolated compounds

The extracts, fractions and isolated compounds were assessed for their antibacterial activity against seven bacteria strains: *Salmonella typhi CPC, S. enterica NR13555, Staphylococcus aureus ATCC43300, S. aureus ATCC25923, Klebsiella pneumoniae clinical isolate, K. pneumoniae NR41388* and *Pseudomonas aeruginosa HM801*.

The minimum inhibitory concentration (MIC) was defined as the lowest concentration of the sample that prevents bacterial growth. The criteria of evaluation of the antibacterial activity of an isolated compound or a plant extract is classified in Table 48 (Kuete *et al*., 2011).

Table 48: Criteria of evaluation of the antibacterial activity of extracts and pure compounds from *S. globulifera* and *R. nepalensis*

Antibacterial activity of pure compounds		**Antibacterial activity of extracts**	
MIC (μg/mL)	Qualification	MIC (μg/mL)	Qualification
MIC ≤ 10	Strong activity	MIC < 100	Significant activity
10 < MIC ≤ 100	Moderate activity	100 < MIC ≤ 625	Moderate activity
MIC >100	Weak activity	MIC > 625	Weak activity

II.4.2.1. *S. globulifera*

The methanol crude extract, the *n*-hexane, EtOAc and *n*-butanol soluble fractions along with some the isolated coumpounds were assessed for their antibacterial activity against seven bacterial strains: *S. typhi CPC, S. enterica NR13555, S. aureus ATCC43300, S. aureus ATCC25923, K. pneumoniae clinical isolate, K. pneumoniae NR41388*, and *P. aeruginosa HM801* (Table 49).

Table 49: Antibacterial activity of extract, fractions, and compounds from *S. globulifera* (MIC in μg.mL^{-1})

Extracts/ compounds	Antibacterial activity (MIC in μg.mL^{-1})						
	St	***Se***	***Sa***	***Sau***	***Kpc***	***Kp***	***Pa***
ME	250	-	250	250	250	1000	125
HF	15.7	62.5	250	62.5	31.2	125	31.2
EF	62.5	500	1000	31.2	31.2	500	31.2
BF	500	-	-	500	1000	1000	500
112	3.9	62.5	125	3.9	3.9	62.5	3.9
113 and **114**	15.6	62.5	500	62.5	15.6	62.5	15.6
116	31.2	125	500	62.5	31.2	62.5	31.2
115	3.9	125	250	31.2	3.9	62.5	3.9
Gentamycin	0.048	0.07	0.07	0.03	0.048	0.07	0.048

St: *Salmonella typhi* CPC; **Se**: *S. enterica* NR13555; ***Sa***: *Staphylococcus aureus* ATCC43300; ***Sau***: *S. aureus* ATCC25923; ***Kpc***: *Klebsiella pneumoniae* Clinical isolate; ***Kp***: *K. pneumoniae* NR41388; ***Pa***: *Pseudomonas aeruginosa* HM801; -: >1000 μg/mL; **BF**: *n*-butanol fraction; **HF**: *n*-hexane fraction; **ME**: methylene chloride/methanol extract; **EF**: ethyl acetate fraction.

Strong activity Moderate activity

The MeOH crude extract and the *n*-BuOH fraction of *S. globulifera* exhibited moderate activity, while, the *n*-hexane and EtOAc fractions exhibited good antibacterial activities on at least two strains with MIC values ranging from 15.7 to 31.2 μg.mL^{-1}, except on *S. aureus* ATCC25923, which was not susceptible to the EtOAc fraction. Compounds **112** and **113−116** displayed good to moderate activity against these strains, with MIC values ranging from 3.9 to 62.5 μg.mL^{-1}, except for *S. aureus* ATCC25923, which was not susceptible.

These results highlighted the knowledge on the potential of guttiferone derivatives as potent antileishmanial and antibacterial agents (Azebaze *et al*., 2008; Iinuma *et al*., 1996) and thus, justify the use of this plant in traditional medicine to treat skin and bacterial diseases (Ssegawa *et al*., 2007; Gupta *et al*., 2005).

II.4.2.2. *R. nepalensis*

The CH_2Cl_2−MeOH (1:1, v/v) root extract of *R. nepalensis* was subjected to preliminary screening on seven bacteria strains: *S. typhi CPC, S. enterica NR13555, S. aureus ATCC43300, S. aureus ATCC25923, P. aeruginosa HM801, K. Pneumoniae NR41388* and *K. Pneumoniae* (clinical isolate). This extract exhibited significant antibacterial activities with 31.25 ≤MIC≤

62.5 $\mu g.mL^{-1}$ against five of the tested strains (Table 50) and was subjected to a liquid-liquid partition using *n*-hexane, ethyl acetate and *n*-butanol, successively. The three fractions obtained were also screened for their antibacterial potential and the EtOAc fraction was the most active against the tested strains with MICs ranging from 31.25 to 3.9 $\mu g.mL^{-1}$ (Table 50) (Kuete *et al*. 2011).

All the isolated compounds from the active EtOAc fraction were assessed *in vitro* for their antibacterial activity on the above mentioned strains and compounds **117, 120, 122, 124, 126** and **127** exhibited strong to moderate antibacterial activities ranging from 1.9 to 62.5 $\mu g.mL^{-1}$ against *S. typhi*, *S. aureus* ATCC25923, *K. Pneumonie* NR41388 and *P. aeruginosa* HM801 (Table 50). Emodin (**117**) showed the best antibacterial activity, particularly against *S. typhi CPC*, *P. aeruginosa HM801* and *K. Pneumoniae* Clinical isolate with MICs value of 1.9 $\mu g.mL^{-1}$, while compounds **120, 122, 124, 126** and **127** displayed good activities on at least one of the tested strains. The result obtained with the anthraquinone, emodin (**117**), corroborate with those reported by Chukwujekwu and collaborators (2006) against *S. aureus* with an MIC value of 3.9 $\mu g.mL^{-1}$. 1,8-Dihydroxyanthraquinones are known to possess good antibacterial activity. Their antibacterial activity is due to their interaction with the cell wall and cell membrane by which it increases the permeability of the cell envelope and leads to the leakage of cytoplasm and the deconstruction of cell (Wei *et al*. 2015).

While comparing the activity of the isolated compounds, the crude extract and the EtOAc fraction, it was observed that apart from *S. enterica* strain, the partition led to an increase in the activity of the EtOAc against six strains of bacteria and a decrease in the activity of *n*-hexane and *n*-BuOH soluble fractions. The increase or the decrease of activity may be due to the synergistic effect and antagonistic of the constituents of the fractions, respectively.

Apart from compound **117** that was more active than all the extracts and fractions, compounds **120, 122, 124, 126** and **127** were more active than the EtOAc soluble fraction on at least one of the assayed strains. In addition, the good activity of the crude extract, EtOAc soluble fractions and that of compounds **111, 117, 120, 122, 124, 126** and **127** against *S. aureus, K. Pneumonia*, *S. typhi and Salmonella enterica* may partially justify the use of this plant in traditional medicine in the treatment of typhoid, fever, skin diseases and respiratory tract infections.

Table 50: Antibacterial activity of extract, fractions, and compounds (1−20) from *R. nepalensis* (MIC in $\mu g.mL^{-1}$)

	St	***Se***	***Sa***	***Sau***	***Pa***	***Kp***	***Kpc***
CH_2Cl_2/MeOH	62.5	250	31.2	31.2	31.2	250	31.2
n-hexane	500	500	250	250	250	500	500
EtOAc	15.6	500	7.80	15.6	7.8	250	3.9
n-BuOH	200	500	250	125	250	500	125
111	-	-	-	-	-	-	-
117	1.9	250	500	15.7	1,9	250	1,9
120	15.9	125	500	31.2	125	ND	ND
124	15.6	500	125	31.2	ND	ND	ND
122	31.2	250	500	250	ND	ND	ND
126 + 127	15.6	250	500	1000	62.5	-	31.2
119	-	-	-	-	-	-	-
118	-	-	-	1000	-	1000	1000
121	500	1000	1000	-	ND	ND	-
128	125	500	500	250	ND	ND	500
123	1000	1000	125	1000	500	-	500
125	-	-	-	-	-	-	-
140	-	-	-	500	1000	-	-
141	-	-	1000	1000	1000	1000	1000
142	-	-	-	-	-	-	-
137	100	> 100	> 100	100	ND	ND	ND
138	250	> 500	500	500	ND	ND	500
130	1000	-	1000	1000	1000	-	1000
129	500	-	500	1000	500	-	1000
Gentamycin	0.048	0.07	0.07	0.03	0.03	0.07	0.048

***St**: Salmonella typhi* CPC; ***Se** : Salmonella enterica* NR13555; ***Sa**: Staphylococcus aureus* ATCC43300; ***Sau**: Staphylococcus aureus* ATCC25923; ***Pa**: Pseudomonas aeruginosa* HM801; ***Kp**: Klebsiella Pneumoniae* NR41388; ***Kpc**: Klebsiella Pneumoniae* Clinical isolate; ND : not determined; **CH_2Cl_2/MeOH**: methylene chloride/methanol extract; **EtOAc**: Ethyl acetate fraction; ***n*-BuOH**: *n*-butanol fraction.

Strong activity Moderate activity

Analogues **143**–**147** were also assessed *in vitro* for their antibacterial activity against the aforementioned bacteria strains and all the derivatives were inactive (Table 51). These results confirm that bioactivity of emodin is attributable to the hydroxy groups, and this is in accordance with previous findings (Chalothorn *et al*. 2019). Thus, the absence of the hydroxy group at C-6 or C-8 may justified the inactivity of questin (**122**), chrysophanol (**119**), physcion (**118**), questinol (**121**) and emodin-6-*O*-*β*-D-glucoside (**125**) (Omosa *et al*. 2016) on some strains. In addition, the absence of the hydroxy group at the position-8 in questinol (**121**) could justify the fact that this compound was also inactive against all the tested bacteria strains except for the *S. typhi CPC strain* with a MIC value of 31.2 $\mu g.mL^{-1}$. Despite the absence of the hydroxy groups at C-8 and C-6 in the mixture of physcionin (**126**) and chrysophanein (**127**), it

exhibited moderate activity against *S. typhi*, *P. aeruginosa HM801* and *K. Pneumoniae* Clinical isolate and this is probably due to the synergistic effect of these two compounds.

Also, nitro and amino derivatives were prepared (Scheme 36). In fact, the treatment of compound **117** with concentrated HNO_3 in concentrated H_2SO_4 (Teich *et al*. 2004) produced 1,6,8-trihydroxy-3-methyl-2,4,5,7-tetranitro anthraquinone **(148)**. Furthermore, this analogue was treated with H_2 in palladium (Carturan *et al*. 1983) and led to 5-amino-1,6,8-trihydroxy-3-methyl-2,4,7-trinitro anthraquinone **(149)**. Compounds **148** and **149** were also assessed for their antibacterial activity against the above-mentioned strains. While comparing the activity of emodin (**117**) and the analogue (**148**), it was observed that the presence of nitro groups has considerably increased the potency of emodin (**117**) against *K. Pneumoniae NR41388* strain and *S. aureus ATCC43300* (Table 51). This result could be considered as an additional information to those reported by Chalothorn *et al*. (2019), which showed that the presence of secondary amine at C-4 increased the anti-methicillin-resistant *S. aureus*. Interestingly, the analogue **149** was most potent that **117** against *S. enterica NR13555* (Table 51). Thus, in addition to findings previously reported by Chalothorn *et al*. (2019), the presence of an amino group at position C-5 also increases the antibacterial activity (Table 51).

Table 51 : Antibacterial activity of emodin (2) and derivatives (21−27) (MIC in $\mu g.mL^{-1}$)

	St	***Se***	***Sa***	***Sau***	***Pa***	***Kp***	***Kpc***
117	1.9	250	500	15.7	1.9	250	1.9
143	-	-	-	1000	-	-	-
144	-	-	-	1000	-	-	-
145	1000	-	-	1000	1000	1000	500
146	-	-	-	500	-	-	-
147	500	-	-	250	500	1000	500
148	250	500	250	250	250	15.6	125
149	125	125	500	250	125	250	250
Gentamycin	0.048	0.07	0.07	0.03	0.03	0.07	0.048

Strong activity Moderate activity

CONCLUSION AND PERSPECTIVES

The objective of this work was to search for potential extracts, fractions from two Cameroonian medicinal plants namely *R. nepalensis* (Polygonaceae) Spreng and *S. globulifera* Linn. f. (Clusiaceae) and compounds which can serve as lead for the development of new drugs against leishmaniasis and bacterial diseases.

The chemical investigation of the active extracts, fractions led to the isolation of thirty-two (32) compounds characterized using usual spectroscopic techniques (IR, HRESI mass spectrometry, 1D and 2D NMR). Four of the compounds isolated from *S. globulifera* and named guttiferone U (**112**), guttiferone V (**113**), guttiferone W (**114**) and globuliferanol (**116**) are new derivatives. From *R. nepalensis,* one new derivative named berquaertiide (**111**), and two others 5-Hydroxy-7-methoxy-1(3*H*)-isobenzofuranone (**137**) and 3-hydroxy-*γ*-butyrolactone (**138**) are isolated for the first time from natural source were also reported. The twenty five remaining compounds were grouped into three classes of secondary metabolites including twenty-one phenolic derivatives, three steroids and one triterpenoid.

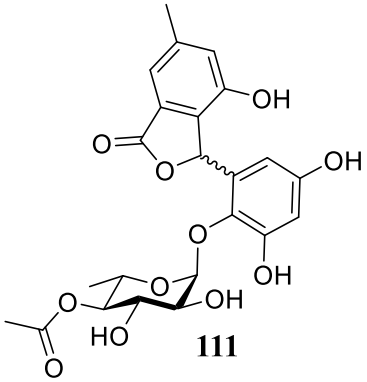

111

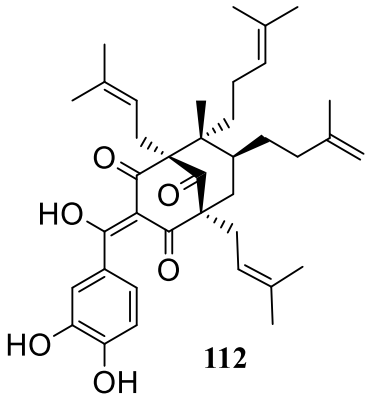

112

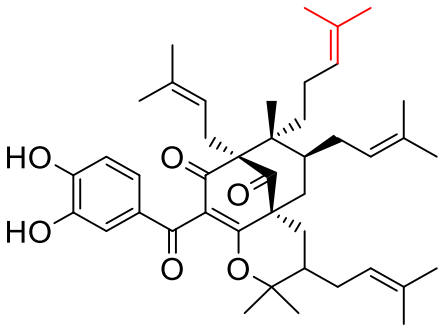

113

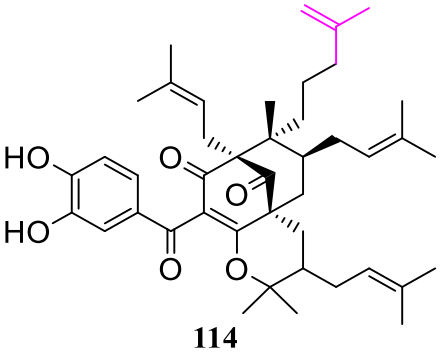

114

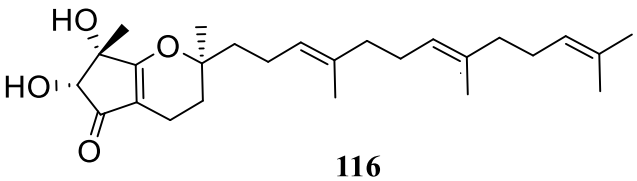

116

In addition to enriching the knowledge on the chemistry of these plants, this study represents a significant chemophenetic contribution to these species. It has provided further information about possible chemophenetic markers of these species and showed the presence of uncommon metabolites encountered in these species. Among the isolated compounds, the phenylisobenzofuranone derivative named berquaertiide (**111**) was found to be a new compound and two others 5-Hydroxy-7-methoxy-1(3*H*)-isobenzofuranone (**137**) and 3-hydroxy-γ-butyrolactone (**138**) are isolated for the first time from Polygonaceae family. These results support the uses of this plant in traditional medicine and confirm the antibacterial potential of anthraquinones known as biomarkers of the Polygonaceae family. Moreover, the study also confirmed the role of the hydroxy group on the activity of emodin, a secondary metabolite that could be a lead in the search of new antibacterial agents. The results obtained for the biological evaluation of isolated compounds support the use of *S. globulifera* in folk medicine.

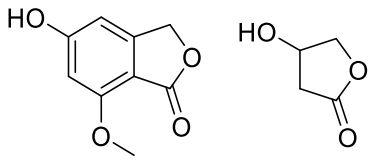

137 **138**

The results obtained show also the antileishmanial, the antibacterial and cytotoxicity potencies of some extracts, fractions and compounds.

The *n*-hexane fraction from the methanol extract of the stem bark of *S. globulifera*, which displayed good in vitro activity against *Leishmania donovani* NR-48822 promastigotes (IC50 43.11 μg.mL^{-1}) led to the isolation of Guttiferone K (**115**) which exhibited the best antileishmanial activity against the parasite with an IC_{50} value of 3.30 ± 0.51 μg.mL^{-1} but with weak selectivity toward Raw 264.7 macrophage cells (SI > 1.25). The EtOAc soluble fraction from the CH_2Cl_2-MeOH (1:1) extract of roots of *R. nepalensis* displayed a significant activity against seven bacterial strains with MICs (31.2–3.9 μg.mL^{-1}). The purification of this fraction yielded emodin (**117**) which was the most active against all the tested strains (15.7 to 1.9 μg.mL^{-1}).

In addition, seven analogues (6-allyloxyemodin (**143**), 6,8-diallyloxyemodin (**144**), 1,6-diallyloxyemodin (**145**), 1,6,8-triallyloxyemodin (**146**), 1,6,8-triacetylemodin (**147**), 1,6,8-trihydroxy-3-methyl-2,4,5,7-tetranitro anthraquinone (**148**) and 5-amino-1,6,8-trihydroxy-3-methyl-2,4,7-trinitro anthraquinone (**149**)) of compound **2** were prepared and further assessed

for their antibacterial activity. Compounds 1,6,8-trihydroxy-3-methyl-2,4,5,7-tetranitro anthraquinone (**148**) and 5-amino-1,6,8-trihydroxy-3-methyl-2,4,7-trinitro anthraquinone (**149**) were most active than emodin (**117**) against *Salmonella enterica* and *Klebsiella pneumoniae* with MIC (125 and 15.6 μg.mL^{-1}, respectively). These leading us to conclude that all hydroxy groups are essential for antibacterial activity of emodin, The methyl group is crucial for antibacterial activity and The amino and nitro groups at position C4 enhance antibacterial activity (strains SE NR1355; KP NR41388).

These results show that *S. globulifera* and *R. nepalensis* could be sources of leishmaniacidal and bactericidal agents and contribute to the valorisation of the Cameroonian biodiversity.

In our future work, we intend to:

- synthesize the active molecules;
- do the networking on *Symphonia* for the isolation of benzophenones only, as they have shown good antileishmanial and antibacterial activity.

PART III:

MATERIAL AND METHODS

III.1. APPARATUS AND PLANT MATERIALS

III.1.1. Apparatus

III.1.1.1. Evaporation, weighing and chromatographies

For this study, an OHAUS Pionneer type balance (precision 0.001) was used to weigh the isolated compounds. The crude extracts were freed from solvents using a HEIDOLPH brand rotary evaporator connected to a VACUUBRAND pump and a LAUDA chiller.

Test tubes of 500 mL, 100 mL, 10 mL of the respective brands Pobel, Dagra, Fortuna were used for the preparation of the different solvent systems.

The extracts were dissolved in distillated water and successively partitioned with *n*-hexane, EtOAc, and *n*-BuOH, while column chromatographies were carried out on 230–400 mesh silica gel (Merck, Darmstadt, Germany), 70–230 mesh silica gel (Merck, Darmstadt, Germany) and Sephadex LH-20 (Sigma-Aldrich, Munich, Germany). MPLC (BÜCHI Reveleris X2 Flash Chromatography System) normal phase with pre-packed silica-gel columns as stationary was used for the purifications.

The dimensions of the pre-packed silica-gel columns were chosen based on the amount of extract to be separated. The different eluents used were adapted to the stationary phases depending on the polarity of the compounds to be separated or analyzed. Analytical thin layer chromatography (TLC) was performed on Merck pre-coated silica gel (60 F254) aluminium foil (Merck, 20 × 20 cm) 0.2 mm thick. The identification of compound spots on TLC plates was carried out by visualizing under a UV lamp of type Spectroline, model VL-4-LC, with wavelength 254 and 366 nm, then pulverizing with sulphuric acid diluted at 20%, and heating the plate in an oven at about 100°C. L-rhamnose (Sigma-Aldrich, Munich, Germany) and glucose was used for comparison of sugar moieties.

III.1.1.2. Mass spectra

High resolution mass spectra were obtained with a QTOF Compact Spectrometer (Bruker, Germany) equipped with a HRESI source. The spectrometer was operated in positive and negative modes (mass range: 50–1500, with a scan rate of 1.00 Hz) with automatic gain control to provide high-accuracy mass measurements within 0.4 ppm deviation using Na formate as calibrant. The following parameters were used for experiments: spray voltage of 4.5 kV, capillary temperature of 200°C. Nitrogen was used as sheath gas (4 L/min). The optical rotations were measured using a PerkinElmer polarimeter.

III.1.1.3. Nuclear Magnetic Resonance (NMR) spectra

The ^{1}H and ^{13}C NMR spectra were recorded on Bruker DRX 500 MHz and 600 MHz NMR spectrometers (Bruker Corporation, Brussels, Belgium) in deuterated solvents. Chemical shifts were reported in δ (ppm) using tetramethylsilane (TMS) (Sigma-Aldrich) as an internal standard, while coupling constants (J) were measured in Hz.

III.1.1.4. Optical rotation measurement and Infrared spectrum

The optical rotation were measured using a PerkinElmer polarimeter. Infrared (IR) spectra were recorded on Bruker Tensor 27 FTIR-spectrometer equipped with a diamond ATR.

III.1.2. Plant materials

The roots of *R. nepalensis* were harvested in May 2016 in Bamenda, Northwest Region of Cameroon, and identified at the Cameroon National Herbarium, Yaoundé, with voucher specimen number Nº 7665/SRFCam.

The stem bark of *S. globulifera* was harvested in May 2016 in Bangangte (West region of Cameroon) and identified by Mr. Nana Victor, a retired botanist at the National Herbarium of Cameroon, where a voucher specimen (29529 SRFK) was already available.

III.2. SOME CHARACTERISTIC TESTS USED IN THE IDENTIFICATION OF SECONDARY METABOLITES

III.2.1. Ferric chloride test

The purpose of this test is to identify phenolic compounds. The reagents used are ethanol and iron (III) chloride ($FeCl_3$).

Procedure: In 5 mL of ethanol contained in a test tube, a small amount of the compound was dissolved. Then a few drops of the ferric chloride ($FeCl_3$) solution were added to the solution obtained.

Results and interpretation: Gradually, the reaction medium turns to a greenish blue or purple color (transient or permanent) due to the formation of a complex of the type $[Fe\ (OAr)_6]^{3-}$, which indicates the presence of free phenolic hydroxy groups. The formation of this complex is done according to the following equation:

$$6\ Ar\text{-}OH + FeCl_3 \longrightarrow [Fe(Ar\text{-}O)_6]^{3-} + 3H^{+} + 3HCl$$

III.2.2. Shinoda test

The purpose of this test is to identify flavonoids. The reagents used are methanol, hydrochloric acid (HCl) and magnesium shaves (Mg).

Procedure: In 5 mL of methanol in a test tube, a small amount of the extract or compound was dissolved. To the resulting solution, a few drops of concentrated hydrochloric acid (HCl) and a few shaves of magnesium were added.

Results and Interpretation: The presence of flavonoids was confirmed by the appearance of a purple color.

III.2.3. Bornträger test

The purpose of this test is to identify quinones and anthraquinones. The reagents used are sodium hydroxide (NaOH) and methylene chloride (CH_2Cl_2).

Procedure: In 5 mL of methylene chloride contained in a test tube, a small amount of the compound was dissolved. Then 10% of an aqueous sodium hydroxide solution was added to the resulting solution.

Results and interpretation: A red coloration developed in the aqueous phase is characteristic of anthraquinones, while a pink or purple coloration occurs in the aqueous phase for benzoquinones.

III.2.4. Libermann-Burchard test

The purpose of this test is to identify triterpenoids and steroids. The reagents used are chloroform ($CHCl_3$), acetic anhydride [$(CH_3CO)_2O$] and concentrated sulfuric acid (H_2SO_4).

Procedure: The dry residue was dissolved in 3 mL of chloroform. After having stirred it, the mixture were filtered and then distributed into 2 test tubes, the first of which serves as a control. Two drops of acetic anhydride were added to the second tube. The mixture was slightly stirred, then a few drops of 36 N H_2SO_4 wass added to it.

Results and interpretation: The presence of terpenoids is indicated by a purplish red stain, while that of steroids are confirmed by a bluish green stain.

III.3. EXTRACTION, FRACTIONATION, ISOLATION AND PURIFICATION OF COMPOUNDS

III.3.1. Extraction

III.3.1.1. Preparation of *R. nepalensis* crude extract

The air-dried root of *R. berquaertii* (8.5 kg) was powdered and macerated three times at room temperature (26 °C) with 30 L of CH_2Cl_2−MeOH (1:1, v/v) for 48 h. The solvent was removed under vacuum to yield the root crude extract (500.7 g).

III.3.1.2. Preparation of *S. globulifera* crude extract

The stem bark of *S. globulifera* was chopped, air-dried, and then ground to give 10.3 kg of powder, which was extracted by maceration using methanol for 48 h, three times each. The extract was freed from the solvent using a rotavapor to yield 638.7 g of MeOH extract.

III.3.2. Fractionnation of crude extracts and isolation of compounds

III.3.2.1. Fractionnation of crude extract and isolation of compounds from *R. nepalensis*

Part of the extract (490.1 g) was suspended in water and successively partitioned with *n*-hexane, EtOAc, and *n*-BuOH to provide 20.5 g, 130.1 g, and 110.5 g of each fraction, respectively. Part of the EtOAc soluble fraction (125 g), which was the most active fraction was subjected to silica gel column chromatography (CC), eluted with a gradient of EtOAc in CH_2Cl_2 followed by a gradient of MeOH in EtOAc to afford four main sub-fractions F1–F4. The purification of these sub-fractions over silica gel, sephadex LH-20 and MPLC (BÜCHI Reveleris X2 Flash Chromatography System) normal phase with pre-packed silica-gel columns twenty compounds.

III.3.2.1.1. Study of the sub-fraction F1

The sub-fraction F1 (35.7 g) was subjected to CC over silica gel and eluted successively with mixtures of CH_2Cl_2−EtOAc, (1:0, v/v) and (9:1, v/v), respectively to afford compounds **RBR1a** (**119**) (50.5 mg; CH_2Cl_2−EtOAc, 1:0, v/v), **RBR2** (**118**) (25.5 mg; CH_2Cl_2−EtOAc, 1:0, v/v), **RBR3C** (**2**) (3.1 mg; CH_2Cl_2−EtOAc, 1:0, v/v), **RBR5** (**140**) (5.2 mg; CH_2Cl_2−EtOAc, 9:1, v/v) and **RBR4** (**141**) (10.0 mg; CH_2Cl_2−EtOAc, 9:1, v/v).

III.3.2.1.2. Study of the sub-fraction F2

F2 (17.5 g) was subjected to CC over silica gel with mixtures of CH_2Cl_2−EtOAc, (9:1 to 17:3, v/v). The fractions collected were grouped according to their TLC profiles into three main sub-fractions coded F2a-F2c. F2a (2.1 g) was subjected to MPLC using normal phase pre-packed silica gel columns as stationary phase with CH_2Cl_2−EtOAc (1:1, v/v) to afford compounds **RBR6b** (**120**) (5.2 mg; CH_2Cl_2−EtOAc, 1:0, v/v) and **RBR15** (**124**) (5.2 mg;

CH_2Cl_2−EtOAc, 1:0, v/v). The purification of F2b (3.7 g) by CC over Sephadex LH-20 and eluted with methanol led to the isolation of **RBR10R1** (**5**) (5.4 mg) and **RBR9a** (**128**) (5.1 mg). F2c (1.8 g) was purified using MPLC equipped with normal phase pre-packed silica gel columns as stationary phase and eluted with the mixture of CH_2Cl_2−EtOAc (17:3, v/v) to afford **RBR9N2** (**138**) (5.4 mg; CH_2Cl_2−EtOAc, 17:3, v/v) and **RBR9N1** (**137**+**138**) (5.1 mg; CH_2Cl_2−EtOAc, 17:3, v/v).

III.3.2.1.3. Study of the sub-fraction F3

The CC of F3 (20.4 g) over silica gel using mixtures of CH_2Cl_2−EtOAc (17:3 to 1:1, v/v) of increasing polarities followed by MPLC using normal phase pre-packed silica-gel columns as stationary phase and a CH_2Cl_2−EtOAc gradient solvent system (3:1 to 1:1, v/v) yielded compounds **RBR7a2** (**121**) (5.5 mg; CH_2Cl_2−EtOAc, 3:1, v/v), **RBR17** (**130**) (15.4 mg; CH_2Cl_2−EtOAc, 1:1, v/v) and **RBR147-19** (**123**) (8.2 mg; CH_2Cl_2-EtOAc 1:1, v/v).

III.3.2.1.4. Study of the sub-fraction F4

Finally, F4 (31.3 g) was equally subjected to CC over silica gel using mixtures of CH_2Cl_2-EtOAc (1:1, v/v) to (CH_2Cl_2−EtOAc, 4:1, v/v) to afford four subfractions F4a-F4d. F4a (3.7 g) was chromatographed over MPLC using normal phase pre-packed silica gel columns as stationary phase with CH_2Cl_2−MeOH (CH_2Cl_2−MeOH, 7:3 to 1:1, v/v) solvent systems of increasing polarities to yield **RBR48-1** (**111**) (15.5 mg; CH_2Cl_2−MeOH, 1:1, v/v). The purification of F4b (1.5 g) and F4d on CC over Sephadex LH-20 (2.7 g) using methanol as eluent afforded the mixture **RBR95-23a/b** (**126+127**) (8.5 mg) and **RBR64** (**129**) (5.4 mg), respectively. F4c (5.2 g) was subjected to MPLC using normal phase pre-packed silica-gel columns as stationary phase and eluted with CH_2Cl_2−EtOAc (19:1 to 1:1, v/v) to yield **RBR95-35b** (**13**) (7.3 mg; CH_2Cl_2−EtOAc, 1:1, v/v) and **RBR87-56D** (**142**) (30.4 mg; CH_2Cl_2−EtOAc, 1:1, v/v). F4d was not studied because of its complexity.

III.3.2.2. Fractionnation of crude extract and isolation of compounds from *S. globulifera*

Part of the extract (628.2 g) was dissolved in water and successively partitioned with *n*-hexane, EtOAc, and *n*-BuOH. After removal of solvent under reduced pressure, 146.8 g of *n*-hexane, 76.2 g of EtOAc, and 42.3 g of *n*-BuOH fractions were obtained. A part of the soluble *n*-hexane fraction of *S. globulifera* (140.1 g), which was the most active fraction, was subjected to CC over a silica gel using a mixture of *n*-hexane-EtOAc solvent systems of increasing polarities. Ninety-eight (98) sub-fractions were obtained and combined based on their TLC profiles into five sub-fractions labeled F1 (34.8 g; *n*-hexane/EtOAc, 19:1–4:1, v/v), F2 (30.2 g;

n-hexane/EtOAc, 9:1–3:1, v/v), F3 (25.2 g; *n*-hexane/EtOAc, 4:1–3:2, v/v), F4 (15.7 g; *n*-hexane/EtOAc, 3:2–1:1, v/v) and F5 (15.6 g; *n*-hexane/EtOAc, 1:1–0:1, v/v). The purification of these fractions over silica gel, sephadex LH-20 and MPLC (BÜCHI Reveleris X2 Flash Chromatography System) normal phase with pre-packed silica-gel columns led to the isolation of fifteen compounds.

Table 52: Chromatogram of the *n*-hexane fraction

Fractions	Elution systems	Observation
1–25 (F1, 34.8 g)	*n*-hexane/EtOAc (19:1–4:1, v/v)	Mixture of at least five compounds including **SYE22-22** and **SYEF12b**
26–46 (F2, 30.2 g)	*n*-hexane/EtOAc (9:1–3:1, v/v)	Complex mixture of at least twelve compounds including **SYE26-28-16Ma/b**, **SYE25-6M**, **SYE137**, **SYE171**, **SYEF26-48D**, **SYE26-8M** and **SYEF23**
47–64 (F3, 25.2 g)	*n*-hexane/EtOAc (4:1–3:2, v/v)	Mixture of at least five compounds including **SYE44-4-5mi** and **SYEF1310b**
65–84 (F4, 15.7 g)	*n*-hexane/EtOAc (3:2–1:1, v/v)	Oily mixture of at least nine compounds including **SYE70-45-48**
85–98 (F5, 15.6 g)	*n*-hexane/EtOAc (1:1–0:1, v/v)	Mixture of at least four compounds including **SYE85-38-39**

The purification of fraction F1 (34.8 g) over silica gel CC using mixtures of *n*-hexane/EtOAc (19:1–4:1, v/v) gave compounds **SYE22-22** (**139**) (5.5 mg; *n*-hexane/EtOAc, 4:1, v/v) and **SYEF12b** (**140+141**) (5.8 mg; *n*-hexane/EtOAc, 4:1, v/v).

The purification of fraction F2 (30.2 g) over Sephadex LH-20 CC eluting with MeOH followed by MPLC using normal phase pre-packed silica-gel columns as the stationary phase with the *n*-hexane/EtOAc (9:1–3:2, v/v) gradient solvent system and a second purification by repeated Sephadex LH-20 CC yielded **SYE26-28-16Ma/b** (**113+114**) (10.5 mg; *n*-hexane/EtOAc, 3:2, v/v), **SYE25-6M** (**112**) (5.2 mg; *n*-hexane/EtOAc, 3:2, v/v), **SYE137** (**131**) (15.0 mg; *n*-hexane/EtOAc, 3:2, v/v), **SYE171** (**132**) (5.6 mg; *n*-hexane/EtOAc, 3:2, v/v), **SYEF26-48D** (**135**) (6.3 mg; *n*-hexane/EtOAc, 3:2, v/v), **SYE26-8M** (**133**) (5.3 mg; *n*-hexane/EtOAc, 3:2, v/v) and **SYEF23** (**136**) (5.1 mg; *n*-hexane/EtOAc, 3:2, v/v).

F3 (25.2 g) was subjected to CC over Sephadex LH-20, eluting with MeOH, followed by MPLC using normal phase pre-packed silica-gel columns as the stationary phase with the

mixture of *n*-hexane/EtOAc (9:1–3:2, v/v) gradient solvent systems and purified a second time by repeated CC over Sephadex LH-20 to afford compounds **SYE44-4-5mi** (**115**) (20.5 mg; *n*-hexane/EtOAc, 3:2, v/v) and **SYEF1310b** (**134**) (5.0 mg; *n*-hexane/EtOAc, 3:2, v/v).

The CC of sub-fraction F4 (15.7 g) over Sephadex LH-20 eluting with MeOH followed by MPLC using normal phase pre-packed silica-gel columns as the stationary phase with *n*-hexane/EtOAc (7:3–1:1, v/v) gradient solvent system afforded compound **SYE70-45-48** (**116**) (10.4 mg; *n*-hexane/EtOAc, 1:1, v/v).

The CC of sub-fraction F5 (15.6 g) over silica gel using mixtures of *n*-hexane/EtOAc (1:1–0:1, v/v) gave compound **SYE85-38-39** (**142**) (7.4 mg; *n*-hexane/EtOAc, 1:1, v/v).

III.4. EVALUATION OF BIOLOGICAL ACTIVITIES

III.4.1. Antileishmanial assay

The cryopreserved promastigote form of *Leishmania donovani* 1S (MHOM/SD/62/1S) was obtained from Bei Resources and was routinely maintained at the Antimicrobial and Biocontrol Agents Unit, University of Yaoundé 1, in M199 medium supplemented with 10% Heat-Inactivated Fetal Bovine Serum (HIFBS) (Sigma) with 100 IU/mL penicillin and 100 µg/mL streptomycin. The culture was maintained in 75 cm^2 cell culture flask at 28°C (Khanjani *et al*., 2015) and checked for growth daily and sub-cultured everyday 72 h.

The antileishmanial effect of *R. berquaertii* and *S. globulifera* crude extracts, some fractions and some of the isolated compounds on cultured *L. donovani* 1S (MHOM/SD/62/1S) promastigotes was evaluated using the resazurin colorimetric method as described by Siqueira-Neto *et al*. (2010) with little modifications. For this purpose, 4.10^5 promastigotes/mL/well were seeded in a 96 wells microtiter plate and treated with different concentrations of extracts, fractions and isolated compounds for 72 h at 28°C. The viability rate of promastigotes had a direct relationship with the amount of pink resorufin that was produced through the reduction of blue resazurin by the dehydrogenase enzyme in the inner mitochondrial membrane of the living parasites. Briefly, the promastigotes from a logarithmic phase culture (4.10^5 cells/mL; 90 μL) were seeded in 96 wells microtiter plate and were treated with 10 μL of inhibitors at different concentrations. They were all assessed in triplicate at final concentrations of 100–0.16 μg/mL for extracts/fractions and 50–0.08 μg/mL for compounds and test plates were incubated for 28 h at 28°C, followed by the addition of 1 mg/mL resazurin. The negative and positive controls were 0.1% DMSO and amphotericin B (10–0.016 μg/mL). After an additional

incubation for 44 h, plates were then read on a Magelan Infinite M200 fluorescence multi-well plate reader (Tecan) at an excitation and emission wave lengths of 530 and 590 nm.

III.4.2. Antibacterial assay

Antibacterial activity assay was conducted on a total of eleven bacterial strains, including four clinical isolates including *S. typhi* CPC (S1), *E. coli* (clinical isolate) (S5), *K. pneumoniae* (clinical isolate) (S10) and *E. cloacae* (clinical isolate) (S11) and seven reference strains namely *S. enterica* NR13555 (S2), *E. coli* ATCC25322 (S3), *E. coli* ATCC35218 (S4), *S. aureus* ATCC43300 (S6), *S. aureus* ATCC25923 (S7), *P. aeruginosa* HM801 (S8), *K. pneumoniae* NR41388 (S9).

The bacterial strains were maintained on agar slant at 4℃ and subcultured on a fresh appropriate agar plate 24 h prior to any antibacterial test. The minimal inhibitory concentration (MIC) of extracts and compounds were assessed using the broth microdilution method as described by Eloff (1998), with slight modifications. The assays were performed in triplicates and reproduced twice. Each test sample was dissolved in DMSO to give a stock solution. In all wells of a 96 wells microplate, 100 μL of sterile culture broth (MHB) were introduced. Then, 100 μL of each mother solution (2000 μg/mL) was added to the first well, and then distributed to all other wells according to a geometric progression of reason 2, with final concentrations varying from 500 to 3.9 μg/mL and from 50 to 0.15 μg/mL for ciprofloxacin (reference antibiotic) used as positive control. Then, 100 μL of the liquid culture medium (MHB) inoculated with the test germ (2.10^6 CFU/mL) were introduced into the wells to obtain a final concentration of 10^6 CFU/mL. The negative controls consisted of wells containing only the culture medium on the one hand and wells containing a mixture of culture broth and germ on the other hand. The microtiter plates were covered and incubated at 37℃ for 18 h. After incubation, 20 μL of resazurin were then introduced into all wells and the microplates were incubated again at 37℃ for 30 min (Mativandlela *et al*., 2006). The colour shift from blue to pink indicated the presence of viable cells. The MIC was the lowest concentration of the extract that did not permit any visible growth compared to the control wells.

III.4.3. Cytotoxicity assay

The cytotoxicity profile of the crude extract, fractions and compounds was assessed using the Alamar blue assay (Mosman, 1983) against Raw 264.7 cells duly cultivated in complete Dulbecco's Modified Eagle's Medium (DMEM) containing 13.5 g/L DMEM (Sigma Aldrich), 10% Fetal Bovine Serum (Sigma Aldrich), 0.2% sodium bicarbonate (w/v) (Sigma

Aldrich) and 50 μg/mL gentamycin (Sigma Aldrich). Globally, macrophages were seeded into 96-wells cell-culture flat-bottomed plates at a density of 104 cells in 100 μL of complete medium/well and incubated for 24 h at 37°C, 5% CO_2 to allow cell adhesion. 10 μL of each serially diluted test sample solutions were added and assay plates were then incubated for 48 h in same experimental conditions. Growth control (0.1% DMSO-100% growth) and positive control wells (Podophyllotoxin at 20 μM) were included in the experiment plates. Cell proliferation was checked by adding 10 μL of a stock solution of resazurin (0.15 mg/mL in sterile PBS) to each well followed by plates incubation during 4 h. Fluorescence was then read on a Tecan Infinite M200 fluorescence multi-well plate reader (Tecan) at an excitation/emission of 530/590 nm. Results were expressed as 50% cytotoxic concentration (CC_{50}) and selectivity indices (SI) (CC_{50} Mammalian cell/IC_{50} *Leishmania donovani*) were calculated for each tested substance.

The data were subjected to one-way analysis of variance (ANOVA) and results were presented as means ± SD of the replicated values. Significant differences for multiple comparisons were determined by Waller Duncan post-Hoc test at $p \leq 0.05$ using the Statistical Package for the Social Sciences (SPSS, version 16.0) program.

III.5. PHYSICAL AND CHEMICAL CHARACTERISTICS OF THE ISOLATED COMPOUNDS

Berquaertiide

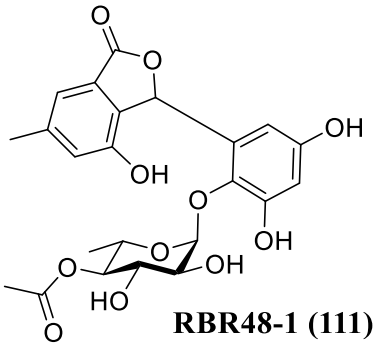

RBR48-1 (111)

Molecular formula:	$C_{23}H_{24}O_{11}$
HRESI: $[M+Na]^+$	*m/z* 499.1205
Optical rotatory power	$[\alpha]_{589}^{20}$ +6.1
IR: OH	3264-3733 cm^{-1}
C=O ester conjugated	1733 cm^{-1}
Aromatic ring	1615 cm^{-1}
Physical aspect:	Brown oil
^{1}H RMN (DMSO-d_6, 600 MHz):	Table 19
^{13}C RMN (DMSO-d_6,150 MHz):	Table 19

Guttiferone U

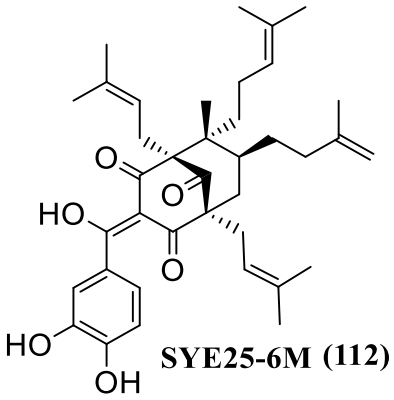

SYE25-6M (112)

Molecular formula:	$C_{38}H_{50}O_6$
HRESI: $[M+Na]^+$	*m/z* 625.3494
Optical rotatory power	$[\alpha]_{589}^{20}$ +93
IR: OH	3735 cm^{-1}
Vinyl	2974 cm^{-1}
C=O ketone conjugated	1725 cm^{-1}
Aromatic ring	1646 cm^{-1}
Physical aspect:	Yellowisch finely divided solid
^{1}H RMN (acetone-d_6, 600 MHz):	Table 20
^{13}C RMN (acetone-d_6,150 MHz):	Table 20

Guttiferone V

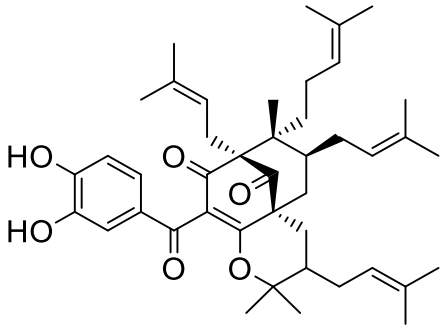

SYE27-28-16Ma (113)

Guttiferone W

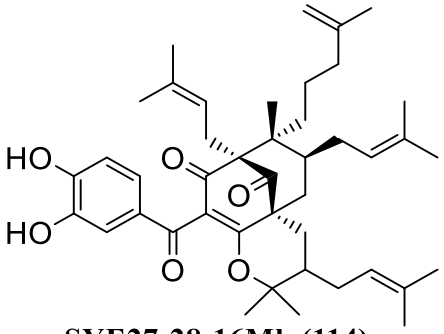

SYE27-28-16Mb (114)

Molecular formula:	$C_{38}H_{50}O_6$
HRESI: $[M+Na]^+$	*m/z* 693.4141
Optical rotatory power	$[\alpha]_{589}^{20}$ +93
IR: OH	3300 cm^{-1}
C=O ketone non-conjugated	1729 cm^{-1}
C=O ketone conjugated	1669 cm^{-1}
Aromatic ring	1699 cm^{-1}
Physical aspect:	Yellowisch finely divided solid
^{1}H RMN (acetone-d_6, 600 MHz):	Table 21
^{13}C RMN (acetone-d_6,150 MHz):	Table 21

Guttiferone K

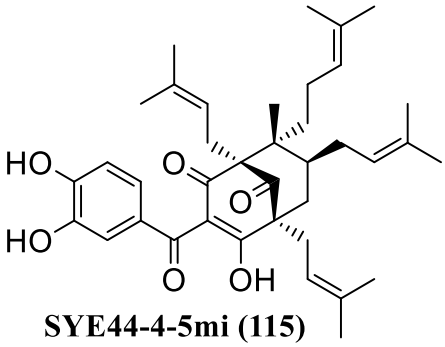

SYE44-4-5mi (115)

Molecular formula:	$C_{38}H_{50}O_6$
ESI: $[M+Na]^+$	*m/z* 603.4
Physical aspect:	Yellowisch finely divided solid
^{1}H RMN (acetone-d_6, 600 MHz):	Table 22
^{13}C RMN (acetone-d_6,150 MHz):	Table 22

Globuliferanol

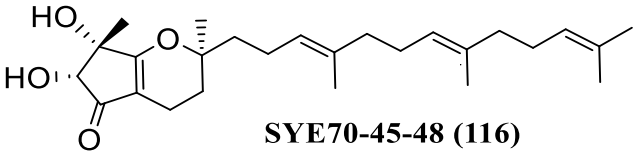

SYE70-45-48 (116)

Molecular formula:	$C_{26}H_{40}O_4$
HRESI: $[M+Na]^+$	*m/z* 439.2816
Optical rotatory power	$[\alpha]_{589}^{20}$ +21.5
IR: OH	3364 cm^{-1}
C=O ketone conjugated	1685 cm^{-1}
Aromatic ring	1620 cm^{-1}
Physical aspect:	Brown oil
^{1}H RMN (DMSO-d_6, 600 MHz):	Table 23
^{13}C RMN (DMSO-d_6, 150 MHz):	Table 23

Emodin

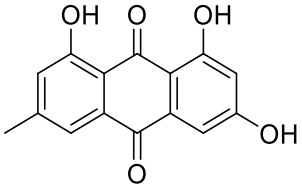

RBR3C (117)

Molecular formula:	$C_{15}H_{10}O_5$
ESI: $[M-2H]^-$	*m/z* 268.8
Physical aspect:	Red finely divided solid
^{1}H RMN (DMSO-d_6, 600 MHz):	Table 24
^{13}C RMN (DMSO-d_6, 150 MHz):	Table 24

Physcion

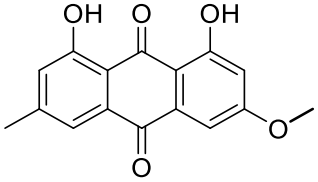

RBR2 (118)

Molecular formula:	$C_{15}H_{10}O_6$
ESI: $[M-2H]^-$	*m/z* 282.9
Physical aspect:	Yellow powder
^{1}H RMN (DMSO-d_6, 600 MHz):	Table 25
^{13}C RMN (DMSO-d_6, 150 MHz):	Table 25

Chrisophanol

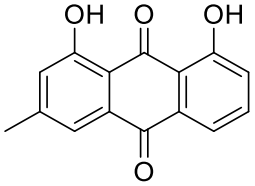

RBR1a (119)

Molecular formula:	$C_{15}H_{10}O_4$
ESI: $[M-H]^-$	*m/z* 253.0
Physical aspect:	Light yellow amorphous powder
^{1}H RMN (DMSO-d_6, 600 MHz):	Table 26
^{13}C RMN (DMSO-d_6, 150 MHz):	Table 26

Citreorosein

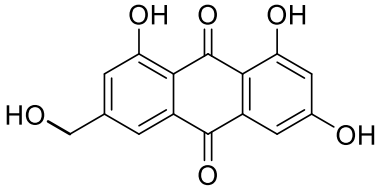

RBR6b (120)

Molecular formula:	$C_{16}H_{12}O_5$
ESI: $[M-2H]^-$	*m/z* 284.8
Physical aspect:	Yellow powder
^{1}H RMN (DMSO-d_6, 600 MHz):	Table 27
^{13}C RMN (DMSO-d_6, 150 MHz):	Table 27

Questinol

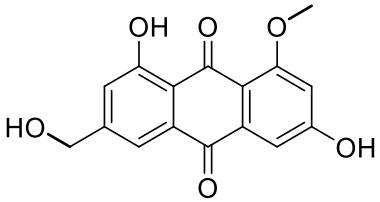

RBR7a2 (121)

Molecular formula:	$C_{16}H_{12}O_6$
HRESI: $[M-2H]^-$	*m/z* 299.0559
Physical aspect:	Light yellow amorphous powderin
^{1}H RMN (DMSO-d_6, 600 MHz):	Table 28
^{13}C RMN (DMSO-d_6, 150 MHz):	Table 28

Questin

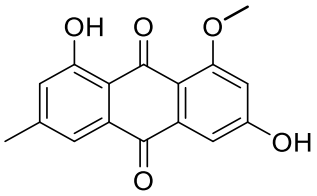

RBR10R1 (122)

Molecular formula:	$C_{16}H_{12}O_5$
HRESI: $[M-H]^-$	*m/z* 283.0608
Physical aspect:	Yellow needles
^{1}H RMN (DMSO-d_6, 600 MHz):	Table 29
^{13}C RMN (DMSO-d_6, 150 MHz):	Table 29

Emodic acid

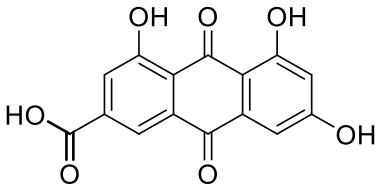

RBR147-19 (123)

Molecular formula:	$C_{15}H_8O_7$
HRESI: $[M-2H]^-$	*m/z* 299.0198
Physical aspect:	Yellow finely divided solid
^{1}H RMN (DMSO-d_6, 600 MHz):	Table 30
^{13}C RMN (DMSO-d_6, 150 MHz):	Table 30

1,3,6-Trihydroxy-8-methyl-anthraquinone

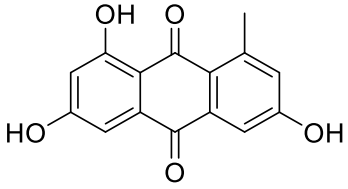

RBR15 (124)

Molecular formula:	$C_{15}H_{10}O_5$
ESI: $[M-2H]^-$	*m/z* 268.818
Physical aspect:	Yellow needles
^{1}H RMN (DMSO-d_6, 600 MHz):	Table 31
^{13}C RMN (DMSO-d_6, 150 MHz):	Table 31

Emodin-6-*O*-*β*-D-glucopyranoside

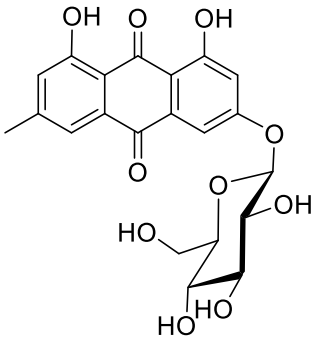

RBR95-35b (125)

Molecular formula:	$C_{21}H_{20}O_{10}$
ESI: $[M-2H]^-$	*m/z* 430.923
Physical aspect:	Yellow finely divided solid
^{1}H RMN (DMSO-d_6, 600 MHz):	Table 32
^{13}C RMN (DMSO-d_6, 150 MHz):	Table 32

Physcionin

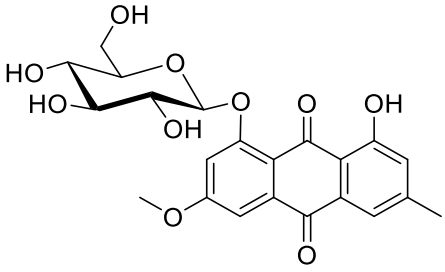

RBR95-23a (126)

Molecular formula:	$C_{22}H_{22}O_{10}$
Physical aspect:	Yellow finely divided solid
^{1}H RMN (DMSO-d_6, 600 MHz):	Table 33
^{13}C RMN (DMSO-d_6, 150 MHz):	Table 33

Chrysophanein

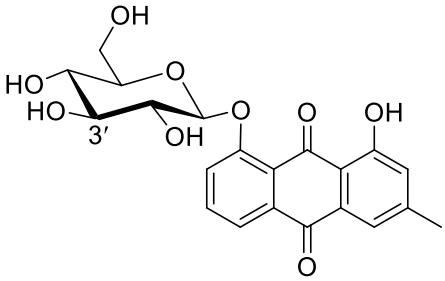

RBR95-23b (127)

Molecular formula:	$C_{21}H_{20}O_9$
ESI: $[M+Na]^+$	*m/z* 439.1
Physical aspect:	Yellow finely divided solid
^{1}H RMN (DMSO-d_6, 600 MHz):	Table 33
^{13}C RMN (DMSO-d_6, 150 MHz):	Table 33

Emodin bianthrone

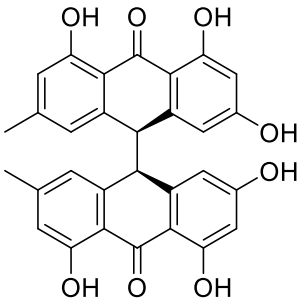

RBR9a (128)

Molecular formula:	$C_{30}H_{22}O_8$
ESI: $[M+H]^+$	*m/z* 511.287
Physical aspect:	Brown oil
^{1}H RMN (DMSO-d_6, 600 MHz):	Table 34
^{13}C RMN (DMSO-d_6, 150 MHz):	Table 34

Epicatechin 3-*O*-gallate

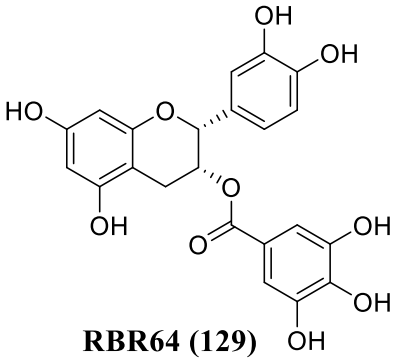

RBR64 (129)

Molecular formula:	$C_{22}H_{18}O_{10}$
ESI: $[M+Na]^+$	*m/z* 465.1
Physical aspect:	Yellow white oil
^{1}H RMN (DMSO-d_6, 600 MHz):	Table 35
^{13}C RMN (DMSO-d_6, 150 MHz):	Table 35

Epicatechin 3-(6''-*O*-methyl) gallate

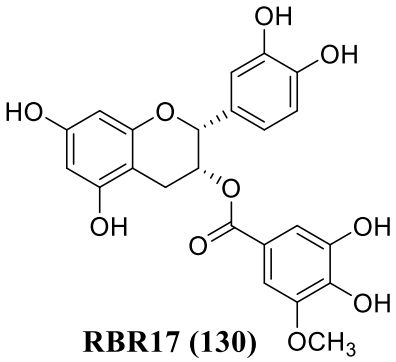

RBR17 (130)

Molecular formula:	$C_{23}H_{20}O_{10}$
ESI: $[M+Na]^+$	*m/z* 479.1
Physical aspect:	Colorless amorphous
^{1}H RMN (DMSO-d_6, 600 MHz):	Table 36
^{13}C RMN (DMSO-d_6, 150 MHz):	Table 36

Gaboxanthone

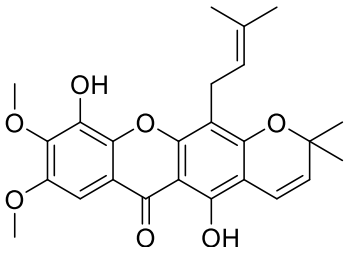

SYE137 (131)

Molecular formula:	$C_{25}H_{26}O_7$
ESI: $[M+K]^+$	*m/z* 477.43
Physical aspect:	Yellow finely divided solid
^{1}H RMN (DMSO-d_6, 500 MHz):	Table 37
^{13}C RMN (DMSO-d_6, 125 MHz):	Table 37

Xanthone V2

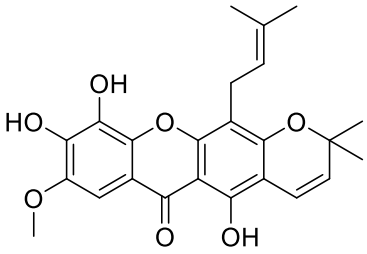

SYE171 (132)

Molecular formula:	$C_{24}H_{24}O_7$
HRESI: $[M+K]^+$	*m/z* 463.4534
Physical aspect:	Yellow finely divided solid
^{1}H RMN (DMSO-d_6, 500 MHz):	Table 38
^{13}C RMN (DMSO-d_6, 125 MHz):	Table 38

Symphonin

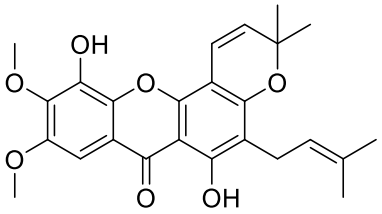

SYE26-8M (133)

Molecular formula:	$C_{25}H_{26}O_7$
HRESI: $[M+Na]^+$	*m/z* 461.1480
Physical aspect:	Yellow finely divided solid
^{1}H RMN (DMSO-d_6, 500 MHz):	Table 39
^{13}C RMN (DMSO-d_6, 125 MHz):	Table 39

1,5-Dihydroxy-3-methoxyxanthone

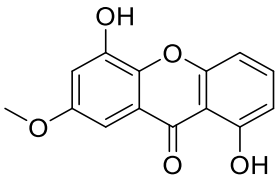

SYE1310b (134)

Molecular formula:	$C_{14}H_{10}O_5$
ESI: $[M+Na]^+$	*m/z* 281.0
Physical aspect:	Yellow finely divided solid
^{1}H RMN (acetone-d_6, 600 MHz):	Table 40
^{13}C RMN (acetone-d_6, 150 MHz):	Table 40

Pyranojacareubin

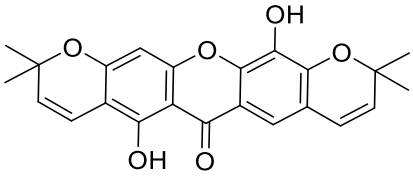

SYE26-48D (135)

Molecular formula:	$C_{23}H_{20}O_6$
ESI: $[M+Na]^+$	*m/z* 415.2
Physical aspect:	Yellow finely divided solid
^{1}H RMN (DMSO-d_6, 500 MHz):	Table 41
^{13}C RMN (DMSO-d_6, 125 MHz):	Table 41

Kaempferol

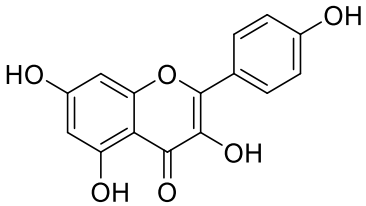

SYE23 (136)

Molecular formula:	$C_{15}H_{10}O_6$
ESI: $[M-2H]^-$	*m/z* 284.894
Physical aspect:	Yellow finely divided solid
^{1}H RMN (acetone-d_6, 600 MHz):	Table 42
^{13}C RMN (acetone-d_6, 150 MHz):	Table 42

5-Hydroxy-7-methoxy-1(3*H*)-isobenzofuranone

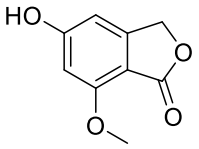

RBR9N1 (137)

Molecular formula:	$C_9H_8O_4$
ESI: $[M-2H]^-$	*m/z* 178.8
Physical aspect:	Bright shiny needle
^{1}H RMN (DMSO-d_6, 600 MHz):	Table 43
^{13}C RMN (DMSO-d_6, 150 MHz):	Table 43

3-Hydroxy-*γ*-butyrolactone

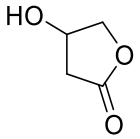

RBR9N2 (138)

Molecular formula:	$C_4H_6O_3$
ESI: $[M-2H]^-$	*m/z* 124.9
Physical aspect:	Yellowish oil
^{1}H RMN (DMSO-d_6, 600 MHz):	Table 44
^{13}C RMN (DMSO-d_6, 150 MHz):	Table 44

Lupeol

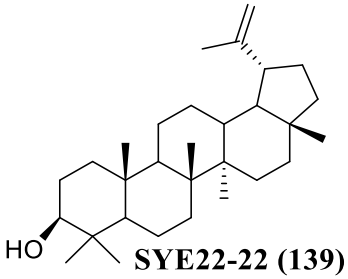

SYE22-22 (139)

Molecular formula:	$C_{30}H_{50}O$
Physical aspect:	Finely divided solid

β-Sitosterol

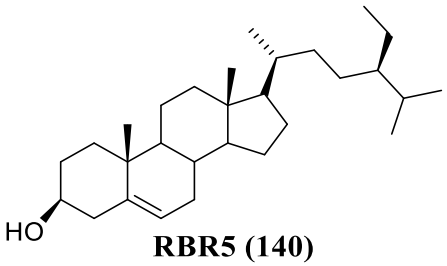

RBR5 (140)

Molecular formula:	$C_{29}H_{50}O$
Physical aspect:	White powder

Stigmasterol

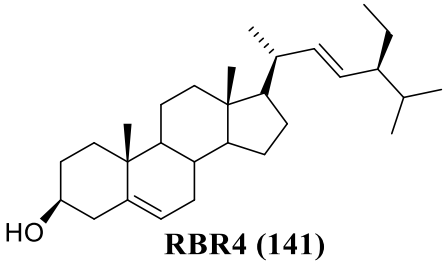

RBR4 (141)

Molecular formula:	$C_{29}H_{48}O$
Physical aspect:	White powder

β-sitosterol-3-*O*-*β*-D-glucopyranoside

Molecular formula: $C_{35}H_{60}O_6$
Physical aspect: White powder

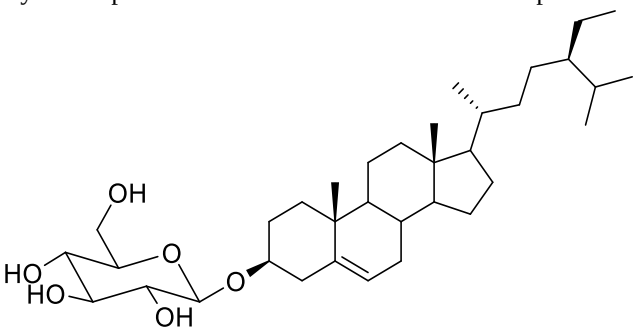

RBR86-57D (142)

REFERENCES

- Abbasi, A. M., Shah, M. H., Khan, M. A. (2015). *Wild edible vegetables of lesser Himalayas*. Switzerland: Springer International Publishing.
- Abdel-Aal, E. S. M., Young, J. C., Rabalski, I., Hucl, P., Fregeau-Reid, J. (2007). Identification and quantification of seed carotenoids in selected wheat species. *Journal of Agricultural and Food Chemistry*, *55*(3), 787-794.
- Abdul-Salim, K. (2002). *Systematics and biology of Symphonia* L. f. (Clusiaceae). Harvard University, USA, 132–137.
- Adam, P., Arigoni, D., Bacher, A., Eisenreich, W. (2002). Biosynthesis of Hyperforin in *Hypericum perforatum*. *Journal of Medicinal Chemistry*, *45*(21), 4786–4793.
- Agati, G., Azzarello, E., Pollastri, S., Tattini, M. (2012). Flavonoids as antioxidants in plants: location and functional significance. *Plant science*, *196*, 67–76.
- Agrawal PK. 1992. NMR spectroscopy in the structural elucidation of oligosaccharides and glycosides. *Phytochemistry*, *31*(10), 3307–3330.
- Akendengue, B., Louis, A. M. (1994). Medicinal plants used by the Masango people in Gabon. *Journal of ethnopharmacology*, *41*(3), 193–200.
- Akhoundi, M., Kuhls, K., Cannet, A., Votýpka, J., Marty, P., Delaunay, P., Sereno, D. (2016). A historical overview of the classification, evolution, and dispersion of Leishmania parasites and sandflies. *PLoS Neglected Tropical Diseases*, *10*(3), 366–402.
- Al Easa, H. S., Rizk, A. F. M., Hussiney, H. A. (1995). Constituents of Plants Growing in Qatar, Part XXVI: *Phytochemical investigation of Rumex vesicarius*, Qatar University Digital Hub, Qatar, 562–580.
- Alvar J., Vélez I. D., Bern C., Herrero M., Desjeux P., Cano J., Jannin J., Boer M. (2012). Leishmanisis and global estimates of its incidence. *Public Library of Science ONE* **7**, 1–12.
- Alvar, J., Yactayo, S., Bern, C. (2006). Leishmaniasis and poverty. *Trends in Parasitology*, *22*(12), 552–557.
- Alvi, K. A., Nair, B., Gallo, C., Baker, D. (1997). Screening of microbial extracts for tyrosine kinase inhibitors. *The Journal of Antibiotics*, *50*(3), 264–266.
- Andrade, T. M., Carvalho, E. M., Rocha, H. (1990). Bacterial infections in patients with visceral leishmaniasis. *Journal of infectious diseases*, *162*(6), 1354-1359.

- Angiosperm Phylogeny Group, Chase, M. W., Christenhusz, M. J., Fay, M. F., Byng, J. W., Judd, W. S., Stevens, P. F. (2016). An update of the Angiosperm Phylogeny Group classification for the orders and families of flowering plants: APG IV. *Botanical Journal of the Linnean Society*, *181*(1), 1–20.
- Ankita, S., Tribhuwan, S., Rekha, V. (2015). GC-MS Analysis of bioactive phytoconstituents from *Rumex vesicarius*. L. *International Journal of Pharmaceutical Research*, *6*, 269–72.
- Asakawa, T., Kawabe, Y., Yoshida, A., Aihara, Y., Manabe, T., Hirose, Y., Kan, T. (2016). Syntheses of methylated catechins and theaflavins using 2-nitrobenzenesulfonyl group to protect and deactivate phenol. *The Journal of Antibiotics*, *69*(4), 299–312.
- Aslam, B., Wang, W., Arshad, M. I., Khurshid, M., Muzammil, S., Rasool, M. H., Baloch, Z. (2018). Antibiotic resistance: a rundown of a global crisis. *Infection and Drug Resistance*, 1645–1658.
- Azebaze, A. G. B., Ouahouo, B. M. W., Vardamides, J. C., Valentin, A., Kuete, V., Acebey, L., Meyer, M. (2008). Antimicrobial and antileishmanial xanthones from the stem bark of *Allanblackia gabonensis* (Guttiferae). *Natural Product Research*, *22*(4), 333–341.
- Bailey, W. R., Scott, E. G. (1986). "Diagnostic Microbiology." C.V. Mosby Company.
- Bailly, C., Vergoten, G. (2021). Anticancer properties and mechanism of action of oblongifolin C, guttiferone K and related polyprenylated acylphloroglucinols. *Natural Products and Bioprospecting*, *11*(6), 629–641.
- Barbee, L. A., St. Cyr, S. B. (2022). Management of *Neisseria gonorrhoeae* in the United States: Summary of evidence from the development of the 2020 gonorrhea treatment recommendations and the 2021 Centers for Disease Control and Prevention sexually transmitted infection treatment guidelines. *Clinical Infectious Diseases*, *74*, S95–S111.
- Bayma, J. C., Arruda, M. S., Neto, M. S. (1998). A prenylated xanthone from the bark of *Symphonia globulifera*. *Phytochemistry*, *49*(4), 1159–1160.

- Bélanger, J., Balakrishna, M., Latha, P., Katumalla, S., Johns, T. (2010). Contribution of selected wild and cultivated leafy vegetables from South India to lutein and beta-carotene intake. *Asia Pacific Journal of Clinical Nutrition*, *19*(3), 417–424.
- Bicker, J., Petereit, F., Hensel, A. (2009). Proanthocyanidins and a phloroglucinol derivative from *Rumex acetosa* L. *Fitoterapia*, *80*(8), 483–495.
- Borghi, S. M., Fattori, V., Conchon-Costa, I., Pinge-Filho, P., Pavanelli, W. R., Verri, W. A. (2017). Leishmania infection: painful or painless? *Parasitology Research*, *116*, 465–475.
- Botta, B., Delle Monachè, F., Delle Monache, G., Kabangu, K. (1986). Acetylvismione D from *Psorospermum febrifugum*. *Phytochemistry*, *25*(3), 766–775.
- Bruneton, J. (1999). *Pharmacognosie, phytochimie, plantes médicinales*, 3ème édition Lavoisier*, Paris*, *1120*.
- Cabral, F. N., Bittrich, V., Estanislau do Amaral, M. D. C. (2016). Two new species and one new record of *Caraipa* (Calophyllaceae) from Colombia. *Systematic Botany*, *41*(2), 348–353.
- Cabral, F. N., Bittrich, V., Hopkins, M. J. G. (2017). Clusiaceae sl (Calophyllaceae, Clusiaceae ss and Hypericaceae) in the Viruá National Park, Roraima, Brazil. *Phytotaxa*, *329*(1), 1–27.
- Camacho, M. D. R., Phillipson, J. D., Croft, S. L., Solis, P. N., Marshall, S. J., Ghazanfar, S. A. (2003). Screening of plant extracts for antiprotozoal and cytotoxic activities. *Journal of Ethnopharmacology*, *89*(2–3), 185–191.
- Cao, S. G., Lim, T. B., Sim, K. Y., Goh, S. H. (1997). A highly prenylated xanthone from the bark of *Calophyllum gracilipes* (Guttiferae). *Natural Product Letters*, *10*(1), 55–58.
- Cao, S., Brodie, P. J., Miller, J. S., Ratovoson, F., Birkinshaw, C., Randrianasolo, S., Kingston, D. G. (2007). Guttiferones K and L, antiproliferative compounds of *Rheedia calcicola* from the Madagascar rain forest. *Journal of Natural Products*, *70*(4), 686–688.
- Cardona, M. L., Fernández, I., Pedro, J. R., Serrano, A. (1990). Xanthones from *Hypericum reflexum*. *Phytochemistry*, *29*(9), 3003–3006.

- Carturan, G., Facchin, G., Cocco, G., Navazio, G., Gubitosa, G. (1983). Hydrogenation of nitrocompounds with supported palladium catalysts: Influence of metal dispersion and nitrocompound nature. *Journal of Catalysis*, *82*(1), 56–65.
- Chalothorn, T., Rukachaisirikul, V., Phongpaichit, S., Pannara, S., Tansakul, C. (2019). Synthesis and antibacterial activity of emodin and its derivatives against methicillin-resistant *Staphylococcus aureus*. *Tetrahedron Letters*, *60*(35), 151004.
- Choe, S. G., Hwang, B. Y., Kim, M. S., Oh, G. J., Lee, K. S., Ro, J. S. (1998). Chemical Components of *Rumex acetosella* L. *Korean Journal of Pharmacognosy*, *29*(3), 209–216.
- Chukwujekwu, J. C., Coombes, P. H., Mulholland, D. A., Van Staden, J. (2006). Emodin, an antibacterial anthraquinone from the roots of *Cassia occidentalis*. *South African Journal of Botany*, *72*(2), 295–297.
- Ciochina, R., Grossman, R. B. (2006). Polycyclic polyprenylated acylphloroglucinols. *Chemical Reviews*, *106*(9), 3963–3986.
- Collakova, E., DellaPenna, D. (2001). Isolation and functional analysis of homogentisate phytyltransferase from *Synechocystis* sp. PCC 6803 and Arabidopsis. *Plant Physiology*, *127*(3), 1113–1124.
- Collee, J. G., Fraser, A. G., Marmino, B. P., Simons, A. (1996). *Mackin and McCartney Practical Medical Microbiology*. The Churchill Livingstone. *Inc. USA*.
- Cox, F. E. (Ed.). (2009). *Modern parasitology: a textbook of parasitology*. John Wiley Sons, London, 7–8.
- Craig C. Freeman and James L. Reveal. (2005). "Polygonaceae" pages 216–601. In: Flora of North America Editorial Committee (editors). *Flora of North America* vol. 5. Oxford University Press: New York, NY, USA.
- Croft, S. L., Yardley, V. (2002). Chemotherapy of leishmaniasis. *Current Pharmaceutical design*, *8*(4), 319–342.
- Cronquist, A. (1981). *An integrated system of classification of flowering plants*. Columbia University Press, Columbia, 220–231.

- Cuesta-Rubio, O., Velez-Castro, H., Frontana-Uribe, B. A., Cárdenas, J. (2001). Nemorosone, the major constituent of floral resins of *Clusia rosea*. *Phytochemistry*, *57*(2), 279–283.
- D'Amelia, V., Aversano, R., Chiaiese, P., Carputo, D. (2018). The antioxidant properties of plant flavonoids: their exploitation by molecular plant breeding. *Phytochemistry Reviews*, *17*, 611–625.
- Dacosta, Y. (2003). *Bioactive phytonutrients: 669 Bibliographic references*. Ed. Yves Dacosta.
- Demirezer, L. Ö., Kuruüzüm-Uz, A., Bergere, I., Schiewe, H. J., Zeeck, A. (2001). The structures of antioxidant and cytotoxic agents from natural source: anthraquinones and tannins from roots of *Rumex patientia*. *Phytochemistry*, *58*(8), 1213–1217.
- Demirezer, Ö., Kuruüzüm, A., Bergere, I., Schiewe, H. J., Zeeck, A. (2001). Five naphthalene glycosides from the roots of *Rumex patientia*. *Phytochemistry*, *56*(4), 399–402.
- Dénes, A., Papp, N., Babai, D., Czúcz, B., Molnár, Z. (2013). Edible, wild-growing plants and their utilization among Hungarians living in the Carpathian Basin based on ethnographic and ethnobotanical research: Trans-Danubian Studies A: *Natural Sciences Series*, *13*, 35–76.
- Desjeux, P. (2004). Leishmaniasis: current situation and new perspectives. *Comparative Immunology, Microbiology and Infectious Diseases*, *27*(5), 305–318.
- Dick, C. W., Abdul-Salim, K., Bermingham, E. (2003). Molecular systematic analysis reveals cryptic tertiary diversification of a widespread tropical rain forest tree. *The American Naturalist*, *162*(6), 691–703.
- Dick, C. W., Heuertz, M. (2008). The complex biogeographic history of a widespread tropical tree species. *Evolution*, *62*(11), 2760–2774.
- Diel, K. A. P., Marinho, L. C., von Poser, G. L. (2022). The ethnobotanical relevance of the tribe Symphonieae (Clusiaceae) around the world. *Journal of Ethnopharmacology*, *284*, 114745.
- Ekpo, B. A., Bala, D. N., Essien, E. E., Adesanya, S. A. (2008). Ethnobotanical survey of Akwa Ibom state of Nigeria. *Journal of Ethnopharmacology*, *115*(3), 387–408.

- El-Feraly, F. S., Cheatham, S. F., McChesney, J. D. (1985). Total synthesis of notholaenic acid. *Journal of Natural Products*, *48*(2), 293–298.
- El-Hawary, S. A., Sokkar, N. M., Ali, Z. Y., Yehia, M. M. (2011). A profile of bioactive compounds of *Rumex vesicarius* L. *Journal of Food Science*, *76*(8), C1195–C1202.
- Eloff, J. N. (1998). A sensitive and quick microplate method to determine the minimal inhibitory concentration of plant extracts for bacteria. *Planta medica*, *64*(08), 711–713.
- Elzaawely, A. A., Xuan, T. D., Tawata, S. (2005). Antioxidant and antibacterial activities of *Rumex japonicus* H OUTT. aerial parts. *Biological and Pharmaceutical Bulletin*, *28*(12), 2225–2230.
- Fan, P., Lou, H., Yu, W., Ren, D., Ma, B., Ji, M. (2004). Novel flavanol derivatives from grape seeds. *Tetrahedron Letters*, *45*(15), 3163-3166.
- Fredimoses, M., Zhou, X., Ai, W., Tian, X., Yang, B., Lin, X., Liu, Y. (2019). Emerixanthone E, a new xanthone derivative from deep sea *fungus Emericella* sp SCSIO 05240. *Natural Product Research*, *33*(14), 2088–2094.
- Fromentin, Y., Cottet, K., Kritsanida, M., Michel, S., Gaboriaud-Kolar, N., Lallemand, M. C. (2015). *Symphonia globulifera*, a widespread source of complex metabolites with potent biological activities. *Planta Medica*, *81*(02), 95–107.
- Fromentin, Y., Gaboriaud-Kolar, N., Lenta, B. N., Wansi, J. D., Buisson, D., Mouray, E., Michel, S. (2013). Synthesis of novel guttiferone A derivatives: in-vitro evaluation toward *Plasmodium falciparum*, *Trypanosoma brucei* and *Leishmania donovani*. *European Journal of Medicinal Chemistry*, *65*, 284–294.
- Fuentes, R. G., Pearce, K. C., Du, Y., Rakotondrafara, A., Valenciano, A. L., Cassera, M. B., Kingston, D. G. (2018). Phloroglucinols from the roots of *Garcinia dauphinensis* and their antiproliferative and antiplasmodial activities. *Journal of Natural Products*, *82*(3), 431–439.
- Gales, L., Damas, A. M. (2005). Xanthones-a structural perspective. *Current medicinal chemistry*, *12*(21), 2499–2515.
- Gautam, R., Karkhile, K. V., Bhutani, K. K., Jachak, S. M. (2010). Anti-inflammatory, cyclooxygenase (COX)-2, COX-1 inhibitory, and free radical scavenging effects of *Rumex nepalensis*. *Planta Medica*, *76*(14), 1564–1569.

- Gautam, R., Srivastava, A., Jachak, S. M. (2011). Simultaneous determination of naphthalene and anthraquinone derivatives in *Rumex nepalensis* Spreng. Roots by HPLC: comparison of different extraction methods and validation. *Phytochemical Analysis*, *22*(2), 153–157.
- Getie, M., Gebre-Mariam, T., Rietz, R., Höhne, C., Huschka, C., Schmidtke, M., Neubert, R. H. H. (2003). Evaluation of the anti-microbial and anti-inflammatory activities of the medicinal plants Dodonaea viscosa, *Rumex nervosus* and *Rumex abyssinicus*. *Fitoterapia*, *74*(1–2), 139–143.
- Ghosh, L., Gayen, J. R., Sinha, S., Pal, S., Pal, M., Saha, B. P. (2003). Antibacterial efficacy of *Rumex nepalensis* Spreng. roots. *Phytotherapy Research*, *17*(5), 558–559.
- Gontijo, V. S., Dos Santos, M. H., Viegas Jr, C. (2017). Biological and chemical aspects of natural biflavonoids from plants: a brief review. *Mini Reviews in Medicinal Chemistry*, *17*(10), 834–862.
- Goss, K. U., Schwarzenbach, R. P. (2001). Linear free energy relationships used to evaluate equilibrium partitioning of organic compounds. *Environmental Science & Technology*, *35*(1), 1–9.
- Grenand, P., Moretti, C., Jacquemin, H., Prévost, M. F. (2004). Pharmacopées traditionnelles en guyane, créoles, wayasi, palikur. *IRD, Paris*, 293–298.
- Gunaydin, K., Topcu, G., Ion, R. M. (2002). 1, 5-Dihydroxyanthraquinones and an anthrone from roots of *Rumex crispus*. *Natural product letters*, *16*(1), 65–70.
- Guo, S., Feng, B., Zhu, R., Ma, J., Wang, W. (2011). Preparative isolation of three anthraquinones from *Rumex japonicus* by high-speed counter-current chromatography. *Molecules*, *16*(2), 1201–1210.
- Gupta, M. P., Solis, P. N., Calderón, A. I., Guinneau-Sinclair, F., Correa, M., Galdames, C., Ocampo, R. (2005). Medical ethnobotany of the Teribes of Bocas del Toro, Panama. *Journal of ethnopharmacology*, *96*(3), 389–401.
- Gusakova, S. D., Khomova, T. V., Glushenkova, A. I. (1990). Lipids of the fruit of *Rumex paulsenianus*. *Chemistry of Natural Compounds*, *26*(5), 512–518.
- Gustafson, K. R., Blunt, J. W., Munro, M. H., Fuller, R. W., McKee, T. C., Cardellina II, J. H., Boyd, M. R. (1992). The guttiferones, HIV-inhibitory benzophenones from

Symphonia globulifera, *Garcinia livingstonei*, *Garcinia ovalifolia* and *Clusia rosea*. *Tetrahedron*, *48*(46), 10093–10102.

- Gustafsson, M. H., Bittrich, V., Stevens, P. F. (2002). Phylogeny of Clusiaceae based on rbc L sequences. *International Journal of Plant Sciences*, *163*(6), 1045–1054.
- Habib, M. R., Nikkon, F., Rahman, M., Haque, M. E., Karim, M. R. (2007). Isolation of stigmasterol and beta-sitosterol from methanolic extract of root bark of *Calotropis gigantea* (Linn). *Pakistan Journal of Biological Sciences: PJBS*, *10*(22), 4174–4176.
- Hayasaka S, Koseki T, Murayama T, Kwon E, Shiono Y. 2011. Phenylisobenzofuranones from *Fungicolous Nodulisporiu*m sp. SH-1. Z Naturforsch B. 66(9):961–964.
- Humphries, R., Bobenchik, A. M., Hindler, J. A., & Schuetz, A. N. (2021). Overview of changes to the clinical and laboratory standards institute performance standards for antimicrobial susceptibility testing, M100. *Journal of Clinical Microbiology*, *59*(12), 10–1128.
- Iinuma, M., Tosa, H., Tanaka, T., Kanamaru, S., Asai, F., Kobayashi, Y., Shimano, R. (1996). Antibacterial activity of some *Garcinia* benzophenone derivatives against methicillin-resistant *Staphylococcus aureus*. *Biological and Pharmaceutical Bulletin*, *19*(2), 311–314.
- Irvine, F. R. (1961). Woody plants of Ghana. *Woody plants of Ghana.*
- Jang, D. S., Kim, J. M., Kim, J. H., Kim, J. S. (2005). 24-nor-Ursane type triterpenoids from the stems of *Rumex japonicus*. *Chemical and Pharmaceutical Bulletin*, *53*(12), 1594–1596.
- John A. S., Mary L. B. (2020). Triterpenes: Biosynthesis, Biological Importance, and Their Role in Medicinal Chemistry. *Natural Product Reports, 15*(2), 320–334.
- John Brandbyge. (1993). "Polygonaceae". pages 531-544. In: Klaus Kubitzki (editor); Jens G. Rohwer, and Volker Bittrich (volume editors). *The Families and Genera of Vascular Plants* volume II. Springer-Verlag: Berlin; Heidelberg, Germany ISBN 978-3-540-55509-4 (Berlin) ISBN 978-0-387-55509-6 (New York).
- Jug, U., Vovk, I., Glavnik, V., Makuc, D., Naumoska, K. (2021). Off-line multidimensional high performance thin-layer chromatography for fractionation of

Japanese knotweed rhizome bark extract and isolation of flavan-3-ols, proanthocyanidins and anthraquinones. *Journal of Chromatography A*, *1637*, 461802.

- Karppinen, K., Hokkanen, J., Tolonen, A., Mattila, S., Hohtola, A. (2007). Biosynthesis of hyperforin and adhyperforin from amino acid precursors in shoot cultures of *Hypericum perforatum*. *Phytochemistry*, *68*(7), 1038–1045.
- Kerem, Z., Bilkis, I., Flaishman, M. A., Sivan, L. (2006). Antioxidant activity and inhibition of α-glucosidase by trans-resveratrol, piceid, and a novel trans-stilbene from the roots of Israeli *Rumex bucephalophorus* L. *Journal of Agricultural and Food Chemistry*, *54*(4), 1243–1247.
- Kevric, I., Cappel, M. A., Keeling, J. H. (2015). New world and old world Leishmania infections: a practical review. *Dermatologic Clinics*, *33*(3), 579–593.
- Khanjani Jafroodi, S., Farazmand, A., Amin, M., Doroodgar, A., Shirzadi, M. R., Razavi, M. R. (2015). Methanolic Extract's Activity of *Artemisia absinthium*, *Vitexagnus-castus* and Phytolacaamericana Against Leishmania major; in vitro and *in vivo*. *International Archives of Health Sciences*, *2*(2).
- Khare, C. P. (2007). *Indian medicinal plants: An Illustrated Dictionary*. Springer-Verlag. *Berlin pg*, 699–700.
- Kim, K. J., Liu, X., Komabayashi, T., Jeong, S. I., Selli, S. (2016). Natural products for infectious diseases. *Evidence-Based Complementary and Alternative Medicine, 2016*.
- Kimutai, A., Ngure, P., Tonui, W., Gicheru, M., Nyamwamu, L. (2009). Leishmaniasis in Northern and Western Africa: a review. *African Journal of Infectious Diseases*, *3*(1).
- Klingauf, P., Beuerle, T., Mellenthin, A., El-Moghazy, S. A., Boubakir, Z., Beerhues, L. (2005). Biosynthesis of the hyperforin skeleton in *Hypericum calycinum* cell cultures. *Phytochemistry*, *66*(2), 139–145.
- Kobets, T., Grekov, I., Lipoldova, M. (2012). Leishmaniasis: prevention, parasite detection and treatment. *Current Medicinal Chemistry*, *19*(10), 1443–1474.
- Köser, C. U., Ellington, M. J., Peacock, S. J. (2014). Whole-genome sequencing to control antimicrobial resistance. *Trends in Genetics*, *30*(9), 401–407.
- Kuete, V., Alibert-Franco, S., Eyong, K. O., Ngameni, B., Folefoc, G. N., Nguemeving, J. R., Pagès, J. M. (2011). Antibacterial activity of some natural products against

bacteria expressing a multidrug-resistant phenotype. *International Journal of Antimicrobial Agents*, *37*(2), 156–161.

- Kumar, S., Sharma, S., Chattopadhyay, S. K. (2013). The potential health benefit of polyisoprenylated benzophenones from *Garcinia* and related genera: Ethnobotanical and therapeutic importance. *Fitoterapia*, *89*, 86–125.
- Kuruüzüm, A., Demirezer, L. Ö., Bergere, I., Zeeck, A. (2001). Two new chlorinated Naphthalene Glycosides from *Rumex patientia*. *Journal of Natural Products*, *64*(5), 688–690.
- Lee, N. J., Choi, J. H., Koo, B. S., Ryu, S. Y., Han, Y. H., Lee, S. I., Lee, D. U. (2005). Antimutagenicity and cytotoxicity of the constituents from the aerial parts of *Rumex acetosa*. *Biological and Pharmaceutical Bulletin*, *28*(11), 2158–2161.
- Lee, Y. K., Hwang, B. S., Hwang, Y., Lee, S. Y., Oh, Y. T., Kim, C. H., ... & Jeong, Y. T. (2021). Melanogenesis inhibitory activities of Epicatechin-3-*O*-gallate isolated from *Polygonum amphibium* L. *Microbiology and Biotechnology Letters*, 49(1), 24-31.
- Lenta, B. N., Ngouela, S., Noungoue, D. T., Tsamo, E., Connolly, J. D. (2004). Symphonin: A new prenylated pyranoxanthone with antimicrobial activity from the seeds of *Symphonia globulifera* (Guttiferae). *Bulletin of the Chemical Society of Ethiopia*, *18*(2).
- Lenta, B. N., Vonthron-Sénécheau, C., Weniger, B., Devkota, K. P., Ngoupayo, J., Kaiser, M., Sewald, N. (2007). Leishmanicidal and cholinesterase inhibiting activities of phenolic compounds from *Allanblackia monticola* and *Symphonia globulifera*. *Molecules*, *12*(8), 1548–1557.
- Li, J. J., Li, Y. X., Li, N., Zhu, H. T., Wang, D., Zhang, Y. J. (2022). The genus *Rumex* (Polygonaceae): an ethnobotanical, phytochemical and pharmacological review. *Natural Products and Bioprospecting*, *12*(1), 21.
- Liang, H. X., Dai, H. Q., Fu, H. A., Dong, X. P., Adebayo, A. H., Zhang, L. X., Cheng, Y. X. (2010). Bioactive compounds from *Rumex* plants. *Phytochemistry Letters*, *3*(4), 181–184.
- Lin, C. N., Chung, M. I., Lu, C. M. (1990). Anthraquinones from *Rhamnus formosana*. *Phytochemistry*, *29*(12), 3903–3905.

- Liu, B., Falkenstein-Paul, H., Schmidt, W., Beerhues, L. (2003). Benzophenone synthase and chalcone synthase from *Hypericum androsaemum* cell cultures: cDNA cloning, functional expression, and site-directed mutagenesis of two polyketide synthases. *The Plant Journal*, *34*(6), 847–855.
- Locksley, H. D., Moore, I., & Scheinmann, F. (1966). Extractives from guttiferae. Part III. The isolation and structure of symphoxanthone and globuxanthone from *Symphonia globulifera* L. *Journal of the Chemical Society C: Organic*, 2186–2190.
- Loi, M. C., Poli, F., Sacchetti, G., Selenu, M. B., Ballero, M. (2004). Ethnopharmacology of ogliastra (Villagrande Strisaili, Sardinia, Italy). *Fitoterapia*, *75*(3–4), 277–295.
- Lopez, A., Hudson, J. B., Towers, G. H. N. (2001). Antiviral and antimicrobial activities of Colombian medicinal plants. *Journal of Ethnopharmacology*, *77*(2–3), 189–196.
- Madigan, M. T., Martinko, J. M., & Parker, J. (1997). *Brock biology of microorganisms* (Vol. 11). Upper Saddle River, NJ: Prentice hall.
- Mai, L. P., Guéritte, F., Dumontet, V., Tri, M. V., Hill, B., Thoison, O., Sévenet, T. (2001). Cytotoxicity of rhamnosylanthraquinones and rhamnosylanthrones from *Rhamnus nepalensis*. *Journal of Natural Products*, *64*(9), 1162–1168.
- Majekodunmi, S. O., Aliga, U. L. (2017). A systematic study on flow ability and compressibility of *Symphonia globulifera* stem bark powder for tablet dosage form. *American Journal of Biomedical Engineering*, *7*, 1–8.
- Malik, K., Ahmad, M., Öztürk, M., Altay, V., Zafar, M., Sultana, S. (2021). *Herbals of Asia: prevalent diseases and their treatments*. Springer, Berlin, 499–507.
- Mandell, G. L., Bennett, J. E., Dolin, R. (2014). "Principles and Practice of Infectious Diseases." Elsevier, Saunders, 2285–2287.
- Markham, K. R. (1982). *Techniques of flavonoid identification*. Academic press, London, 100-113.
- Marques, E. D. J., Ferraz, C. G., dos Santos, I. B., dos Santos, I. I., El-Bachá, R. S., Ribeiro, P. R., Cruz, F. G. (2021). Chemical constituents isolated from *Clusia criuva* subsp. *Criuva* and their chemophenetics significance. *Biochemical Systematics and Ecology*, *97*, 104293.

- Marti, G., Eparvier, V., Moretti, C., Prado, S., Grellier, P., Hue, N., Litaudon, M. (2010). Antiplasmodial benzophenone derivatives from the root barks of *Symphonia globulifera* (Clusiaceae). *Phytochemistry*, *71*(8–9), 964–974.
- Mativandlela, S. P. N., Lall, N., Meyer, J. J. M. (2006). Antibacterial, antifungal and antitubercular activity of (the roots of) *Pelargonium reniforme* (CURT) and *Pelargonium sidoides* (DC)(Geraniaceae) root extracts. *South African Journal of Botany*, *72*(2), 232–237.
- Mbaveng, A.T.; Kuete, V. Nguemeving, J.R. Penlap, B.V. Nkengfack, A.E. Meyer, J.M. Krohn, K. Antimicrobial activity of the extracts and compounds obtained from *Vismia guineensis* (Guttiferae). *Asian Journal of Traditional Medicines*, **2008**, *3*, 211–223.
- Mei, R., Liang, H., Wang, J., Zeng, L., Lu, Q., Cheng, Y. (2009). New seco-anthraquinone glucosides from *Rumex nepalensis*. *Planta Medica*, *75*(10), 1162–1164.
- Mkounga, P., Fomum, Z. T., Meyer, M., Bodo, B., Nkengfack, A. E. (2009). Globulixanthone F, a new polyoxygenated xanthone with an isoprenoid group and two antimicrobial biflavonoids from the stem bark of *Symphonia globulifera*. *Natural Product Communications*, *4*(6), 218–237.
- Molnár, P., Ősz, E., Zsila, F., Deli, J. (2005). Isolation and structure elucidation of anhydroluteins from cooked sorrel (*Rumex rugosus* Campd.). *Chemistry and Biodiversity*, *2*(7), 928–935.
- Mosmann, T. (1983). Rapid colorimetric assay for cellular growth and survival: application to proliferation and cytotoxicity assays. *Journal of Immunological Methods*, *65*(1–2), 55–63.
- Muganga, R., Angenot, L., Tits, M., Frederich, M. (2010). Antiplasmodial and cytotoxic activities of Rwandan medicinal plants used in the treatment of malaria. *Journal of Ethnopharmacology*, *128*(1), 52–57.
- Munavu, R. M., Mudamba, L. O., Ogur, J. A. (1984). Isolation and characterization of the major anthraquinone pigments from *Rumex abysinica*. *Planta medica*, *50*(01), 111–123.
- Murray, C. J., Barber, R. M., Foreman, K. J., Ozgoren, A. A., Abd-Allah, F., Abera, S. F., Del Pozo-Cruz, B. (2015). Global, regional, and national disability-adjusted life years (DALYs) for 306 diseases and injuries and healthy life expectancy (HALE) for

188 countries, 1990–2013: quantifying the epidemiological transition. *The Lancet*, *386*(10009), 2145–2191.

- Newman, D. J., Cragg, G. M. (2012). Natural products as sources of new drugs over the 30 years from 1981 to 2010. *Journal of Natural Products*, *75*(3), 311–335.
- Ngamba, D., Tane, P., Bezabih, M., Awouafack, M., Abegaz, B. (2007). Two new anthraquinones from *Gladiolus psittascinus*. *Biochemical Systematics and Ecology*, 35(10), 709–713.
- Ngouela, S., Lenta, B. N., Noungoue, D. T., Ngoupayo, J., Boyom, F. F., Tsamo, E., Connolly, J. D. (2006). Anti-plasmodial and antioxidant activities of constituents of the seed shells of *Symphonia globulifera* Linn f. *Phytochemistry*, *67*(3), 302–306.
- Nguyen, H. T., Nguyen, T. T., Duong, T. H., Tran, N. M. A., Nguyen, C. H., Nguyen, T. H. A., Sichaem, J. (2022). α-Glucosidase inhibitory and antimicrobial benzoylphloroglucinols from *Garcinia schomburgakiana* fruits: *In vitro* and *in silico* studies. *Molecules*, *27*(8), 2574.
- Nkengfack, A. E., Mkounga, P., Meyer, M., Fomum, Z. T., Bodo, B. (2002). Globulixanthones C, D and E: three prenylated xanthones with antimicrobial properties from the root bark of *Symphonia globulifera*. *Phytochemistry*, *61*(2), 181–187.
- Noman, O. M., Mothana, R. A., Al-Rehaily, A. J., Nasr, F. A., Khaled, J. M., Alajmi, M. F., Al-Said, M. S. (2019). Phytochemical analysis and anti-diabetic, anti-inflammatory and antioxidant activities of *Loranthus acaciae* Zucc. grown in Saudi Arabia. *Saudi Pharmaceutical Journal*, *27*(5), 724–730.
- Nwaka, S., Hudson, A. (2006). Innovative lead discovery strategies for tropical diseases. *Nature Reviews Drug Discovery*, *5*(11), 941–955.
- Ohnmacht, S., West, R., Simionescu, R., Atkinson, J. (2008). Assignment of the ^{1}H and ^{13}C NMR of tocotrienols. *Magnetic Resonance in Chemistry*, *46*(3), 287–294.
- Omosa, L. K., Midiwo, J. O., Mbaveng, A. T., Tankeo, S. B., Seukep, J. A., Voukeng, I. K., Kuete, V. (2016). Antibacterial activities and structure–activity relationships of a panel of 48 compounds from Kenyan plants against multidrug resistant phenotypes. *SpringerPlus*, *5*, 1–15.

- Orbán-Gyapai, O., Lajter, I., Hohmann, J., Jakab, G., Vasas, A. (2015). Xanthine oxidase inhibitory activity of extracts prepared from Polygonaceae species. *Phytotherapy Research*, *29*(3), 459–465.
- Orbán-Gyapai, O., Liktor-Busa, E., Kúsz, N., Stefkó, D., Urbán, E., Hohmann, J., Vasas, A. (2017). Antibacterial screening of *Rumex* species native to the Carpathian Basin and bioactivity-guided isolation of compounds from *Rumex aquaticus*. *Fitoterapia*, *118*, 101–106.
- Oryan A., 2015. Plant-derived compounds in treatment of leishmaniasis. *Iranian Journal of Veterinary Research*, 16, 1–19.
- Oyen L.P.A., (2005). Basic list of species and commodity grouping. *Plant Resources of Tropical Africa*, 12, 110–113.
- Pavia DL, Lampman MG, Kriz GS, Vyvyan JR. Introduction to spectroscopy. 5th edition, Washington, USA. p 235.
- Persing, D. H., Tenover, F. C., Versalovic, J., Tang, Y. W., Unger, E. R., Relman, D. A., White, T. J. (1993). "Molecular Microbiology: Diagnostic Principles and Practice." *American Society for Microbiology*, *16*(2), 59-67.
- Pizzolatti, M. G., Venson, A. F., Júnior, A. S., Smânia, E. D. F., Braz-Filho, R. (2002). Two epimeric flavalignans from Trichilia catigua (Meliaceae) with antimicrobial activity. *Zeitschrift für Naturforschung C*, *57*(5-6), 483-488.
- Rao, K. N. V., Sunitha, C. H., Banji, D., Sandhya, S., Mahesh, V. (2011). A study on the nutraceuticals from the genus *Rumex*. *Hygeia Journal for Drugs and Medicines*, *3*(1), 76–88.
- Reithinger, R., Dujardin, J. C. (2007). Molecular diagnosis of leishmaniasis: current status and future applications. *Journal of Clinical Microbiology*, *45*(1), 21–25.
- Rivero-Cruz, I., Acevedo, L., Guerrero, J. A., Martínez, S., Pereda-Miranda, R., Mata, R., Timmermann, B. N. (2005). Antimycobacterial agents from selected Mexican medicinal plants. *Journal of pharmacy and Pharmacology*, *57*(9), 1117–1126.
- Ruhfel, B. R., Bittrich, V., Bove, C. P., Gustafsson, M. H., Philbrick, C. T., Rutishauser, R., Davis, C. C. (2011). Phylogeny of the *clusioid clade* (Malpighiales): evidence from the plastid and mitochondrial genomes. *American Journal of Botany*, *98*(2), 306–325.

- Ruhfel, B. R., Stevens, P. F., Davis, C. C. (2013). Combined morphological and molecular phylogeny of the *clusioid clade* (Malpighiales) and the placement of the ancient rosid macrofossil Paleoclusia. *International Journal of Plant Sciences*, *174*(6), 910–936.
- Sahreen, S., Khan, M. R., Khan, R. A. (2014). Comprehensive assessment of phenolics and antiradical potential of *Rumex hastatus* D. Don. roots. *BMC Complementary and Alternative Medicine*, *14*, 1–11.
- Seng, P., Drancourt, M., Gouriet, F., La Scola, B., Fournier, P. E., Rolain, J. M., Raoult, D. (2009). Ongoing revolution in bacteriology: routine identification of bacteria by matrix-assisted laser desorption ionization Time-of-Flight mass spectrometry. *Clinical Infectious Diseases*, *49*(4), 543–551.
- Silva, A. M. S., Pinto, D. C. G. A. (2005). Structure elucidation of xanthone derivatives: studies of nuclear magnetic resonance spectroscopy. *Current Medicinal Chemistry*, *12*(21), 2481–2497.
- Singh, N., Mishra, B. B., Bajpai, S., Singh, R. K., Tiwari, V. K. (2014). Natural product-based leads to fight against leishmaniasis. *Bioorganic and Medicinal Chemistry*, *22*(1), 18–45.
- Singh, R. K., Pandey, H. P., Sundar, S. (2006). Visceral leishmaniasis (kala-azar): challenges ahead. *Indian Journal of Medical Research*, *123*(3), 331.
- Siqueira-Neto, J. L., Song, O. R., Oh, H., Sohn, J. H., Yang, G., Nam, J., Freitas-Junior, L. H. (2010). Antileishmanial high-throughput drug screening reveals drug candidates with new scaffolds. *PLoS Neglected Tropical Diseases*, *4*(5), e675.
- Slonczewski, J. L., Foster, J. W., Foster, E. (2020). *Microbiology: An Evolving Science Fifth International Student Edition with Ebook, Smartwork 5, Animations, eTopics and eAppendices*. WW Norton & Company, New York City, 1200-1250.
- Sosa, A. M., Amaya, S., Salamanca Capusiri, E., Gilabert, M., Bardón, A., Giménez, A., Borkosky, S. A. (2016). Active sesquiterpene lactones against *Leishmania amazonensis* and *Leishmania braziliensis*. *Natural Product Research*, *30*(22), 2611–2615.
- Ssegawa, P., Kasenene, J. M. (2007). Medicinal plant diversity and uses in the Sango bay area, Southern Uganda. *Journal of Ethnopharmacology*, *113*(3), 521–540.

- Stafford, A. M. (2002). Plant cell cultures as a source of bioactive small molecules. *Current Opinion in Drug Discovery and Development*, *5*(2), 296–303.
- Suffredini, I. B., Paciencia, M. L. B., Díaz, I. E., Frana, S. A., Bernardi, M. M. (2017). Mice behavioral phenotype changes after administration of Anani (*Symphonia globulifera*, Clusiaceae), an alternative Latin American and African medicine. *Pharmacognosy Magazine*, *13*(52), 617.
- Süleyman, H. A. L. İ. S., Demirezer, L. Ö., Kuruüzüm, A., Banoğlu, Z. N., Göçer, F. A. T. I. M. A., Özbakir, G., Gepdiremen, A. (1999). Antiinflammatory effect of the aqueous extract from *Rumex patientia* L. roots. *Journal of Ethnopharmacology*, *65*(2), 141–148.
- Tala, M. F., Ansary, M. W. R., Talontsi, F. M., Kowa, T. K., Islam, M. T., Tane, P. (2018). Anthraquinones and flavanols isolated from the vegetable herb *Rumex abyssinicus* inhibit motility of *Phytophthora capsici zoospores*. *South African Journal of Botany*, *115*, 1–4.
- Tamokou, J. D. D., Chouna, J. R., Fischer-Fodor, E., Chereches, G., Barbos, O., Damian, G., Silaghi-Dumitrescu, R. (2013). Anticancer and antimicrobial activities of some antioxidant-rich Cameroonian medicinal plants. *PLoS One*, *8*(2), e55880.
- Tan, X., Han, X., Teng, H., Li, Q., Chen, Y., Lei, X., Yang, G. (2021). Structural elucidation of garcipaucinones A and B from *Garcinia paucinervis* using quantum chemical calculations. *Journal of Natural Products*, *84*(4), 972–978.
- Tavares, L., Carrilho, D., Tyagi, M., Barata, D., Serra, A. T., Duarte, C. M. M., Dos Santos, C. N. (2010). Antioxidant capacity of Macaronesian traditional medicinal plants. *Molecules*, *15*(4), 2576–2592.
- Teich, L., Daub, K. S., Krügel, V., Nissler, L., Gebhardt, R., Eger, K. (2004). Synthesis and biological evaluation of new derivatives of emodin. *Bioorganic and Medicinal Chemistry*, *12*(22), 5961–5971.
- Téné, D.G.; Tih, A.E.; Kamdem, M.H.K.; Talla, R.M.; Diboue, P.H.B.; Melongo, Y.K.D.; Ghogomu, R.T. (2021). Antibacterial and antioxidant activities of compounds isolated from the leaves of *Symphonia globulifera* (Clusiaceae) and their chemophenetic significance. *Biochemical Systematics and Ecology*, *99*, 104345.

- Torres-Guerrero, E., Quintanilla-Cedillo, M. R., Ruiz-Esmenjaud, J., Arenas, R. (2017). Leishmaniasis: a review. *F1000Research, 6*.
- Tsamo, L. D. F., Yimgang, L. V., Wouamba, S. C. N., Mkounga, P., Nkengfack, A. E., Voutquenne-Nazabadioko, L., ... & Sewald, N. (2021). A new ceramide (rumexamide) and other chemical constituents from Rumex abyssinicus jacq (polygonaceae): isolation, characterization, antibacterial activities and chemophenetic significance. *Advances in Biological Chemistry*, *11*(05), 266–282.
-
- Valentão, P., Andrade, P. B., Silva, E., Vicente, A., Santos, H., Bastos, M. L., Seabra, R. M. (2002). Methoxylated xanthones in the quality control of small centaury (*Centaurium erythraea*) flowering tops. *Journal of Agricultural and Food Chemistry*, *50*(3), 460–463.
- Van den Berg, A. J. J., Labadie, R. P. (1981). The production of acetate derived hydroxyanthraquinones, -dianthrones, -naphthalenes and-benzenes in tissue cultures from *Rumex alpinus*. *Planta Medica*, *41*(02), 169–173.
- Vasas, A., Orbán-Gyapai, O., Hohmann, J. (2015). The Genus *Rumex*: Review of traditional uses, phytochemistry and pharmacology. *Journal of Ethnopharmacology*, *175*, 198-228.
- Vázquez, F. M., Suarez, M. A., Pérez, A. (1997). Medicinal plants used in the Barros Área, Badajoz province (Spain). *Journal of Ethnopharmacology*, *55*(2), 81–85.
- Ventola, C. L. (2015). The antibiotic resistance crisis: part 1: causes and threats. *Pharmacy and Therapeutics*, *40*(4), 277.
- Wegiera, M. A. G. D. A. L. E. N. A., Smolarz, H. D., Wianowska, D., Dawidowicz, A. L. (2007). Anthracene derivatives in some species of *Rumex* L. genus. *Acta Societatis Botanicorum Poloniae*, *76*(2).
- Wei, Y., Liu, Q., Yu, J., Feng, Q., Zhao, L., Song, H., Wang, W. (2015). Antibacterial mode of action of 1, 8-dihydroxy-anthraquinone from Porphyra haitanensis against *Staphylococcus aureus*. *Natural Product Research*, *29*(10), 976–979.
- Wei, Y., Xie, Q., Fisher, D., Sutherland, I. A. (2011). Separation of patuletin-3-*O*-glucoside, astragalin, quercetin, kaempferol and isorhamnetin from *Flaveria bidentis*

(L.) Kuntze by elution-pump-out high-performance counter-current chromatography. *Journal of Chromatography A*, *1218*(36), 6206–6211.

- Weinstein, M. P., Lewis, J. S. (2020). The clinical and laboratory standards institute subcommittee on antimicrobial susceptibility testing: background, organization, functions, and processes. *Journal of Clinical Microbiology*, *58*(3), 10–1128.
- World Health Organization. (2017). Global leishmaniasis update, 2006-2015: a turning point in leishmaniasis surveillance. *Weekly Epidemiological Record*, *92*(38), 557–565.
- World Health Organization. (2020). Global leishmaniasis surveillance, 2017–2018, and first report on 5 additional indicators. *Weekly Epidemiological Record 95*(25), 265–279.
- World Health Organization. https://www.who.int/features/qa/typhoid-fever/fr/, 2020.
- Wu, S. B., Long, C., Kennelly, E. J. (2014). Structural diversity and bioactivities of natural benzophenones. *Natural Product Reports*, *31*(9), 1158–1174.
- Wurdack, K. J., Davis, C. C. (2009). Malpighiales phylogenetics: gaining ground on one of the most recalcitrant clades in the angiosperm tree of life. *American Journal of Botany*, *96*(8), 1551–1570.
- Xiao, Z. P., Wu, H. K., Wu, T., Shi, H., Hang, B., Aisa, H. A. (2006). Kaempferol and quercetin flavonoids from *Rosa rugosa*. *Chemistry of Natural Compounds*, *42*, 736–737.
- Xu, Z., Deng, M., Xu, Z., Deng, M. (2017). Polygonaceae. *Identification and Control of Common Weeds: Volume 2*, 171–243.
- Yadav, S., Kapley, A. (2021). Antibiotic resistance: Global health crisis and metagenomics. *Biotechnology Reports*, *29*, e00604.
- Yang, X., Kang, M. C., Li, Y., Kim, E. A., Kang, S. M., Jeon, Y. J. (2014). Anti-inflammatory activity of questinol isolated from marine-derived fungus *Eurotium amstelodami* in lipopolysaccharide-stimulated RAW 264.7 macrophages. *Journal of Microbiology and Biotechnology*, *24*(10), 1346–1353.
- Yang XD, Li ZY, Mei SX, Zhao JF, Zhang HB, Li L. 2003. Two new phenylpropanoid esters of rhamnose from *Lagotis yunnanensis*. *Journal of Asian Natural Products Research*, 5(3), 223–226.

- Yang, Y., Yan, Y. M., Wei, W., Luo, J., Zhang, L. S., Zhou, X. J., Cheng, Y. X. (2013). Anthraquinone derivatives from Rumex plants and endophytic *Aspergillus fumigatus* and their effects on diabetic nephropathy. *Bioorganic and Medicinal Chemistry Letters*, *23*(13), 3905–3909.
- Yoon, H. M., Park, J. Y., Oh, M. H., Kim, K. H., Han, J. H., Whang, W. K. (2005). A new acetophenone of aerial parts from *Rumex aquatica*. *Natural Product Sciences*, *11*(2), 75–78
- Yoshikawa, T., Naito, Y. (2002). What is oxidative stress? *Japan Medical Association Journal*, *45*(7), 271–276.
- Yuan, Y., Chen, W. S., Zheng, S. Q., Yang, G. J., Zhang, W. D., Zhang, H. M. (2001). Studies on chemical constituents in root of *Rumex patientia* L. *Zhongguo Zhong yao za zhi = Zhongguo zhongyao zazhi = China Journal of Chinese Materia Medica*, *26*(4), 256–258.
- Yuniati, Y., Rollando, R. (2018). Isolation of antibacterial compounds from endophyte fungal of *fusarium* sp. In *phyllanthus niruri* linn. Leaves. *Journal of Pharmaceutical Sciences and Research*, *10*(2), 260–264.
- Zee, O. P., Kim, D. K., Kwon, H. C., Lee, K. R. (1998). A new epoxynaphthoquinol from *Rumex japonicus*. *Archives of Pharmacal Research*, *21*, 485–486.
- Zeutsop, J. F., Zébazé, J. N., Nono, R. N., Frese, M., Chouna, J. R., Lenta, B. N., Sewald, N. (2021). Antioxidant and cytotoxicity activities of *δ*-tocotrienol from the seeds of *Allophylus africanus*. *Natural Product Research*, *36*(18), 4655–4665.
- Zhang, Y., Xia, Y., Lai, Y., Tang, F., Luo, Z., Xue, Y., Zhang, J. (2014). Efficient synthesis of kinsenoside and goodyeroside a by a chemo-enzymatic approach. *Molecules*, *19*(10), 16950–16958.
- Zhen-li, L. I. U., Lin-fu, L. I., Zhi-mao, C. H. A. O., Zhi-qian, S. O. N. G., Chun, W. A. N. G., Ling, Z. H. A. N. G. (2009). Chemical constituents from *Radix Polygoni multiflori* Thunb. after Preparing. *Natural Product Research and Development*, *21*(2), 239–241.
- (2012). Leishmanisis and global estimates of its incidence. *Public Library of Science ONE* **7**, 1–12.

ANNEXE

PUBLICATIONS RESULTING FROM THIS WORK:

1. **Nguengang, R. T**., Tchegnitegni, B. T., Ateba, J. E. T., Tabekoueng, G. B., Awantu, A. F., Bankeu, J. J. K., Lenta, B. N. (2022). Antibacterial constituents of *Rumex nepalensis* spreng and its emodin derivatives. *Natural Product Research*, 1-12.
2. **Nguengang, R. T**., Tchegnitegni, B. T., Nono, E. C. N., Bellier Tabekoueng, G., Fongang, Y. S. F., Bankeu, J. J. K., Lenta, B. N. (2023). Constituents of the Stem Bark of *Symphonia globulifera* Linn. f. with Antileishmanial and Antibacterial Activities. *Molecules*, *28*(6), 2473.

PARTICIPATION IN NATIONAL AND INTERNATIONAL CONFERENCES:

1. Yaoundé-Bielefeld SDG Graduate School of Natural Products with antiparasitic and Antimicrobial activity (YaBiNaPa) Network Meeting (from 12th to 15th February 2019).
2. 4th Scientific Conference of Ph.D. Candidates and Young Researchers from State Universities/Private Institutes of Higher Education and Research (CDJEC) (from 11th to 13th July 2019).
3. DAAD Alumni conference (Genetic resources, research and innovation from 24th to 26th July 2019).